

The Design and Synthesis of Small Molecule Bromodomain Inhibitors

Simon Christopher Cranko Alcock Lucas

PhD Thesis

2018

Supervisors: Dr. Stephen Atkinson and Professor Nicholas Tomkinson

Department of Pure & Applied Chemistry, University of Strathclyde, 295 Cathedral Street, Glasgow G1 1XL

Epigenetics Discovery Performance Unit, GSK Medicines Research Centre, Gunnels Wood Road, Stevenage, Hertfordshire, SG1 2NY

GSK Confidential – Do not copy

This thesis is the result of the author's original research. It has been composed by the author and has not been previously submitted for examination which has led to the award of a degree.

The copyright of this thesis belongs to GSK in accordance with the author's contract of engagement with GSK under the terms of the United Kingdom Copyright Acts. Due acknowledgement must always be made of the use of any material contained in, or derived from, this thesis.

Signed:

Date:

Acknowledgements

I would like to thank Stephen Atkinson for all his dedicated help, support and guidance throughout my PhD. Without your knowledge, insight and encouragement I would not be the scientist that I am today. Thank you to my academic supervisor Nick Tomkinson for your guidance and insightful support of this work, and, to you and your group, for welcoming me to Glasgow for an enjoyable three months.

I am deeply grateful to everyone in the Epigenetics DPU for making me feel at home for the duration of the PhD. I am particularly grateful to Alex, Bob (Woof!), Frankie, Jon, and Kayleigh for their input into this work. Thanks to Manu for your support, enthusiasm and interest in all my PhD work and to Rab for his support of this work. Also thank you to Kaan, who survived his IP year with me and taught me a lot of valuable lessons!

Thank you to Harry Kelly and William Kerr for accepting me onto the PhD programme.

I am grateful to all those at GSK who have assisted me in anyway throughout my time on the PhD programme; Paul Bamborough and Chun-wa Chung for their help with X-ray crystallography and modelling; James Gray for running DMPK experiments; Richard Briers, Eric Hortense, Steve Jackson, and Andy Knaggs for chiral HPLC analysis and purification; Tony Cook and Esme Clarke for HRMS analysis; Sean Lynn for help interpreting and assigning NMR spectra; Alex Phillipou for teaching me about nanoBRET assays; and finally thank you to Laurie Gordon for teaching me to run TR-FRET assays and for her help with generating data.

Thank you to all the other PhD students and graduates at GSK who have created a fun and vibrant environment over the last three and half years; in particular, thanks to Mike for surviving our cosy work environment and being a joy to work with; and to Ross and Heather for putting up with me on the commute!

Thank you to Mum and Dad for their continued support and encouragement, and to Lorna and Steve, for all their help over the last three years.

Finally, thank you to my ginger monsters, Rex and Toby, for always bringing a smile to my face. And most importantly, thank you Jen, without your continued love and understanding I would not be where I am today.

Abstract

Pan-BET inhibitors show profound anti-proliferative and anti-inflammatory activity and, as such, several compounds have entered clinical trials for oncology indications. However, dose-limiting toxicities have been observed in patients which could limit their use. As the BET family consists of 4 bromodomain containing proteins (BRD2, 3, 4, and T), each of which contain 2 bromodomains (a BD1 and a BD2 domain), there is the potential that inhibitors which selectively target a single protein or domain, will retain efficacy and mitigate the dose-limiting toxicity observed with pan-BET inhibitors.

This work describes the development of a series of BD2 selective 2,3-dihydrobenzofurans as highly potent BD2 inhibitors with 1000-fold selectivity over BD1. Investment in the development of two orthogonal routes delivered inhibitors which were potent and selective but had raised *in vitro* clearance and low solubility. An *in silico* Metasite prediction identified dehydrogenation of the 2,3-dihydrobenzofuran as a metabolic weakness. Insertion of a synthetically challenging quaternary centre into the 2,3-dihydrobenzofurans blocked the predicted site of metabolism and improved solubility. This led to the development of GSK852; a potent, 1000-fold selective, highly soluble compound with good *in vivo* rat and dog PK as a promising pre-candidate molecule.

Whilst the BET family has generated much excitement in drug discovery, it contains only 8 of the 61 known bromodomains. The function of many of the non-BET bromodomains is currently unknown and there is significant interest in the development of selective chemical probes which will enable elucidation their biological roles and identify new therapeutic targets. This work also details the identification of a chemical probe for the CECR2 bromodomain. Starting from a promiscuous template, work was carried out to improve the potency, selectivity and physico-chemical properties of the chemotype. Structure based optimisation of a hydantoin lead to the development of GSK232, a highly potent, selective and soluble chemical probe for CECR2.

Abbreviations

Ac	Acetyl
ALARM NMR	A La assay to detect reactive molecules by NMR
AMP	Artificial membrane permeability
Amphos	Bis(di- <i>tert</i> -butyl(4-dimethylaminophenyl)phosphine)dichloropalladium(II)
aq.	Aqueous
Arg	Arginine
Asn	Asparagine
Asp	Aspartate
ATAD2	ATPase family, AAA domain containing 2
AUC	Area under curve
aq.	Aqueous
BET	Bromo and Extra Terminal Domain
Bn	Benzyl
Boc	<i>tert</i> -Butyloxycarbonyl protecting group
BPTF	Bromodomain PHD finger transcription factor
BRD	Bromodomain
BRET	Bioluminescence resonance energy transfer
c	Cyclo
c-MYC	MYC proto-oncogene
CAD	Charged aerosol detection
CECR2	Cats Eye Syndrome chromosome region, candidate 2
CIA	Collagen Induced Arthritis
CL _b	Blood Clearance
CL _{FU}	Unbound Clearance
CLND	Chemiluminescent nitrogen detection
CNS	Central nervous system
Cp	Cyclopentadienyl
CREBBP	CREB binding protein
Cys	Cysteine
DBF	2,3-Dihydrobenzofuran
DBU	1,8-Diazabicyclo[5.4.0]undec-7-ene

GSK Confidential – Do not copy

DIAD	Diisopropyl azodicarboxylate
DIPEA	<i>N,N</i> -Diisopropyl ethylamine
DLT	Dose limiting toxicity
DMF	<i>N,N</i> - Dimethylformamide
DMQ	3,4-Dihydro-3-methyl-2(1 <i>H</i>)-quinazolinone
DMSO	Dimethyl sulfoxide
DNA	Deoxyribonucleic acid
eq.	Equivalent
Et	Ethyl
FaSSIF	Fasted state simulated intestinal fluid
FLS	Fibroblast-like synoviocytes
FRAP	Fluorescence recovery after photobleaching
FRET	Fluorescence resonance energy transfer
%Fpo	Oral bioavailability
GCN5	General control nonderepressible 5
Gly	Glycine
Glu	Glutamate
h	Hour(s)
H-bond	Hydrogen bond
HAC	Heavy atom count
HAT	Histone acetyl transferase
HATU	(1-[Bis(dimethylamino)methylene]-1 <i>H</i> -1,2,3-triazolo[4,5- <i>b</i>]pyridinium 3-oxide hexafluorophosphate)
HDAC	Histone deacetylase
HDL	High density lipoprotein
hERG	Human Ether-à-go-go-Related Gene
His	Histidine
HPH	High pH
HRMS	High resolution mass spectrometry
HTRF	Homogeneous time resolved fluorescence
HTS	High throughput screen
hWB	Human whole blood
IL-6	Interleukin 6

GSK Confidential – Do not copy

Ile	Isoleucine
<i>i</i> Pr	Isopropyl
IV	Intravenous
IVC	<i>in vitro</i> clearance
JAK	Janus kinase 2
KAc	Acetylated lysine
%LBF	Percentage liver blood flow
LCMS	Liquid chromatography mass spectrometry
LE	Ligand efficiency
LLE _{at}	Lipophilic ligand efficiency (Astex)
LPS	Lipopolysaccharide
M	Molar
MBTE	Methyl <i>tert</i> -butyl ether
Me	Methyl
MeCN	Acetonitrile
Met	Methionine
MCP-1	Monocyte chemoattractant protein-1
<i>m</i> CPBA	<i>meta</i> -Chloroperbenzoic acid
min	Minute(s)
mmol	Millimole
m.p.	Melting point
mRNA	Messenger Ribonucleic Acid
Ms	Methane sulfonyl
MTS	Mid throughput screen
MW	Molecular weight
mw	Microwave
<i>m/z</i>	mass/charge ratio
NBS	<i>N</i> -Bromosuccinimide
NHC	<i>N</i> -heterocyclic carbene
NIS	<i>N</i> -Iodosuccinimide
NMC	NUT midline carcinoma
NMR	Nuclear magnetic resonance
NOE	Nuclear Overhauser effect

GSK Confidential – Do not copy

nr	No reaction
NUT	Nuclear protein in testis
PB1	Polybromo 1
PBMC	Peripheral blood mononucleated cell
PCAF	P300/CBP-associated factor
PEPPSI <i>iPr</i>	[1,3-Bis(2,6-Diisopropylphenyl)imidazol-2-ylidene](3-chloropyridyl) palladium(II) dichloride
PFI	Property forecast index
Ph	Phenyl
Phe	Phenylalanine
PK	Pharmacokinetics
PLK1	Polo-like kinase 1
PMP	1,2,2,6,6,-Pentamethylpiperidine
Pro	Proline
PROTAC	Proteolysis targeting chimera
PTM	Post translational modification
R	Generic group
RA	Rheumatoid Arthritis
rt	Room temperature
RVF	Arginine-Valine-Phenylalanine
SAR	Structure activity relationship
Sat.	Saturated
SEC	Size exclusion chromatography
SGC	Structural genomics consortium
SLAD	Solubility limited absorbable dose
SM	Starting material
STAB	Sodium triacetoxyborohydride
<i>t</i>	Tertiary
$t_{1/2}$	Half-life
TAF1	Transcription initiation factor TFIID subunit 1
TBAF	Tetrabutylammonium fluoride
TEA	Triethylamine
TFA	Trifluoroacetic acid

GSK Confidential – Do not copy

TfOH	Triflic Acid
THF	Tetrahydrofuran
THQ	Tetrahydroquinoline
THQx	Tetrahydroquinoxaline
TLC	Thin layer chromatography
t_R	Retention time
TR-FRET	Time resolved fluorescence resonance energy transfer
tRNA	Transfer Ribonucleic Acid
Trp	Tryptophan
TsOH	Tosic acid
Tyr	Tyrosine
Val	Valine
V_{ss}	Volume at steady state
WPF	Tryptophan-Proline-Phenylalanine
w/w	Weight by weight
Xantphos	4,5-Bis(diphenylphosphino)-9,9-dimethylxanthene
XPhos Pd G2	Chloro(2-dicyclohexylphosphino-2',4',6'-triisopropyl-1,1'-biphenyl)[2-(2'-amino-1,1'-biphenyl)]palladium(II)

Contents

Acknowledgements.....	iii
Abstract.....	iv
Abbreviations.....	v
1. Introduction	1
1.1. Medicinal Chemistry	1
1.1.1. The Application of Medicinal Chemistry Principles	1
1.1.2. Exposure at the Site of Action.....	3
1.1.3. Target Engagement.....	7
1.1.4. Functional Pharmacology.....	11
1.2. An Introduction to Epigenetics and Bromodomains.....	12
1.2.1. The Role of DNA	12
1.2.2. The Structure of Chromatin	14
1.2.3. Post Translational Histone Modification.....	15
1.2.4. Histone Acetylation.....	16
1.3. The role of the BET family of BRDs in Disease	20
1.3.1. Oncology	21
1.3.2. Autoimmune Inflammation	23
1.4. Small Molecule Inhibitors of the BET Family	25
1.4.1. The structure of Bromodomains.....	25
1.4.2. pan-BET Inhibitors.....	27
1.4.3. Bivalent BET Inhibitors	33
1.4.4. Dual BET Inhibitors.....	36
1.4.5. Degradation of BRD4 by bifunctional molecules	39
1.5. Domain Selective BET inhibitors	42
1.5.1. Clinical Limitations of pan-BET inhibition	42
1.5.2. Structural differences between BET BD1 and BD2 domains	42
1.5.3. BD1 Biased BET inhibitors	45
1.5.4. BD2 Selective BET inhibitors	46
1.6. Pursuing a BD2 Selective BET inhibitor	49
1.6.1. Development of a Highly Potent and BD2 Selective BET Inhibitor	49
1.6.2. Overcoming the Genotoxic Risk of 1.43	51
1.6.3. Discovery of 2,3-Dihydrobenzofurans as BD2 Selective BET Inhibitors	52

2.	Synthetic Strategies Towards DBFs as BD2 Selective BET Inhibitors	56
2.1.	Aims.....	56
2.2.	Synthetic Approaches Targeting DBFs as BET Selective BET Inhibitors	57
2.2.1.	Initial Synthesis of DBFs (S,S)-1.46 and (±)-2.011	57
2.2.2.	Reimagining the Retrosynthetic Approach to DBF 2.011	59
2.2.3.	Initial Studies towards a Synthetic Route to DBF (±)-2.011	61
2.2.4.	Optimisation of the Hydroboration	63
2.2.5.	Insertion of the Methyl Amide Warhead.....	65
2.2.6.	Optimisation of the Suzuki Coupling to form <i>ortho</i> Vinyl Phenols	68
2.2.7.	Scale up of 2.029 and Exploration of the Amide Vector	71
2.2.8.	Late Stage Functionalisation of the C3 Position.....	73
2.3.	Investigating the SAR of the 2-unsubstituted DBFs	77
2.3.1.	SAR of the Amide Vector.....	77
2.3.2.	SAR of the C2 DBF Substituent.....	80
2.3.3.	X-ray Crystallography of DBF (S)-2.056	82
2.3.4.	<i>In Vivo</i> PK profiling of DBFs (S)-2.011 , (S)-2.056 and (S)-2.067	84
2.3.5.	<i>In Silico</i> Analysis of DBF 2.039	86
2.4.	Synthetic Approaches Targeting a DBF Quaternary Centre.....	87
2.4.1.	Reductive Heck cyclisation.....	87
2.4.2.	Further Functionalisation of the Quaternary Centre.....	90
2.4.3.	Synthesis of DBFs 2.101-2.103	95
2.4.4.	Targeting a CH_2F Quaternary centre.....	97
2.5.	Investigating the SAR of the DBFs with a Quaternary Centre.....	99
2.5.1.	SAR of the Quaternary Vector.....	99
2.5.2.	X-ray Crystallography of 2.101	101
2.5.3.	<i>In Vivo</i> PK Profile of DBFs (S)-2.101 , (S,S,S)-2.108 and (S)-2.103	103
2.6.	Conclusions and Future Work on the DBF Series.....	105
3.	Development of a Chemical Probe for CECR2	107
3.1.	Chemical Probes for Target Validation	107
3.2.	Small Molecule inhibitors of non-BET BRDs.....	108
3.2.1.	ATAD2	110
3.2.2.	CECR2	113
3.2.3.	Structural Features of the CECR2 BRD	116
3.3.	Discovery of the Phenylsulfonamide Series.....	118

GSK Confidential – Do not copy

3.3.1.	Displacing the Water: The Binding Mode of (S,S)-3.013	119
3.4.	Aims.....	124
3.5.	Evaluating the Importance of the Aryl Substituent	125
3.6.	Optimisation of the Sulfonamide Vector	128
3.7.	Targeting Selectivity Through Interactions with the WPF Residues	134
3.7.1.	Understanding the Role of the Hydantoin Group.....	134
3.7.2.	Identification of 5,6 Biaryls with CECR2 Selectivity	137
3.7.3.	Exploration of 5,6 Biaryl Systems.....	142
3.7.4.	Decreasing the PFI and Improving the LLE _{at} of the Benzotriazole	148
3.7.5.	Investigating Triazole Substitution.....	150
3.7.6.	Conformational restriction of triazole amides.....	156
3.8.	Greater Selectivity Through Sulfonamide Modification	164
3.9.	Selectivity and Cellular Target Engagement	168
3.10.	Conclusions and Future Work on CECR2	171
4.	Experimental	174
4.1.	General Experimental	174
4.2.	General Procedures	176
4.3.	Optimisation Procedures	177
4.4.	Chemistry Experimental.....	178
4.4.1.	BD2 Experimentals	178
4.4.2.	CECR2 Experimentals	206
4.5.	Biological Data Experimental	264
5.	Appendix	266
6.	References	270

1. Introduction

1.1. Medicinal Chemistry

1.1.1. The Application of Medicinal Chemistry Principles

Fundamentally, medicinal chemistry is the discipline of developing a candidate drug molecule capable of successfully testing a disease hypothesis in clinical trials, hopefully resulting in the launch of a new medicine. The development of a drug from target validation through to market launch, is a long, difficult, and expensive process, throughout which the disease hypothesis will be thoroughly tested in clinical trials, more often than not leading to failure of the drug candidate in question (Figure 1.01).¹ It is the job of the medicinal chemist to use an interdisciplinary approach to reduce the high attrition rate associated with drug discovery by identifying the optimal drug candidate which has the highest chance of success during lead optimisation.

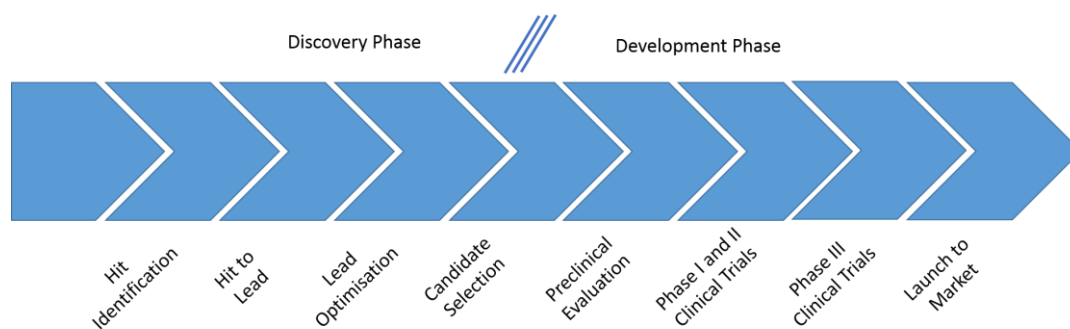


Figure 1.01. The drug discovery journey from target identification to market launch.

The development of a clinical candidate is a multiparameter optimisation, usually carried out through an iterative cycle of design-make-test, whereby each iteration provides marginal improvements to the template until the desired criteria are met (Figure 1.02). It is rarely a straightforward progression from hit to candidate. Therefore, decision making is key, and must be based on robust data, generated in a time-efficient manner and backed up by a suitable synthetic strategy which all serve to reduce the cycle time and identify a clinical candidate in a short time frame.¹

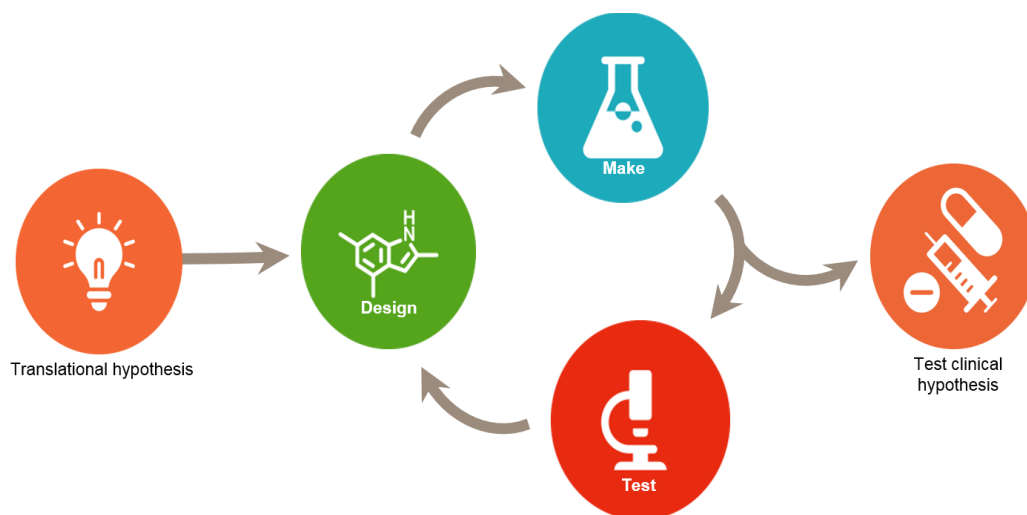


Figure 1.02. The medicinal chemistry design-make-test cycle.

Once the optimal compound has been identified, a drug company must decide whether to progress the drug candidate to clinical trials for which there is a high attrition rate.^{2,3} Drugs fail in the clinic for two main reasons: lack of safety and efficacy. That is, either they do not work, or they do not work at a safe dose. Due to high drug attrition rates, there has been discussion in the literature about the most effective way to improve the chances of success. AstraZeneca have recently developed principles termed the 5R framework from an analysis of 142 projects carried out between 2005 and 2011.^{4, 5} The aim was to identify and understand which features of projects gave successful outcomes and what caused project closure. From this arose the 5 Rs which were: right target; right tissue, right safety, right patients, right commercial potential. Firstly, these factors show the importance of choosing the right target. A good target needs to show a strong link between target and disease (*i.e.* inhibition or activation of a protein or pathway results in the desired phenotype) ideally through genetic validation, show differentiated efficacy, meet clinical and commercial needs and importantly be druggable. Target validation is essential for drug discovery and will be discussed further in Section 3.1. The authors also highlight the importance of bioavailability and tissue exposure, which will come from a clear understanding of preclinical pharmacokinetics (PK) and pharmacodynamics (PD). The authors later showed that implementation of this framework had a positive impact on AstraZeneca's pipeline.⁶

Other companies have also looked at their own drug attrition rates. In 2012, Pfizer carried out an analysis of 44 programmes which had been through a phase II clinical trial.⁷ The

majority of failures were caused by lack of efficacy however, in only 43% of the trials was it felt that the disease hypothesis had been adequately tested. Only 8 of the 44 programmes progressed to phase III trials. From their analysis, Pfizer developed the three pillars of survival which need to be demonstrated for the highest chance of success. They are: exposure at the site of action, target engagement and functional pharmacology (Figure 1.03).

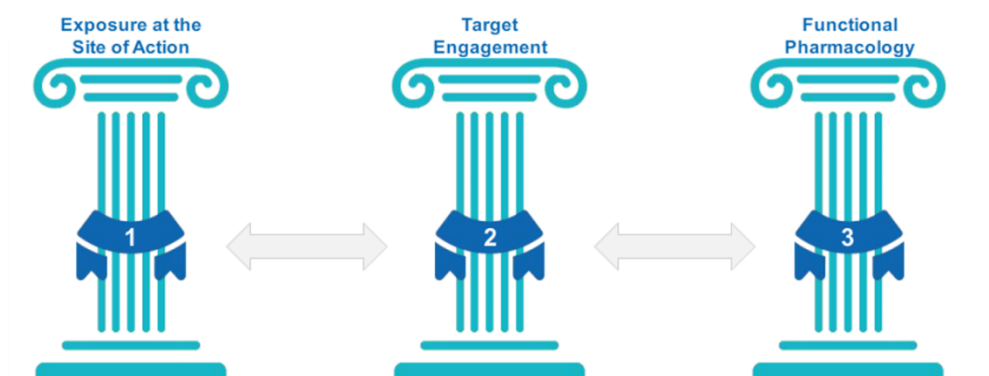


Figure 1.03. The Pfizer three pillars.

Adherence to the three pillars gives confidence that the disease hypothesis has been successfully tested. Therefore, even when progression is halted through lack of efficacy, this is because the pharmacological target is not relevant to the disease. To achieve the objectives set out in these frameworks, medicinal chemists must ensure that drug candidates are efficacious at the protein target and have the correct chemical properties that will allow them to reach the site of action for a sufficient duration to cause a phenotypic effect and if that phenotype is not observed. It is not through a lack of target engagement. Therefore, the data which medicinal chemists use to develop drug candidates must be examined to ensure that these aims are met.

1.1.2. Exposure at the Site of Action

Pharmacokinetics

Pfizer's 3 pillars and AstraZeneca's 5Rs both highlighted the importance of ensuring that the compound of interest reaches the desired site of action.^{5, 7} Understanding the pharmacokinetics (PK), of a molecule is crucial for drug development. PK is concerned with measuring and understanding absorption, distribution, metabolism, excretion and toxicity (ADMET) of a pharmaceutical agent. As these properties can't be directly measured in

GSK Confidential – Do not copy

humans before the onset of a clinical trial, PK is predicted from animal models and *in vitro* hepatocyte preparations from animal species and humans. The aim is to establish an *in vitro/in vivo* correlation between animal *in vitro* and *in vivo* data and then scale this data to predict human PK.

Due to ethical considerations, which strive to minimise the number of animals used, *in vitro* studies are conducted first to establish a rationale for progression to *in vivo* studies. *In vitro* clearance (IVC) is used to determine how quickly a compound is broken down by the body. In this work, the hepatocyte metabolic stability was assessed. Isolated hepatocytes of three species (rat, dog and human) were utilised. Hepatocytes are cells which constitute most of the liver tissue and contain both phase I (P450 enzymes) and phase II drug metabolising enzymes which allows for the metabolic profile of the potential drug to be assessed. Approximately 60% of marketed compounds are cleared by CYP-mediated metabolism, so assessing this at an early stage is crucial to understanding the PK.⁸ A low value for IVC is desirable, as this provides confidence that metabolism will be low. It is hoped that this will correlate with lower clearance *in vivo*. Achieving a suitable clearance and bioavailability in two species is crucial as this will permit the building of an *in vitro/in vivo* model. Additionally, two animal species (rodent and non-rodent) need to be dosed at multiples above the predicted efficacious exposure to establish safety margins.

Animals are given both an intravenous (IV) and oral dose and the concentration of the compound in the blood is measured over time (Figure 1.04). From these plots an understanding of the PK can be achieved. The half-life ($t_{1/2}$) or the time taken for the concentration to decline by 50% can be determined from the terminal gradient of the curves. The area under the curve (AUC) is the total amount of drug reaching systemic circulation and is used to determine exposure. Oral bioavailability (%Fpo) looks at the normalised ratio of exposure from an oral dose compared to an intravenous (IV) dose and can be calculated using the equation in Figure 1.04. %Fpo is dependent on absorption and first pass liver metabolism.

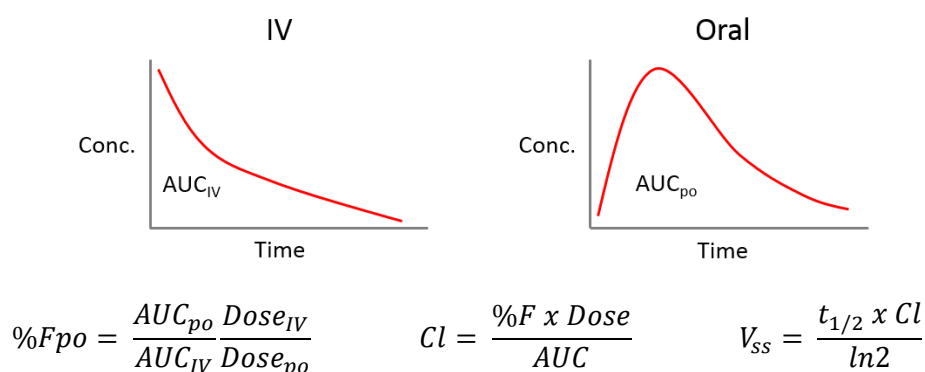


Figure 1.04. Concentration time graphs for both IV and oral administration to animals. Important equations used to determine %F_{po}, CL_b and V_{ss} are shown beneath.

The rate at which a compound is removed from the body will affect both the %F_{po} and t_{1/2}. Clearance (CL_b) is a measure of the volume of plasma/blood irreversibly cleared of drug per unit time and can be calculated using the equation in Figure 1.04. The theoretical maximum rate for drug removal is given by the rate of circulation through the liver, termed the liver blood flow. The rate of CL_b can therefore also be expressed as percentage liver blood flow (%LBF). The volume of distribution at steady state (V_{ss}) is the theoretical volume the total drug in the body would occupy at steady state if the concentration is uniform throughout the body (Figure 1.04). A higher V_{ss} indicates a greater degree of distribution of the drug in the body tissue rather than the plasma. Clearance along with volume of distribution define the exposure profile of the molecule. By factoring in protein binding, these parameters determine the free blood concentration available to engage the target. For a clinical candidate, a high unbound blood concentration with a low predicted human dose from oral delivery is desired and a low unbound clearance is vital for this.

Measuring Physico-chemical Properties

The physico-chemical properties of a molecule are essential to its success as a drug. Following the three pillars, a molecule needs to have suitable physico-chemical properties to reach the site of action within the human body. First and foremost, amongst the physico-chemical measurements is lipophilicity. Generally, a more lipophilic compound will be more potent against the target protein; this is because the active site of the target is more hydrophobic than the surrounding aqueous environment. However, this is usually associated with raised metabolism, due to increased affinity for metabolic enzymes such as P450s.⁹ Lipophilic

GSK Confidential – Do not copy

compounds are also normally more promiscuous, leading to a greater risk of toxicity. For example, inhibition of human Ether-à-go-go-gene (hERG), a potassium ion channel which coordinates the heartbeat, is more likely with more lipophilic compounds. Inhibition of hERG should be avoided as it can potentially be fatal.¹⁰ Furthermore, high lipophilicity correlates with higher plasma protein binding. In order to interact with the target protein a drug must be unbound. Therefore, clearance should be considered in terms of plasma protein binding, in order to derive a meaningful picture of free concentration available to the target.¹¹ If the lipophilicity is too low and a compound becomes very hydrophilic, this usually correlates with a low permeability, although this will also depend on the molecular weight and number of H-bond donors and acceptors. The bioavailability of the drug, which depends on the rate of absorption through the gut, may therefore also decrease as the lipophilicity is lowered.^{12, 13} Lipophilicity is therefore a balance, but an important indicator of the desirable properties of a drug. Throughout this work ChromLogD_{7.4} was used as a measurement of lipophilicity at physiological pH.¹⁴ This is a chromatographic variant of logD, which is a measure of the partition coefficient of the concentration of the drug in a mixture of octanol and water at a specific pH. ChromLogD_{7.4} is therefore a useful indicator of the properties of a drug. To eliminate charge effects caused by protonation, ChromLogD_{10.5} can be used as a surrogate for logP. The Property Forecast Index (PFI) [ChromLogD_{7.4} + aromatic ring count] is a related measurement which is generally considered to be a good predictor of solubility and off-target activity (e.g. P450).¹⁵ A PFI of <6 is desired as this has been shown to correlate well with good solubility.¹⁵ During this work, a well validated model for ChromLogD_{7.4} was also utilised to predict the lipophilicity of molecules. As a result, compounds outside of the targeted space did not have to be prepared.

Solubility is another important parameter for drug discovery. Insufficient solubility may compromise assay data as the compound cannot be dissolved to the necessary aqueous concentration.¹⁶ Poor solubility is a risk factor for low oral absorption. An oral drug has a finite time and volume (length of gut) to be absorbed. Absorption can only happen if a compound is dissolved, therefore, if a compound does not have sufficient solubility only a portion will dissolve and can be absorbed. This is known as the solubility limited absorbable dose (SLAD). If SLAD is reached, the only way to improve absorption is to bioenhance the drug (i.e. change the form/version or particle size). Therefore, poor solubility correlates with higher development costs due to the additional time and effort it takes to make a suitable

GSK Confidential – Do not copy

formulation. Assessing and optimising solubility during lead optimisation is critically important.^{17, 18} Throughout this work, high throughput chemiluminescence nitrogen detection (CLND) or charged aerosol detection (CAD) solubility assays were used to measure kinetic solubility.^{19, 20} Work within our laboratories has demonstrated that these two methods are equivalent (see Figure 5.01, Section 5) and can be used interchangeably. Kinetic solubility is the maximum solubility of the fastest precipitating form of a compound, as measured from a stock solution. Kinetic solubility is usually over predictive of the thermodynamic solubility, which measures the solubility of a solid in an aqueous solution and is dependent on form. However, given CAD solubility represents a best-case scenario, this was utilised to exclude compounds with poor solubility. This work used fasted state simulated intestinal fluid (FaSSIF) solubility to measure the thermodynamic solubility, which aims to understand the solubility of the molecule in a physiologically relevant system (for oral delivery). Although this is usually considered the gold standard for solubility measurements, the value generated will depend on the crystalline form of the compound as well as its physico-chemical properties. Generally, crystalline molecules have lower solubilities as a lattice enthalpy must be overcome prior to solvation. That is why establishing a developable crystalline form is important prior to developing a candidate.

Good permeability and absorption are crucial in order to achieve good bioavailability. Permeability is a complex property in drug discovery and there is discussion in the literature about the application of measurements of properties such as artificial membrane permeability (AMP) which measures a compound's ability to cross a lipid infused membrane.²¹ AMP is a high throughput method which only looks at passive diffusion of a compound and not active transport and is therefore only an estimate for what occurs *in vivo*.²² Although this measure appears to correlate well with oral absorption through the intestine with some series, it is rarely predictive of cellular permeability. To address this, cellular concentration assays and cellular target engagement assays are used.^{23, 24}

1.1.3. Target Engagement

Biochemical Assays

In target-based drug discovery, assessing the potency of your series against the protein of interest is of paramount importance. Time-resolved Fluorescence Resonance Energy Transfer (TR-FRET) assays are an effective high throughput method to do this and will be used to

assess potency against a target protein throughout this thesis.²⁵ TR-FRET assays are artificial constructs where excitation of a donor (usually a lanthanide e.g. Eu or Tb) promotes Förster resonance energy transfer to a fluorescent tag and subsequent emission at a different wavelength (Figure 1.05). This energy transfer is distance dependent and so will only occur when the tag is brought into proximity to the donor through a binding event to the target. When an inhibitor is added, a concentration-dependent loss of emission can be measured leading to the generation of an IC_{50} value, or the concentration at which 50% of maximal inhibition is achieved. The \log_{10} of this, or pIC_{50} , is usually used to assess and compare potency.

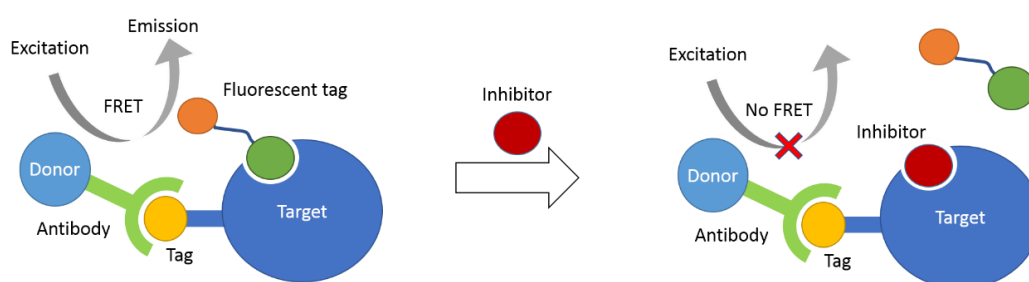


Figure 1.05. TR-FRET assays are used to measure protein binding. Excitation of a donor (light blue), usually a lanthanide, causes FRET to a fluorescent tag (orange) held in close proximity to the donor by binding the target (dark blue). FRET is distance dependent and dosing in an inhibitor (red sphere) will result in a loss of fluorescent.

For an antagonist, high levels of target engagement are desirable. Jacqmin *et al.* showed that for the antiviral agent Maraviroc, just 1.2% of free activated receptors on a target cell were able to elicit 50% of the maximum response.^{26, 27} Therefore, high affinity and target occupancy are important for drug candidates otherwise they may not display the expected pharmacology. However, it is important to remember that these methods only show that a binding event has occurred and are not predictive of efficacy. None the less, TR-FRET assays are still a useful tool in drug discovery.

Ligand Efficiency

When optimising potency, it is often important to understand how efficient the ligand-protein interaction is. Increasing the size and lipophilicity of a molecule will generally increase potency because a ligand will prefer the hydrophobic environment of the protein to the aqueous environment.²⁸ However, these interactions can be non-specific and increased

GSK Confidential – Do not copy

lipophilicity is undesirable for reasons discussed previously (Section 1.1.2). Therefore, many companies and academic groups have started using ligand efficiency (LE) metrics, particularly during hit optimisation, to identify the most efficient protein-ligand interactions. LE is measured as the binding energy per heavy atom (HAC) and can be calculated from the Gibbs free binding energy (Equation 1.01).²⁹ Often only an IC₅₀ value is available and so ΔG is approximated. A LE of greater than 0.3 is desirable to show efficient binding.

Equation 1.01. Derivation Ligand Efficiency

$$LE = \frac{-\Delta G}{HAC} = \frac{-RT\ln(K_d)}{HAC}$$

$$LE \approx \frac{-RT\ln(IC_{50})}{HAC} \approx \frac{1.37x pIC_{50}}{HAC}$$

Terms: LE, Ligand efficiency; ΔG, Gibbs free energy; HAC, Heavy atom count; R, Boltmann constant; T, Temperature; K_d, Dissociation constant; IC₅₀, 50% Inhibition concentration.

Astex later proposed the Astex lipophilic ligand efficiency (LLE_{at}) which factors in the calculated partition coefficient (clogP) to adjust the value of ΔG to account for non-specific hydrophobic interactions (Equation 1.02).³⁰ The metric was then adjusted so that it uses the same scale as LE, therefore, a value of greater than 0.3 is also desirable for LLE_{at}. Both LE and LLE_{at} will be used to assess efficiency in this work.

Equation 1.02. Derivation of Lipophilic Ligand Efficiency.

$$LLE_{AT} = 0.11 - \frac{\Delta G^*}{HAC}$$

Where:

$$\Delta G^* \approx RT\ln(IC_{50}) + RT\ln(P)$$

Terms: LLE_{at}, Astex lipophilic ligand efficiency; ΔG, Gibbs free energy corrected for lipophilicity; HAC, Heavy atom count; R, Boltmann constant; T, Temperature; IC₅₀, 50% Inhibition concentration; P, partition coefficient.

Cellular Target Engagement

Whilst biochemical assays are a useful high throughput determinant of ligand-protein binding, this will not necessarily translate into living systems. Determining the level of cellular target engagement enables confirmation of the desired mode of action and can determine the affinity for the target protein in a more relevant setting. There are multiple ways of

measuring target engagement, however, most of the methods developed rely on artificial constructs within a cell and this must be taken into account when the data is analysed.²³ Bioluminescence resonance energy transfer (BRET) has become a common technique to measure protein-protein interactions and can be used as evidence of cellular target engagement.³¹ This work used a nanoBRET system developed by Promega® (Figure 1.06).³² In the presence of a luciferin substrate, luciferase enzymes will emit bioluminescence. If the luciferase is in proximity to a fluorophore, the resulting photon can excite the acceptor fluorophore by resonance energy transfer resulting in fluorescence at a different wavelength to the bioluminescence. In the nanoBRET assay a small HaloTag protein is transfected onto one of the proteins of interest, and the luciferase transfected onto the other. The HaloTag then binds the fluorescent ligand which is held close to the luciferase through the protein-protein interaction. Like in TR-FRET assays, BRET is distance dependent and so will only occur when the tag is brought into proximity of the luciferase. When an inhibitor capable of disrupting the protein-protein interaction is added, a concentration-dependent loss of BRET can be measured to give a pIC₅₀ value for inhibition.

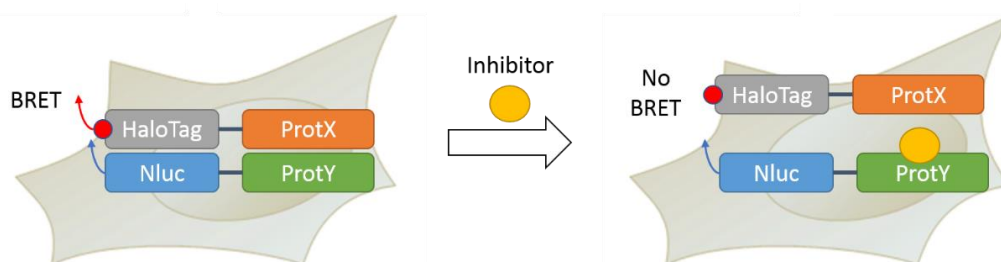


Figure 1.06. BRET assays are used to measure cellular target engagement. A luciferase (Nluc, blue) will emit bioluminescence in the presence of its substrate, resulting in energy transfer to a fluorophore (Red sphere) leading to emission. The fluorophore is modified so that it binds to a HaloTag protein (grey). The HaloTag and Nluc are then attached to Protein X (ProtX, orange) and Protein Y (ProtY, green) respectively. BRET is distance dependent and dosing in an inhibitor (yellow sphere) will result in a loss of fluorescent.

Another technique which has commonly been used to display cellular target engagement is fluorescence recovery after photobleaching (FRAP).³³ In a FRAP assay, a cell is labelled with a fluorescent molecule or protein. A green fluorescent protein (GFP) can be fused to the protein of interest. Then, a high intensity laser pulse photobleaches a portion of the cell and the migration of the GFP label back into the bleached area is monitored over time. For

protein-protein complexes, a slow diffusion rate is observed. Small molecule inhibitors capable of disrupting the protein-protein interaction, will therefore increase the $t_{1/2}$ if they can permeate the cell.

Cellular target engagement experiments are powerful tools to understand cellular penetration and target affinity however, they are not a measure of efficacy or proof of the desired pharmacology.

1.1.4. Functional Pharmacology

Phenotypic Assays

To provide confidence that a molecule will be efficacious if it reaches the site of action, phenotypic assays are used. Phenotypic assays do not confirm target engagement, but it is inferred if there is a strong relationship between target inhibition and phenotypic response. If the phenotype can be measured clinically this may become a biomarker. During this work a phenotypic assay was used to establish efficacy and show cellular target engagement. Peripheral blood mononuclear cells (PBMCs), a term used to describe any peripheral blood cell with a round nucleus (e.g. lymphocytes and monocytes) were stimulated with lipopolysaccharide (LPS) which are endotoxins able to elicit a strong immune response in animal cells.³⁴ Upon stimulation, the cells release chemokines and cytokines, the levels of which can be measured. For this work, the concentration of monocyte chemoattractant protein-1 (MCP-1 / CCL2), a small chemokine which recruits monocytes, memory T-cells, and dendritic cells to the site of inflammation, was measured. Blocking MCP-1 has been shown to play a beneficial role in inflammatory diseases.^{35, 36} Therefore, if a compound is able to induce a concentration-dependent reduction of MCP-1 without loss of cell count, then its pharmacology should be functionally relevant to immuno-inflammation disorders. Additionally, a human whole blood (hWB) assay was run using the same LPS stimulated mechanism. This causes a chemokine/cytokine storm and the concentration of MCP-1 can again be measured to determine whether a compound is efficacious.

The first chapter of this thesis will describe synthetic efforts towards enabling the identification of a clinal candidate for an epigenetic modulator protein.

1.2. An Introduction to Epigenetics and Bromodomains

The term epigenetics, literally meaning ‘above genetics’, was first introduced by the embryologist Conrad Waddington in the 1950s.³⁷ He was studying the mechanisms by which a single fertilised cell can give rise to thousands of different cell types. During his work, it became clear that the same genetic material could encode for multiple distinct cell types, therefore, demonstrating that a given phenotype is not solely driven by an organism’s Deoxyribose Nucleic Acid (DNA) but by the way that this genetic blueprint is interpreted. Over time this definition evolved to denote chemical or physical changes which manipulate gene expression without altering the underlying genetic code.^{38, 39} Therefore, in order to understand epigenetics; the molecular basis of DNA, how it is stored and accessed within the cell, and how physical and chemical changes influence this, must be examined.

1.2.1. The Role of DNA

DNA is one of the essential components of life, whereby all the information necessary for the expression of the genome is stored within a cell. The structure of DNA was first fully characterised by Watson and Crick in 1953, building upon the work of Franklin, identifying its unique double helix structure.⁴⁰⁻⁴² They found that it is formed from two strands of a negatively charged polyphosphate-sugar backbone which are linked by complementary pairs of purine and pyrimidine bases (Figure 1.07). There are four bases; purines Adenine (A) and Guanine (G), and pyrimidines Thymine (T), and Cytosine (C). The specific pairings of A + T and C + G link the two strands of backbone together through a network of complimentary H-bonds. These non-covalent interactions link the two strands together inducing a twist, due to the 3D structure of the sugars that form the backbone, which gives rise to the famous DNA double helix.⁴³

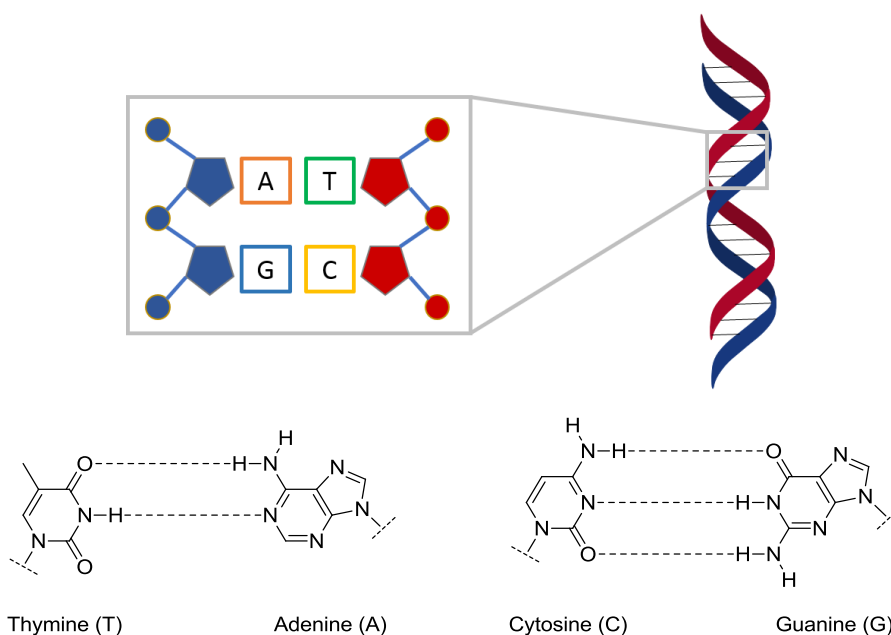


Figure 1.07. The famous DNA double helix is formed from a polyphosphate sugar backbone (complementary strands are shown in red and blue) interconnected by pairing of bases; Adenine (A), Thymine (T), Cytosine (C) and Guanine (G). These bases form pairs of A+T and C+G, which are connected by non-covalent H-bonding interactions.

The 'central dogma' of molecular biology revolves around the idea that a gene encodes a message, which builds a protein, which then has some kind of function within a cell (Figure 1.08).⁴⁴ The information which encodes for the production of proteins is stored within DNA in the form of the specific sequence of bases. Sequences of three bases (named codons: i.e. CAG) code for a specific amino acid, which couple to form peptide chains and subsequently proteins. Protein biosynthesis begins with the opening of the double stranded DNA, which is catalysed by RNA polymerase, and formation of messenger ribonucleic acid (mRNA) in a process called transcription. The sequence of bases in mRNA mirrors the parent DNA with the exception of T which is replaced by Uracil (U). Once the DNA has been copied into mRNA, it can be translated into proteins through the assembly of amino acids. This process is mediated by the ribosome which facilitates the synthesis of a transfer ribonucleic acid (tRNA) anti-codon sequence, thereby bringing together amino acid units, which form proteins (Figure 1.08). The specific sequence of DNA which codes for a protein is called a gene. This only gives a very simplistic view of how our genetic material functions. It is estimated that the human genome contains 20,000-25,000 protein encoding genes, roughly the same number as the common earthworm, therefore, the number of protein encoding genes alone

GSK Confidential – Do not copy

cannot possibly account for the wide variety of functionality observed in human cells.⁴⁵ In fact, protein encoding genes only constitute about 2% of the human genome, therefore, additional levels of complexity must be present.

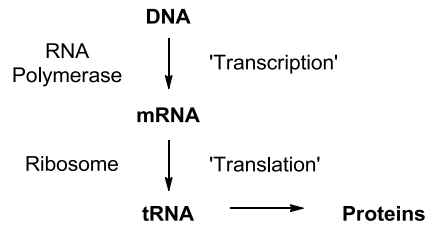


Figure 1.08. The formation of a complementary strand of mRNA provides the blue print for the assembly of amino acids into proteins and is the process by which the DNA encodes for proteins.

One additional layer of complexity is epigenetics, which refers to changes in gene transcription which are not caused by the underlying genetic code. To understand how epigenetic changes arise, the way in which DNA is stored and accessed in the nucleus must be examined.

1.2.2. The Structure of Chromatin

The entire genome is contained within each nucleus of every cell in the body. To fit into the nucleus, the DNA must be tightly packed. The basic unit by which DNA is stored in a cell is called a nucleosome. Nucleosomes pack closely together to form chromatin fibre which coils-up to form chromosomes (Figure 1.09). Every cell within the human body contains 23 pairs of chromosomes, which are necessary for the storage of our genetic information. However, in this tightly packed state, known as heterochromatin, the genes cannot be expressed and are silenced. In order for a gene to be transcribed it must be made accessible. This occurs through unwinding of the chromatin fibre to form a more open state known as euchromatin. In this form the DNA strand is more readily accessible and can be expressed.

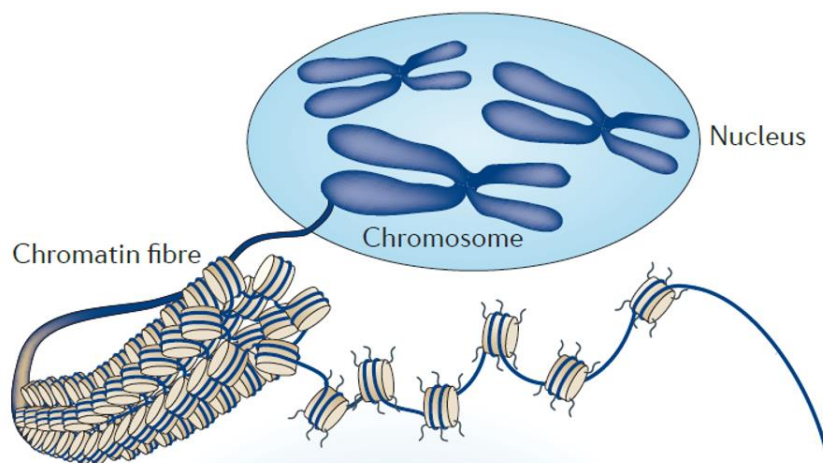


Figure 1.09. Chromosomes are formed from coils of chromatin fibre, which in turn are comprised of nucleosome units. Reproduced with permission from Nat. Rev. Drug Discov.⁴⁶

1.2.3. Post Translational Histone Modification

The conversion of chromatin between its hetero- and euchromatin states is controlled in part by the post translational modification (PTM) of histone proteins, which are a key structural component of nucleosomes (Figure 1.10). Nucleosome units are composed of 147 base pairs of DNA wrapped in two super helical turns around an octamer of four core histone proteins (H3, H4, H2A, and H2B).⁴⁷ The histone proteins are globular in structure except for the N-terminus, which sticks out into solvent, termed the histone tail.

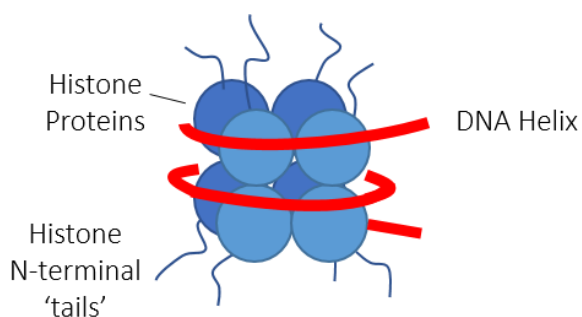


Figure 1.10. The structure of the nucleosome, formed from an octomer of 8 histone proteins (blue) around which wraps 147 base pairs of DNA (red). The N-terminus of the histones (tails) are solvent exposed.

The availability of the histone tails of the nucleosome unit makes them susceptible to a wide range of PTMs, that is, small chemical changes to specific amino acid residues such as

methylation or acetylation. It is the PTM of the histone tails that orchestrates chromatin stability and therefore controls gene expression or repression.⁴⁶ As such, the histone tail can be considered as a barcode, which can be modified by multiple PTMs. Depending on the type of modification, the location, and the presence of other PTMs; the recruitment of transcriptional machinery and the unwinding of sections of chromatin can be controlled. Importantly, it is now recognised that this process is both highly dynamic and highly specific. Genes can be selectively expressed or silenced in response to stimuli. For example, it is believed certain genes (e.g. coding for inflammatory cytokines) sit in a primed state, such that chemical modification of a histone tail (e.g. Lys acetylation) rapidly activates gene expression.⁴⁸

The PTM of histone tails is controlled by three families of proteins (Figure 1.11). Writers tag the histone tails with an epigenetic mark, which can subsequently be removed by an eraser protein. The third class of epigenetic modulators are the reader domains, which recognise specific PTMs on histone tails.

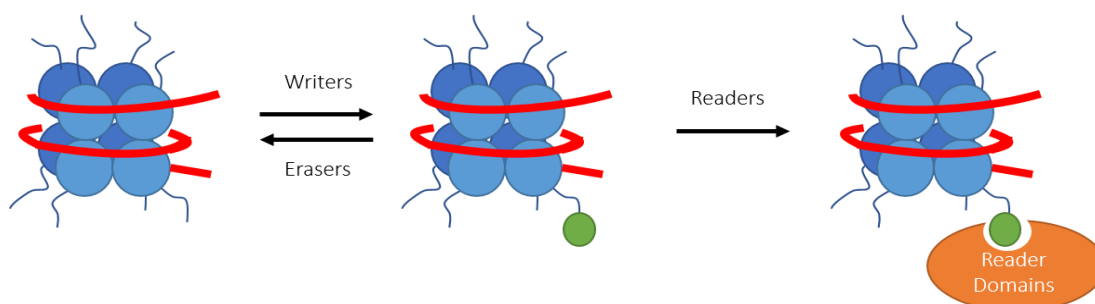


Figure 1.11. PTMs (green spheres) of histone tails (blue) are epigenetic marks which can be written, erased or read by reader domains (orange).

1.2.4. Histone Acetylation

Lys acetylation is an important PTM and has a role in transcription, repair, and replication.⁴⁹ It is thought to be responsible for controlling gene expression through the weakening of DNA-histone interactions. Histone tails typically contain a significant number of positively charged Lys residues, which are attracted to the negatively charged DNA.⁵⁰ Acetylation serves to neutralise the charge on the Lys amino acid and increase steric hindrance, which in turn relaxes the chromatin structure, making the DNA accessible for recognition by transcription

factors (Figure 1.12).^{51, 52} Acetylation is a reversible process which occurs at the terminal amine of Lys residues of histone tails.

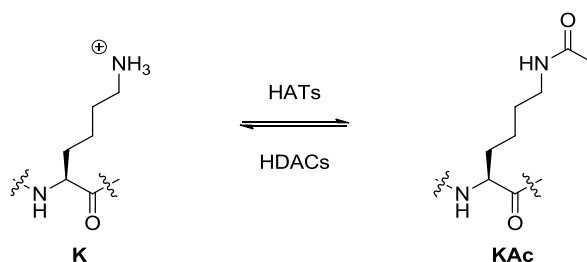


Figure 1.12. The acetylation of positively charged Lys residues serves to neutralise the charge and increase the steric demands of the residue.

Analysis of the ‘histone code’ has highlighted that many active genes are associated with nucleosomes with high levels of acetylated Lys and a more relaxed chromatin state.¹² Conversely, silent genes are associated with nucleosomes with little histone acetylation and a more condensed chromatin state.^{53, 54} The degree of Lys acetylation on histone tails, like most PTMs, is controlled by writer and eraser proteins.

1.2.4.1. Histone Acetyl Transferases

Histone acetyl transferases (HATs) are epigenetic writer domains which place KAc marks on histone tails by transferring an acetyl group from acetyl-CoA to the Lys side chain. HATs can be divided into two classes based on their localisation within a cell. Type A HATs are found in the nucleus and regulate gene expression through acetylation of histones.⁵⁵ Typically the HAT domain in these proteins is accompanied by a reader domain capable of recognising the KAc mark and recruiting transcription factors. Type B HATs are less well characterised.⁵⁵ They are located in the cytoplasm and acetylate histones prior to nucleosome assembly.

Recently, links to the pathology of cancer,⁵⁶ asthma,⁵⁷ COPD,⁵⁸ viral infection,⁵⁹ and neurological disorders⁶⁰ have been reported, however, the role of prominent HATs such as p300 (a type A HAT) remains under debate as contradicting articles on their role in cancer have been published.⁶¹ One article reports p300 as a tumour suppressor gene, whereas the other shows a link between tumour growth and p300 upregulation.^{56, 62} This may, in part, be due to the lack of suitable tool compounds.⁶³ Multiple HAT inhibitors have been published, however, Dahlin *et al.* recently used a La assay to detect reactive molecules by NMR (ALARM

NMR) to show that 15 out of the 23 known inhibitors were nonselective interference compounds.⁶⁴⁻⁶⁸ Follow-up studies showed thiol reactivity and aggregation as well as demonstrating non-specific effects in cell assays. Additionally, as HAT domains are usually part of complex proteins, effects seen in knock-down experiments may not be driven by the HAT domain. Further work is needed to develop the tool compounds needed to fully elucidate the role of HATs in disease and establish whether there might be any clinical utility of these enzymes.⁶⁴

1.2.4.2. Histone Deacetylases

Histone deacetylases (HDACs) are epigenetic eraser domains which remove KAc markers from histone tails. There are 11 known HDACs (1-11), which are divided into four major classes (I, II, III and IV), which differ in function and structure. Classes I, II and IV all contain a Zn²⁺ ion in the active site, unlike class III.⁶⁹ It was initially believed that all HDACs could deacetylate lysine substrates, however, only a subset of HDACs (1, 2, 3, and 6) show significant catalytic activity towards KAc.⁷⁰ The role of HDACs in disease is well validated by suitable tool compounds and a clear link between pan-HDAC inhibition and cancer therapy has already been established.^{53, 71} However, the precise role of specific HDAC isoforms is not currently well understood. The first small molecule epigenetic regulator to be approved was the HDAC inhibitor Vorinostat (**1.01**, Figure 1.13), which has been marketed by Merck since 2006 for the treatment of cutaneous T-cell lymphoma.⁷² Vorinostat (**1.01**) contains a hydroxamic acid moiety, which acts as a zinc chelator allowing it to bind to the active site of HDACs. This structural feature is preserved in Panobinostat (**1.02**) and Belinostat (**1.03**) which are marketed HDAC inhibitors approved for the treatment of T-Cell lymphoma and multiple myeloma respectively.^{73, 74} Inhibitors which contain a hydroxamic acid binder are generally promiscuous and bind to multiple class I, II, and IV HDACs. Alternatively, Chidamide (**1.04**) and Entinostat (**1.05**) employ an amino-benzamide moiety capable of acting as the zinc chelator.⁷⁵⁻⁷⁷ This structural change improves selectivity towards class I HDACs. Finally, Romidepsin (**1.06**), a natural product isolated from the bacterium *Chromobacterium violaceum*, which was shown to act through HDAC inhibition, has been approved for the treatment of T-Cell lymphoma.^{78, 79}

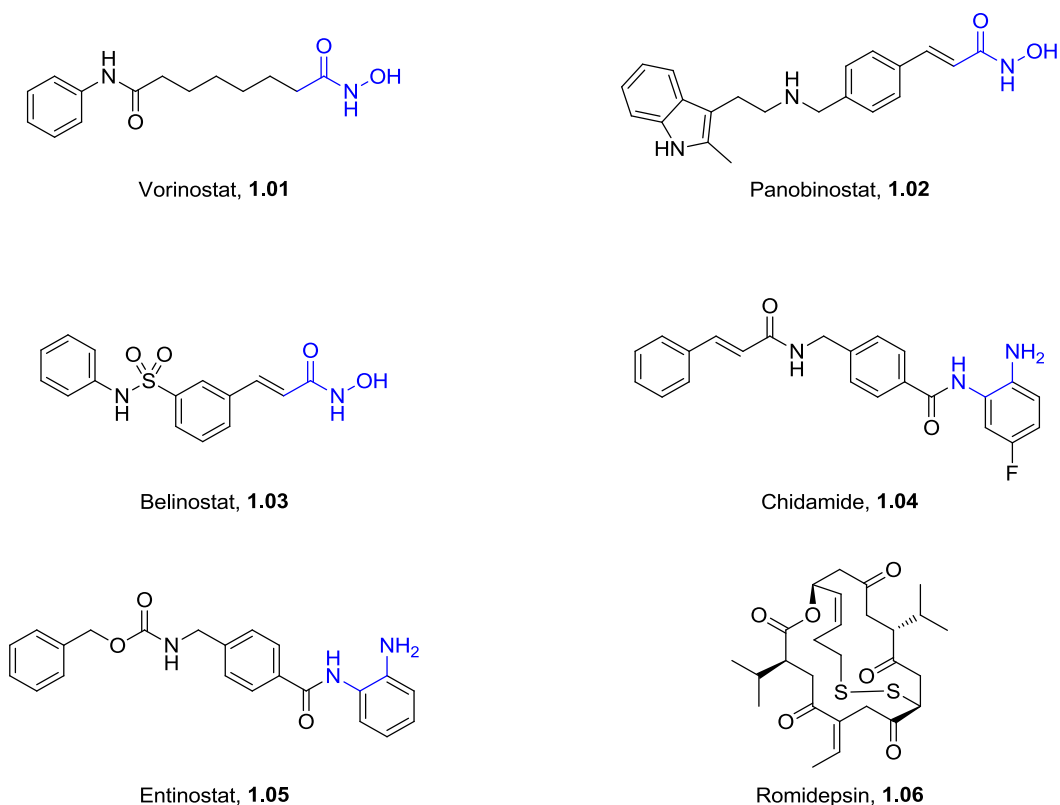


Figure 1.13. HDAC inhibitors marketed for the treatment of cancer. Zinc binders are shown in Blue.

These HDAC inhibitors show a clear link between HDAC inhibition and disease, however, clinical toxicities and poor PK associated with zinc binders has led to poor tolerability and narrow therapeutic windows.⁸⁰ Further work is needed to improve the potency and selectivity of HDAC inhibitors and fully elucidate the biological role of specific HDACs.

1.2.4.3. Bromodomains

KAc marks on histone tails are read by epigenetic reader domains called bromodomains (BRDs). BRDs are usually found within large multi-domain nuclear proteins, which control transcriptional co-activation by binding to modified DNA histones. The bound BRDs then recruit transcription factors and activate replication mechanisms. Since it is possible for proteins to contain multiple BRDs, proteins which contain a BRD are referred to as BRD containing proteins (BCPs). The first BRD structure was identified in 1992 from the *Brahma drosophila* fruit fly.⁸¹ Since then, 61 human BRDs have been identified, which are contained within 46 chromatin regulator proteins.⁸² These have been placed in a phylogenetic tree

BRDT, each of which contain two BRDs (labelled BD1 and BD2) and an extra terminal domain (Figure 1.15). Three of the BET BCPs (BRD2, 3 and 4) are ubiquitously expressed within the human body, however, expression of BRDT is restricted to the testes. Due to the high sequence homology between the 8 BRDs, most small molecule inhibitors published to date are generally classed as pan-BET and are equipotent at each domain (small molecule BET inhibitors will be outlined in Section 1.4.). The role of BET inhibitors as therapeutic agents in oncology and immuno-inflammation is rapidly being established and will be delineated further in the following sections.

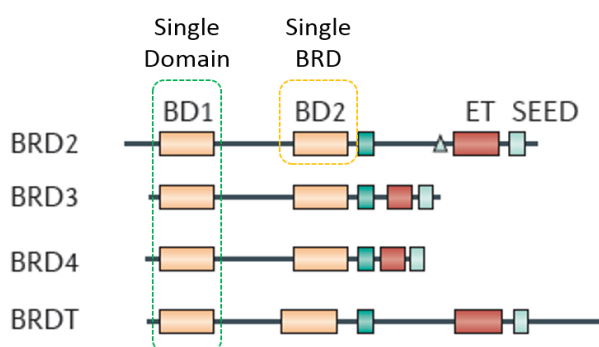


Figure 1.15. The BET family of 8 BRDs contained within 4 BRD containing proteins. The BD1 (single domain) is circled in green and a single BRD (BRD2 BD2) is circled in yellow.

1.3.1. Oncology

Nuclear protein *in testis* (NUT) midline carcinoma (NMC) is a rare but lethal cancer. It is caused by the translocation of the NUT protein and BRD4, which fuse to form the BRD4-NUT oncogene leading to aggressive tumour growth.⁹⁰ It is believed that the BRD4-NUT fusion protein is capable of binding to chromatin resulting in modification of gene expression, which maintains cells in a perpetual state of proliferation.⁹¹ There is currently no treatment for NMC but small molecule BET inhibitors have caused apoptosis in NMC derived cell lines and are currently in clinical trials for its treatment.⁹²

The discovery of a direct link between NMC and inhibition of the BET family, led to significant interest in BET inhibitors as a potential therapy in multiple cancer types.⁹³ BRD4 was identified as a therapeutic target in acute myeloid leukaemia (AML) using an siRNA screen.⁹⁴ BET inhibitors (e.g. (+)-JQ1 **1.08**, see Section 1.4.) showed anti-proliferative effects in multiple

GSK Confidential – Do not copy

in vitro AML cell lines and *in vitro* mouse AML xenograft models.^{95, 96} Antileukemic effects have also been observed in mixed lineage leukaemia (MLL) cell lines, where I-BET151 (**1.11**) (see Section 1.4.1) inhibited the transcription of genes critical to cell cycle progression leading to apoptosis, an effect also observed in melanoma cell lines. Furthermore, BET inhibitors have shown potential therapeutic benefits in Burkitt's lymphoma,⁹⁷ ovarian cancer,⁹⁸ prostate cancer,⁹⁹ medulloblastoma,¹⁰⁰ glioblastoma,¹⁰¹ non-Hodgkin's lymphoma,^{102, 103} and neuroblastoma, amongst others.¹⁰⁴⁻¹¹²

It is theorised that the role of the BET family in oncology is primarily driven by suppression of the c-Myc oncogene.^{97, 113, 114} c-Myc is a gene family which encodes multipurpose transcription factors vital to healthy cell growth and differentiation. However, amplification of c-Myc is among the most common genetic abnormalities observed in cancer genomes and deregulation of normal function can lead to aggressive cell proliferation. Targeting c-Myc is a well validated hypothesis in oncology but strategies to directly modulate it do not exist. BET inhibitors are capable of suppressing the expression of c-Myc and show efficacy in c-Myc driven cell lines.⁹²

Based on this evidence, BET inhibitors might be expected to cause general repression of gene transcription and cell cycle arrest. However, BET proteins, in particular BRD4, appear to localise specifically to super-enhancers, which are non-coding regions of DNA capable of binding to transcription factors important for cell-type speciation.^{115, 116} The c-Myc oncogene is activated by a super enhancer region of DNA which recruits significantly more BRD4 than normal, therefore, it is believed that BRD4 acts as a regulatory co-factor, which activates c-Myc leading to oncogenesis.¹¹⁷

However, it is clear that BET inhibition is more complex than simply suppression of c-Myc. Puissant *et al.* found that only 4 of the 99 cell lines sensitive to (+)-JQ1 (**1.08**) in a high throughput pharmacogenic screen were c-Myc amplified.¹⁰⁷ Interestingly, BET inhibition was also shown to be effective against primary effusion lymphoma, a cancer type which is not driven by abhorrent c-Myc expression.^{99, 102, 118} Further work is required to understand the precise mechanism of action of BET inhibitors. Notwithstanding this, multiple BET inhibitors have now entered the clinic for oncology indications.¹¹⁹

1.3.2. Autoimmune Inflammation

The BET family has also been shown to play an important role in autoimmune inflammation and BET inhibitors are a promising target for the treatment of rheumatoid arthritis (RA).^{120, 121} The molecular pathology of RA is complex, however, BET inhibitors have been shown to target RA through multiple mechanisms (Figure 1.16).¹²² For example, RA is characterised by the appearance of fibroblast-like synoviocytes (FLS) in the synovium. FLS cells cause joint damage and bone destruction, but these effects are decreased by BET inhibitors.^{120, 123} Osteoclasts are bone cells critical for the maintenance, repair and remodelling of bones. Abhorrent osteoclast function is typical in patients with RA.^{124, 125} BET inhibitors are able to suppress the detrimental effects of mis-regulated osteoclasts in macrophage cell lines. Furthermore, Nicodeme *et al.* stimulated mouse bone marrow derived macrophages with LPS, inducing the production of a variety of cytokines and chemokines and showed that I-BET762 (**1.07**, Section 1.4.) reduced the immune response in a dose-dependent manner.¹²⁶ Schilderink *et al.* used another BET inhibitor, I-BET151 (**1.11**, Section 1.4.), to demonstrate similar effects in LPS-stimulated dendritic cells derived from bone marrow.¹²⁷ They showed that BET inhibition reduced the production of pro-inflammatory cytokines and T cell activation.¹²⁸ Evidence for the therapeutic effect of BET inhibition has also been demonstrated *in vivo*. (+)-JQ1 (**1.08**) was capable of reducing inflammation using a mouse collagen induced arthritis model in a dose-dependent manner.¹²⁹ These combined factors provide a strong rationale for the therapeutic potential of BET inhibitors in RA and other immune mediated inflammatory diseases.

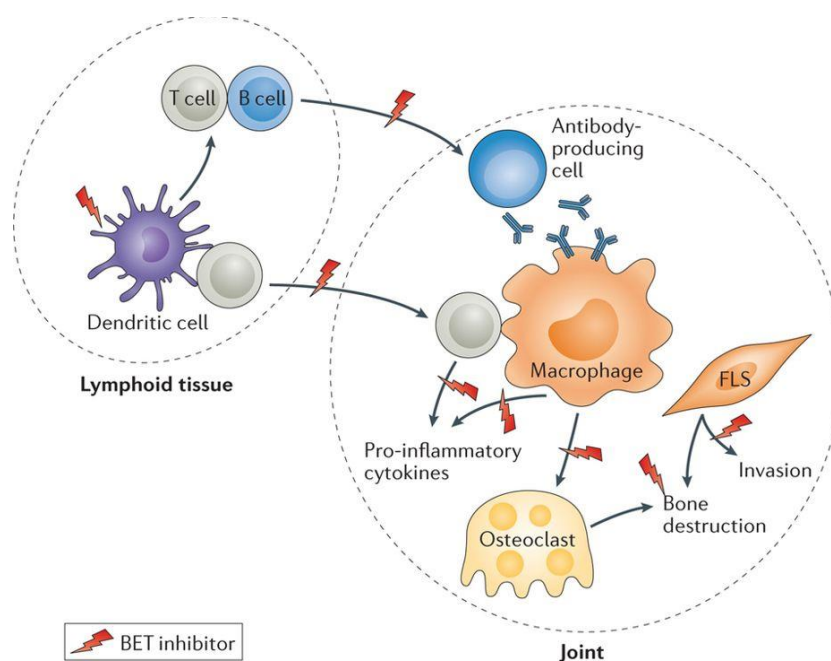


Figure 1.16. The molecular mechanism of RA is complex, and inflammation is driven by multiple mechanisms. BET inhibitors have been shown to effect multiple different signalling pathways vital to disease progression. Reproduced with permission from Nat. Rev. Drug Discov.¹²²

BET inhibitors have also been shown to play a significant role in other inflammatory diseases. Atherosclerosis is a cardiovascular condition caused by hardening of the arteries. Elevated levels of high density lipoprotein (HDL) cholesterol are thought to decrease the risk of atherosclerosis, which is a significant cause of mortality. Apolipoprotein A1 (ApoA1) is a major component of HDL, therefore, it is believed that ApoA1 up-regulation is a potential therapeutic strategy and an alternative to lipid modifying drugs such as statins. The first BET inhibitors were developed by phenotypic targeting of ApoA1 upregulation, indicating a direct link between BET inhibition and treatment of atherosclerosis.^{126, 130} Furthermore, there is also evidence that the BET family plays a role in other inflammatory disorders such as psoriasis.¹³¹

BET inhibitors together with gene knock-out and knock-down approaches have shown that the BET family contributes to the expression of multiple inflammatory genes.^{122, 132} There is evidence that the BET family plays a role in the recruitment of nuclear factor kappa-light-chain-enhancer of activated B cells (NF- κ B), a transcription factor that controls cytokine production and is involved in the immune response to infection.¹³³ Deregulation of NF- κ B has been linked to immuno-inflammation disorders.^{85, 134} BRD4 is believed to localise on the

super-enhancer region which controls the expression of NF- κ B and other transcription factors capable of inducing an immune response.¹³⁴

It is clear that the BET family plays a prominent role in disease. Based on this, a large number of pan-BET inhibitors have been discovered by academics and pharmaceutical companies to capitalise and further expand on this exciting group of therapeutic targets.

1.4. Small Molecule Inhibitors of the BET Family

1.4.1. The structure of Bromodomains

BRDs engage KAc residues of histone tails *via* a protein-protein interaction (PPI). Traditionally, PPIs have been difficult to inhibit due to the shallow nature of the binding pockets typically associated with this kind of interaction and the requirement for a small molecule to disrupt a large number of surface interactions made by two macromolecules.¹³⁵ However the PPI interactions of BRDs with histones have proved to be highly amenable targets for small molecule intervention. The structure of the 61 human BRDs is well conserved throughout the family.¹³⁶ The basic unit of each BRD consists of 4 α -helices (labelled α Z, α A, α B, and α C) which are linked by three loop regions (ZA, AB, and BC). A large hydrophobic cavity capable of binding KAc is formed by the four alpha helices and the ZA and BC loops (Figure 1.17).¹³⁷

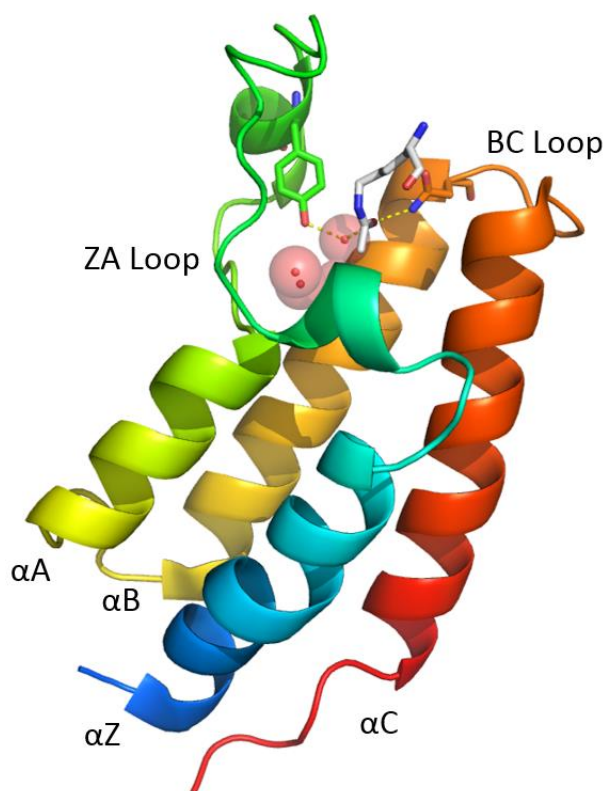


Figure 1.17. KAc (silver) in BRD4 BD2 (pdb4kv1). The 4 alpha helices are displayed as a coloured cartoon. The waters are shown as red spheres and key H-bonds are shown as dashed yellow lines.

Within the hydrophobic binding pocket are structural features conserved throughout most BRDs which are critical for KAc recognition. Typical BRDs such as the BET family have an Asn (Asn433 in BRD4 BD2, Figure 1.18) residue on their BC loop which can make a H-bond to KAc.^{132, 138} The other key structural feature is a Tyr residue (Tyr390 in BRD4 BD2,) located on the ZA loop. The KAc can make a water mediated H-bond to this residue which provides further stability to the binding interaction. This water molecule is part of a network of 4 water molecules which are found within the base of most BRD binding pockets and are well conserved throughout the family. Displacement of these water molecules have generated a lot of interest in the search for selectivity towards different BRDs and will be discussed further in Section 3.3.1. Another important structural feature is the 'WPF' shelf region named after the Trp374, Pro375 and Phe376 residues which form this region in the BET family (BRD4 BD2 numbering). These residues can differ considerably in different BRDs and provide opportunities for gaining selectivity between family members. In the BET family, the shelf is a distinct hydrophobic pocket which is not engaged by KAc. Its proximal location to the KAc

binding site offers opportunities for small molecule affinity. Furthermore the 'gate-keeper' residue is also important as it controls how accessible the WPF shelf is. In BRD4 BD2 the gatekeeper is the Ile439 residue.

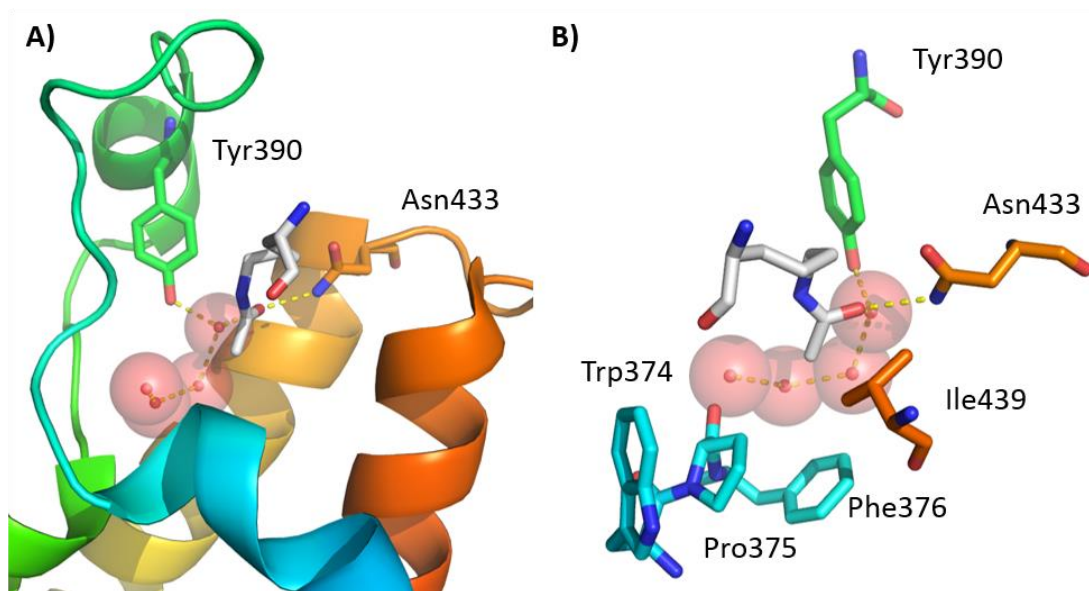


Figure 1.18. Binding site of BRD4 BD2 (pdb4kv1) with KAc (silver) bound. The waters are shown as red spheres and key H-bonds are shown as dashed yellow lines. A) The 4 alpha helices are displayed as a coloured cartoon with key residues depicted as stick. B) The WPF shelf consisting of Trp374, Pro375, and Phe376 in shown as sticks along with the Ile439 gatekeeper residue.

The structural features of BRDs, with a well-defined, deep, and narrow binding pocket, make them amenable to small molecule inhibition. Most small molecule inhibitors mimic the interactions of the natural KAc substrate to bind to BRDs, the challenge is then finding and maintaining selectivity.

1.4.2. pan-BET Inhibitors

1.4.2.1. Triazolodiazepine Inhibitors

Evidence of the significant role that the BET family has in a range of diseases has been driven by the availability of suitable tool molecules and this interest in turn has led to the development of more high-quality inhibitors of the BET family ultimately leading to clinical candidates.⁸³ The BET family resides on a single branch of the phylogenetic tree (Figure 1.14, section 1.3) and as such the 8 BRDs are highly homologous. Due to the difficulty associated with inhibition of a single BRD, the majority of compounds developed are pan-BET inhibitors,

which are equally potent at all 8 BRDs of the BET family.¹³⁹ The first BET inhibitors, I-BET762 **1.07** and (+)-JQ1 **1.08** (Figure 1.19), were reported in 2010 by Nicodeme *et al.* and Filippakopoulos *et al.*, respectively.^{126, 140}

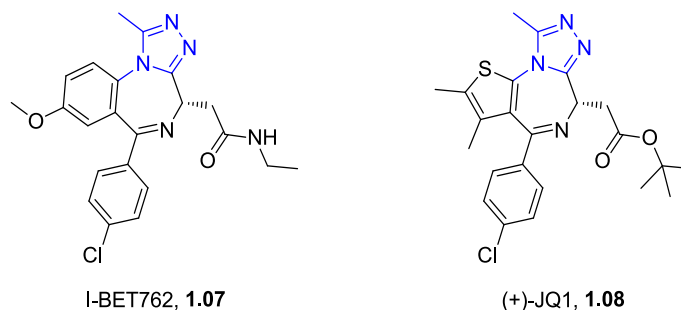


Figure 1.19. I-BET762 (**1.07**) and (+)-JQ1 (**1.08**), published in 2010 were the first example of small molecule BRD inhibitors which make key interactions to the conserved Asn140 residue through the triazolyl warhead highlighted in blue.

Both molecules contain the triazolodiazepine core structure, which acts as the KAc mimetic by making key interactions with the conserved Asn140 and Tyr97 (Figure 1.11). Selectivity over non-BET BRDs is thought to come from the interactions made with the ZA channel, where the fused phenyl group is positioned, and the WPF shelf, where the pendant phenyl ring resides (Figure 1.20). The ZA channel is a lipophilic pocket formed from the ZA loop which changes in size and shape between different BRDs. The steric constraints of the ZA channel can accommodate the methoxy phenyl ring of **1.07** leading to increased affinity for the BET family. As discussed previously (Section 1.4.1), there is a lack of sequence conservation observed for the WPF shelf region of the non-BET BRDs. For example, in the ATPase family, AAA domain containing 2 protein (ATAD2) the shelf region is defined by Arg, Val and Phe leading to a very different pocket shape and electronics (see Section 3.2.3 for more details). In BET, the Trp, Pro and Phe residues create a shelf which provides good shape complementarity for the 4-chloro phenyl ring. The chloro substituent was also shown to be important for removing off target activity. The favourable interactions of the pendant phenyl with the WPF shelf and the methoxy phenyl in the ZA channel are thought to be the main driving force for high BET affinity relative to other BRDs.¹⁴¹ The chirality of the carbonyl substituent was also shown to be important. The opposite enantiomer of (+)-JQ1 (**1.08**), (-)-JQ1, showed no significant activity at any of the BET proteins and as such provided an excellent negative control (see Section 3.1).

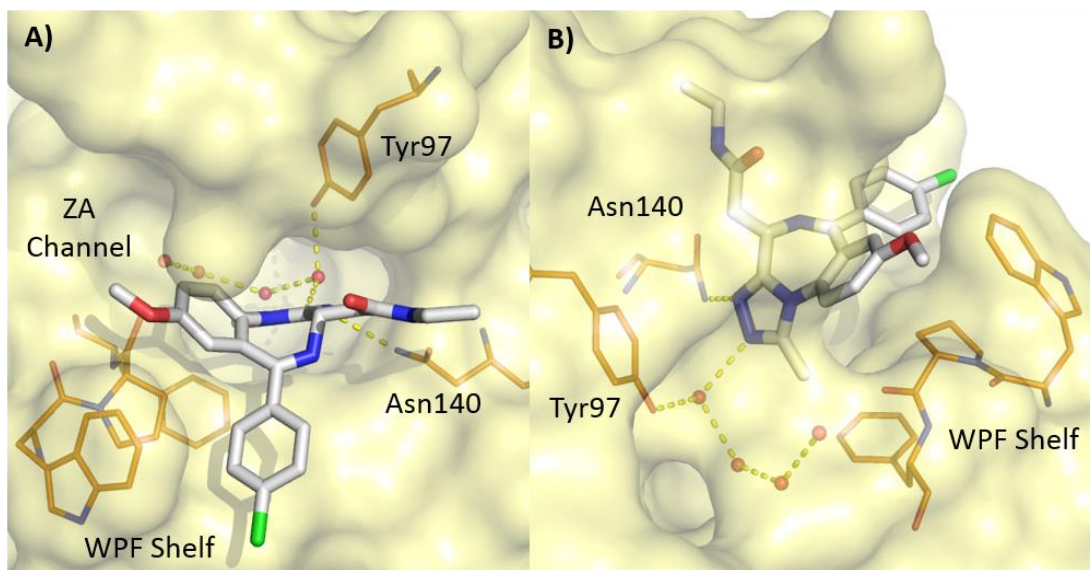


Figure 1.20. X-ray crystallography (pdb3p5o) of iBET762 (**1.07**, silver) in BRD4 BD1 (yellow). Key residues, Tyr97 and Asn140 and the WPF shelf region, are shown as orange lines. Water molecules are depicted as red spheres and H-bonds are shown as yellow dashed lines. A) The chlorophenyl group sits on the WPF shelf and the methoxyphenyl points into the ZA channel. B) The interactions of the triazolo warhead with the conserved Asn140 and Tyr97 can be seen.

Building on this work, two further clinical candidates based on the triazolodiazepine framework have been reported (Figure 1.21). OTX015 (**1.09**) and TEN-010 (**1.10**) are both based on (+)-JQ1 (**1.08**) and contain the thienophenone ZA-channel substituent but have converted the *t*-butyl ester to a secondary phenolic amide and a primary amide respectively.¹⁴²⁻¹⁴⁴ They have both entered the clinic for oncology indications.

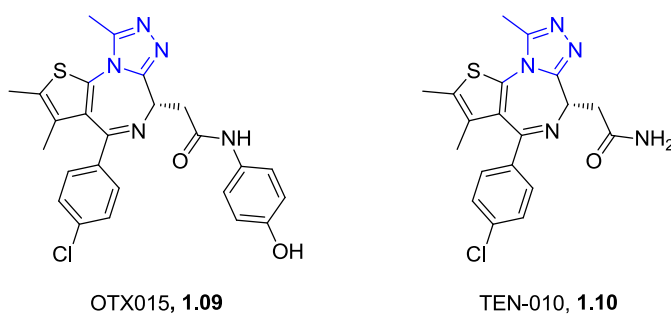


Figure 1.21. OTX015 (**1.09**) and TEN-010 (**1.10**) are triazolodiazepine based pan-BET inhibitors which have progressed to clinical trials. The triazole KAc mimetic is shown in blue.

1.4.2.2. Isoxazole based Scaffolds

Since the discovery of triazolodiazepines as BET inhibitors, other key pharmacophores have been reported which can mimic the BRD-KAc interaction. The first example, I-BET151 (**1.11**), was reported by GSK in 2012 (Figure 1.22).^{145, 146} They identified the dimethyl isoxazole from a high throughput screen (HTS) targeting ApoA1 upregulation. Further work to improve potency at BET, conformationally locked the benzylic pyridine, through formation of a cyclic urea, ultimately leading to a sub-micromolar inhibitor.

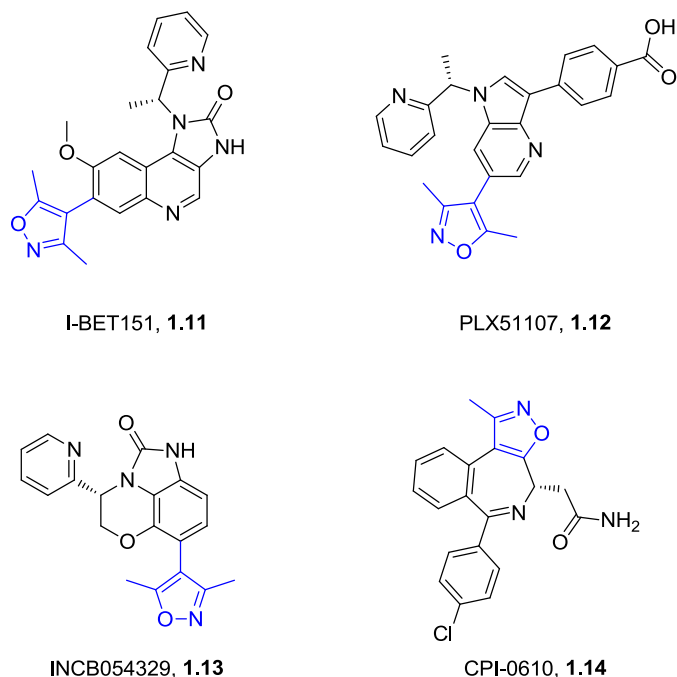


Figure 1.22. Small molecule BET inhibitors (**1.11–1.14**) which contain an isoxazole KAc mimetic. KAc mimetics shown in blue.

X-ray crystallography of I-BET151 (**1.11**) in BRD2 BD1 revealed how the dimethyl isoxazole binds to the BRD (Figure 1.23). The isoxazole oxygen makes a H-bond to the conserved Asn140 (BRD2 BD1 numbering) and both the isoxazole heteroatoms are capable of making a through water interaction to the conserved Tyr97. The two methyl groups then both occupy small lipophilic pockets within the binding site, allowing for excellent shape complementary of the ligand with the protein. I-BET151 (**1.11**) was optimised to conformationally deliver the pyridine on to the WPF shelf. The quinoline nitrogen also makes a H-bond to a water

molecule stabilising the binding further. Due to the success of I-BET151 (**1.11**), further compounds based on a dimethyl isoxazole warhead have since been reported.

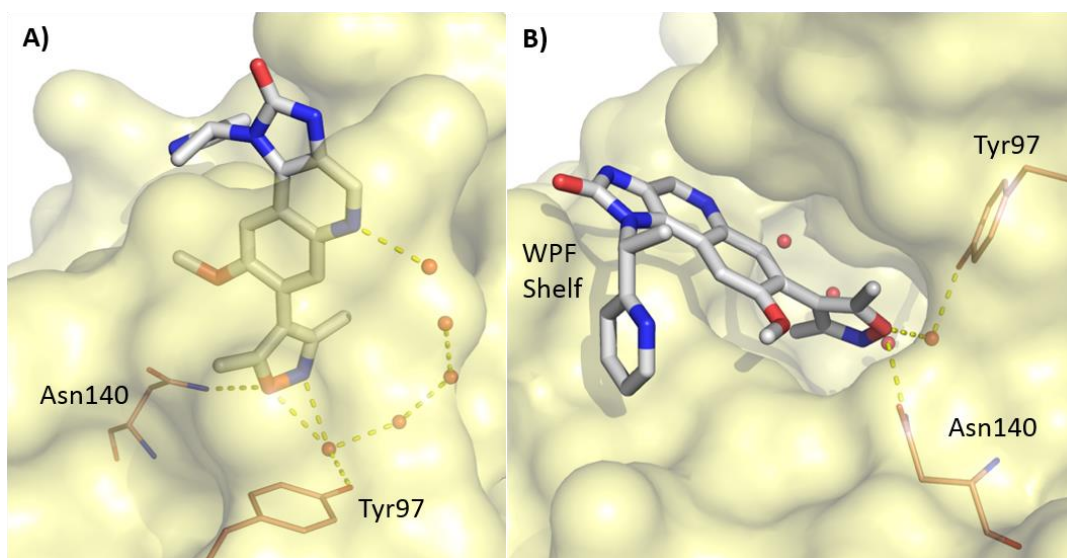


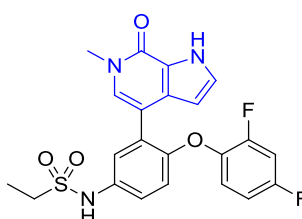
Figure 1.23. X-ray crystal structure (pdb3zyu) of I-BET151 (**1.11**, silver) in BRD2 BD1 (yellow). Key residues are shown in orange, H-bonds are depicted as yellow dashed lines and binding pocket waters are red spheres. A) The dimethyl isoxazole interacts with the conserved Asn140 and Tyr97 residues. B) The benzylic pyridone sits on the lipophilic WPF shelf region.

PLX51107 (**1.12**) is currently in clinical trials for the treatment of solid tumours and AML (Figure 1.22). Compound **1.12** was shown to be a potent nanomolar BET inhibitor which bound to BET through the dimethyl isoxazole warhead.¹⁰⁶ Additionally, INCB054329 (**1.13**), another isoxazole-based BET inhibitor has entered the clinic for oncology indications (Figure 1.22).¹⁴⁷ Multiple other small molecule inhibitors bearing this moiety have been reported, highlighting the importance of this pharmacophore as an KAc mimetic.¹⁴⁸

Interestingly, Gehring *et al.* combined the isoxazole warhead with the thienozepine present in (+)-JQ1 (**1.08**) to develop CPI-0610 (**1.14**, Figure 1.22).¹⁴⁹ They identified the isoxazole warhead from a fragment screen and took a scaffold hopping approach to optimise potency for the BET family. Isoxazole **1.14** is a highly potent BET inhibitor (BRD4 BD1 $pIC_{50} = 7.6$) which showed efficacy against c-Myc driven cancer cell lines. Compound **1.14** is currently in the clinic for multiple oncology indications.¹⁵⁰

1.4.2.3. Pyridone based scaffold

Researchers at AbbVie have developed pyrrolopyridones as potent BET BRD inhibitors. Their work started from a fragment screen which identified a pyridazinone fragment which was subsequently optimised into ABBV-075 (**1.15**, figure 1.24).^{151, 152} The pyridone moiety acts as the KAc mimetic and makes a bidentate H-bonding interaction with the conserved Asn through both the carbonyl lone pair and pyrrole NH. The pyridone methyl group then sits in the pocket formed by the network of waters in the base of the binding pocket. ABBV-075 (**1.15**) showed activity in an AML mouse xenograft model and has subsequently progressed to phase I clinical trials.

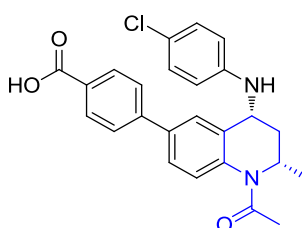


ABBV-075, **1.15**

Figure 1.24. ABBV-075 (**1.15**), a pyrrolopyridone based pan-BET inhibitor. KAc mimetic shown in blue.

1.4.2.4. Tetrahydroquinoline inhibitors

The tetrahydroquinoline (THQ) KAc mimetic was first disclosed by Bamborough *et al.* as an efficient fragment for BET inhibition.¹⁵³ This fragment was optimised to give I-BET726 (**1.16**), a potent and selective BET BRD inhibitor (Figure 1.25).¹⁵⁴



I-BET726, **1.16**

Figure 1.25. I-BET726 (**1.16**), a THQ based pan-BET inhibitor. KAc mimetic shown in blue.

The THQ acetamide made key interactions to the conserved Asn residue and a through water interaction with the conserved Tyr (Figure 1.26). The stereogenic methyl group then filled a

small lipophilic pocket providing excellent shape complementarity between the ligand and BRD.

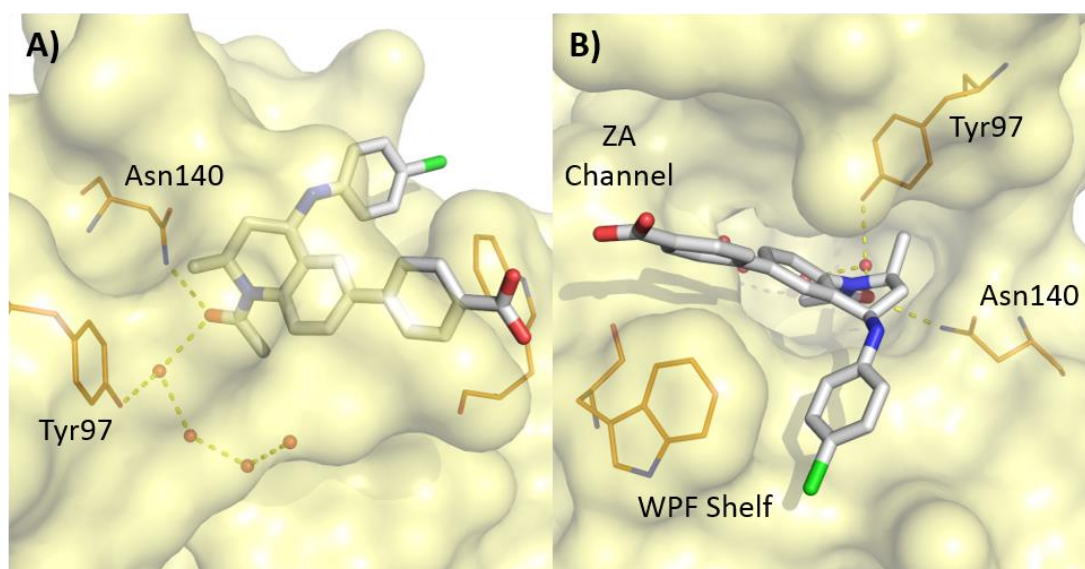


Figure 1.26. X-ray crystal structure (pdb4bjx) of I-BET726 (**1.16**, silver) in BRD4 BD1 (yellow). Key residues are shown. Water molecules are depicted as red spheres and H-bonds as dashed yellow lines. A) The key interactions with Asn140 and Tyr97 are depicted; B) The chlorophenyl can be seen on the WPF shelf with the phenyl carboxylic acid placed in the ZA channel. The stereogenic methyl occupies then occupies a small lipophilic pocket.

Overall, excellent progress has been made in the development of small molecule BET inhibitors. Multiple compounds have progressed to clinical trials for oncology indications and the outcomes of these trials will determine whether there is a therapeutic potential for pan-BET inhibition to treat inflammatory disorders. With it has come a detailed knowledge of the structural requirements for BET inhibition. Further developments are now being made to target the BET family through differentiated approaches.

1.4.3. Bivalent BET Inhibitors

The BET family of BCPs all contain 2 BRDs which are separated by a flexible protein unit without a defined domain structure. Theoretically, it should be possible to design a compound with 2 separate KAc mimetics that could bring both domains into proximity. The fact that multivalent binding is of critical importance for specific, high affinity chromatin recognition is increasingly being recognised.¹⁵⁵⁻¹⁵⁷ Miller *et al.* showed that BRDT recognises

the nucleosome solely through the BD1 domain but that the BD2 domain can then make a bidentate interaction with the nucleosome, suggesting that this kind of inhibition would be possible.¹⁵⁸ Waring *et al.* reported AZD5153 (**1.17**, Figure 1.27) which was the first example of a bivalent BET inhibitor capable of *in cis* binding to both BRDs (BD1 and BD2) of the BET family simultaneously, resulting in exquisite potency against BRD4 through an avidity effect (Figure 1.27).^{159, 160} The cellular SAR observed during their optimisation was suggestive of binding 2 BRDs simultaneously and when **1.17** was crystallised in BRD4, it induced dimerization indicating that both ends of the molecule were able to act as KAc mimetics. They then used ¹H NMR analysis to show that their binding mode was inconsistent with monovalency in solution phase. To show further evidence of bivalency they used analytical centrifugation, a technique whereby UV light absorption is used to map the sample concentration *versus* the axis of rotation as a result of the applied centrifugal field, to establish that there is a change in the conformation of the protein in the presence of the ligand **1.17**. Finally, they used a BRET system (see Section 1.1.3) to show a bidentate engagement of **1.17** in cells. AZD5153 has shown efficacy in tumour xenograft models of acute myeloid leukaemia, multiple myeloma and diffuse B-cell lymphoma and has entered the clinic to treat haematological malignancies.¹¹¹

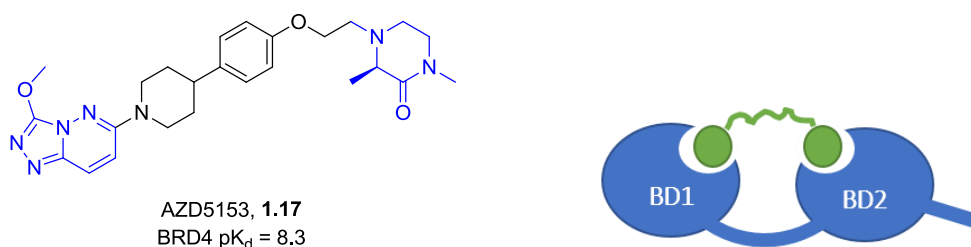
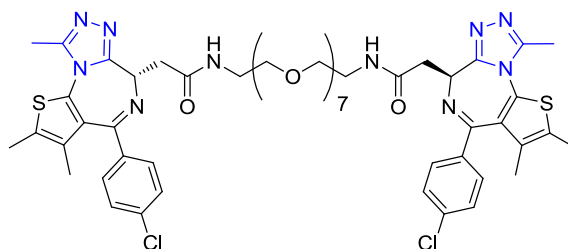


Figure 1.27. Left: AZD5153 (**1.17**), the first bivalent BET inhibitor with both KAc mimetics shown in blue. Right: Diagram showing *in cis* binding between a bivalent inhibitor (green) and both the BD1 and BD2 domains of a single BCP.

Around the same time, Tanaka *et al.* reported MT1 (**1.18**, Figure 1.28) as a bivalent BET inhibitor.¹⁶¹ They designed their inhibitor by linking from the *t*-butyl ester present in (+)-JQ1 (**1.08**) with an amide PEG7 linker. In this case *in cis* bivalency was shown using size exclusion chromatography (SEC), in which the monomeric peak was shifted when the bivalent ligand was added in a 1:2 ratio, consistent with change in protein shape. This was consistent with intramolecular inhibition of BRD4 which was further validated by X-ray crystallography. MT1

(**1.18**) also showed efficacy in a mouse xenograft model of leukaemia, making it a high-quality tool to assess the role of bivalent inhibition. The linker length required for bivalency in this case was significantly longer than in **1.18** suggesting that the optimal vectors were not being utilised.



MT1, **1.18**
BRD4 pIC₅₀ = 8.5

Figure 1.28. MT1 (**1.18**), a bivalent BET inhibitor based on (+)-JQ1 (**1.08**).

Interestingly, bivalent probes are beginning to be utilised for non-BET bromodomain inhibition. Suh *et al.* recently reported a bivalent ligand capable of binding simultaneously to both bromodomains of transcription initiation factor TFIID subunit 1 (TAF1).¹⁶² Ligand **1.19** was 100-fold more potent than the monovalent ligand (Figure 1.29), which is based on a promiscuous BRD inhibitor Bromosporine (**1.20**).¹⁶³ To show bivalent inhibition of their ligand, they used SEC, to demonstrate dose-dependent dimerization of the two BRDs by their ligand. Their work demonstrated that bivalent BRD inhibitors could potentially be used for any BCP with multiple BRDs.

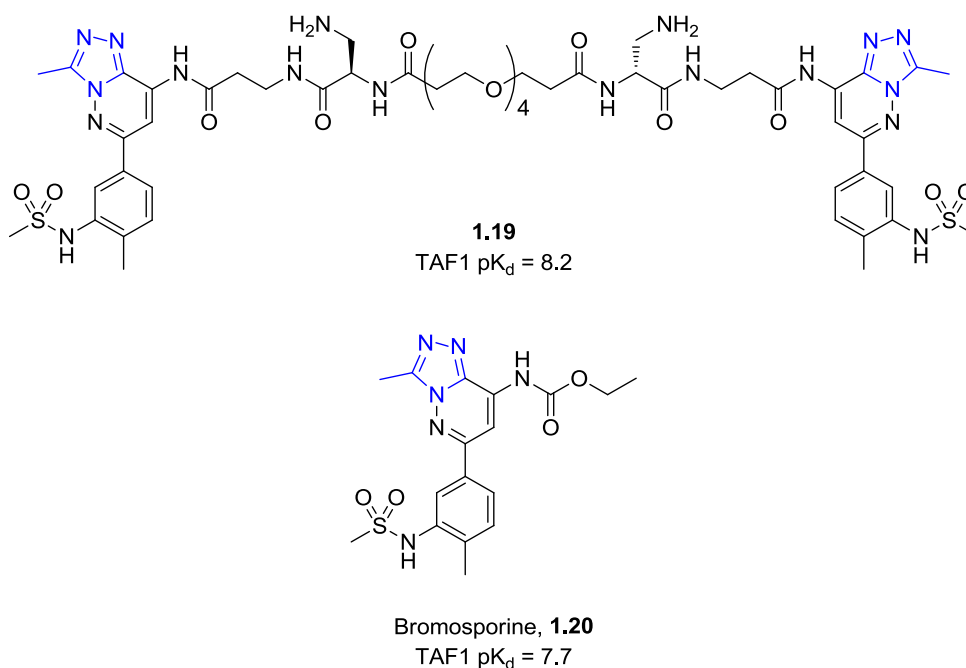


Figure 1.29. A bivalent TAF1 inhibitor (**1.19**) capable of binding to both BRDs of TAF1. It is based on the pan-bromodomain inhibitor Bromosporine (**1.20**).

1.4.4. Dual BET Inhibitors

An attractive strategy for targeting complex, multifactorial diseases such as cancer has been to develop dual inhibitors which display polypharmacology. That is, they show potency at multiple disease relevant proteins to achieve a synergistic effect. Designing polypharmacology can be challenging, due to the increased difficulty of optimising a template to target multiple proteins simultaneously. However, the strategy can ultimately lead to a more efficacious single agent without the need for combination therapies.¹⁶⁴ Indeed, examples of BET inhibitors which display efficacy at additional targets are beginning to appear in the literature. For example, BET and HDAC inhibitors have been shown to have overlapping phenotypes and can synergise to target c-Myc induced murine lymphoma.¹⁶⁵ This suggests that molecules capable of inhibiting both the HDAC and BET families could provide a novel strategy for oncology.

Atkinson *et al.* reported THQ **1.21** (Figure 1.30) which combined a pan-BET scaffold (Section 1.4.2) developed within the group with a hydroxamic acid linker known to bind to the zinc-containing HDAC (see Section 1.2.4).¹⁶⁶ Careful consideration of the optimal vector led to the development of a molecule that was able to engage both the BET family and HDAC family *in*

vitro. They then demonstrated cellular target engagement using LPS stimulated PBMCs where **1.21** was able to induce a dose-dependent response, hence demonstrating an immuno-inflammation relevant phenotype. Compound **1.21** also inhibited growth of both NMC and AML cell lines, however, no marked increase in potency was demonstrated compared to the parent compounds suggesting little synergy in the mechanism targeted. Other dual BET/HDAC inhibitors have subsequently been released which will allow for a full evaluation of their therapeutic potential. Amemiya *et al.* reported adenine **1.22**, which showed human leukaemia cell line-60 growth inhibition (Figure 1.30).¹⁶⁷ Additionally, Shoa *et al.* reported a dual BET/HDAC inhibitor **1.23** based on the BD2 biased scaffold present in RVX-208 (**1.38**, see Section 1.5.4) and the marketed HDAC inhibitor Panobinostat. They showed that **1.23** had a greater effect than the single agents (+)-JQ1 (**1.08**) and Vorinostat (**1.01**) against c-Myc driven AML.¹⁶⁸ Lastly, Zhang *et al.* reported dimethyl isoxazole **1.24**.¹⁶⁹ These compounds showed potent antiproliferative effects against a range of human leukaemia cell lines and represent an interesting approach to exploit the synergistic effect of dual HDAC and BET inhibition, although to date, no such inhibitor has progressed to the clinic.

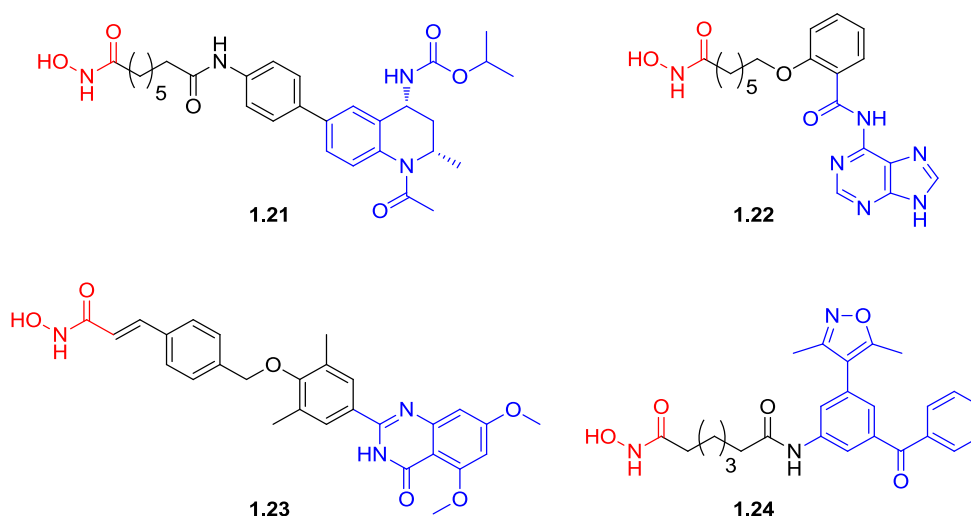


Figure 1.30. Dual BET/HDAC inhibitors **1.21–1.24**. The BET KAc mimetic is shown in blue and the hydroxamic acid HDAC zinc binder is shown in red.

Dual BET/kinase inhibitors are also starting to be developed as agents for oncology indications.¹⁷⁰ Ciceri *et al.* showed that the efficacy of many kinase inhibitors was driven, at least partially, by BET inhibition. They demonstrated that two clinical candidates, BI-2536 (**1.25**), a polo-like kinase 1 (PLK1) inhibitor, and TG101348 (**1.26**), a Janus kinase 2 (JAK2)

inhibitor, both display nanomolar activity for the BET family (Figure 1.31).^{171,172} Further work was initiated to understand the SAR of BI-2536 (**1.25**) at both BET and PLK1. Chen *et al.* demonstrated the importance of the aniline as being key for kinase binding. The ether analogue (i.e. changing the *NH* to *O*) reduced activity at PLK1 by 1000-fold leading to a selective BRD4 inhibitor.¹⁷³ Compound **1.25** was shown to bind to BRD4 BD1 through the methylated lactam which is capable of acting as an KAc mimetic.¹⁷⁴ Conversely, with TG101348 (**1.26**), the kinase pyrazine-aniline hinge binder is also capable of acting as a KAc mimetic.¹⁷¹ A crystal structure of **1.26** in BRD BD1 showed the hinge binder unit making two H-bonds to the conserved Asn residue.

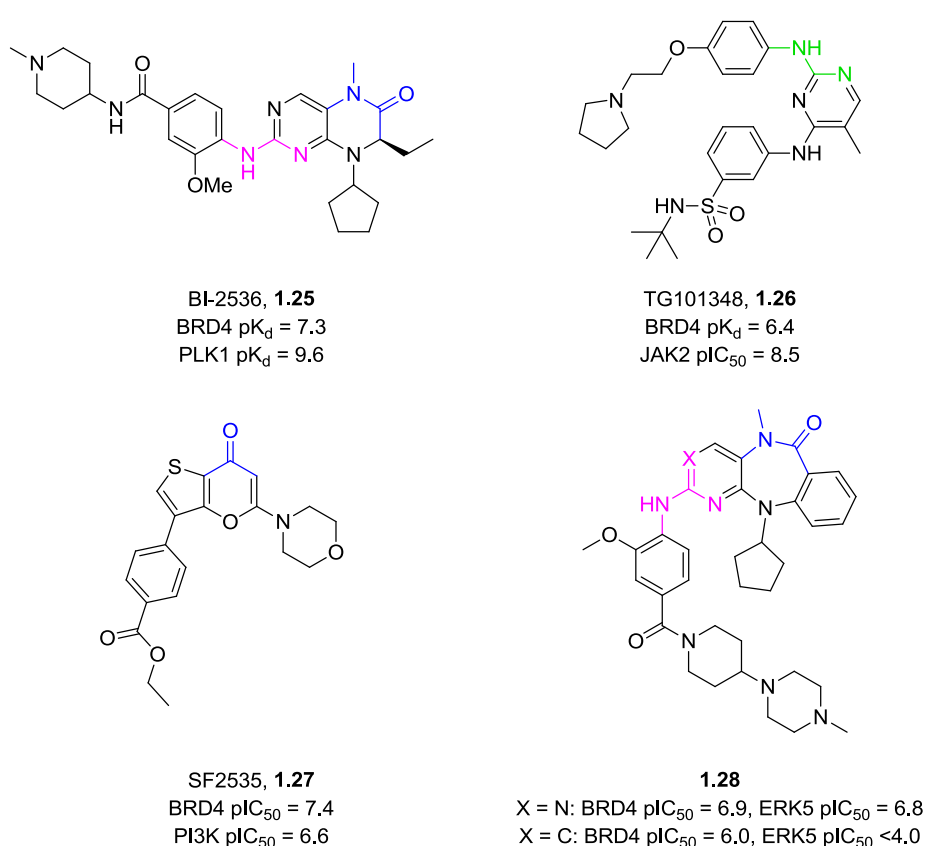


Figure 1.31. Dual BRD kinase inhibitors **1.25–1.28**. KAc mimetics are shown in blue. Kinase hinge binders are shown in pink. Functionality that can act as both a kinase hinge and KAc mimetic are shown in green.^{171-173, 175, 176}

Dual inhibitors of BET and other kinases are starting to be rationally designed. Andrews *et al.* targeted downregulation of c-Myc using a dual BET/PI3K inhibitor SF2535 (**1.27**) to block tumour growth and metastasis (Figure 1.31).¹⁷⁵ The thienopyranone template was capable

of binding to both PI3K and BET with sub micromolar affinity. In this case the pyrone carbonyl group was shown to act as the KAc mimetic by making a H-bond to the conserved asparagine.¹⁷⁷ Wang *et al.* then reported a pyrimido-benzodiazepinone scaffold (**1.28**) which bound to BRD4 BD1 through the diazepinone lactam.¹⁷⁶ They went on to demonstrate that through structural modifications to the template they could gain selectivity for either ERK5 or BRD4. For example, when X = C, the compounds were inactive against ERK5 at 40 μ M, however, this was also detrimental to BRD4 potency. They also showed that the KAc mimetic (Figure 1.31) was vital for both BRD4 and ERK5 activity. Through the exploration of the SAR, the authors were able to develop a chemical probe with selectivity for ERK5. This will be a useful tool to determine the different phenotypes of ERK5, BRD4 and dual inhibition respectively. Dual BET inhibitors represent an interesting opportunity for targeting polypharmacology through multiple synergistic pathways. However, it remains to be seen if this offers advantages to classical two agent combination therapies.

1.4.5. Degradation of BRD4 by bifunctional molecules

Alternative modalities to small molecule inhibitors are becoming increasingly prevalent in drug discovery.¹⁷⁸ One example is bifunctional molecules capable of first recognition and then inducing degradation of the target proteins, more commonly known as PROteolysis TArgeting Chimeras (PROTACs).^{179, 180} Rather than inhibit the function of their target, PROTACs eliminate the protein entirely through recruitment of the cellular proteasome (Figure 1.32). PROTAC molecules are bifunctional; one end is capable of binding to the protein of interest and the other engages a family of proteins called E3 ubiquitin ligases. This interaction results in the transfer of small proteins called ubiquitin onto the target protein. These markers are recognised by the proteasome which subsequently degrades the target. As PROTACs eliminate the protein of interest their pharmacology is more akin to protein knock-down than small molecule inhibition and could provide an alternative approach for drug discovery.¹⁸⁰

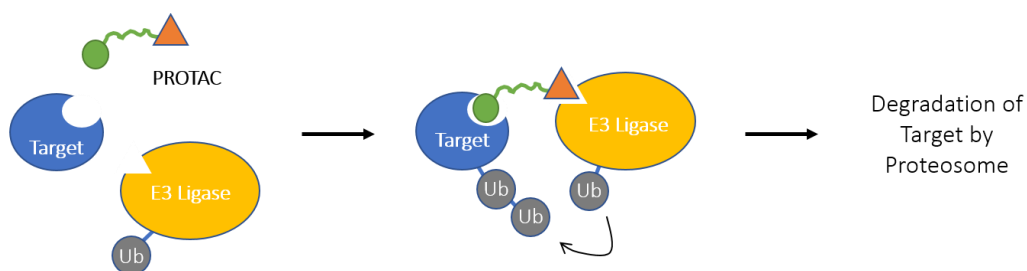


Figure 1.32. PROTACs are bifunctional molecules which bring a target protein and an E3 ligase into proximity. This results in a ubiquitination event, ultimately causing the degradation of the target protein by the proteasome.

The first BET PROTAC, reported by Winter *et al.*, was based on the small molecule inhibitor (+)-JQ1 (**1.08**).¹⁸⁰ They then used a C₄ linker to connect thalidomide, a known small molecule inhibitor of Cereblon (an E3 ligase). They showed that dBET1 (**1.29**, Figure 1.33) could bring BRD4 and Cereblon into proximity using a donor-acceptor luminescence assay and that loss of BRD4 could be detected in an AML cell line assay. They also used a known proteasome inhibitor (carfilzomib) to demonstrate that degradation of BRD4 was caused by the proteasome. Interestingly, dBET1 (**1.29**) was also able to reduce c-Myc expression and show efficacy in a leukemic cell lines. Other Cereblon ligand-based BET inhibitors which utilise different BET inhibitor warheads have since been reported showing a wider applicability to this approach.¹⁸¹⁻¹⁸⁵

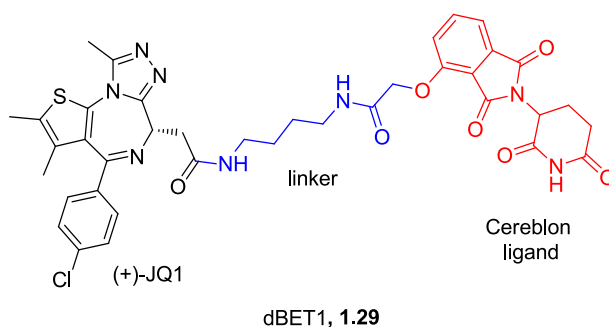


Figure 1.33. dBET1 (**1.29**) was the first PROTAC developed which targeted degradation of the BET family. It is based on a (+)-JQ1 (**1.08**) BET inhibitor which is linked to thalidomide, a small molecule which is recognised by the E3 ligase Cereblon.

Degradation of the BET family has also been achieved by engaging other E3 ligases. Cuilli *et al.* linked (+)-JQ1 (**1.08**) to a known VHL ligand using a PEG linker to give MZ1 (**1.30**, Figure 1.34).¹⁸⁶ They investigated a range of different linkers and identified the PEG3 chain present

in MZ1 (**1.30**) to be the most optimal. Isothermal calorimetry (ITC) measurements showed that MZ1 (**1.30**) could engage both BET and VHL independently and still function as ligands for the respective proteins. They were then able to demonstrate that a VHL based PROTAC approach can decrease concentrations of BRD2, BRD3 and BRD4 in HeLa cells, using Western blotting to analyse protein abundance. Interestingly, MZ1 (**1.30**) showed differential results to (+)-JQ1 (**1.08**) when the expression of selected genes was investigated. For example, expression of apoptosis antigen 1 (FAS), a cell surface receptor involved in apoptosis, is downregulated by (+)-JQ1 (**1.08**) but not MZ1 (**1.30**) compared to the control. Cuilli *et al.* then went on to crystallise the entire BRD4(BD2)-PROTAC-E3 Ligase construct, providing excellent evidence for the structural basis of protein degradation.¹⁸⁷ Their work also suggested that due to differences in ternary complex stability and the availability of a position suitable for ubiquitination, it may be possible to selectively degrade different BET isoforms using a pan-BET PROTAC.¹⁸⁸ They demonstrated this using the structurally related compound AT1 (**1.31**). Since MZ1 (**1.30**) was first published, other inhibitors which employ different BET inhibitors with VHL ligands to induce degradation of the BET family have been reported.^{189, 190}

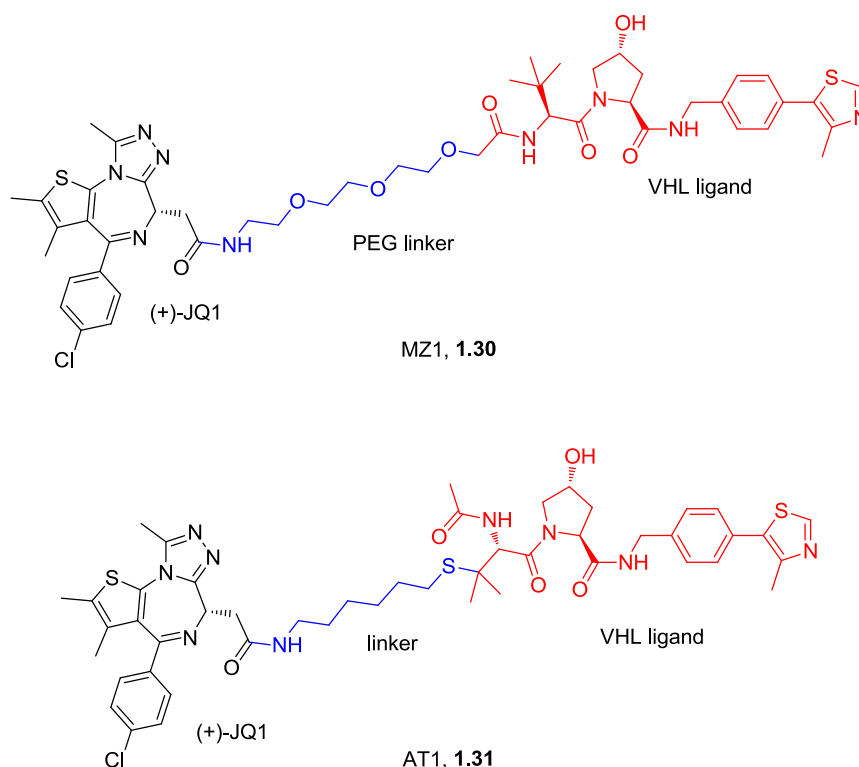


Figure 1.34. MZ1 (**1.30**) and AT1 (**1.31**), the first bifunctional BET degraders which contain a VHL E3 ligase binder. Both BET warheads are based on (+)-JQ1 (**1.08**).

1.5. Domain Selective BET inhibitors

1.5.1. Clinical Limitations of pan-BET inhibition

The small molecule BET inhibitors discussed so far are all classed as pan-BET inhibitors. Pan-BET inhibitors target all 8 BRDs of the BET family and show little or no selectivity for a single BRD or domain. The BET family plays a critical role in gene transcription vital for essential cellular processes and because of this show a strong oncology and immuno-inflammation phenotype. To date, 20 BET inhibitors have entered the clinic, however, pre-clinical safety study data and early clinical trial results could prevent or restrict their progression.¹¹⁹ BRD4 knock-down experiments lead to loss of stem cells in the gastrointestinal tract as well as loss of hematopoietic stem cells.¹⁹¹ The loss of important stem cells observed *in vivo* is likely to be recapitulated in patients and is the cause of one of the most significant dose-limiting toxicities (DLTs): thrombocytopenia. Thrombocytopenia is a condition where the blood platelet count is lowered, resulting in mucocutaneous bleeding which can ultimately be life threatening.¹⁹² Although a low platelet count appears to be reversible in the case of BET inhibitors, thrombocytopenia has been cited as a DLT for studies involving OTX015 (**1.09**).⁹² With I-BET762 (**1.07**) and CPI-0610 (**1.14**) thrombocytopenia was observed but was not dose limiting. Additionally, neutropenia, a low neutrophil (a type of white blood cell) count, and hyponatremia, a low sodium blood level, were observed as DLTs for OTX015 (**1.09**).¹⁴² Other side-effects include, fatigue, nausea, abdominal pain, diarrhoea, anaemia, and vomiting.⁹² The side effects could seriously impact the progression of pan-BET inhibitors as single agent therapies.

1.5.2. Structural differences between BET BD1 and BD2 domains

As there is cross activity, it is unknown which of the 8 BET BRDs is responsible for the different phenotypes observed and it is theorised that the disease relevant phenotype is driven by a different mechanism to the observed dose-limiting findings. Work by Cuilli *et al.* used a bump-and-hole approach to further investigate the unique role of individual BRDs (Figure 1.35).¹⁹³⁻¹⁹⁵ In the bump-and-hole approach, a known inhibitor is modified to create a 'bump' which clashes with the wild type protein. A selective 'hole' can then be engineered on the protein of interest by mutation of a conserved hydrophobic residue. In this case Leu94 was chosen and converted to a less sterically encumbered alanine residue to accommodate the modified ligand (**1.32**, figure 1.35). They achieved 160-fold selectivity for the first domain

using this approach and used it to demonstrate that inhibition of BD1 is sufficient to displace BRD4 from chromatin using a FRAP assay (see Section 1.1.3). The idea that the BET family primarily binds to histones through the BD1 domain is further validated by the work of Miller *et al.* Their work on BRDT using biophysical methods, including ITC, indicated that BRDT recognises the nucleosome solely through the BD1 domain but that the BD2 domain can then make a bidentate interaction with the nucleosome.¹⁵⁸

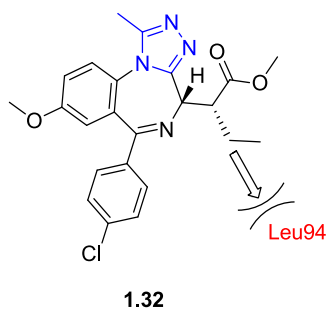
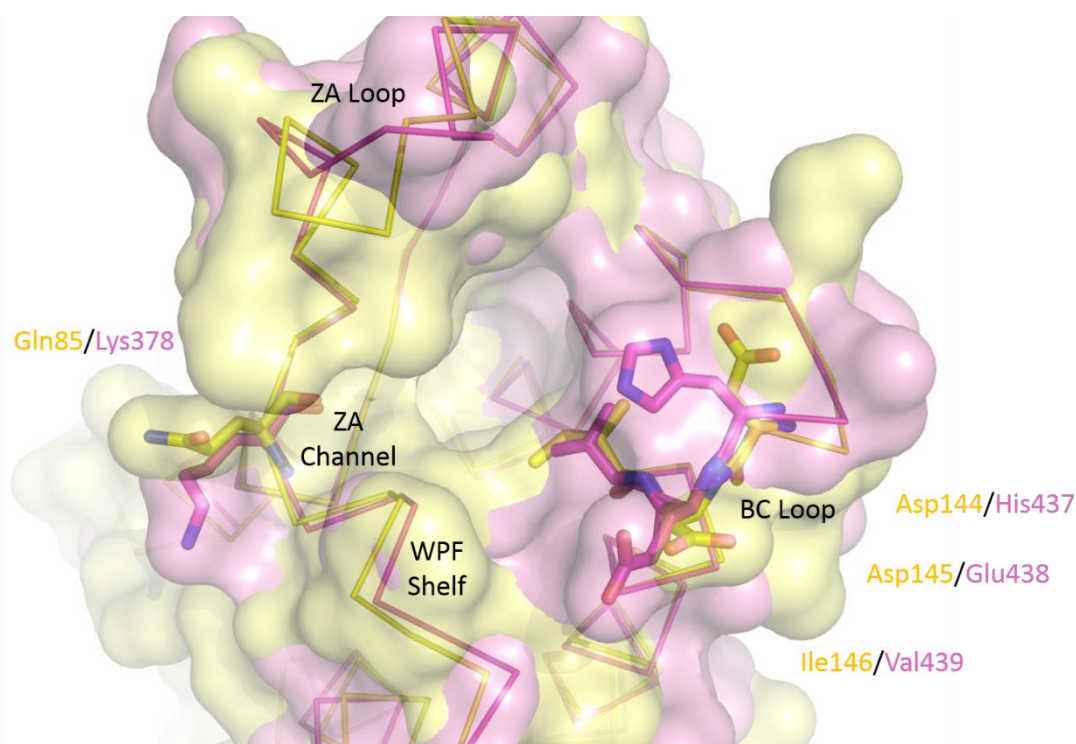


Figure 1.35. A bump-and-hole approach to target selectivity within the BET family.

The work of Cuilli *et al.* served to provide insight into the mechanism of action, however, as it was based on artificial constructs it may not translate to a wild-type system. Therefore, it is desirable to design small molecules which can elucidate the role of each specific BRD. Given the significant degree of sequence homology between BRDs within each domain (i.e. BRD2 BD1 and BRD3 BD1), targeting a single member of the family is incredibly challenging. However, domain selectivity (i.e. BD1 vs. BD2) is a more achievable approach due to minor differences between the BD1 and BD2 domains.

The sequence homology of the two domains (BD1 and BD2) is generally high, although there are several key differences which may be exploited when searching for selectivity (Figure 1.36). Arguably the greatest differences lie on the BA loop. Here, a number of changes are clustered close together which is advantageous for designing small molecule inhibitors. In BRD4 Asp144 in BD1 is replaced by His437 in BD2. The BD2 specific His is a key residue bordering the WPF shelf, which could be exploited for selectivity. Additionally, Asp145 in BD1 is replaced by Glu438 in BD2 and the Ile146 gatekeeper residue in BD1 changes to the slightly larger Val439 in BD2. Furthermore, there are key differences on the ZA loop which affect the shape and potential interactions in the ZA channel. Notably, Glu85 in BD1 is replaced by

either a Lys or Arg in the BD2 domain. These structural features of the two BRDs are starting to be exploited in the development of domain selective BET inhibitors.



				<i>αZ</i>		<i>ZA loop</i>		<i>αA</i>
BRD2	BD1	61	PPPEVSNPKKGRVTNQLQYLHKVVMKALWK	---	HQFAWPF	QPVD	AVKLG	LPDYHKIIKQPM
BRD3	BD1	21	PPPEVSNPSKGRKTNQLQYMQNVVVKTLWK	---	HQFAWPF	YPVDA	IKLNL	PDYHKIIKPNMD
BRD4	BD1	45	PPPEVSNPKPKRQTNQLQYLLRVVVKTLWK	---	HQFAWPF	QPVD	AVKLG	LPDYHKIIKQPM
BRD1	BD1	14	PPPEYINTKKNGRLTNQLQYLQKVVVKDLWK	---	HSFSWPF	CRPVD	AVKLG	LPDYHTI
BRD2	BD2	339	-----QSSKKGKLS	EQLKHC	NGILKELLS	SKHAAY	AWPFY	QPVDA
BRD3	BD2	301	-----HAGKKGKLS	EHLYCDS	ILREML	SKHAAY	AWPFY	QPVDA
BRD4	BD2	343	-----APEKSSKVS	EQLKCC	SGILKEM	FAKHAAY	AWPFY	QPVDA
BRD1	BD2	262	-----NVVKT	VKVT	EQLRHC	SEILKEM	LAKKHF	SYAWPFY
			<i>αA</i>	<i>αB</i>	<i>BC</i>	<i>αC</i>		
BRD2	BD1	128	RRLENNYYWAASE	CMQDFNT	MTN	CIYINK	PTDDIV	LMAQ
BRD3	BD1	88	KRLENNYYWSASE	CMQDFNT	MTN	CIYINK	PTDDIV	LMAQ
BRD4	BD1	112	KRLENNYYWNAQ	ECIQDFNT	MTN	CIYINK	PGDDIV	LMAE
BRD1	BD1	81	KRLENKYYAKASE	CIQDFNT	MTN	CIYINK	PGDDIV	LMAQ
BRD2	BD2	401	RKMENRDYRDAQ	EFAADV	RLMFS	NCYKYN	PPDHEV	VAMAR
BRD3	BD2	363	RKMDGREYPDAQ	EFAADV	RLMFS	NCYKYN	PPDHEV	VAMAR
BRD4	BD2	405	SKLEAREYRDAQ	EFGADV	RLMFS	NCYKYN	PPDHEV	VAMAR
BRD1	BD2	324	EKMDNQEYKDAY	KFAADV	RLMFM	NCYKYN	PPDHEV	VTMAR

Figure 1.36. A comparison of residue changes between BRD4 BD1 (pdb4kv1) and BRD4 BD2 (pdb3uw9). BRD4 BD1 residues are shown in yellow and BRD4 BD2 residues are shown in pink. Below are the sequences of the BET family with key residue changes between the BD1 and BD2 domains highlighted.

1.5.3. BD1 Biased BET inhibitors

Reports of molecules with a bias for BD1 are starting to appear in the literature (Figure 1.37). One of the first examples was reported by Zhou and co-workers who released MS436 (**1.33**), a low nanomolar BET inhibitor with a preference for the first BRD.¹⁹⁶ The selectivity is believed to come from a water mediated interaction with the BD1 specific Gln85 located on the ZA loop and the unique azo moiety within MS436 (**1.33**). This is anchored in place by the phenol warhead and its *meta*-aniline which binds through a network of H-bonds, and is crucial for high potency and BD1 bias.

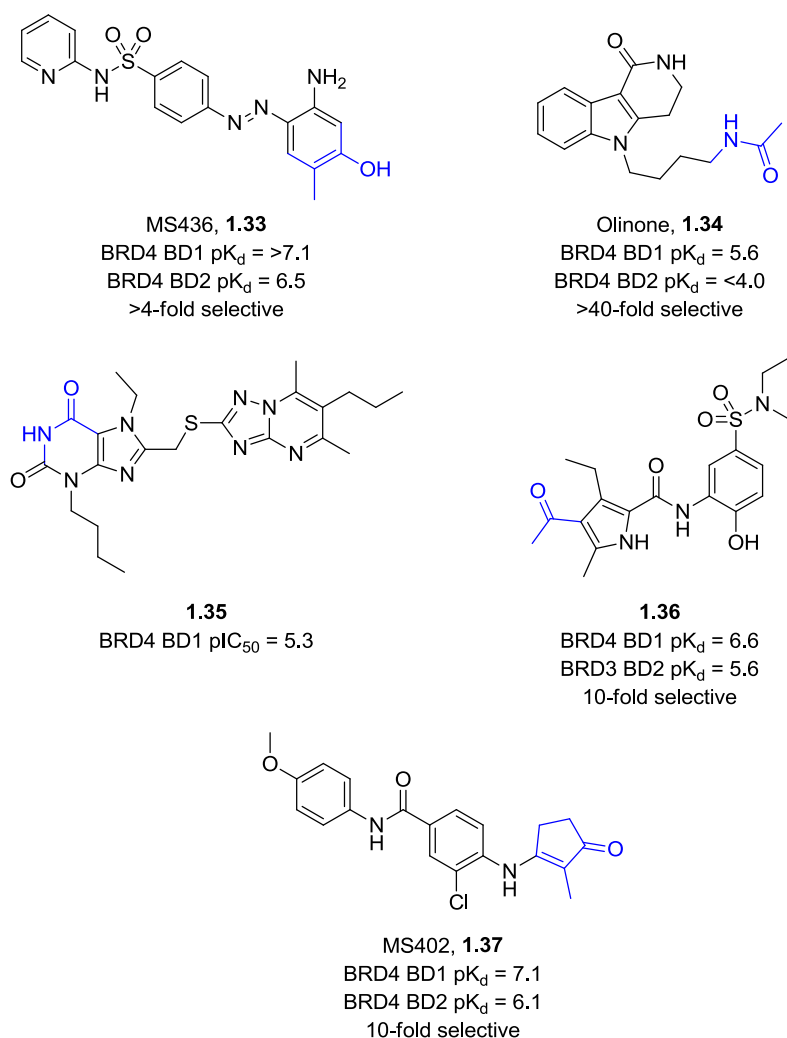


Figure 1.37. Small molecule BET inhibitors **1.33–1.37** with bias for BD1.

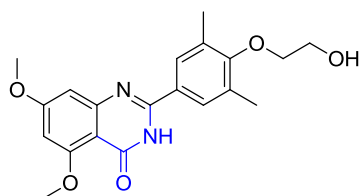
Further work by Zhou then disclosed Olinone (**1.34**) which only bound to the first BRD ($pK_d = 5.6$) and possessed no detectable affinity for BD2, as assessed by ITC measurements (Figure

1.37).¹⁹⁷ The tricyclic structure interacts with the BD1 specific Asp144 which drives selectivity. Two additional BD1 biased inhibitors were reported in early 2015 by Raux and Hügler respectively. Raux *et al.* reported xanthine **1.35** which was identified from a medium-throughput screen (MTS) using a protein-protein interaction inhibition orientated library.¹⁹⁸ Using a homogenous time resolved fluorescence (HTRF) experiment, **1.35** was identified as a 5 μ M (pIC₅₀ = 5.3) inhibitor of BRD BD1 with >10-fold selectivity over other members of the BET family tested, despite its weak binding. It should be noted that the data for inhibition of the BD2 domain did not converge and selectivity is impossible to ascertain. Hügler *et al.* then reported 4-acyl pyrrole **1.36** as a potent BRD4 BD1 inhibitor (pK_d = 6.6).¹⁹⁹ The inhibitor shows 10-fold bias for BRD4 BD1, although binding affinity is only given for BRD4 (BD1) and BRD3 (BD1 and BD2). Zhou has now reported another structurally differentiated BD1 biased inhibitor MS402 (**1.37**).²⁰⁰ Compound **1.37** contains a cyclic enone warhead which binds as the KAc mimetic. Again, the selectivity for this series comes from exploiting the residue change in the ZA loop. The amide makes a H-bond to the BD1 specific Gln85 thought to be responsible for the 10-fold selectivity observed. These compounds represent the first steps towards BD1 selective BET inhibitors, however, they are not currently selective enough to confidently identify the phenotype of BD1 inhibition. 100 or indeed 1000-fold selective inhibitors remain a desirable challenge to the medicinal chemistry community in order to achieve this goal.

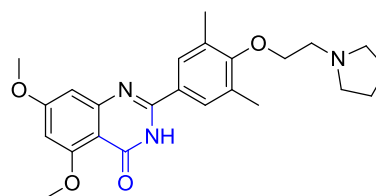
1.5.4. BD2 Selective BET inhibitors

BD2 selective BET inhibitors have also drawn increasing interest and reports of selective compounds are beginning to appear in the literature (Figure 1.38). RVX-208 (**1.38**) was developed by Resverlogix for the treatment of cardiovascular disease associated with atherosclerosis, through phenotypic screening against ApoA1 upregulation. This is the same mechanism which led to the serendipitous discovery of I-BET762 (**1.07**) as a BET inhibitor (Section 1.4.2).²⁰¹ Intriguingly, with RVX-208 (**1.38**) no anti-proliferative effects were observed. On further investigation, it became clear that RVX-208 (**1.38**) had a bias for the second BRD of the BET family, with the highest selectivity window observed for BRD2 of 23-fold. Compound **1.38** constituted one of the first indications of differentiated phenotypes between the two domains. The selectivity is believed to come from an interaction with the BD2 specific His433 (BRD2 numbering) which flips into the KAc binding pocket and makes a π -stacking interaction with the inhibitor. RVX-208 (**1.38**) was improved upon to deliver RVX-

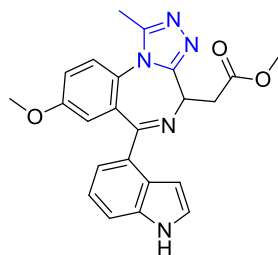
297 (**1.39**), which is an orally bioavailable BET inhibitor which shows 50-fold preference for BD2 in an alpha screen assay.^{202, 203} Compound **1.39** was efficacious in a collagen induced arthritis model. Molecular dynamic simulations identified the BC loop changes, which include His433, as the most influential factors for selectivity in studies on RVX-208 (**1.38**) and RVX-297 (**1.39**).^{204, 205}



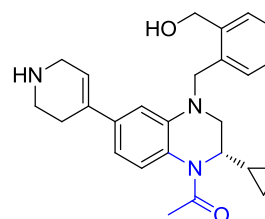
RVX-208, **1.38**
BRD4 BD1 $pK_d = 6.0$
BRD4 BD2 $pK_d = 6.9$
8-fold selective



RVX-297, **1.39**
BRD4 BD1 $pIC_{50} = 5.9$
BRD4 BD2 $pIC_{50} = 7.7$
63-fold selective



1.40
BRD4 BD1 $pK_d = 6.3$
BRD4 BD2 $pK_d = 7.3$
10-fold selective



1.41
BRD4 BD1 $pIC_{50} = 5.5$
BRD4 BD2 $pIC_{50} = 7.2$
50-fold selective

Figure 1.38. BET inhibitors with selectivity for BD2 (**1.38–1.41**). KAc mimetics are shown in blue.

During their work developing the bump-and-hole approach Cuilli *et al.* reported **1.40** which was *c.a.* 10-fold selective for the second BRD in both BRD2 and BRD4.¹⁹⁴ They believed that the electron rich indole was able to form an edge-to-face interaction with the BD2 specific His leading to greater stabilisation in BD2. More recently, Law *et al.* have reported tetrahydroquinoxaline (THQx) **1.41** as a BET inhibitor with selectivity for the second BRD.²⁰⁶ THQx **1.41** showed a 50-fold bias towards BD2 in BRD4 biochemical FRET assays and >300-fold selectivity against all other tested BRDs, in DiscoverX's BROMOscan panel. THQx **1.41** has an analogous binding mode to THQ **1.41**. Again, the acetamide warhead mimics the key interaction of KAc with Asn429 and Tyr386, but here, the cyclopropyl group occupies the small lipophilic pocket. The benzyl group occupies the shelf region between the WPF shelf

region and the benzylic alcohol then makes a H-bond to the BD2 specific His433 residue which is believed to enhance the bias for the second domain. The semi-saturated heterocycle then points into the ZA channel (Figure 1.39).

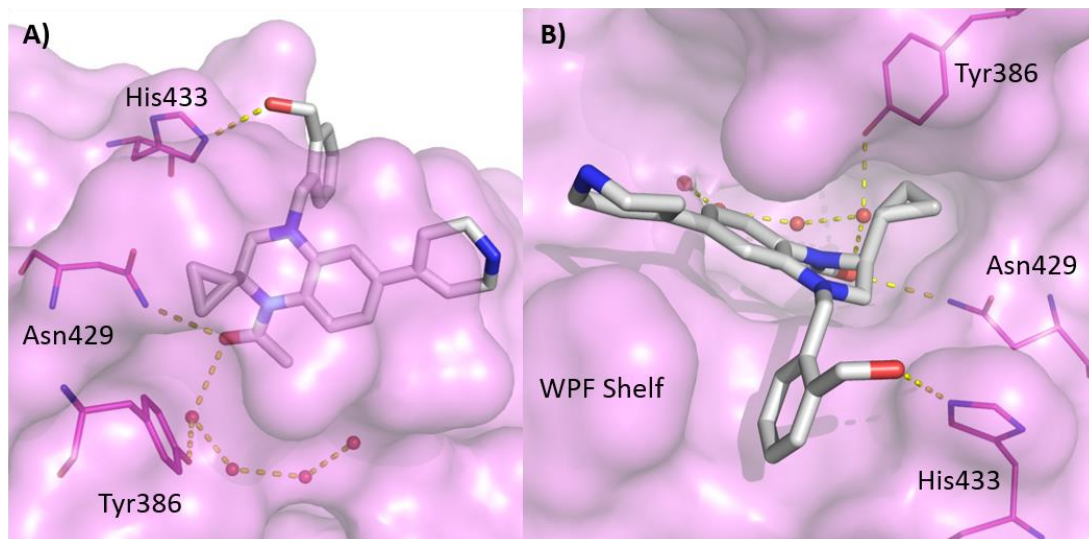


Figure 1.39. X-ray crystallography (pdb6ffg) of THQx (**1.41**, silver) in BRD2 BD2 (pink). Key residues are depicted as magenta lines, waters as red spheres and H-bonds are shown as yellow dashed lines. A) THQx **1.41** makes interactions with Asn429 and Tyr386. B) The aromatic group benzyl group sits between the WPF shelf and the BD2 specific His433 which the benzyl alcohol makes a H-bond to. This interaction is believed to be a key driver of selectivity for the second BRD of the BET family.

With the development of molecules capable of distinguishing between domains, clarity about the unique role of each domain is starting to occur. RVX-297 (**1.39**) maintains a range of immune relevant efficacies *in vitro* and *in vivo*, for example, it downregulates interleukin 6 expression in FLS.^{202, 203} However, due to the high dose used, the selectivity of **1.39** is insufficient to determine whether the effects observed are caused solely by inhibition of BD2. Furthermore, THQx **1.41** inhibited the release of the MCP-1 cytokine in human PBMCs and whole blood following induction of an immune response by treatment with LPS.²⁰⁶ Furthermore, it is still unclear what role the specific BET isoforms (BRD2, 3, 4 and T) play in gene transcription. Further work is needed both on domain selective and single domain selective inhibitors to understand their individual biological roles.

1.6. Pursuing a BD2 Selective BET inhibitor

1.6.1. Development of a Highly Potent and BD2 Selective BET Inhibitor

Although several BD2 selective inhibitors have been reported, it was felt that the level of selectivity obtained may not be sufficient to disconnect the safety and efficacy of BD1 and BD2. This was particularly important in this class of inhibitor due to the extent of the efficacy and toxicity associated with pan-BET inhibition. As such, work towards the development of BD2 selective BET inhibitors with enhanced selectivity was undertaken by our group.

A HTS of 2 million compounds was undertaken, screening against the BRD4 BD2 domain at a single concentration. Mutated TR-FRET assays, which used a truncated BRD4 protein (residues 1-477) and either a Y390A mutation or a Y97A mutation to assess BD2 or BD1 potency respectively, were used to determine affinity for a single domain. Mutation of the conserved Tyr to an Ala residue completely removed the ability of small molecule BRD inhibitors to interact with that domain. Hits which preferentially bound to the BD2 domain of BRD4 were selected. This identified acetamide derivative **1.42** (Figure 1.40), which displayed 13-fold selectivity over BD1 in a biochemical TR-FRET assay. Notably, this selectivity was also observed for BRD2, BRD3, and BRD4. Optimisation of the amide vector, insertion of a benzylic methylene unit and fluorination of the phenyl core lead to GSK046 (**1.43**, figure 1.40): a potent BET inhibitor (BRD4 BD2 $pIC_{50} = 7.3$) with 1300-fold selectivity for BD2 (BRD4 BD1 $pIC_{50} = 4.2$).²⁰⁷

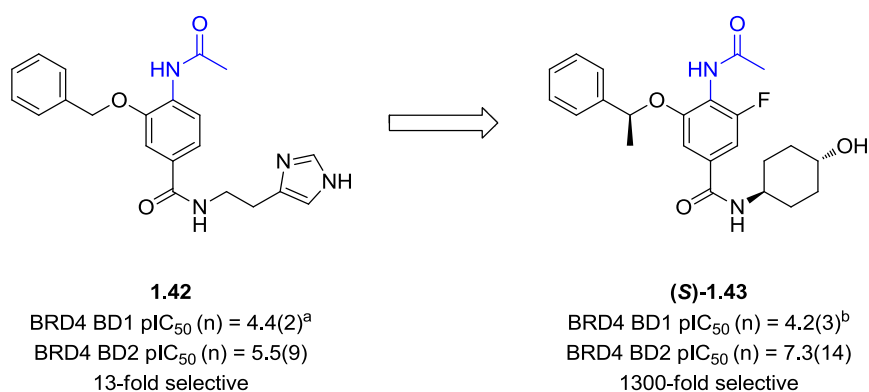


Figure 1.40. Development of GSK046 (**1.43**) from initial hit to potent and BD2 selective BET inhibitor.

^aalso <4.3 (n = 7); ^balso <4.3 (n = 10).

GSK Confidential – Do not copy

The exquisite selectivity could be understood by evaluation of the GSK046 (**1.43**) crystal structure in BRD2 BD2 (Figure 1.41). Here, the acetamide acts as the KAc mimetic, whilst the benzyloxy group occupies the WPF shelf, with the benzylic methyl pointing into the ZA-channel. Crystallographic evidence shows that the fluorine substituent changes how the core is positioned in the binding pocket meaning that the cyclohexanol amide *NH* can form a bidentate interaction to Asn429 (BRD2 BD2 numbering). Although this interaction also occurs in BD1, the BD2 specific His433 makes an edge-to-face interaction with the benzyl group. In BD1 this residue is replaced with an Asp residue which cannot make this interaction and these combined factors are believed to drive the excellent selectivity.

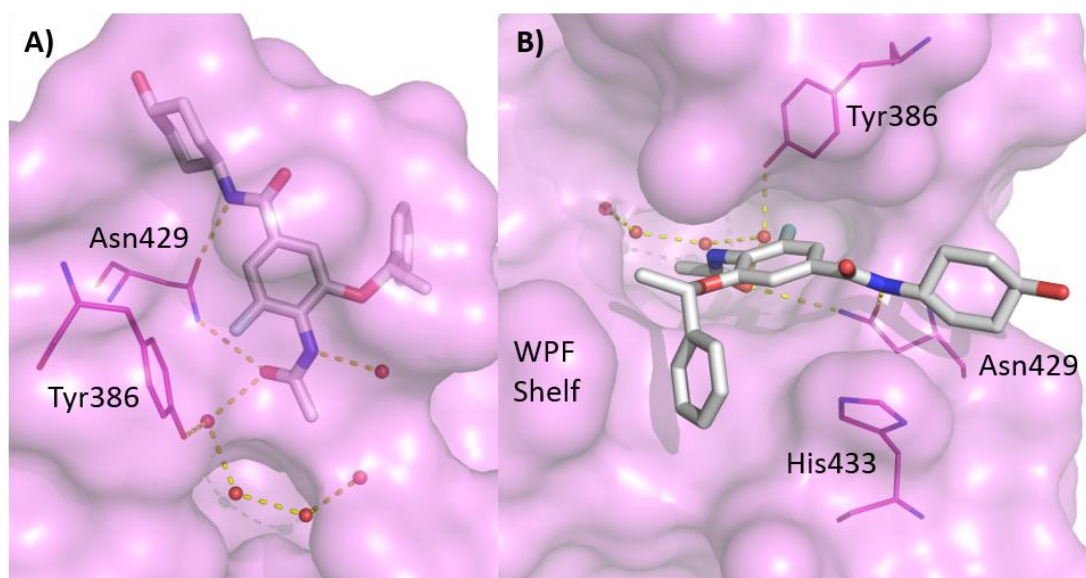


Figure 1.41. X-ray crystallography of GSK046 (**1.43**, silver) in BRD2 BD2 (pink). Key residues are shown in magenta, water as red spheres and H-bonds as yellow dashes. A) **1.43** interacts with Asn429 and Tyr386 through the methylamide. The second amide makes a bidentate interaction to Asn429. B) The phenyl ring sits between the WPF shelf region and BD2 specific His433.

GSK046 (**1.43**) represents an excellent tool to probe mechanistically the roles of the BD1 and BD2 domains both *in vitro* and *in vivo*. To investigate whether a highly selective BD2 BET inhibitor could maintain an immuno-inflammation phenotype, **1.43** was tested in an LPS stimulated PBMC cellular assay. Pleasingly, acetamide **1.43** caused concentration-dependent inhibition of MCP-1, demonstrating for the first time that a BD2 selective BET inhibitor could be progressed to treat inflammatory diseases. Unfortunately, acetamide **1.43** contained an

embedded aniline and was considered of high genotoxic potential, so progression beyond a tool was not possible.

1.6.2. Overcoming the Genotoxic Risk of **1.43**

Despite the exquisite selectivity of GSK046 (**1.43**), the genotoxic liability meant that an alternative chemotype was sought for the development of a BD2 selective clinical candidate. In parallel, pyridone **1.44**, which showed a marginal degree of selectivity towards the second BRD of BRD4 after optimisation of another hit from the same HTS as **1.42**, was identified as an alternative starting point (Figure 1.41).²⁰⁸ Despite the initially poor selectivity profile of pyridone **1.44**, X-ray crystallography suggested that a scaffold hopping approach from GSK046 (**1.43**) could be used to improve selectivity. Addition of a *meta*-amide and optimisation of this vector led to GSK620 (**1.45**), a 200-fold selective BD2 BET inhibitor.

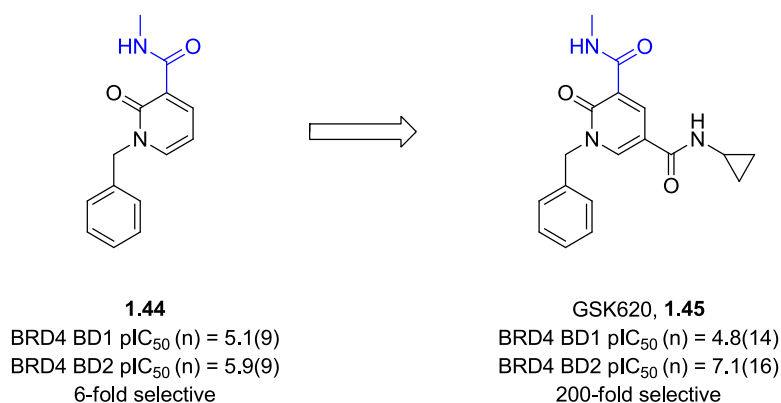


Figure 1.41. Optimisation of GSK620 (**1.45**) from fragment hit to potent and BD2 selective BET inhibitor.

An X-ray crystal structure of **1.45** in BRD2 BD2 was solved and overlaid with that of GSK046 (**1.43**). Unsurprisingly, the methylamide warhead is the KAc binding mimetic, with the amide carbonyl making a H-bond to Asn429 and Tyr386 (Figure 1.42). A portion of the binding potency is believed to arise from an intramolecular H-bond between the pyridone carbonyl group and the methylamide *NH* which stabilises the required bioactive conformation of the warhead. The binding of pyridone **1.45** exploits the same BD2 residues as acetamide **1.43** (Figure 1.42). The two amides participate in a bidentate interaction with Asn429 which places the benzyl group on the WPF shelf where it forms an edge-to-face interaction with His433 in BD2. When the X-ray crystal structure of acetamide **1.43** and pyridone **1.45** were overlaid,

the phenyl rings are co-located, suggesting that this interaction is integral for the high selectivity observed.

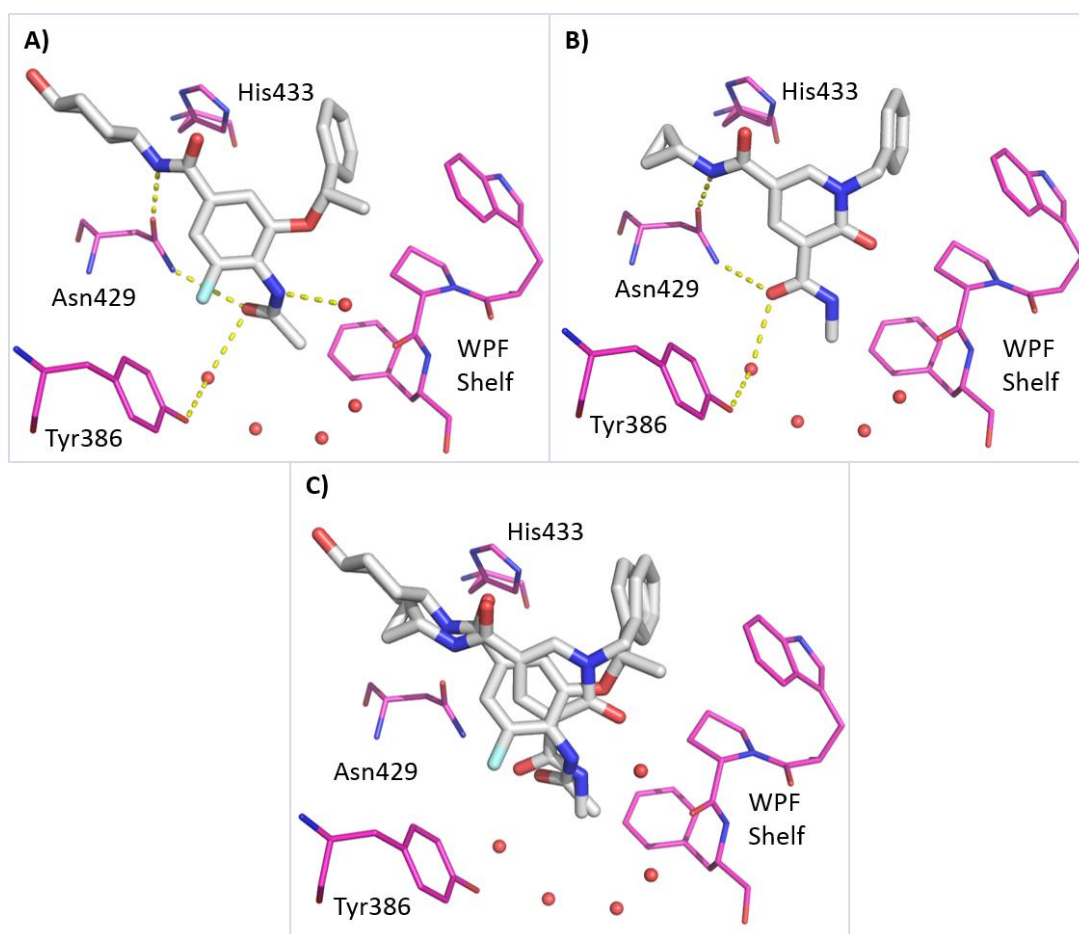


Figure 1.42. X-ray crystallography of **1.43** (A) and **1.45** (B) showing interactions with key residues (magenta) and waters (red spheres). H-bonds are dashed yellow lines. C) **1.43** and **1.45** both form a bidentate interaction with Asn429 and the phenyl rings of both sit between His433 and the WPF shelf.

1.6.3. Discovery of 2,3-Dihydrobenzofurans as BD2 Selective BET Inhibitors

GSK620 (**1.45**) showed that achieving >100-fold selectivity was possible in multiple chemotypes, unfortunately, **1.45** had poor CAD and FaSSIF solubility (see Section 1.1.2). In addition to this, it was noted that pyridone **1.45** readily crystallised. The low FaSSIF solubility was therefore, at least partially, driven by a high lattice enthalpy. Additionally, a higher selectivity of 1000-fold was considered preferential. Therefore, improving both the selectivity and solubility of the series was desirable. It was hypothesised that conformational

restriction of the phenyl group would provide an entropically more favourable interaction with BD2. Lowering the number of potential free energy states of this group in solution means that there would be a smaller entropic penalty on binding the protein, potentially leading to an improvement in potency and therefore selectivity.²⁰⁹ Benzylic methylene groups had been well tolerated in the pyridone series and so it was envisioned that cyclisation from the benzylic position to the pyridone carbonyl group, to form a 2,3-dihydrobenzofuran (DBF) core, would fit in the BD2 binding pocket and be able to mimic the key interactions of pyridone **1.45** for selectivity (Figure 1.43). This strategy proved effective and culminated in GSK973 (**(S,S)**-**1.46**), a DBF analogue which showed excellent potency against BRD4 BD2 $pIC_{50} = 7.8$, and greater than 1000-fold selectivity over BRD4 BD1. This BD2 selectivity profile was recapitulated against the other BET BD1 family members.

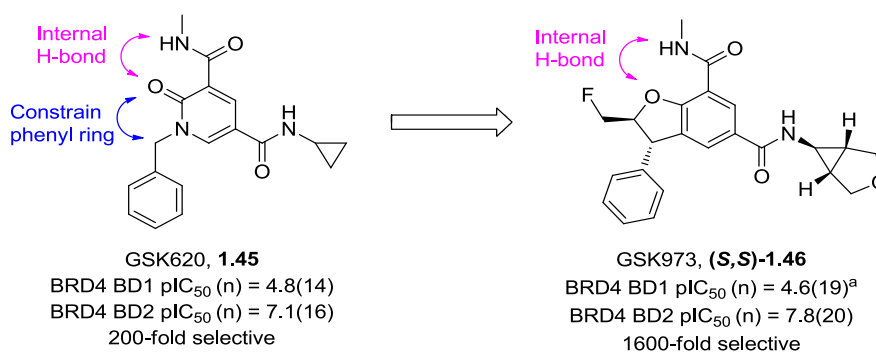


Figure 1.43. Constraining pyridone **1.45** affords DBF GSK973 (**(S,S)**-**1.46**) an exquisitely selective BD2 inhibitor. ^aalso <4.3 (n = 1).

To understand the drivers of domain selectivity in the DBF series, an X-ray crystal structure of DBF (**(S,S)**-**1.46**) was solved and overlaid with the structure of bound pyridone **1.45** (Figure 1.44). As expected, both templates contain the same basic pharmacophore with the key interactions being identical to GSK620 (**1.45**). The bicyclic lock of the DBF ring serves to place the phenyl ring between the WPF shelf region and the BD2 specific His433 as had been desired. The *trans* configuration of the C2/C3 substituents of the DBF ring places the CH_2F group into the ZA channel with excellent shape complementarity. A *cis* conformation would induce a clash with the protein, a fact reflected by the lower potency of this diastereomer.

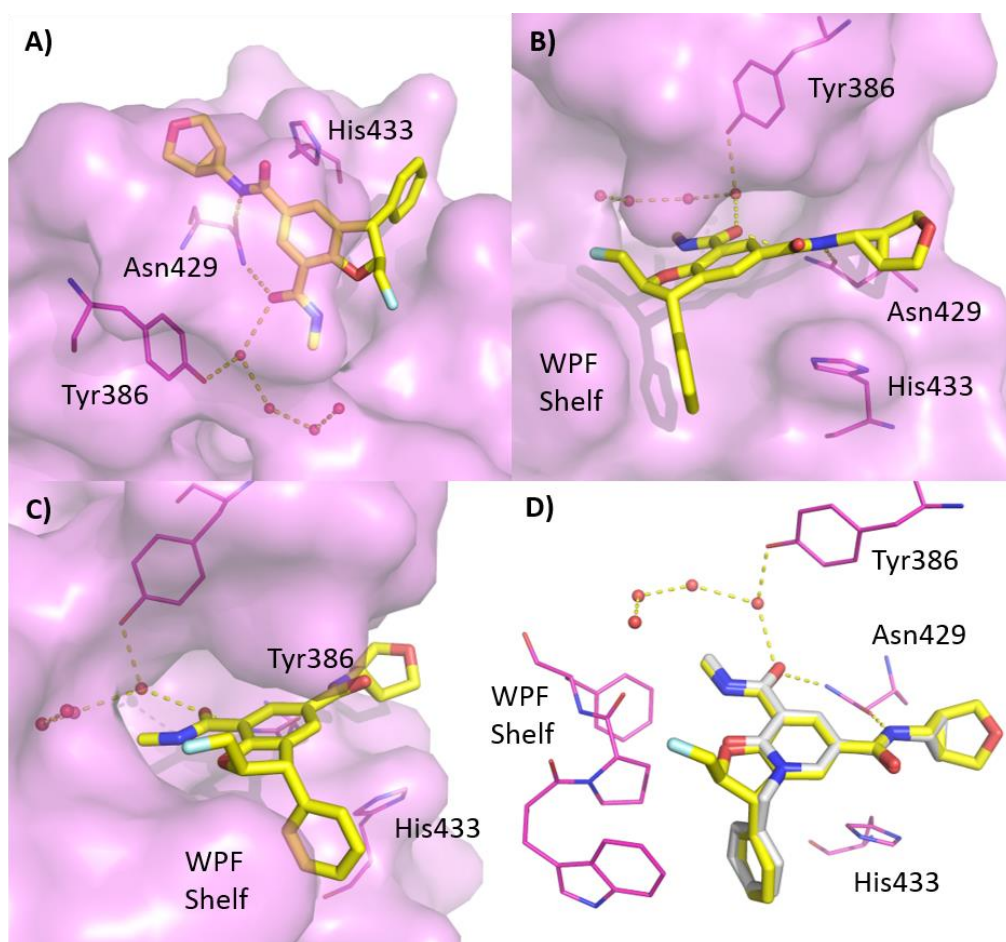


Figure 1.44. Crystal structure of GSK973 (**1.46**, yellow) overlaid with pyridone **1.45** (grey) in BRD2 BD2 (pale pink). The key residues are present (magenta) and the H-bonding interactions are shown by yellow dotted lines. Water molecules are visible as red spheres. A-C) DBF **1.46** makes a bidentate interaction with Asn429 and place a phenyl ring between the BD2 specific His433 and the WPF shelf. D) The two inhibitors are shown to have significant overlap.

Whilst DBF (**S,S**)-**1.46** displayed excellent potency and selectivity, the DBF series had an inherently more lipophilic core, meaning that even with a more polar amide group, the ChromLogD of (**S,S**)-**1.46** was higher than **1.45** (3.3 vs. 3.1, Table 1). SAR data showed that the DBF compounds such as (**S,S**)-**1.46** were required to occupy a narrow physico-chemical range (ChromLogD = 3.0 – 4.0) to maintain a good overall developability profile. Analogues of (**S,S**)-**1.46** which were of higher lipophilicity suffered from poor rodent PK, whilst lower lipophilicity negatively impacted permeability and bioavailability. GSK973 ((**S,S**)-**1.46**) did improve the poor solubility of pyridone **1.45** by CAD (≥ 152 vs. $87 \mu\text{g mL}^{-1}$) but this was not recapitulated in FaSSIF (25 vs. $47 \mu\text{g mL}^{-1}$) assays. Additionally, GSK973 ((**S,S**)-**1.46**) was

GSK Confidential – Do not copy

cleared more readily than pyridone **1.45** (1.8 vs. 1.0 mL min⁻¹g⁻¹) in a rat hepatocyte *in vitro* clearance (IVC) assay.

Table 1.01. Comparison of the properties of pyridone **1.45** and DBF GSK973 ((**S,S**)-**1.46**).

	1.45	(S,S)-1.46
BRD4 BD2 pIC ₅₀ (n) / BD1 pIC ₅₀ (n)	7.1(16) / 4.8(14)	7.8(20) / 4.6(19) ^a
Selectivity	200x	1600x
ChromLogD	3.1	3.6
CAD solubility (μg mL ⁻¹)	87	≥206
FaSSIF solubility (μg mL ⁻¹)	25	47
Rat hepatocyte IVC (mL min ⁻¹ g ⁻¹)	1.0	1.8

^aAlso <4.3 (n = 7).

One limitation to the SAR work for this series was the synthetic tractability of changing the pendent C3 phenyl substituent. There was the potential that introduction of further embedded polarity on this vector would allow access to the desired physico-chemical space. Additionally, the removal of the 2-CH₂F substituent from the DBF core had not been investigated. This potentially offered a method to reduce lipophilicity and molecular weight, whilst potentially reducing synthetic complexity and allowing a wider variety of shelf substituents to be prepared. To achieve this goal a new synthetic strategy was needed, and this is the subject of the first part of this thesis.

2. Synthetic Strategies Towards DBFs as BD2 Selective BET Inhibitors

2.1. Aims

The aim for this project was to develop synthetic methodology to allow for a full SAR analysis of the two key vectors of the DBF series, namely the shelf group and the amide vector on the DBF template (Figure 2.01). The methodology developed should allow for late stage functionalisation of the two key vectors with the aim of delivering a candidate quality molecule which fulfils the following criteria (see Section 1.1 for more details):

- Potent and BET family selective molecule (BRD4 BD2 $pIC_{50} > 7.0$) with 1000-fold selectivity over BRD4 BD1.
- Efficacy in *in vitro* immuno-inflammation disease models (hWB and PBMC $pIC_{50} > 6.0$).
- Suitable physico-chemical profile.
- High solubility (FaSSIF $>100 \mu\text{g mL}^{-1}$).
- Suitable human PK predicted properties to drive a high unbound blood concentration ($>IC_{90}$ for 4 H), with a low predicted human dose from oral administration.
- Able to dose to two animal species (rat and dog) at multiples above predicted efficacious concentration.

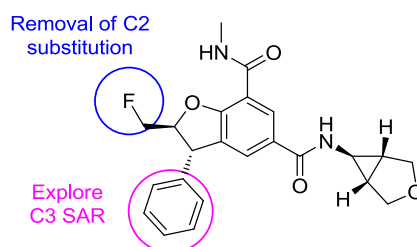


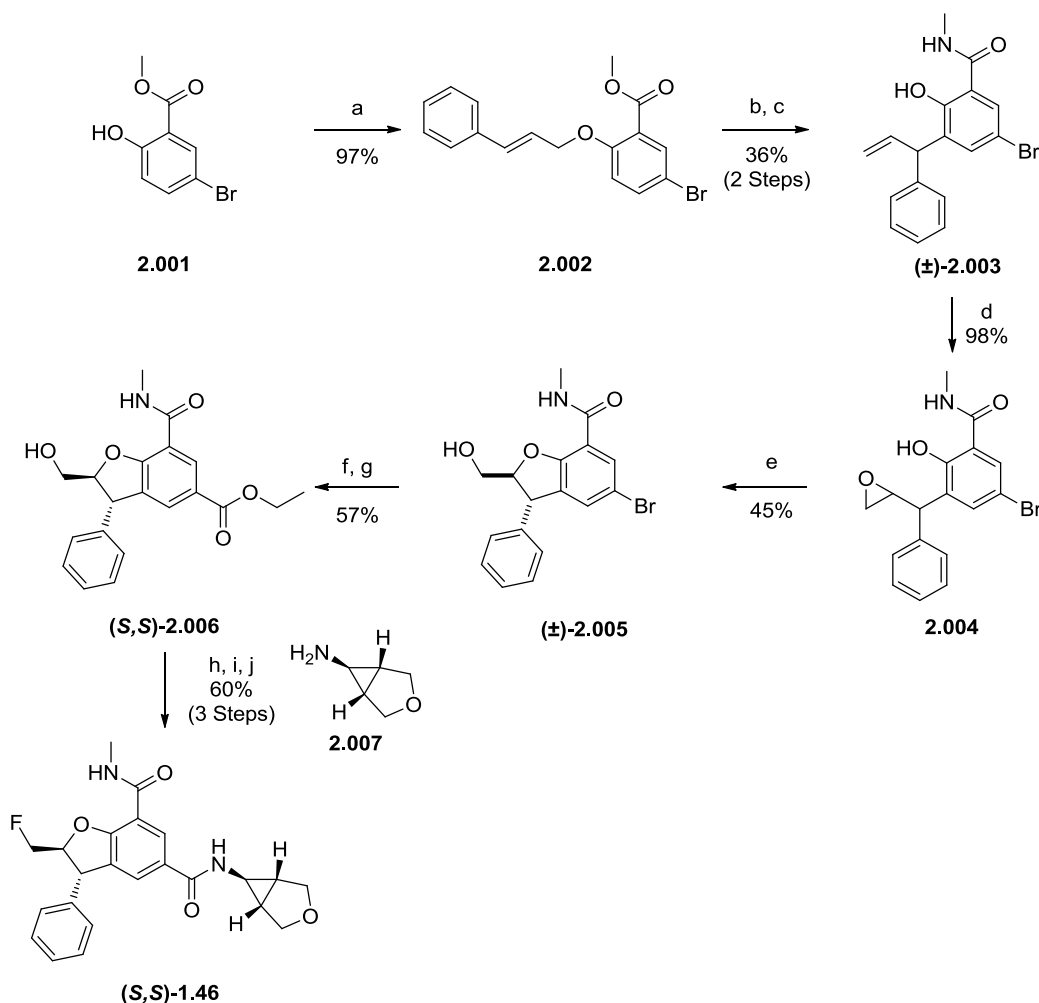
Figure 2.01. Strategic aims of investigating the DBF template.

2.2. Synthetic Approaches Targeting DBFs as BET Selective BET Inhibitors

2.2.1. Initial Synthesis of DBFs (*S,S*)-1.46 and (±)-2.011.

The starting point in the investigation of the DBF core without a C2 substituent was to examine the synthesis of DBF (*S,S*)-1.46.

Scheme 2.01. Synthesis of (*S,S*)-1.46

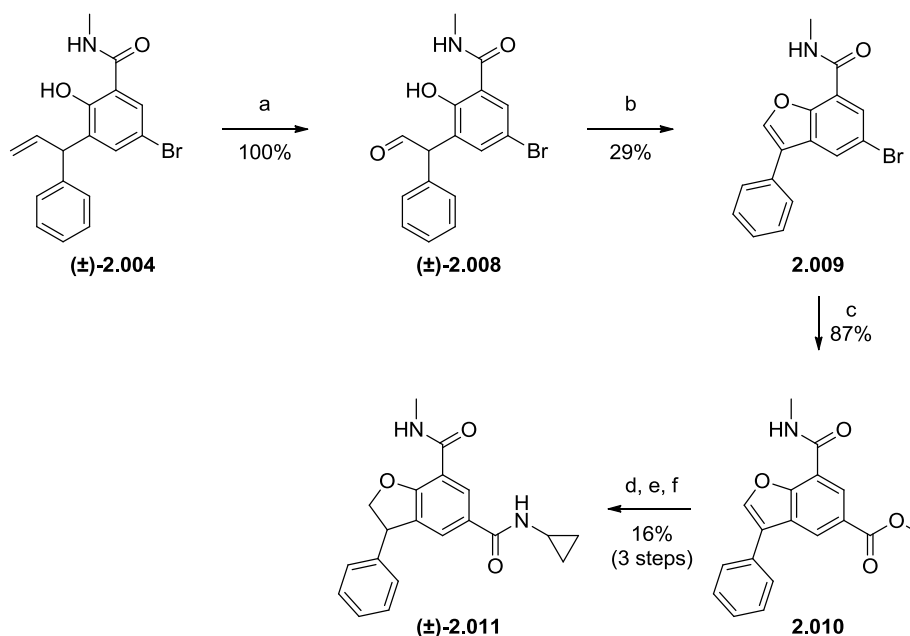


a) (*E*)-(3-Chloroprop-1-en-1-yl)benzene (1.2 eq.), K₂CO₃ (1.6 eq.), KI (1.0 eq.), acetone, reflux, 16 h, 97%; b) *N,N*-dimethylaniline, 200 °C, 4 h, 71%; c) methylamine (40% w/w in water), THF, rt, 16 h, 50%; d) *m*CPBA, CH₂Cl₂, 0 °C, 98%; e) KOH (2 eq.), DMSO:H₂O, 0 °C, 45%; f) Pd(OAc)₂ (10 mol%), Xantphos (10 mol%), CO, TEA (5 eq.) MeOH:DMF, 70 °C, 57%; g) Separation of the two enantiomers by chromatography using a chiral stationary phase; H), Deoxo-Fluor® (2.5 eq.), CH₂Cl₂, 0 °C to rt, 16 h, 80%; i) NaOH (3 eq.), EtOH:THF, H₂O, rt, 18 h, 92%; j) (1*R*,5*S*,6*R*)-3-oxabicyclo[3.1.0]hexan-6-amine (**2.007**, 1.2 eq.), HATU (1.3 eq.), TEA (1.3 eq.), CH₂Cl₂, rt, 16 h, 82%.

GSK Confidential – Do not copy

Starting from the commercially available methyl 5-bromo-2-hydroxybenzoate **2.001**, alkylation of the phenol with (*E*)-(3-chloroprop-1-en-1-yl)benzene gave **2.002** in a 97% yield (Scheme 2.01). When phenol ether **2.002** was heated at reflux, a key Claisen rearrangement occurred which installed the necessary terminal olefin in a yield of 71%. An amide formation with methylamine in water/THF inserted the methyl amide warhead (**±**)-**2.003** in a 50% yield. This direct amidation is likely facilitated by the phenol and is discussed in more detail in Section 2.2.5. The terminal olefin (**±**)-**2.003** could then be epoxidised using *m*CPBA in 98% yield. A 5-*exo*-tet cyclisation induced by deprotonation of the phenol by KOH, formed DBF (**±**)-**2.005**. Subsequent deprotonation of the dibenzylic centre led to formation of the more thermodynamically stable *trans* stereochemistry. A Pd catalysed carbonylation reaction installed an ethyl ester in 57% yield. At this point the two enantiomers were separated by chromatography using a chiral stationary phase. Deoxo-Fluor® could then convert the terminal alcohol to a fluorine atom in 80% yield. Quantitative hydrolysis of the ester using LiOH and a subsequent amide coupling gave DBF (**S,S**)-**1.46**.

The initial synthesis of DBF (**±**)-**2.011**, where the CH₂F group had been deleted, was carried out by other members of our laboratories (Scheme 2.01) and relied on terminal olefin intermediate (**±**)-**2.004** used in the synthesis of GSK973 (**(S,S)**-**1.46**).²¹⁰ Deletion of a methylene unit was undertaken by dihydroxylation using osmium tetroxide and diol cleavage with sodium periodate to give aldehyde (**±**)-**2.008** quantitatively (Scheme 2.02). This was cyclised using acid catalysis to give benzofuran **2.009**. This step gave the desired product in a low yield of 29% and proved a major obstacle to the scalability of this route. Nevertheless, a carbonylation was carried out in an 87% yield to insert the methyl ester giving **2.010**. This was then hydrolysed to afford the acid and subsequently coupled with H₂NcPr using HATU as the coupling agent in a 94% yield. The final step was a hydrogenation of the double bond using 10 mol% Pd/C in MeOH. The reaction was carried out in a flow H-cube apparatus, but the 16% yield for this step was disappointingly low, and suggested that an alternative approach to hydrogenation may be necessary to optimise this sequence.

Scheme 2.02. Initial synthesis of DBF (\pm)-**2.011** by colleagues at GSK.

a) OsO₄ (0.05 eq.), NaIO₄ (4 eq.), water, acetone, rt, 10 min, 100%; b) *p*TsOH (0.2 eq.), toluene, reflux, 24 h, 29%; c) CO, Pd(OAc)₂ (11 mol%), Xantphos (15 mol%), TEA (5 eq.), MeOH, DMF, 70 °C, 18 h, 87%; d) 2 M NaOH, MeOH, rt, 2 h, 100%; e) HATU (1.5 eq.), TEA (2 eq.), H₂NcPr (2 eq.), DMF, rt, 1 h, 94%; f) H₂, Pd/C (10 mol%), H-cube, MeOH, 17%.

Overall, this route was 9 steps with a poor overall yield of 0.7%. In addition, the C3 phenyl group which needs to be varied as part of the SAR strategy is installed in step 1. Therefore, a new route was required.

2.2.2. Reimagining the Retrosynthetic Approach to DBF **2.011**

To establish a shorter, more efficient route to the target DBF (\pm)-**2.011** the retrosynthetic approach was re-visited. A 5-step retrosynthesis was envisioned (Figure 2.02) which allowed for late-stage functionalisation of the amide vector. Despite the poor yield of the hydrogenation of **2.010** in Scheme 2.02, it was believed that optimisation of this reaction through screening of catalysts and conditions would provide higher yields, making benzofuran **2.010** an attractive intermediate. The methyl amide warhead could be installed through an amino carbonylation reaction from bromide **2.013**. NBS bromination, controlled by the *ortho* directing electron donating oxygen and the *meta* directing electron withdrawing ester, should form bromide **2.013** from benzofuran **2.014**. The key disconnection hinged upon epoxidation and cyclisation of alkene **2.016**. The alkene could be prepared from

commercially available iodide **2.017** and boronic acid **2.018**. Although this strategy also inserted the C3 substituent in the first step, it tested the key step of the retrosynthesis in the next step and was a much shorter overall route.

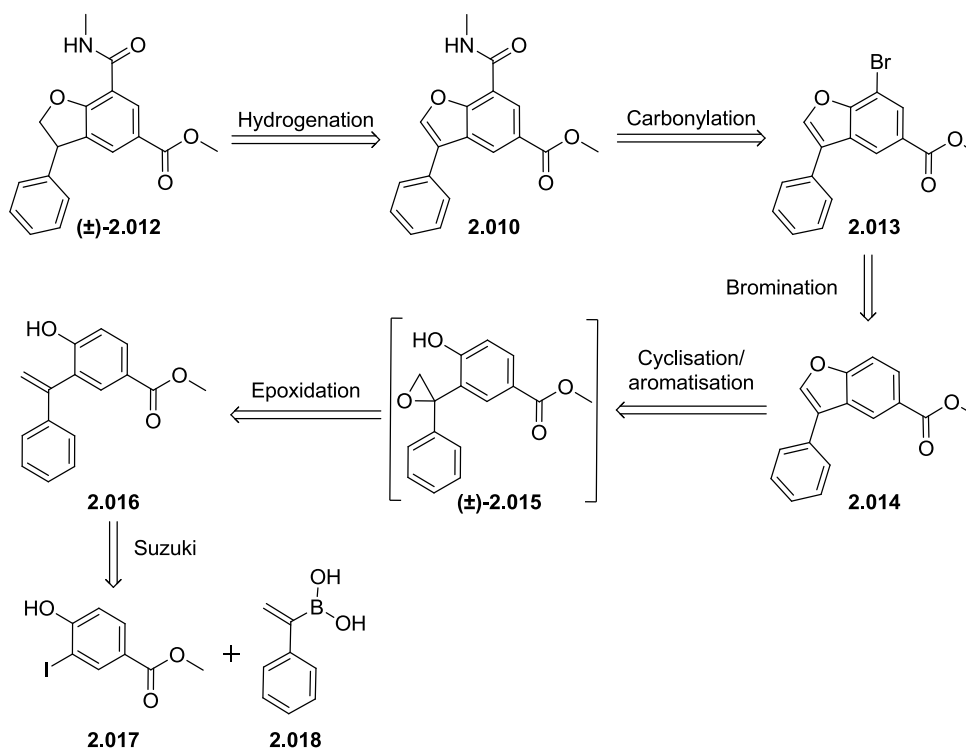
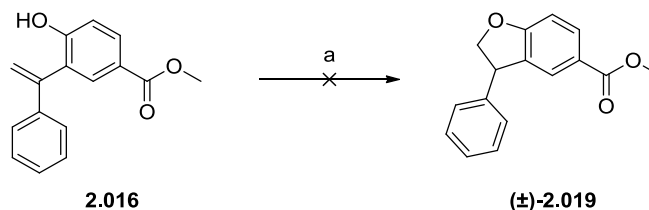


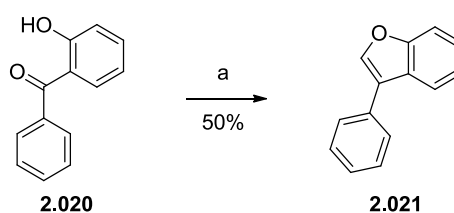
Figure 2.02. Retrosynthesis of DBF **2.012** which identified the key cleavage of the benzofuran ring to give a vinylic phenol precursor.

Phenols can add directly to alkenes in the presence of sulfuric acid.²¹¹ However, direct cyclisation onto the double bond would formally be a 5-*endo*-trig, which is disfavoured by Baldwin's rules.²¹² The epoxide mediated cyclisation is a favoured 5-*exo*-trig reaction which should allow access to benzofuran **2.014**.^{212, 213} For completeness, a 5-*endo*-trig cyclisation mediated by TfOH was attempted to prove this was correct and indeed only SM was observed after refluxing for 24 h (Scheme 2.03).

Scheme 2.03. Attempted 5-*endo-trig* cyclisation to form DBF (\pm)-**2.019** using TfOH.

a) TfOH, toluene, reflux, 24 h, no reaction observed.

Chittimalla *et al.* have published a synthesis of benzofurans which relies on a Corey-Chaykovsky epoxidation.²¹⁴ Once the sulfur ylide had added into ketone **2.020** and subsequently formed the epoxide, *in situ* cyclisation and dehydration gave benzofuran **2.021** in a 50% yield (Scheme 2.04). This was good precedent therefore, that if phenolic epoxide (\pm)-**2.015** could be formed in the reaction, cyclisation and dehydration would follow to afford the desired benzofuran (Figure 2.02).^{215, 216}

Scheme 2.04. Literature precedent for the Corey-Chaykovsky epoxidation/cyclisation method to synthesise benzofuran **2.021**.

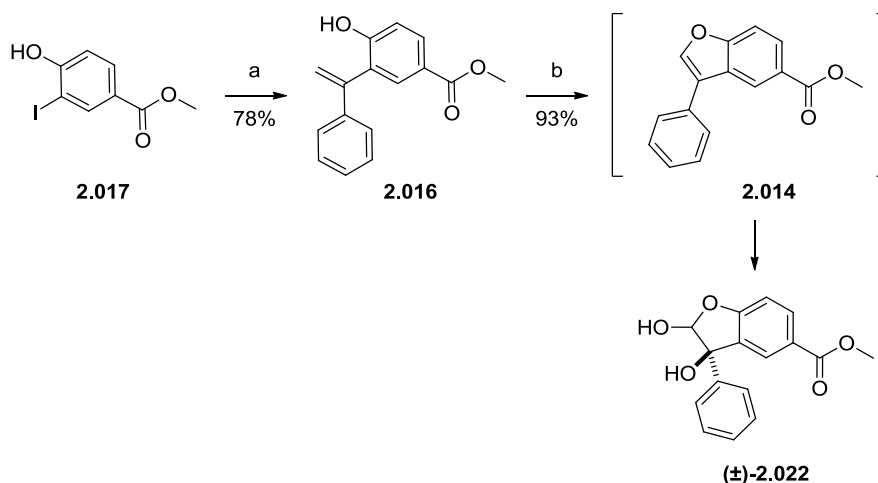
a) $(\text{CH}_3)_3\text{SOI}$, *n*BuLi, THF, 60 °C, 4 h, 50%.

2.2.3. Initial Studies towards a Synthetic Route to DBF (\pm)-**2.011**

To test the key benzofuran cyclisation proposal, simplified vinyl phenol **2.016** was prepared using a Suzuki coupling reaction (Scheme 2.05). The commercially available iodide **2.017** was reacted with (1-phenylvinyl)boronic acid **2.018**, using $\text{PdCl}_2(\text{dppf})$ as a catalyst, to afford the desired product **2.016** in 78% yield. This was then reacted with *m*CPBA in CH_2Cl_2 at rt overnight in an attempt to form the benzofuran **2.014**. However, only diol (\pm)-**2.022** was isolated from the reaction mixture as, what appeared by ^1H and ^{13}C NMR to be, a single compound of undefined stereochemistry. This diol is thought to arise due to the desired benzofuran **2.014** reacting with *m*CPBA to afford another epoxide which is then opened by water. Initially, the reaction was carried out with 2 eq. of *m*CPBA, but this was reduced to 1 eq. in an attempt to stop the by-product formation. Unfortunately, upon analysis of the crude

reaction mixture by LCMS, only SM and diol (\pm)-**2.022** were observed, suggesting that epoxidation of benzofuran **2.014** is faster than vinyl phenol **2.016**. This is perhaps unsurprising as the oxygen of the benzofuran may increase the nucleophilicity of the double bond enabling it to react more readily with the electrophilic *m*CPBA.

Scheme 2.05. Attempted synthesis of benzofuran **2.014** by epoxidation and subsequent ring opening.

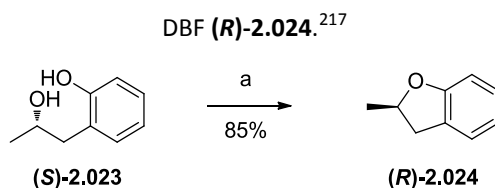


a) (1-Phenylvinyl) boronic acid (**2.018**, 1.0 eq.), PdCl₂(dppf) (10 mol%), K₂CO₃ (3.0 eq.), 1,4-dioxane:water, 90 °C, 4 h, 78%; b) *m*CPBA (2.0 eq.), CH₂Cl₂, rt, 16 h, 93%.

Attempts were then made to find another method of activating the terminal olefin. Bromine was used as it was thought that formation of a bromonium ion would facilitate the ring closure. This ultimately proved unsuccessful as none of the desired benzofuran product **2.014** was observed. This led to the search for an alternative strategy.

It is well known in the literature that, given the appropriate precursors, DBFs can be synthesised using Mitsunobu conditions. Gotor-Fernandez *et al.* used this methodology to synthesise benzofuran (*R*)-**2.024** in 85% yield using a precursor (*S*)-**2.023** made by enzymatic methods (Scheme 2.06).²¹⁷ The drawback of this approach was the ability to synthesise the required β -hydroxyphenol (*S*)-**2.023**. Given the structure of phenol **2.016**, it was thought that hydroboration of the olefin would afford primary alcohol (\pm)-**2.25** in readiness for the Mitsunobu reaction. Importantly, this would form the DBF core directly and avoid the requirement for a subsequent hydrogenation of the benzofuran, which had previously been low yielding.

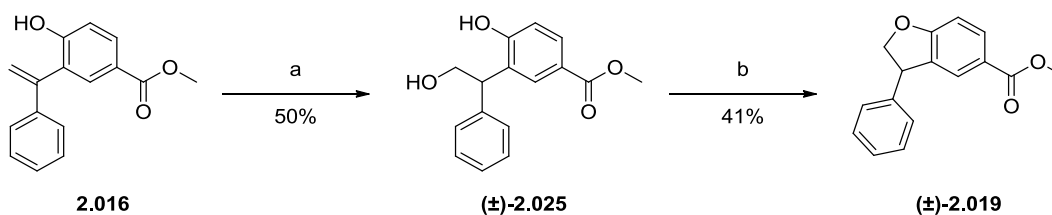
Scheme 2.06. Literature precedent for the Mitsunobu approach to cyclise diol **(S)**-2.023 into



a) PPh₃, DIAD, THF, rt, 3 h, 85%.

The hydroboration of styrene was pioneered by H. C. Brown in the 1960s and 1970s, however, there are no examples in the literature where a hydroboration has been attempted on a vinyl group *ortho* to a phenol.²¹⁸ Initial studies were therefore conducted using borane (1 M in THF). Two equivalents of borane are necessary as the first equivalent should react with the phenol before the second equivalent carries out the hydroboration reaction (Scheme 2.07). The reaction gave a separable mixture of two regioisomers in a 3:2 ratio, of which the desired isomer **(±)**-2.025 was isolated in a 50% yield by mass directed auto preparation (MDAP). The other regioisomer was a 34% impurity by LCMS analysis of the reaction and was isolated in 21% yield. Before this reaction was optimised, the Mitsunobu reaction was carried out to check that this route was appropriate for this substrate. A Mitsunobu reaction using the classic reagents of triphenyl phosphine and DIAD was undertaken and afforded the desired benzofuran **(±)**-2.019 in an isolated yield of 41% (Scheme 2.07).

Scheme 2.07. Alternative strategy using hydroboration and a subsequent Mitsunobu reaction.



a) Borane (1 M in THF, 2.0 eq.), 0 °C, 4 h, *then* NaOH (2 M, 3 eq.), H₂O₂ (33% w/w in water, 1.0 eq.) rt, 1.5 h, 50%; b) PPh₃ (1.2 eq.), DIAD (1.2 eq.), THF, rt, 16 h, 41%.

2.2.4. Optimisation of the Hydroboration

As this route had now been used to synthesise the required DBF framework, attention was turned to optimisation of the hydroboration reaction. As previously discussed, the first attempt using borane (1 M in THF) gave a mixture of alcohols **(±)**-2.025 and **(±)**-2.026 (Scheme 2.07). Given the mechanism of hydroboration it was thought that the required *anti*-

Markovnikov product (\pm)-**2.025** would be favoured by both the electronics and sterics of the reaction. The *anti*-Markovnikov (\pm)-**2.025** product would arise from a transition state with the δ^+ charge on the benzylic position and the boron at the least hindered end of the double bond (Figure 2.03). This is seen in the hydroboration of styrene where the required *anti*-Markovnikov product is formed favourably in an 80:20 mixture over the other regioisomer.²¹⁸ The selectivity for phenol (\pm)-**2.016** was lower with a 60:34 mixture observed. This reaction clearly needed further investigation.

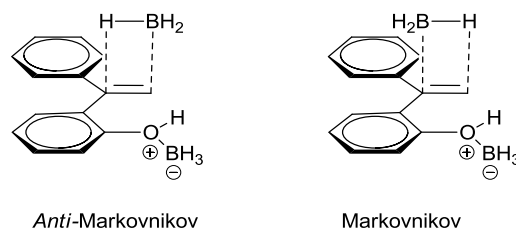


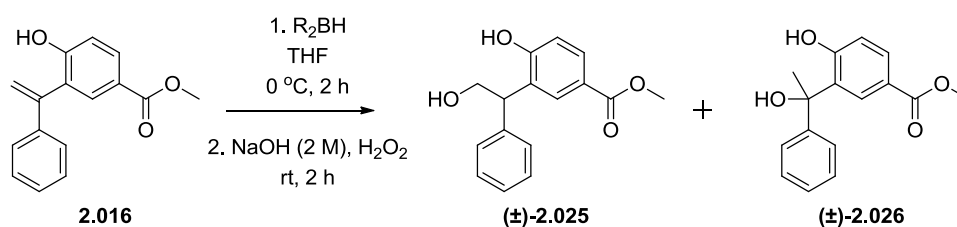
Figure 2.03. Two transition states for the hydroboration of a vinylic phenol: The theoretically favoured *anti*-Markovnikov (left) and the theoretically disfavoured Markovnikov (right).

Firstly, alcohol (\pm)-**2.025** was exposed once more to the hydroboration work up conditions (NaOH/H₂O₂) to determine whether the product was stable to the reaction conditions and to ensure that the ratio observed was not due to a rearrangement of the product. This proved to be the case as no formation of regioisomer (\pm)-**2.026** was observed. An alternative work-up procedure was then investigated. NaOH and H₂O₂ were replaced with sodium perborate tetrahydrate, however, little of the desired product (\pm)-**2.025** was formed.²¹⁹ There was no evidence to suggest a rearrangement of the product was occurring, so it was probable that regioselectivity was governed by the initial hydroboration. A selection of hydroborating agents were therefore employed to understand and influence the outcome of the reaction (Table 2.01).

Initially, it was thought that increasing the bulk of the boron species would favour formation of the desired regioisomer. 9-BBN is a well-known bulky boron reagent.²²⁰ However, when the hydroboration was attempted using 9-BBN no reaction was observed (Table 2.01, Entry 2). The reason for this is likely to be because the first equivalent will react with the phenol, which may then make the double bond too sterically hindered to undergo the hydroboration. It was thought that an intermediate sized boron species may help overcome

this problem. Thexylborane was synthesised from borane and 2,3-dimethylbut-2-ene by a known literature procedure, and was used directly as a 0.66 M solution in THF.^{221, 222} Upon exposing phenol **2.016** to thexylborane, a much more selective reaction was observed (Entry 3), favouring the formation of (\pm)-**2.025** in an 83:17 ratio. (+)-(Ipc)₂BH is a well-known chiral hydroboration reagent first pioneered by H. C. Brown.²²³ In order to try and synthesise DBF (\pm)-**2.025** as a single enantiomer, (+)-(ipc)₂BH was synthesised from (+)-pinene and borane. No reaction was observed when this reagent was exposed to phenol **2.016** (Entry 4) and this was again thought to be due to steric hindrance. An alternative approach could be to synthesise (+)-(ipc)BH₂ as this less bulky borane may be more effective. However, given the thexylborane result this was not attempted.

Table 2.01. Optimisation of Hydroboration of vinyl phenol **2.025**.



	Borane (R ₂ BH)	(\pm)- 2.025 (%) ^a	(\pm)- 2.027 (%) ^a	2.016 (%) ^a
1	BH ₃ (1 M in THF)	60	34	6
2	9-BBN (1 M in THF)	0	0	100
3	Thexylborane (0.66 M in THF)	83	17	0
4	(+)-(Ipc) ₂ BH	0	0	100

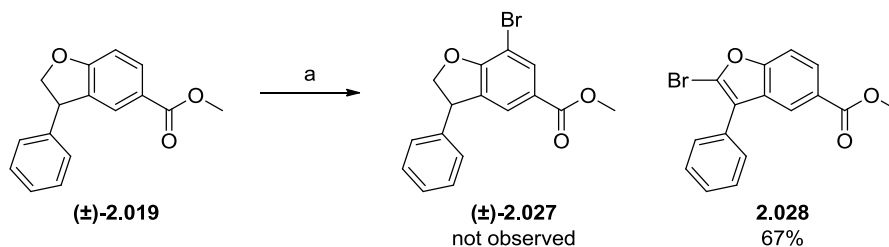
^aRatio calculated from LCMS analysis of the crude reaction mixture.

2.2.5. Insertion of the Methyl Amide Warhead

Now that a scalable route to DBF (\pm)-**2.019** had been established, the methyl amide warhead needed to be installed (Scheme 2.08). Bromination of the benzofuran, using an electrophilic source of bromine such as NBS, should be directed *ortho* to the oxygen and *meta* to the carbonyl group to afford the bromide (\pm)-**2.027**. Unfortunately, when DBF (\pm)-**2.019** was reacted with NBS in CH₂Cl₂ at rt only the 2-bromobenzofuran **2.028** (64%) was isolated from the reaction. Rather than bromination, an oxidation bromination sequence occurred which

placed a bromine at the 2-position of the furan ring. This transformation has been reported in the literature although these reactions normally require a radical initiator (typically AIBN),²²⁴ therefore, this outcome was surprising.

Scheme 2.08. Attempted NBS bromination of DBF (\pm)-**2.019**.



a) NBS (1.2 eq.), CH₂Cl₂, rt, 16 h.

As late stage functionalisation to insert the warhead was proving problematic, an alternative route was devised which relied on carrying out the hydroboration/Mitsunobu reactions with the methyl amide already in place. An updated retrosynthesis was proposed which built up the more functionalised vinylic phenol **2.029** over 4 steps (Figure 2.04). A Suzuki reaction similar to that in Scheme 2.05 should yield the desired advanced intermediate **2.029** primed for the hydroboration/Mitsunobu sequence from the highly functionalised aromatic bromide **2.030**.

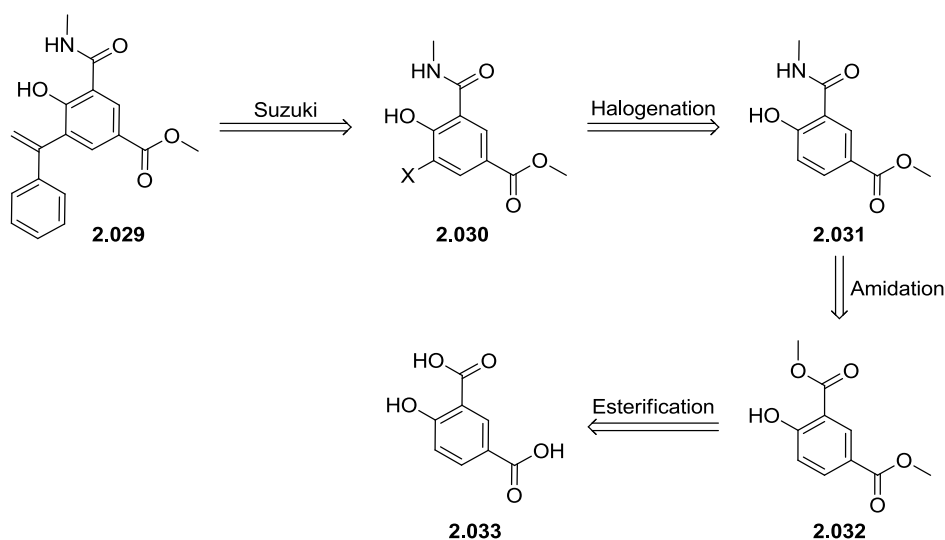
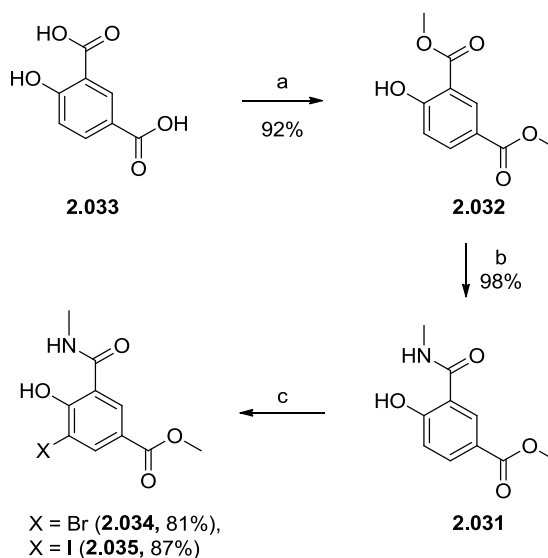


Figure 2.04. Retrosynthesis of phenol **2.029** which incorporates the methyl amide warhead at an earlier stage.

This in turn could be formed from phenol **2.031** where halogenation using NXS (X = Br, I) should be directed *ortho* to the phenol and *meta* to both the electron-withdrawing carbonyl groups. There was some evidence in the literature and earlier work on the DBF series that amide **2.032** could be prepared from methyl ester **2.032**, simply using methylamine 40% w/w in water.^{225, 226} The diester **2.032** could in turn be accessed by methylation of the readily available hydroxyisophthalic acid **2.033**.

The forward synthesis was carried out using the conditions in Scheme 2.09. Dimethyl 4-hydroxyisophthalate **2.032** was prepared from commercially available 4-hydroxyisophthalic acid (**2.033**), using thionyl chloride in MeOH.²²⁷ Upon addition of thionyl chloride to 4-hydroxyisophthalic acid **2.033** in MeOH, dimethyl sulfite is formed, a process which forms HCl and upon heating facilitates esterification to form **2.032**. Once the reaction is cooled to rt, the product precipitated out of solution in a 92% yield (Scheme 2.09). Methylamine (40% w/w in water) was then added to **2.032** in THF and a precipitate formed. The suspension was stirred until full dissolution, at which point the reaction was complete. Only a single product was observed and the target **2.031** was isolated in a 98% yield. Halogenation was then achieved using either NBS (**2.034**, 81%) or NIS (**2.035**, 87%). Overall, **2.035** was prepared from **2.033** in 3 steps and 78% overall yield.

Scheme 2.09. Synthesis of highly functionalised phenols **2.031** and **2.035**.



a) SOCl₂ (7.5 eq.), MeOH, reflux, 6 h, 92%; b) NH₂Me (40% w/w in water, 5 eq.), THF, rt, 16 h, 98%; c) NXS (1.2 eq.), CH₂Cl₂, rt, 2-16 h.

In order to rationalise the outcome of the regioselective amidation, the ^{13}C NMR was examined as a means of understanding the electronic properties of each ester. Theoretically, the carbonyl carbon of the more electrophilic ester should have a higher chemical shift as it is more deshielded. In this instance, the inferred H-bonding interaction between the phenol and the *ortho* ester group should remove electron density from the carbonyl group increasing the dipole, therefore, deshielding the carbonyl carbon and increasing the chemical shift. When the ^{13}C NMR of phenol **2.032** was fully assigned the *ortho* ester group did indeed have a higher chemical shift with a difference of 2.7 ppm when compared to the *para* ester group (Figure 2.05).

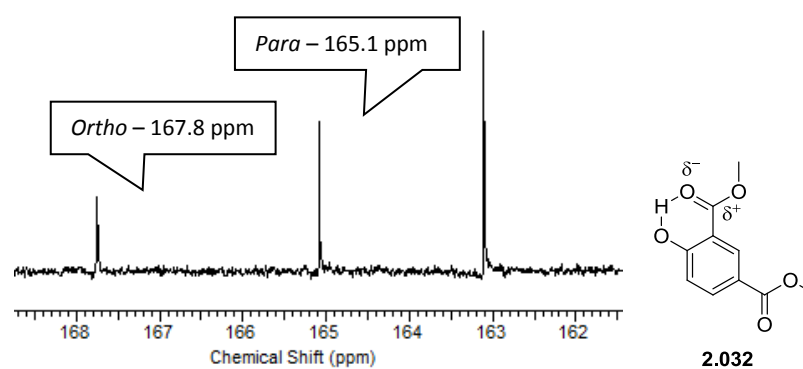


Figure 2.05. Comparison of ^{13}C NMR shifts of the two esters in phenol 2.44.

2.2.6. Optimisation of the Suzuki Coupling to form *ortho* Vinyl Phenols

Bromide **2.034** was then exposed to standard Suzuki conditions used previously to synthesise vinyl phenol **2.016** (Scheme 2.05). Unfortunately, this reaction had a low conversion of 17% by LCMS and an isolated yield of only 10% after purification by column chromatography (Scheme 2.10). The major side product observed in the reaction mixture was *trans*-alkene **2.036**. There are several possibilities which might explain the formation of this side-product. One option was that protodeborylation of boronic ester **2.018** was occurring and instead a Heck reaction, which would lead to the *trans*-alkene **2.036** with styrene is taking place. The presence of an additional EWG *ortho* to the phenol could cause this in two ways: by altering the electronics of the halide-carbon bond group (although this might be expected to enhance the rate of oxidative addition and transmetalation), or by providing a chelating group which could poison the catalyst. It is believed that the methyl amide chelating group slows down the reaction, which gives time for protodeborylation to occur before oxidative addition takes

To investigate if the halide could be altered to improve reactivity, the corresponding iodide **2.035** was used (Entries 2 vs. 1). This improved reactivity in the Suzuki reaction (54%), but a major side-product **2.036** (17%) was still observed. Pd(amphos)Cl₂ had been used to catalyse analogous reactions in the literature, albeit without the *ortho* methyl amide.²²⁹ The dimethylamine groups on the phosphine ligands, increase electron density at the Pd, aiding oxidative addition (Figure 2.05).²³⁰ However, these conditions only gave a conversion of 19% (Entry 3) with bromide **2.034** which constituted no significant improvement over Pd(dppf)Cl₂.

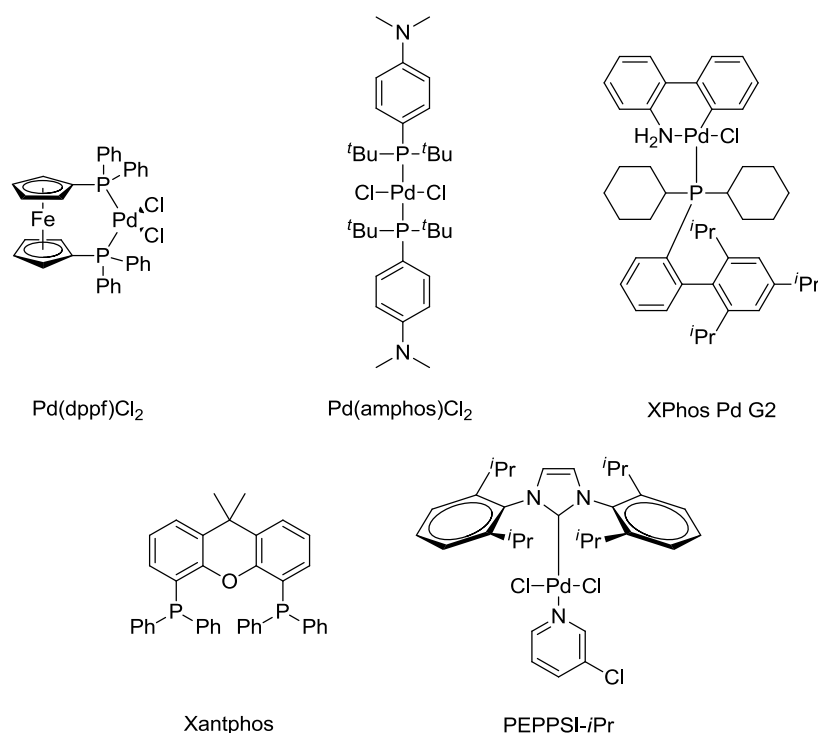


Figure 2.06. Structures of the different ligands, catalysts and pre-catalysts used in the exploration of Suzuki reaction summarised in Table 2.02.

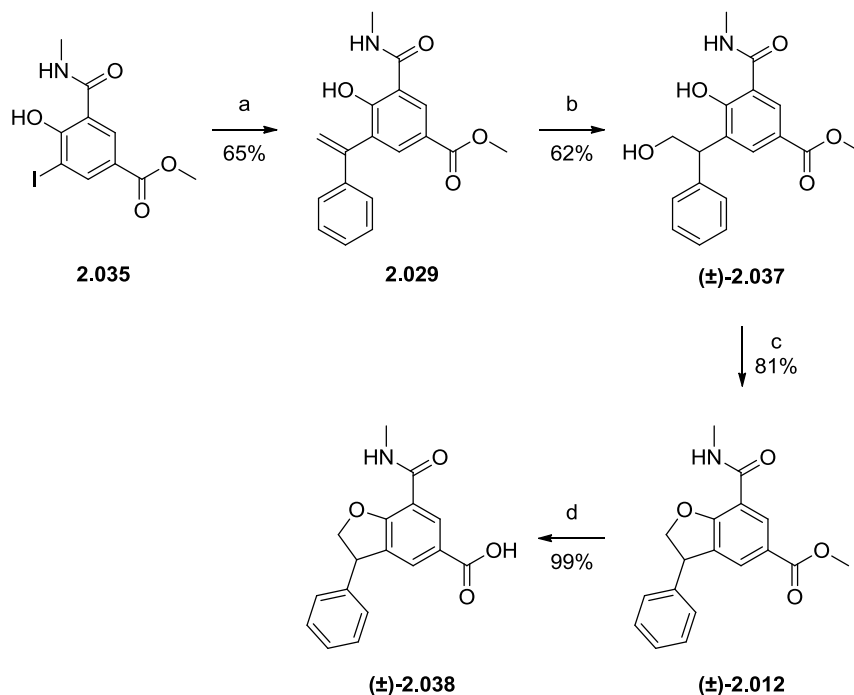
Xantphos also showed no further improvement on the original conditions (48%, entry 4). As the reaction appeared to work better with iodide **2.035** and gave less side-product, it was thought that the oxidative addition step may be crucial. Buchwald *et al.* have reported pre-catalysts which form the catalytically active species *in situ* under conditions where boronic acid decomposition is slow.²³¹ The monodentate phosphine ligand XPhos is highly reactive in both C-C and C-N bond forming reactions.²³² However, in this case XPhos Pd G2 offered only minor improvements (Entry 5) with bromide **2.034** (30% conversion) and showed poorer conversion with iodide **2.035** as a coupling partner (43% conversion) relative to Entries 1 and

2.²³³ When the reaction was run in toluene (Entry 5) none of the desired product **2.029** was observed suggesting this solvent was not tolerated. Another pre-catalyst which is known to work well for aryl chlorides where oxidative addition is often rate-limiting is PEPPSI-*i*Pr, an *N*-heterocyclic carbene (NHC) based catalyst (Figure 2.06).²³⁴ The NHC ligand makes PEPPSI-*i*Pr more electron rich which aids the oxidative addition step. The bulk of the NHC ligand also ensures that reductive elimination occurs quickly. Remarkably, when PEPPSI-*i*Pr was used as a catalyst with a potassium phosphate base in 1,4-dioxane/water a conversion of 88% was observed (Entry 8). To complete the study, the PEPPSI-*i*Pr conditions were repeated with bromide **2.034** (Entry 9), where the conversion was only 45% supporting the argument that oxidative addition is the rate limiting stage of the catalytic cycle.

2.2.7. Scale up of **2.029** and Exploration of the Amide Vector

Having established optimal conditions for the Suzuki coupling, the reaction was then scaled up to 2.0 g and an isolated yield of 65% was achieved for **2.029** (Scheme 2.11).

Scheme 2.11. Synthesis of acid (\pm)-**2.038** by hydroboration/Mitsunobu reactions, to allow for exploration of the amide vector.

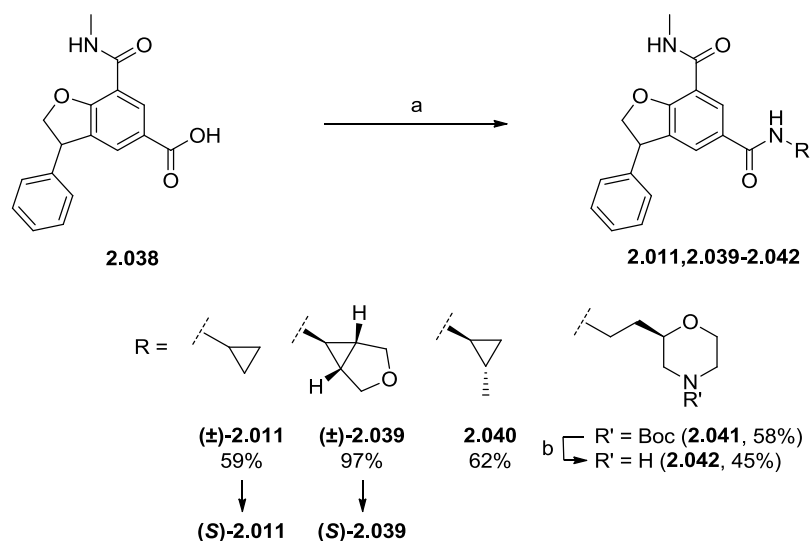


a) (1-Phenylvinyl)boronic acid (1.2 eq.), K_3PO_4 (3.0 eq.), PEPPSI-*i*Pr (10 mol%), 1,4-dioxane:water, 70 °C, 2 h, 65%;
 b) (i) thexylborane (0.66 M in THF, 2.0 eq.), THF, 0 °C, 16 h; (ii) NaOH, H_2O_2 , rt, 2 h, 62%; c) PPh_3 (1.2 eq.), DIAD (1.2 eq.), THF, rt, 16 h, 81%; d) LiOH (2 eq.), THF:water, 50 °C, 2 h, 99%.

In tandem with the other route improvements the advanced intermediate **2.029** was prepared on 1.2 g scale in 53% overall yield. Vinyl phenol **2.029** was then hydroborated with thexylborane to afford, after oxidative work-up, primary alcohol (\pm)-**2.037** in 62% yield as a single regioisomer. Following this, a Mitsunobu reaction using triphenylphosphine and DIAD gave the functionalised DBF (\pm)-**2.012** in an 87% yield. Now that a suitable route to form the DBF core had been established the methyl ester was hydrolysed quantitatively using lithium hydroxide to form carboxylic acid (\pm)-**2.038** which was used to make a range of amides (Scheme 2.11).

A range of different amides (\pm)-**2.011**, (\pm)-**2.039–2.042**) were synthesised using HATU as the coupling reagent (Scheme 2.12). The amide couplings proceeded in yields of 58–97%. In the case of DBF **2.042**, the Boc protected morpholine derivative (**2.041**) was coupled in a 58% yield and subsequently deprotected using TFA in a 45% yield to afford amide **2.042** as a mixture of diastereomers. Compound **2.040** was prepared as a mixture of diastereomers after being synthesised from (1*S*,2*S*)-2-methylcyclopropanamine. The single enantiomer, (*S,S,S*)-**2.040** was prepared by colleagues at GSK.

Scheme 2.12. Synthesis of final compounds: variation of the amide vector.



The single enantiomers of (\pm)-**2.011** and (\pm)-**2.039** were obtained by separation through chromatography using a chiral stationary phase. The absolute configuration of the most active enantiomer was assigned as (*S*) based on previous crystallographic evidence of GSK973

((S,S)-1.46, see Figure 1.44, Section 1.6.3). Overall DBF **(±)-2.011** was synthesised over 8 steps in 17% yield, a marked improvement on the original route (Scheme 2.02). The SAR of these analogues along with further examples synthesised by other members of the team will be discussed in Section 2.3.

2.2.8. Late Stage Functionalisation of the C3 Position

Whilst the synthetic route discussed above had delivered the desired amide alterations, one major disadvantage to this approach was that differentiation of the C3 phenyl group must happen at an early stage and the vinylic boronic acids required were not all commercially available. A novel approach which would allow for functionalisation of the shelf group was desirable, therefore, a new retrosynthesis was envisioned (Figure 2.07).

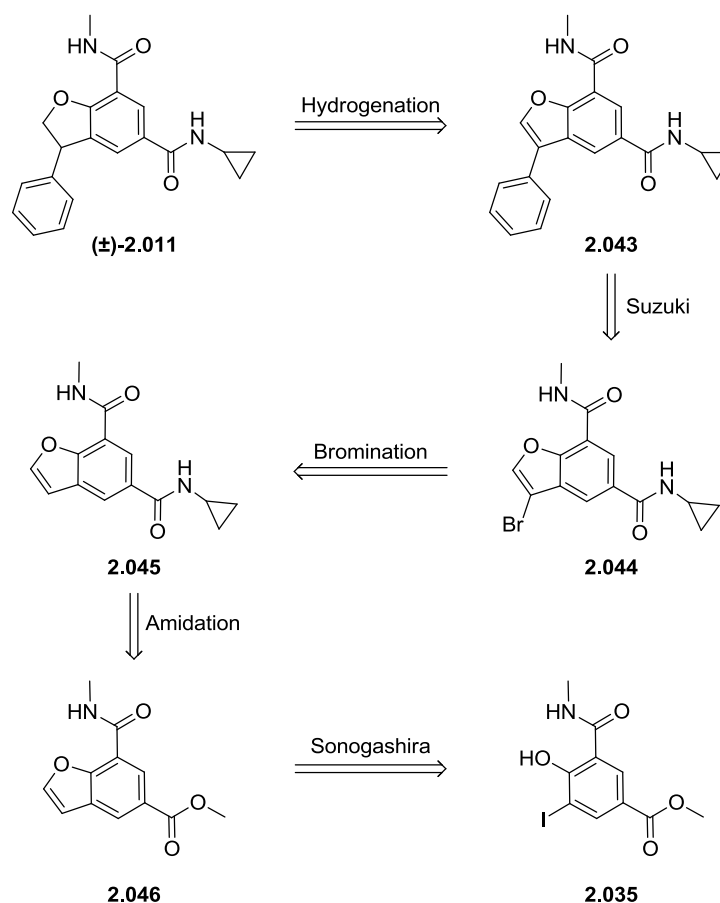


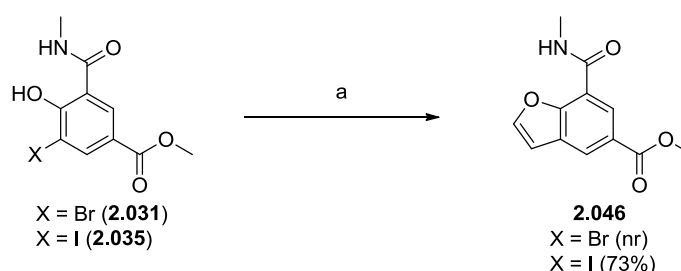
Figure 2.07. Retrosynthetic plan which hinges upon a late stage insertion of the C3 aryl group.

The last step of this route would be a hydrogenation of a benzofuran to DBF **(±)-2.011**. It was anticipated that optimisation of reaction conditions would afford improvements to the

original 10% yield (see Scheme 2.02). The C3 substituent could then be functionalised by late-stage cross-coupling to the respective boronic esters, from bromide **2.044**. Regioselective bromination of benzofuran **2.045** should furnish the necessary synthetic handle for these couplings. The benzofuran **2.046**, in turn, could be synthesised by a Sonogashira reaction from key intermediate **2.035**, the synthesis of which was optimised previously (Scheme 2.09). It is well known in the literature that if a Sonogashira reaction is carried out on a halogen *ortho* to a phenol, *in situ* cyclisation will occur to give the benzofuran leading to the direct synthesis of **2.046**.²³⁵

To investigate the key disconnection in the new synthetic strategy, the Sonogashira reaction was attempted (Scheme 2.13) using TMS acetylene and previously prepared phenols **2.031** and **2.035**. Once again, the iodide proved a more appropriate substrate, likely for similar reasons of higher turnover of the oxidative addition stage. Initially, when using bromide **2.031**, no reaction was observed, however, on switching to iodide **2.035** the desired benzofuran **2.046** was isolated in a yield of 73% after *in situ* TMS deprotection using TBAF.

Scheme 2.13. Using the Sonogashira reaction to build up the benzofuran ring.



a) (i) TMS acetylene (2.2 eq.), PdCl₂(PPh₃)₂ (5 mol%), CuI (10 mol%), TEA (3.0 eq.), DMF, 80 °C, 16 h; (ii) TBAF (2 M in THF), rt, 2 h, 73%.

In order to brominate at the 3-position, benzofuran **2.046** was reacted with bromine in CH₂Cl₂ to afford dibromide (\pm)-**2.047**. After removal of the excess bromine and solvent *in vacuo*, KOH in EtOH was added to facilitate the selective elimination of the bromide from the 2 position to afford 3-bromobenzofuran **2.048** in a yield of 94% (Scheme 2.14).²³⁶ The selectivity arises through formation of an oxonium ion intermediate followed by loss of a proton (Figure 2.08).

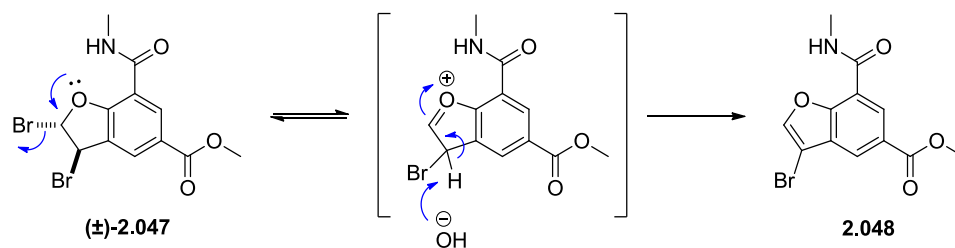
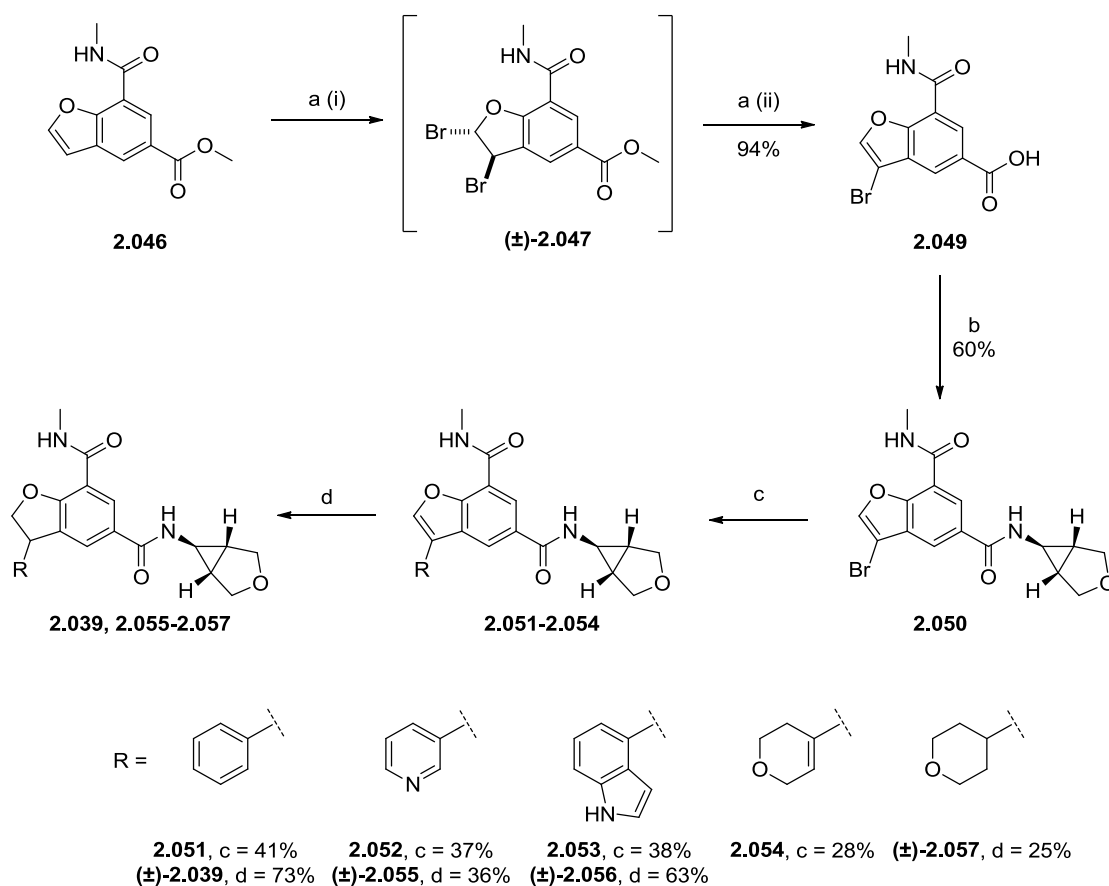


Figure 2.08. Proposed mechanism which explains the regioselectivity for the debromination of DBF **2.048**.

Addition of the base also hydrolysed the ester to afford the (desired) corresponding carboxylic acid **2.049**. A HATU mediated amide coupling, using DIPEA as a base, gave amide **2.050** in a 60% yield (Scheme 2.14).

Scheme 2.14. Functionalisation of the DBF scaffold to insert a range of different C3 substituents.



a) i) Br₂ (1.5 eq.), CH₂Cl₂, rt, 2 h; ii) KOH (2.0 eq.), EtOH, 40 °C, 24 h, 94%; b) HATU (1.2 eq.), DIPEA (3 eq.), (1*R*,5*S*,6*R*)-3-oxabicyclo[3.1.0]hexan-6-amine **2.007** (1.4 eq.), DMF, rt, 16 h, 60%; c) boronic acid (1.2 eq.), Pd Cat (10 mol%), K₃PO₄ (3.0 eq.), 1,4-dioxane:water, 40 °C, 2 h, 28–41%; d) Pd/C type 424 (10 mol%), EtOH, H₂, rt, 16 h, 25–73%.

GSK Confidential – Do not copy

The *meso* oxabicyclic **2.007** was chosen as these compounds were predicted to occupy the desired physico-chemical space. Bromide **2.050** was then diversified *via* Suzuki couplings. The Suzuki reactions used PEPPSI-*i*Pr or XPhos Pd G2 as a catalyst and proceeded in yields of up to 41%. Subsequent hydrogenation of the biaryl products (**2.051–2.054**) using the heterogeneous Pd/C type 424 under a hydrogen atmosphere gave DBFs (\pm)-**2.039**, (\pm)-**2.055–2.0257** in yields of up to 73%. Pd/C type 424²³⁷ was used in previous in-house work where these conditions proved superior.²³⁸ Sufficient material was synthesised for the generation of the initial data for each compound and so the reactions were not optimised further. For indole (\pm)-**2.056**, the single enantiomer was prepared by another member of the team upon scale-up using the same route. The absolute stereochemistry of the most active enantiomer was assigned from X-ray crystallography (Figure 2.09, section 2.3.3.). Compounds (\pm)-**2.055** and (\pm)-**2.057** were tested as a racemic mixture.

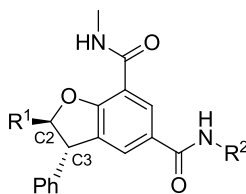
With a synthetic strategy that allowed for functionalisation of both the amide and C3 aryl vectors established, synthesis of analogues **2.011**, **2.039–2.042**, and **2.055–2.057** along with further examples synthesised by other members of our laboratory was enabled. It was now possible to fully explore the SAR of the DBF template.

2.3. Investigating the SAR of the 2-unsubstituted DBFs

2.3.1. SAR of the Amide Vector

As outlined previously, the flexible synthetic strategy developed has allowed the synthesis of analogues to establish the effect of deletion of the C2 substituent and to explore a wider range of C3 substituents. Selected examples are shown in Table 2.03. First, the effect of removing the CH_2F substituent was examined, by comparison of historical DBF systems where $C2 = CH_2F$. Overall, potency and selectivity was generally well maintained in all examples (Entries 1–10 and 14–15) and an average reduction in ChromLogD of 0.2 log units was observed. The primary amide **(S)-2.059** (Entry 2) was potent at BRD4 BD2 ($pIC_{50} = 7.3$), however, removal of the amide substituent negatively impacted on selectivity (200-fold). These trends were mirrored for the CH_2F variant **(S,S)-2.058** (Entry 1). The methyl amide **(S)-2.061**, increased potency at BRD4 BD2 by 0.4 log units which was concomitant with a minor improvement in selectivity (320-fold), however, this was still below the desired 1000-fold threshold. With an aim to improve the selectivity, the cyclopropyl derivative which had been optimised for the pyridone series (Section 1.6.2) was tested. DBF **(S)-2.011** showed excellent potency at BRD4 BD2 ($pIC_{50} = 7.7$) and was 800-fold selective over BD1. This compound occupied the desired physico-chemical space (ChromLogD = 3.6) and deletion of the CH_2F substituent raised the CLND solubility from 8 to $\geq 141 \mu\text{g mL}^{-1}$ (Entry 6 vs. 5). Progression to a rat hepatocyte IVC assay showed minor improvements in metabolic stability ($2.0 \text{ mL min}^{-1} \text{ g}^{-1}$) compared to the CH_2F DBF **(S,S)-2.062** ($3.2 \text{ mL min}^{-1} \text{ g}^{-1}$). As discussed in the introduction, the elevated rat clearance had been a major flaw for the fluorinated DBFs, therefore, because of its promising profile, DBF **(S)-2.011** was progressed to *in vivo* PK studies which will be discussed in Section 2.3.4. The methyl cyclopropyl amide **(S,S,S)-2.040** (Entry 8) improved potency at BD2 ($pIC_{50} = 8.0$) and selectivity (1600-fold) over BD1. However, this increase in potency was likely driven by the log unit increase in ChromLogD to 4.5 which was outside the desired range for this series and as such submission for IVC analysis was not undertaken. A marked improvement in the solubility was also observed on deletion of the CH_2F group with this example (Entry 7 vs. entry 8).

Table 2.03. Comparison of the '973 series with 3-substituted DBFs.



	R ¹	R ²	BRD4 BD2(n) / BD1(n) pIC ₅₀ Selectivity	Chrom LogD _{7.4}	CLND Solubility (μg mL ⁻¹)	Rat IVC (mL min ⁻¹ g ⁻¹)
1 ^a	CH ₂ F (S,S)-2.058	H	6.9(2) / 4.7(2) 160x	2.9	≥128	-
2 ^a	H (S)-2.059		7.3(3) / 5.0(2) 200x	2.7	≥144 ^e	-
3 ^a	CH ₂ F (S,S)-2.060	Me	7.5(3) / 4.9(2) 400x	3.3	≥149	3.0
4 ^a	H (S)-2.061		7.7(2) / 5.2(2) 320x	3.2	≥130 ^e	-
5 ^a	CH ₂ F (S,S)-2.062		7.6(3) / <3.3(2) ^d >20000x	3.9	8	3.2
6	H (S)-2.011		7.7(10) / 4.8(10) 800x	3.6	≥141	2.0
7 ^a	CH ₂ F (S,S,S,S)- 2.063		8.0(3) / 5.0(1) ^b 1000x	4.5	7	-
8	H (S,S,S)- 2.040		8.0(2) / 4.8(2) 1600x	4.5	≥76	-
9 ^a	CH ₂ F (S,S)-1.46		7.8(20) / 4.6(19) ^c 1600x	3.6	≥206 ^e	1.8
10	H (S)-2.039		7.8(8) / 4.8(8) 1000x	3.3	≥143	8.6
11 ^a	H (S)-2.064		7.9(3) / 4.6(3) 2000x	2.9	≥124 ^e	3.3
12 ^a	H (S)-2.065			7.9(3) / 4.9(3) 1000x	3.4	≥163
13	H 2.042^f		7.3(2) / <4.3(2) >1000x	2.1	≥166	-
14 ^a	CH ₂ F (S,S)-2.066		7.3(3) / 4.4(1) ^b 790x	2.7	165	1.1
15 ^a	H (S)-2.067		7.3(3) / 4.6(3) 500x	2.5	≥201	1.8

^aPrepared by colleagues at GSK; ^bAlso <4.3 (n = 2); ^cAlso <4.3 (n = 1); ^dAlso <4.3 (n = 4); ^eCAD solubility; ^fA 1:1 diastereomeric mixture of C3 epimers.

GSK Confidential – Do not copy

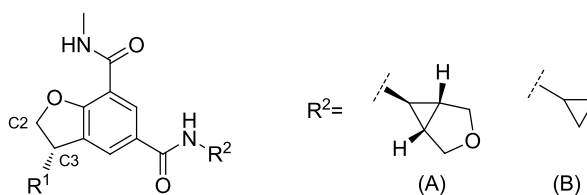
The *meso* oxabicyclic amide was used successfully in the development of DBF **(S,S)-1.46** (Section 1.6.3) to lower the lipophilicity by introducing polarity into the amide substituent. DBF **(S)-2.039** (Table 2.03, Entry 9) was well tolerated ($pIC_{50} = 7.8$) and was 1000-fold selective over BRD4 BD1. The lower ChromLogD (3.3) and high CLND solubility ($\geq 143 \mu\text{g mL}^{-1}$) made progression to IVC desirable. Interestingly, DBF **(S)-2.039** had high clearance in rat hepatocytes ($8.6 \text{ mL min}^{-1} \text{ g}^{-1}$), which was raised relative to the CH_2F DBF **(S,S)-1.46** ($1.8 \text{ mL min}^{-1} \text{ g}^{-1}$). Therefore, progression of this compound was halted. Due to the decrease in ChromLogD observed (relative to DBF **(S,S)-1.46**) it was believed that the increase in clearance was not driven by lipophilicity but by a metabolic liability in the new core. An exploration of other bicyclic amides was then conducted with the hope that the excellent potency and selectivity of DBF **(S)-2.039** could be maintained alongside a reduction in IVC. The *exocyclic* alcohol **(S)-2.039** and azabicyclic amide **2.065** were both investigated. Both bicycles **(S)-2.064** and **(S)-2.065** were potent against BRD BD2 ($pIC_{50} = 7.9$) and highly selective (2000-fold and 1000-fold respectively) over BD1. Both were in a suitable physico-chemical space (ChromLogD = 2.9 and 3.4). Unsurprisingly, the addition of an additional hydrogen-bond donor in DBF **(S)-2.064** decreased the lipophilicity compared to oxabicyclic **(S)-2.039**. Due to the initial promising profile, both compounds were progressed to *in vitro* PK studies. Unfortunately, both DBF **(S)-2.064** and DBF **(S)-2.065** showed raised hepatocyte clearance (3.3 and $6.8 \text{ mL min}^{-1} \text{ g}^{-1}$ respectively) and progression to *in vivo* PK studies was not warranted. Weakly basic amides had been well tolerated in the pyridone series and their utility in the DBF series was assessed next. Morpholine **2.042** showed lower potency at BRD4 BD2 ($pIC_{50} = 7.3$) although it maintained 1000-fold selectivity over BD1. DBF **2.042** had high CLND solubility ($\geq 166 \mu\text{g mL}^{-1}$), however, it was thought that the low ChromLogD (2.1) would negatively impact bioavailability and so was not progressed further. As the low ChromLogD was believed to be driven by the basicity of the morpholine amine, the *trans*-1,3-dioxan-5-amide **(S)-2.067**, which was first reported by Ndubaku *et al.* during the development of a selective p21 activated kinase 1 (PAK1), was explored.²³⁹ The *trans*-1,3-dioxan-5-amide moiety had a pK_a of 6.8, where the amine basicity is modulated by the two oxygens of the acetal, and as such was predicted to provide the right balance of properties in the DBF series. DBFs **(S)-2.066-2.067** were well tolerated, both with and without a C_2 CH_2F substituent, had a high potency against BD2 in both series ($pIC_{50} = 7.3$) and were ≥ 500 -fold selective over BD1. Due to a desirable physico-chemical profile, DBF **2.067** was progressed to understand its

metabolic stability. Pleasingly, DBF **2.067** had lower clearance ($1.8 \text{ mL min}^{-1} \text{ g}^{-1}$) relative to the other DBF analogues tested and was therefore progressed to *in vivo* studies.

2.3.2. SAR of the C2 DBF Substituent

Having established that the CH_2F group was not required for potency and selectivity, a greater range of C3 substituents were prepared and the SAR examined. The high BD2 potency of the DBF series is believed to be partly driven by an edge-to-face π -stacking interaction between the phenyl ring and the BD2 specific His433 (Section 1.6.3, Figure 1.44). Therefore, replacement of this substituent with a non-aromatic group should lead to a decrease in activity at BD2, but it was felt important to test this hypothesis as the removal of an aromatic ring is known to be beneficial to solubility.¹⁵ As expected, THP (\pm)-**2.057** showed a 10-fold drop in potency relative to the phenyl substituent (**S**)-**2.039** (Table 2.04). Additionally, all three regioisomers of the electron-deficient pyridyls were poorly tolerated (Entries 2–4) relative to the phenyl derivative (**S**)-**2.039**. The reduction in activity was attributed to two probable causes; either the polarity of the pyridine rings was poorly tolerated, or a more electron-rich aromatic ring is required to maximize the potency obtained from the edge-to-face interactions with Trp370 and His433. To investigate this further, an electron donating *ortho* methoxy group was examined with both a cyclopropyl amide (\pm)-**2.070** and an oxabicyclic amide (\pm)-**2.071**. Both (\pm)-**2.070** and (\pm)-**2.071** (Entries 5 and 6) were potent at BRD4 BD2 ($\text{pIC}_{50} = 7.5$ and 7.2 respectively), however, this offered no improvements over the phenyl ring (**S**)-**2.039** (Table 2.03, Entry 10), therefore, progression was halted. It was interesting to note that the additional electron density of the ring did not cause an increase in potency or selectivity. Any increase in potency that came from the increased aromaticity was possibly counterbalanced by a detrimental effect caused by the polarity or steric bulk of the substituent. The effect of polarity was further explored by examination of a 4-fluoro substituent. DBFs (**S**)-**2.072** and (**S**)-**2.073** were both potent (BRD4 BD2 $\text{pIC}_{50} = 7.5$ and 7.6 respectively) and selective (630-fold). Both sat in the desired physico-chemical space (ChromLogD = 3.8 and 3.6 respectively), however, DBF (**S**)-**2.072** had lower kinetic solubility ($40 \mu\text{g mL}^{-1}$). Despite this both 4-fluoro phenyls (**S**)-**2.072** and (**S**)-**2.073** were progressed to assess the IVC. Disappointingly, both DBF **2.072** and **2.073** were rapidly cleared in rat hepatocytes (6.1 and $15.0 \text{ mL min}^{-1} \text{ g}^{-1}$ respectively) and were therefore not assessed *in vivo*.

Table 2.04. Exploration of C3 substituent SAR.



	R ¹	R ²	BRD4 BD2 pIC ₅₀ (n) / BD1 pIC ₅₀ (n) Selectivity	Chrom LogD _{7.4}	CLND Solubility (μg mL ⁻¹)	IVC rat (mL min ⁻¹ g ⁻¹)
1	4-THP	(A) (±)-2.057	6.6(3) / 4.7(3) 80x	2.1	≥177	-
2 ^a	2-pyridyl	(A) (±)-2.068	6.7(3) / <4.3(3) >250x	1.6	≥158	-
3	3-pyridyl	(A) (±)-2.055	6.6(3) / 4.8(1) ^c 63x	1.4	≥104	-
4 ^a	4-pyridyl	(A) (±)-2.069	6.8(2) / 4.8(1) ^d 100x	1.3	≥184	-
5 ^a	3-OMe- C ₆ H ₄	(B) (±)-2.070	7.2(3) / 4.7(3) 320x	3.8	≥161	-
6 ^a		(A) (±)-2.071	7.5(3) / 4.6(3) 790x	3.2	≥186	-
8 ^a		(B) (S)-2.072	7.5(4) / 4.7(4) 630x	3.8	40	6.1
9 ^a	4-F- C ₆ H ₄	(A) (S)-2.073	7.6(3) / 4.8(3) 630x	3.6	≥176	14.8
10 ^a	2-Me- C ₆ H ₄	(A) (S)-2.074	7.6(3) / 4.9(3) 500x	4.0	≥103	30.9
11 ^a	4-indole	(B) (S)-2.075	8.1(2) / 5.0(2) 1300x	3.5	≥142	4.6
12 ^b		(A) (S)-2.056	8.2(8) / 5.3(8) 790x	3.1	≥137	3.6

^aPrepared by colleagues at GSK; ^bSingle enantiomer prepared by a colleague at GSK; ^cAlso <4.3 (n = 2); ^dAlso <4.3 (n = 1).

Fluoro groups are known to block metabolic soft spots, therefore, the raised clearance of DBFs **(S)-2.072** and **(S)-2.073**, suggested that metabolism of the 4-position of the phenyl ring was not responsible for the raised clearance of DBFs **(S)-2.072** and **(S)-2.073** (Table 2.04, entry 8–9). It was proposed that *ortho* substitution of the phenyl ring could restrict rotation around the C3 position, potentially providing an entropic driving force for binding if the low energy state matched the desired binding conformation. However, DBF **(S)-2.074** (Table 2.04, Entry 10) offered no improvements in either potency or selectivity compared to the unsubstituted phenyl ring (Table 2.03, Entry 10). This suggests that *ortho* substitution is tolerated but not beneficial. DBF **(S)-2.074** was just within the acceptable ChromLogD range (4.0) and just over the desired solubility threshold ($\geq 103 \mu\text{g mL}^{-1}$), therefore, was progressed to assess IVC. Again, DBF **(S)-2.074** showed raised clearance in rat hepatocytes ($31.0 \text{ mL min}^{-1} \text{ g}^{-1}$). Cuilli *et al.* had identified a BD2 selective triazoloazepene by exploiting the edge-to-face interaction of an indole shelf group with the BD2 specific His433 (Section 1.5.4).¹⁹⁴ An indole aryl substituent had increased both potency and selectivity in the pyridone series relative to a phenyl substituent. Therefore, to optimise for higher potency and selectivity in the DBF series, indoles **(S)-2.075** and **(S)-2.056** were prepared. As predicted, both indoles **(S)-2.075** and **(S)-2.056** were highly potent against BRD4 BD2 ($\text{pIC}_{50} = 8.1$ and 8.2 respectively) and selective over BD1 (1300 and 790-fold respectively). The additional H-bond donor and increased polarity of the C3 substituent relative to the phenyl ring caused a reduction in lipophilicity of both indoles. Additionally, both indoles **(S)-2.075** and **(S)-2.056** had high CLND solubility (≥ 142 and $\geq 137 \mu\text{g mL}^{-1}$ respectively) and were therefore progressed to assess IVC. Both indoles showed a raised hepatocyte clearance of 3.6 and $4.6 \text{ mL min}^{-1} \text{ g}^{-1}$ respectively. However, this was an improvement over any other C3 substituents tested. Therefore, due to the high potency, and reduced clearance (compared to DBF **(S)-2.039**), DBF **(S)-2.056** was progressed to *in vivo* PK and will be discussed further in Section 2.3.4.

2.3.3. X-ray Crystallography of DBF **(S)-2.056**

To further understand the key interactions of the DBF ligand with the BD2 BRD, and to further probe the increased potency obtained from the indole C3 substituent, an X-ray crystal structure of DBF **(S)-2.056** was resolved and compared with DBF **(S,S)-1.46** (Figure 2.08). The methyl amide warhead mimics the interactions of the natural KAc substrate, making a through water interaction with the conserved Tyr386 and a H-bond to the conserved Asn429. The second amide then makes a further bidentate interaction to Asn429. This places the

indole between the WPF shelf and the BD2 specific histidine (His433). Interestingly, Cuilli *et al.* attribute the increased BD2 potency of indole (**S**)-**2.056** (see Section 1.5.4) to the increased aromaticity of the pyrrole ring relative to the phenyl ring.²⁰³ Furthermore, a through water H-bond to Asp434 is also visible.

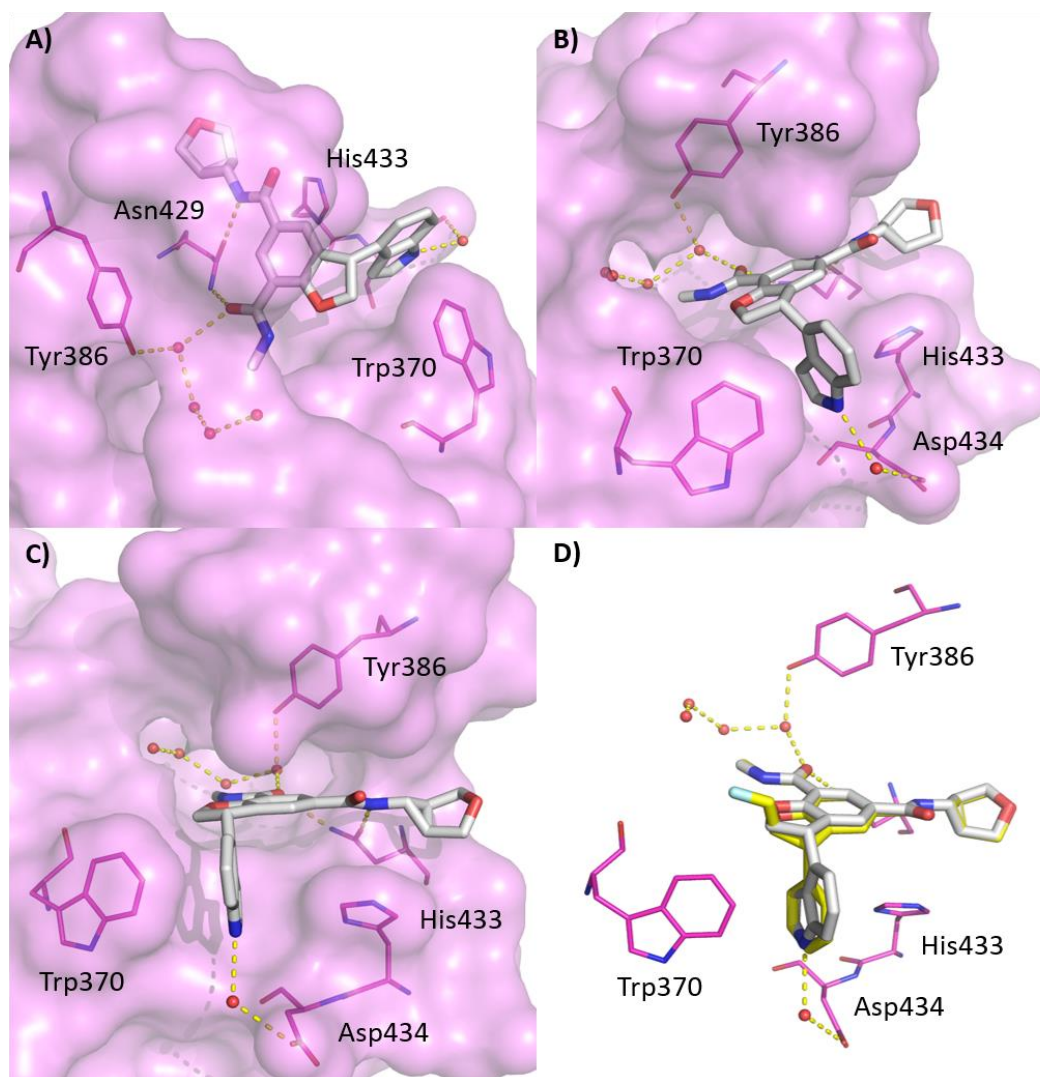


Figure 2.09. X-ray crystallography of (**S**)-**2.056** (grey) in BRD2 BD2. The key residues are shown in magenta and H-bonds as dashed yellow lines. Waters are red dots. A) The methylamide warhead and amide vector make a bidentate interaction with Asn429. The carbonyl group of the warhead makes an additional through water interaction to Tyr386. B-C) These interactions place the indole substituent between the WPF shelf and BD2 specific His433, where it is further stabilized by a through water interaction to Asp434. D) DBF (**S**)-**2.056** overlaid with GSK973 ((**S,S**)-**1.46**).

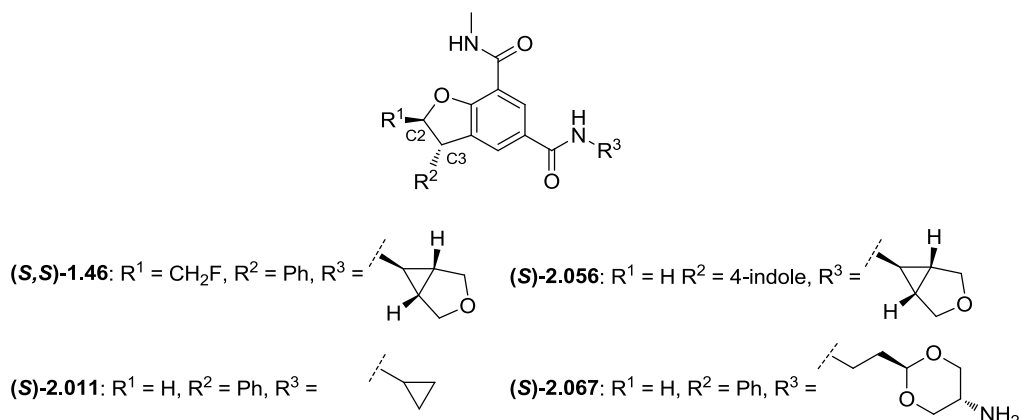
When DBF **(S,S)-1.46** and indole **(S)-2.056** were overlaid, they exhibited the same mode of binding, however, there is a slight movement in DBF **(S)-2.056** relative to **(S,S)-1.46** which places the indole pyrrole ring on top of the phenyl ring between Trp370 and His433. It was believed that this optimises the edge-to-face π -stacking between the ligand, His433 and Trp370. Additionally, the indole *NH* forms a through water interaction to Asp434, further stabilising this interaction.

2.3.4. *In Vivo* PK profiling of DBFs **(S)-2.011**, **(S)-2.056** and **(S)-2.067**

The potency and selectivity of the DBF series was now well understood, but, despite careful control of the lipophilicity of the series, achieving suitable IVC had been challenging. The lead compounds (**(S)-2.011**, **(S)-2.056** and **(S)-2.067**), which had demonstrated potency, selectivity and low clearance were progressed to understand their *in vivo* PK, cellular target engagement and thermodynamic (FaSSIF) solubility when compared to DBF **(S,S)-1.46** (Table 2.05). DBF **(S)-2.011** maintained excellent potency in both LPS stimulated PBMC and hWB assays measuring reduction of MCP-1 (Section 1.1.3), demonstrating that this series could reduce inflammation *in vitro*. Pleasingly, the low clearance in hepatocytes translated into a low *in vivo* clearance of 34 mL min⁻¹ kg⁻¹. However, the unbound clearance was 723 mL min⁻¹ kg⁻¹ (c.f. 184 mL min⁻¹ kg⁻¹ for **(S,S)-1.46**) suggesting that the apparent low clearance is a function of high protein binding. When dosed orally, DBF **(S)-2.011** showed a good bioavailability of 47%. Unfortunately, a low FaSSIF solubility of 28 $\mu\text{g mL}^{-1}$ meant it was not progressed to dog *in vivo* PK studies. DBFs **(S)-2.056** and **(S)-2.067** were then investigated. Both were active in PBMC ($\text{pIC}_{50} \geq 7.4$) and hWB blood assays ($\text{pIC}_{50} \geq 6.7$). Interestingly, DBF **(S)-2.056** was 10-fold more potent in the biochemical TR-FRET assay and this trend was also observed in the cellular assays. Pleasingly, **(S)-2.056** and **(S)-2.067** were more soluble than **(S)-2.011** with FaSSIF solubility $\geq 269 \mu\text{g mL}^{-1}$. It is interesting to note that there was a poor correlation between CLND and FaSSIF solubility. Given the excellent profile of both **(S)-2.056** and **(S)-2.067**, *in vivo* PK studies were conducted. DBF **(S)-2.056** showed low blood clearance of 39 mL min⁻¹ kg⁻¹. However, unlike DBF **(S)-2.011**, a low blood clearance did not translate into good bioavailability ($F_{\text{po}} = 6\%$). This is suggestive of poor absorption, however, DBF **(S)-2.056** showed good permeability in an AMP assay (133 nm s⁻¹) so this result is perhaps surprising. DBF **(S)-2.067** was highly cleared in the rat (177 mL min⁻¹ kg⁻¹) and as expected this led to poor oral bioavailability ($F_{\text{po}} = 10\%$).

GSK Confidential – Do not copy

Table 2.05. Further profiling of DBFs (**(S)**-2.011, (**(S)**-2.056 and (**(S)**-2.067.



		((S,S) -1.46 ^a)	((S) -2.011)	((S) -2.056 ^b)	((S) -2.067 ^a)
BRD4 BD1 pIC₅₀ (n) / BD2 pIC₅₀ (n)		7.8(20) / 4.6(19) ^c	7.7(10) / 4.8(10)	8.2(8) / 5.3(8)	7.3(3) / 4.6(3)
Selectivity		1600x	790x	790x	500x
LE / LLE_{at}		0.36 / 0.38	0.42 / 0.40	0.36 / 0.40	0.32 / 0.40
PBMC MCP-1 pIC₅₀ (n)^f		-	7.7(2)	≥8.7(3)	7.4(3)
hWB MCP-1 pIC₅₀ (n)^f		7.2(2)	6.9(2)	7.9(2)	6.7(2)
CLND Solubility (μg mL⁻¹)		≥206 ^e	≥141	≥137	≥202
FaSSIF Solubility (μg mL⁻¹)		47	28	269	845 ^d
AMP (nm s⁻¹)		165	300	133	53
IVC (mL min⁻¹ g⁻¹)	Rat	1.8	2.0	3.6	1.8
	Dog	<0.7	<0.7	0.8	<0.7
	Human^f	<0.5	<0.5	<0.5	<0.5
Rat IV PK^g	CL_b / CL_{FU} (mL min⁻¹ kg⁻¹)	73 / 184	34 / 723	39 / -	177 / 1311
	%LBF	89	43	43	>100
	V_{ss} (L kg⁻¹)	2.1	0.6	1.2	3.7
	T_{1/2} (h)	0.6	0.3	0.6	0.4
Rat Oral PK^g	Fpo (%)	48	47	6	10

^aPrepared by colleagues at GSK; ^bSingle enantiomer prepared by a colleague at GSK; ^cAlso <4.3 (n = 1); ^dData was >1000 on 1 / 2 test occasions; ^eCAD solubility; ^fThe human biological samples were sourced ethically and their research use was in accord with the terms of the informed consents under an IRB/EC approved protocol; ^gAll animal studies were ethically reviewed and carried out in accordance with Animals (Scientific Procedures) Act 1986 and the GSK Policy on the Care, Welfare and Treatment of Animals.

The poor oral bioavailability of **(S)-2.056** and **(S)-2.067** and the poor FaSSIF solubility of **(S)-2.011**, meant the search for a more suitable lead compound must continue. The challenge for this series was balancing high solubility with a suitable *in vitro* and *in vivo* PK profile. Over 150 compounds with this scaffold were synthesised and none had met the desired criteria of solubility and metabolic stability, therefore, a novel approach was required.

2.3.5. *In Silico* Analysis of DBF **2.039**

The synthetic strategy developed in Section 2.2, had allowed an investigation into an improved C3 substituent and the effect of removing the C2 CH₂F group from the DBF core. However, suitable PK and high solubility remained challenging. Therefore, a new strategy which could improve on both these areas was sought. To aid rational design moving forward, an *in silico* Metasite ID was used to predict the metabolic liabilities of the template (Figure 2.10).²⁴⁰

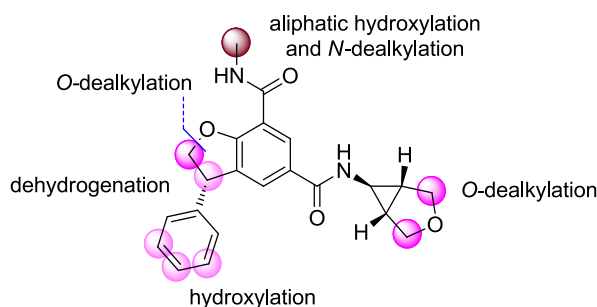


Figure 2.10. *In silico* Metasite ID of **(S)-2.039** which highlights vulnerable groups which are most likely to be metabolised. The darker circles represent the positions most likely to be oxidised.

This suggested that the amide warhead would be the most easily metabolised site. However, as other series which contained the same warhead had demonstrated good PK (Section 1.6) with a similar ChromLogD, it was hypothesised that this was in fact more metabolically stable than predicted. Moreover, previous SAR work had shown that the methyl amide was critical for potency. Additionally, the oxabicyclo amide was predicted to be a metabolic liability through *O*-dealkylation of the ether. However, a range of structurally diverse amides were well tolerated but they all showed raised hepatocyte clearance. Hydroxylation of the aryl ring was also indicated, however, 4-fluoro **(S)-2.072–2.073** did not improve metabolic stability relative to the unsubstituted aryl ring. This pointed towards the DBF core as the main driver for metabolism, with aromatisation to the benzofuran a likely metabolic fate for this type of compound. This is consistent with **(S,S)-1.46** vs **(S)-2.039** data where between the matched

pairs, the IVC increases from 1.8 to 8.6 mL min⁻¹ g⁻¹ (Table 2.03, Entries 9–10). It is possible that the increased steric hindrance of the CH₂F potentially helps to limit metabolism at this position. Therefore, a strategy was envisioned which inserted a quaternary centre into the molecule at the 3-position to stop aromatisation/cleavage of the DBF ring and potentially lead to a more metabolically stable compound. Additionally, it was theorised that the increased sp³ character and 3D structure of a quaternary centre would increase solubility.

2.4. Synthetic Approaches Targeting a DBF Quaternary Centre

2.4.1. Reductive Heck cyclisation

To improve the solubility and address the metabolic liabilities of DBF (**S**)-**2.011**, an alternative approach was proposed which targeted insertion of a quaternary centre within the DBF core (Figure 2.11). Retrosynthetically, the quaternary DBF (**S**)-**2.076** could be accessed from ester (\pm)-**2.077** *via* a chiral separation, hydrolysis and amide coupling. To install the quaternary centre, a reductive Heck cyclisation of iodide **2.078** was envisioned which would form a bond between an aryl iodide and an ether linked alkene. This could itself be prepared *via* alkylation of phenol **2.035** which had previously been prepared (Section 2.2.5.).

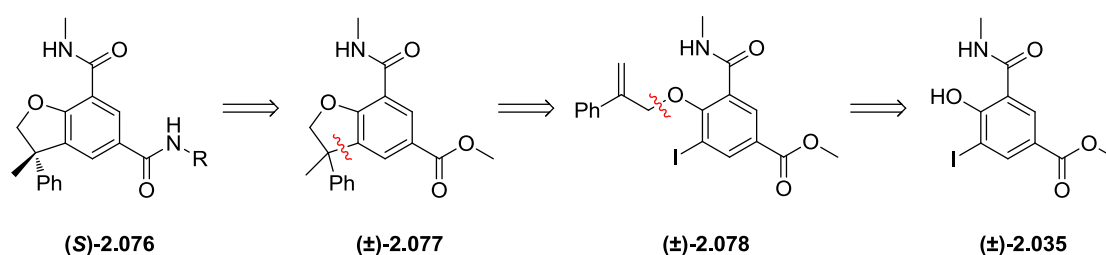
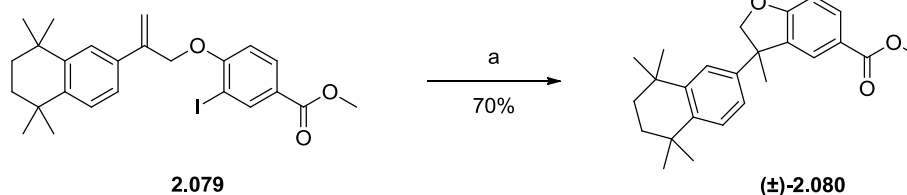


Figure 2.11. Retrosynthetic approach to target a DBF quaternary centre.

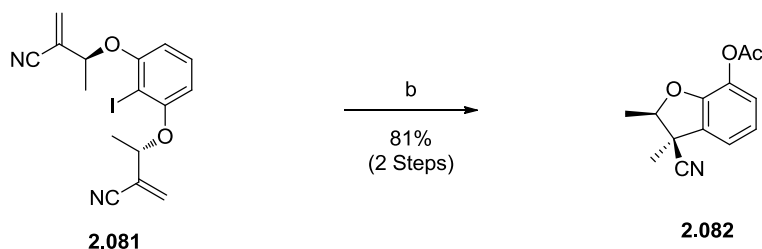
Precedent for a reductive Heck cyclisation came from two main sources. Diaz *et al.* used a reductive Heck to synthesise new synthetic retinoids (Scheme 2.15).²⁴¹ Their procedure reacted iodide **2.079** with Pd(OAc)₂, tributylamine as the base and formic acid as the reductant, which worked in yields of up to 70%. Another example was reported by Trost *et al.* in their total syntheses of Furaquinocin A, B, and E.²⁴² Again, a formic acid reductant was used to facilitate the transformation of *meso*-iodide **2.081** in the presence of a palladium catalyst and 1,2,2,6,6-pentamethyl piperidine (PMP) base.

Scheme 2.15. Literature precedent for a reductive Heck cyclisation.^{241, 242}

Diaz:



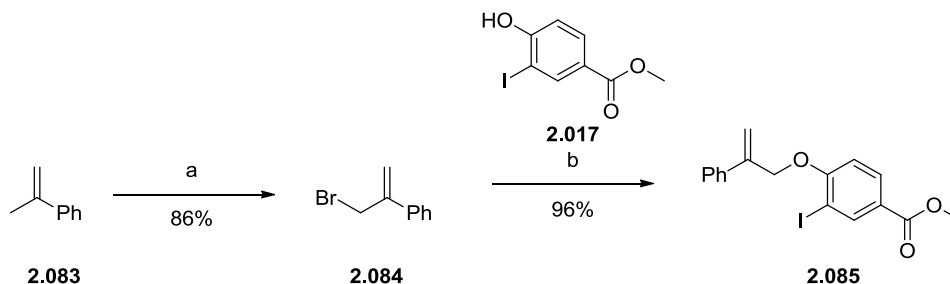
Trost:



a) Pd(OAc)₂ (10 mol%), Bu₃N (2.2 eq.), HCO₂H (1.1 eq.), MeCN, 65 °C, 4 h, 70%; b) PdCl₂(MeCN)₂ (10 mol%), PMP (6.0 eq.), HCO₂H (4.0 eq.), DMF, 50 °C, then Ac₂O (2.4 eq.), TEA (3.8 eq.), DMAP (cat.), CH₂Cl₂, rt, 1 h, 81% (2 steps).

To test the utility of this methodology, the necessary precursor **2.085** was synthesised (Scheme 2.16). Starting from 1-methylstyrene (**2.083**), NBS bromination using catalytic TsOH at 100 °C gave bromide **2.084** in 86% yield according to the literature procedure.²⁴³ A more truncated DBF was chosen as a test substrate for proof of concept studies for the cyclisation reaction. Accordingly, alkylation using phenol **2.017** and K₂CO₃ as a base in acetone gave complete conversion to the desired ether **2.085** which was isolated in 96% yield.

Scheme 2.16. Synthesis of the precursor alkene for the reductive Heck cyclisation.

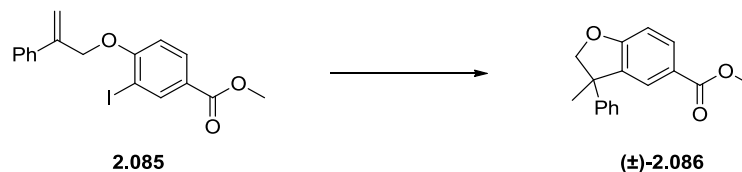


a) NBS (1.05 eq.), TsOH (0.1 eq.), THF, 100 °C, 4 h, 86%; b) K₂CO₃ (3.0 eq.), acetone, 80 °C, 1 h, 96%.

Aryl iodide **2.085** was then taken forward to investigate a reductive Heck cyclisation (Table 2.06). The literature conditions from Diaz and Trost were chosen as a starting point for the

investigation.^{241, 242} The first experiment examined, using Diaz's conditions of Bu₃N and Pd(OAc)₂, showed 33% conversion by LCMS but then did not progress further with significant unreacted iodide **2.085** remaining. Concurrently, Trost's conditions using PMP and PdCl₂(MeCN)₂ were investigated and this reaction showed complete conversion to (±)-**2.086** by LCMS and the product was isolated in 83% yield. These conditions appeared superior and were taken forward in this work.

Table 2.06. Investigation into conditions to facilitate a reductive Heck to access DBF (±)-**2.086**.

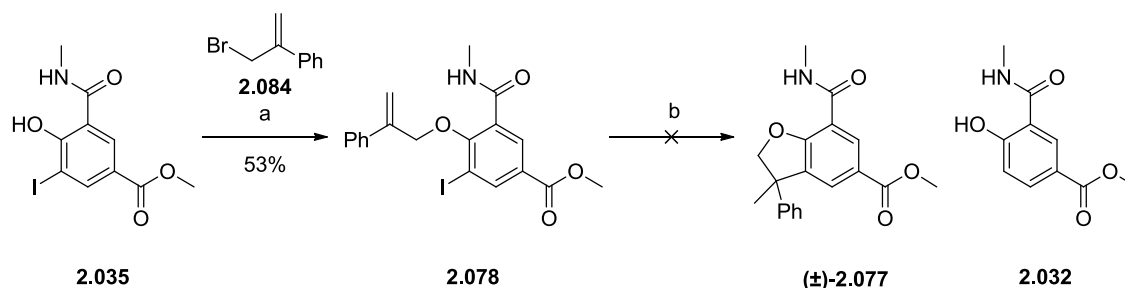


Conditions	HCO ₂ H (2.2 eq.), Bu ₃ N (3.3 eq.) Pd(OAc) ₂ (20 mol%) MeCN, 65 °C, 4 h	HCO ₂ H (4.0 eq.), PMP (6.0 eq.) PdCl ₂ (MeCN) ₂ (10 mol%) DMF, 50 °C, 2 h
Conversion (%) ^a	33%	100%
Isolated Yield (%)	-	83%

^aConversion measured as (area product/(area product + area starting material)) in LCMS trace of reaction mixture.

The next step was to investigate the reductive Heck cyclisation of the more functionalised aryl iodide **2.078** (Scheme 2.17). Compound **2.035**, a key intermediate in the synthesis of (±)-**2.011** (Section 2.2), was alkylated using bromide **2.084** and K₂CO₃ in 53% yield. Attempts were then made to affect the cyclisation to form DBF (±)-**2.077**.

Scheme 2.17. Exploration of reductive Heck cyclisation on a more functionalised substrate.



a) K₂CO₃ (3.0 eq.), acetone, 100 °C, 16 h, 53%; b) Formic acid (4.0 eq.), PMP (6.0 eq.) PdCl₂(MeCN)₂ (10 mol%), DMF, 2 h, 50 °C.

Using the same conditions which were successful for (\pm)-**2.086**, only a small amount of desired product (\pm)-**2.077** was observed in the reaction mixture. The major product was the formation of dealkylated and dehalogenated phenol **2.032**. It is believed that loss of the allyl group occurs first, *via* a Tsuji-Trost like mechanism through Pd insertion into the allyl system.²⁴⁴

The Tsuji-Trost like elimination of the phenol is facilitated by the electron withdrawing methyl amide which stabilises the phenolate leaving group to aid addition (Figure 2.12). Once the allyl group has been lost insertion into the aryl iodide will solely lead to dehalogenation through a reductive mechanism as there is no scope for an intramolecular cyclisation before reductive elimination. Additionally, previous work (Section 2.2.6) had shown that the addition of the amide group slowed down oxidative addition into the aryl iodide bond. Therefore, no further investigation into this route was carried out as it was believed that insertion of the methylamide warhead would be more facile at a later stage and this will be discussed in section 2.4.3.

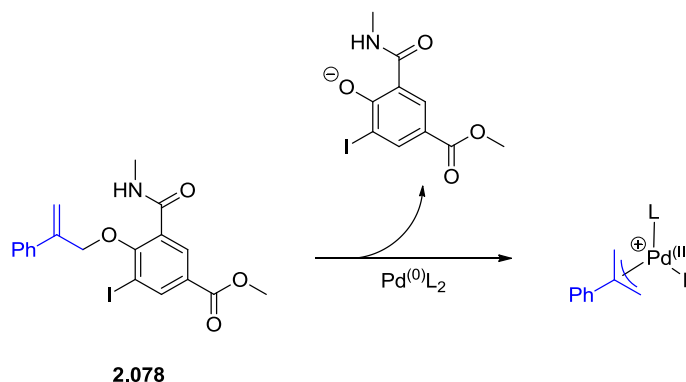


Figure 2.12. Tsuji-Trost like insertion of Pd(0) into an allyl group. The stabilised phenoxide anion can act as a leaving group to facilitate this addition.

2.4.2. Further Functionalisation of the Quaternary Centre

With the successful installation of a methyl quaternary centre to afford DBF (\pm)-**2.086**, attention then turned to inserting other functionality onto this new vector which could provide an additional handle to balance the physico-chemical properties of the series. DBFs (\pm)-**2.087** and (\pm)-**2.088** were designed to add polarity onto the quaternary centre using an alcohol and fluorine respectively (Figure 2.13).

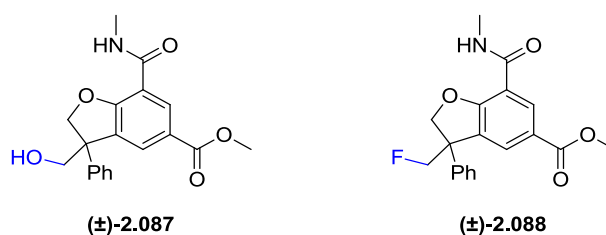


Figure 2.13. Desired targets to probe the tolerability of polarity at the quaternary vector.

To access DBF based systems **(±)-2.087** and **(±)-2.088**, the Heck cyclisation strategy which had synthesised DBF **(±)-2.086** was re-examined. In the successful reductive Heck reaction, it was thought that cyclisation (a *pseudo* 5-*exo*-trig) occurred at a far greater rate than the reductive cleavage of the Pd-C bond. Evidence for this came from the fact that the dehalogenated material (ether **2.089**) had not been observed in the reaction mixture (Figure 2.14). This suggests that if oxidative addition does occur, cyclisation happens at a much faster rate than reductive elimination. Therefore, if an alternative catalytic cycle is employed e.g. a Miyaura borylation reaction, then the cyclisation should occur before the transmetallation and reductive elimination steps leading to *exo*-cyclic functionalisation.

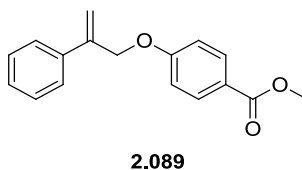


Figure 2.14. Proposed by-product that would be expected to be observed if cyclisation was slower than reduction.

Intercepting cyclised Pd intermediate **(±)-2.085a** with a Miyaura borylation catalytic cycle (Figure 2.15) offered a promising strategy for the installation of a boronic ester for use as a synthetic handle. The boronic ester could be oxidised to afford alcohol **(±)-2.090**, which could in turn afford the corresponding fluoride through a deoxo fluorination reaction.

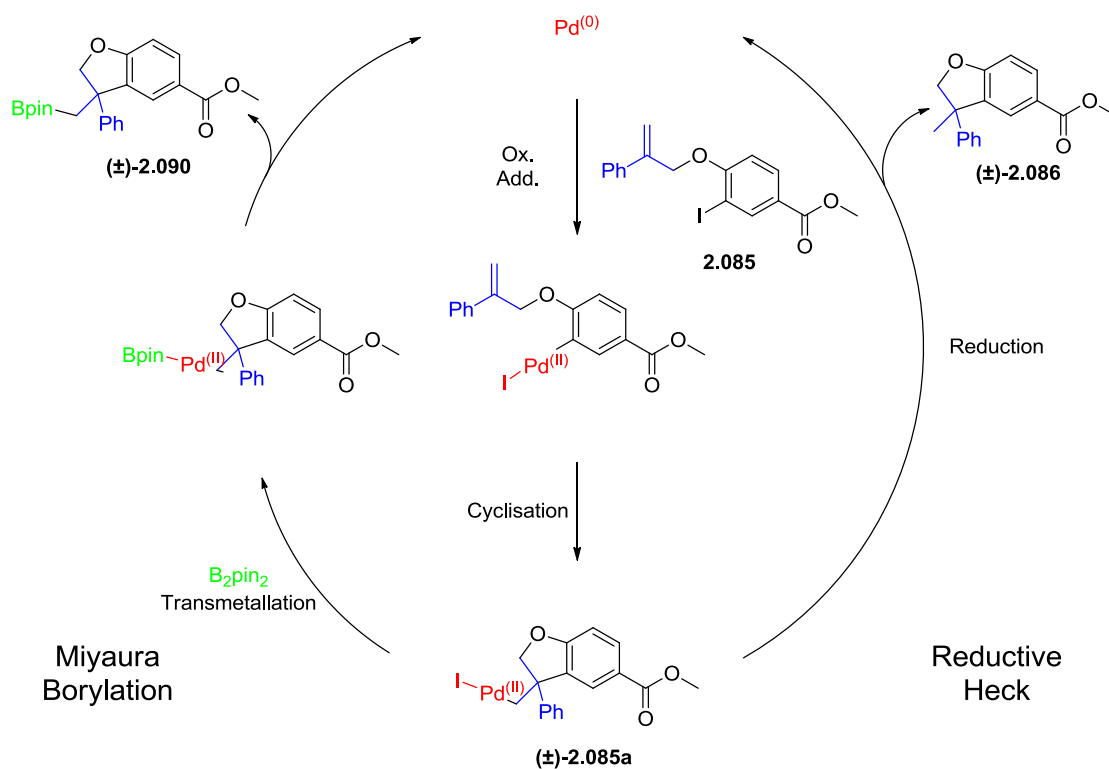
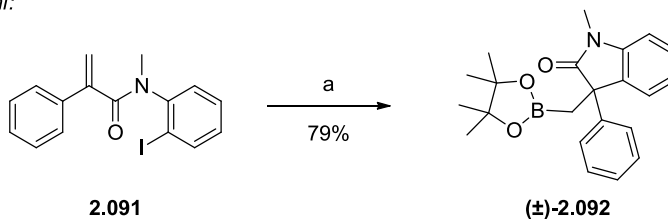


Figure 2.15. Proposed catalyst cyclic of the reductive Heck and intramolecular Heck/Miyaura borylation reactions.

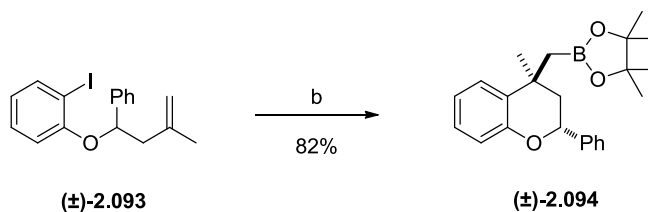
There was precedent for a tandem cyclisation/borylation reaction in the literature (Scheme 2.18). Vachhani *et al.* reported the formation of borylated lactams such as boronic ester **(±)-2.092** using B₂Pin₂ and a Pd catalyst in yields of up to 79%.²⁴⁵ Additionally, Lautens *et al.* reported a cyclisation to form tetrahydropyrans such as **(±)-2.094** with an *exo*-cyclic boronic ester, again using B₂Pin₂ and a Pd catalyst in up to 82% yield.²⁴⁶ These two reactions showed that it was possible to achieve both a 5-membered cyclisation and a cyclisation to form an *O*-containing heterocycle, therefore, it was reasoned that under similar reaction conditions it should be possible to affect this transformation onto aryl iodide **2.085**.

Scheme 2.18. Literature precedent for a Heck/Miyaura Borylation cascade reaction.^{245, 246}

Vachhani:



Lautens:

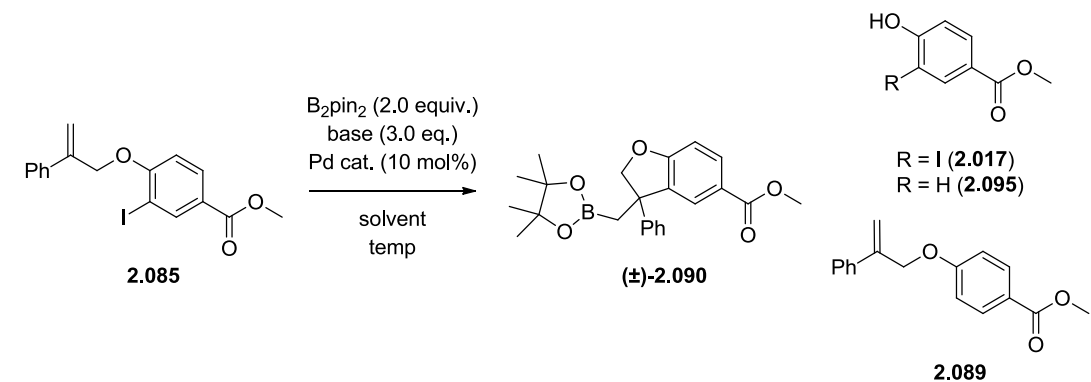


a) Pd(PPh₃)₄ (2 mol%), B₂pin₂ (2.0 eq.), Na₂CO₃ (2.0 eq.), MeCN:water, mw, 120 °C, 40 min, 79%; b) Pd₂(dba)₃ (2 mol%), B₂pin₂ (1.5 eq.), KOAc (1.5 eq.), DMF, 80 °C, 2 h, 82%.

An investigation was then initiated to find optimal conditions for the synthesis of boronic ester **(±)-2.090** (Table 2.07). Initially, the literature conditions reported by Vachhani and Lautens were recapitulated. It was encouraging that immediate evidence for boronate **(±)-2.090** was observed, however, neither of these conditions gave high enough conversion to the desired product to be considered practical moving forward (Entries 1–2). Several side-products were observed in the reaction mixture which were consistent with dehalogenation to form **2.017** as well as subsequent deallylation to form **2.095**. In addition, deallylation of the starting iodide to form **2.089** was also observed. As neither set of literature conditions had given sufficient conversion, alternative conditions were looked for. It was believed that the rate of cyclisation was far greater than the rate of transmetallation, therefore, it was hypothesised that conditions which had been optimised for the Miyaura borylation reaction would lead to higher conversion to the desired product **(±)-2.090**. To adopt this strategy, the conditions for direct cross-coupling of haloarenes to B₂pin₂, which used a Pd(dppf)Cl₂ catalyst and KOAc base, originally reported by Miyaura *et al.* were then examined.²⁴⁷ However, no improvements were seen over the initial reactions (Entry 3). Changing the base to TEA, gave no conversion to the desired product **(±)-2.090** (Entry 4).²⁴⁸ Literature conditions for the borylation of unreactive substrates were then investigated. Molander *et al.* had reported the use of XPhos Pd G2 for the synthesis of aryl boronic esters from aryl chlorides in high yield.²⁴⁹ These conditions overcame the lower reactivity observed with aryl chlorides and it was

hoped they would prove efficient in the synthesis of DBF (\pm)-**2.090**. A higher conversion to boronic ester (\pm)-**2.090** was observed (49%) with minimal side-product formation.

Table 2.07. Optimisation of a Heck/Miyaura borylation cascade reaction

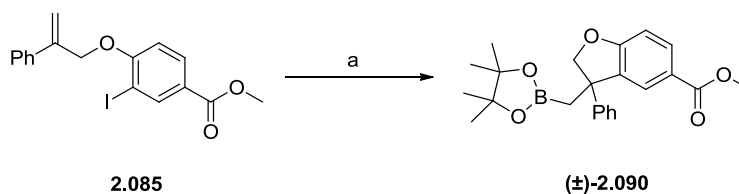


	Catalyst	Base	Solvent	Temp (°C)	2.090 (%)	2.017 (%)	2.094 (%)	2.089 (%)	2.085 (%)
1	Pd(PPh ₃) ₄	Na ₂ CO ₃	MeCN:water (10:1)	100	20	4	1	22	0
2	Pd ₂ (dba) ₃	KOAc	DMF	100	14	15	9	23	15
3	Pd(dppf)Cl ₂	KOAc	1,4-dioxane	100	17	21	4	14	22
4	Pd(dppf)Cl ₂	TEA	1,4-dioxane	100	0	9	3	0	81
5	XPhos Pd G2	KOAc	EtOH	100	49	0	0	6	12

Peak areas calculated from LCMS trace of reaction mixture.

The one-pot cyclisation/borylation reaction was then conducted on a 50 mg scale using the optimised conditions to isolate and characterise boronic ester (\pm)-**2.090** (Scheme 2.19). The reaction proceeded in 84% isolated yield to afford the desired boronic ester (\pm)-**2.090** which could be utilised as a synthetic handle to further functionalise the quaternary centre.

Scheme 2.19. One-pot Heck cyclisation and Miyaura borylation.

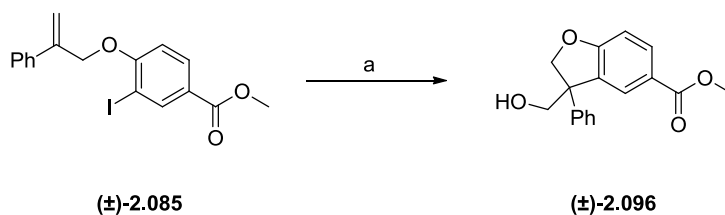


a) XPhos Pd G2 (10 mol%), KOAc (3.0 eq.), B₂pin₂ (2.0 eq.), EtOH, 100 °C, 4 h, 84%.

To insert a CH₂OH quaternary centre, oxidation to the alcohol was considered. However, exploration of a one-pot cyclisation/borylation/oxidation reaction was seen as a more

expedient approach which would streamline the synthesis of DBF (**±**)-**2.095**. The Heck cyclisation/Miyaura borylation was repeated with iodide **2.085**, however, upon consumption of the starting material, the reaction was cool to 0 °C before hydrogen peroxide and NaOH were added to the reaction (Scheme 2.20). This furnished desired alcohol (**±**)-**2.096** in 85% yield. Oxone[®] was also investigated as the oxidising agent, but no conversion to the desired alcohol was observed.²⁵⁰

Scheme 2.20. One-pot Heck cyclisation, Miyaura borylation and oxidation procedure.



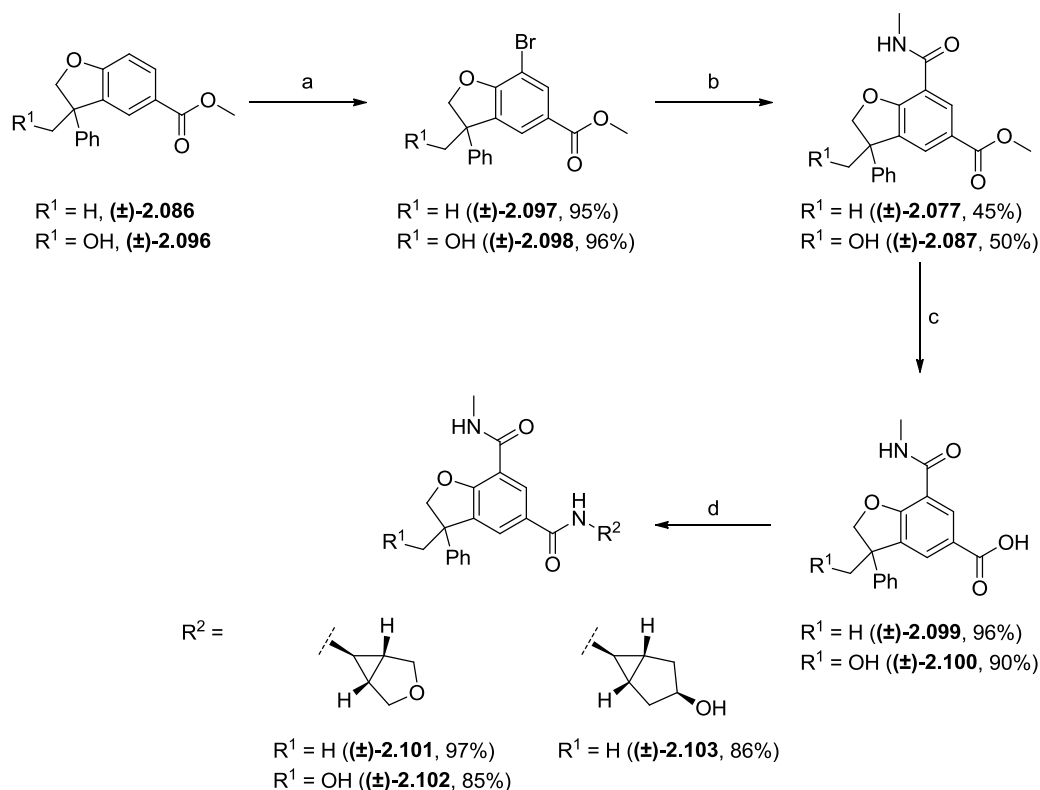
a) i) XPhos Pd G2 (10 mol%), KOAc (3.0 eq.), B₂pin₂ (2.0 eq.), EtOH, 100 °C, 4 h; ii) H₂O₂ (10 eq.), NaOH (1.0 eq.), 0 °C, 4 h, 85%.

2.4.3. Synthesis of DBFs **2.101-2.103**

Having optimised the installation of both the Me and CH₂OH quaternary centres, it was now necessary to introduce the key methylamide warhead and amide vector substituents onto the DBF core (Scheme 2.21). Fluorination would be attempted at a later stage to provide the most convergent route. Bromination of the core was directed to the 7-position by the *ortho* electron donating phenolic ether and the *meta* electron withdrawing ester to give a single regioisomer. In this case only bromination occurred, as oxidation to the benzofuran (which occurred when bromination of DBF (**±**)-**2.019** was examined) was not possible (*c.f.* Scheme 2.08, Section 2.2.5). Subsequently, the methylamide warhead could be installed directly through a Pd catalysed aminocarbonylation reaction. Mechanistically, the CO inserts into the Pd-aryl bond after the initial oxidative addition step, which subsequently undergoes reductive elimination with the amine nucleophile to form an amide.^{251, 252} There has been considerable work in this area looking for conditions suitable to lower CO pressures or which do not require CO gas. In this case, CO is released *in situ* by cobalt carbonyl, negating the need to use CO gas.²⁵³ Overall the reaction proceeded in 30-45% yield. Hydrolysis of the ester was achieved using LiOH in water and THF in high yield. The *meso* oxabicyclic amine was then installed using a HATU mediated amide coupling to give (**±**)-**2.101** and (**±**)-**2.102** in 97% and 85% yield respectively. The oxabicycle was chosen as the optimal substituent from previous

SAR as it provided a good balance of properties whilst also providing a matched pair for analysis of the SAR. The single enantiomers of DBF (\pm)-**2.101** was then obtained by purification using a chiral stationary phase and the absolute stereochemistry of the most potent enantiomer was assigned as (*S*) based on X-ray crystallography of this compound (Figure 2.16, Section 2.5.2). The single enantiomer of DBF (\pm)-**2.102** was synthesised by another member of the team but used in the SAR analysis for clarity.

Scheme 2.21. Synthesis of Quaternary DBFs (\pm)-**2.101**–**2.103**.



a) Bromine (5.0 eq.), CH_2Cl_2 , rt, 1h, 95-96%; b) Methylamine hydrochloride (2.4 eq.), $\text{Pd}(\text{OAc})_2$ (20 mol%), Xantphos (20 mol%), $\text{Co}(\text{CO})_8$ (0.5 eq.), DMAP (4.0 eq.), 1,4-dioxane, mw, 100 °C, 4 h, 45-50%; c) LiOH (2.0 eq.), THF:water, 50 °C, 2-3 h, 90-96%; d) (1*R*,5*S*,6*R*)-3-oxabicyclo[3.1.0]hexan-6-amine (1.1 eq.), HATU (1.2 eq.), DIPEA (3.0 eq.), CH_2Cl_2 , rt, 85-97%.

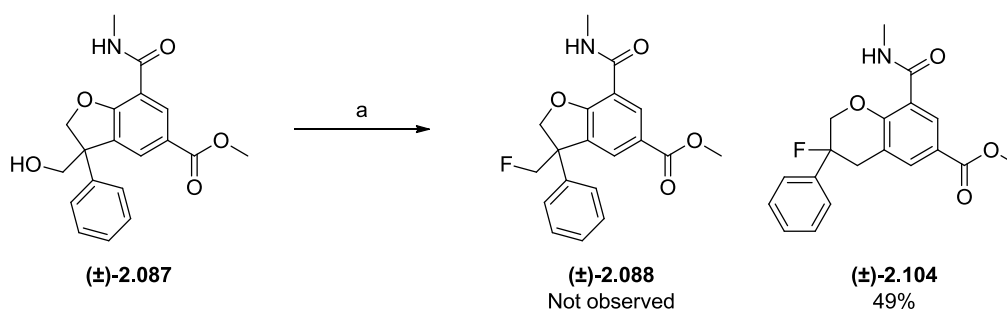
Bicyclic hexanol (\pm)-**2.103**, which was predicted to reside in a desirable physico-chemical space, was synthesised in 86% yield. Earlier work had shown that *exo*-cyclic alcohol (*S*)-**2.064** was potent and selective and lowered the lipophilicity of the DBF, it was therefore hypothesised to mitigate the ChromLogD increase caused by the methyl quaternary centre (see Table 2.03). The single enantiomers of DBF (\pm)-**2.101** were then obtained by purification

using a chiral stationary phase. The absolute configuration of the most potent enantiomer of (\pm)-**2.103** was assigned as (*S*) in accordance with X-ray crystallography of DBF (*S,S*)-**2.101**.

2.4.4. Targeting a CH_2F Quaternary centre

Early work on the DBF series had identified GSK973 (*S,S*)-**1.46**, which contained a CH_2F substituent at the 2-position of the DBF. The fluoro group was a useful tool to balance the physico-chemical properties of the series without inserting an additional H-bond donor.^{254, 255} Although not expected to be as polar as alcohol (\pm)-**2.102**, the fluorinated quaternary centre was predicted to reduce the ChromLogD compared to the methyl (\pm)-**2.102**. Therefore, DBF (\pm)-**2.088** was a desirable target. The synthesis of DBF (*S,S*)-**1.46** had installed the fluorine atom through a deoxy fluorination reaction in 71% yield (see Scheme 2.01, Section 2.2.1). It was hypothesised that a similar strategy could be employed to convert alcohol (\pm)-**2.087** into fluoride (\pm)-**2.088**.²⁵⁶ However, when this was attempted using Deoxo-Fluor[®] only 6-membered dihydropyran (\pm)-**2.104** was isolated from the reaction mixture (Scheme 2.22). Formation of any of the desired product (\pm)-**2.088** was not observed.

Scheme 2.22. Proposed synthesis of fluoro compound **2.088**.



a) Deoxo-Fluor[®] (50% w/w in THF, 2.0 eq.), CH_2Cl_2 , 40 °C, 1 h.

The formation of the 6-membered ring can be rationalised by looking at the reaction mechanism (Figure 2.16). Firstly, the oxygen attacks the sulfur trifluoride to displace a fluoride ion. The nitrogen lone pair eliminates another fluoride to form activated alcohol (\pm)-**2.087b** which is primed as a stable leaving group. Normally, one of the displaced fluorides would act as a nucleophile at this stage and displace the oxygen in a S_N2 process, however, this is not observed. In this instance it is possible that the *neopentyl*ic oxygen is too sterically hindered to undergo nucleophilic substitution. Instead a pinacol-like rearrangement occurs

to form a stabilised tertiary, benzylic carbocation (**(±)**-2.087c.²⁵⁷ The carbocation can then be quenched by fluoride in the reaction mixture leading to the observed product.

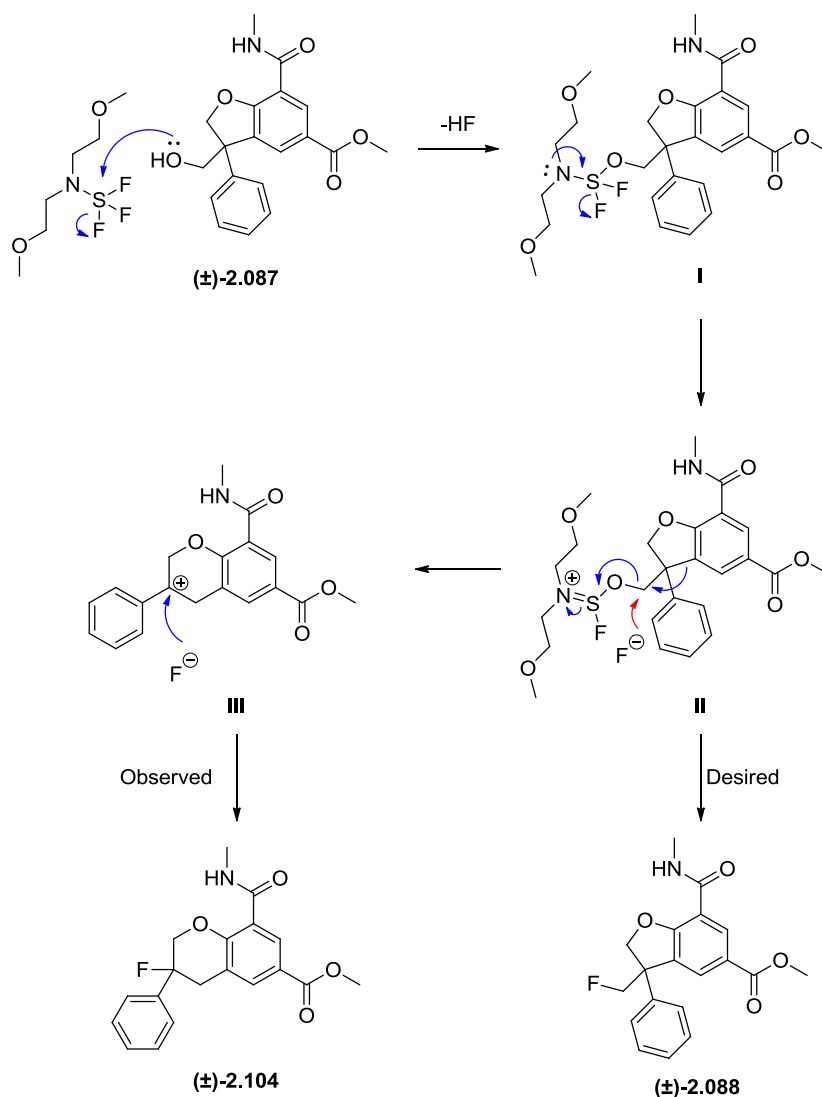


Figure 2.16. Proposed mechanism for the fluorination/rearrangement of DBF (**(±)**-2.087) to form fluoride (**(±)**-2.104). The rearrangement is shown by the blue arrows and the desired attack of the fluoride ion through an S_N2 mechanism, by the red arrow.

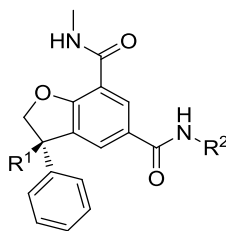
Alternative approaches which looked at other deoxy-fluorinating reagents were explored within the group. However, they still led to a rearrangement rather than the desired product. Future work will look at alternative routes to install the fluorine from a boronic ester intermediate, for example, using copper catalysis as pioneered by the Sandford lab.²⁵⁸

2.5. Investigating the SAR of the DBFs with a Quaternary Centre

2.5.1. SAR of the Quaternary Vector

With a suitable synthetic strategy established, the effect of inserting a quaternary centre at the C3 position of the DBF series could now be explored (Table 2.08). Firstly, a comparison of the matched molecular pairs utilising the oxabicyclic amide was conducted. The methyl quaternary centre (DBF **(S)**-2.101, Entry 2) maintained potency at BRD4 BD2 ($pIC_{50} = 7.5$) relative to the unsubstituted DBF **(S)**-2.039 (Entry 1, $pIC_{50} = 7.8$) albeit with a slight reduction in selectivity to 630-fold. This trend was mirrored with a CH_2OH substituent (**(S)**-2.102, Entry 3) which was equipotent and selective to DBF **(S)**-2.101. Unsurprisingly, the additional methyl group present in DBF **(S)**-2.101 increased the ChromLogD by 0.4 log units from 3.3 to 3.7 relative to DBF **(S)**-2.039 (Entry 1). Addition of an alcohol served to lower the lipophilicity through introduction of polarity and a hydrogen-bond donor (ChromLogD = 2.4) although these factors were predicted to limit bioavailability. Both DBFs (**(S)**-2.101 and **(S)**-2.102) had high solubility ($\geq 147 \mu g mL^{-1}$) and were therefore progressed to rat IVC, to assess whether a quaternary centre was able to mitigate the metabolic liabilities of the DBF core. Pleasingly, both 3,3-disubstituted DBFs **(S)**-2.101 and **(S)**-2.102 showed improved rat hepatocyte stability (Entries 2-3, $\leq 1.4 mL min^{-1} g^{-1}$) compared to DBF **(S)**-2.039. This validated the hypothesis that insertion of the quaternary centre would improve the metabolic stability of the template. DBF **(S)**-2.101 was chosen for *in vivo* PK studies due to its preferential ChromLogD (Section 1.6.3). The SAR of the amide vector with a quaternary DBF core was then explored. Methyl amide **(S)**-2.105 (Entry 4) was less potent at BRD4 BD2 ($pIC_{50} = 7.1$) and more active at BRD4 BD1 ($pIC_{50} = 5.3$) than the oxabicyclic amide **(S)**-2.101, which was concomitant with a reduction in selectivity to 63-fold. As seen previously (Section 2.3), the selectivity of the series could be increased by insertion of a cyclopropyl (**2.106**) or methyl cyclopropyl (**(S,S,S)**-2.107) amide which were 630 and 790-fold selective respectively. However, due to the additional quaternary methyl, both compounds were highly lipophilic (ChromLogD ≥ 4.0). Compound **2.106** was tested in rat hepatocytes and had a raised clearance of $6.7 mL min^{-1} g^{-1}$ which was likely a function of this increased lipophilicity. Therefore, **(S,S,S)**-2.107 was not progressed to assess rat IVC.

Table 2.08. Exploration of the effect of a quaternary centre at the 3-position of the DBF.



	R ¹	R ²	BRD4 BD2 pIC ₅₀ (n) / BD1 pIC ₅₀ (n) Selectivity	Chrom LogD _{7.4}	CAD Solubility (μg mL ⁻¹)	Rat IVC (mL min ⁻¹ g ⁻¹)
1	H (S)-2.039		7.8(8) / 4.8(8) 1000x	3.3	≥143 ^b	8.6
2	Me (S)-2.101		7.5(8) / 4.7(8) 630x	3.7	≥147	1.2
3	CH ₂ OH (S)-2.102		7.4(6) / 4.6(7) 630x	2.4	≥202	1.4
4 ^a	Me (S)-2.105	Me	7.1(4) / 5.3(4) 63x	3.4	≥132	8.9
5 ^a	Me (S)-2.106		7.3(4) / 4.5(4) 630x	4.0	≥138	6.7
6 ^a	Me (S,S,S)- 2.107		7.6(4) / 4.7(4) 790x	4.7	3	-
7 ^a	CH ₂ OH (S,S,S)- 2.108		7.5(5) / 4.6(7) 790x	3.3	≥123	2.7
8 ^a	Me (S)-2.109		6.5(4) / <4.3(4) >130x	3.3	≥161	-
9	Me (S)-2.103		7.8(8) / 4.8(8) 1000x	3.3	≥133	1.0
10 ^a	Me (S)-2.110		7.9(2) / 4.7(2) 1600x	3.7	≥151	6.4

^aPrepared by colleagues at GSK; ^bCLND solubility.

GSK Confidential – Do not copy

The lipophilicity of the methyl cyclopropyl amide **(S,S,S)-2.107** could be reduced (ChromLogD = 3.3) by installation of the CH₂OH quaternary centre to afford DBF **(S,S,S)-2.108**. Pleasingly, potency and selectivity were maintained and the high CLND solubility ($\geq 123 \mu\text{g mL}^{-1}$) provided a strong rationale to assess the rat IVC. Although the rat hepatocyte clearance was slightly raised ($2.7 \text{ mL min}^{-1} \text{ g}^{-1}$), DBF **(S,S,S)-2.108** was progressed to study the *in vivo* PK which will be discussed in Section 2.5.3. The cyclohexanol amide had been optimal in the development of **(S)-1.43** (GSK046, Section 1.6.1), therefore, the DBF analogue **(S)-2.109** was examined. Interestingly, the cyclohexanol amide was not well tolerated in this series and had sub optimal potency at BRD4 BD2 ($\text{pIC}_{50} = 6.4$). However, DBFs **(S,S,S)-2.108** and **(S)-2.109** showed that the addition of another H-bond donor placed the series in the optimal physico-chemical space (ChromLogD = 3.3 for both examples). Therefore, the exo-cyclic alcohol amide group which had been well tolerated previously (Table 2.03, Entry 11) was investigated as it combined the cyclopropyl moiety vital for potency and selectivity with a more polar alcohol. Both diastereomers of the alcohol were prepared. DBF **(S)-2.103** was potent at BRD4 BD2 ($\text{pIC}_{50} = 7.8$) and 1000-fold selective. As predicted, it had a desirable ChromLogD value of 3.3 and a high CAD solubility of $\geq 133 \mu\text{g mL}^{-1}$ and was therefore progressed to rat IVC studies. Pleasingly, DBF **(S)-2.103** showed the lowest rat clearance of all the DBFs tested ($1.0 \text{ mL min}^{-1} \text{ g}^{-1}$) and was therefore progressed to *in vivo* PK (Section 2.5.3). Interestingly, the diastereomer, DBF **(S)-2.110** was more potent (BRD4 BD2 $\text{pIC}_{50} = 7.9$) and selective (1600-fold). However, IVC data on this diastereomer showed that it had high clearance in rat hepatocytes and was therefore not progressed.

2.5.2. X-ray Crystallography of **2.101**

To understand whether the quaternary C3 carbon impacted the binding mode of the DBF series, an X-ray crystal structure of **(S)-2.101** in BRD2 BD2 was solved and compared to DBF analogues **(S)-2.056** and **(S,S)-1.46**. Figure 2.17 shows that the quaternary DBF **(S)-2.101** makes the same interactions as previous DBF examples. The methylamide warhead mimics the interactions of KAc whilst the bidentate interaction of the second amide to Asn429 still forces the phenyl group between the WPF shelf and BD2 specific His433 conferring BD2 potency and selectivity. The quaternary methyl group occupies a space between the lipophilic WPF shelf region and a lipophilic region of the ZA loop, although the SAR (Table 2.08, Entry 2 vs. Entry 1) suggests this is only tolerated and not optimal for potency. The X-ray crystal structures of DBFs **(S,S)-1.46** and **(S)-2.056** were then overlaid to compare how

they interacted with BRD2 BD2. As shown in Figure 2.16, the nature of binding is highly homologous between the three DBFs.

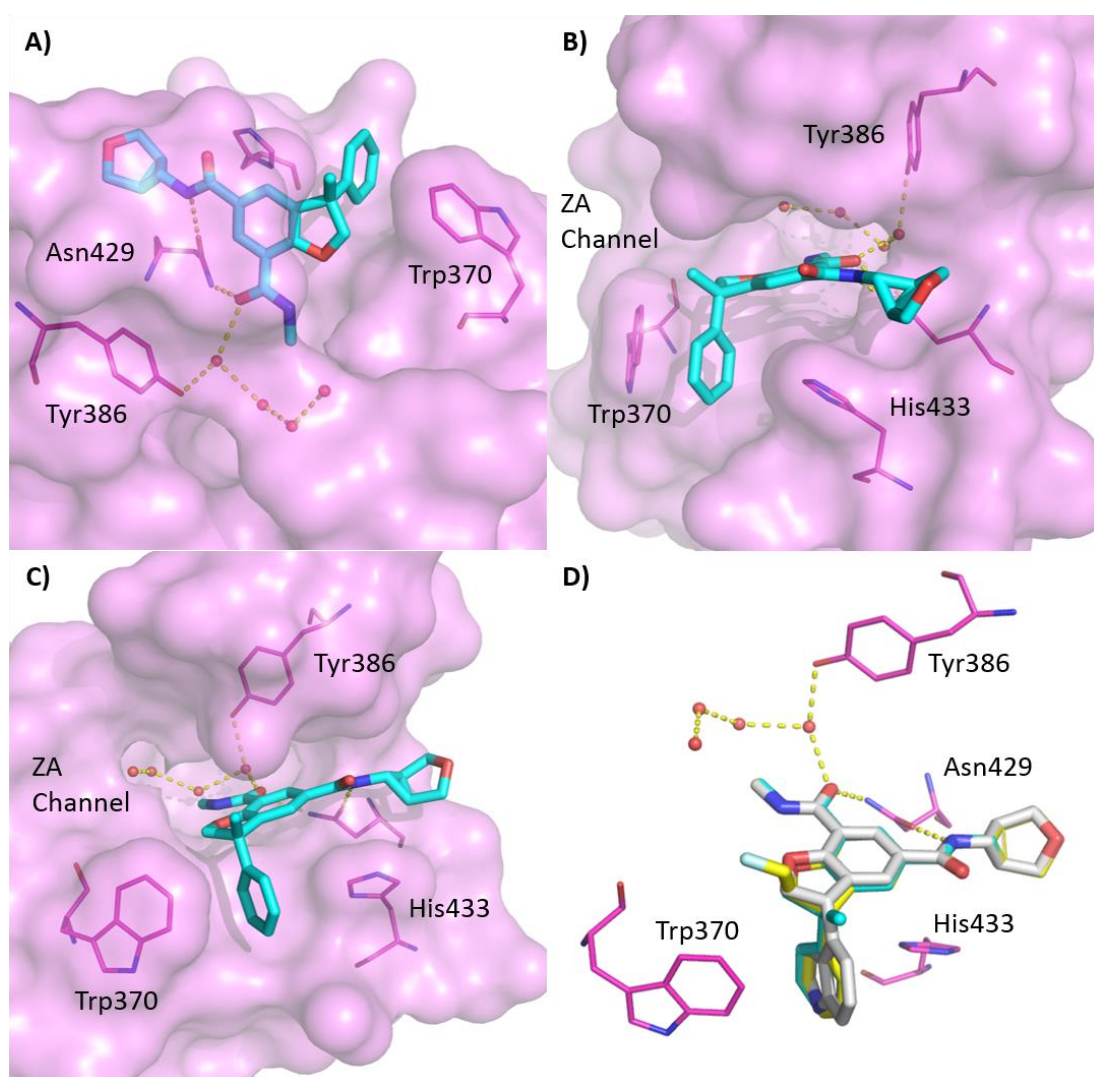
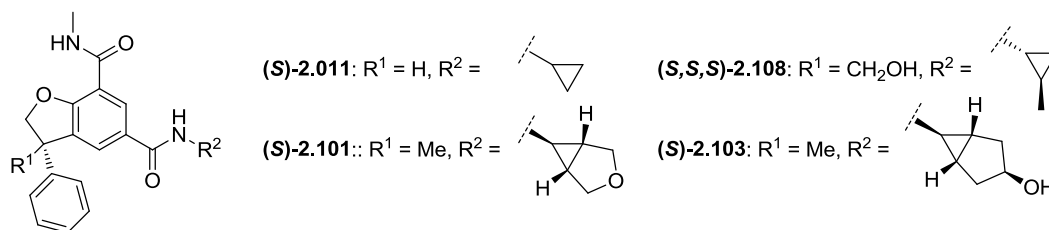


Figure 2.17. X-ray crystallography of (S)-2.101 (teal) in BRD2 BD2 (pink). Key residues are shown as magenta lines, H-bonds as dashed yellow lines and waters as red spheres. A) DBF (S)-2.101 makes a through water interaction with Tyr386 and a bidentate H-bonding interaction to Asn429. B-C) The phenyl C3 group is then placed between the BD2 specific His433 and Trp370 of the WPF shelf. The C3 methyl occupies a lipophilic area adjacent to the WPF shelf. D) DBF (S,S)-1.46 (yellow) and DBF (S)-2.056 (silver) are shown for comparison and a high degree of overlay is observed.

2.5.3. *In Vivo* PK Profile of DBFs **(S)-2.101**, **(S,S,S)-2.108** and **(S)-2.103**

The reduced IVC values observed for DBFs **(S)-2.101**, **(S,S,S)-2.108** and **(S)-2.103** were promising, as they validated the initial hypothesis that a quaternary centre could improve the metabolic stability of the series. The *in vivo* PK, cellular target engagement and thermodynamic solubility could now be assessed and compared to DBF **(S)-2.011** (Table 2.09). DBF **(S)-2.101** was potent in both the phenotypic LPS stimulated PBMC ($pIC_{50} = 8.1$) and hWB assays ($pIC_{50} = 6.8$). To understand whether the improved IVC for this compound would translate *in vivo*, the rat PK was investigated. DBF **(S)-2.101** had a moderate blood clearance of $61 \text{ mL min}^{-1} \text{ kg}^{-1}$, or 77% of the liver blood flow, however, the CL_{FU} was $274 \text{ mL min}^{-1} \text{ kg}^{-1}$, which was significantly lower than for **(S)-2.011**. DBF **(S)-2.101** had good oral bioavailability of 54%. Unfortunately, the FaSSIF solubility of DBF **(S)-2.101** was still sub-optimal ($82 \text{ } \mu\text{g mL}^{-1}$). DBF **(S,S,S)-2.108** was also potent in the hWB assay ($pIC_{50} = 7.0$). Importantly, **(S,S,S)-2.108** had a high FaSSIF solubility ($>1000 \text{ } \mu\text{g mL}^{-1}$), most likely caused by the reduced lipophilicity and additional H-bond donor compared to DBF **(S)-2.101**. Therefore, despite the slightly raised IVC ($2.7 \text{ mL min}^{-1} \text{ g}^{-1}$), DBF **(S,S,S)-2.108** was investigated *in vivo*. Although, the IVC of DBF **(S,S,S)-2.108** was raised relative to DBF **(S)-2.101**, they had the same blood clearance *in vivo*, although the higher protein binding of **(S,S,S)-2.108** meant a higher unbound clearance. Interestingly, the bioavailability of DBF **(S,S,S)-2.108** was reduced compared to DBF **(S)-2.101** although this was still consistent with the observed clearance and was likely a first pass effect. Nonetheless the rat *in vivo* data looked promising, however, due to elevated dog IVC data, progression into dog PK studies was halted. Finally, DBF **(S)-2.103** was highly potent in PBMC ($pIC_{50} = 7.7$) and hWB assays ($pIC_{50} = 7.8$). Previously, DBFs **(S)-2.011** and **(S)-2.101** had shown a 10-fold reduction in potency between PBMC and hWB assays, but, **(S)-2.103** was equipotent in the two assays. Pleasingly, **(S)-2.103** was highly soluble by both FaSSIF ($>1000 \text{ } \mu\text{g mL}^{-1}$) and CAD ($\geq 133 \text{ } \mu\text{g mL}^{-1}$) assessment. The low IVC data gave strong rationale for progression into *in vivo* PK studies. Again, a moderate blood clearance of $55 \text{ mL min}^{-1} \text{ kg}^{-1}$ was observed equating to 69% LBF, the lowest unbound clearance was observed for **(S)-2.103**. The oral bioavailability (32%) is once again consistent with the %LBF observed, and was sufficient for progression into a second species. Overall, the excellent profile of DBF **(S)-2.103** made it a suitable candidate for progression into dog *in vivo* PK studies. **(S)-2.103** had a low clearance in dog ($5 \text{ mL min}^{-1} \text{ kg}^{-1}$) and was 64% orally bioavailable. Thus, **(S)-2.103** demonstrated suitable *in vivo* PK in two species.

Table 2.09. Further profiling of DBFs (S)-2.101, (S,S,S)-2.108 and (S)-2.103.



Compound		(S)-2.011	(S)-2.101	(S,S,S)-2.108	(S)-2.103
BRD4 BD2 pIC ₅₀ (n) / BD1 pIC ₅₀ (n)		7.7(10) / 4.8(10)	7.5(8) / 4.7(8)	7.5(5) / 4.6(7)	7.8(8) / 4.8(8)
Selectivity		790x	630x	790x	1000x
BRD4 BD2 LE/LLE _{at}		0.42 / 0.40	0.35 / 0.36	0.37 / 0.39	0.36 / 0.40
PBMC pIC ₅₀ (n) ^b		7.7(2)	8.1(2)	-	7.7(2)
hWB MCP-1 pIC ₅₀ (n) ^b		6.9(2)	6.8(2)	7.0(2)	7.7(2)
CAD Solubility (µg mL ⁻¹)		≥141 ^a	≥147	≥123	≥133
FaSSiF Solubility (µg mL ⁻¹)		28	82	>1000	>1000
AMP (nm s ⁻¹)		300	153	210	82
IVC (mL min ⁻¹ g ⁻¹)	Rat	2.0	1.2	2.7	1.0
	Dog	<0.7	<0.7	1.0	<0.7
	Human ^b	<0.5	<0.5	<0.5	<0.5
Rat IV PK ^c	CL _b / CL _{FU} (mL min ⁻¹ kg ⁻¹)	34 / 723	61 / 274	60 / 340	55 / 260
	%LBF	43	77	60	69
	V _{ss} (L kg ⁻¹)	0.6	1.6	1.2	2.3
Rat Oral PK ^c	T _{1/2} (h)	0.3	0.3	0.3	0.7
	Fpo (%)	47	54	38	32
	CL _b / CL _{FU} (mL min ⁻¹ kg ⁻¹)	-	-	-	5 / 27
Dog IV PK ^c	%LBF	-	-	-	8
	V _{ss} (L kg ⁻¹)	-	-	-	0.9
	T _{1/2} (h)	-	-	-	2.9
Dog Oral PK ^c	Fpo (%)	-	-	-	64

^aCLND solubility; ^bThe human biological samples were sourced ethically and their research use was in accord with the terms of the informed consents under an IRB/EC approved protocol; ^cAll animal studies were ethically reviewed and carried out in accordance with Animals (Scientific Procedures) Act 1986 and the GSK Policy on the Care, Welfare and Treatment of Animals.

(S)-2.103 also has human hepatocyte IVC of <0.5 (along with all of the other leads). Here it has been shown that rat and dog correlate *in vitro* and *in vivo*, which is suggestive of a low/moderate human clearance prediction.

2.6. Conclusions and Future Work on the DBF Series

The aim of this work was to develop a highly potent BET inhibitor with 1000-fold selectivity for the BD2 domain which had suitable PK and solubility for progression as a pre-candidate. This was achieved by investing in the development of a new, robust, synthetic strategy to access the DBF template. The routes developed allowed for a full exploration of the SAR of the DBF C3 substituent. Due to metabolic liabilities of this series attributed to oxidation of the DBF ring, a quaternary DBF was envisioned which was also predicted to improve the sub-optimal FaSSIF solubility of DBF **(S)-2.011**. A novel route to synthesise the complex DBF core was developed which relied on a key reductive Heck cyclisation to install the methylated quaternary centre. Further functionalisation of the quaternary vector was achieved through a tandem cyclisation/borylation/oxidation procedure to access a CH₂OH group. The routes developed allowed access to a series of DBFs which showed improved metabolic stability and higher FaSSIF solubility relative to the DBFs profiled previously. This work identified GSK852 **((S)-2.103)** a potent, 1000-fold selective, highly soluble compound with good *in vivo* rat and dog PK as a promising pre-candidate molecule (Figure 2.18). As such, work to understand the dose prediction, pre-clinical safety and efficacy in both oncology and immuno-inflammation indications has been initiated.

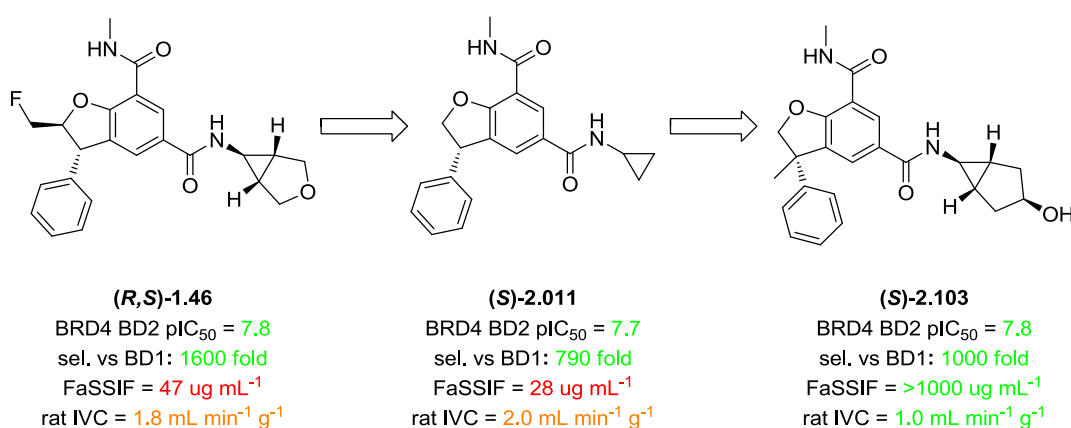
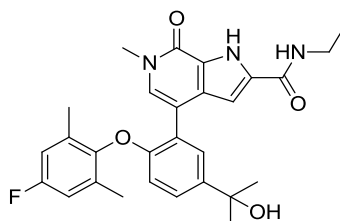


Figure 2.18. Development of DBF **(S)-2.103** a highly potent and selective BD2 BET inhibitor with improved solubility and rat PK.

GSK Confidential – Do not copy

It is clear that BET inhibitors exhibit a strong potential to treat both oncology and inflammatory conditions. However, the development of a marketable medicine will rely on being able to achieve efficacy at a safe dose. DBF (**S**)-**2.103** represents an exciting opportunity to understand whether highly BD2 selective BET inhibitors will offer a different clinical outlook from pan-BET compounds. Interestingly, whilst carrying out this work AbbVie reported ABBV-744 (**2.111**, Figure 2.19), a BD2 selective BET inhibitor which has recently entered the clinic for advanced prostate cancer and relapsed/refractory AML.²⁵⁹ ABBV-744 (**2.111**) is reportedly 300-fold selective and the clinical end points of this study will be closely monitored to assess whether improved safety margins are observed based on this improved selectivity profile.



ABBV-744, **2.111**

Figure 2.19. ABBV-744 (**2.111**); a BD2 selective BET inhibitor reported by AbbVie for the treatment of advanced prostate cancer and AML.

3. Development of a Chemical Probe for CECR2

Whilst the BET family represent well validated targets in drug discovery, they represent just 8 of the 61 known human BRDs.⁸² Due to the mechanism by which BET inhibitors are believed to work (*i.e.* by regulating gene expression of enhancer regions critical to the molecular mechanism of disease), it has been hypothesised that other BCPs are likely to control the expression of genes crucial to other diseases.^{83, 260} Despite this promising hypothesis, the pharmacological relevance of inhibiting these BRDs using small molecules is still largely unknown. Therefore, before investment in a full drug discovery programme, these targets need to be fully validated.²⁶¹

3.1. Chemical Probes for Target Validation

Target validation, or proving that the target protein has a key role in disease, is critical for successful target-based drug discovery. Commonly, the up- and down-regulation of specific genes, proteins or biomarkers in disease is investigated to identify potential therapeutic targets. The effect of deactivating entire proteins through protein knockdown experiments, using RNA interference techniques, can be explored to further validate the targets identified.²⁶² However, protein knock-down experiments block the action of an entire protein complex including multiple domains and scaffolding functions and may not be representative of the effect of small molecule inhibition. This is particularly important when studying BRDs which are usually part of much larger BCPs which contain multiple domains of different function, for example, the BET family of proteins contain 2 BRDs and an extra terminal domain. Due to the limitations of protein knock-down experiments, chemical probes are increasingly being developed to validate potential drug targets. The expectation is that this effort will lead to new therapeutic targets. However, there is a degree of ambiguity when it comes to a description of what makes a good chemical probe.

Chemical probes differ from drug candidates in a few different ways. As discussed previously (Section 1.1) high levels of target engagement, suitable PK for exposure at the site of action and functional pharmacology are just some of the requirements for a drug candidate. For a chemical probe, suitability for *in vivo* experiments is not a requirement, therefore, demonstrating good PK is not necessary *per se*. However, good PK would lead to the potential for use *in vivo*, which could be valuable to further delineate the target role in a given disease.

For a chemical probe to fulfil its purpose it must display high potency and selectivity for the target of interest. On the other hand, polypharmacology may be acceptable for a drug candidate if it delivers functional pharmacology and is safe. High enough solubility and permeability to prevent assay interference and allow cellular studies are also desirable properties for a chemical probe. There has been discussion in the literature as to the specific criteria which a chemical probe should possess.²⁶³ As such, a list of guidelines based on this discussion can be drawn out which state that probes should display:²⁶⁴

- <100 nM activity in a biological assay ($pIC_{50} > 7.0$)
- 10–100-fold selectivity over significant off-targets
- <1 μ M *in vivo* cell assay potency²⁶⁴

One caveat here is how selectivity is definitively assessed. In the case of a BRD inhibitor, activity at other BRD proteins can be routinely examined. However, there are predicted to be thousands of druggable targets in the human proteasome, therefore, a causative correlation between target engagement and a robust phenotype cannot be confirmed with a single compound. For full target validation, the use of multiple chemical probes with distinct chemotypes will give weight to any discoveries. Confidence in a target is therefore only increased when structurally dissimilar compounds of equal potency both show disease modifying efficacy. Additionally, a structurally similar negative control which is inactive against the target protein is desirable. This is ideally an enantiomer of the tool. For example, in the case of (+)-JQ1 (**1.08**, Section 1.4.2) the opposite enantiomer, (-)-JQ1, can be used as a negative control.²⁶⁵

3.2. Small Molecule inhibitors of non-BET BRDs

Due to the interest in BRDs as therapeutic targets, there has been an explosion of tool molecules being published in the literature.^{49, 52, 83, 137, 139, 260} There are now small molecule inhibitors for 30 of the 61 known human BRDs (Figure 3.01), although it should be noted that this includes inhibitors which display activity at multiple BRDs and therefore their utility as a suitable chemical tool is questionable. For example, PFI-3 (**3.014**, Figure 3.11, Section 3.3.1) is active at all 6 human polybromo 1 (PB1) BRDs. This is due, in part, to the high sequence homology of closely related BRDs and so finding selectivity can be challenging. P300/CBP-

associated factor (PCAF) probes L-Moses and GSK4027 (Figure 5.02, Section 5) are both equipotent at the homologous general control nonderepressible 5 (GCN5) BRD.^{266, 267} Interestingly, the development of chemical probes has not been uniform (Figure 3.01). Significant attention has been given to the development of tools for specific BRDs such as CREB binding protein (CREBBP)/E1a-associated protein p300 (EP300)²⁶⁸⁻²⁷⁶ and BRD7/9.²⁷⁷⁻²⁸¹ This asymmetry in development is most likely caused by multiple factors. The promising results of gene knock-down experiments will encourage the development of the first inhibitor, which leads to a deeper understanding for the requirements of potency and selectivity for a specific BRD. Furthermore, the development of suitable assays during initial probe discovery makes future work on this target more tractable, encouraging others to develop orthogonal tools.

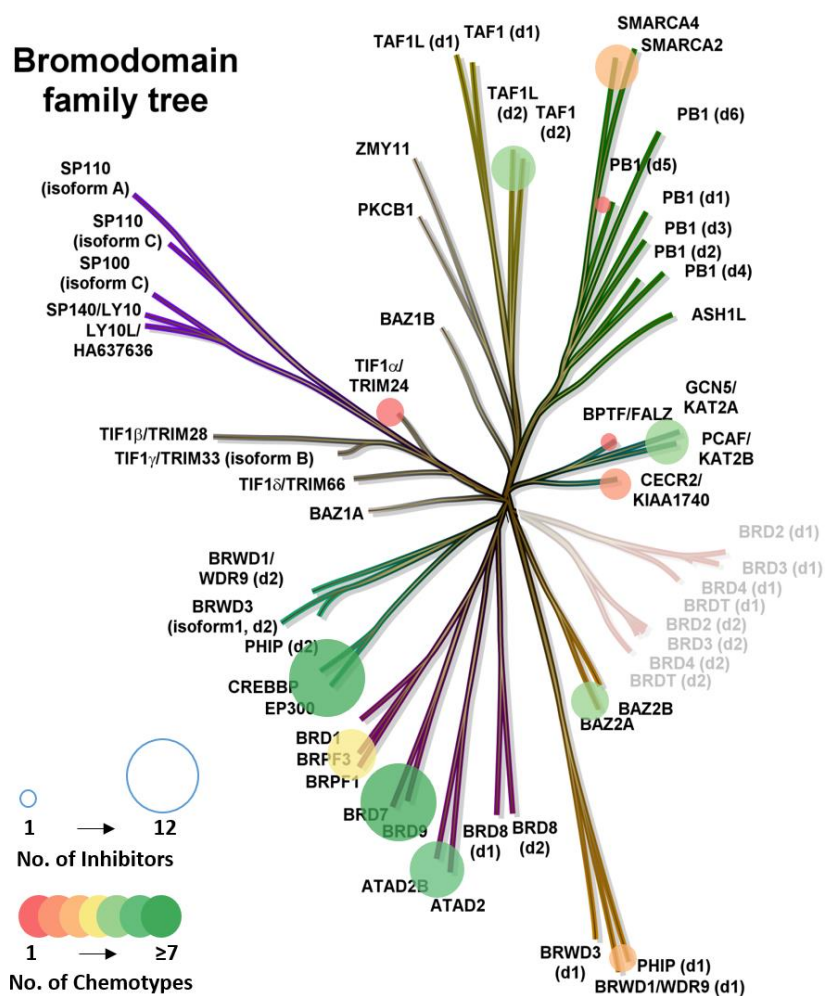


Figure 3.01. BRD phylogenetic tree showing no. of inhibitors and number of distinct chemotypes reported for each non-BET BRD.²⁸²

One BRD of interest for which chemical probes are still desirable is the Cats Eye Chromosome region, candidate 2 (CECR2) BRD. In the search for a CECR2 tool molecule, this thesis details the optimisation of a series of dual ATAD2/CECR2 inhibitors.

3.2.1. ATAD2

ATAD2 is a non-BET BRD containing protein which has been linked to prostate, lung and breast cancer.^{283, 284} It is believed to regulate the transcription of the c-Myc oncoprotein which stimulates aggressive cell proliferation and is strongly linked to the development of cancer.²⁸⁵ As such, small molecule inhibitors of ATAD2 are desirable in order to investigate the phenotype of inhibition and determine its therapeutic potential. There has been discussion and hypotheses generated about the relative druggability of the non-BET BRDs.²⁸⁶⁻²⁸⁸ Vidler *et al.* analysed the BRD family using SiteMap, which gives an *in silico* prediction of druggability based on pocket size and accessibility, and highlighted ATAD2 as one of the least tractable due to its shallow binding site. However, this hypothesis has slowly been discredited, beginning with Fesik *et al.* and Knapp *et al.* publishing fragments **3.001** and **3.002** as weak inhibitors (Figure 3.02).^{288, 289}

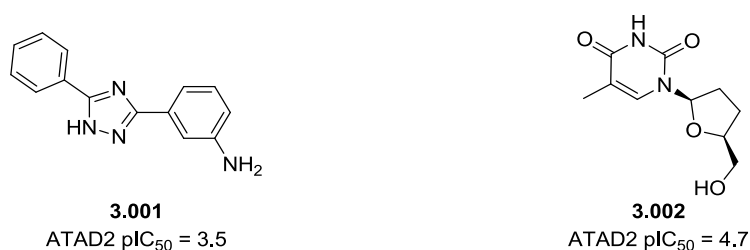


Figure 3.02. Fragments with ATAD2 affinity.

The first small molecule inhibitor of ATAD2 was naphthyridone **3.003** (Figure 3.03), a low micromolar inhibitor, which utilises a methyl pyridone as the AcK mimetic (discussed below).²⁹⁰ Despite showing relatively modest activity compared to the leading BET inhibitors (ATAD2 pIC₅₀ = 5.9) this was a significant step forward against what was predicted to be a low tractability target.²⁸⁶ This initial probe was optimised by targeting interactions with the RVX shelf (*vide infra*) to afford **3.004**, which was more potent (ATAD2 pIC₅₀ = 6.9) and displayed 160-fold selectivity over the BET family.²⁹¹ Further improvement of physico-chemical properties culminated in the identification of the chemical probe GSK8814 (**3.005**), a cell-permeable and selective tool molecule.²⁹² The conformation of the piperidine ring was found

to be pivotal; maintaining the difluoro cyclohexyl moiety in the correct orientation to interact with the RVF shelf in ATAD2 was crucial to maintain potency. Bamborough *et al.* then went on to show that the correct conformation could also be achieved using tropane **3.006** (ATAD2 $pIC_{50} = 7.0$).²⁹³

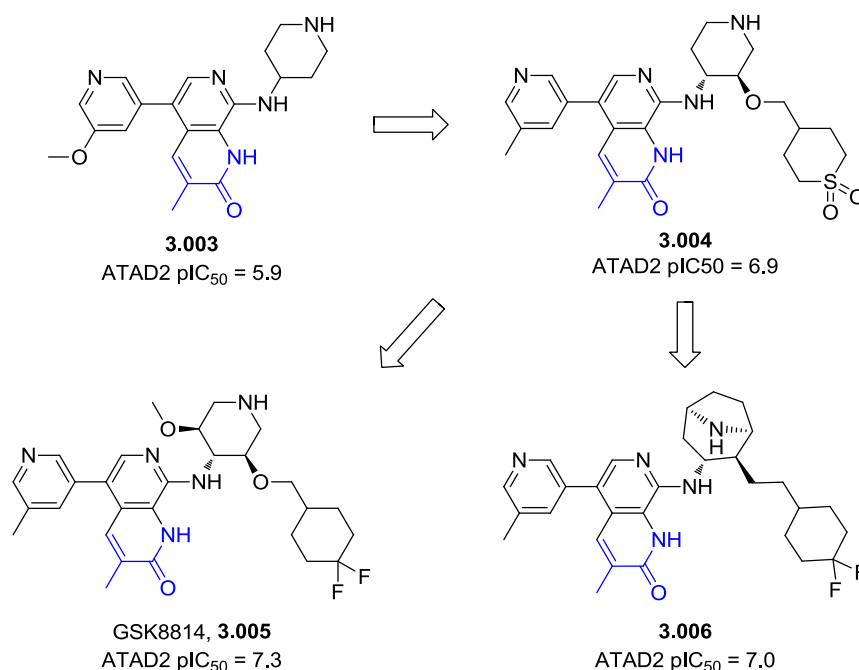


Figure 3.03. Naphthyridone ATAD2 inhibitors with KAc mimetic shown in blue.

Naphthyridones **3.003–3.006** mimic the KAc by making H-bonding interactions through the pyridone carbonyl and nitrogen to Asn1064 (Figure 3.04). The carbonyl group then makes a through water interaction with Tyr1021. The importance of the piperidine conformation is obvious in the crystal structure. The equatorial conformation of the substituents places the methoxy group into a pocket formed by the BC loop and then points the difluoro cyclohexane group towards the RVF residues where it occupies a lipophilic pocket formed by the Ile1074 gatekeeper residue.

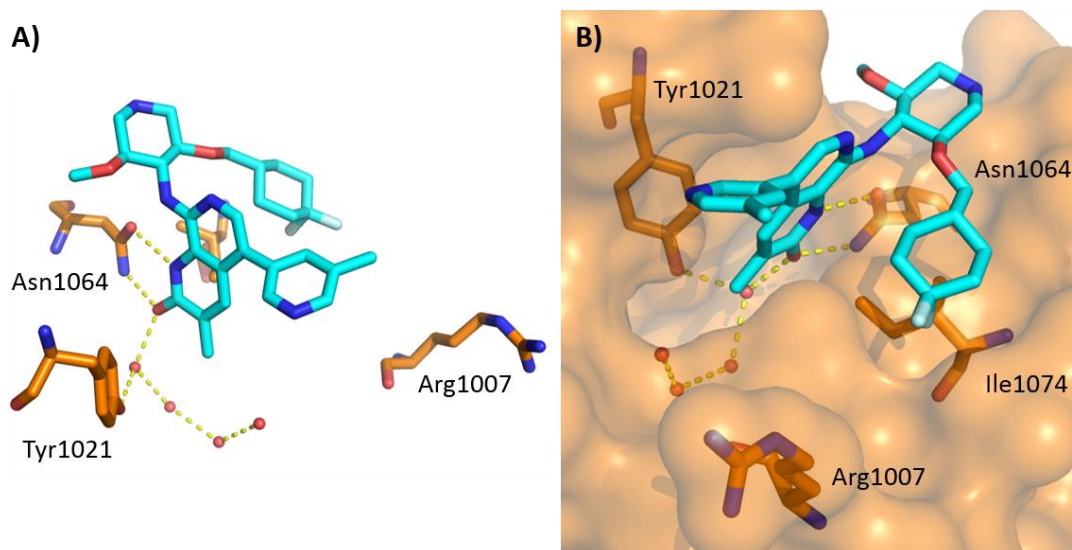
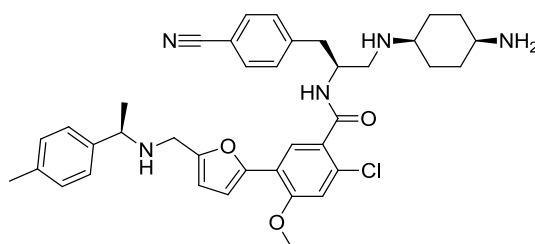


Figure 3.04. X-ray crystal structure (pdb5lj0) of GSK8814 (teal) in ATAD2 (orange) with key residues shown. Water molecules are depicted at red spheres and H-bonds as dashed yellow lines.

More recently, an isoform selective ATAD2 inhibitor, BAY-850 (**3.007**) was published.²⁹⁴ This showed excellent ATAD2 potency ($pIC_{50} = 6.8$) and no inhibition of other BRDs. Whilst evaluating the potency using a thermal shift assay, the authors noted the melting curve was consistent with a shift from mono- to biphasic, suggesting the formation of a new protein species. They further investigated this phenomenon using mass spectrometry and interestingly, they only observed signals consistent with one molecule of **3.007** binding to an ATAD2 dimer. SEC was also consistent with the formation of an ATAD2 dimer although an X-ray crystal structure was not solved to delineate the precise mode of binding. Despite its large size and the presence of 3 basic centres in the structure, **3.007** was shown to be cell permeable using a FRAP assay and as such is a suitable tool compound.



BAY-850, **3.007**
ATAD2 $pIC_{50} = 6.8$

Figure 3.05. BAY-850 (**3.007**), a small molecule ATAD2 inhibitor.

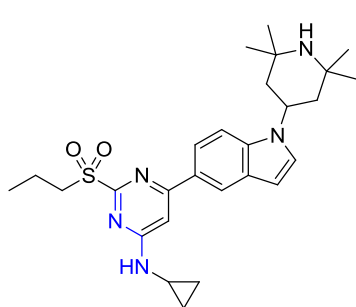
3.2.2. CECR2

CECR2 is a BRD containing transcription factor which was first identified through an examination of the 22q11 chromosome region. Patients with Cats Eye Syndrome are characterised by multiple congenital defects and all have multiple copies of the 22q11 chromosome region present in their DNA. CECR2 is a protein encoded by a gene found in this region of DNA, although the exact role of CECR2 in the development and prognosis of patients with Cats Eye Syndrome is unknown. Down-regulation of CECR2 does cause neural tube defects during development, potentially suggesting that aberrant CECR2 expression is a contributing factor to Cats Eye Syndrome.^{295, 296} The neural tubes developed will later constitute the brain and spinal cord, forming the central nervous system. The process by which neural tubes form during embryo development is called neurulation. CECR2 has been shown to be involved in neurulation through the chromatin remodeling complex SNF2L.²⁹⁷⁻²⁹⁹ Furthermore, CECR2 has also been implicated in the response to DNA double strand breaks, using RNA knockdown experiments.³⁰⁰ If left unchecked, DNA double strand breaks can contribute to the development of cancer. Additionally, CECR2 was linked to c-Myc driven cancer through a functional genomics approach.³⁰¹ Despite the apparent links to diseases such as Cats Eye Syndrome and oncology, the precise role of CECR2 remains unknown. Therefore, high quality chemical probes for CECR2 are desirable to further investigate its biological function.

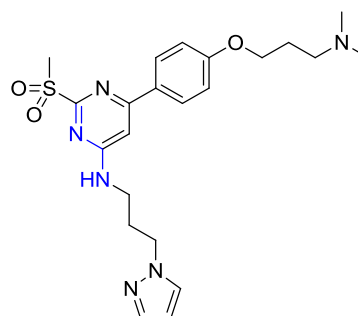
There are currently three published small molecule inhibitors of CECR2 (Figure 3.06) with two distinct chemotypes. The first, NVS-CECR2-1 (**3.008**) is a highly selective tool molecule which is highly selective against 48 other BRDs, although no data has been published to date. It has nanomolar affinity against CECR2 using ITC ($pK_d = 7.1$) and maintains activity in a cellular FRAP assay at $0.1 \mu\text{M}$ (see Section 1.1.3). Compound **3.008** was also potent in the GSK CECR2 assay ($pIC_{50} = 7.4$). The authors describe the probe as being poorly soluble and this was observed in a CAD solubility assay ($5 \mu\text{g mL}^{-1}$). The poor solubility is likely driven by the high PFI. More recently, the SGC and Takeda have worked to improve this chemotype and disclosed TP-238 (**3.009**), a chemical probe based on the same pharmacophore as NVS-CECR2-1 (**3.008**) with improved solubility. The improved solubility is most likely a function of the addition of further basicity. Compound **3.009** is potent at CECR2 ($pIC_{50} = 7.5$) but also displays activity at the BRD PHD finger transcription factor (BPTF) BRD ($pIC_{50} = 6.5$). Despite poor permeability ($AMP = 28 \text{ nm s}^{-1}$), cellular target engagement was demonstrated using nanoBRET experiments (CECR2

GSK Confidential – Do not copy

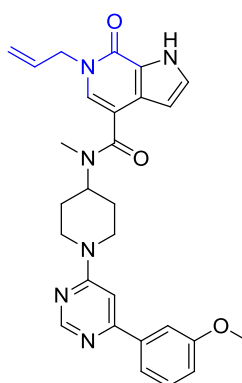
$pEC_{50} = 6.5$). In cells **3.009** was equipotent against BPTF ($pEC_{50} = 6.5$) which is a limitation of its use. The other available tool is GNE-886 (**3.010**), which has a CECR2 TR-FRET pIC_{50} of 7.8 equating to a 100-fold selectivity window over the closest BRDs.³⁰² Compound **3.010** had a high PFI (7.9) and sub-optimal solubility ($80 \mu\text{g mL}^{-1}$). The authors demonstrated cellular permeability and target engagement, by showing displacement of an artificial CECR2-ZsGreen fusion protein from chromatin. The displaced protein aggregates can be visualised by microscopy and quantified. The CECR2 pEC_{50} is 5.4 which equates to a 250-fold drop-off from the biochemical data, suggesting poor cellular permeability.



NVS-CECR2-1, **3.008**
CECR2 $pK_d = 7.1$
GSK CECR2 $pIC_{50} = 7.4(4)$
ChromLogD / PFI = 4.3 / 7.3
CAD solubility = $3 \mu\text{g mL}^{-1}$



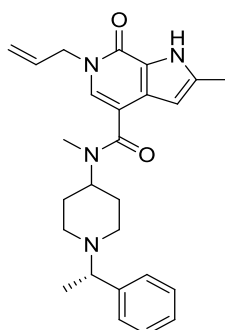
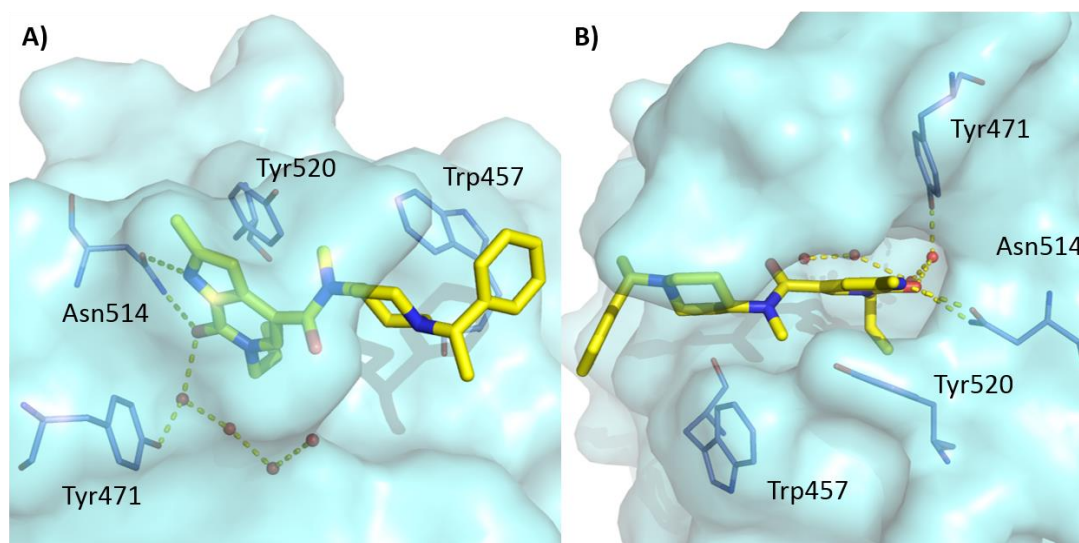
TP-238, **3.009**
CECR2 $pIC_{50} = 7.5$
BPTF $pIC_{50} = 6.5$
CECR2 nano BRET $pEC_{50} = 6.5$
BPTF nanoBRET $pEC_{50} = 6.5$
AMP = 28 nm s^{-1}



GNE-886, **3.010**
CECR2 $pIC_{50} = 7.8$
GSK CECR2 $pIC_{50} = 7.5(6)$
ChromLogD / PFI = 3.9 / 7.9
CAD solubility = $80 \mu\text{g mL}^{-1}$
CECR2 $pEC_{50} = 5.4$

Figure 3.06. Small molecule inhibitors of the CECR2 BRD (**3.008–3.010**) with KAc mimetics shown in blue.

During the development of GNE-886 (**3.010**), Crawford *et al.* disclosed the X-ray crystal structure (Figure 3.07) of the close analogue **3.011** (CECR2 pIC_{50} = 6.7). The pyrrolopyridine H-bonds to the conserved Asn514 residue, and the carbonyl group makes a through water interaction to the conserved Tyr471. The allyl group, which was shown to be critical for CECR2 potency and selectivity, induces a small lipophilic pocket beneath the Tyr520 gatekeeper residue. The amide then points out into the channel formed by the ZA loop and the aromatic ring is placed in proximity to Trp457.



3.011
CECR2 pIC_{50} = 6.9

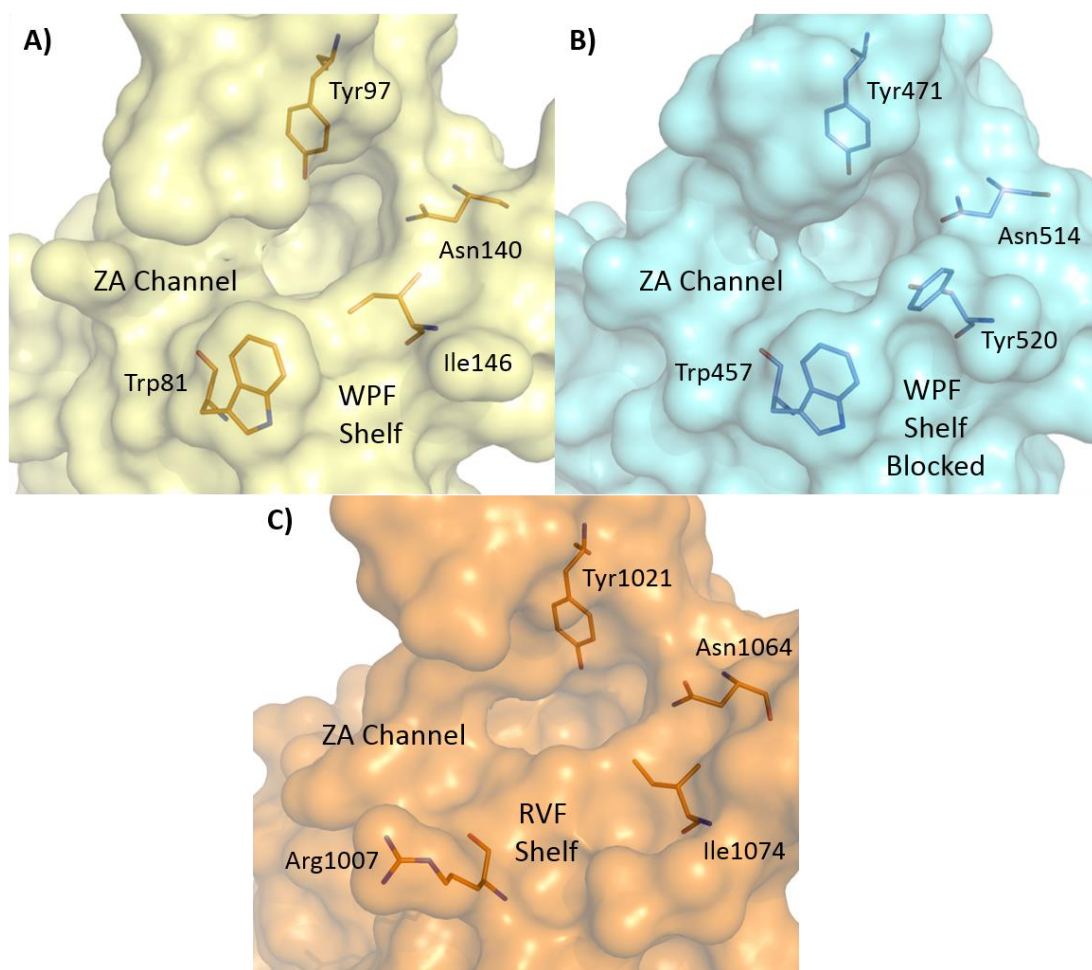
Figure 3.07. X-ray crystal structure (pdb5v84) of **3.011** (yellow) in CECR2 (blue) with key residues shown. Pocket waters are shown as red spheres and H-bonds as yellow dashed lines. A) Hydrogen bonding interactions with Asn514 and Tyr461 are depicted. B) Aromatic group place in proximity to Trp457.

Despite the availability of selective chemical probes for CECR2, none of the probes reported to date match the desired profile of a tool molecule (Section 3.1). NVS-CECR2-1 (**3.008**) and

GNE-886 (**3.010**) both have solubility issues which may be a limitation to their use. GNE-886 is also significantly less potent in cells. TP-238 (**3.009**) is from the same series as **3.008**, therefore, does not constitute a distinct chemotype. Furthermore, **3.009** does not maintain the desired 30-fold selectivity window over BPTF. Therefore, the phenotype of CECR2 remains largely unexplored. Any results obtained would also be questionable until they have been repeated with a small molecule inhibitor with a different chemotype or a negative control (Section 3.1). A further tool molecule with a differentiated chemotype was therefore considered desirable.

3.2.3. Structural Features of the CECR2 BRD

CECR2 resides in the same family of BRDs as BPTF, GCN5L2 and PCAF as classified by whole sequence homology as shown by the phylogenetic tree (Figure 1.14, Section 1.2.4). Importantly, for this work, there are distinct features of the CECR2 KAc recognition site which differentiate it both from the BET family and ATAD2. As previously discussed (see Section 1.4.1), the BET family are characterised by the presence of a WPF shelf region, a lipophilic shelf adjacent to Trp81 (BRD4 BD1). CECR2 also contains WPF residues in this region (Trp457), however, access to the shelf is restricted by the Tyr520 gatekeeper residue. Therefore, whilst the Trp457 residue can still be engaged through the ZA channel, exploitation of the shelf region in CECR2 is limited. Evidently, there is some flexibility associated with the Tyr520 gatekeeper residue, as demonstrated by GNE-886 (**3.010**), which can induce a small lipophilic pocket to accommodate the allyl group (Figure 3.07). The shelf region is even more differentiated in ATAD2, the WPF residues are replaced with RVF residues which leads to a shallower shelf region, with no defined pocket. This is exaggerated by the Ile1074 gatekeeper residues, which helps make for a poorly defined binding pocket. There are also structural changes in other areas of the binding pocket. For instance, the ZA loop in CECR2 is 2 amino acids shorter compared to the BET family which creates a slightly smaller ZA channel. As access to the shelf region is blocked in CECR2, accessing the ZA channel may be necessary to achieve the desired potency.



BRD	WPF Shelf Residues			Gate-keeper
ATAD2	Arg1007	Val1008	Phe1009	Ile1074
BRD4 (BD1)	Trp81	Pro82	Phe83	Ile146
BRD4 (BD2)	Trp374	Pro375	Phe376	Val439
CECR2	Trp457	Pro458	Phe459	Tyr520

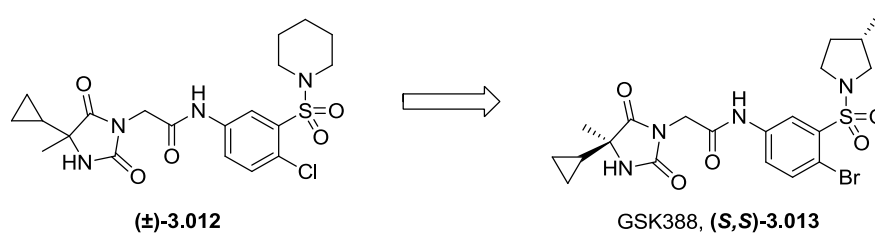
Figure 3.08. Comparison of the Apo structures of BRD4 BD1 (A, yellow, pdb3uw9), CECR2 (B, blue, pdb3nxb) and ATAD2 (C, orange, pdb3dai). The shelf (WPF or RVF) and gatekeeper residues are shown. Table: Comparison of the key residues in the WPF/RVF shelf region and gate keeper parts of BRD4 BD1 and BD2, ATAD2 and CECR2.

The significant number of structural differences between the gatekeeper and shelf residues make it a promising region for gaining selectivity. For example, Arg1007 is capable of making different interactions to Trp457 and could be exploited for selectivity between the 2 BRDs. Overall, the well-defined CECR2 binding pocket makes it an attractive target for development of a chemical probe.

3.3. Discovery of the Phenylsulfonamide Series

The strategy to find a novel chemical probe for CECR2 to further investigate its biological role began with an analysis of historical projects targeting orthogonal BCPs (e.g. TAF1, ATAD2 etc.) to identify a molecule with CECR2 activity. This approach took advantage of the large data set that had generated within our laboratories and the considerable number of BRD inhibitors historically prepared. This identified GSK388 ((*S,S*)-**3.013**), a tool molecule developed to target the ATAD2 BRD, which contained a unique phenyl sulfonamide chemotype (discussed fully in Section 3.3.1). This series was first discovered from a HTS against the ATAD2 BRD, which identified **3.012** as a promising hit. Optimisation of the sulfonamide and aryl substituent to increase affinity for ATAD2 delivered GSK388 ((*S,S*)-**3.013**) as a potent ATAD2 inhibitor. This made an attractive starting point for the development of a chemical probe for CECR2 for a number of reasons (Table 3.01). Firstly, both **3.012** and (*S,S*)-**3.013** showed no appreciable activity against the BET family, using BRD4 BD1 as a representative example ($pIC_{50} < 4.3$). Due to the strong phenotype observed for BET inhibitors, high selectivity over this family was considered of fundamental importance for a non-BET probe. Additionally, (*S,S*)-**3.013** was soluble ($129 \mu\text{g mL}^{-1}$) and permeable in an AMP assay (99 nm s^{-1}) with a suitable lipophilicity ($\text{ChromLogD} = 4.7$). Also, although (*S,S*)-**3.013** exhibited significant ATAD2 potency ($pIC_{50} = 7.2$), there were enough residue and conformational differences between CECR2 and ATAD2 that it was felt that selectivity could be engineered.

Table 3.01. Optimisation of GSK388 (**3.013**) a potent ATAD2 inhibitor from a HTS hit **3.012**.



	(±)-3.012	(<i>S,S</i>)-3.013
CECR2 pIC_{50} (n) / ATAD2 pIC_{50} (n)	5.0(4) / 5.7(6)	6.7(4) / 7.2(6)
Selectivity^a	5x(A)	3x(A)
CECR2 LE / LLE_{at}	0.22 / 0.20	0.30 / 0.28
BRD4 BD1 pIC_{50} (n)	<4.3(4)	<4.3(2)
ChromLogD_{7.4}	4.8	4.7
CLND Solubility ($\mu\text{g mL}^{-1}$)	136	129
AMP	125	99

^a(A) denotes selectivity for ATAD2.

At the outset of this project, an analysis of the ATAD2 vs. CECR2 selectivity of the phenyl sulfonamide template was conducted. All small molecules with this template which had been tested against both CECR2 and ATAD2 in our in-house TR-FRET assays were examined. Figure 3.09 revealed the relationship between ATAD2 and CECR2 potency. None of the compounds in the collection showed any significant selectivity for CECR2, albeit these analogues had been designed to favour ATAD2, so this is perhaps unsurprising. In order to engineer CECR2 selectivity into this template, structural insights into its binding mode were required, especially as at first glance, this series has no obvious KAc mimetic.

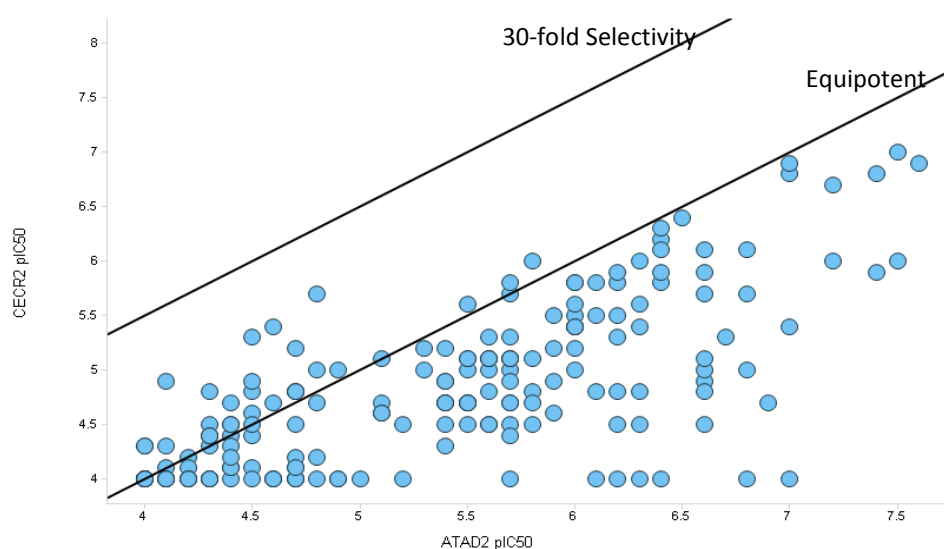


Figure 3.09. ATAD2 vs. CECR2 selectivity of the phenyl sulfonamide template at the onset of the project.

3.3.1. Displacing the Water: The Binding Mode of **(S,S)-3.013**

Most small molecule BRD inhibitors mimic the interactions of the natural KAc substrate through key interactions with the conserved Asn and Tyr residues. Initially, it was not obvious how the phenyl sulfonamide series interacted with the ATAD2 BRD. X-ray crystallography in CECR2 proved problematic, but an X-ray crystal structure of **(R,S)-3.013** (the opposite enantiomer to **(S,S)-3.013**, data for **(R,S)-3.013** is in Table 5.02, Section 5) in ATAD2 was solved and revealed a unique mode of binding (Figure 3.10).

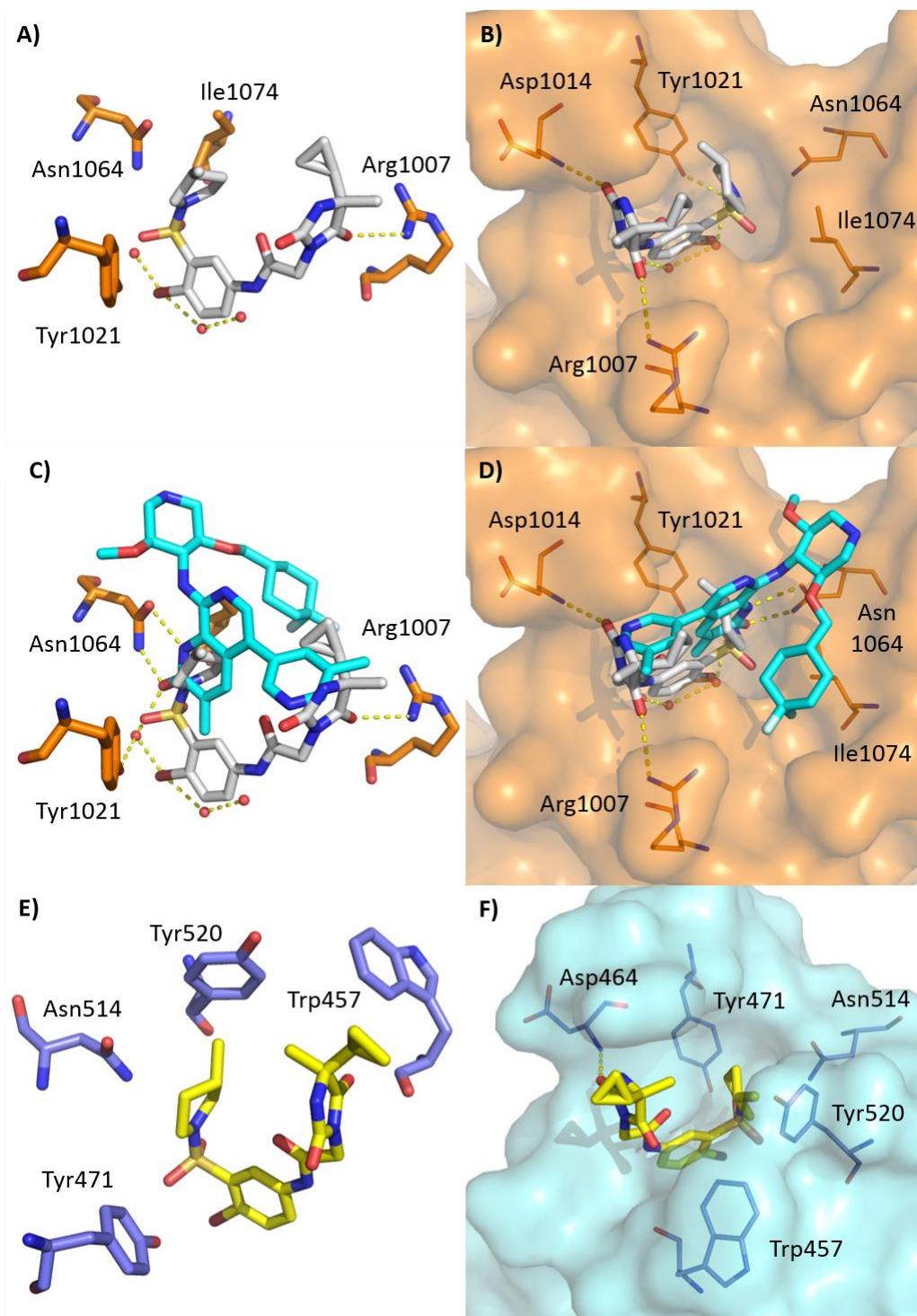


Figure 3.10. A and B: X-ray crystal structure of **(R,S)-3.013** (silver, data in Table 5.02, Section 5) in ATAD2 (orange) overlaid with H-bonds to key residues shown as dashed yellow lines. The water network is shown as red spheres. **(R,S)-3.013** can be seen sitting much deeper in the binding pocket displacing the canonical waters. C and D: X-ray crystal structure of **(R,S)-3.013** (silver) in ATAD2 (orange) overlaid with GSK8814 (**3.005**, pdb5lj0, teal) in ATAD2 (orange). E and F: Docking model of GSK388 (**(S,S)-3.013**, yellow) in the *apo* crystal structure of CECR2 (blue).

Phenylsulfonamide **(R,S)-3.013** bound much deeper in the binding pocket than a typical inhibitor, wholly displacing the network of water molecules normally found in the base of the KAc recognition site (Figure 3.10, (a)–(b)). For comparison, an X-ray crystal structure for GSK8814 (**3.005**, Figure 3.10, (c)–(d)) shows the classical interactions of KAc made by a KAc mimetic (i.e. a H-bond from the pyridone carbonyl group to the conserved Asn1064 and a through water interaction to Tyr1021). Interestingly, **(R,S)-3.013** does not appear to make any direct interactions with either Asn1064 or Tyr1021 in ATAD2. The sulfonamide occupies a lipophilic pocket formed in part by the Ile1074 gatekeeper residue, for which the (S)-methyl pyrrolidine provides good shape complementarity. The hydantoin moiety then vectors towards the ZA channel where it makes H-bonds to the backbone NH of Asp1014 on the ZA loop and Arg1007 of the RVF shelf.

As CECR2 crystallography remained problematic, a docking model of GSK388 (**(S,S)-3.013**) in the *apo* structure of CECR2 was solved (Figure 3.10, (E)–(F)). This showed that **(S,S)-3.013** could fit in the binding pocket of CECR2, although it must be remembered that this is not proof of the actual binding conformation. However, throughout this work, the SAR of the series in CECR2 was consistent with displacement of the water and it is believed to bind in this manner. Like in ATAD2, **(S,S)-3.013** sits deeper in the KAc recognition site than a typical inhibitor although it does not appear to make any specific interactions in this region. The (S)-methyl cyclopropyl moiety is still well tolerated despite the significant change in the shape induced by the change in gatekeeper residue from Ile1074 in ATAD2 to Tyr520 in CECR2. Interestingly, the pyrrolidine sulfonamide appears to be flipped 180° in CECR2 relative to ATAD2, although it is difficult to know whether this is significant or not. One of the hydantoin carbonyl groups then makes a H-bond to the backbone NH of Asp464, although it cannot make another H-bond to Trp457 in CECR2.

There are only a few examples in the literature where the BRD canonical water network has been wholly or partially displaced by an inhibitor. ATAD2 fragment **3.001** (Figure 3.02, Section 3.2.1) which contains a tricyclic structure was shown to displace the water network.²⁸⁸ Although it is worth noting that the low potency of this fragment and the high concentration required to generate X-ray crystallography limits the reliability of this data. Most success has come from the development of family VIII inhibitors (see phylogenetic tree, Figure 3.01, Section 3.2). Fedorov *et al.* reported that salicylic acid could displace the water network from

family VIII members.³⁰³ The salicylic fragment was then optimised to deliver PFI-3 (**3.014**, Figure 3.11), a pan-family VIII inhibitor.³⁰⁴ Compound **3.014** contains a phenol warhead which displaces the 4 conserved water molecules. The *ortho* ketone then makes a H-bonding interaction to the conserved Asn707 (PB1). Subsequently, Ley *et al.* reported dihydropyrrolo[1,2-*a*]quinazolone **3.015** as another pan-family VIII inhibitor.³⁰⁵ Compound **3.015** was also shown to displace the water network from the BRD binding pocket. A significant increase in potency was observed upon the addition of the chloride which makes a halogen bond (see Section 3.5) to a carbonyl group of Met731 in PB1(5). The carbonyl oxygen then makes a H-bond to the conserved Asn residue. Lastly, Myrianthopoulos *et al.* used a virtual screening approach to identify **3.016** which also bound to family VIII BRDs through displacement of the canonical water molecules.³⁰⁶

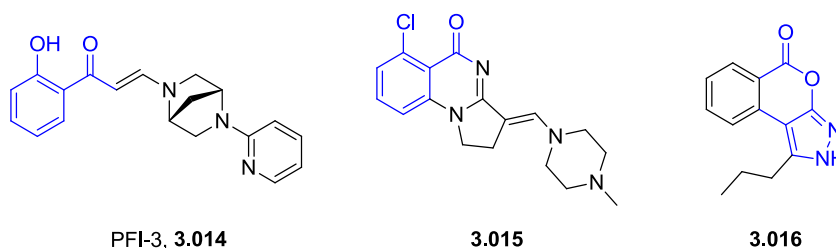


Figure 3.11. Small molecule inhibitors (**3.014–3.016**) of family VIII which have been shown to disrupt the network of water molecules ordinarily found in BRD binding pockets.

More recently, Crawford *et al.* have shown that it is possible to disrupt, or partially displace the water network to drive selectivity for a particular BRD.³⁰⁷ They worked on a promiscuous *N*-methyl pyrrolopyridone **3.017** and showed that different *N*-pyridone substituents were able to bind preferentially to certain BRDs (Figure 3.12). Insertion of an allyl group and a but-2-en-1-yl substituent were able to induce the formation of a lipophilic channel between the gatekeeper residue and the shelf region in CECR2 and BRD9. Pyrrolopyridone **3.018** was further optimised to deliver GNE-886 (**3.010**, Section 3.2.2). Furthermore, crystallography of but-3-en-1-yl **3.020** (Figure 2) was shown to rearrange the network of water molecules (removing one molecule entirely) in TATA-Box Binding Associated Factor 1 (TAF1) and BRD4. This work built on the observations made by Flynn *et al.* who noticed that butyryl and crotyl Lys bound preferentially to different BRDs.³⁰⁸ BRD9 and CECR2 both recognise butyryl Lys and

this was attributed to the Tyr gatekeeper residue in these two BRDs which is capable of moving to induce a small lipophilic pocket to accommodate the allyl group.

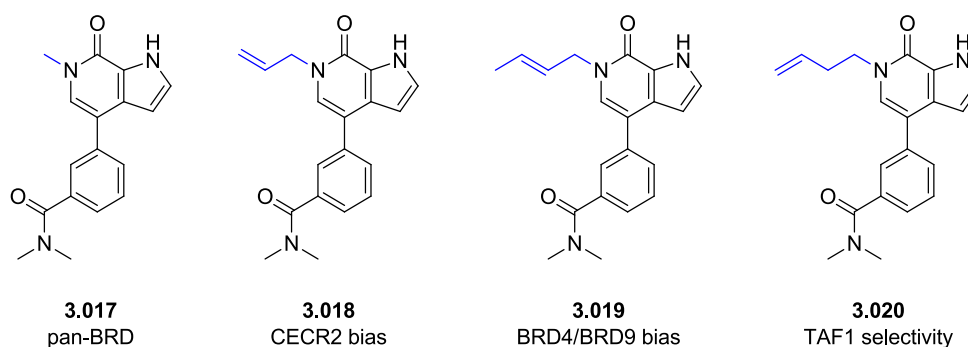


Figure 3.12. *N* substitution of pyrrolopyridones **2.017–2.020** can induce a bias towards different BRDs.

The tantalising evidence published by Flynn *et al.* and Crawford *et al.* suggesting that affinity and selectivity for different BRDs can be gained through disruption of the water network, has led to an increased interest in calculating the stability of the respective water networks. Zhang *et al.* studied the protein dynamics of 4 BRDs including ATAD2 and BRD2 BD1.³⁰⁹ Their work showed that the increased flexibility of the ZA loop in ATAD2 leads to a more open binding pocket and consequently, a reduction in the stability of the water network. These results were consistent with those of Biggin *et al.* who used grand canonical Monte Carlo simulations to calculate the free binding energy of the 4 conserved water molecules.³¹⁰ They calculated the stability of each water separately and amalgamated their results to understand the overall stability. Their work showed that the water network present in ATAD2 is amongst the least stable along with, unsurprisingly, the members of family VIII (PB1(1-4) etc.). Given these results, it is perhaps not surprising that a small molecule inhibitor which displaces the water network from ATAD2 has been discovered. However, it is interesting that phenylsulfonamide (**S,S**)-**3.013** can displace one of the most stable water networks from the binding pocket of CECR2. Therefore, the phenyl sulfonamide series presented an interesting opportunity for optimisation of a potent and selective chemical probe for CECR2.

3.4. Aims

The aim of this work was to deliver a potent and selective chemical probe for CECR2 from the phenylsulfonamide series. As discussed previously, a chemical probe for CECR2 should satisfy the following criteria:

- CECR2 TR-FRET $pIC_{50} > 7.0$
- >100-fold selectivity over the BET family
- >30 selectivity over another non-BET BRDs
- CAD solubility $> 100 \mu\text{g mL}^{-1}$
- Evidence of cellular target engagement (nanoBRET $pEC_{50} > 6.0$)

To achieve these aims, the phenyl sulfonamide series would be thoroughly explored. Full SAR optimisation of the 3 key vectors; the halide, sulfonamide and hydantoin vectors, would strive to deliver the desired profile (Figure 3.14). This work built upon the understanding and insights gained from the development of an ATAD2 inhibitor which had optimised all three vectors with respect to ATAD2. The previous SAR would be revisited to understand the relationship between the two BRDs and identify any opportunities for CECR2 selectivity. Although no crystallography was available in CECR2, a docking model would be used to exploit structural changes between the two BRDs.

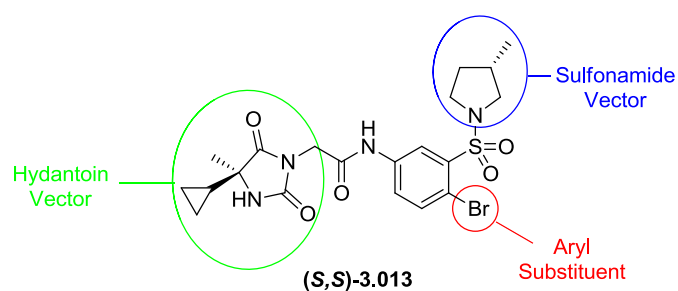
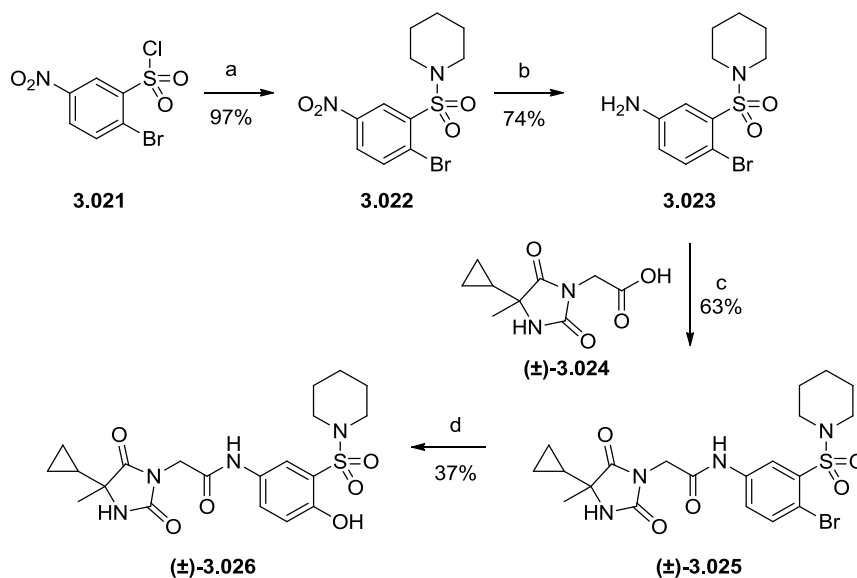


Figure 3.14. Phenylsulfonamide **3.013** with the 3 primary areas for SAR exploration, namely the sulfonamide vector, the halogen vector and the hydantoin vector.

3.5. Evaluating the Importance of the Aryl Substituent

Due to the unique binding mode of the phenyl sulfonamide series, which displaces the water network from the BRD bind pocket, understanding the contribution of the bromide was a sensible starting point, especially as bromine is a large lipophilic atom. In addition, it was hoped this would aid our understanding of the binding mode of this series with respect to CECR2. To probe the tolerability of the binding pocket, a range of substituents were investigated. The compounds were either obtained from the GSK compound collection or synthesised using the route in Scheme 3.01.

Although the most obvious halide replacements had already been prepared, given the series had displaced a water network, phenol **3.026** was seen as an important analogue to test. The synthesis of phenyl sulfonamide **3.026** started from commercially available sulfonyl chloride **3.021** (Scheme 3.01). Synthesis of sulfonamide **3.022** was achieved by dropwise addition of piperidine to a stirred solution of sulfonyl chloride **3.021** and DIPEA at 0 °C. Subsequently, reduction of the nitro group to afford aniline **3.023** proceeded by treatment with iron and NH₄Cl in 74% yield. The hydantoin group was then installed using the commercially available 2-(4-cyclopropyl-4-methyl-2,5-dioxoimidazolidin-1-yl)acetic acid ((±)-**3.024**) and HATU as a coupling agent in 63% yield. With the hydantoin in place it was possible to use bromide (±)-**3.025** as a synthetic handle to install the desired alcohol (±)-**3.026**. Indeed, a Miyaura borylation reaction developed previously (Section 2.4.2, Scheme 2.20) was used to convert bromide (±)-**3.025** into the corresponding boronic ester, followed by a subsequent one-pot oxidation to phenol (±)-**3.026** using hydrogen peroxide and NaOH in 37% yield.

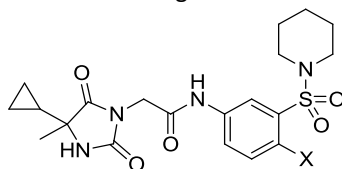
Scheme 3.01. Synthesis of phenol **3.026**.

a) Piperidine (1.2 eq.), DIPEA (2.2 eq.), CH₂Cl₂, 0 °C, 1 h, 97%; b) Iron (3.0 eq.), NH₄Cl (1.5 eq.), EtOH:water (3:1), 70 °C, 2 h, 74%; c) 2-(4-Cyclopropyl-4-methyl-2,5-dioximidazolidin-1-yl)acetic acid (**3.024**, 1.2 eq.), HATU (1.2 eq.), DIPEA (3.0 eq.), CH₂Cl₂, rt, 2 h, 63%; d) XPhos Pd G2 (10 mol%), KOAc (3.0 eq.), B₂pin₂ (2.0 eq.), EtOH, 100 °C, 2 h; ii) H₂O₂ (10 eq.), NaOH (1.0 eq.), 0 °C, 10 min, 37%.

The effect of replacing the bromide with phenyl sulfonamide (**±**)-**3.026**, synthesised in Scheme 3.01, and historical compounds (**±**)-**3.012**, (**±**)-**3.025**, and (**±**)-**3.027–3.030**, is shown in Table 3.02. Interestingly, the same trends in potency were observed for both ATAD2 and CECR2, which gave confidence that the phenyl sulfonamide series inhibited both BRDs through the same binding mode. When the aryl substituent was changed from bromide (**±**)-**3.025** to chloride (**±**)-**3.012**, a 4-fold decrease in activity and a reduction in LE was observed against CECR2 (Entry 1 vs. Entry 2) suggesting that the size of the pocket is more accommodating to the larger bromine atom. Pleasingly, neither compound showed any BET activity at the concentrations tested. Altering to the methyl (**±**)-**3.028** and trifluoromethyl (**±**)-**3.027** substituents (Entries 3 and 4) gave a significant drop in potency against CECR2, suggesting that the halogen atoms may be providing a specific interaction with the protein (*vide infra*). Alkyne (**±**)-**3.029** (Entry 5) showed poor affinity for both CECR2 (pIC₅₀ = <4.0) and ATAD2 (pIC₅₀ = 4.5). As discussed, phenol (**±**)-**3.026** was designed to mimic the interactions of the water molecule it was displacing through the availability of a H-bond donor. The poor activity of this substituent reinforced the belief that the pocket is mainly hydrophobic and that releasing crystallographic waters provides a gain in entropy. Therefore, replacing a single

interaction with a polar functional group is not favourable. Unsurprisingly, removal of the substituent gave phenylsulfonamide (**(±)**-**3.030** which was inactive at ATAD2 (Entry 6, $pIC_{50} = <4.0$).

Table 3.02. Investigation into the halogen vector in the phenylsulfonamides.



	X	CECR2 pIC_{50} (n) / ATAD2 pIC_{50} (n) Selectivity ^a	CECR2 LE / LLE _{at}	BRD4 BD1 pIC_{50} (n)	Chrom LogD _{7.4}	CLND solubility ($\mu\text{g mL}^{-1}$)
1 ^b	Cl (±) - 3.012	5.0(4) / 5.7(6) 5x(A)	0.22 / 0.20	<4.3(4)	4.8	136
2 ^c	Br (±) - 3.025	5.6(2) / 6.3(5) 5x(A)	0.25 / 0.23	4.3(1) ^f	4.8	93
3 ^b	CF ₃ (±) - 3.027	4.5(4) / 5.0(2) 3x(A)	0.18 / 0.17	<4.3(2)	5.3	66
4 ^b	Me (±) - 3.028	<4.0(4) / 4.6(4) >4x(A)	<0.18 / 0.16	<4.3(2)	4.6	$\geq 152^d$
5 ^b	C \equiv CH (±) - 3.029	<4.0(4) / 4.5(4) >3x(A)	<0.17 / 0.17	<4.3(2)	4.4	≥ 182
6	OH (±) - 3.026	<4.0(4) / <4.0(4) -	<0.18 / <0.19	<4.3(2)	3.7	176 ^d
7 ^b	H (±) - 3.030	4.4(2) ^e / <4.0(4) -	0.20 / <0.20	<4.3(4)	4.2	$\geq 169^d$

^a(A) denotes selectivity for ATAD2 over CECR2; ^bPrepared by colleagues at GSK; ^cCompound previously prepared by colleagues at GSK; ^dCAD solubility; ^eAlso <4.0 (n = 2); ^fAlso <3.3 (n = 2).

Due to the increased potency observed with halides (**(±)**-**3.012** and (**(±)**-**3.025**, the possibility of a halogen bonding interaction was investigated. Halogen bonds are a non-covalent interaction formed between an electron deficient region of a C-X bond (where X = F, Cl, Br, I) termed a σ hole and negative electron density such as the lone pairs of Lewis bases or anions.^{311, 312} σ holes are areas of positive electrostatic potential which arise in halogen atoms as a result of covalent bonding.³¹³ The larger the σ hole, the stronger the halogen bonding interaction potential. The increase in potency observed from Me to Cl to Br in the phenyl sulfonamide series is consistent with reports of halogen bonds in the literature.³¹⁴ Methyl groups are unable to form halogen bonds and the size of the σ hole increases from Cl to Br consistent with the observed increase in potency. Therefore, the X-ray crystal structure of

(R,S)-3.013 in ATAD2 was re-examined to search for possible halogen bonding interactions. The carbonyl group of Ile1056 is 3.2 Å away from the aryl bromide, this is shorter than the sum of the van der Waals distances (3.35 Å) and therefore suggestive of a non-covalent interaction. Additionally, the Ar–Br---O bond angle is 158.3° and the Br---O–C angle is 126.6°, both of which are close to the optimal 180.0° and 120.0° angles for halogen bonds respectively.^{311, 314, 315} Based on this evidence, it is possible that the increased affinity of the **(±)-3.012** and **(±)-3.025** is driven by a halogen bonding interaction. Alternatively, the increased affinity could simply be driven by the larger size of the bromide substituent for which the pocket size is more accommodating.

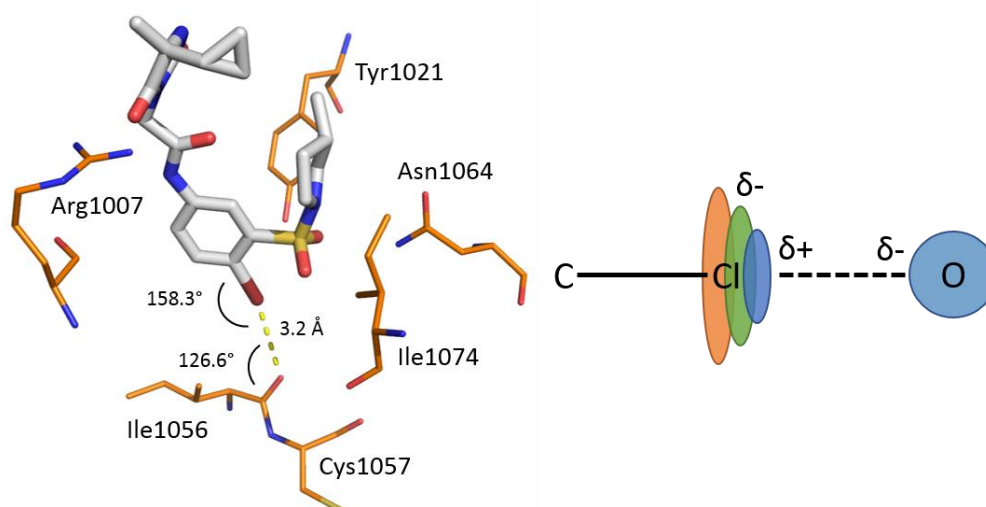


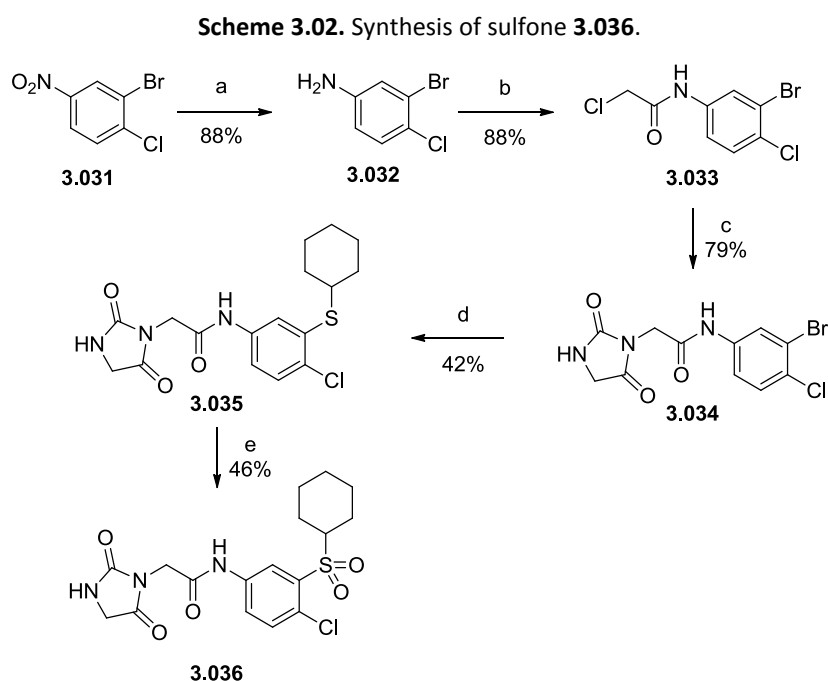
Figure 3.15. Left: X-ray crystal structure of **(R,S)-3.013** (silver) in ATAD2 with key residues shown in orange. Dashed line denotes the potential halogen bond interaction between the aryl bromide and the carbonyl of Ile1056. Right: Diagram of halogen bonding interaction formed by a δ^+ sigma hole in a halogen (Cl, Br or I) and an electronegative oxygen atom.

3.6. Optimisation of the Sulfonamide Vector

Having been unable to replace the bromide with an alternative substituent or gain any CECR2 selectivity, focus turned to the sulfonamide vector. Again, the sulfonamide vector had been investigated with respect to ATAD2 but given the previously discussed gatekeeper differences between ATAD2 and CECR2, it was felt that the SAR may be divergent in this region. Therefore, the historical data was re-examined and additional substituents (**3.036**, **3.040–3.042**) were designed and prepared to further understand the SAR and exploit the differences between the two BRDs. Throughout this work, the chloride substituent was used

to aid synthetic tractability and the unsubstituted hydantoin removed chirality from the hydantoin vector.

There was no obvious interaction made by the sulfonamide oxygens, however, the characteristic 110.5° angle was believed to be key to deliver the alkyl substituent into the lipophilic pocket formed in part by the Tyr520 gatekeeper residue (see Figure 3.10). To investigate whether removal of the sulfonamide nitrogen was tolerated, sulfone **3.036** was synthesised *via* the route shown in Scheme 3.02. Nitro-aromatic **3.031** was first reduced to the corresponding aniline **3.032**, using iron and NH₄Cl. Aniline **3.032** was then subjected to amidation using 2-chloroacetyl chloride and DIPEA. Subsequent alkylation of alkyl halide **3.033** with hydantoin using potassium carbonate in DMF gave bromide **3.034** in 79% yield.



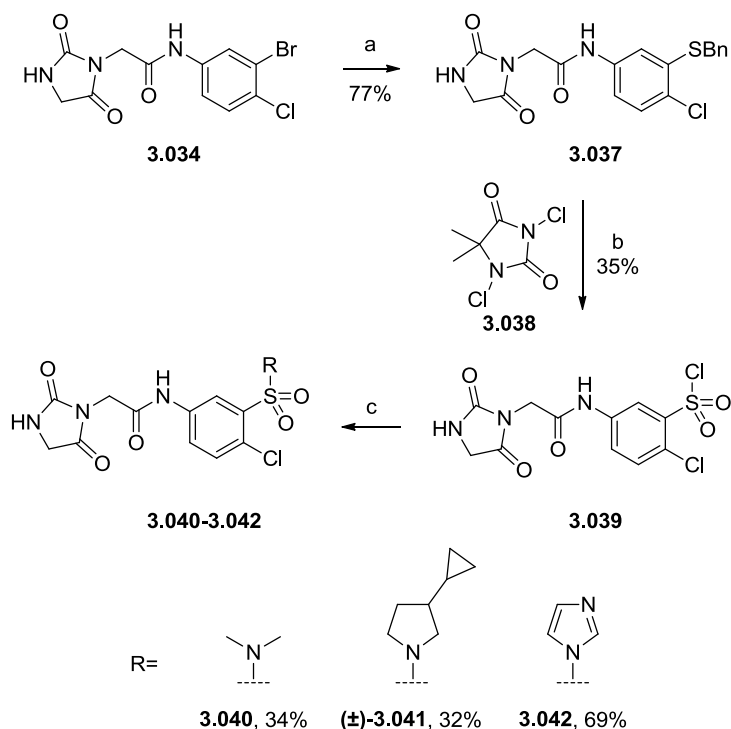
a) Iron (3.0 eq.), NH₄Cl (1.5 eq.), EtOH:Water (3:1), 70 °C, 16 h, 88%; b) 2-chloroacetyl chloride (1.0 eq.), DIPEA (1.0 eq.), CH₂Cl₂, rt, 1 h, 88%; c) Hydantoin (1.2 eq.), K₂CO₃ (3.0 eq.), DMF, 70 °C, 1 h, 79%; d) Cyclohexane thiol (1.5 eq.), Xantphos (20 mol%), Pd₂dba₃ (10 mol%), DIPEA (3.0 eq.), 1,4-dioxane:DMF (3:2), 100 °C, 1 h, 42%; e) *m*CPBA (2.0 eq.), CH₂Cl₂, rt, 16 h, 46%.

A chemoselective Pd-mediated coupling then afforded thioether **3.035**, using Xantphos ligands in a 1,4-dioxane:DMF (3:2) solvent mixture at 100 °C. These conditions were first reported by Mispelaere-Canivet *et al.* in 2005 and optimised further in our own laboratories.^{316, 317} The reaction proceeded in good yield despite the notoriety of sulfur

compounds for deactivating palladium reactions. It is thought that the drop-wise addition of thiol was paramount for a high yield, as it provided time for each catalytic cycle to complete and oxidative addition to occur. The reaction was complete as soon as thiol addition had finished. Sulfide **3.035** was then oxidised to sulfone **3.036**, using two equivalents of *m*CPBA in CH₂Cl₂ at rt.

To introduce diversity at the sulfonamide vector, three further sulfonamides were prepared from sulfonyl chloride **3.039** (Scheme 3.03). This was undertaken starting from the bromide **3.034**. Sulfide **3.037** was synthesised in a 77% yield using the same palladium coupling conditions utilised in Scheme 3.02 but employing benzyl thiol. Sulfide **3.037** could then be oxidised directly to sulfonyl chloride **3.039** using 1,3-dichloro-5,5-dimethylimidazolidine-2,4-dione **3.038** as an oxidant.³¹⁸ The low yield (35%) of this reaction was attributed to the reactivity and instability of sulfonyl chloride **3.039**. Sulfonyl chloride **3.039** could then be employed to synthesise sulfonamides (\pm)-**3.040–3.042** using the commercial amines and DIPEA as a base in yields of 32-69%.

Scheme 3.03. Synthesis of sulfonyl chloride **3.039** for use in a sulfonamide array.



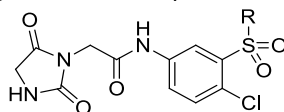
a) Benzyl mercaptan (1.5 eq.), Xantphos (20 mol%), Pd₂dba₃ (10 mol%), DIPEA (3.0 eq.), 1,4-dioxane:DMF (3:2), 100 °C, 1 h, 77%; b) 1,3-dichloro-5,5-dimethylimidazolidine-2,4-dione **3.038** (2.0 eq.), water, AcOH, MeCN, rt, 2 h, 35%; c) amine (1.0 – 1.2 eq.), DIPEA (3.0 eq.), CH₂Cl₂, rt, 4 h, 32–69%.

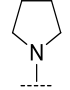
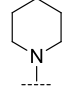
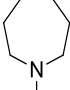
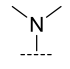
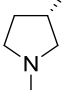
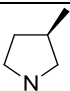
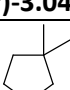
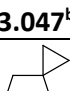
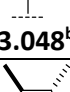
GSK Confidential – Do not copy

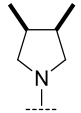
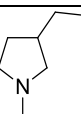
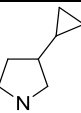
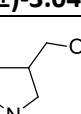
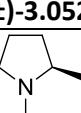
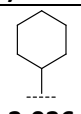
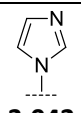
It was proposed that the potency of GSK388 ((*S,S*)-**3.013**) against ATAD2 was driven by the good shape complementarity between the (*S*)-methyl pyrrolidine sulfonamide substituent and the lipophilic pocket of the protein formed by the Ile1074 gatekeeper residue. The Tyr520 gatekeeper changes the shape of the binding pocket, therefore, it was unknown whether the (*S*)-methyl pyrrolidine was the optimal substituent for CECR2 potency. To explore this area of the protein, unsubstituted heterocycles **3.043–3.045** were examined first. Increasing the size of the ring from pyrrolidine **3.043** ($pIC_{50} = 5.4$), to piperidine **3.044** ($pIC_{50} = 4.7$) and azepane **3.045** ($pIC_{50} = 4.9$) was detrimental to both potency and LE. Pyrrolidine **3.043** was the most active of the saturated heterocycles and had an improved LE vs. Entries 2 and 3. This was attributed to an excellent shape complementarity with the binding pocket. Despite the differences in the protein homology, interestingly, these potency trends were repeated against ATAD2. Dimethyl sulfonamide **3.040** was less active against CECR2 ($pIC_{50} = 4.2$) and it was thought that this truncated substituent didn't adequately fill the binding pocket. Substitution at the 3- position of the pyrrolidine ((*S*)-**3.046**, Entry 5) was tolerated but no increase in potency or selectivity was observed with a methyl group. Interestingly, the two enantiomers were equipotent (Entries 5 and 6) therefore 3,3-disubstituted pyrrolidines **3.047–3.048** were examined. *Gem*-dimethyl analogue **3.047** was 0.8 log units less potent against CECR2, suggesting that the increased size induces a clash with the protein. However, cyclopropyl **3.048** was equipotent with pyrrolidine **3.043** ($pIC_{50} = 5.5$, LE = 0.28) albeit with a decrease in LE. X-ray crystallography of ATAD2 and a docking model of CECR2 (Figure 3.10, Section 3.3.1) had suggested that the pyrrolidine might be able to flip orientation in the binding pocket. Therefore, 3,4-disubstituted pyrrolidines **3.049–3.050** were examined. The racemic *trans*-pyrrolidine (\pm)-**3.049** was well tolerated ($pIC_{50} = 5.7$, LE = 0.28) and gave a moderate increase in potency but no increase in LE compared to (*S*)-**3.046**, although a marginal increase in ATAD2 selectivity was also observed. Interestingly, the *cis*-conformation (**2.050**) was 10-fold less potent against CECR2 ($pIC_{50} = 4.7$) suggesting that this substitution pattern is not tolerated. Extending the chain length of the methyl pyrrolidine to ethyl pyrrolidine (\pm)-**3.051** increased the potency and LE at CECR2 (Entry 11, $pIC_{50} = 5.9$, LE = 0.29), however, this was accompanied by a 0.5 log unit increase in ChromLogD and increased ATAD2 potency. Increasing the bulk and lipophilicity of the ethyl substituent to cyclopropyl pyrrolidine (\pm)-**3.041** gave a further increase in potency and LE at CECR2 (Entry 12, $pIC_{50} = 6.5$, LE = 0.30) without a concomitant increase in ATAD2 potency. However, there was still no significant selectivity for CECR2. The potency of this compound was attributed to

the sp² character of the cyclopropyl ring, which could interact with the Tyr520 gatekeeper in CECR2 preferentially over the Ile1074 gatekeeper in ATAD2.

Table 3.03. Investigation into the optimal sulfonamide for CECR2.



	R	CECR2 pIC ₅₀ (n) / ATAD2 pIC ₅₀ (n) / Selectivity ^a	CECR2 LE / LLE _{at}	BRD4 BD1 pIC ₅₀ (n)	Chrom LogD _{7.4}	CLND solubility (μg mL ⁻¹)
1	 3.043^b	5.4(4) / 6.0(4) 4x(A)	0.28 / 0.34	<4.3(4)	2.6	≥259
2	 3.044^b	4.5(4) / 5.6(6) 13x(A)	0.23 / 0.26	<4.3(2)	3.5	≥176
3	 3.045^b	4.9(4) / 5.9(6) 10x(A)	0.24 / 0.25	<4.3(4)	3.7	≥174
4	 3.040	4.1(4) ^d / 4.9(6) 6x(A)	0.23 / 0.33	4.4(2)	2.2	≥129 ^c
5	 (S)-3.046^b	5.5(8) / 6.1(8) 4x(A)	0.28 / 0.32	<4.3(2)	3.2	≥153
6	 (R)-3.046^b	5.3(2) / 6.0(6) 5x(A)	0.27 / 0.31	<4.3(4)	3.2	175
7	 3.047^b	4.6(3) / 5.5(6) 8x(A)	0.23 / 0.24	<3.3(2)	3.8	≥153 ^c
8	 3.048^b	5.4(4) / 6.0(8) 4x(A)	0.26 / 0.31	<4.3(2)	3.3	≥158
9	 (±)-3.049^b	5.7(2) / 6.6(6) 8x(A)	0.28 / 0.29	4.7(1) ^f	3.8	167

10	 3.050^b	4.7(2) / 5.7(6) 10x(A)	0.23 / 0.24	<4.3(2)	3.7	156
11	 (±)-3.051^b	5.9(4) / 6.2(8) 2x(A)	0.29 / 0.30	<4.3(4)	3.8	≥175
12	 (±)-3.041	6.3(3) / 6.3(4) -	0.30 / 0.32	<4.3(2)	4.0	≥169 ^c
13	 (±)-3.052^b	5.4(2) / 6.0(4) 4x(A)	0.26 / 0.36	<4.3(2)	2.6	≥352
14	 (R)-3.053^b	5.1(4) / 5.6(6) 3x(A)	0.26 / 0.29	4.5(1) ^e	3.1	≥201
15	 3.036	<4.0(6) / <4.0(2) -	<0.20 / <0.21	<4.3(2)	3.6	116
16	 3.042	<4.0(6) / <4.0(4) -	<0.21 / <0.29	<4.3(2)	2.1	≥155

^a(A) denotes selectivity for ATAD2 over CECR2; ^bPrepared by colleagues at GSK; ^cCAD solubility; ^dAlso <4.0 (n = 1); ^eAlso <4.3 (n = 2); ^fAlso <4.3 (n = 2).

Polarity at the 3-position was poorly tolerated, the most potent example, ether **(±)-3.052** (Entry 13, CECR2 pIC₅₀ = 5.4), offered no advantages over pyrrolidine **3.043**. Substitution at the 2-position to afford pyrrolidine **(R)-3.053** (Entry 14) was less well tolerated, with a drop in pIC₅₀ to 5.1. This may be because 2-substitution induces a twist in the conformation of the sulfonamide or because the methyl group clashes with the protein. Changing from a sulfonamide to a cyclohexyl sulfone (**3.036**, entry 7, pIC₅₀ <4.0) was not tolerated in either BRD in accordance with the prediction regarding the importance of the directionality provided by the sulfonamide (*vide supra*). Likewise, the aromatic variant **3.042** (Entry 16), which was designed to form an edge-to-face interaction with Tyr520, was inactive against ATAD2 and CECR2 at the concentrations tested. Importantly, phenyl sulfonamides **3.036**,

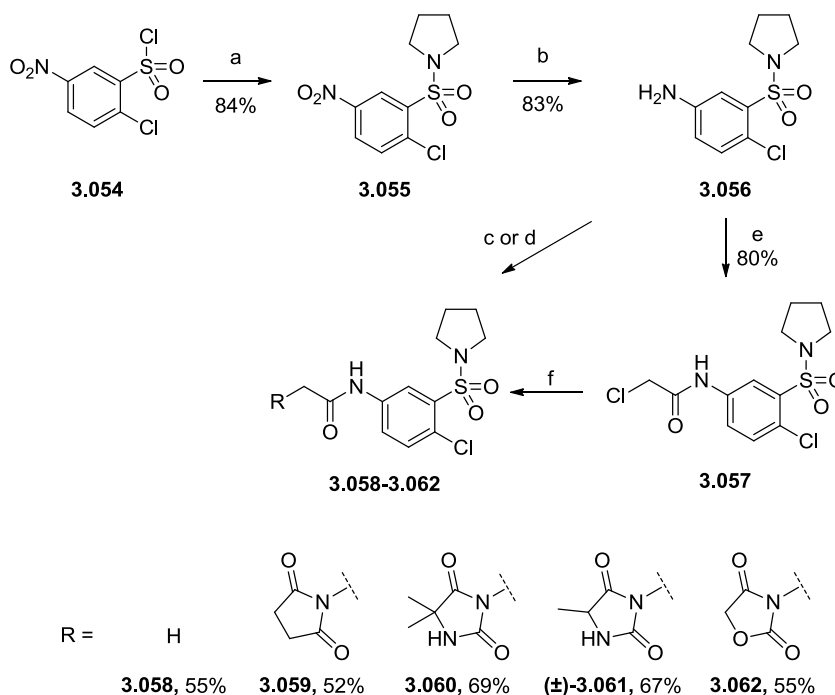
3.040–3.053 had poor affinity for BRD4 BD1, increasing the belief that this series would deliver a probe with appropriate selectivity over the BET family. Additionally, the phenyl sulfonamides **3.036**, **3.040–3.053** were highly soluble (CLND/CAD solubility >100 µg mL⁻¹). However, it appeared that to obtain significant selectivity over ATAD2, a step change in structure elsewhere in the molecule would be required.

3.7. Targeting Selectivity Through Interactions with the WPF Residues

3.7.1. Understanding the Role of the Hydantoin Group

Work to optimise the aryl and sulfonamide substituents had led to an increased understanding of the SAR and how to target potency for CECR2. However, throughout this work, perhaps surprisingly, selectivity over ATAD2 had not been forthcoming. Attention then turned to the amide vector which directed the hydantoin moiety towards the ZA channel bordering the WPF residues in CECR2 and the RVF residues in ATAD2.³¹⁹ This was the region of the protein where the greatest number of residue changes had been identified (Section 3.2.3), and as such modification of the hydantoin moiety offered the most potential to obtain selectivity. The hydantoin had offered appropriate potency for ATAD2 and had not previously been altered. However, the SAR of this vector with regards to CECR2 was poorly understood. As such, historical compounds **3.043** and **3.063–3.064** were re-examined, and, in order to fully probe this vector, hydantoin analogues (**3.058–3.062**) were synthesised using the route in Scheme 3.04. The chloro aryl substituent and pyrrolidine sulfonamide were chosen for this investigation as this template had the greatest range of historical data.

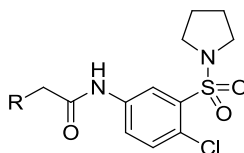
Starting from commercially available sulfonyl chloride **3.054**, a sulfonamide coupling using pyrrolidine and DIPEA as a base gave sulfonamide **3.055** in 84% yield. The nitro group could then be reduced using the conditions adopted previously (Scheme 3.01) to afford aniline **3.056** in 83% yield. To afford acetamide **3.058**, aniline **3.056** was acetylated using acetic anhydride and DIPEA in 55% yield. Succinamide **3.059** could also be prepared directly from aniline **3.056** using 2-(2,5-dioxopyrrolidin-1-yl)acetic acid and HATU as a coupling agent in 52% yield. Alternatively, chloride **3.057** was prepared using 2-chloroacetyl chloride (see Scheme 3.02). Subsequent alkylation of alkyl chloride **3.057** with the respective hydantoin furnished **3.060–3.062** in 55-69% yield.

Scheme 3.04. Synthesis of phenyl sulfonamides **3.059–3.063**.

a) Pyrrolidine (1.0 eq.), DIPEA (2.2 eq.), CH_2Cl_2 , 0 °C, 2 h, 84%; b) iron (5.0 eq.), NH_4Cl (1.5 eq.), EtOH:water (3:1), 70 °C, 2 h, 83%; c) R = **3.058**, Ac_2O (1.0 eq.), DIPEA (3.0 eq.), CH_2Cl_2 , rt, 1 h, 55%; d) R = **3.059**, 2-(2,5-dioxopyrrolidin-1-yl)acetic acid (1.1 eq.), HATU (2.2 eq.), DIPEA (3.0 eq.), CH_2Cl_2 , rt, 1 h, 52%; e) 2-chloroacetyl chloride (1.2 eq.), DIPEA (3.0 eq.), CH_2Cl_2 , 0 °C-rt, 1 h, 80%; f) *amedione* (1.1 eq.), K_2CO_3 (1.5 eq.), acetone, 70 °C, 1 h, 55-69%.

The 4-cyclopropyl-4-methyl hydantoin (**(±)-3.063**) had given high ATAD2 potency during the development of GSK388 (**(S,S)-3.013**). Interestingly, (**(±)-3.063**) was equipotent at ATAD2 and CECR2 (pIC_{50} = 6.0 and 5.8 respectively). The unsubstituted hydantoin had been prepared historically and was 0.4 log units less potent at CECR2 (Entry 2, pIC_{50} = 5.4), although equipotent against ATAD2 relative to (**(±)-3.063**). Therefore, sequential removal of the substitution at the 4-position of the hydantoin was investigated. *Gem*-dimethyl analogue **3.060** was 0.5 log units less potent at CECR2 than hydantoin (**(±)-3.063**), a drop-off not observed in ATAD2, suggesting that the cyclopropyl was more important for CECR2 potency. Removal of one of the methyl groups to give 4-methyl hydantoin (**(±)-3.061**) had a negligible effect on potency at CECR2 suggesting that this was not of pivotal importance. Furthermore, truncation back to hydantoin **3.043** had no effect on potency. The LE was maintained across this set of analogues (Entries 1–4).

Table 3.04. Investigation of the substituent targeting the RVF shelf



	R	CECR2 pIC ₅₀ (n) / ATAD2 pIC ₅₀ (n) Selectivity ^a	CECR2 LE / LLE _{at}	BRD4 BD1 pIC ₅₀ (n)	Chrom LogD _{7.4}	CAD solubility (μg mL ⁻¹)
1	 (±)-3.063^b	5.8(2) / 6.0(4) 2x(A)	0.26 / 0.27	<3.3(2) ^e	4.2	148 ^c
2	 3.043^b	5.4(4) / 6.0(4) 4x(A)	0.28 / 0.34	<4.3(4)	2.6	≥259 ^c
3	 3.060	5.3(6) / 5.8(8) 3x(A)	0.26 / 0.27	<4.3(2)	3.4	≥158
4	 (±)-3.061	5.2(6) / 5.8(8) 4wx(A)	0.26 / 0.30	<4.3(2)	3.0	≥343
5	 3.062	5.8(6) / 5.9(8) 1x(A)	0.31 / 0.37	<4.3(2)	3.6	94
6	 3.059	5.4(6) / 5.9(8) 3x(A)	0.28 / 0.32	<4.3(2)	3.3	≥106
7	 3.064^b	4.8(4) / 4.3(6) 3x	0.26 / 0.28	<4.3(2)	3.4	181 ^c
8	H 3.058	4.1(4) ^d / 4.4(4) 2x(A)	0.30 / 0.26	3.7(2) ^f	3.5	≥122

^a(A) denotes selectivity for ATAD2 over CECR2; ^bPrepared by colleagues at GSK; ^cCLND solubility; ^dAlso <4.0 (n = 2); ^eAlso <4.3 (n = 1); ^fAlso <4.3 (n = 4).

Interestingly, 2,4-oxazolidinedione **3.062** (Entry 5, pIC₅₀ = 5.8) was also well tolerated with CECR2 potency increased over the *NH* analogue, hinting that the hydantoin *NH* was not

making any specific interactions in CECR2. Further evidence of the superficial role of the hydantoin *NH* in binding to CECR2 was shown by pyrrolidine-dione **3.059** (Entry 6) which maintained a similar potency of 5.4 (*c.f.* hydantoin **3.043**). Interestingly, the potency at ATAD2 remained largely unchanged for these modifications, also suggesting that the *NH* was not vital here either. Previous work had further simplified the hydantoin substituent back to 2-pyrrolidinone **3.064** (Entry 7) which saw a 5-fold decrease in CECR2 potency and decreased LE ($pIC_{50} = 4.7$, $LE = 0.26$) suggesting that both carbonyl groups are important for activity. However, 2-pyrrolidinone **3.064** had a 3-fold bias for CECR2 suggesting that the carbonyl groups are more important in ATAD2. In fact, the 2-pyrrolidinone **3.064** offered little difference in ATAD2 potency compared to truncated acetamide **3.058** (Entry 8, $pIC_{50} = 4.5$). It is also important to note that acetamide **3.058** has improved CECR2 LE relative to most of the hydantoins prepared. This is suggestive that the hydantoin is by no means optimal for CECR2. Again, none of the compounds tested showed any significant activity at BRD4 BD1 and were mostly in an acceptable ChromLogD range (2.6 – 4.2) with suitable solubility ($\geq 94 \mu\text{g mL}^{-1}$).

3.7.2. Identification of 5,6 Biaryls with CECR2 Selectivity

It was clear from Table 3.04 that the hydantoin moiety was not optimal for CECR2 potency. To aid rational design, the X-ray crystal structure of the compound (*S,R*)-**3.013** was revisited. GSK388 ((*S,S*)-**3.013**) was docked into the *apo* structure of CECR2 (Figure 3.016) and the two structures compared. SAR work had shown that the two carbonyl groups were vital for ATAD2 potency and that moderate selectivity for CECR2 could be gained through removal of one of them, albeit with a significant reduction in potency (Table 3.04). In ATAD2, the hydantoin makes H-bonds using both carbonyl groups; one to the backbone *NH* of Asp1014 and the other to Arg1007 on the RVF shelf (Figure 3.16, A). The decrease in ATAD2 potency observed for **3.064** (Entry 7, Table 3.04) relative to **3.059** is consistent with the reduction in viable H-bonds. In CECR2, according to the model, one of the hydantoin carbonyl groups can still make a H-bond to the backbone *NH* of Asp 464. However, there is no suitable donor engaged from the WPF region due to the residue change from Arg1007 to Trp457. Therefore, a strategy was adopted which aimed to build out towards the WPF residues with a substituent which would interact more favourable with Trp457.

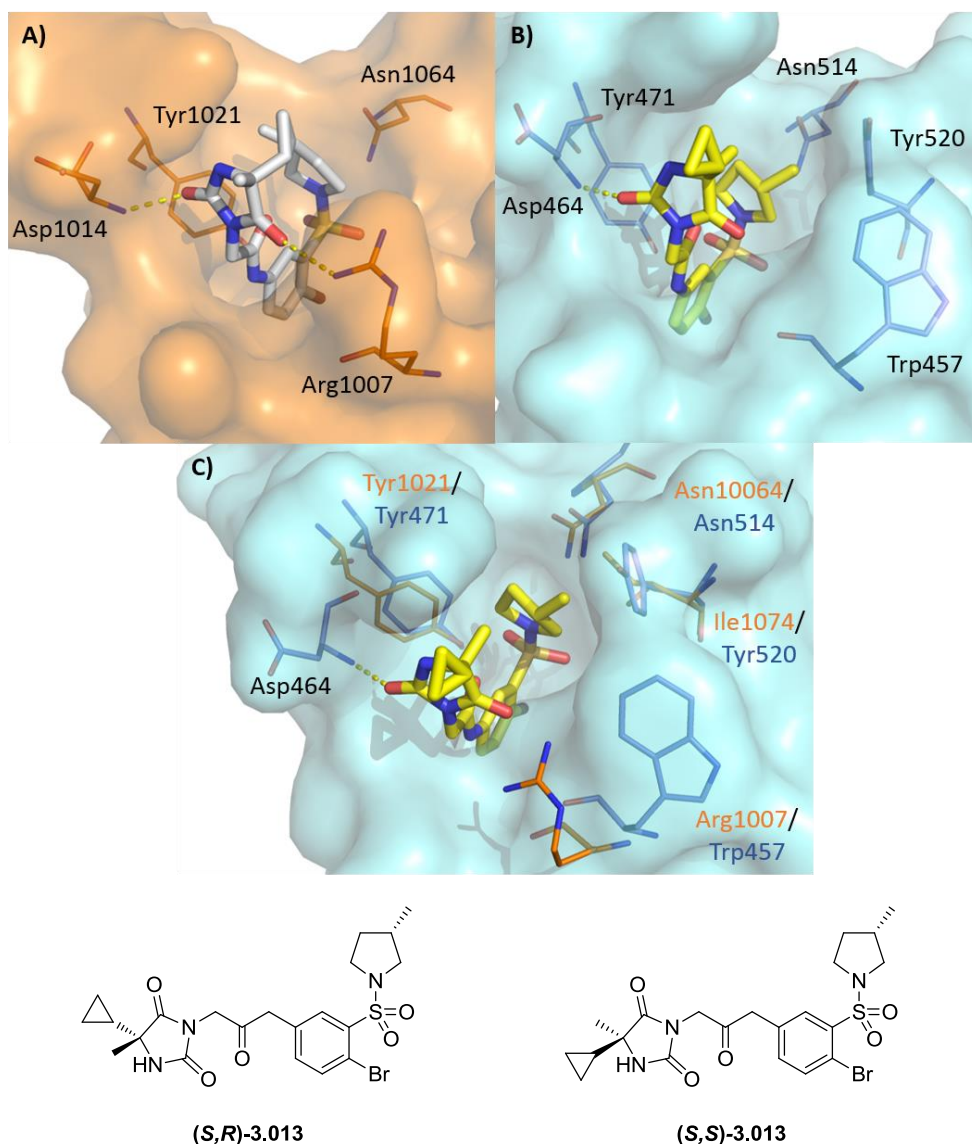


Figure 3.16. A) X-ray crystallography of **(S,R)-3.013** (silver) in ATAD2 (orange) with key residues shown. **(S,R)-3.013** makes H-bonds to both Asp1014 and Arg1007. B) A docking model of **(S,S)-3.013** (yellow) in the *apo* crystal structure of CECR2 (blue, pdb3nxb). **(S,S)-3.013** makes a H-bond to Asp464 but cannot interact with Trp457. C) A docking model of **(S,R)-3.013** (yellow) in the *apo* crystal structure of CECR2 (blue) with point changes between the CECR2 and ATAD2 domains annotated.

Aromatic rings have been shown to form π -stacking interactions with the WPF shelf in the BET family.⁴⁹ Therefore, it was hypothesised that substituents such as benzimidazolinone **(S)-3.065** might interact favorably with Trp457 whilst maintaining a H-bond with the *NH*. This would also remove one of the carbonyl groups which had appeared crucial for ATAD2 activity, hopefully leading to an increase in selectivity. To test this hypothesis biaryls **(S)-3.065**, and **(S)-3.069–3.075** were synthesised using the route in Scheme 3.05. In this case, the more

active (*S*)-methyl pyrrolidine sulfonamide group was employed together with the bromide substituent, which should lead to the best opportunity for highly potent CECR2 inhibitors.

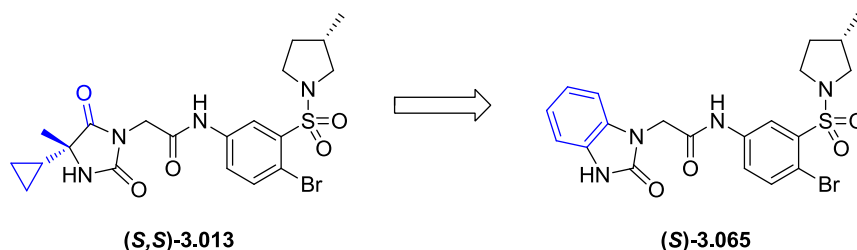
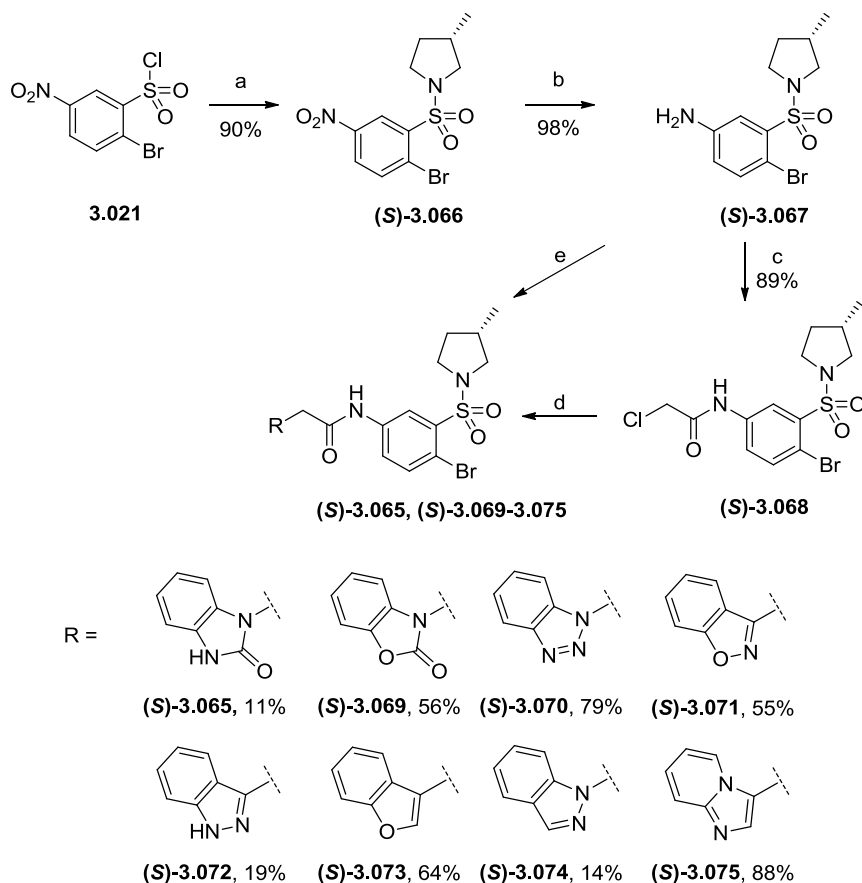


Figure 3.17. Strategy for exploiting residues in the WPF region of CECR2.

Starting from commercially available sulfonyl chloride **3.021**, a sulfonamidation reaction with (*S*)-methyl pyrrolidine and DIPEA furnished nitro aromatic (**S**)-**3.066**. This could be reduced to the desired aniline ((**S**)-**3.067**) using iron and NH₄Cl in 98% yield. The desired biaryls could then be accessed through two methods. *N*-linked heteroaryls ((**S**)-**3.065** and (**S**)-**3.070**) could be prepared from chloride (**S**)-**3.068**, which was synthesised in turn from aniline (**S**)-**3.067** using 2-chloroacetyl chloride in 89% yield. Subsequent alkylation of chloride (**S**)-**3.067** with the desired biaryl gave phenyl sulfonamides (**S**)-**3.065** and (**S**)-**3.069** in 11–56% yield. Alternatively, for (**S**)-**3.069–3.075**, the required carboxylic acid was commercially available. Therefore, a HATU mediated amide coupling gave the desired products ((**S**)-**3.069–3.075**) in 19–88% yields.

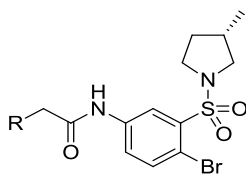
Scheme 3.05. Synthesis of 5,6-biaryls (**S**)-**3.066**, and (**S**)-**3.070–3.076**.

a) (*S*)-methyl pyrrolidine (1.0 eq.), DIPEA (2.2 eq.), CH₂Cl₂, 0 °C, 1 h, 90%; b) iron (5.0 eq.), NH₄Cl (1.5 eq.), EtOH:water (3:1), 70 °C, 2 h, 98%; c) 2-Chloroacetyl chloride (1.2 eq.), DIPEA (3.0 eq.), CH₂Cl₂, 0 °C-rt, 1 h, 89%; d) R = **(S)-3.065** and **(S)-3.069**, 5,6 biaryl (1.1 eq.), K₂CO₃ (1.5 eq.), acetone, 70 °C, 1 h, 11–56%; e) R = **(S)-3.070–3.075**, (5,6-biaryl)-CH₂COOH (1.1 eq.), HATU (2.2 eq.), DIPEA (3.0 eq.), CH₂Cl₂, rt, 1 h, 14–88%.

Pleasingly, benzimidazolinone **3.065** (Table 3.05, entry 2) maintained potency at CECR2 (pIC₅₀ = 6.4) relative to hydantoin (**(S,S)**-**3.013** whilst activity at ATAD2 dropped 20-fold. The corresponding benzoxazolidine **(S)-3.069** (Entry 3) showed a further 10-fold increase in potency towards CECR2 (pIC₅₀ = 7.4) whilst no increase in ATAD2 potency was observed, leading to a 50-fold selective inhibitor. Interestingly, there was only a marginal increase in LLE_{at} for **(S)-3.069** relative to **(S,S)**-**3.013**, despite the 0.7 log unit increase in potency. Compound **(S)-3.069** was also more potent at BRD4 BD1 (pIC₅₀ = 5.0) although it still maintained a 250-fold selectivity window.

GSK Confidential – Do not copy

Table 3.05. Investigation of 5,6-biaryls designed to target Trp457 in CECR2.



	R	CECR2 pIC ₅₀ (n) / ATAD2 pIC ₅₀ (n) Selectivity ^a	CECR2 LE / LLE _{at}	BRD4 BD1 pIC ₅₀ (n)	Chrom LogD _{7.4} / PFI	CAD (μg mL ⁻¹)
1	 (S,S)-3.013^b	6.7(4) / 7.2(6) 3x(A)	0.30 / 0.28	<4.3(2)	4.7 / 5.7	129 ^c
2	 (S)-3.065	6.4(6) / 5.8(8) 4x	0.29 / 0.23	<4.3(3)	4.6 / 7.6	25
3	 (S)-3.069	7.3(8) / 5.7(8) 40x	0.33 / 0.29	5.0(2)	5.7 / 8.7	21
4	 (S)-3.070	6.6(6) / 5.6(6) 10x	0.31 / 0.26	4.8(1) ^d	5.3 / 8.3	18
5	 (S)-3.071	6.5(6) / 6.0(4) 3x	0.31 / 0.26	4.6(1) ^e	6.2 / 9.2	3 ^c
6	 (S)-3.072	5.5(4) / 5.7(6) 2x(A)	0.26 / 0.21	4.7(1) ^f	5.3 / 8.3	7 ^{c,g}
7	 (S)-3.073	5.0(5) / 5.6(2) 4x	0.24 / 0.13	<4.3(2)	6.7 / 9.7	0 ^c
9	 (S)-3.074	5.9(4) / 5.5(6) 3x	0.28 / 0.24	<4.3(2)	4.5 / 7.5	38
8	 (S)-3.075	6.4(4) / 5.9(2) 3x	0.30 / 0.23	4.9(2) ^f	5.8 / 8.8	16 ^c

^a(A) denotes selectivity for ATAD2 over CECR2; ^bPrepared by colleagues at GSK; ^cCLND solubility; ^dAlso <4.3 (n = 1); ^eAlso <4.3 (n = 1); ^fAlso <4.3 (n = 1); ^gData is <0 on 1 test occasion.

Based on previously discussed ATAD2 crystallography and CECR2 modelling (Section 3.3.1), it was thought that the carbamate in **(S)-3.069** was retaining a H-bonding interaction with the protein. Therefore, benzotriazole **(S)-3.070** and benzisoxazole **(S)-3.071** (Entries 4 and 5) were designed to explore whether this interaction could be maintained when the H-bond acceptor was located within an aromatic ring. Both compounds showed good potency for CECR2 (pIC_{50} = 6.7 and 6.6 respectively) and were somewhat selective over ATAD2 and highly selective over BRD4 BD1. Changing the H-bond donor-acceptor pattern to give indazole **(S)-3.072** lowered CECR2 potency 10-fold (pIC_{50} = 5.6) suggesting that a H-bond donor is poorly tolerated at this position. Further investigation of the optimal positioning of the H-bond donor pattern was then conducted. Removal of one of the heteroatoms to give benzofuran **(S)-3.073** (Entry 7) showed a 32-fold drop-off in CECR2 potency, suggesting that a H-bond acceptor at the 2-position was crucial. However, fused imidazolopyridine **(S)-3.074** with a nitrogen at the 3-position was more potent (pIC_{50} = 6.0). Although this is still 0.7 log units lower than benzotriazole **(S)-3.070**, which supported the importance of a lone-pair in the 2-position. The poor tolerability of benzofuran **(S)-3.073** is potentially the result of the furan oxygen being a weaker H-bond acceptor.³²⁰ Interestingly, *N*-linked indazole **(S)-3.075** (pIC_{50} = 6.5) which only features the H-bond acceptor at the 2-position, had a similar profile to benzotriazole **(S)-3.070** with a reduced selectivity window over ATAD2 (4-fold). Overall, this SAR shows that a H-bond donor to acceptor change at the 3-position is highly beneficial for CECR2, whilst neutral for ATAD2 (Entry 3 vs 2). It also shows that an H-bond acceptor at the 2-position is very important (e.g. Entry 5 vs Entry 7). Indeed, benzoxazolidine **(S)-3.069** and benzotriazole **(S)-3.070** showed the greatest potency and selectivity, however, the addition of 2 further aromatic rings to the template was detrimental to both ChromLogD and solubility. The increased ChromLogD and greater number of aromatic rings is likely the cause of the poor solubility observed (solubility $\leq 38 \mu\text{g mL}^{-1}$). As a result, none of the compounds tested were suitable for further progression.

3.7.3. Exploration of 5,6 Biaryl Systems

Whilst improvements had been made to the selectivity, none of the initial 5,6 biaryls tested had the desired physico-chemical profile (Table 3.05). The high lipophilicity was likely causing the reduced solubility; PFI (ChromLogD + Ar ring count) has previously been inversely correlated with solubility.^{321, 322} Therefore, an analysis of the physico-chemical properties of the phenylsulfonamide series was conducted. Figure 3.18 shows the solubility (Log_{10}) plotted

against PFI, and the compounds are coloured according to their AMP. A PFI of <6 is considered optimal for improving solubility although the desired solubility could still be achieved for compounds where the PFI < 7.2. It was also feared that high lipophilicity may increase the likelihood of non-specific binding and therefore reduce selectivity over other BRDs or unknown off-targets. Furthermore, decreasing the PFI to < 5.5 appeared to be detrimental to permeability, therefore, a window of 5.5–7.2 was considered optimal to balance the physico-chemical properties.

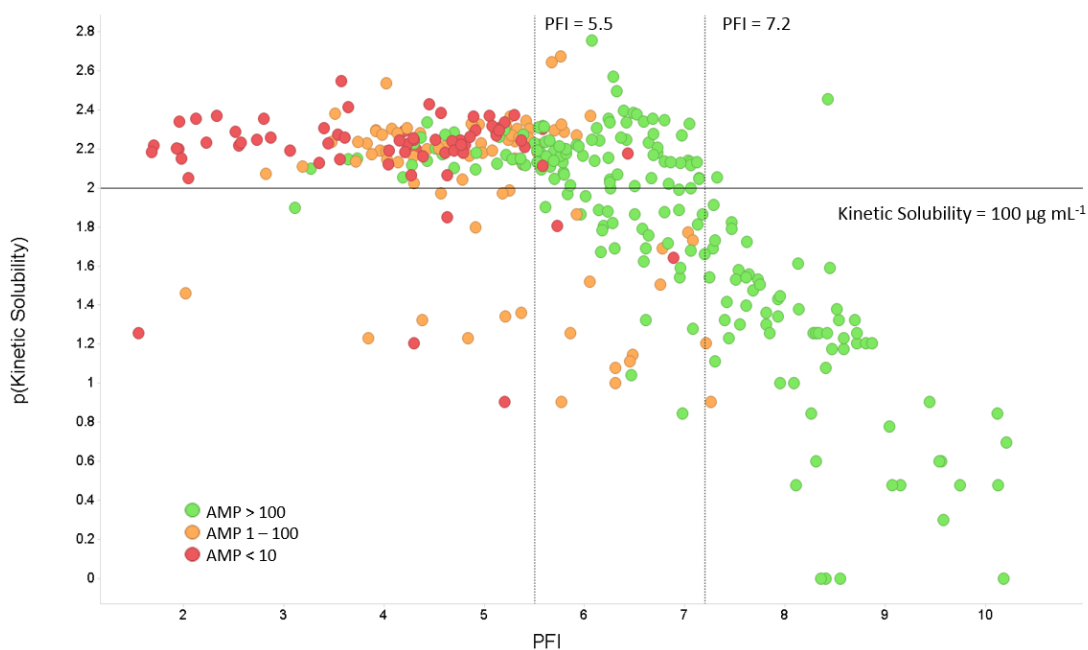
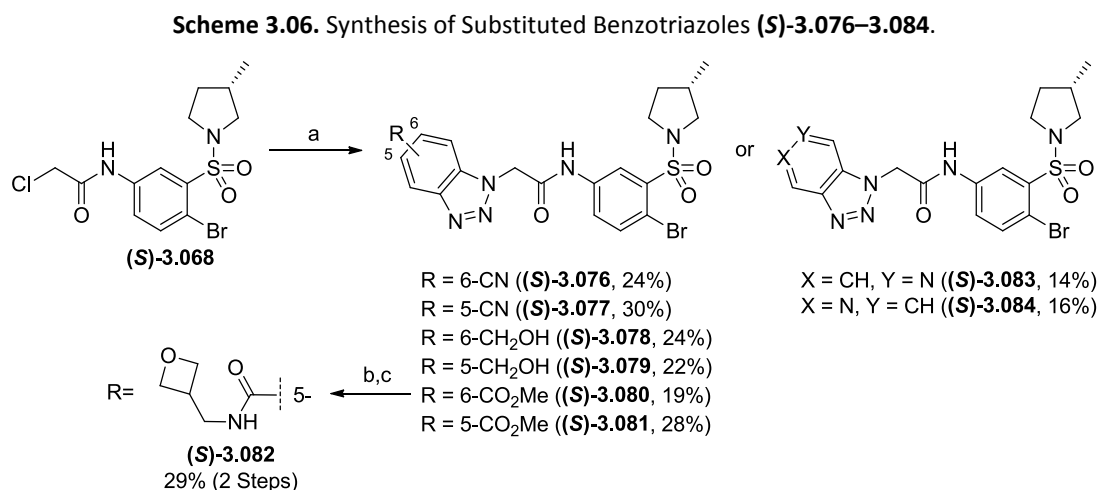


Figure 3.18. An analysis of the logarithmic solubility vs. PFI of the phenylsulfonamide series with the data points coloured according to permeability.

Phenyl sulfonamides **(S)-3.076–3.084**, **3.091** and **(S)-3.093** (Table 3.06) were substituted benzotriazoles designed to be of lower ChromLogD (and PFI), in order to establish whether this did indeed correlate with improved solubility. Furthermore, increased potency and selectivity at CECR2 was also desirable and it was hoped that elaboration of the benzotriazole might deliver this. The benzotriazole was chosen for this exploration due to the synthetic tractability of the desired compounds.

Benzotriazoles **(S)-3.076–3.081** could be prepared from alkyl chloride **(S)-3.068** (Scheme 3.06) described in Scheme 3.05. Alkylation using substituted benzotriazoles gave a mixture

of two regioisomers in a 1:1 ratio. Purification by MDAP delivered a mixture of the two regioisomers which could then be separated using chromatography on a chiral stationary phase. Further functionalisation of the 5-position was achieved by hydrolysis of ester **(S)-3.080** using LiOH and subsequent amidation to afford oxetane amide **(S)-3.082**. Triazolopyridines **(S)-3.083–3.084** could also be synthesised from alkyl chloride **(S)-3.068** (Scheme 3.06). Using K₂CO₃ as a base, alkylation gave both possible regioisomers which could be separated using MDAP to afford **(S)-3.083–3.084** without the need for further purification.

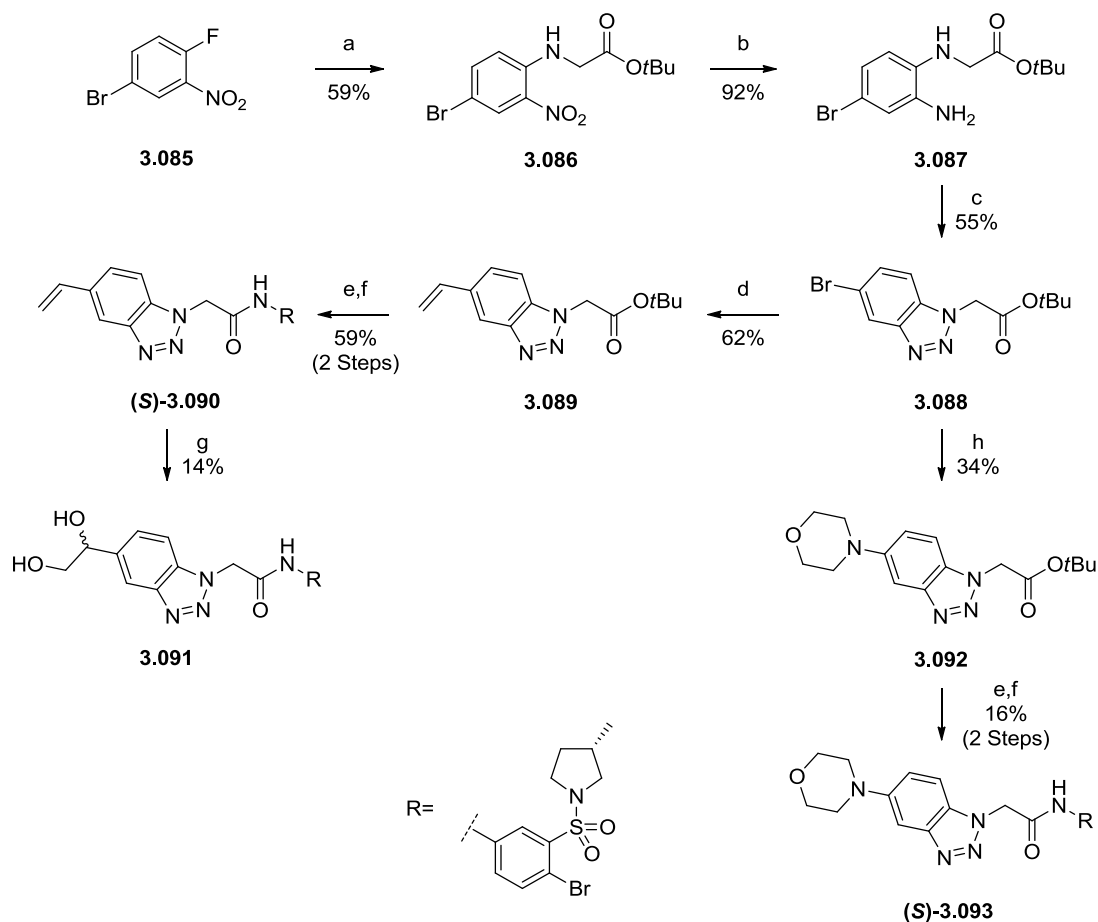


a) Benzotriazole or triazolopyridine (1.2 eq.), K₂CO₃ (1.3 eq.), acetone, 60 °C, 1 h, 14–30%; b) LiOH (2.0 eq.), THF:water (1:1), 50 °C, 2 h, 86%; c) oxetan-3-ylmethanamine hydrochloride (1.4 eq.), HATU (1.1 eq.), DIPEA (3.0 eq.), CH₂Cl₂, 34%.

Where the required benzotriazole was not commercially available, an alternative strategy was required. Bromide **3.088** was synthesised using the route outlined in Scheme 3.07 and could then be used as a synthetic handle to insert the desired functionality. Starting from the commercially available fluoride **3.085**, an S_NAr reaction, activated by the *ortho*-nitro group, was used to introduce *tert*-butyl glycinate.³²³ Reduction to aniline **3.086** was then effected using iron and NH₄Cl (92%). To afford benzotriazole **3.088**, aniline **3.087** was reacted with sodium nitrite to afford the diazonium species which cyclised *in situ* to form the triazole ring. A Suzuki reaction with the potassium salt of trifluoro(vinyl)borate, using the XPhos Pd G2 catalyst installed a vinyl group to give benzotriazole **3.089**.³²⁴ Functionalisation of the bromide was necessary at this stage, before coupling to aryl bromide **3.067**, to mitigate any chemoselectivity issues involved with Pd catalysis at a late stage. Benzotriazole **3.089** could then be coupled to aniline **3.067** after acid hydrolysis of the *tert* butyl ester using HATU to

afford phenyl sulfonamide (**S**)-**3.090**. Finally, a Sharpless asymmetric dihydroxylation reaction using AD-mix- β gave the desired diol **3.091** in 14% yield.^{325, 326} It was unknown whether the diol would be tolerated, therefore, AD-Mix was only used for synthetic feasibility and the diastereoselectivity was not determined due to the poor yield obtained and **3.091** was tested as an unknown mixture of diastereomers.

Scheme 3.07. Synthesis of benzotriazole **3.090** and functionalisation of the bromide synthetic handle through Pd catalysed cross-coupling



Alternatively, a Buchwald Hartwig amination was used to install a morpholine group. The RuPhos ligand used was developed by Buchwald for the coupling of secondary amines to aryl

bromides.³²⁷ Temperatures greater than 80 °C led to high levels of protodebromination, whilst Cs₂CO₃ as a base was also found to be important for high conversion. Purification of the desired product was problematic and led to a low 34% yield. However, this was sufficient to complete the synthesis of benzotriazole **3.092**. The desired phenylsulfonamide **(S)-3.093** could again be synthesised through ester hydrolysis and subsequent amidation in good yields.

The solubility of both the substituted 5,6-biaryls (**(S)-3.076–3.084**, **3.091** and **(S)-3.093**) and the 5,6-biaryls (**(S)-3.065** and **(S)-3.069–3.075**) prepared previously (Table 3.05) was examined (Figure 3.19). There was a limited correlation between decreasing PFI and increasing solubility ($r^2 = 0.637$), suggesting that this was a viable strategy for targeting an improved profile. However, only one of the compounds synthesised met the desired threshold despite a general trend towards a lower PFI and improved solubility.

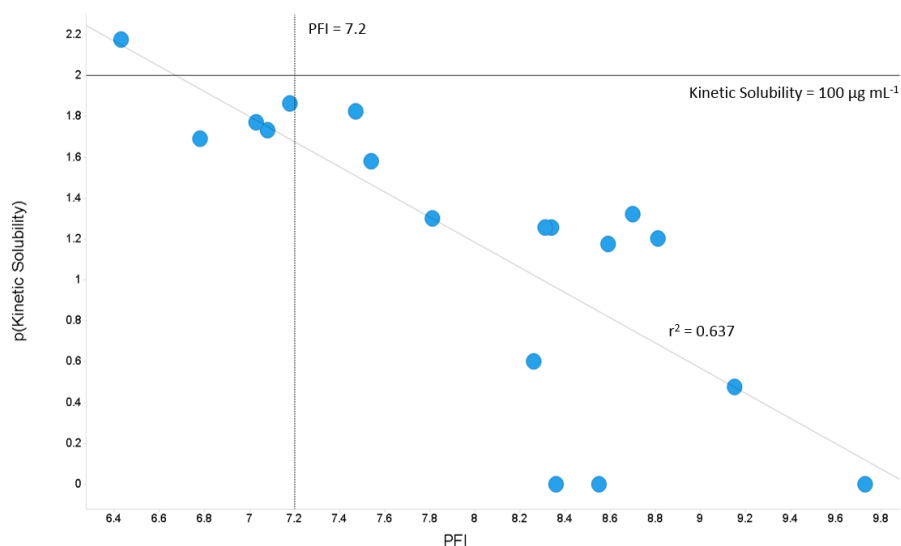
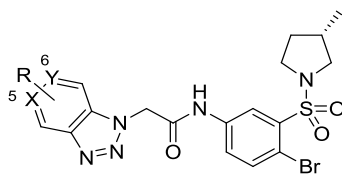
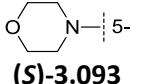
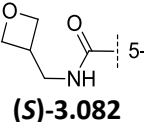
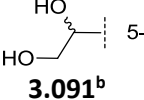


Figure 3.19. An analysis of the logarithmic solubility vs. PFI of the compounds in tables 3.05 and 3.06.

When the benzotriazoles synthesised were tested in the TR-FRET assays, clear SAR was observed between substitution at the 5- or 6-position (Table 3.06). Substitution at the 6-position (Entries 2, 4, and 6) offered no advantage over benzotriazole **(S)-3.070**. Nitrile **(S)-3.076** had no effect on CECR2 potency (Entry 2) whilst both alcohol **(S)-3.078** and ester **(S)-3.080** (Entries 4 and 6) were less potent. However, the reverse was true for substitution at the 5-position (Entries 3, 5, and 7) which led to increased potency at CECR2 and selectivity over ATAD (16–32-fold) with all three examples.

Table 3.06. Exploring substitution of the benzotriazole to improve the physico-chemical profile.



	R	X	Y	CECR2 pIC ₅₀ (n) / ATAD2 pIC ₅₀ (n) Selectivity ^a	CECR2 LE / LLE _{at}	BRD4 BD1 pIC ₅₀	Chrom LogD _{7.4} / PFI	CAD (μg mL ⁻¹)
1	- (S)-3.070	CH	CH	6.6(6) / 5.6(6) 13x	0.31 / 0.26	4.8(1) ^d	5.3 / 8.3	18
2	6-CN (S)-3.076	CH	CR	6.5(6) / 6.0(6) 6x	0.29 / 0.26	<4.3(1) ^e	5.4 / 8.4	<1
3	5-CN (S)-3.077	CR	CH	7.1(6) / 5.8(6) 20x	0.31 / 0.28	<4.3(2)	5.3 / 8.3	18
4	6-CH ₂ OH (S)-3.078	CH	CR	6.0(6) / 5.5(6) 4x	0.27 / 0.27	<4.3(2)	4.1 / 7.1	54
5	5-CH ₂ OH (S)-3.079	CR	CH	6.8(6) / 5.6(6) 16x	0.30 / 0.30	4.4(2)	4.0 / 7.0	59
6	6-CO ₂ Me (S)-3.080	CH	CR	6.2(6) / 6.1(6) 1x	0.26 / 0.22	<4.3(2)	5.6 / 8.6	15
7	5-CO ₂ Me (S)-3.081	CR	CH	7.3(6) / 5.8(5) ^c 32x	0.30 / 0.26	<4.3(2)	5.6 / 8.6	<1
8	 (S)-3.093	CR	CH	7.1(6) / 5.6(6) 32x	0.28 / 0.27	5.0(2)	4.8 / 7.8	20
9	 (S)-3.082	CR	CH	7.1(4) / 5.9(2) 16x	0.26 / 0.31	4.6(2)	3.8 / 6.8	49
10	 3.091^b	CR	CH	6.6(5) / 5.8(4) 6x	0.27 / 0.32	4.4(2)	3.4 / 6.4	150
11	- (S)-3.083	N	CH	6.8(5) / 5.7(4) 13x	0.32 / 0.31	4.5(2)	4.2 / 7.2	73
12	- (S)-3.084	CH	N	6.1(4) / 5.8(4) 2x	0.29 / 0.28	4.4(1) ^d	4.5 / 7.5	67

^a(A) denotes selectivity for ATAD2 over CECR2; ^bAn unknown diastereomeric mixture of hydroxy epimers; ^cAlso <4.0 (n = 1); ^dAlso <4.3 (n = 1); ^eAlso <4.8 (n = 1);

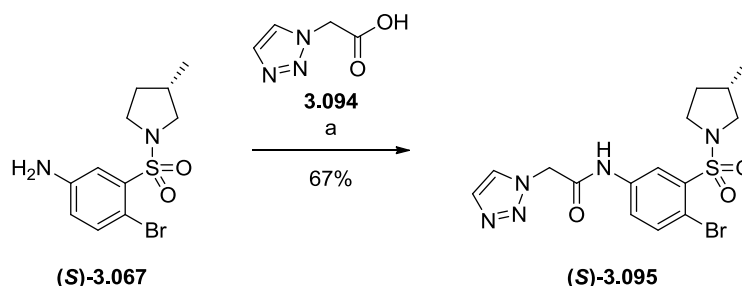
Having established that substitution at the 5-position of the benzotriazole was well tolerated, attention then turned to groups that would further reduce the PFI to aid in the search for a soluble compound. Morpholine derivative **(S)-3.093** was well tolerated (Table 3.06, Entry 8, CECR2 $\text{pIC}_{50} = 7.3$) and was 40-fold selective over ATAD2, however, did not significantly increase solubility ($20 \mu\text{g mL}^{-1}$) compared to **(S)-3.070**. Oxetanes are well known for their ability to increase solubility, but, surprisingly, only marginal improvements were observed for oxetane **(S)-3.082** (Entry 9, $49 \mu\text{g mL}^{-1}$).³²⁸ Compound **(S)-3.082** also did not display the desired 30-fold selectivity window over ATAD2. Of the benzotriazoles tested, only alcohol **3.091** (Entry 10) gave significant improvements in solubility, which was most likely driven by the additional H-bond donors, albeit it also had the lowest PFI. Despite the improved solubility **3.091** was not potent enough at CECR2 to warrant further study ($\text{pIC}_{50} = 6.6$). Triazolopyridines **(S)-3.083–3.084** were both designed to lower the ChromLogD and increase solubility without adding additional molecular weight. Pleasingly, **(S)-3.084** maintained potency and selectivity compared to benzotriazole **(S)-3.070** (Entries 11 vs 1). The reduction in lipophilicity did indeed increase the solubility, however, this was still below the desired threshold. The other regioisomer **(S)-3.83** was 0.6 log units less potent at CECR2.

3.7.4. Decreasing the PFI and Improving the LLE_{at} of the Benzotriazole

As further substitution of the benzotriazole had not delivered the desired physico-chemical profile, an alternative strategy was considered. Whilst the use of an aromatic phenyl ring increased potency at CECR2 it was unclear whether this was indeed the optimal substituent. Potentially, a smaller, less lipophilic substituent could provide the same boost in potency. Furthermore, removal of one aromatic ring would improve the PFI, therefore, it was reasonable to suggest that if tolerated these changes would improve the physico-chemical profile of the series.

As a starting point triazole **(S)-3.095** was synthesised from aniline **(S)-3.067** using the commercially available acid **3.094**, HATU and DIPEA in 67% yield (Scheme 3.08).

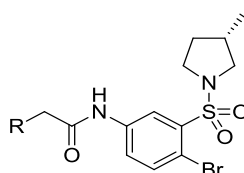
Scheme 3.08. Synthesis of triazole **3.095**.

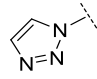
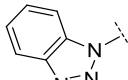


a) 2-(1H-1,2,3-triazol-1-yl)acetic acid hydrochloride (1.2 eq.), HATU (1.5 eq.), DIPEA (3.0 eq.), CH₂Cl₂, rt, 2h, 67%.

As expected triazole **(S)-3.095** was 1.3 log units less potent at CECR2 ($pIC_{50} = 5.4$) relative to benzotriazole **(S)-3.070**. Interestingly, both compounds were similarly potent at ATAD2 confirming that selectivity was being derived from the phenyl group of the benzotriazole. This is due to the polar Arg1007 residue in this region of ATAD2 which does not interact favourably with a hydrophobic group. Triazole **(S)-3.095** had a lower ChromLogD and PFI (3.9 and 5.9) compared to benzotriazole **(S)-3.070** and improved solubility (166 $\mu\text{g mL}^{-1}$) in agreement with previous analyses of the series (Figure 3.18).

Table 3.07. Exploration of triazole substitution.



	R	CECR2 pIC_{50} (n) / ATAD2 pIC_{50} (n) Selectivity	CECR2 LE / LLE _{at}	BRD4(1) pIC_{50}	Chrom LogD _{7.4} / PFI	CAD Solubility $\mu\text{g mL}^{-1}$
1	 (S)-3.095	5.4(6) / 5.4(6) -	0.30 / 0.30	<4.3(2)	3.9 / 5.9	≥ 166
2	 (S)-3.070	6.6(6) / 5.6(6) 10x	0.31 / 0.26	4.8(1) ^a	5.3 / 8.3	18

^aAlso <4.3 (n = 1)

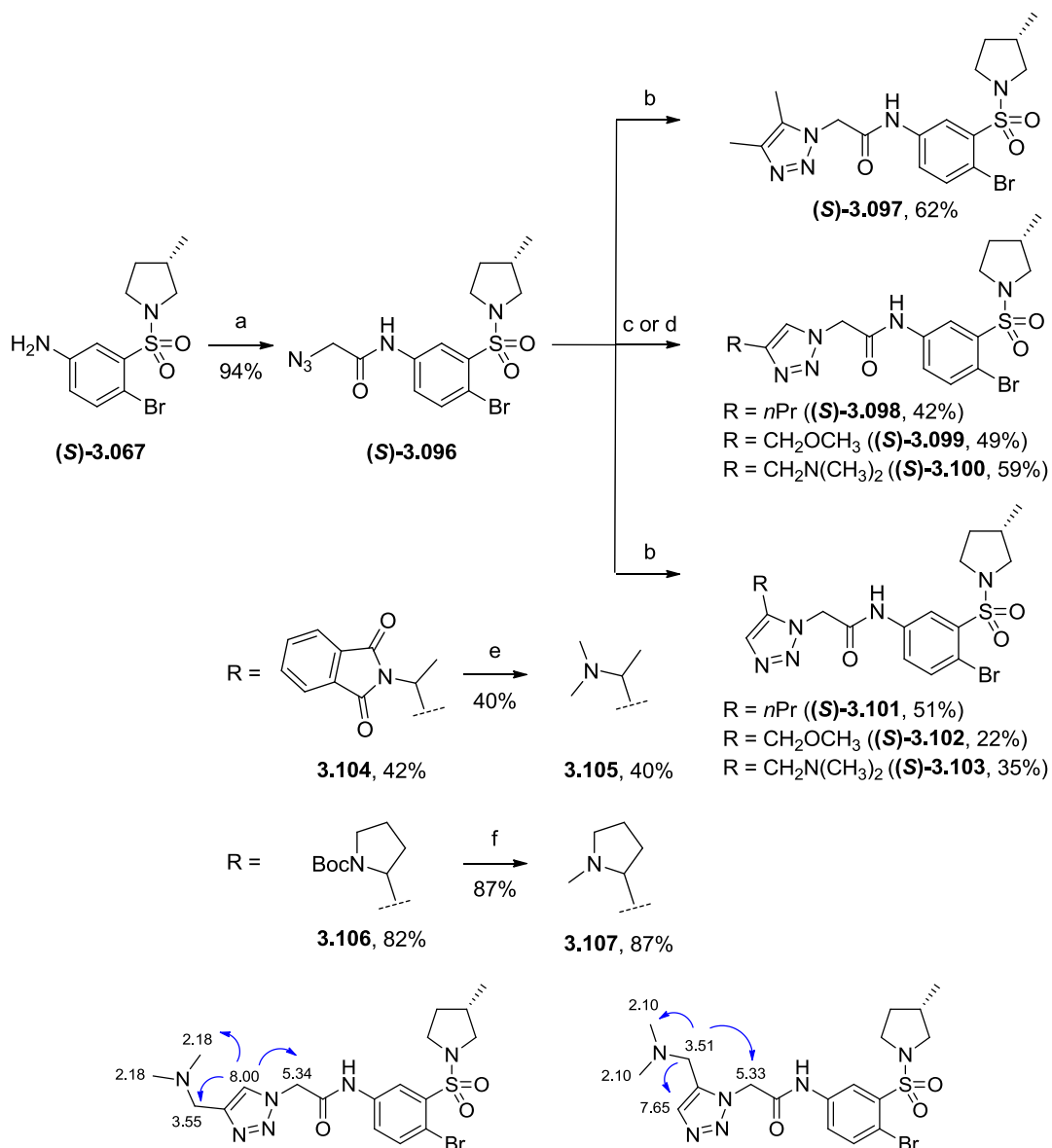
Both the LE and LLE_{at} of **(S)-3.095** and **(S)-3.070** were calculated and the values were intriguing. Whilst the addition of a phenyl ring to benzotriazole **(S)-3.070** increased CECR2 potency by 1.3 log units, the LE had only increased by 0.02. The LLE_{at} decreased on addition of the phenyl ring suggesting that the increase in potency was not justified by the concomitant increase in lipophilicity.

3.7.5. Investigating Triazole Substitution

It was proposed that it might be possible to maintain potency and selectivity whilst replacing the aromatic ring present in benzotriazole **(S)-3.070** with alternative substituents. However, without X-ray crystallography to aid design, rationally identifying interactions to target was difficult. Therefore, a diversity orientated approach was used. The substituents chosen were commercially available alkynes covering a range of functionality including alkyl chains, ethers and amines. The synthetic tractability of regioselectively forming substituted triazoles made this a desirable strategy for investigating a wide range of groups.

Triazole substituents **(S)-3.097–3.103**, **3.105** and **3.107** were prepared regioselectively by the route in Scheme 3.09. The late-stage azide **(S)-3.096** was prepared from aniline **(S)-3.067** and 2-azidoacetic acid, *via* a HATU mediated amide coupling, in 94% yield. The products could be synthesised in a regioselective fashion using click chemistry. A copper catalysed click reaction with the desired alkyne gave 4-substituted triazoles **(S)-3.098–3.100** in up to 59% yield.³²⁹ Alternatively, a ruthenium catalysed click reaction gave the 5-substituted triazoles **(S)-3.101–3.103** in up to 62% yield.³³⁰ Although there was excellent literature precedent for the regioselective nature of the two orthogonal metal catalysts employed, the regiochemistry of the dimethylamine triazoles (**3.100** and **3.103**) was also confirmed by NOESY NMR (Scheme 3.09, for spectra see Section 5). For **3.100**, irradiation of the signal at 8.00 ppm, corresponding to the triazole CH, showed enhancement of the signals at 2.18, 3.55, and 5.34; corresponding to the dimethylamine protons, the methylene between the triazole and dimethylamine group, and the methylene between the triazole and carbonyl, respectively. For **3.103**, irradiation of the signal at 3.51 ppm, corresponding to the methylene between the triazole and dimethylamine group, showed enhancement of the signals at 2.10, 5.33, and 7.65; corresponding to the dimethylamine protons, the methylene between the triazole and carbonyl and the triazole CH, respectively.

Scheme 3.09. Regioselective synthesis of triazoles (**(S)**-**3.097**–**3.103**, **3.105** and **3.107** and NOE correlations of **3.100** and **3.103**..

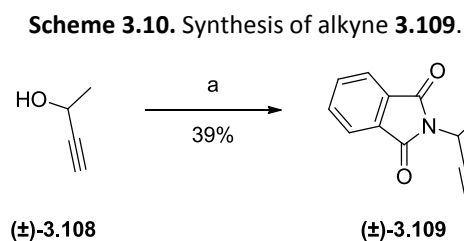


a) 2-Azidoacetic acid (1.0 eq.), HATU (1.2 eq.), DIPEA (3.0 eq.), CH_2Cl_2 , rt, 2 h, 94%; b) alkyne (1.5 eq.), $\text{Cp}^*\text{RuCl}(\text{PPh}_3)_2$ (3 mol%), THF, 65 °C, 2 h, 22–82%. c) alkyne (1.1 eq.), $\text{CuSO}_4 \cdot 5\text{H}_2\text{O}$ (5 mol%), sodium ascorbate (0.15 eq.), CH_2Cl_2 :water (1:1), rt, 16 h, 49–59%; d) alkyne (2.0 eq.), $\text{Cu}(\text{OAc})_2 \cdot \text{H}_2\text{O}$ (10 mol%), sodium ascorbate (0.15 eq.), MeOH, 100 °C, mw, 30 min, 42%; e) $\text{NH}_2\text{NH}_2 \cdot \text{H}_2\text{O}$ (1.5 eq.), EtOH, reflux, 30 min, then formaldehyde (37 w/w% in water, 2.5 eq.), STAB (2.5 eq.), MeOH, rt, 2 h, 40%; f) HCl (4 M in 1,4-dioxane, 4.5 eq.), rt, 4 h, then formaldehyde (37% w/w in water, 1. eq.), STAB (1.3 eq.), MeOH, rt, 2 h, 87%.

The phthalimide protecting group of **3.104**, was removed using hydrazine monohydrate to give the free amine which could be methylated using Eschweiler Clarke conditions to afford **3.105** in 40% yield as a 1:1 mixture of diastereomers. For **3.106**, Boc deprotection was

facilitated using HCl (4 M in 1,4-dioxane) and the free amine could again be methylated using Eschweiler Clarke conditions to afford pyrrolidine **3.107** in 87% yield as a 1:1 mixture of diastereomers. The two diastereomers of **3.107** were obtained by column chromatography using a chiral stationary phase, to give (*S,S**)-**3.107** and (*S,R**)-**3.107** of undefined absolute configuration at the new chiral centre.

Alkyne (\pm)-**3.109** was not commercially available, but could be synthesised *via* the route outlined in Scheme 3.10.³³¹ Mesylation of alcohol (\pm)-**3.108** was achieved using methane sulfonic anhydride and TEA base. Alkylation of the mesylate intermediate using potassium phthalimide gave (\pm)-**3.109** in 39% yield.



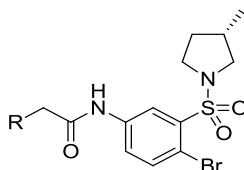
a) TEA (3.0 eq.), Ms₂O (1.5 eq.), CH₂Cl₂, rt, 1 h, *then* potassium 1,3-dioxoisindolin-2-ide (1.4 eq.), DMF, 80 °C, 1 h, 39%.

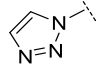
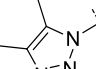
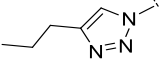
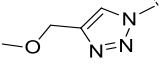
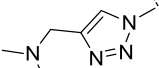
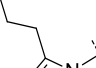
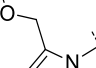
With a selection of substituted triazoles in hand, the potency, selectivity and physico-chemical properties were evaluated. As discussed, triazole (*S*)-**3.095** (Table 3.08, Entry 1) had shown reduced CECR2 potency (*c.f.* benzotriazole (*S*)-**3.070**, Table 3.07, Entry 2). However, 4,5-dimethyltriazole (*S*)-**3.097** showed increased CECR2 inhibition ($pIC_{50} = 6.0$) whilst maintaining reduced affinity for ATAD2 (Table 3.07, Entry 2). Importantly, this suggested that the aromatic ring could be replaced by sp^3 groups with similar overall efficiency. A range of substituents at the 4-position were then investigated ((*S*)-**3.098–3.100**). Neither a propyl or ether group at the 4-position of the triazole increased potency or selectivity for CECR2 ((*S*)-**3.098** and (*S*)-**3.099**, Entries 3 and 4). However, the installation of a methylene linked dimethylamine afforded compound (*S*)-**3.100** (Entry 5, $pIC_{50} = 6.6$) which was equipotent with benzotriazole (*S*)-**3.070** and 2.2 log units more polar. Unfortunately, (*S*)-**3.100** was only 5-fold selective over ATAD2 but it did give confidence in this approach. Substitution at the 5-position was then explored. Interestingly, the same substituents at the 5-position ((*S*)-**3.101–3.103**) all showed increased potency and selectivity (Entries 6–8). In particular,

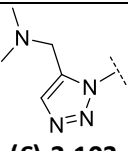
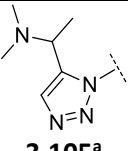
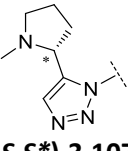
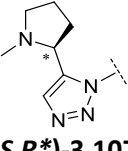
GSK Confidential – Do not copy

dimethylamine **(S)-3.103** was potent at CECR2 ($pIC_{50} = 7.1$) and displayed 40-fold selectivity over ATAD2. It was also highly soluble ($224 \mu\text{g mL}^{-1}$) despite being 1.4 log units more lipophilic than dimethylamine **(S)-3.100** (discussed in more detail subsequently). Importantly, **(S)-3.103** demonstrated for the first time that CECR2 selectivity was possible with compounds that had a suitable physico-chemical profile. Dimethylamine **(S)-3.103** was progressed into downstream assays and will be discussed further in Section 3.9.

Table 3.08. Exploration of triazole substitution.



	R	CECR2 pIC_{50} (n) / ATAD2 pIC_{50} (n) Selectivity	CECR2 LE / LLE _{at}	BRD4 BD1 pIC_{50} (n)	Chrom LogD _{7.4} / PFI	CAD solubility ($\mu\text{g mL}^{-1}$)
1	 (S)-3.095	5.4(6) / 5.4(6) -	0.30 / 0.30	<4.3(2)	3.9 / 5.9	≥ 166
2	 (S)-3.097	6.0(6) / 5.2(6) 6x	0.30 / 0.30	<4.3(2)	4.4 / 6.4	≥ 181
3	 (S)-3.098	5.8(6) / 5.8(8) -	0.28 / 0.24	4.4(2)	5.1 / 7.1	48
4	 (S)-3.099	5.8(6) / 5.6(8) 2x	0.28 / 0.31	<4.3(2)	4.1 / 6.1	≥ 235
5	 (S)-3.100	6.6(4) / 5.9(6) 5x	0.31/ 0.34	<4.3(2)	3.1 / 5.1	≥ 234
6	 (S)-3.101	7.1(5) / 5.5(6) 40x	0.35 / 0.30	5.1(2)	5.1 / 7.1	19
7	 (S)-3.102	6.6(6) / 6.0(6) 4x	0.32 / 0.35	4.3(1) ^b	4.3 / 6.3	≥ 216

8	 (S)-3.103	7.1(5) / 5.4(6) 50x	0.34 / 0.37	<4.3(2)	4.6 / 6.6	≥219
9	 3.105^a	7.0(4) / 5.6(4) 25x	0.32 / 0.34	4.6(2)	5.1 / 7.1	≥213
10	 (S,S*)-3.107	7.8(3) / 5.6(4) 160x	0.34 / 0.35	5.2(2)	4.7 / 6.7	≥226
11	 (S,R*)-3.107	7.4(3) / 5.5(4) 80x	0.33 / 0.33	4.9(2)	4.7 / 6.7	≥189

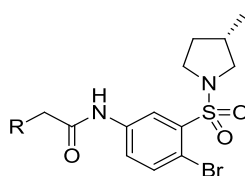
^aA 1:1 diastereomeric mixture of methylene epimers; ^bAlso <4.3 (n = 1).

Additional amine substituents were then investigated. α -Substitution of the methylene unit to give amine **3.105** was well tolerated, although it offered no benefits over **(S)-3.103**. The additional methyl group increased the ChromLogD by 0.6 log units relative to **(S)-3.103**, however, this did not significantly lower the solubility. This suggests that the reduction in aromatic ring count and the presence of a polar amine is sufficient to drive solubility. Pyrrolidines **(S,S*)-3.107** and **(S,R*)-3.107** significantly increased potency at CECR2 ($pIC_{50} \geq 7.6$) and were 126-fold and 200-fold selective, respectively. Interestingly, the ChromLogD only increased by 0.2 log units for **(S,S*)-3.107** and **(S,R*)-3.107** compared to dimethylamine **(S)-3.103**. This is potentially due to an increase in polarity driven by cyclisation. Pleasingly, both **(S,S*)-3.107** and **(S,R*)-3.107** were highly soluble ($CAD \geq 189 \mu g mL^{-1}$). Pyrrolidines **(S,S*)-3.107** and **(S,R*)-3.107** will also be discussed further in Section 3.9.

The difference in lipophilicity of the dimethylamine regioisomers **(S)-3.100** and **(S)-3.103** was interesting and warranted further investigation. It was thought that the difference in lipophilicity was either a function of basicity or polarity, therefore, the basicity of the amine nitrogen was examined (Table 3.09). Firstly, the difference between $ChromLogD_{7.4}$ and $ChromLogD_{10.5}$ was established. Interestingly, the greatest difference was observed for dimethylamine **(S)-3.100** ($\Delta = 1.0$) suggesting that at physiological pH the amine is protonated

and therefore basic. Furthermore, the difference observed for dimethylamine (**(S)**-**3.103**) was negligible suggesting that in this case the amine is not basic. There is the possibility that the adjacent *N*-lone pair in (**(S)**-**3.100**), is capable of stabilising the protonated species in this example. There is still a 0.7 log unit difference in ChromLogD_{10.5}, suggesting that polarity is also a contributing factor to the overall lipophilicity. α -Substitution of the methylene unit (**3.105**) also showed no difference between ChromLogD_{7.4} and ChromLogD_{10.5} suggesting no formation of a protonated species. As expected, ChromLogD did increase relative to (**(S)**-**3.103**) with the addition of the methyl group.

Table 3.09. Exploration of triazole substitution.



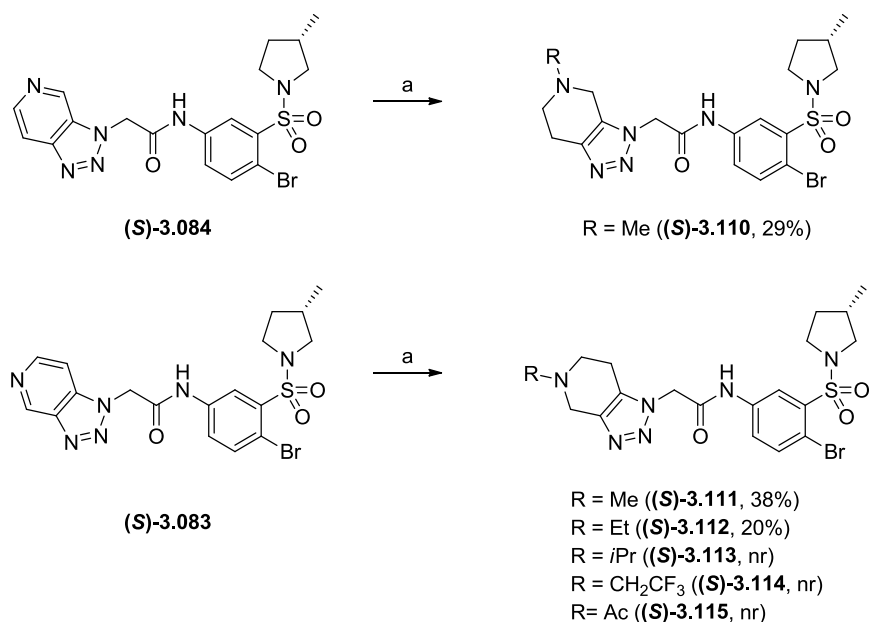
	R	Chrom LogD _{7.4}	Chrom LogD _{10.5}	Δ	Chemaxon pKa
4	 (S) - 3.100	3.1	4.1	1.0	6.6
7	 (S) - 3.103	4.6	4.5	-0.1	6.6
9	 3.105	5.1	5.1	0.0	6.9
10	 (S,S*) - 3.107	4.7	5.0	0.3	7.0
11	 (S,R*) - 3.107	4.7	5.0	0.3	7.0

There was a minor difference between ChromLogD_{7.4} and ChromLogD_{10.5} for pyrrolidines **(S,S*)-3.107** and **(S,R*)-3.107** ($\Delta = 0.3$) suggesting a weakly basic amine. To further investigate the amine basicity, the pKa was predicted using Chemaxon. Surprisingly, this was unable to distinguish between the two regioisomers, suggesting that the software does not give an accurate prediction in this case.

3.7.6. Conformational restriction of triazole amides

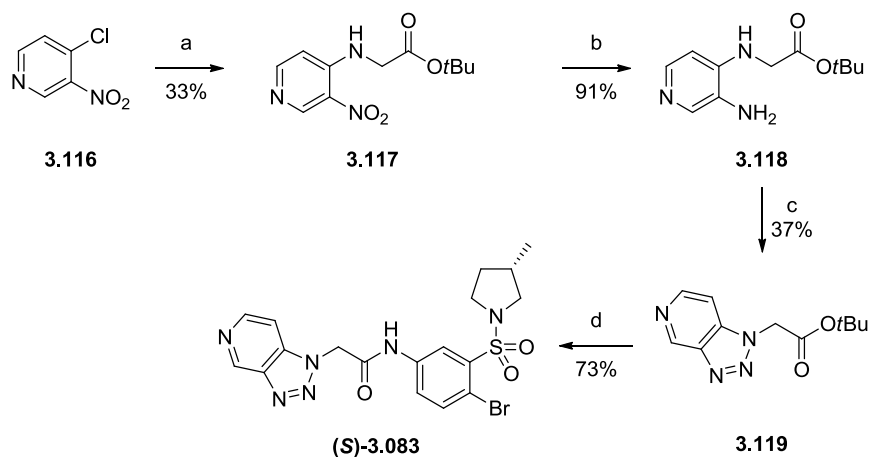
Secondary amine derivatives (**(S)-3.103**, **(S,S*)-3.107** and **(S,R*)-3.107**) had demonstrated that the desired chemical probe profile was achievable. However, the most favourable conformation of the flexible amine groups, and whether they made any specific interactions with the protein, was unknown. To probe this, further rigidification of the amine groups was proposed. If rigidification locked the amine group in a desirable conformation, then, binding to CECR2 would become entropically more favourable leading to an increase in potency. Triazole **(S)-3.097** had demonstrated that substitution at both the 4- and 5- position was tolerated simultaneously, therefore, cyclisation of the amines back into the triazole ring to form triazolopiperidines **(S)-3.110–3.111** was proposed.

Triazolopiperidines **(S)-3.110–3.112** were prepared *via* the route in Scheme 3.11 from triazolopyridines **(S)-3.084** and **(S)-3.083** (which had been prepared previously by separation of the two regioisomers; see Scheme 3.06, Section 3.7.3). Firstly, the triazolopyridines **(S)-3.084** and **(S)-3.083**, were refluxed with an alkylating agent (either methyl or ethyl iodide) to form an intermediate pyridinium ion. After a solvent switch to MeOH:water, reduction of the intermediate pyridinium was then achieved using sodium borohydride to afford the desired product in 20–38% yield.

Scheme 3.11. Synthesis of triazolopiperidines (**S**)-3.10–3.115.

a) Alkyl iodide or anhydride (1.2 eq.), MeCN, 80 °C, 4 h, then NaBH₄ (2.2 eq.), MeOH:water (1:1), rt, 1 h, 20-38%.

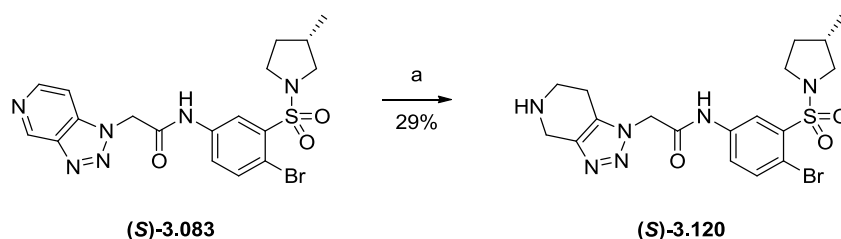
Unfortunately, this route was not feasible for a wider range of substituents. 2-Iodopropane, 2,2,2-trifluoroethyl iodide and acetic anhydride all failed to form the desired pyridinium intermediate and only SM was observed in the reaction mixture. This suggested that either the electrophiles were not strong enough to promote attack by the pyridine lone pair or that the intermediate pyridinium was unstable. Therefore, an alternative approach was targeted which involved hydrogenation of triazolopyridine (**S**)-3.083 to form triazolopiperidine (**S**)-3.120. From here, a series of alkylations/acylations would afford the desired substituents ((**S**)-3.113–3.115). However, the previous synthesis of triazolopyridines (**S**)-3.084 and (**S**)-3.083 had required the separation of the two regioisomers (Scheme 3.06, Section 3.7.3). Whilst this was appropriate for the concise synthesis of both desired triazolopyridine regioisomers, the low yield was not optimal for further functionalisation. Therefore, a regioselective synthesis of the desired triazolopyridine (**S**)-3.083 was investigated using a route analogous to the synthesis of benzotriazole (**S**)-3.088 (Scheme 3.07, Section 3.7.3).

Scheme 3.12. Synthesis of late stage intermediate (**S**)-**3.084**.

a) *tert*-butyl glycinate (1.1 eq.), TEA (1.0 eq.), EtOH, reflux, 6 h, 33%; b) iron (5.0 eq.), NH₄Cl (1.5 eq.), EtOH:water (3:1), 70 °C, 2 h, 91%; c) NaNO₂ (1.2 eq.), AcOH:water (1:1), 0 °C-80 °C, 37%; d) HCl (4 M in dioxane, 8.3 eq.), 40 °C, overnight *then* **3.068** (0.83 eq.), HATU (1.0 eq.), DIPEA (2.5 eq.), rt, 2 h, 73%.

An S_NAr reaction of 3-nitro-4-chloropyridine (**3.116**) using *tert*-butyl glycinate gave aryl nitro derivative **3.117** (Scheme 3.12). This could be reduced to the corresponding aniline **3.118** using iron and NH₄Cl in 91% yield. Formation of the diazonium salt using sodium nitrite followed by *in situ* cyclisation gave the desired triazolopyridine **3.119**. Hydrolysis of the *tert*-butyl ester followed by an amide coupling gave triazolopyridine (**S**)-**3.083** in 8% yield over 4 steps which could now be used as a late stage intermediate.

With a route to triazolopyridine (**S**)-**3.083** that could be performed at scale in place, the hydrogenation to afford (**S**)-**3.120** could be investigated. The hydrogenation conditions used needed to be compatible with the functionality already in place. Of immediate concern was the aromatic bromide which could be susceptible to hydrogenolysis (e.g. with a Pd/C catalyst). Reports in the literature suggested that Rh/C catalysts were optimal for the hydrogenation of triazolopyridines therefore this was chosen as a starting point for this investigation.³³² Hydrogenation of triazolopiperidine (**S**)-**3.083** was carried out using a 5% Rh/C catalyst in a H-cube apparatus at rt and atmospheric pressure. AcOH was also used, as protonation of the pyridine ring is known to promote reduction.³³² Unfortunately, the conversion was disappointingly low even after 24 h, leading to an isolated yield of just 29%. This low yield was insufficient for progression and so an investigation into more suitable conditions was conducted.

Scheme 3.13. Initial attempts at the hydrogenation of triazolopyridine **3.120**.

a) Rh/C, H₂, MeOH:EtOH:AcOH (1:1:1), H-cube flow apparatus, 24 h, 29%.

To improve the efficiency of the hydrogenation, a catalyst screen was carried out. The catalysts were chosen from the internal heterogeneous catalyst collection available in our laboratory. All Pd containing catalysts were omitted to try and mitigate the formation of debrominated product. This left 10 catalysts from Johnson Matthey's (JM's) primary screening collection. Additionally, two Rh/C catalysts from Evonik's primary catalyst collection were also chosen for investigation. The reaction screen was carried out in a CAT96 instrument.³³³ This is a semi-automated piece of equipment which can accurately control temperature, pressure and stirring rate for up to 96 reactions. The hydrogenation was first run at rt under 15 bars of hydrogen, in MeOH:AcOH (10:1). After 22 h only JM26 B103032-5 (Table 3.10, Entry 2), a 5% Pt/C catalyst, showed any appreciable conversion (22%) to the desired product. Most reactions were mainly mixtures of starting material **(S)-3.083** and desired product **(S)-3.120** only, showing at least, that formation of undesirable side-products was being kept to a minimum.

GSK Confidential – Do not copy

Table 3.10. HPLC analysis of hydrogenation catalyst screen run in MeOH:AcOH (10:1) at 15 bar H₂ for 22 h at rt.

	Type	Supplier	Name	(S)-3.120 Area % ^a	(S)-3.083 Area % ^a	(S)-3.120 + (S)-3.083 Area % ^a
1	3% Pt/C	JM25	B103032-3	12	50	62
2	5% Pt/C	JM26	B103032-5	22	47	69
3	5% Pt/C	JM27	5R18	12	50	62
4	5% Pt/C	JM28	5R128M	9	65	74
5	5% Pt/C	JM29	B501032-5	7	69	76
6	10% Pt/C	JM31	10R128M	11	63	74
7	5% Rh/C	JM34	C101023-5	5	83	88
8	5% Rh/C	JM35	5R594	4	68	72
9	5% Rh/Al ₂ O ₃	JM36	C301099-5	11	65	76
10	5% Rh/C	JM38	5R619	6	86	92
11	5% Rh/C	Evonik	P3051	1	92	93
12	5% Rh/C	Evonik	P3053	0	94	94

^aPeak areas were analysed by HPLC.

To improve conversion, the temperature of the reaction was increased. After 28 h at 50 °C, the reaction mixture was analysed (Table 3.11). Unfortunately, none of the Rh/C catalysts investigated gave sufficient conversion to the desired product (Entries 7-8 and 10-12, <33%). Pleasingly, use of a Rh/Al₂O₃ catalyst, JM36 C301099-5 (Entry 9), gave 67% conversion to **(S)-3.120** leaving 10% remaining starting material **(S)-3.083**. Two Pt/C catalysts, JM26 B103032-5 and JM31 10R128M, also gave good conversion (Entries 2 and 6). 10% Pt/C JM31 10R128M (63%) was slightly inferior to 5% Pt/C JM26 B103032-5, which gave the greatest conversion (80%) to the desired product **(S)-3.120**. This represented almost complete consumption of the starting material (3% remaining) and minimal side-product formation. Therefore, JM26 B103032-5 was chosen as the optimal catalyst for the hydrogenation. Interestingly, none of the other Pt/C catalysts were comparable (Entries 1 and 3–5) which emphasizes the complex factors governing the choice of heterogeneous catalyst.

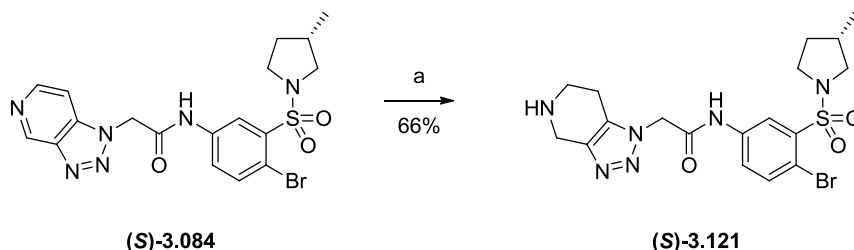
Table 3.11. HPLC analysis of hydrogenation catalyst screen run in MeOH:AcOH (10:1) at 15 bar H₂ for 22 h at rt and 28 h at 50 °C. Peak areas were measured by HPLC.

	Type	Supplier	Name	(S)-3.120 Area % ^a	(S)-3.083 Area % ^a	(S)-3.120 + (S)-3.083 Area % ^a
1	3% Pt/C	JM25	B103032-3	50	16	66
2	5% Pt/C	JM26	B103032-5	80	3	83
3	5% Pt/C	JM27	5R18	47	20	67
4	5% Pt/C	JM28	5R128M	48	42	80
5	5% Pt/C	JM29	B501032-5	51	30	81
6	10% Pt/C	JM31	10R128M	63	10	73
7	5% Rh/C	JM34	C101023-5	19	70	89
8	5% Rh/C	JM35	5R594	29	26	55
9	5% Rh/Al ₂ O ₃	JM36	C301099-5	67	10	77
10	5% Rh/C	JM38	5R619	33	40	73
11	5% Rh/C	Evonik	P3051	7	80	87
12	5% Rh/C	Evonik	P3053	4	83	87

^aPeak areas were analysed by HPLC.

With the discovery of a suitable catalyst, the hydrogenation of triazolopyridine **(S)-3.083** could now be carried out on a 750 mg scale to give the desired product **(S)-3.120** in 66% yield (Scheme 3.14).

Scheme 3.14. Hydrogenation of triazolopyridine **3.084** to afford triazolopiperidine **3.121**.

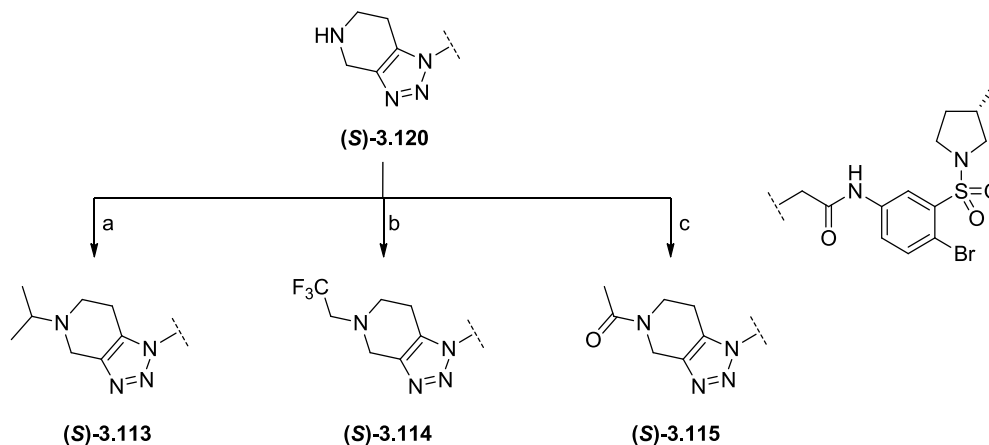


a) 5% Pt/C (JM26, B103032-5, 10% w/w), H₂ (240 psi), MeOH, 50 °C, 16 h; 66%.

With a suitable route to triazolopiperidine **(S)-3.120** established, further functionalisation of the amine could now be conducted (Scheme 3.15). *Isopropyl* amine **(S)-3.113** was synthesised through alkylation of amine **(S)-3.120** using 2-iodopropane and K₂CO₃ as a base in 58% yield. The fluorinated amine **(S)-3.114** was prepared in 43% yield using methodology developed by Denton *et al.* for the late stage trifluoroethylation of amines.³³⁴ Their work used TFA as a trifluoroethyl source and phenylsilane as a reductant to give the desired

trifluoroethylamines in high yields. Lastly, amide (**S**)-**3.115** was prepared using acetic anhydride and DIPEA to furnish the desired product in 53% yield.

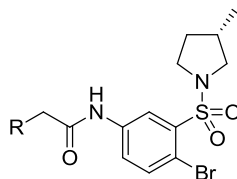
Scheme 3.15. Synthesis of triazolopiperidines (**S**)-**3.113–3.115**.



a) Iodopropane (1.5 eq.), K_2CO_3 (3.0 eq.), acetone, 80 °C, 4 h, 58%; b) $PhSiH_3$ (2.0 eq.), TFA (1.75 eq.), THF, 70 °C, 1 h, 43%; c) Ac_2O (1.5 eq.), DIPEA (3.0 eq.), CH_2Cl_2 , rt, 1 h, 53%.

Having the dimethylamine substituent at the 5-position (**S**)-**3.103** had afforded higher potency relative to the 4-substituent (**S**)-**3.100** during the exploration of the triazole vectors (Table 3.08, Section 3.7.5). Therefore, conformational restriction of this amine was investigated first. Interestingly, triazolopiperidine (**S**)-**3.110** was 0.4 log units less potent at CECR2 ($pIC_{50} = 6.7$) relative to dimethylamine (**S**)-**3.103**. This suggested that conformational restriction did not keep the dimethylamine in its favoured binding conformation. It was also possible that the methyl group at this position induced a clash with the protein. Therefore, the regioisomer was prepared and pleasingly, triazolopiperidine (**S**)-**3.111** was both highly potent (Entry 2, CECR2 $pIC_{50} = 7.4$) and 32-fold selective for CECR2. Additionally, (**S**)-**3.111** had a low ChromLogD (3.7) and was highly soluble ($440 \mu g mL^{-1}$). The methyl group could be extended to give ethylamine (**S**)-**3.112** (Entry 3) which had a comparable profile to (**S**)-**3.111** albeit with a slight increase in ChromLogD. Branching of the alkyl group gave *isopropyl* amine (**S**)-**3.113** which was also highly potent at CECR2 (Entry 4, $pIC_{50} = 7.6$), equating to 79-fold selectivity over ATAD2. Despite the increased lipophilicity compared to (**S**)-**3.111** and (**S**)-**3.112**, *isopropyl* amine (**S**)-**3.113** was still highly soluble ($238 \mu g mL^{-1}$). None of these alkylated triazolopiperidines ((**S**)-**3.111–3.113**) showed any significant activity at BRD4 BD1 ($pIC_{50} \leq 4.5$) and will therefore be discussed further in Section 3.9.

Table 3.12. Exploring cyclic saturated triazoles.



	R	CECR2 pIC ₅₀ (n) / ATAD2 pIC ₅₀ (n) Selectivity	CECR2 LE / LLE _{at}	BRD4 BD1 pIC ₅₀ (n)	Chrom LogD _{7.4} / PFI	CAD Solubility (μg mL ⁻¹)
1	 (S)-3.110	6.6(4) / 5.7(4) 8x	0.30 / 0.33	<4.3(2)	3.9 / 5.9	≥186
2	 (S)-3.111	7.3(8) / 5.7(10) 40x	0.33 / 0.37	<4.3(4)	3.7 / 5.7	≥211
3	 (S)-3.112	7.3(8) / 5.6(10) 50x	0.32 / 0.34	4.5(3) ^a	4.1 / 6.1	569
4	 (S)-3.113	7.5(3) / 5.7(4) 63x	0.32 / 0.32	4.3(1) ^a	4.5 / 6.5	238
5	 (S)-3.114	6.8(3) / 5.6(4) 16x	0.27 / 0.28	4.5(2)	5.3 / 7.3	49
6	 (S)-3.115	7.0(3) / 5.8(4) 16x	0.30 / 0.40	<4.3(2)	3.4 / 5.4	182
7	 (S)-3.120	6.6(5) / 5.6(6) 10x	0.31 / 0.37	4.8(2)	2.9 / 4.9	≥233

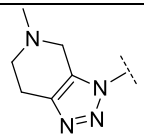
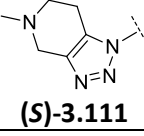
^aAlso <4.3 (n = 1).

In an effort to further understand the tolerated substitution of the amine, trifluoroethylamine **(S)-3.114** was tested. Interestingly, a 0.5 log unit reduction in CECR2 potency was observed relative to ethylamine **(S)-3.112**. The increased lipophilicity of **3.114** was also detrimental to the solubility (49 μg mL⁻¹). Acylation of the amine gave acetamide **3.115** which was potent at CECR2 (Entry 6, pIC₅₀ = 7.1) but was only 20-fold selective over

ATAD2. The unsubstituted triazolopiperidine (**S**)-**3.120** was poorly tolerated in CECR2 (Entry 7, $pIC_{50} = 6.6$) but still maintained a 10-fold selectivity window.

The basicity of the triazolopiperidine nitrogen was examined. Interestingly, there was little difference between the ChromLogD_{7.4} and ChromLogD_{10.5} for both methyl triazolopiperidine regioisomers (Table 3.13), suggesting that the amine is not highly protonated at physiological pH. Therefore, the desirable ChromLogD of (**S**)-**3.110** and (**S**)-**3.111** is most likely a function of polarity caused by the nitrogen dipoles. It is interesting that conformational restriction of (**S**)-**3.100** decreases the degree of protonation, which might be in keeping with an inability of the adjacent triazole *N*-lone pair to stabilise the protonated form of these cyclic examples.

Table 3.13. Assessing the basicity of triazolopiperidines (**S**)-**3.111-3.112**.

	R	Chrom LogD _{7.4}	Chrom LogD _{10.5}	Δ	Chemaxon pKa
1	 (S)-3.110	3.9	4.1	0.2	6.1
2	 (S)-3.111	3.7	3.7	0.0	8.4

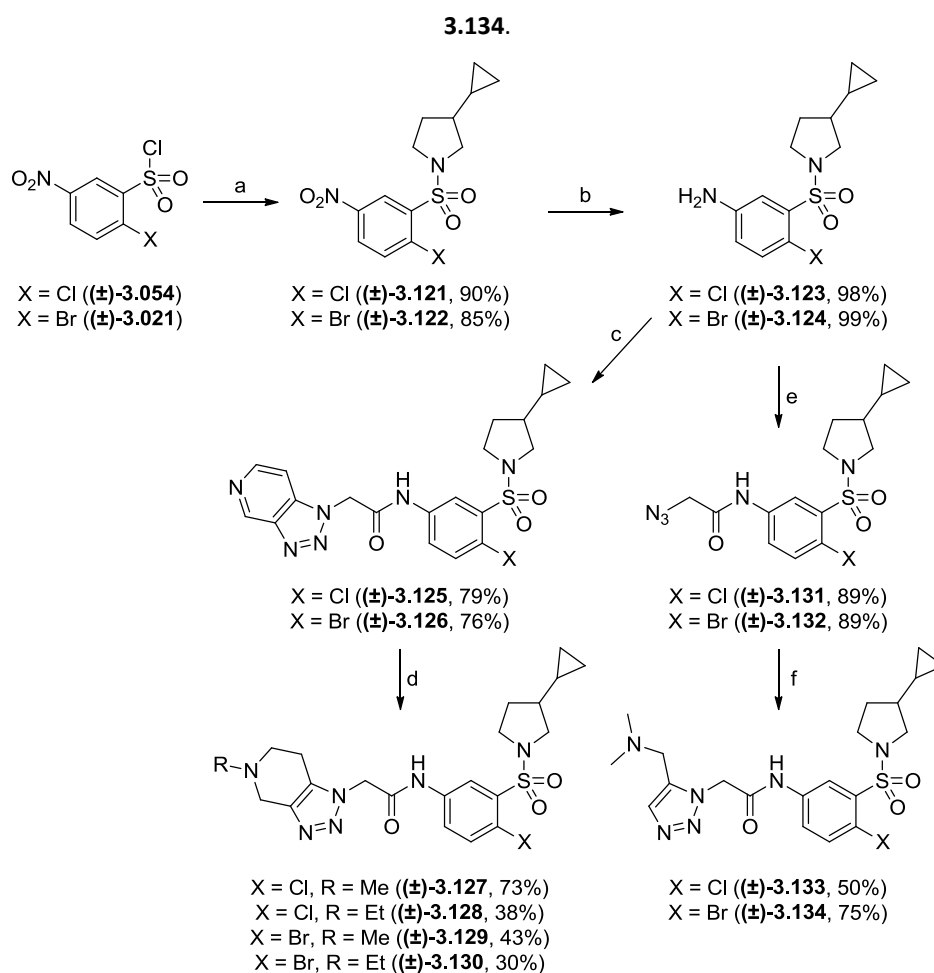
3.8. Greater Selectivity Through Sulfonamide Modification

The discovery of dimethylamine (**S**)-**3.103** and triazolopiperidines (**S**)-**3.111–3.113** was encouraging, as they met most of the desired criteria set out at the onset of the project and could be progressed to understand their wider bromodomain selectivity and cellular target engagement. However, it was thought that by revisiting the most promising sulfonamides (Section 3.6), that potency and selectivity could be increased further. As shown in Table 3.03, (Section 3.6) further extending the substitution at the pyrrolidine 3-position from methyl to cyclopropyl, increased potency at CECR2, albeit with only minor increases in LE. It was felt that the improved physico-chemical profile of the triazole moiety would make the series much more tolerant of the increased lipophilicity associated with moving to a 3-cyclopropyl pyrrolidine and that this substituent would further increase potency at CECR2 without

affecting ATAD2 potency. In addition, the chloride had been shown to be an appropriate replacement of the bromide and therefore both halides were included in this final iteration.

To test this hypothesis, sulfonamides (**±**)-**3.127–3.130** and (**±**)-**3.133–3.134** were synthesised using established routes. The cyclopropyl group had no detrimental impact on reactivity and the reactions proceeded in good yields (Scheme 3.16). Where sufficient material was obtained the two enantiomers were separated by chromatography on a chiral stationary phase. The most potent enantiomer of each compound was assigned as (*S**) and the least potent enantiomer assigned as (*R**) for clarity throughout this work.

Scheme 3.16. Synthesis of 3-cyclopropylpyrrolidine sulfonamides (**±**)-**3.127–3.130** and (**±**)-**3.133–**



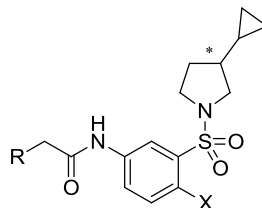
a) 3-cyclopropylpyrrolidine (1.0 eq.), DIPEA (2.2 eq.), CH₂Cl₂, 0 °C, 2 h, 85–90%; b) iron (3.0 eq.), NH₄Cl (1.5 eq.), 3:1 EtOH:water, 70 °C, 2 h, 98–99%; c) Acid **3.120** (1.2 eq.), HATU (1.2 eq.), DIPEA (3.0 eq.), CH₂Cl₂, rt, 2 h, 76–79%; d) R-I (1.0–5.0 eq.), MeCN, 80 °C, 2 h, then NaBH₄ (2.2 eq.), 1:1 MeOH:water, rt, 30–73%; e) 2-azidoacetic acid (1.1 eq.), HATU (1.2 eq.), DIPEA (3.0 eq.), CH₂Cl₂, rt, 1 h, 89%; f) *N,N*-dimethylprop-2-yn-1-amine (1.5 eq.), Cp**Ru*Cl(PPh₃)₂ (3 mol%), THF, 65 °C, 2 h, 50–75%.

GSK Confidential – Do not copy

Methyl triazolopiperidines (**±**)-**3.127** and (**±**)-**3.129** were prepared as single enantiomers with both a chloro and bromo aryl substituent. With the increase in potency gained from the cyclopropyl group, the most active enantiomer, (**S**^{*})-**3.127** retained high potency at CECR2 ($\text{pIC}_{50} = 8.2$) even with chloride substitution on the aromatic ring. Interestingly, the opposite enantiomer was 20-fold less potent at CECR2, a trend which was also observed for (**S**^{*})-**3.129** vs. (**R**^{*})-**3.129**. This is significant as both enantiomers of methyl pyrrolidine ((**S**)-**3.046** and (**R**)-**3.046**) were equipotent at CECR2 (Table 3.03, Section 3.6). It is likely that the increased size of the cyclopropyl group means that the pocket is more accommodating to one enantiomer and less accommodating to the other. Chlorides (**S**^{*})-**3.127** and (**R**^{*})-**3.127** were in the desirable physico-chemical space and were highly soluble. Changing the aryl substituent to bromide (**S**^{*})-**3.130** (Table 3.14, Entry 3) did not give the additive increase in potency normally associated with this point change (Table 3.02, Section 3.5). However, both enantiomers were potent ($\text{pIC}_{50} \geq 7.4$), greater than 63-fold selective and highly soluble ($\geq 177 \mu\text{g mL}^{-1}$). Changing the triazolopiperidine substitution to ethyl was well tolerated. In this case, only the racemates were tested, but they were potent ($\text{pIC}_{50} \geq 7.6$) and >150-fold selective for CECR2, with a slightly lower LE compared to the comparative methyl analogue. Furthermore, both chloride (**±**)-**3.128** and bromide (**±**)-**3.130** were highly soluble and showed low affinity for BRD4 BD1. However, it was not obvious at this stage if the ethyl group was really differentiating relative to (**S**^{*})-**3.127** and (**S**^{*})-**3.129**. Next the triazoles **3.133–3.134** were investigated. An additive loss in potency is usually associated with the bromide to chloride switch, however, for the most active cyclopropyl enantiomer ((**S**^{*})-**3.133**), this is mitigated by an increase in potency caused by the cyclopropyl substituent. This delivered a potent probe ($\text{pIC}_{50} = 7.3$) with 160-fold selectivity over ATAD2. As expected, a 0.4 log unit increase in potency from chloride (**S**^{*})-**3.133** to bromide (**S**^{*})-**3.134** is still observed. The most active enantiomer of (**S**^{*})-**3.134** had a CECR2 pIC_{50} of 7.7 and maintained 130-fold selectivity over ATAD2. Triazoles **3.133–3.134** had a higher ChromLogD (5.1) than the triazolopiperidines **3.133–3.134**, however, they were still highly soluble ($\geq 111 \mu\text{g mL}^{-1}$). Overall, a set of potential tool compounds ((**S**)-**3.103**, (**S,S**^{*})-**3.107**, (**S,R**^{*})-**3.107**, (**S**)-**3.111–3.113**, (**S**^{*})-**3.127**, **3.128**, (**S**^{*})-**3.129**, **3.130**, (**S**^{*})-**3.133**, (**S**^{*})-**3.134**) had now been identified, however, it was now necessary to evaluate their wider BRD selectivity and demonstrate cellular target engagement.

GSK Confidential – Do not copy

Table 3.14. Investigating the addition of a 3-cyclopropyl pyrrolidine sulfonamide.



	R	X	Cmpd No.	CECR2 pIC ₅₀ (n) / ATAD2 pIC ₅₀ (n) Selectivity	CECR2 LE / LLE _{at}	BRD4 BD1 pIC ₅₀ (n)	Chrom LogD _{7.4}	CAD Solubility (µg mL ⁻¹)
1		Cl	(S*)- 3.127	7.7(4) / 5.5(2) 160x	0.33 / 0.36	4.6(4)	4.3	207
2			(R*)- 3.127	6.9(5) / 5.2(4) 50x	0.30 / 0.32	4.4(2)	4.3	≥312
3		Br	(S*)- 3.129	8.2(3) / 5.7(4) 320x	0.35 / 0.38	4.9(2)	4.4	177
4			(R*)- 3.129	7.4(3) / 5.5(4) 79x	0.32 / 0.35	4.6(2)	4.4	248
5		Cl	(±)- 3.128	7.5(5) / 5.3(6) 160x	0.31 / 0.32	4.7(3)	4.6	171
6		Br	(±)- 3.130	7.9(5) / 5.7(6) 160x	0.33 / 0.34	4.9(2)	4.7	152
7		Cl	(S*)- 3.133	7.3(3) / 5.2(4) 130x	0.32 / 0.34	4.8(2)	5.1	131
8			(R*)- 3.133	6.8(3) / 5.1(4) 50x	0.30 / 0.32	4.5(2)	5.1	136
9		Br	(S*)- 3.134	7.6(3) / 5.6(4) 100x	0.34 / 0.36	4.9(2)	5.1	112
10			(R*)- 3.134	7.3(3) / 5.5(4) 63x	0.32 / 0.34	4.8(2)	5.1	111

*Absolute stereochemistry of centre undefined

3.9. Selectivity and Cellular Target Engagement

The 12 compounds ((*S*)-**3.103**, (*S,S**)-**3.107**, (*S,R**)-**3.107**, (*S*)-**3.111–3.113**, (*S**)-**3.127**, **3.128**, (*S**)-**3.129**, **3.130**, (*S**)-**3.133**, (*S**)-**3.134**) identified which met the established criteria for a CECR2 chemical probe were sent to DiscoverRx for screening against a panel of 32 BRDs. The compounds were tested at 10 μ M concentration against each BRD and the percentage inhibition calculated. The results were then represented as a box and whisker plot (Figure 3.20) to determine whether there were any overall trends (For full results see Appendix 5). Pleasingly, only 4 BRDs: ATAD2, CECR2, GCN5 and TAF1, showed 100% inhibition for every compound tested against it. That ATAD2 showed 100% inhibition for 11 of the compounds tested, each of which had previously been shown to be \geq 30-fold selective, gave confidence that BRDs where 100% was not observed would not have appreciable inhibition. This was compelling evidence that obtaining a pK_d on these BRDs would give a valuable insight into whether the optimised phenylsulfonamides had a suitable selectivity profile. Therefore, as selectivity data had already been generated for ATAD2, (*S*)-**3.103**, (*S,S**)-**3.107**, (*S,R**)-**3.107**, (*S*)-**3.111–3.113**, (*S**)-**3.127**, (\pm)-**3.128**, (*S**)-**3.129**, (\pm)-**3.130**, (*S**)-**3.133**, and (*S**)-**3.134**, were submitted to DiscoverRx’s GCN5 and TAF1 assay as well as CECR2 for comparison. These 12 compounds were also submitted to GSK’s TAF1 TR-FRET assay.

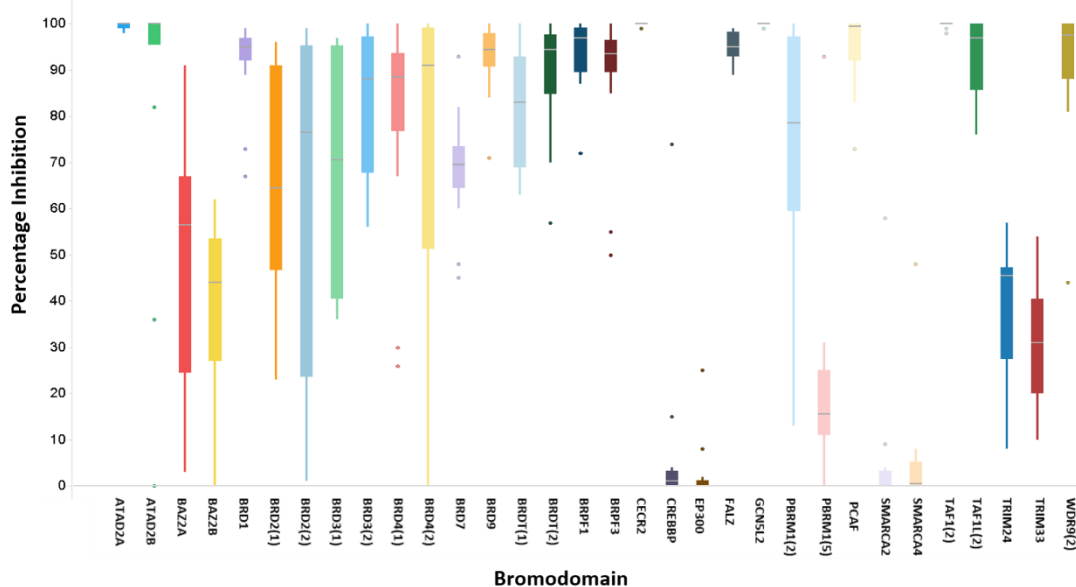


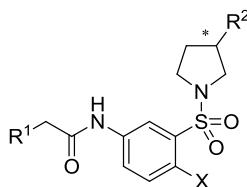
Figure 3.20. Box plot of BRD inhibition at 10 μ M concentration using DiscoverRx’s single shot panel.

The mean is represented as a grey bar.

GSK Confidential – Do not copy

The results of the wider BRD profiling are shown in Table 3.15. Pleasingly, DiscoverRx's CECR2 assay showed a strong correlation with GSK's CECR2 TR-FRET assay, with the greatest difference observed of 0.5 log units. This correlation gave confidence that **(S)-3.103**, **(S,S*)-3.107**, **(S,R*)-3.107**, **(S)-3.111–3.113**, **(S*)-3.127**, **(±)-3.128**, **(S*)-3.129**, **(±)-3.130**, **(S*)-3.133**, **(S*)-3.135** were highly potent CECR2 inhibitors. Triazolopiperidines **(S)-3.111–3.113**, **(S*)-3.127**, **(±)-3.128**, **(S*)-3.129**, and **(±)-3.130** showed good selectivity over GCN5 (≥ 30 -fold) with the exception of **(S*)-3.129**, which had a slightly reduced selectivity of 20-fold. Interestingly, dimethylamines **(S)-3.103**, **(S,S*)-3.107**, **(S,R*)-3.107**, **(S*)-3.133**, and **(S*)-3.134** did not show adequate selectivity for CECR2 over GCN5. The most selective example was **(S,R*)-3.107** which was 10-fold selective over GCN5. This suggests that the more flexible amine is capable of making a specific interaction in GCN5 which cannot be recapitulated with conformational restriction of the dimethylamine moiety. However, without the support of an adequate docking model or X-ray crystal structure this theory was difficult to pursue further. Unfortunately, this meant that **(S)-3.103**, **(S,S*)-3.107**, **(S,R*)-3.107**, **(S)-3.111**, **(S*)-3.133**, **(S*)-3.134** would not be suitable tool compounds. Disappointingly, **(S)-3.103**, **(S,S*)-3.107**, **(S,R*)-3.107**, **(S)-3.111–3.113**, **(S*)-3.127**, **(S*)-3.129**, **(±)-3.130**, **(S*)-3.133**, **(S*)-3.134** showed reduced selectivity against TAF1 using DiscoverRx's data. Only **(S)-3.103** and **(±)-3.128** showed the required selectivity for further progression. However, phenylsulfonamides **(S)-3.103**, **(S,S*)-3.107**, **(S,R*)-3.107**, **(S)-3.111**, **(S*)-3.127**, **(±)-3.128**, **(S*)-3.129**, **(±)-3.130**, **(S*)-3.133**, **(S*)-3.134** were all ≥ 50 -fold selective over TAF1 using the TR-FRET assays, with only **(S)-3.112** and **(S)-3.113** showing sub-optimal selectivity. The disconnect between GSK selectivity and DiscoverRx selectivity was intriguing and warranted further investigation.

Table 3.15. Assessing the wider BRD selectivity of the lead compounds.



	R ¹	X	R ²	CECR2 pIC ₅₀ (n)	BROMOscan			TAF1 pIC ₅₀ (n) / Sel ^b
					CECR2 pK _d (n)	GCN5 pK _d (n) / Sel ^a	TAF1 pK _d (n) / Sel ^a	
1		Cl	(S*)-cyPr (S*)- 3.127	7.7(4)	8.0(2)	6.5(2) 30x	7.0(2) 10x	6.0(3) 50x
2		Br	(S*)-cyPr (S*)- 3.129	8.2(3)	8.1(2)	6.8(2) 20x	7.2(2) 8x	6.1(3) 130x
3			(S)-Me (S)- 3.111	7.3(8)	7.8(2)	6.2(2) 40x	6.7(2) 13x	5.6(3) 50x
4		Cl	(Rac)-cyPr (±)- 3.128	7.5(5)	7.9(2)	6.2(2) 50x	<5.0(2) >790x	5.8(3) 50x
5		Br	(Rac)-cyPr (±)- 3.130	7.9(5)	8.4(2)	6.7(2) 50x	7.3(2) 13x	6.1(3) 63x
6			(S)-Me (S)- 3.112	7.3(8)	7.5(2)	6.0(2) 32x	6.8(2) 5x	6.0(3) 25x
7		Br	(S)-Me (S)- 3.113	7.5(3)	7.7(2)	6.1(2) 40x	7.1(2) 4x	6.3(3) 20x
8		Cl	(S*)-cyPr (S*)- 3.133	7.3(3)	7.3(2)	7.0(2) 2x	6.1(2) 16x	4.9(3) 250x
9		Br	(S*)-cyPr (S*)- 3.134	7.6(3)	7.9(2)	7.2(2) 5x	6.6(2) 22x	5.4(3) 160x
10			(S)-Me (S)- 3.103	7.1(5)	7.2(2)	6.7(2) 3x	<5.0(2) >200x	4.8(3) 200x
11		Br	(S)-Me (S,S*)- 3.107	7.8(3)	7.7(2)	7.0(2) 5x	6.8(2) 8x	5.2(3) 400x
12			(S)-Me (S,R*)- 3.107	7.4(3)	7.8(2)	6.7(2) 13x	6.6(2) 16x	5.1(3) 200x

^aCalculated using CECR2 pK_d; ^bCalculated using CECR2 pIC₅₀.

GSK TAF1 TR-FRET assay data was plotted against DiscoverRx's TAF1 assay data (Figure 3.21) using data points from every compound which had been tested in both assays and not restricted to the phenylsulfonamide series. Pleasingly, there was a strong correlation between the data points ($r^2 = 0.775$). However, there was a disconnect between the internal and external data, whereby compounds appear more potent when tested at DiscoverRx. The line of best fit ($y = 1.23x + 0.21$) shows that the gap widens for more potent compounds. The reasons behind this disconnect are not clear, however, the TAF1 data must be treated with caution due to this.

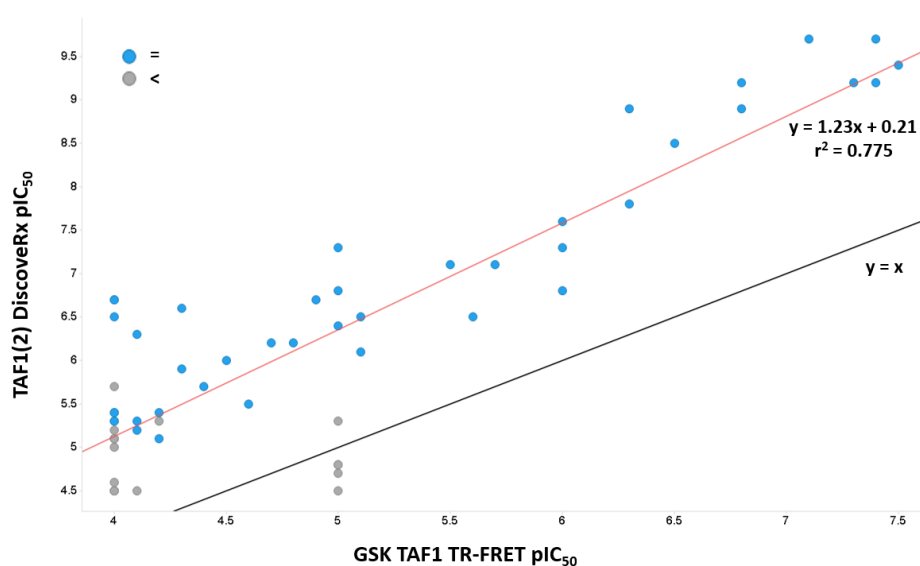


Figure 3.21. Correlation between GSK's TAF1 TR-FRET assay data and DiscoverRx's TAF1(2) assay data.

Overall triazolopiperidine (**S***)-**3.127** had the best wider BRD profile of the lead compounds. It fulfills all of the probe selectivity requirements with the exception of the disconnected external TAF1 data.

3.10. Conclusions and Future Work on CECR2

The aim of this work was to develop a chemical probe for the CECR2 BRD which was potent and selective, soluble and displayed cellular target engagement. To achieve this aim, the SAR of the phenyl sulfonamide series was thoroughly interrogated, starting with an investigation of historical data. This identified that bromide and chloride were the optimal aryl substituents, most likely due to their ability to form a halogen bond in the binding pocket. It also showed that pyrrolidine sulfonamides provide the optimal shape complementarity with

the binding pocket and that some substitution was tolerated. By targeting the gatekeeper residue, a 3-cyclopropyl pyrrolidine was identified as optimal. A structural analysis of the X-ray crystal structure of **(S,R)-3.013** in ATAD2 and the docking model of **(S,S)-3.013** in CECR2 identified targeting of the WPF residues in CECR2 as a promising strategy to obtain selectivity. This ultimately led to the discovery of the triazolopiperidine group which balanced the desired potency and selectivity with a suitable physico-chemical profile. This ultimately led to the nomination of triazolopiperidine **(S*)-3.127** as a chemical probe for the CECR2 BRD (Figure 3.22).

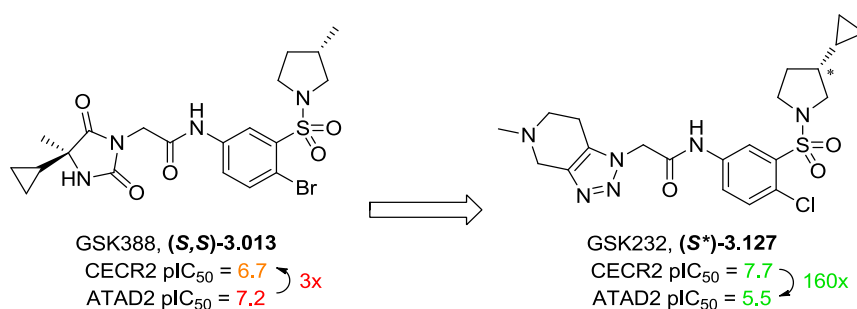
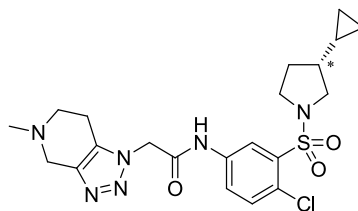


Figure 3.22. Development of GSK232 **(S*)-3.127** as highly potent CECR2 inhibitor with 500-fold selectivity over the ATAD2 BRD.

GSK232 (**(S*)-3.127**, Table 3.16) was a highly potent CECR2 inhibitor (pIC₅₀ = 8.2) and was >160-fold selective over the other non-BET BRDs examined (500-fold selective over ATAD2 and 160-fold selective over TAF1(internal data)). Pleasingly, **(S*)-3.127** was 4000-fold selective against BRD4 BD1 and 1600-fold selective over BRD4 BD2. **(S*)-3.127** has now been submitted to DiscoverRx to obtain complete dose response selectivity data against its panel of 32 BRDs to support the single shot data already generated. **(S*)-3.127** also showed an excellent physico-chemical profile. It was highly soluble (207 µg mL⁻¹) and showed good AMP (135 nm s⁻¹) which gives confidence this molecule will be cell penetrant. A nanoBRET assay will be used to determine whether GSK232 **(S*)-3.127** is capable of displacing CECR2 from chromatin in cells. This work is currently ongoing. Lastly, vibrational circular dichroism will be used to determine the absolute stereochemistry of **(S*)-3.127**.

Table 3.16. Full analysis of GSK232 (**(S*)-3.127**).

Compound	(S*)-3.127
CECR2 pIC₅₀ (n)	7.7(4)
CECR2 LE/LLE_{at}	0.33 / 0.36
ATAD2 pIC₅₀ (n) / Selectivity	5.5(2) / 160x
BRD4 BD1 pIC₅₀ (n) / Selectivity	4.6(4) / 1300x
BRD4 BD2 pIC₅₀ (n) / Selectivity	5.0(4) / 500x
TAF1 pIC₅₀ (n) / Selectivity	6.0(3) / 50x
ChromLogD_{7.4} / PFI	4.3 / 6.3
CAD Solubility (µg mL⁻¹)	207
AMP (nm s⁻¹)	135

As previously discussed (Section 3.2.2), the current state of the art chemical probe for CECR2 is GNE-886 (**3.010**), which was reported whilst this work was being undertaken. Whilst both GSK232 (**(S*)-3.127**) and GNE-886 (**3.010**) have comparable potency and selectivity profiles, GSK232 improves on the sub-optimal solubility of GNE-886 (**3.010**). When GSK232 (**(S*)-3.127**) is used in conjunction with GNE-886 (**3.010**), NVS-CECR2-1 (**3.008**) and TP238 (**3.009**), the chemical probe toolset for CECR2 has the capability to drive full target validation experiments as there are now potent and selective chemical probes with three distinct chemotypes.

4. Experimental

4.1. General Experimental

Unless otherwise stated, all reactions were carried out under an atmosphere of nitrogen using anhydrous solvents. Solvents and reagents were purchased from commercial suppliers and used as received.

Reactions were monitored by thin layer chromatography (TLC) or LCMS. TLC was carried out on glass or aluminium-backed 60 silica plates coated with UV254 fluorescent indicator. Spots were visualised using UV light (254 or 365 nm) or common staining methods as appropriate. Silica flash chromatography was carried out using Biotage SP4 or Isolera One apparatus using SNAP KP and SNAP ULTRA or RediSep® pre-packed silica cartridges. Ion exchange chromatography was carried out using Biotage Isolute cartridges and extracted organic mixtures were dried using Biotage PTFE hydrophobic phase separator frits unless otherwise stated.

NMR spectra were recorded at rt (unless otherwise stated) using standard pulse methods on a Bruker AV-400 ($^1\text{H} = 400 \text{ MHz}$, $^{13}\text{C} = 101 \text{ MHz}$) or a Bruker AV-500 ($^1\text{H} = 500 \text{ MHz}$, $^{13}\text{C} = 151 \text{ MHz}$). Chemical shifts are referenced to trimethylsilane (TMS) or the residual solvent peak, and are reported in ppm. Coupling constants are quoted to the nearest 0.1 Hz and multiplicities are given by the following abbreviations and combinations thereof: s (singlet), d (doublet), ABq (AB quartet), t (triplet), q (quartet), quin (quintet), sxt (sextet), m (multiplet), br. (broad).

IR spectra were obtained on a Perkin Elmer Spectrum 1 FTIR apparatus, with major peaks reported (cm^{-1}). Optical rotation of chiral products was measured using a Jasco P1030 polarimeter. Melting point analysis was carried out using a Stuart SMP40 melting point apparatus, melting points are uncorrected. HRMS spectra were recorded on a Micromass Q-ToF Ultima hybrid quadrupole time-of-flight mass spectrometer, with analytes separated on an Agilent 1100 Liquid Chromatograph equipped with a Phenomenex Luna C18(2) reversed phase column (100 mm x 2.1 mm, 3 μm packing diameter). LC conditions were 0.5 mL/min flow rate, 35 $^\circ\text{C}$, injection volume 2-5 μL . Gradient elution with (A) water containing 0.1% (v/v) formic acid and (B) acetonitrile containing 0.1% (v/v) formic acid. Gradient conditions

GSK Confidential – Do not copy

were initially 5% B, increasing linearly to 100% B over 6 min, remaining at 100% B for 2.5 min then decreasing linearly to 5% B over 1 min followed by an equilibration period of 2.5 min prior to the next injection.

LCMS analysis was carried out on a Waters Acquity UPLC instrument equipped with a BEH or CSH column (50 mm x 2.1 mm, 1.7 µm packing diameter) and Waters micromass ZQ MS using alternate-scan positive and negative electrospray. Analytes were detected as a summed UV wavelength of 210 – 350 nm. Two liquid phase methods were used:

Formic: 40 °C, 1 mL/min flow rate. Gradient elution with the mobile phases as (A) water containing 0.1% volume/volume (v/v) formic acid and (B) acetonitrile containing 0.1% (v/v) formic acid. Gradient conditions were initially 1% B, increasing linearly to 97% B over 1.5 min, remaining at 97% B for 0.4 min then increasing to 100% B over 0.1 min.

High pH: 40 °C, 1 mL/min flow rate. Gradient elution with the mobile phases as (A) 10 mM aqueous ammonium bicarbonate solution, adjusted to pH 10 with 0.88 M aqueous ammonia and (B) acetonitrile. Gradient conditions were initially 1% B, increasing linearly to 97% B over 1.5 min, remaining at 97% B for 0.4 min then increasing to 100% B over 0.1 min.

Mass directed automatic purification (MDAP):

Formic MDAP: The HPLC separation was conducted on an Xselect CSH C18 column (150 mm x 30 mm i.d. 5 µm packing diameter) at ambient temperature, eluting with 0.1% formic acid in water (solvent A) and 0.1% formic acid in acetonitrile (solvent B) using an elution gradient of between 0 and 100% solvent B over 15 or 25 min. The UV detection was an averaged signal from wavelength of 210 nm to 350 nm. The mass spectra were recorded on a Waters ZQ Mass Spectrometer using alternate-scan positive and negative electrospray. Ionisation data was rounded to the nearest integer.

High pH MDAP: The HPLC analysis was conducted on an Xselect CSH C18 column (150 mm x 30 mm i.d. 5 µm packing diameter) at ambient temperature, eluting with 10 mM ammonium bicarbonate in water adjusted to pH 10 with ammonia solution (solvent A) and acetonitrile (solvent B) using an elution gradient of between 0 and 100% solvent B over 15 or 25 min. The UV detection was an averaged signal from wavelength of 210 nm to 350 nm. The mass spectra were recorded on a Waters ZQ Mass Spectrometer using alternate-scan positive and negative electrospray. Ionisation data was rounded to the nearest integer.

4.2. General Procedures

General Procedure A: Amide Coupling

HATU (1.2 eq.) was added to the *carboxylic acid* (1.0 eq.) and DIPEA (3.0 eq.) in DMF or CH₂Cl₂ at rt under nitrogen. The resulting solution was stirred at rt for 5 min, before the *amine* (1.1 eq.) was added. The resulting solution was stirred at rt for 2 h. The reaction was diluted with water (20 mL) and extracted with CH₂Cl₂ (2 x 20 mL). The combined organic extracts were washed with LiCl solution (20 mL), passed through a hydrophobic frit and concentrated *in vacuo* to afford the crude product.

General Procedure B: Suzuki Coupling

The *boronic acid/ester* (1.2 eq.), *aromatic bromide* (1.0 eq.), *base* (3.0 eq.) and *Pd catalyst* (10 mol%) were dissolved in water (0.5 mL) and 1,4-dioxane (2.0 mL). The solution had nitrogen bubbled through it for 5 min and was then stirred at *temperature* until complete. The reaction was diluted with water (10 mL) and extracted with CH₂Cl₂ (3 x 10 mL). The combined organics were passed through a hydrophobic frit and concentrated *in vacuo* to afford the crude product.

General Procedure C: Hydrogenation

The *benzofuran* (1 eq.) in EtOH (10 mL) was added to a hydrogenation flask containing Pd/C, type 424 (5 mol%). The vessel was evacuated and back-filled with hydrogen (x3) and allowed to stir under a hydrogen atmosphere at rt for 24 h. Once complete, the reaction was filtered through a Celite plug, washing with EtOH (60 mL) and concentrated *in vacuo* to afford the crude product.

General Procedure D: T3P Amide Coupling Array

(*S*)-4-bromo-3-((3-methylpyrrolidin-1-yl)sulfonyl)aniline (0.032 g, 0.1 mmol) was dissolved in CH₂Cl₂ (0.5 mL) and added to the preweighed *carboxylic acid* (0.140 mmol). DIPEA (0.052 mL, 0.300 mmol) was added and the reaction stirred at rt for 5 mins. T3P (50% in EtOAc) (0.080 mL, 0.140 mmol) was added and the solution stirred at rt for 2 h. Solvent was removed from all sample until dry. The samples were purified by HPH MDAP. The solvent was dried under a stream of nitrogen to give the required product amides.

4.3. Optimisation Procedures

Optimisation Procedure A: Hydroboration Screen (Table 2.01, Section 2.2.4)

The *borane* (0.5 – 1.0 M in THF, 2.0 eq.) was added to methyl 4-hydroxy-3-(1-phenylvinyl)benzoate in THF (1 mL) at 0 °C under nitrogen. The resulting solution was stirred at rt overnight. Water (0.10 mL) was added, followed by sodium hydroxide (2 M, 0.5 mL, 1.00 mmol) and hydrogen peroxide (35% w/w in water, 0.5 mL, 5.71 mmol). The resulting solution was stirred at rt for 2 h. The reaction mixture was then analysed by LCMS.

Optimisation Procedure B: Suzuki Screen (Table 2.02, Section 2.2.6)

Methyl 4-hydroxy-3-iodo-5-(methylcarbamoyl)benzoate or methyl 4-hydroxy-3-bromo-5-(methylcarbamoyl)benzoate (50 mg, 0.149 mmol), (1-phenylvinyl) boronic acid (24 mg, 0.164 mmol), *Pd catalyst* (10 mol%, 0.015 mmol), and *base* (3.0 eq., 0.448 mmol) were dissolved in *solvent* (1 mL) and degassed under nitrogen. The resulting solution was heated to *temperature* and stirred for *time*. The reaction mixture was then analysed by LCMS.

Optimisation Procedure C: Cyclisation/Borylation Screen (Table 2.07, Section 2.4.2)

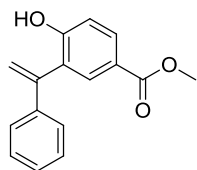
Methyl 3-iodo-4-((2-phenylallyl)oxy)benzoate (20 mg, 0.051 mmol), *bis*(pinacolato) diboron (26 mg, 0.101 mmol), *base* (3.0 eq., 0.152 mmol), and *Pd catalyst* (2-10 mol%) were dissolved in *solvent* (1 mL) at rt under nitrogen. The resulting solution was heated to 100 °C for 2 h. The reaction mixture was then analysed by LCMS.

Optimisation Procedure D: Hydrogenation Screen (Tables 3.10–3.11, Section 3.7.6)

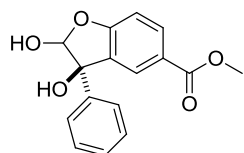
(*S*)-2-(1*H*-[1,2,3]triazolo[4,5-*c*]pyridin-1-yl)-*N*-(4-bromo-3-((3-methylpyrrolidin-1-yl)sulfonyl)phenyl)acetamide (**S**)-**3.083** (240 mg, 0.501 mmol) was suspended in MeOH (3.60 mL) and 0.30 mL aliquots were pipetted across 12 reaction vessels containing *hydrogenation catalysts* (0.050 mmol). AcOH (0.36 mL) was added across the 12 reaction vessels in 0.03 mL aliquots. The reactions vials were then placed in a Cat96 and stirred under 15 bar of hydrogen at rt for 22 h. The reactions were analysed by HPLC. The reactions were then stirred at 50 °C under 15 bar of hydrogen at rt for a further 28 h. The reactions were analysed by HPLC.

4.4. Chemistry Experimental

4.4.1. BD2 Experimentals

Methyl 4-hydroxy-3-(1-phenylvinyl)benzoate (2.016)²²⁸

Methyl 4-hydroxy-3-iodobenzoate (1.50 g, 5.39 mmol) (1-phenylvinyl)boronic acid (0.878 g, 5.93 mmol), Pd(dppf)Cl₂ (0.396 g, 0.54 mmol), and K₂CO₃ (2.23 g, 16.2 mmol) were dissolved in 1,4-dioxane (20 mL) and water (4.0 mL) at rt and degassed under nitrogen. The resulting solution was heated to 90 °C and stirred for 4 h. The reaction was allowed to cool before diluting with CH₂Cl₂ (50 mL) and washing with sat. aq. Na₂CO₃ (20 mL). The organic layer was passed through a hydrophobic frit and concentrated *in vacuo* to afford the crude product. The crude product was purified by silica chromatography, eluting with 0-30% EtOAc/cyclohexane. The pure fractions were concentrated *in vacuo* to afford methyl 4-hydroxy-3-(1-phenylvinyl)benzoate **2.016** (1.07 g, 4.21 mmol, 78% yield) as an orange gum. LCMS (Formic, ES⁺): t_R = 1.15 min; m/z = 255.1; HRMS (C₁₆H₁₄O₃): [M+H]⁺ calculated 255.1016, found 255.1014; ¹H NMR (CDCl₃-d, 400 MHz): δ (ppm) 7.97 (dd, J=8.6, 2.0 Hz, 1H), 7.89 (d, J=2.0 Hz, 1H), 7.32–7.38 (m, 5 H), 6.99 (d, J=8.6 Hz, 1H), 5.93 (d, J=1.0 Hz, 1H), 5.58 (s, 1H), 5.46 (d, J=1.0 Hz, 1H), 3.88 (s, 3H); ¹³C NMR (CDCl₃-d, 101 MHz): δ (ppm) 166.7, 157.2, 144.3, 138.7, 132.4, 131.4, 128.9, 128.8, 127.5, 126.9, 122.7, 117.6, 115.9, 51.9; IR ν_{max} (cm⁻¹) 3335, 1685, 1601, 1438, 1257, 1191, 1116, 909, 771, 704.

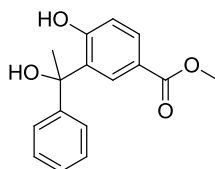
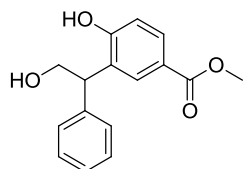
(±)-Methyl 2,3-dihydroxy-3-phenyl-2,3-dihydrobenzofuran-5-carboxylate ((±)-2.022)

*m*CPBA (0.705 g, 3.15 mmol) was added to methyl 4-hydroxy-3-(1-phenylvinyl) benzoate **2.016** (0.400 g, 1.57 mmol) in CH₂Cl₂ (10 mL) at rt under nitrogen. The resulting solution was stirred at rt for 16 h. The reaction was quenched with sat. aq. sodium thiosulfate (20 mL) and extracted with CH₂Cl₂ (20 mL). The organic layer was washed with sat. aq. NaHCO₃, passed through a hydrophobic frit and concentrated *in vacuo* to afford (±)-methyl 2,3-dihydroxy-3-phenyl-2,3-dihydrobenzofuran-5-carboxylate ((±)-**2.022**) (0.420 g, 1.467 mmol, 93% yield). LCMS (Formic, ES⁻): t_R = 0.93 min; m/z = 285.1; HRMS (C₁₆H₁₄O₅): [2M+Na]⁺ calculated 595.1580, found 595.1568; ¹H NMR (CDCl₃-d, 400 MHz): δ (ppm) 7.97 (dd, J=8.6, 2.0 Hz, 1H), 7.78 (d, J=2.0 Hz, 1H), 7.34–7.44 (m, 5 H), 6.90 (d, J=8.6 Hz, 1H), 5.77 (s, 1H), 5.00 (br. s., 1H), 3.82 (s, 3H), 1.60–1.78 (m, 1H); ¹³C NMR (CDCl₃-d, 101 MHz): δ (ppm) 166.7, 162.1, 141.0, 133.5, 131.1, 128.7,

GSK Confidential – Do not copy

128.6, 128.1, 127.5, 125.8, 123.8, 110.5, 108.4, 52.0; m.p. 111.0 – 114.6 °C; IR ν_{\max} (cm⁻¹) 3462, 3384, 2956, 1694, 1613, 1416, 1349, 1295, 1139, 762, 706.

(±)-Methyl 4-hydroxy-3-(2-hydroxy-1-phenylethyl)benzoate ((±)-2.025) and **(±)-methyl 4-hydroxy-3-(1-hydroxy-1-phenylethyl)benzoate ((±)-2.056)**



Borane (1 M in THF, 0.787 mL, 0.787 mmol) was added dropwise to methyl 4-hydroxy-3-(1-phenylvinyl)benzoate **2.016** (0.100 g, 0.393 mmol) in THF (5 mL) at 0 °C under

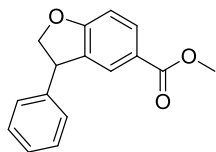
nitrogen. The resulting solution was stirred for 4 h. After this time a solution of 10% water in THF (2 mL) was added followed by 2 M NaOH (3 mL), and hydrogen peroxide (35% w/w in water, 2 mL, 0.393 mmol). The resulting solution was stirred at rt for 1.5 h. The reaction was acidified with 2 M HCl and extracted with EtOAc (2 x 20 mL). The combined organics were passed through a hydrophobic frit and concentrated *in vacuo* to afford the crude product. The crude product was purified by formic MDAP. The solvent was evaporated *in vacuo* to give (±)-methyl 4-hydroxy-3-(2-hydroxy-1-phenylethyl)benzoate **(±)-2.025** (54 mg, 0.198 mmol, 50% yield) as a white solid and (±)-methyl 4-hydroxy-3-(1-hydroxy-1-phenylethyl)benzoate **(±)-2.056** (23 mg, 0.084 mmol, 21% yield) as a yellow gum.

(±)-Methyl 4-hydroxy-3-(2-hydroxy-1-phenylethyl)benzoate ((±)-2.025):

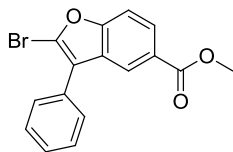
LCMS (Formic, ES⁺): t_R = 0.89 min; m/z = 273.1; HRMS (C₁₆H₁₆O₄): [M+H]⁺ calculated 273.1121, found 273.1110; ¹H NMR (CDCl₃-d, 400 MHz): δ (ppm) 7.78 (d, J =2.2 Hz, 1H), 7.67 (dd, J =8.5, 2.2 Hz, 1H), 7.21-7.30 (m, 4H), 7.14-7.19 (m, 1H), 6.87 (d, J =8.5 Hz, 1H), 4.45 (t, J =7.2 Hz, 1H), 3.87-3.98 (m, 2H), 3.77 (s, 3H); *Alcohol and phenol OH not visible*; ¹³C NMR (DMSO-*d*₆, 101 MHz): δ (ppm) 166.7, 160.2, 142.8, 130.4, 129.6, 129.4, 128.8, 128.5, 126.4, 120.5, 115.5, 63.9, 52.1, 46.3; m.p. 150.2 – 152.0 °C; IR ν_{\max} (cm⁻¹) 3405, 3176, 2870, 1685, 1607, 1429, 1285, 785, 701.

(±)-Methyl 4-hydroxy-3-(1-hydroxy-1-phenylethyl)benzoate ((±)-2.026):

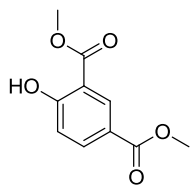
LCMS (Formic, ES⁺): t_R = 0.89 min; m/z = 255.1 (-H₂O); ¹H NMR (CDCl₃-d, 400 MHz): δ (ppm) 7.86 (dd, J =8.6, 2.0 Hz, 1H), 7.77 (d, J =2.0 Hz, 1H), 7.25–7.41 (m, 5H), 6.86 (d, J =8.6 Hz, 1H), 3.85 (s, 3H), 2.03 (s, 3H); *Alcohol and phenol OH not visible*; IR ν_{\max} (cm⁻¹) 3262, 2951, 1687, 1590, 1493, 1437, 1230, 1112, 765, 698.

(±)-Methyl 3-phenyl-2,3-dihydrobenzofuran-5-carboxylate ((±)-2.019)

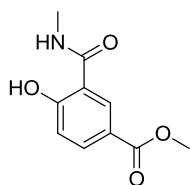
DIAD (0.014 mL, 0.071 mmol) was added dropwise to (±)-methyl 4-hydroxy-3-(2-hydroxy-1-phenylethyl)benzoate **(±)-2.025** (0.016 g, 0.059 mmol) and triphenyl phosphine (0.018 g, 0.071 mmol) dissolved in THF (2 mL). The resulting solution was stirred at rt overnight. The reaction was concentrated *in vacuo*, re-dissolved in CH₂Cl₂ (10 mL), and washed with sat. aq. NaHCO₃ (10 mL). The organic layer was passed through a hydrophobic frit and concentrated *in vacuo* to afford the crude product. The crude product was purified by formic MDAP. The solvent was evaporated *in vacuo* to give (±)-methyl 3-phenyl-2,3-dihydrobenzofuran-5-carboxylate **(±)-2.019** (6 mg, 0.024 mmol, 40% yield) as a white solid. LCMS (Formic, ES⁺): t_R = 1.23 min; m/z = 255.1; ¹H NMR (CDCl₃-d, 400 MHz): δ (ppm) 7.94 (dd, J=8.4, 1.6 Hz, 1H), 7.71 (d, J=1.5 Hz, 1H), 7.27–7.37 (m, 3H), 7.18–7.22 (m, 2H), 6.90 (d, J=8.4 Hz, 1H), 4.97–5.03 (m, 1H), 4.66–4.72 (m, 1H), 4.53 (dd, J=8.9, 7.5 Hz, 1H), 3.83 (s, 3H).

Methyl 2-bromo-3-phenylbenzofuran-5-carboxylate ((±)-2.027)

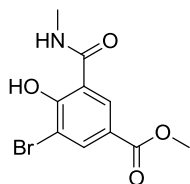
NBS (6 mg, 0.038 mmol) was added to (±)-methyl 3-phenyl-2,3-dihydrobenzofuran-5-carboxylate **(±)-2.019** (8 mg, 0.031 mmol) in CH₂Cl₂ (1 mL) at rt under nitrogen. The resulting solution was stirred at rt overnight. The reaction was quenched with sat. aq. NaHCO₃ (20 mL) and extracted with CH₂Cl₂ (2 x 10 mL). The combined organics were passed through a hydrophobic frit and concentrated *in vacuo* to afford the crude product. The crude product was purified using silica chromatography, eluting with 0-10% EtOAc/cyclohexane. The pure fractions were concentrated *in vacuo* to afford (±)-methyl 2-bromo-3-phenylbenzofuran-5-carboxylate **(±)-2.027** (7 mg, 0.021 mmol, 67% yield) as a white solid. LCMS (Formic, ES⁻): t_R = 1.47 min; no m/z; ¹H NMR (CDCl₃-d, 400 MHz): δ (ppm) 8.34 (d, J=1.5 Hz, 1H), 8.06 (dd, J=8.8, 1.5 Hz, 1H), 7.63–7.68 (m, 2H), 7.52–7.58 (m, 3H), 7.43–7.50 (m, 1H), 3.94 (s, 3H); ¹³C NMR (CDCl₃-d, 101 MHz): δ (ppm) 166.9, 157.8, 130.0, 128.9, 128.9, 128.3, 128.2, 127.5, 126.4, 126.0, 121.9, 121.2, 111.0, 52.2.

Dimethyl 4-hydroxyisophthalate (2.032)

Thionyl chloride (15 mL, 206 mmol) was added dropwise to a solution of 4-hydroxyisophthalic acid **2.033** (5 g, 27.5 mmol) in MeOH (50 mL) at 0 °C under nitrogen. The resulting solution was stirred at rt for 30 min before heating gently to reflux for 6 h. The reaction was allowed to cool. Upon cooling, a precipitate formed which was collected by filtration to afford dimethyl 4-hydroxyisophthalate **2.032** (5.32 g, 25.3 mmol, 92% yield) as a white solid. LCMS (Formic, ES⁺): t_R = 1.02 min; no m/z; HRMS (C₁₀H₁₀O₅): [M+H]⁺ calculated 211.0601, found 211.0602; ¹H NMR (DMSO-*d*₆, 400 MHz): δ (ppm) 11.01 (s, 1H), 8.36 (d, *J*=2.4 Hz, 1H), 8.04 (dd, *J*=8.6, 2.4 Hz, 1H), 7.10 (d, *J*=8.6 Hz, 1H), 3.91 (s, 3H), 3.83 (s, 3H); ¹³C NMR (DMSO-*d*₆, 101 MHz): δ (ppm) 168.3, 165.6, 163.6, 136.1, 132.5, 121.2, 118.5, 114.4, 53.1, 52.5.

Methyl 4-hydroxy-3-(methylcarbamoyl)benzoate (2.031)

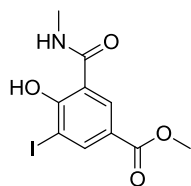
Methylamine (40% w/w in water, 20.59 mL, 238 mmol) was added to dimethyl 4-hydroxyisophthalate **2.032** (10 g, 47.6 mmol) in THF (100 mL) at rt. A precipitate formed and the resulting suspension was stirred at rt overnight. After this time the precipitate had dissolved. The reaction was quenched with sat. aq. NaHCO₃ (50 mL) and extracted with EtOAc (2 x 100 mL) and CH₂Cl₂ (2 x 100 mL). The combined organics were passed through a hydrophobic frit and concentrated *in vacuo* to afford methyl 4-hydroxy-3-(methylcarbamoyl)benzoate **2.031** (9.8 g, 46.8 mmol, 98% yield) as a pink solid. LCMS (Formic, ES⁺): t_R = 0.80 min; m/z = 210.1; HRMS (C₁₀H₁₁NO₄): [M+H]⁺ calculated 210.0761, found 210.0756; ¹H NMR (DMSO-*d*₆, 400 MHz): δ (ppm) 11.55 (q, *J*=4.6 Hz, 1H), 8.35 (d, *J*=2.8 Hz, 1H), 7.44 (dd, *J*=8.9, 2.8 Hz, 1H), 6.21 (d, *J*=8.9 Hz, 1H), 3.67 (s, 3H), 2.75 (d, *J*=4.6 Hz, 3H); *Phenol OH not visible*; ¹³C NMR (DMSO-*d*₆, 101 MHz): δ (ppm) 176.8, 168.9, 167.5, 133.5, 132.4, 122.5, 118.8, 108.3, 51.0, 25.4; m.p. 128.2 – 130.9 °C; IR ν_{max} (cm⁻¹) 2964, 1728, 1679, 1586, 1435, 1350, 1307, 1206, 1239, 1110, 763, 698.

Methyl 3-bromo-4-hydroxy-5-(methylcarbamoyl)benzoate (2.034)

NBS (3.57 g, 20.08 mmol) was added to methyl 4-hydroxy-3-(methylcarbamoyl)benzoate **2.031** (3.50 g, 16.73 mmol) in CH₂Cl₂ (15 mL) at rt. The resulting solution was stirred at rt for 2 h. The reaction was quenched with sat. aq. NaHCO₃ (50 mL) and extracted with CH₂Cl₂ (2 x 50 mL) and EtOAc (50 mL). The combined organics were passed through a hydrophobic frit and

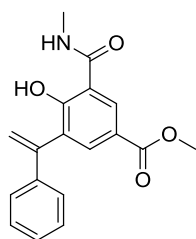
concentrated *in vacuo* to afford methyl 3-bromo-4-hydroxy-5-(methylcarbamoyl)benzoate **2.034** (3.89 g, 13.50 mmol, 81% yield) as a yellow solid. LCMS (Formic, ES⁺): $t_R = 1.06$ min; $m/z = 287.9, 289.9$; HRMS (C₁₀H₁₀BrNO₄): [M+H]⁺ calculated 287.9866, found 287.9861; ¹H NMR (DMSO-*d*₆, 400 MHz): δ (ppm) 9.38 (br. s., 1H), 8.46 (d, $J=2.0$ Hz, 1H), 8.13 (d, $J=2.0$ Hz, 1H), 3.79 (s, 3H), 2.78 (d, $J=4.4$ Hz, 3H); *Phenol OH not visible*; ¹³C NMR (DMSO-*d*₆, 101 MHz): δ (ppm) 179.8, 169.4, 165.1, 162.9, 137.2, 128.8, 115.8, 112.0, 52.6, 26.6; m.p. 113.7 – 115.3 °C; IR ν_{max} (cm⁻¹) 3376, 1776, 1699, 1567, 1426, 1363, 1287, 1187, 934, 816, 770, 727.

Methyl 4-hydroxy-3-iodo-5-(methylcarbamoyl)benzoate (2.035)



NIS (3.36 g, 14.91 mmol) was added to methyl 4-hydroxy-3-(methylcarbamoyl)benzoate **2.031** (2.6 g, 12.43 mmol) in CH₂Cl₂ (15 mL) at rt. The resulting solution was stirred at rt overnight. The reaction was diluted with water (20 mL) before sodium hydrosulfite was added until the reaction was almost colourless. The solution was extracted with CH₂Cl₂ (2 x 50 mL) and the combined organics were passed through a hydrophobic frit and concentrated *in vacuo* to afford methyl 4-hydroxy-3-iodo-5-(methylcarbamoyl)benzoate **2.035** (3.62 g, 10.80 mmol, 87% yield) as a cream solid. LCMS (Formic, ES⁺): $t_R = 1.11$ min; $m/z = 335.9$; HRMS (C₁₀H₁₀INO₄): [M+H]⁺ calculated 335.9727, found 335.9725; ¹H NMR (CDCl₃-*d*, 400 MHz): δ (ppm) 8.50 (d, $J=2.0$ Hz, 1H), 8.18 (d, $J=2.0$ Hz, 1H), 7.09 (br. s., 1H), 3.89 (s, 3H), 3.04 (d, $J=4.9$ Hz, 3H); *Phenol OH not visible*; ¹³C NMR (DMSO-*d*₆, 101 MHz): δ (ppm) 179.8, 169.5, 164.9, 164.6, 143.6, 129.3, 122.0, 87.4, 52.7, 26.7; m.p. 138.9 – 142.2 °C; IR ν_{max} (cm⁻¹) 3394, 2510, 1687, 1251, 696.

Methyl 4-hydroxy-3-(methylcarbamoyl)-5-(1-phenylvinyl)benzoate (2.029)

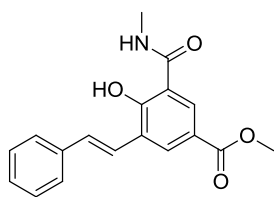


(1-Phenylvinyl)boronic acid **2.018** (1.06 g, 7.16 mmol), methyl 4-hydroxy-3-iodo-5-(methylcarbamoyl)benzoate **2.035** (2.00 g, 5.97 mmol), K₃PO₄ (3.80 g, 17.91 mmol) and PEPPSI-*i*Pr (0.406 g, 0.597 mmol) were dissolved in 1,4-dioxane (21 mL) and water (9 mL) at rt and degassed under nitrogen. The resulting solution was stirred at 70 °C for 2 h. The reaction was allowed to cool to rt and diluted with water (50 mL) and then extracted with CH₂Cl₂ (2 x 50 mL). The combined organics were passed through a hydrophobic frit and concentrated *in vacuo* to afford the crude product. The crude product was purified by silica chromatography, eluting with 0-30% EtOAc/cyclohexane. The pure fractions were concentrated *in vacuo* to afford

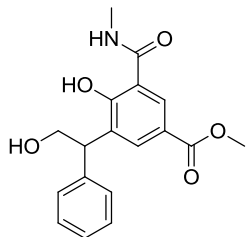
GSK Confidential – Do not copy

methyl 4-hydroxy-3-(methylcarbamoyl)-5-(1-phenylvinyl)benzoate **2.029** (1.21 g, 3.89 mmol, 65% yield) as a cream gum. LCMS (Formic, ES⁺): t_R = 1.23 min; m/z = 312.3; HRMS (C₁₇H₁₇NO₄): [M+H]⁺ calculated 312.1230, found 312.1232; ¹H NMR (MeOD-*d*₄, 400 MHz): δ (ppm) 8.45 (d, *J*=2.2 Hz, 1H), 7.96 (d, *J*=2.2 Hz, 1H), 7.22–7.34 (m, 5H), 5.78 (d, *J*=1.2 Hz, 1H), 5.38 (d, *J*=1.2 Hz, 1H), 3.90 (s, 3H), 2.93 (s, 3H); Phenol OH and amide NH not visible; ¹³C NMR (MeOD-*d*₄, 101 MHz): δ (ppm) 170.3, 166.4, 163.0, 145.9, 140.4, 135.3, 131.3, 128.2, 127.8, 127.2, 126.1, 119.8, 115.5, 114.4, 51.1, 25.1; m.p. 140.3 – 142.1 °C; IR ν_{max} (cm⁻¹) 3389, 2514, 1715, 1624, 1589, 1549, 1493, 1433, 1589, 1256, 1160, 995, 910, 862, 769, 685.

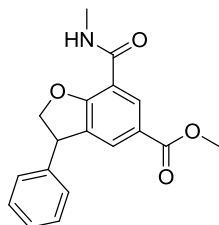
(*E*)-Methyl 4-hydroxy-3-(methylcarbamoyl)-5-styrylbenzoate (**2.036**)



(*E*)-Styrylboronic acid (26 mg, 0.179 mmol), methyl 4-hydroxy-3-iodo-5-(methylcarbamoyl)benzoate **2.035** (50 mg, 0.149 mmol), K₃PO₄ (95 mg, 0.448 mmol) and PEPPSI-*i*Pr (10 mg, 0.015 mmol) were dissolved in 1,4-dioxane (2.0 mL) and water (0.9 mL) at rt and degassed under nitrogen. The resulting solution was stirred at 70 °C for 2 h. The reaction was allowed to cool, diluted with water (10 mL) and then extracted with CH₂Cl₂ (2 x 10 mL). The combined organics were passed through a hydrophobic frit and concentrated *in vacuo* to afford the crude product. The crude product was purified by formic MDAP. The pure fractions were concentrated *in vacuo* to afford (*E*)-methyl 4-hydroxy-3-(methylcarbamoyl)-5-styrylbenzoate **2.036** (31 mg, 0.100 mmol, 67% yield) as a white solid. LCMS t_R = 1.32 min; m/z = 312.2; HRMS (C₁₈H₁₇NO₄): [M+H]⁺ calculated 312.1230, found 312.1219; ¹H NMR (DMSO-*d*₆, 400 MHz): δ (ppm) 14.67 (s, 1H), 9.33 (q, *J*=4.6), 8.46 (d, *J*=2.0 Hz, 1H), 8.31 (d, *J*=2.0 Hz, 1H), 7.60–7.65 (m, 2H), 7.36–7.44 (m, 4H), 7.26–7.33 (m, 1H), 3.89 (s, 3H), 2.85 (d, *J*=4.6 Hz, 3H); ¹³C NMR (DMSO-*d*₆, 101 MHz): δ (ppm) 170.3, 166.1, 163.2, 137.5, 131.3, 131.0, 129.2, 128.4, 128.1, 127.1, 126.6, 122.1, 120.3, 114.6, 52.5, 26.5; m.p. 166.7 – 169.1 °C; IR ν_{max} (cm⁻¹) 3394, 2511, 1688, 1251, 688.

(±)-Methyl 4-hydroxy-3-(2-hydroxy-1-phenylethyl)-5-(methylcarbamoyl)benzoate**((±)-2.037)**

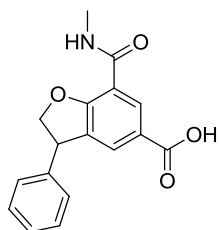
An oven-dried 25 mL round-bottomed flask equipped with a stirrer bar was dried under vacuum and then cooled using a stream of nitrogen. After cooling to 0 °C the reaction flask was charged with borane (1 M in THF, 8.0 mL, 8.00 mmol). 2,3-Dimethylbut-2-ene (2 M in THF, 4.0 mL, 8.00 mmol) was added dropwise and the resulting solution was stirred at rt for 3 h to after which a solution of thexylborane in THF (0.66 M in THF) had formed. Thexylborane (0.66 M in THF, 9.74 mL, 6.43 mmol) was added to methyl 4-hydroxy-3-(methylcarbamoyl)-5-(1-phenylvinyl)benzoate **2.029** (1.3 g, 2.92 mmol) at rt under nitrogen. The resulting solution was stirred at rt overnight. Water (10 mL) was added, followed by 2 M NaOH (10 mL, 20.00 mmol) and hydrogen peroxide (35% w/w in water, 10 mL, 114 mmol). The resulting solution was stirred at rt for 2h. The reaction was quenched by addition of sat. aq. sodium thiosulfate (20 mL) and then acidified using 1 M HCl (20 mL) and extracted with EtOAc (2 x 50 mL) and CH₂Cl₂ (50 mL). The combined organics were passed through a hydrophobic frit and concentrated *in vacuo* to afford (±)-methyl 4-hydroxy-3-(2-hydroxy-1-phenylethyl)-5-(methylcarbamoyl)benzoate **(±)-2.037** (600 mg, 1.822 mmol, 62% yield) as a cream solid. LCMS (Formic, ES⁺): t_R = 0.96 min; m/z = 330.3; HRMS (C₁₈H₁₉NO₅): [M+H]⁺ calculated 330.1336, found 330.1339; ¹H NMR (MeOD-*d*₄, 400 MHz): δ (ppm) 8.33 (d, *J*=2.2 Hz, 1H), 8.03 (d, *J*=2.2 Hz, 1H), 7.26–7.33 (m, 4H), 7.15–7.23 (m, 1H), 4.66 (t, *J*=7.3 Hz, 1H), 4.05–4.19 (m, 2H), 3.89 (s, 3H), 2.92 (s, 3H); *Phenol OH, alcohol OH and amide NH not visible*; ¹³C NMR (MeOD-*d*₄, 101 MHz): δ (ppm) 170.5, 166.6, 163.3, 141.2, 132.8, 131.2, 128.1, 128.0, 126.8, 126.1, 119.5, 114.0, 63.7, 51.1, 45.9, 25.1; m.p. 168.6 – 171.0 °C; IR ν_{max} (cm⁻¹) 2949, 2161, 1714, 1637, 1591, 1546, 1431, 1284, 1019, 767, 699.

(±)-Methyl 7-(methylcarbamoyl)-3-phenyl-2,3-dihydrobenzofuran-5-carboxylate**((±)-2.012)**

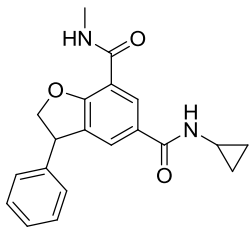
DIAD (0.149 mL, 0.765 mmol) was added dropwise to triphenylphosphine (0.201 g, 0.765 mmol) and (±)-methyl 4-hydroxy-3-(2-hydroxy-1-phenylethyl)-5-(methylcarbamoyl)benzoate **(±)-2.037** (0.210 g, 0.638 mmol) in THF (10 mL) at rt. The resulting solution was stirred at rt overnight. The reaction was quenched with sat. aq. NaHCO₃ (20 mL) and extracted with CH₂Cl₂ (2 x 20 mL). The combined organics were passed through

a hydrophobic frit and concentrated *in vacuo* to afford the crude product. The crude product was purified by silica chromatography, eluting with 0-80% EtOAc/cyclohexane. The pure fractions were concentrated *in vacuo* to afford (±)-methyl 7-(methylcarbamoyl)-3-phenyl-2,3-dihydrobenzofuran-5-carboxylate (**±**)-**2.012** (160 mg, 0.514 mmol, 81% yield). LCMS (Formic, ES⁺): t_R = 1.04 min; m/z = 312.1; HRMS (C₁₈H₁₇NO₄): [M+H]⁺ calculated 312.1230, found 312.1233; ¹H NMR (CDCl₃-d, 400 MHz): δ (ppm) 8.74 (d, J=1.2 Hz, 1H), 7.77–7.85 (m, 1H), 7.44–7.53 (m, 1H), 7.29–7.40 (m, 3H), 7.15–7.22 (m, 2H), 5.16 (dd, J=8.8, 8.8 Hz, 1H), 4.64–4.78 (m, 2H), 3.86 (s, 3H), 3.06 (d, J=4.6 Hz, 3H); ¹³C NMR (MeOD-d₄, 101 MHz): δ (ppm) 166.2, 165.0, 161.3, 141.8, 133.6, 131.4, 129.2, 128.7, 127.4, 127.2, 123.6, 115.6, 81.3, 51.2, 46.8, 25.4; IR ν_{max} (cm⁻¹) 3418, 2985, 275, 1711, 1654, 1608, 1556, 1475, 1430, 1269, 1157, 1031, 993, 927, 767, 699.

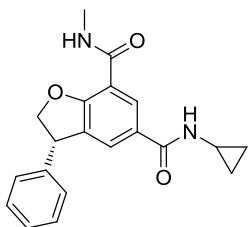
(±)-7-(Methylcarbamoyl)-3-phenyl-2,3-dihydrobenzofuran-5-carboxylic acid ((±)-2.038)



LiOH (15.38 mg, 0.642 mmol) was added to (±)-methyl 7-(methylcarbamoyl)-3-phenyl-2,3-dihydrobenzofuran-5-carboxylate (**±**)-**2.012** (100 mg, 0.321 mmol) in THF (2 mL) and water (2 mL) at rt. The resulting solution was stirred at 50 °C for 2 h. The reaction was allowed to cool, acidified to pH 5 with 1 M HCl and extracted with EtOAc (3 x 20 mL). The combined organics were passed through a hydrophobic frit and concentrated *in vacuo* to afford (±)-7-(methylcarbamoyl)-3-phenyl-2,3-dihydrobenzofuran-5-carboxylic acid (**±**)-**2.038** (95 mg, 0.320 mmol, 99% yield) as a white solid. LCMS (Formic, ES⁺): t_R = 0.89 min; m/z = 298.2; HRMS (C₁₇H₁₅NO₄): [M+H]⁺ calculated 298.1074, found 298.1077; ¹H NMR (DMSO-d₆, 400 MHz): δ (ppm) 12.78 (br. s., 1H), 8.29 (d, J=1.5 Hz, 1H), 7.93 (q, J=4.6 Hz, 1H), 7.61 (d, J=1.5 Hz, 1H), 7.34–7.41 (m, 2H), 7.24–7.33 (m, 3H), 5.19 (dd, J=9.1, 9.0 Hz, 1H), 4.86 (dd, J=9.1, 6.8 Hz, 1H), 4.71 (dd, J=9.0, 6.8 Hz, 1H), 2.85 (d, J=4.6 Hz, 3H); ¹³C NMR (MeOD-d₄, 101 MHz): δ (ppm) 167.4, 165.2, 161.3, 141.8, 133.5, 131.7, 129.5, 128.7, 127.4, 127.1, 126.0, 124.2, 81.2, 46.8, 25.4; m.p. 223.2 – 225.8 °C; IR ν_{max} (cm⁻¹) 2941, 2521, 1712, 1631, 1545, 1474, 1252, 1152, 994, 924, 768, 697, 656.

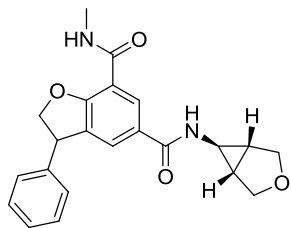
(±)-N⁵-Cyclopropyl-N⁷-methyl-3-phenyl-2,3-dihydrobenzofuran-5,7-dicarboxamide**((±)-2.011)**

(±)-7-(Methylcarbamoyl)-3-phenyl-2,3-dihydrobenzofuran-5-carboxylic acid (90 mg, 0.303 mmol) was reacted with cyclopropanamine (0.021 mL, 0.303 mmol) in DMF (3 mL) according to **general procedure A**. The crude product was purified by silica chromatography eluting with 0-60% EtOAc/cyclohexane. The pure fractions were concentrated *in vacuo* to afford **(±)-2.011** (±)-N⁵-cyclopropyl-N⁷-methyl-3-phenyl-2,3-dihydrobenzofuran-5,7-dicarboxamide (60 mg, 0.179 mmol, 59%) as a cream solid. LCMS (Formic, ES⁺): t_R = 0.91 min; m/z = 337.1; HRMS (C₂₀H₂₀N₂O₃): [M+H]⁺ calculated 337.1547, found 337.1555; ¹H NMR (MeOD-*d*₄, 400 MHz): δ (ppm) 8.32 (d, *J*=1.5 Hz, 1H), 7.62 (d, *J*=1.5 Hz, 1H), 7.32–7.40 (m, 2H), 7.20–7.31 (m, 3H), 5.20 (dd, *J*=9.0, 9.0 Hz, 1H), 4.85 (dd, *J*=9.0, 7.2 Hz, 1H), 4.70 (dd, *J*=9.0, 7.2 Hz, 1H), 3.00 (s, 3H), 2.76–2.84 (m, 1H), 0.73–0.81 (m, 2H), 0.55–0.64 (m, 2H); *Amide NH not visible*; ¹³C NMR (MeOD-*d*₄, 101 MHz): δ (ppm) 169.0, 165.3, 160.2, 141.9, 133.3, 128.8, 128.7, 127.7, 127.4, 127.3, 127.1, 115.3, 81.1, 47.0, 25.4, 22.6, 5.1; m.p. 169.3 – 172.2 °C; IR ν_{max} (cm⁻¹) 3408, 3281, 2955, 1637, 1529, 1452, 1276, 839, 762, 699.

(S)-N⁵-Cyclopropyl-N⁷-methyl-3-phenyl-2,3-dihydrobenzofuran-5,7-dicarboxamide ((S)-2.011)

(±)-N⁵-Cyclopropyl-N⁷-methyl-3-phenyl-2,3-dihydrobenzofuran-5,7-dicarboxamide **(±)-2.011** (55 mg, 0.164 mmol) was dissolved in EtOH (2.5 mL) and injected onto the column (Column: 30 mm x 25 cm Chiralcel OD-H (5 μm, Lot No ODH11158-01) which was eluted with 20% (EtOH + 0.2% isopropylamine)/(heptane + 0.2% isopropylamine), flow rate = 30 mL/min, detection wavelength, 215 nm, 4. Ref 550, 100. Appropriate fractions for isomer 1 were bulked and labelled peak 1. Appropriate fractions for isomer 2 were bulked and labelled peak 2. The bulked pure fractions from peak 1 were concentrated *in vacuo* to afford **(S)-N⁵-Cyclopropyl-N⁷-methyl-3-phenyl-2,3-dihydrobenzofuran-5,7-dicarboxamide ((S)-2.011** (12 mg, 0.036 mmol, 22%) as a white solid. ¹H NMR and LCMS data consistent with *racemate*; Chiral LC: 4.6 mm x 25 cm Chiralcel OD-H column, 20% (EtOH + 0.2% isopropylamine)/(heptane + 0.2% isopropylamine), t_R = 10.899 min, *er* >99:1.

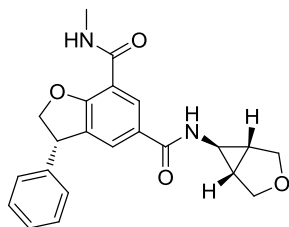
(±)-N⁵-((1R,5S,6r)-3-Oxabicyclo[3.1.0]hexan-6-yl)-N⁷-methyl-3-phenyl-2,3-dihydrobenzofuran-5,7-dicarboxamide ((±)-2.039)



Method 1: (±)-7-(Methylcarbamoyl)-3-phenyl-2,3-dihydrobenzofuran-5-carboxylic acid **(±)-2.038** (60 mg, 0.202 mmol) was reacted with (1R,5S,6r)-3-oxabicyclo[3.1.0]hexan-6-amine **2.007** (28 mg, 0.283 mmol) in DMF (3 mL) according to **general procedure A**. The crude product was purified by silica

chromatography eluting with 0-100% EtOAc/cyclohexane. The pure fractions were concentrated *in vacuo* to afford (±)-N⁵-((1R,5S,6r)-3-oxabicyclo[3.1.0]hexan-6-yl)-N⁷-methyl-3-phenyl-2,3-dihydrobenzofuran-5,7-dicarboxamide (76 mg, 0.196 mmol, 97% yield) as a white solid. **Method 2:** N⁵-((1R,5S,6r)-3-Oxabicyclo[3.1.0]hexan-6-yl)-N⁷-methyl-3-phenylbenzofuran-5,7-dicarboxamide **2.051** (37 mg, 0.098 mmol) was hydrogenated according to **general procedure C**. The crude product was purified by HPH MDAP. Pure fractions were concentrated *in vacuo* to afford (±)-N⁵-((1R,5S,6r)-3-oxabicyclo[3.1.0]hexan-6-yl)-N⁷-methyl-3-phenyl-2,3-dihydrobenzofuran-5,7-dicarboxamide **(±)-2.039** (27 mg, 0.071 mmol, 73% yield) as a white solid. LCMS (Formic, ES⁺): t_R = 0.87 min; m/z = 379.3; HRMS (C₂₂H₂₂N₂O₄): [M+H]⁺ calculated 379.1652, found 379.1659; ¹H NMR (DMSO-*d*₆, 400 MHz): δ (ppm) 8.46 (q, *J*=4.6 Hz, 1H), 8.21 (d, *J*=1.5 Hz, 1H), 7.91 (d, *J*=4.5 Hz, 1H), 7.61 (d, *J*=1.5 Hz, 1H), 7.33–7.40 (m, 2H), 7.21–7.32 (m, 3H), 5.14 (dd, *J*=9.3, 9.0 Hz, 1H), 4.84 (dd, *J*=9.3, 6.8 Hz, 1H), 4.63 (dd, *J*=9.0, 6.8 Hz, 1H), 3.82 (d, *J*=8.4 Hz, 2H), 3.60 (dd, *J*=8.4, 2.7 Hz, 2H), 2.85 (d, *J*=4.6 Hz, 3H), 2.52-2.58 (m, 1H), 1.84 (q, *J*=2.7 Hz, 2H); ¹³C NMR (DMSO-*d*₆, 101 MHz): δ (ppm) 166.3, 164.2, 162.7, 159.7, 142.7, 133.3, 129.4, 129.2, 128.1, 127.6, 127.3, 116.6, 81.0, 69.1, 46.7, 31.4, 26.8, 24.4; m.p. 222.7 – 224.3 °C; IR ν_{max} (cm⁻¹) 3288, 2857, 1639, 1529, 1455, 1263, 1073, 943, 698.

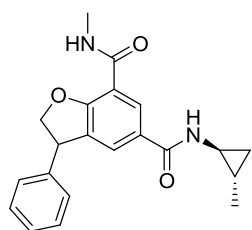
(S)-N⁵-((1R,5S,6r)-3-Oxabicyclo[3.1.0]hexan-6-yl)-N⁷-methyl-3-phenyl-2,3-dihydrobenzofuran-5,7-dicarboxamide ((S)-2.039)



(±)-N⁵-((1R,5S,6r)-3-Oxabicyclo[3.1.0]hexan-6-yl)-N⁷-methyl-3-phenyl-2,3-dihydrobenzofuran-5,7-dicarboxamide **(±)-2.039** (68 mg, 0.180 mmol) was dissolved in EtOH (1.5 mL) and injected onto the column (Column: 30 mm x 25 cm Chiralpak AD-H (5 μm, Lot No ADH13231)) which was eluted with 40% (EtOH + 0.2% isopropylamine)/(heptane + 0.2% isopropylamine), flow rate = 30 mL/min, detection

wavelength, 215 nm, 4. Ref 550, 100. Appropriate fractions for isomer 1 were bulked and labelled peak 1. Appropriate fractions for isomer 2 were bulked and labelled peak 2. The pure fractions from peak 2 were concentrated *in vacuo* to afford (*S*)-*N*⁵-((1*R*,5*S*,6*R*)-3-Oxabicyclo [3.1.0]hexan-6-yl)-*N*⁷-methyl-3-phenyl-2,3-dihydrobenzofuran-5,7-dicarboxamide (**S**)-**2.039** (19 mg, 0.050 mmol, 28%) as a white solid. ¹H NMR and LCMS data consistent with racemate; Chiral LC: 4.6 mm x 25 cm Chiralpak AD-H column, 40% (EtOH + 0.2% isopropylamine)/heptane, *t*_R = 35.857 min, *er* 98:2.

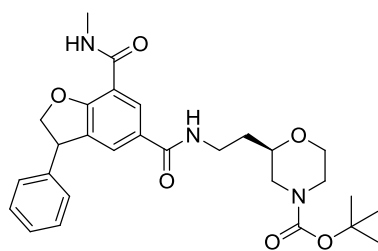
***N*⁷-methyl-*N*⁵-((1*S*,2*S*)-2-methylcyclopropyl)-3-phenyl-2,3-dihydrobenzofuran-5,7-dicarboxamide (2.040) mixture of diastereomers**



(±)-7-(Methylcarbamoyl)-3-phenyl-2,3-dihydrobenzofuran-5-carboxylic acid (**±**)-**2.038** (15 mg, 0.050 mmol) was reacted with (1*S*,2*S*)-2-methylcyclopropanamine (4 mg, 0.050 mmol) in DMF (3 mL) according to **general procedure A**. The crude product was purified by silica chromatography eluting with 0-100% EtOAc/cyclohexane. The

pure fractions were concentrated *in vacuo* to afford *N*⁷-methyl-*N*⁵-((1*S*,2*S*)-2-methylcyclopropyl)-3-phenyl-2,3-dihydrobenzofuran-5,7-dicarboxamide **2.040** (11 mg, 0.031 mmol, 62% yield) as a white solid and a mixture of diastereomers. LCMS (formic, ES⁺) *t*_R = 0.98 min; *m/z* = 351.2; HRMS (C₂₁H₂₂N₂O₃): [M+H]⁺ calculated 351.1703, found 351.1706; ¹H NMR (MeOD-*d*₄, 400 MHz): δ (ppm) 8.31 (d, *J*=2.0 Hz, 1H), 7.60 (d, *J*=2.0 Hz, 1H), 7.33–7.39 (m, 2H), 7.21–7.31 (m, 3H), 5.20 (dd, *J*=9.3, 9.0 Hz, 1H), 4.84 (dd, *J*=9.3, 7.2 Hz, 1H), 4.70 (dd, *J*=9.0, 7.2 Hz, 1H), 3.00 (s, 3H), 2.44–2.50 (m, 1H), 1.11 (d, *J*=6.1 Hz, 3H), 0.91–1.00 (m, 1H), 0.76–0.78 (m, 1H), 0.52–0.55 (m, 1H); *Amide NH not visible*; ¹³C NMR (MeOD-*d*₄, 101 MHz): δ (ppm) 168.9, 165.3, 160.2, 141.9, 133.3, 128.8, 128.7, 127.8, 127.4, 127.3, 127.1, 115.3, 81.1, 47.0, 30.2, 25.4, 16.1, 13.6, 13.4.

(2*R*)-tert-Butyl-2-(2-(7-(methylcarbamoyl)-3-phenyl-2,3-dihydrobenzofuran-5-carboxamido)ethyl)morpholine-4-carboxylate (2.41) mixture of diastereomers

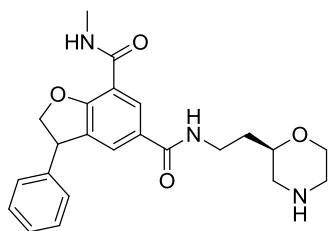


(±)-7-(methylcarbamoyl)-3-phenyl-2,3-dihydrobenzofuran-5-carboxylic acid (**±**)-**2.038** (60 mg, 0.202 mmol) and (*R*)-*tert*-butyl 2-(2-aminoethyl)morpholine-4-carboxylate (55.8 mg, 0.242 mmol) were reacted in DMF according to **general**

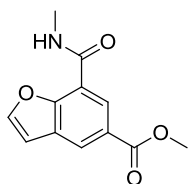
procedure A. The crude product was purified by silica chromatography eluting with 0-100% EtOAc/cyclohexane. The pure fractions were concentrated *in vacuo* to afford (±)-(2*R*)-*tert*-butyl

2-(2-(7-(methylcarbamoyl)-3-phenyl-2,3-dihydrobenzofuran-5-carboxamido)ethyl)morpholine-4-carboxylate **2.41** (60 mg, 0.118 mmol, 58% yield) as a mixture of diastereomers. LCMS (HPH, ES⁺) $t_R = 1.12$ min; $m/z = 510.4$; ¹H NMR (DMSO-*d*₆, 400 MHz): δ (ppm) 8.38–8.50 (m, 1H), 8.23 (s, 1H), 7.86–7.94 (m, 1H), 7.62 (d, $J=1.2$ Hz, 1H), 7.36 (d, $J=7.6$ Hz, 2H), 7.19–7.32 (m, 3H), 5.15 (s, 1H), 4.79–4.89 (m, 1H), 4.57–4.68 (m, 1H), 3.56–3.87 (m, 3H), 3.15–3.31 (m, 5H), 2.86 (d, $J=4.6$ Hz, 3H), 1.53–1.67 (m, 2H), 1.38 (s, 9H), 1.18–1.30 (m, 1H); *Diastereotopic protons not visible*.

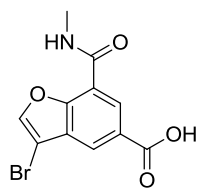
***N*⁷-Methyl-*N*⁵-(2-((*R*)-morpholin-2-yl)ethyl)-3-phenyl-2,3-dihydrobenzofuran-5,7-dicarboxamide (2.042)** mixture of diastereomers



TFA (0.5 mL, 6.49 mmol) was added to (2*R*)-*tert*-butyl 2-(2-(7-(methylcarbamoyl)-3-phenyl-2,3-dihydrobenzofuran-5-carboxamido)ethyl)morpholine-4-carboxylate **2.041** (50 mg, 0.098 mmol) in CH₂Cl₂ (3 mL) at rt under nitrogen. The resulting solution was stirred at rt for 2 h. The reaction was loaded onto a 2 g SCX column and flushed with MeOH (20 mL). The column was then flushed with ammonia (2 M in MeOH, 20 mL). The pure fractions were concentrated *in vacuo* to afford (±)-*N*⁷-methyl-*N*⁵-(2-((*R*)-morpholin-2-yl)ethyl)-3-phenyl-2,3-dihydrobenzofuran-5,7-dicarboxamide **2.042** (18 mg, 0.044 mmol, 45% yield) as a mixture of diastereomers. LCMS (Formic, ES⁺): $t_R = 0.58$ min; $m/z = 410.4$; ¹H NMR (DMSO-*d*₆, 400 MHz): δ (ppm) 8.45 (d, $J=5.6$ Hz, 1H), 8.23 (d, $J=1.5$ Hz, 1H), 7.92 (q, $J=4.6$ Hz, 1H), 7.62 (d, $J=1.5$ Hz, 1H), 7.34–7.42 (m, 2H), 7.22–7.32 (m, 3H), 5.15 (dd, $J=9.7, 9.2$ Hz, 1H), 4.85 (dd, $J=9.7, 6.5$ Hz, 1H), 4.64 (dd, $J=9.2, 6.7$ Hz, 1H), 3.72 (d, $J=10.3$ Hz, 1H), 3.15–3.49 (m, 6H), 2.86 (d, $J=4.6$ Hz, 3H), 2.81 (d, $J=11.5$ Hz, 1H), 2.58–2.75 (m, 2H), 2.37 (t, $J=11.5$ Hz, 1H), 1.55 (q, $J=6.8$ Hz, 2H); ¹³C NMR (DMSO-*d*₆, 101 MHz): δ (ppm) 165.4, 164.2, 159.4, 142.7, 133.3, 129.4, 129.0, 128.1, 127.6, 127.2, 126.5, 116.5, 80.8, 73.8, 66.7, 50.3, 46.7, 45.1, 36.1, 33.3, 26.8; *Diastereotopic protons not visible*.

Methyl 7-(methylcarbamoyl)benzofuran-5-carboxylate (2.046)

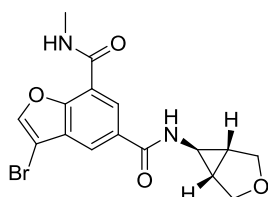
Methyl 4-hydroxy-3-iodo-5-(methylcarbamoyl)benzoate **2.035** (2.96 g, 8.83 mmol), ethynyltrimethylsilane (2.77 mL, 19.43 mmol), copper(I) iodide (0.17 g, 0.883 mmol), TEA (3.69 mL, 26.5 mmol), and Pd(PPh₃)₂Cl₂ (0.31 g, 0.442 mmol) were dissolved in DMF (20 mL) and degassed under nitrogen. The resulting solution was stirred at 80 °C for 18 h. The reaction was cooled, diluted with water (100 mL) and extracted with CH₂Cl₂ (3 x 50 mL). The combined organics were passed through a hydrophobic frit and concentrated in *vacuo* to afford the *crude intermediate*. TBAF (1M in THF, 17 mL, 17.67 mmol) was added to the crude and the resulting solution stirred for 2 hrs. The reaction was quenched with sodium carbonate (50 mL) and extracted with CH₂Cl₂ (2 x 50 mL). The combined organics were washed with sat. aq. LiCl (50 mL), passed through a hydrophobic frit and concentrated in *vacuo* to afford the *crude product*. The crude product was taken up in CH₂Cl₂, at this point a precipitate formed and this was dried *in vacuo* to afford methyl 7-(methylcarbamoyl)benzofuran-5-carboxylate **2.046** (1.50 g, 6.43 mmol, 73% yield) as a pink solid. LCMS (Formic, ES⁺): t_R = 0.75 min; m/z = 234.2; HRMS (C₁₂H₁₁NO₄): [M+H]⁺ calculated 234.0761, found 234.0758; ¹H NMR (DMSO-*d*₆, 400 MHz): δ (ppm) 8.44 (d, *J*=1.7 Hz, 1H), 8.35 (q, *J*=4.6 Hz, 1H), 8.29 (d, *J*=1.7 Hz, 1H), 8.22 (d, *J*=2.2 Hz, 1H), 7.20 (d, *J*=2.2 Hz, 1H), 3.91 (s, 3H), 2.89 (d, *J*=4.6 Hz, 3H); ¹³C NMR (DMSO-*d*₆, 101 MHz): δ (ppm) 166.3, 163.9, 153.9, 148.5, 129.3, 126.1, 126.0, 125.2, 120.0, 108.0, 52.8, 26.9; m.p. 188.8 – 190.2 °C; IR ν_{max} (cm⁻¹) 3327, 1719, 1636, 1552, 1413, 1280, 1174, 1026, 765, 692.

3-Bromo-7-(methylcarbamoyl)benzofuran-5-carboxylic acid (2.49)

Bromine (1.648 mL, 32.2 mmol) was added to methyl 7-(methylcarbamoyl)benzofuran-5-carboxylate **2.46** (5.0 g, 21.44 mmol) in CH₂Cl₂ (50 mL). The resulting solution was stirred at rt for 2 h. The reaction was followed by TLC which appeared to show loss of SM. The reaction was concentrated *in vacuo* to afford an orange gum. KOH (2.65 g, 47.2 mmol) was dissolved in EtOH (50 mL) then added to the crude product, and the resulting solution was stirred at rt overnight. Water (10 mL) was added, then the reaction was warmed to 40 °C and stirred for a further 4 h. The reaction was stirred for a further 2 h. The reaction was quenched with 10% aq. sodium metabisulfate (20 mL) and acidified to pH 5 with 2 M HCl. A white precipitate formed which was filtered and the residue dried under vacuum to afford 3-bromo-7-

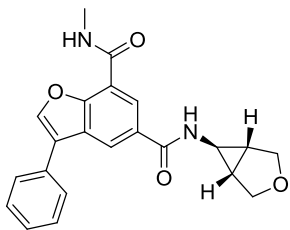
(methylcarbamoyl)benzofuran-5-carboxylic acid **2.49** (6.0 g, 20.13 mmol, 94 % yield) as a white solid. LCMS (Formic, ES⁺): $t_R = 0.77$ min; $m/z = 298.0, 300.0$; HRMS (C₁₁H₈BrNO₄): [M+H]⁺ calculated 297.9710, found 297.9711; ¹H NMR (DMSO-*d*₆, 400 MHz): δ (ppm) 8.32–8.38 (m, 2H), 8.28 (q, $J=4.5$ Hz, 1H), 8.13 (d, $J=1.2$ Hz, 1H), 2.85 (d, $J=4.5$ Hz, 3H), acid CO₂H *not visible*; ¹³C NMR (DMSO-*d*₆, 101 MHz): δ (ppm) 168.0, 164.7, 151.5, 144.6, 137.9, 127.8, 126.9, 122.7, 119.0, 98.4, 26.8; m.p. 203.3 – 205.8 °C; IR ν_{max} (cm⁻¹) 3315, 1663, 1625, 1589, 1552, 1456, 1383, 1267, 1086, 866, 849, 799, 767.

***N*⁵-((1*R*,5*S*,6*r*)-3-Oxabicyclo[3.1.0]hexan-6-yl)-3-bromo-*N*⁷-methylbenzofuran-5,7-dicarboxamide (**2.050**)²⁴³**



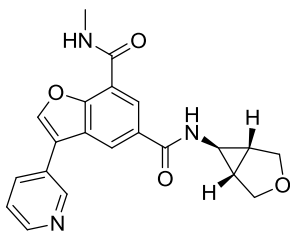
HATU (918 mg, 2.415 mmol) was added to 3-bromo-7-(methylcarbamoyl)benzofuran-5-carboxylic acid **2.049** (600 mg, 2.013 mmol) and DIPEA (1.055 mL, 6.04 mmol) in DMF (5 mL) at rt under nitrogen. The resulting solution was stirred at rt for 5 min before (1*R*,5*S*,6*r*)-3-oxabicyclo[3.1.0]hexan-6-amine **2.007** (239 mg, 2.415 mmol) was added. The resulting solution was stirred at rt overnight. The reaction was diluted with water (20 mL) and extracted with CH₂Cl₂ (2 x 20 mL). The combined organics were washed with sat. aq. LiCl solution (20 mL), passed through a hydrophobic frit and concentrated *in vacuo* to afford the crude product. The crude product was purified by silica chromatography eluting with 0–60% (3:1 EtOAc/EtOH)/EtOAc. The pure fractions were concentrated *in vacuo* to afford *N*⁵-((1*R*,5*S*,6*r*)-3-oxabicyclo[3.1.0]hexan-6-yl)-3-bromo-*N*⁷-methylbenzofuran-5,7-dicarboxamide **2.050** (460 mg, 1.213 mmol, 60% yield) as a cream solid. LCMS (Formic, ES⁺): $t_R = 0.75$ min; 379.1, 381.1; HRMS (C₁₆H₁₅BrN₂O₄): [M+H]⁺ calculated 379.0288, found 379.0286; ¹H NMR (DMSO-*d*₆, 400 MHz): δ (ppm) 8.79 (d, $J=4.4$ Hz, 1H), 8.51 (s, 1H), 8.41 (q, $J=4.6$ Hz, 1H), 8.25 (d, $J=2.0$ Hz, 1H), 8.17 (d, $J=2.0$ Hz, 1H); 3.88–3.90 (m, 2H), 3.62–3.68 (m, 3H), 2.63–2.68 (m, 1H), 1.23–1.27 (m, 4H); ¹³C NMR (DMSO-*d*₆, 101 MHz): δ (ppm) 165.9, 163.7, 151.5, 145.9, 130.3, 128.0, 125.7, 121.5, 120.5, 97.6, 69.1, 38.7, 26.9, 24.5; IR ν_{max} (cm⁻¹) 3673, 3416, 2877, 1666, 1637, 1600, 1549, 1529, 1415, 1393, 1267, 1150, 1065, 1013, 827, 742, 665.

***N*⁵-((1*R*,5*S*,6*r*)-3-oxabicyclo[3.1.0]hexan-6-yl)-*N*⁷-methyl-3-phenylbenzofuran-5,7-dicarboxamide (2.051)**



4,4,5,5-Tetramethyl-2-phenyl-1,3,2-dioxaborolane (64.6 mg, 0.316 mmol), *N*⁵-((1*R*,5*S*,6*r*)-3-oxabicyclo[3.1.0]hexan-6-yl)-3-bromo-*N*⁷-methylbenzofuran-5,7-dicarboxamide **2.050** (100 mg, 0.264 mmol), K₂CO₃ (109 mg, 0.791 mmol) and PEPPSI-*i*Pr (18 mg, 0.026 mmol) were dissolved in 1,4-dioxane (2.0 mL) and water (0.5 mL) and reacted at 40 °C for 2 h according to **general procedure B**. The crude product was purified by formic MDAP. The pure fractions were concentrated *in vacuo* to afford *N*⁵-((1*R*,5*S*,6*r*)-3-oxabicyclo[3.1.0]hexan-6-yl)-*N*⁷-methyl-3-phenylbenzofuran-5,7-dicarboxamide **2.051** (41 mg, 0.109 mmol, 41% yield) as a white solid. LCMS (Formic, ES⁺): t_R = 0.90 min; *m/z* = 377.3; HRMS (C₂₂H₂₀N₂O₄): [M+H]⁺ calculated 377.1496, found 377.1484; ¹H NMR (MeOD-*d*₄, 400 MHz): δ (ppm) 8.38 (d, *J*=1.7 Hz, 1H), 8.32 (d, *J*=1.7 Hz, 1H), 8.16 (s, 1H), 7.64–7.72 (m, 2H), 7.47–7.55 (m, 2H), 7.38–7.46 (m, 1H), 4.04 (d, *J*=8.5 Hz, 2H), 3.76 (d, *J*=8.5 Hz, 2H), 3.05 (s, 3H), 2.67 (t, *J*=2.5 Hz, 1H), 1.94–1.99 (m, 2H); *Amide NHs not visible*; ¹³C NMR (MeOD-*d*₄, 101 MHz): δ (ppm) 169.0, 164.9, 153.9, 143.2, 130.4, 129.6, 128.8, 127.8, 127.4, 127.4, 124.7, 122.7, 122.7, 118.2, 68.9, 30.9, 25.7, 24.5; m.p. 202.2 – 205.8 °C; IR ν_{max} (cm⁻¹) 3264, 2861, 1635, 1521, 1457, 1412, 1330, 1265, 1227, 1095, 1073, 1003, 942, 898, 848, 760, 697, 672.

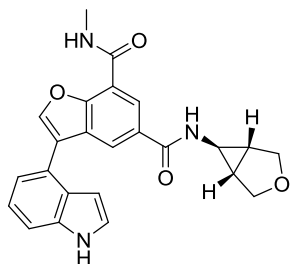
***N*⁵-((1*R*,5*S*,6*r*)-3-oxabicyclo[3.1.0]hexan-6-yl)-*N*⁷-methyl-3-(pyridin-3-yl)benzofuran-5,7-dicarboxamide (2.052)**



Pyridin-3-ylboronic acid (58 mg, 0.475 mmol), *N*⁵-((1*R*,5*S*,6*r*)-3-oxabicyclo[3.1.0]hexan-6-yl)-3-bromo-*N*⁷-methylbenzofuran-5,7-dicarboxamide **2.050** (150 mg, 0.396 mmol), PEPPSI-*i*Pr (27 mg, 0.040 mmol) and K₃PO₄ (252 mg, 1.187 mmol) were dissolved in 1,4-dioxane (2.0 mL) and water (0.5 mL) and reacted at 60 °C for 4 h according to **general procedure B**. The crude product was purified by silica chromatography, eluting with 0-80% (3:1 EtOAc:EtOH)/EtOAc. The pure fractions were concentrated *in vacuo* to afford *N*⁵-((1*R*,5*S*,6*r*)-3-oxabicyclo[3.1.0]hexan-6-yl)-*N*⁷-methyl-3-(pyridin-3-yl)benzofuran-5,7-dicarboxamide **2.052** (55 mg, 0.146 mmol, 37% yield) as a white solid. LCMS (Formic, ES⁺): t_R = 0.53 min; *m/z* = 378.3; ¹H NMR (DMSO-*d*₆, 400 MHz): δ (ppm) 9.04 (d, *J*=1.7 Hz, 1H), 8.77 (q, *J*=4.6 Hz, 1H), 8.68 (s, 1H), 8.66 (dd, *J*=4.9, 1.7 Hz, 1H), 8.46 (d,

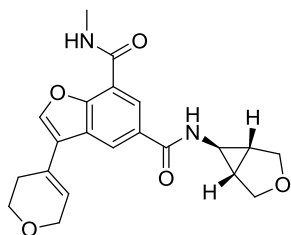
$J=1.7$ Hz, 1H), 8.40–8.44 (m, 1H), 8.26 (d, $J=1.7$ Hz, 1H), 8.19–8.23 (m, 1H), 7.57–7.62 (m, 1H), 3.88 (d, $J=8.3$ Hz, 2H), 3.65 (d, $J=8.3$ Hz, 2H), 2.89 (d, $J=4.6$ Hz, 3H), 2.61–2.66 (m, 1H), 1.91–1.95 (m, 2H).

N^5 -((1*R*,5*S*,6*r*)-3-Oxabicyclo[3.1.0]hexan-6-yl)-3-(1*H*-indol-4-yl)- N^7 -methylbenzofuran-5,7-dicarboxamide (2.053)



4-(4,4,5,5-Tetramethyl-1,3,2-dioxaborolan-2-yl)-1*H*-indole (77 mg, 0.316 mmol), N^5 -((1*R*,5*S*,6*r*)-3-oxabicyclo[3.1.0]hexan-6-yl)-3-bromo- N^7 -methylbenzofuran-5,7-dicarboxamide **2.050** (100 mg, 0.264 mmol), K_2CO_3 (109 mg, 0.791 mmol) and PEPPSI-*i*Pr (18 mg, 0.026 mmol) were dissolved in water (0.5 mL) and 1,4-dioxane (2 mL) and reacted at 40 °C for 2 h according to **general procedure B**. The crude product was purified by formic MDAP. The pure fractions were concentrated *in vacuo* to afford N^5 -((1*R*,5*S*,6*r*)-3-oxabicyclo[3.1.0]hexan-6-yl)-3-(1*H*-indol-4-yl)- N^7 -methylbenzofuran-5,7-dicarboxamide **2.053** (42 mg, 0.101 mmol, 38% yield) as a white solid. LCMS (Formic, ES^+): t_R = 0.86 min; m/z = 416.3; 1H NMR (MeOD- d_4 , 400 MHz): δ (ppm) 8.30-8.38 (m, 1H), 8.19-8.26 (m, 1H), 7.49 (d, $J=8.1$ Hz, 1H), 7.22-7.36 (m, 3H), 6.49-6.58 (m, 1H), 3.95-4.04 (m, 2H), 3.69-3.77 (m, 2H), 3.07 (s, 3H), 2.58-2.65 (m, 1H), 1.86-1.95 (m, 2H); Amide NHs and indole NH not visible.

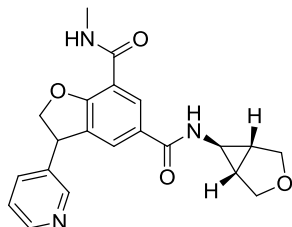
N^5 -((1*R*,5*S*,6*r*)-3-Oxabicyclo[3.1.0]hexan-6-yl)-3-(3,6-dihydro-2*H*-pyran-4-yl)- N^7 -methylbenzofuran-5,7-dicarboxamide (2.054)



2-(3,6-Dihydro-2*H*-pyran-4-yl)-4,4,5,5-tetramethyl-1,3,2-dioxaborolane (67 mg, 0.316 mmol), N^5 -((1*R*,5*S*,6*r*)-3-oxabicyclo[3.1.0]hexan-6-yl)-3-bromo- N^7 -methylbenzofuran-5,7-dicarboxamide **2.050** (100 mg, 0.264 mmol), K_2CO_3 (109 mg, 0.791 mmol) and XPhos Pd G2 (21 mg, 0.026 mmol) were reacted at 40 °C for 16 h according to **general procedure B**. The crude product was purified by formic MDAP. The pure fractions were concentrated *in vacuo* to afford N^5 -((1*R*,5*S*,6*r*)-3-oxabicyclo[3.1.0]hexan-6-yl)-3-(3,6-dihydro-2*H*-pyran-4-yl)- N^7 -methylbenzofuran-5,7-dicarboxamide **2.054** (28 mg, 0.073 mmol, 28% yield) as a white solid. LCMS (Formic, ES^+): t_R = 0.73 min; m/z = 383.3; 1H NMR (MeOD- d_4 , 400 MHz): δ (ppm) 8.40 (d, $J=1.5$ Hz, 1H), 8.30 (d, $J=1.5$ Hz, 1H), 7.97 (s, 1H), 6.44 (s, 1H), 4.38 (d, $J=2.5$ Hz, 2H), 4.05 (d, $J=8.5$ Hz, 2H), 3.96 (t, $J=5.5$

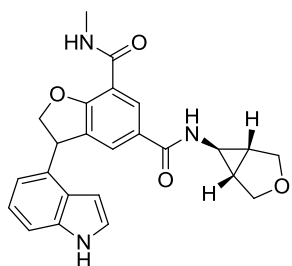
Hz, 2H), 3.77 (d, $J=8.5$ Hz, 2H), 3.04 (s, 3H), 2.69 (t, $J=2.5$ Hz, 1H), 2.52 (d, $J=1.5$ Hz, 2H), 2.00 (t, $J=2.5$ Hz, 2H); Amide NHs not visible.

(±)- N^5 -((1*R*,5*S*,6*r*)-3-oxabicyclo[3.1.0]hexan-6-yl)- N^7 -methyl-3-(pyridin-3-yl)-2,3-dihydrobenzofuran-5,7-dicarboxamide ((±)-2.055)



N^5 -((1*R*,5*S*,6*r*)-3-Oxabicyclo[3.1.0]hexan-6-yl)- N^7 -methyl-3-(pyridin-3-yl) benzofuran-5,7-dicarboxamide **2.052** (50 mg, 0.132 mmol) was hydrogenated according to **general procedure C**. The crude product was purified by formic MDAP. The solvent was evaporated *in vacuo* to afford (±)- N^5 -((1*R*,5*S*,6*r*)-3-oxabicyclo[3.1.0]hexan-6-yl)- N^7 -methyl-3-(pyridin-3-yl)-2,3-dihydrobenzofuran-5,7-dicarboxamide ((±)-**2.055**) (18 mg, 0.047 mmol, 36% yield). LCMS (Formic, ES⁺): t_R = 0.43 min; m/z = 380.1; ¹H NMR (DMSO- d_6 , 400 MHz): δ (ppm) 8.55 (d, $J=2.0$ Hz, 1H), 8.51 (dd, $J=4.5$, 2.0 Hz, 1H), 8.46 (d, $J=4.5$ Hz, 1H), 8.22 (d, $J=2.0$ Hz, 1H), 7.92 (q, $J=4.6$ Hz, 2H), 7.60-7.65 (m, 2H), 7.39 (dd, $J=7.8$, 4.5 Hz, 1H), 5.15 (t, $J=9.8$, 9.0 Hz, 1H), 4.92 (dd, $J=9.8$, 6.5 Hz, 1H), 4.68 (dd, $J=9.0$, 6.5 Hz, 1H), 3.80-3.85 (m, 2H), 3.60 (dd, $J=8.3$, 2.7 Hz, 2H), 2.85 (d, $J=4.6$ Hz, 3H), 2.53-2.57 (m, 1H), 1.80-1.89 (m, 2H); ¹³C NMR (DMSO- d_6 , 101 MHz): δ (ppm) 164.2, 163.6, 159.6, 149.6, 149.0, 138.2, 135.6, 132.4, 129.3, 127.9, 126.9, 124.7, 116.7, 80.5, 69.1, 43.9, 31.4, 26.8, 24.4.

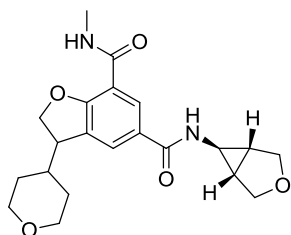
(±)- N^5 -((1*R*,5*S*,6*r*)-3-Oxabicyclo[3.1.0]hexan-6-yl)-3-(1*H*-indol-4-yl)- N^7 -methyl-2,3-dihydrobenzofuran-5,7-dicarboxamide ((±)-2.056)



N^5 -((1*R*,5*S*,6*r*)-3-oxabicyclo[3.1.0]hexan-6-yl)-3-(1*H*-indol-4-yl)- N^7 -methyl benzofuran-5,7-dicarboxamide **2.053** (30 mg, 0.072 mmol) was hydrogenated according to **general procedure C**. The crude product was purified by formic MDAP. The pure fractions were concentrated *in vacuo* to afford (±)- N^5 -((1*R*,5*S*,6*r*)-3-oxabicyclo[3.1.0]hexan-6-yl)-3-(1*H*-indol-4-yl)- N^7 -methyl-2,3-dihydrobenzofuran-5,7-dicarboxamide ((±)-**2.056**) (19 mg, 0.046 mmol, 63% yield) as a white solid. LCMS (Formic, ES⁺): t_R = 0.83 min; m/z = 418.3; HRMS (C₂₄H₂₃N₃O₄): [M+H]⁺ calculated 418.1761, found 418.1764; ¹H NMR (MeOD- d_4 , 400 MHz): δ (ppm) 8.35 (d, $J=1.7$ Hz, 1H), 7.59-7.64 (m, 1H), 7.36 (d, $J=8.1$ Hz, 1H), 7.22 (d, $J=3.0$ Hz, 1H), 7.09 (s, 1H), 6.87 (d, $J=7.1$ Hz, 1H), 6.27 (d, $J=3.0$ Hz, 1H), 5.30 (s, 1H), 5.15-5.23 (m, 1H), 4.92 (s, 1H), 3.97 (dd, $J=8.3$, 1.1 Hz, 2H), 3.70 (d, $J=8.3$ Hz, 2H), 3.03

(s, 3H), 2.55 (s, 1H), 1.87 (s, 2H); Amide NHs and indole NH not visible; ^{13}C NMR (MeOD- d_4 , 101 MHz): δ (ppm) 168.8, 165.3, 160.4, 136.8, 133.2, 132.3, 128.8, 127.5, 127.3, 126.1, 124.5, 121.0, 117.9, 115.1, 110.5, 98.8, 80.0, 68.8, 45.6, 30.8, 25.4, 24.4; m.p. 127.0 – 131.4 °C; IR ν_{max} (cm^{-1}) 2856, 1633, 1394, 751.

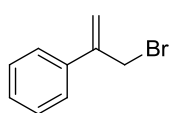
(\pm)- N^5 -((1*R*,5*S*,6*R*)-3-Oxabicyclo[3.1.0]hexan-6-yl)- N^7 -methyl-3-(tetrahydro-2*H*-pyran-4-yl)-2,3-dihydrobenzofuran-5,7-dicarboxamide ((\pm)-2.057**)**



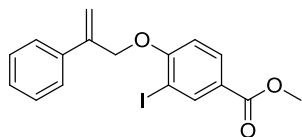
N^5 -((1*R*,5*S*,6*R*)-3-Oxabicyclo[3.1.0]hexan-6-yl)-3-(3,6-dihydro-2*H*-pyran-4-yl)- N^7 -methylbenzofuran-5,7-dicarboxamide **2.050** (8 mg, 0.021 mmol) was hydrogenated according to general procedure C. The crude product was purified by MDAP formic. The pure fractions were concentrated *in vacuo* to afford (\pm)- N^5 -((1*R*,5*S*,6*R*)-

3-oxabicyclo[3.1.0]hexan-6-yl)- N^7 -methyl-3-(tetrahydro-2*H*-pyran-4-yl)-2,3-dihydrobenzofuran-5,7-dicarboxamide (\pm)-**2.057** (2 mg, 5.18 μmol , 25% yield) as a white solid. LCMS (Formic, ES $^+$): t_{R} = 0.68 min; m/z = 387.3; ^1H NMR (MeOD- d_4 , 400 MHz): δ (ppm) 8.29 (d, J =1.8 Hz, 1H), 7.88 (d, J =1.8 Hz, 1H), 4.79 (d, J =7.3 Hz, 2H), 4.04 (d, J =8.6 Hz, 2H), 3.92–4.01 (m, 2H), 3.76 (d, J =8.6 Hz, 2H), 3.48–3.55 (m, 1H), 3.37 (s, 3H), 2.97 (s, 3H), 2.64 (s, 1H), 1.96 (t, J =2.6 Hz, 2H), 1.66–1.74 (m, 1H), 1.45–1.57 (m, 1H), 1.31–1.44 (m, 2H); Amide NHs not visible; ^{13}C NMR (MeOD- d_4 , 101 MHz): δ (ppm) 170.5, 162.1, 132.5, 130.3, 129.0, 128.5, 116.3, 101.5, 77.4, 70.4, 47.2, 40.4, 32.4, 31.2, 29.8, 26.9, 26.1.

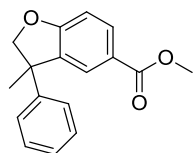
(3-Bromoprop-1-en-2-yl)benzene (2.084)



Prop-1-en-2-ylbenzene **2.083** (5.5 mL, 42.3 mmol) was dissolved in THF (100 mL) at rt under nitrogen. To the resulting solution was added NBS (7.91 g, 44.4 mmol) and TsOH (0.81 g, 4.23 mmol) and the solution was refluxed at 100 °C for 4 h. The reaction was cooled to rt, taken up in Et $_2$ O (20 mL) and washed with water (2 x 20 mL). The organic layer was passed through a hydrophobic frit and concentrated *in vacuo* to afford (3-bromoprop-1-en-2-yl)benzene **2.084** (7.15 g, 36.3 mmol, 86% yield) as a yellow oil. LCMS (Formic, ES $^+$): t_{R} = 1.21 min; does not ionise; ^1H NMR (DMSO- d_6 , 400 MHz): δ (ppm) 7.53–7.59 (m, 2H), 7.32–7.41 (m, 3H), 5.62 (d, J =0.7 Hz, 1H), 5.58 (d, J =0.7 Hz, 1H), 4.64 (s, 2H).

Methyl 3-iodo-4-((2-phenylallyl)oxy)benzoate (2.085)

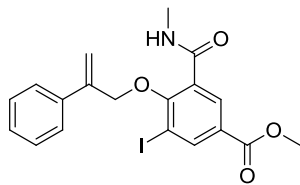
Methyl 4-hydroxy-3-iodobenzoate **2.017** (1.00 g, 3.60 mmol), (3-bromoprop-1-en-2-yl)benzene **2.084** (1.42 g, 7.19 mmol) and K_2CO_3 (1.49 g, 10.79 mmol) were dissolved in acetone (50 mL) and heated to 80 °C for 1 h under nitrogen. The reaction was allowed to cool before quenching with sat. aq. $NaHCO_3$ (50 mL) and extracting with CH_2Cl_2 (3 x 50 mL). The combined organics were passed through a hydrophobic frit and concentrated *in vacuo* to afford the crude product. The crude product was purified by silica column chromatography eluting with 0-30% EtOAc/cyclohexane. The appropriate fractions were collected and concentrated *in vacuo* to afford methyl 3-iodo-4-((2-phenylallyl)oxy)benzoate **2.085** (1.36 g, 3.45 mmol, 96% yield) as a yellow solid. LCMS (Formic, ES⁺): t_R = 1.47 min; m/z = 395.2; ; HRMS ($C_{17}H_{15}O_3$): $[M+H]^+$ calculated 395.0144, found 395.0144; 1H NMR (DMSO- d_6 , 400 MHz): δ (ppm) 8.30 (d, $J=2.2$ Hz, 1H), 7.97 (dd, $J=8.6, 2.2$ Hz, 1H), 7.54–7.60 (m, 2H), 7.33–7.43 (m, 3H), 7.26 (d, $J=8.6$ Hz, 1H), 5.71 (d, $J=1.0$ Hz, 1H), 5.63 (d, $J=1.0$ Hz, 1H), 5.15 (s, 2H), 3.83 (s, 3H); ^{13}C NMR (DMSO- d_6 , 101 MHz): δ (ppm) 165.1, 160.9, 142.4, 140.3, 137.8, 131.7, 128.9, 128.6, 126.4, 124.3, 115.0, 113.1, 86.9, 70.6, 52.6; m.p. 43.1 – 48.3 °C; IR ν_{max} (cm^{-1}) 2948, 1715, 1593, 1308, 1268, 911, 703.

(±)-Methyl 3-methyl-3-phenyl-2,3-dihydrobenzofuran-5-carboxylate ((±)-2.086)

Methyl 3-iodo-4-((2-phenylallyl)oxy)benzoate **2.085** (500 mg, 1.268 mmol) and $PdCl_2(MeCN)_2$ (33 mg, 0.127 mmol) were dissolved in DMF (5 mL) at rt under nitrogen. PMP (1.38 mL, 7.61 mmol) was added followed by formic acid (0.19 mL, 5.07 mmol) and the reaction was heated to 50 °C for 2 h. The reaction was allowed to cool and diluted with Et_2O (50 mL). The organic phase was washed with brine (2 x 50 mL) and the aqueous phase was then extracted with EtOAc (50 mL). The combined organics were passed through a hydrophobic frit and concentrated *in vacuo* to afford the crude product. The crude product was purified by silica chromatography eluting with 0-50% EtOAc/cyclohexane. The pure fractions were concentrated *in vacuo* to afford (±)-methyl 3-methyl-3-phenyl-2,3-dihydrobenzofuran-5-carboxylate ((±)-**2.086**) (281 mg, 1.047 mmol, 83% yield) as a colourless gum. LCMS (Formic, ES⁺): t_R = 1.29 min; m/z = 269.2; HRMS ($C_{17}H_{16}O_3$): $[M+H]^+$ calculated 269.1183, found 269.1178; 1H NMR (DMSO- d_6 , 400 MHz): δ (ppm) 7.86 (dd, $J=8.3, 2.0$ Hz, 1H), 7.66 (d, $J=2.0$ Hz, 1H), 7.21–7.38 (m, 5H), 7.00 (d, $J=8.3$ Hz, 1H), 4.73 (d, $J=9.0$ Hz, 1H), 4.61 (d, $J=9.0$ Hz, 1H), 3.78 (s, 3H), 1.74 (s, 3H). ^{13}C NMR ($CDCl_3-d$, 101 MHz):

δ (ppm) 166.8, 163.7, 145.7, 136.2, 131.4, 128.6, 126.8, 126.3, 126.2, 123.3, 109.7, 87.1, 51.8, 49.5, 26.3; IR ν_{\max} (cm⁻¹) 2951, 1715, 1288, 1251, 772, 700.

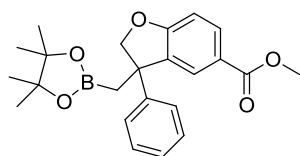
(±)-Methyl 3-iodo-5-(methylcarbamoyl)-4-((2-phenylallyl)oxy)benzoate (2.078)



Methyl 4-hydroxy-3-iodo-5-(methylcarbamoyl)benzoate **2.035** (1.00 g, 2.98 mmol), (3-bromoprop-1-en-2-yl)benzene **2.084** (1.18 g, 5.97 mmol) and K₂CO₃ (1.24 g, 8.95 mmol) were dissolved in acetone (50 mL). The resulting solution was heated at 100 °C

overnight. The reaction was allowed to cool before quenching with sat. aq. NaHCO₃ (50 mL) and extracting with CH₂Cl₂ (3 x 50 mL). The combined organics were passed through a hydrophobic frit and concentrated *in vacuo* to afford the crude product. The crude product was purified by silica chromatography eluting with 0-30% EtOAc/cyclohexane. The pure fractions were concentrated *in vacuo* to afford (±)-methyl 3-iodo-5-(methylcarbamoyl)-4-((2-phenylallyl)oxy)benzoate **2.078** (709 mg, 1.571 mmol, 53% yield) as a yellow oil. LCMS (formic, ES⁺) t_R = 1.27 min, m/z = 452.1; HRMS (C₁₉H₁₈NO₄I): [M+H]⁺ calculated 452.0359, found 452.0356; ¹H NMR (DMSO-*d*₆, 400 MHz): δ (ppm) 8.43 (q, J =4.5 Hz, 1H), 8.38 (d, J =2.0 Hz, 1H), 7.95 (d, J =2.0 Hz, 1H), 7.53–7.58 (m, 2H), 7.30–7.42 (m, 3H), 5.71 (d, J =1.0 Hz, 1H), 5.56 (d, J =1.0 Hz, 1H), 4.92 (s, 2H), 3.86 (s, 3H), 2.73 (d, J =4.5 Hz, 3H); ¹³C NMR (DMSO-*d*₆, 101 MHz): δ (ppm) 166.0, 164.6, 159.3, 142.8, 141.3, 137.9, 131.8, 130.8, 128.9, 128.5, 127.3, 127.0, 126.4, 116.4, 93.9, 75.9, 52.9; m.p. 97.5 – 99.2 °C; IR ν_{\max} (cm⁻¹) 3283, 1718, 1642, 1268, 707.

(±)-Methyl 3-phenyl-3-((4,4,5,5-tetramethyl-1,3,2-dioxaborolan-2-yl)methyl)-2,3-dihydrobenzofuran-5-carboxylate ((±)-2.090)



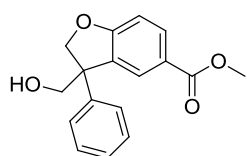
Methyl 3-iodo-4-((2-phenylallyl)oxy)benzoate **2.085** (50 mg, 0.127 mmol), KOAc (37 mg, 0.381 mmol), *bis*(pinacolato) diboron (64 mg, 0.254 mmol) and XPhos Pd G2 (10 mg, 0.013 mmol) were

dissolved in EtOH (1 mL) at rt under nitrogen. The resulting solution was heated to 100 °C for 2 h. The reaction was allowed to cool, then concentrated *in vacuo* before redissolving in CH₂Cl₂ (5 mL) and washing with sat. aq. NaHCO₃ (5 mL). The aqueous layer was washed with CH₂Cl₂ (5 mL). The combined organics were passed through a hydrophobic frit and concentrated *in vacuo* to afford the crude product. The crude product was purified by formic MDAP. The pure fractions were concentrated *in vacuo* to afford (±)-methyl 3-phenyl-3-

GSK Confidential – Do not copy

((4,4,5,5-tetramethyl-1,3,2-dioxaborolan-2-yl)methyl)-2,3-dihydrobenzofuran-5-carboxylate (**±**)-**2.090** (42 mg, 0.107 mmol, 84% yield) as a white solid. LCMS (formic, ES⁺) t_R = 1.46 min, m/z = 313.2, 395.2; HRMS (C₂₃H₂₇BO₅): [M+H]⁺ calculated 395.2030, found 395.2029; ¹H NMR (DMSO-*d*₆, 400 MHz): δ (ppm) 7.79–7.87 (m, 2H), 7.24–7.35 (m, 4H), 7.17–7.24 (m, 1H), 6.91–6.99 (m, 1H), 4.76 (ABq, *J*=9.3 Hz, 2H), 3.79 (s, 3H), 1.81 (d, *J*=15.5 Hz, 1H), 1.62 (d, *J*=15.5 Hz, 1H), 1.00 (d, *J*=2.4 Hz, 12H); ¹³C NMR (DMSO-*d*₆, 101 MHz): δ (ppm) 166.4, 163.8, 147.1, 136.8, 131.3, 128.8, 126.9, 126.8, 126.3, 122.8, 110.1, 86.4, 83.4, 52.2, 50.5, 24.8, 24.7; m.p. 105.9 – 108.4 °C; IR ν_{max} (cm⁻¹) 2978, 1708, 1286, 1254, 1142, 766.

(±)-Methyl 3-(hydroxymethyl)-3-phenyl-2,3-dihydrobenzofuran-5-carboxylate ((±)-2.096)

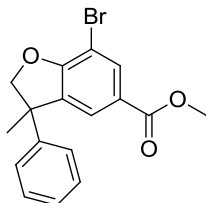


Methyl 3-iodo-4-((2-phenylallyl)oxy)benzoate **2.085** (3.00 g, 7.61 mmol), *bis*(pinacolato) diboron (3.87 g, 15.22 mmol), KOAc (2.24 g, 22.83 mmol) and XPhos Pd G2 (0.59 g, 0.761 mmol) were dissolved in

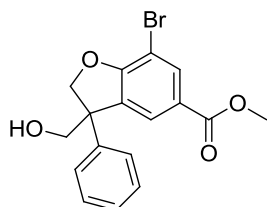
EtOH (50 mL) at rt under nitrogen. The resulting solution was heated to 100 °C and stirred for 4 h. The reaction was allowed to cool to 0 °C before 2 M NaOH (1.90 mL, 3.81 mmol) and aq. hydrogen peroxide (35% w/w in water, 6.66 mL, 76 mmol) were added sequentially and the resulting solution stirred at 0 °C for 10 mins. The reaction was quenched by addition of sat. aq. sodium thiosulfate (50 mL) and extracted with CH₂Cl₂ (2 x 50 mL). The combined organics were passed through a hydrophobic frit and concentrated *in vacuo* to afford the crude product. The crude product was purified by silica chromatography eluting with 0-50% EtOAc/cyclohexane. The pure fractions were concentrated *in vacuo* to afford (±)-methyl 3-(hydroxymethyl)-3-phenyl-2,3-dihydrobenzofuran-5-carboxylate (**±**)-**2.096** (1.84 g, 6.47 mmol, 85% yield) as a cream solid. LCMS (formic, ES⁺) t_R = 1.04 min, m/z = 285.2; HRMS (C₁₇H₁₆O₄): [M+H]⁺ calculated 285.1127, found 285.1135; ¹H NMR (CDCl₃-*d*, 400 MHz): δ (ppm) 8.00 (dd, *J*=8.3, 1.8 Hz, 1H), 7.92 (d, *J*=1.8 Hz, 1H), 7.34–7.41 (m, 2H), 7.28–7.33 (m, 3H), 6.92 (d, *J*=8.3 Hz, 1H), 4.92 (d, *J*=9.1 Hz, 1H), 4.72 (d, *J*=9.1 Hz, 1H), 4.14 (ABq, *J*=11 Hz, 2H), 3.88 (s, 3H); *Alcohol OH not visible*; ¹³C NMR (CDCl₃-*d*, 101 MHz): δ (ppm) 166.8, 164.6, 141.8, 132.2, 130.6, 128.9, 127.4, 127.2, 126.8, 123.2, 110.0, 82.2, 67.2, 55.4, 51.6; m.p. 95.6 – 97.2 °C; IR ν_{max} (cm⁻¹) 3496, 2976, 1708, 1254, 959, 774.

(±)-Methyl-7-bromo-3-methyl-3-phenyl-2,3-dihydrobenzofuran-5-carboxylate ((±)-2.097)

Bromine (0.134 mL, 2.61 mmol) was added to (±)-methyl 3-methyl-3-phenyl-2,3-dihydrobenzofuran-5-carboxylate **(±)-2.086** (140 mg, 0.522 mmol) in CH₂Cl₂ (5 mL) at rt under nitrogen. The resulting solution was stirred at rt for 1 h. The reaction was quenched with aq. sodium thiosulfate (5 mL) and sodium hydrosulfite was added until the reaction turned colourless.

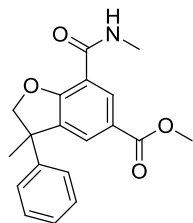


The reaction was then extracted with CH₂Cl₂ (2 x 20 mL). The organics were passed through a hydrophobic frit and concentrated *in vacuo* to afford (±)-methyl 7-bromo-3-methyl-3-phenyl-2,3-dihydrobenzofuran-5-carboxylate **(±)-2.097** (172 mg, 0.495 mmol, 95% yield) as a colourless gum. LCMS (Formic, ES⁺): t_R = 1.40 min; m/z = 347.0, 349.0; HRMS (C₁₇H₁₅O₃Br): [M+H]⁺ calculated 347.0283, found 347.0288; ¹H NMR (DMSO-*d*₆, 400 MHz): δ (ppm) 7.98 (d, *J*=1.5 Hz, 1H), 7.64 (d, *J*=1.5 Hz, 1H), 7.24–7.39 (m, 5H), 4.85 (d, *J*=9.3 Hz, 1H), 4.73 (d, *J*=9.3 Hz, 1H), 3.80 (s, 3H), 1.77 (s, 3H); ¹³C NMR (CDCl₃-*d*, 101 MHz): δ (ppm) 179.2, 165.5, 160.6, 144.6, 137.2, 134.1, 128.6, 127.1, 126.1, 124.8, 102.7, 87.4, 52.2, 50.4, 26.3; m.p. 60.8 – 63.3 °C; IR ν_{max} (cm⁻¹) 2956, 1707, 1432, 1276, 701.

(±)-Methyl 7-bromo-3-(hydroxymethyl)-3-phenyl-2,3-dihydrobenzofuran-5-carboxylate ((±)-2.098)

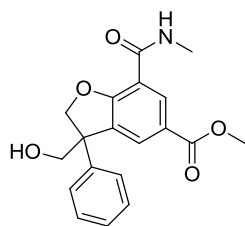
Bromine (0.163 mL, 3.17 mmol) was added to (±)-methyl 3-(hydroxymethyl)-3-phenyl-2,3-dihydrobenzofuran-5-carboxylate **(±)-2.096** (180 mg, 0.633 mmol) in CH₂Cl₂ (5 mL) at rt under nitrogen. The resulting solution was stirred at rt for 1 h. The reaction was quenched with sat. aq. sodium thiosulfate (5 mL) and sodium hydrosulfite was added until the reaction turned colourless. The reaction was then extracted with CH₂Cl₂ (2 x 20 mL). The organics were passed through a hydrophobic frit and concentrated *in vacuo* to afford (±)-methyl 7-bromo-3-(hydroxymethyl)-3-phenyl-2,3-dihydrobenzofuran-5-carboxylate **(±)-2.098** (220 mg, 0.606 mmol, 96% yield) as a colourless gum. LCMS (formic, ES⁺) t_R = 1.18 min, m/z = 363.1, 365.1; HRMS (C₁₇H₁₅O₄Br): [M+H]⁺ calculated 363.0232, found 363.0237; ¹H NMR (DMSO-*d*₆, 400 MHz): δ (ppm) 7.99 (d, *J*=1.8 Hz, 1H), 7.75 (d, *J*=1.8 Hz, 1H), 7.24–7.39 (m, 5H), 4.97 (d, *J*=9.3 Hz, 1H), 4.79 (d, *J*=9.3 Hz, 1H), 3.99 (ABq, *J*=10.8 Hz, 2H), 3.82 (s, 3H); Alcohol OH not visible; ¹³C NMR (DMSO-*d*₆, 101 MHz): δ (ppm) 179.3, 161.6, 143.2, 134.5, 133.6, 129.1, 127.4, 127.3, 126.6, 124.4, 119.6, 102.3, 82.7, 57.0, 52.6; m.p. 136.1 – 137.8 °C; IR ν_{max} (cm⁻¹) 3462, 1694, 1430, 1287, 764.

(±)-Methyl 3-methyl-7-(methylcarbamoyl)-3-phenyl-2,3-dihydrobenzofuran-5-carboxylate ((±)-2.077)



Methanamine hydrochloride (54 mg, 0.806 mmol), (±)-methyl 7-bromo-3-methyl-3-phenyl-2,3-dihydrobenzofuran-5-carboxylate **(±)-2.097** (140 mg, 0.403 mmol), Pd(OAc)₂ (45 mg, 0.202 mmol), Xantphos (117 mg, 0.202 mmol), DMAP (222 mg, 1.814 mmol), and cobalt carbonyl (138 mg, 0.403 mmol) were dissolved in 1,4-Dioxane (10 mL) at rt under nitrogen. The resulting solution was stirred at 100 °C under mw irradiation for 4 h. The reaction was diluted with water (50 mL) and extracted with EtOAc (50 mL) and Et₂O (50 mL). The combined organics were passed through a hydrophobic frit and concentrated *in vacuo* to afford the crude product. The crude product was purified by silica chromatography eluting with 0-70% EtOAc/cyclohexane. The pure fractions were concentrated *in vacuo* to afford methyl (±)-3-methyl-7-(methylcarbamoyl)-3-phenyl-2,3-dihydrobenzofuran-5-carboxylate **(±)-2.077** (79 g, 0.243 mmol, 60% yield) as a white solid. LCMS (Formic, ES⁺): t_R = 1.09 min; m/z = 326.3; HRMS (C₁₉H₁₉NO₄): [M+H]⁺ calculated 326.1392, found 326.1400; ¹H NMR (DMSO-*d*₆, 400 MHz): δ (ppm) 8.34 (d, *J*=1.7 Hz, 1H), 7.92 (q, *J*=4.5 Hz, 1H), 7.75 (d, *J*=1.7 Hz, 1H), 7.23–7.39 (m, 5H), 4.90 (d, *J*=9.0 Hz, 1H), 4.78 (d, *J*=9.0 Hz, 1H), 3.82 (s, 3H), 2.85 (d, *J*=4.5 Hz, 3H), 1.78 (s, 3H); ¹³C NMR (DMSO-*d*₆, 101 MHz): δ (ppm) 165.9, 163.7, 160.8, 145.8, 138.6, 131.5, 129.1, 127.9, 127.3, 126.6, 123.4, 117.3, 87.7, 52.5, 49.0, 26.8, 26.0; m.p. 138.3 – 141.3 °C; IR ν_{max} (cm⁻¹) 3357, 2946, 1707, 1650, 1270, 763.

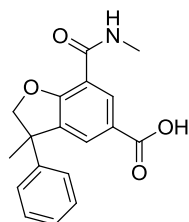
Methyl 3-(hydroxymethyl)-7-(methylcarbamoyl)-3-phenyl-2,3-dihydrobenzofuran-5-carboxylate ((±)-2.087)



(±)-Methyl 7-bromo-3-(hydroxymethyl)-3-phenyl-2,3-dihydrobenzofuran-5-carboxylate **(±)-2.098** (450 mg, 1.239 mmol), methanamine hydrochloride (167 mg, 2.478 mmol), Pd(OAc)₂ (139 mg, 0.619 mmol), Xantphos (358 mg, 0.619 mmol), DMAP (681 mg, 5.58 mmol), and cobalt carbonyl (424 mg, 1.239 mmol) were dissolved in 1,4-dioxane (10 ml) at rt under nitrogen. The resulting solution was stirred at 100 °C under mw irradiation for 4 h. The reaction was passed through a Celite plug, eluting with EtOAc (50 mL). The filtrate was washed with water (50 mL) and the aqueous layer was then extracted with CH₂Cl₂ (50 mL). The combined organics were passed through a hydrophobic frit and concentrated *in vacuo* to afford the crude product. The crude product was purified by silica chromatography

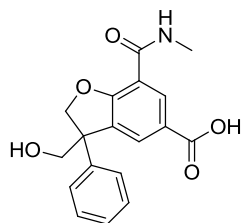
eluting with 0-100% EtOAc/cyclohexane. The pure fractions were concentrated *in vacuo* to afford (±)-methyl 3-(hydroxymethyl)-7-(methylcarbamoyl)-3-phenyl-2,3-dihydrobenzofuran-5-carboxylate (**±**)-**2.087** (210 mg, 0.615 mmol, 50% yield) as a white solid. LCMS (formic, ES⁺) $t_R = 0.89$ min, $m/z = 342.3$; HRMS (C₁₉H₁₉NO₅): [M+H]⁺ calculated 342.1341, found 3342.1350; ¹H NMR (DMSO-*d*₆, 400 MHz): δ (ppm) 8.36 (d, $J=1.8$ Hz, 1H), 7.89 (q, $J=4.5$ Hz, 1H), 7.85 (d, $J=1.8$ Hz, 1H), 7.30–7.40 (m, 4H), 7.23–7.30 (m, 1H), 5.28 (t, $J=5.0$ Hz, 1H), 5.03 (d, $J=9.1$ Hz, 1H), 4.84 (d, $J=9.1$ Hz, 1H), 4.02 (d, $J=5.0$ Hz, 2H), 3.83 (s, 3H), 2.84 (d, $J=4.5$ Hz, 3H); ¹³C NMR (DMSO-*d*₆, 101 MHz): δ (ppm) 166.0, 163.7, 161.7, 143.4, 134.8, 131.7, 129.5, 129.0, 127.3, 122.9, 119.6, 117.0, 83.4, 65.8, 55.3, 52.5, 26.8; m.p. 218.4 – 219.6 °C; IR ν_{max} (cm⁻¹) 3296, 1707, 1651, 1273, 769.

(±)-3-Methyl-7-(methylcarbamoyl)-3-phenyl-2,3-dihydrobenzofuran-5-carboxylic acid ((±)-2.099)



LiOH (10 mg, 0.430 mmol) and (±)-methyl 3-methyl-7-(methylcarbamoyl)-3-phenyl-2,3-dihydrobenzofuran-5-carboxylate (**±**)-**2.077** (70 mg, 0.215 mmol) were dissolved in THF (2 mL) and water (2 mL). The resulting solution was heated to 50 °C and stirred for 2 h. The reaction was allowed to cooled before being acidified with 2 M HCl (20 mL) and extracted with EtOAc (2 x 20 mL). The combined organics were passed through a hydrophobic frit and concentrated *in vacuo* to afford (±)-3-methyl-7-(methylcarbamoyl)-3-phenyl-2,3-dihydrobenzofuran-5-carboxylic acid (**±**)-**2.099** (64 mg, 0.206 mmol, 96% yield) as a white solid. LCMS (formic, ES⁺) $t_R = 0.94$ min, $m/z = 312.3$; HRMS (C₁₈H₁₇NO₄): [M+H]⁺ calculated 312.1236, found 312.1245; ¹H NMR (DMSO-*d*₆, 400 MHz): δ (ppm) 12.81 (br. s., 1H), 8.32 (d, $J=2.0$ Hz, 1H), 7.90 (q, $J=4.6$ Hz, 1H), 7.73 (d, $J=2.0$ Hz, 1H), 7.22–7.39 (m, 5H), 4.89 (d, $J=9.0$ Hz, 1H), 4.76 (d, $J=9.0$ Hz, 1H), 2.85 (d, $J=4.6$ Hz, 3H), 1.78 (s, 3H).

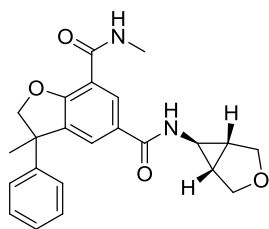
(±)-3-(Hydroxymethyl)-7-(methylcarbamoyl)-3-phenyl-2,3-dihydrobenzofuran-5-carboxylic acid ((±)-2.100)



LiOH (11 mg, 0.469 mmol) and (±)-methyl 3-(hydroxymethyl)-7-(methylcarbamoyl)-3-phenyl-2,3-dihydrobenzofuran-5-carboxylate (**±**)-**2.087** (80 mg, 0.234 mmol) were dissolved in THF (2 mL) and water (2 mL). The resulting solution was stirred at rt for 2 h. The reaction was then heated to 50 °C and stirred for 3 h. The reaction was allowed to

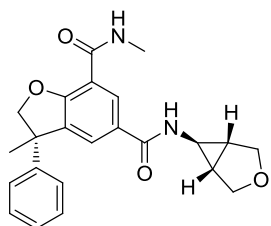
cooled before being acidified with 2 M HCl (20 mL) and extracted with EtOAc (2 x 20 mL). The combined organics were passed through a hydrophobic frit and concentrated *in vacuo* to afford (±)-3-(hydroxymethyl)-7-(methylcarbamoyl)-3-phenyl-2,3-dihydrobenzofuran-5-carboxylic acid (**±**)-**2.100** (69 mg, 0.211 mmol, 90% yield) as a white solid. LCMS (formic, ES⁺) $t_R = 0.76$ min, $m/z = 328.2$; HRMS (C₁₈H₁₇NO₅): [M+H]⁺ calculated 328.1185, found 328.1195; ¹H NMR (DMSO-*d*₆, 400 MHz): δ (ppm) 12.81 (br. s., 1H), 8.34 (d, $J=1.8$ Hz, 1H), 7.87 (q, $J=4.5$ Hz, 1H), 7.83 (d, $J=1.8$ Hz, 1H), 7.31–7.40 (m, 4H), 7.28 (d, $J=6.8$ Hz, 1H), 5.27 (t, $J=4.9$ Hz, 1H), 5.03 (d, $J=9.1$ Hz, 1H), 4.84 (d, $J=9.1$ Hz, 1H), 4.0 (d, $J=4.9$ Hz, 2H), 2.84 (d, $J=4.5$ Hz, 3H); m.p. 259.6 – 262.8 °C; IR ν_{max} (cm⁻¹) 3376, 1716, 1619, 1174, 698.

(±)-N⁵-((1*R*,5*S*,6*r*)-3-oxabicyclo[3.1.0]hexan-6-yl)-N⁷,3-dimethyl-3-phenyl-2,3-dihydrobenzofuran-5,7-dicarboxamide ((±)-2.101**)**



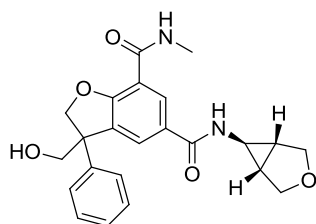
(±)-3-Methyl-7-(methyl carbamoyl)-3-phenyl-2,3-dihydrobenzofuran-5-carboxylic acid (**±**)-**2.099** (60 mg, 0.193 mmol) and (1*R*,5*S*,6*r*)-3-oxabicyclo[3.1.0]hexan-6-amine **2.007** (23 mg, 0.231 mmol) were dissolved in CH₂Cl₂ (4 mL) and reacted according to **general procedure A**. The crude product was purified by silica chromatography eluting with 0-100% (3:1 EtOAc/EtOH)/cyclohexane. Pure fractions were concentrated *in vacuo* to afford (±)-N⁵-((1*R*,5*S*,6*r*)-3-oxabicyclo[3.1.0]hexan-6-yl)-N⁷,3-dimethyl-3-phenyl-2,3-dihydrobenzofuran-5,7-dicarboxamide (**±**)-**2.101** (73 mg, 0.186 mmol, 97% yield) as a white solid. LCMS (formic, ES⁺) $t_R = 0.90$ min; $m/z = 393.4$; HRMS (C₂₃H₂₄N₂O₄): [M+H]⁺ calculated 393.1816, found 393.1814; ¹H NMR (DMSO-*d*₆, 400 MHz): δ (ppm) 8.45 (d, $J=3.9$ Hz, 1H), 8.24 (d, $J=2.0$ Hz, 1H), 7.87 (q, $J=4.6$ Hz, 1H), 7.73 (d, $J=2.0$ Hz, 1H), 7.23–7.39 (m, 5H), 4.83 (d, $J=9.0$ Hz, 1H), 4.72 (d, $J=9.0$ Hz, 1H), 3.84 (d, $J=8.3$ Hz, 2H), 3.62 (dd, $J=8.3$, 2.2 Hz, 2H), 2.84 (d, $J=4.6$ Hz, 3H), 2.55–2.60 (m, 1H), 1.86–1.90 (m, 2H), 1.76 (s, 3H); ¹³C NMR (DMSO-*d*₆, 101 MHz): δ (ppm) 166.4, 164.2, 159.2, 146.1, 137.6, 129.2, 129.0, 128.0, 127.2, 126.6, 126.3, 87.3, 69.1, 49.1, 31.5, 26.7, 26.2, 24.5, 24.5.

(S)-N⁵-((1R,5S,6r)-3-oxabicyclo[3.1.0]hexan-6-yl)-N⁷,3-dimethyl-3-phenyl-2,3-dihydrobenzofuran-5,7-dicarboxamide ((S)-2.101)



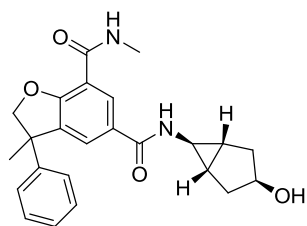
(±)-N⁵-((1R,5S,6r)-3-oxabicyclo[3.1.0]hexan-6-yl)-N⁷,3-dimethyl-3-phenyl-2,3-dihydrobenzofuran-5,7-dicarboxamide (**±**)-**2.101** (42 mg, 0.107 mmol) was dissolved in EtOH (2.0 mL) and injected onto the column (Column: 30 mm x 25 cm Chiralcel OD-H (5 μm, Lot No ODH11158-01) which was eluted with 15% EtOH/heptane, flow rate = 30 mL/min, detection wavelength, 215 nm, 4. Ref 550, 100. Appropriate fractions for isomer 1 were bulked and labelled peak 1. Appropriate fractions for isomer 2 were bulked and labelled peak 2. The bulked pure fractions from peak 1 were concentrated *in vacuo* to afford (S)-N⁵-((1R,5S,6r)-3-oxabicyclo[3.1.0]hexan-6-yl)-N⁷,3-dimethyl-3-phenyl-2,3-dihydrobenzofuran-5,7-dicarboxamide (**S**)-**2.101** (16 mg, 0.041 mmol, 38%) as a white solid. ¹H NMR and LCMS data consistent with racemate; Chiral LC: 4.6 mm x 25 cm Chiralcel OD-H column, 15% EtOH/heptane, t_R = 16.312 min, *er* >99:1.

(±)-N⁵-((1R,5S,6r)-3-oxabicyclo[3.1.0]hexan-6-yl)-3-(hydroxymethyl)-N⁷-methyl-3-phenyl-2,3-dihydrobenzofuran-5,7-dicarboxamide ((±)-2.102)



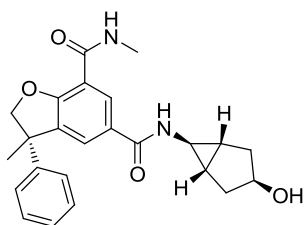
(±)-3-(Hydroxymethyl)-7-(methylcarbamoyl)-3-phenyl-2,3-dihydrobenzofuran-5-carboxylic acid (**±**)-**2.100** (70 mg, 0.214 mmol) and (1R,5S,6r)-3-oxabicyclo[3.1.0]hexan-6-amine **2.007** (25 mg, 0.051 mmol) were dissolved in CH₂Cl₂ (4 mL) and reacted according to general procedure A. The crude product was purified by silica chromatography, eluting with 0-100% (3:1 EtOAc:EtOH)/EtOAc. The pure fractions were concentrated *in vacuo* to afford (±)-N⁵-((1R,5S,6r)-3-oxabicyclo[3.1.0]hexan-6-yl)-3-(hydroxymethyl)-N⁷-methyl-3-phenyl-2,3-dihydrobenzofuran-5,7-dicarboxamide (**±**)-**2.102** (74 mg, 0.181 mmol, 85% yield) as a white solid. LCMS (formic, ES⁺) t_R = 0.75 min; *m/z* = 409.2; HRMS (C₂₃H₂₄N₂O₅): [M+H]⁺ calculated 409.1763, found 409.1759; ¹H NMR (DMSO-*d*₆, 400 MHz): δ (ppm) 8.48 (d, *J*=4.0 Hz, 1H), 8.25 (d, *J*=2.0 Hz, 1H), 7.85 (q, *J*=4.8 Hz, 1H), 7.81 (d, *J*=2.0 Hz, 1H), 7.30–7.39 (m, 4H), 7.23–7.29 (m, 1H), 5.26 (t, *J*=5.2 Hz, 1H), 5.01 (d, *J*=9.1 Hz, 1H), 4.81 (d, *J*=9.1 Hz, 1H), 3.93–4.04 (m, 2H), 3.85 (d, *J*=8.3 Hz, 2H), 3.63 (dd, *J*=8.3, 2.5 Hz, 2H), 2.84 (d, *J*=4.5 Hz, 3H), 2.57–2.59 (m, 1H), 1.87–1.91 (m, 2H); m.p. 155.8 – 160.0 °C; IR ν_{max} (cm⁻¹) 3402, 1640, 1537, 838, 699.

(±)-*N*⁵-((1*R*,3*R*,5*S*,6*r*)-3-hydroxybicyclo[3.1.0]hexan-6-yl)-*N*⁷,3-dimethyl-3-phenyl-2,3-dihydrobenzofuran-5,7-dicarboxamide ((±)-2.103)



HATU (2.56 g, 6.75 mmol) was added to 3-methyl-7-(methylcarbamoyl)-3-phenyl-2,3-dihydrobenzofuran-5-carboxylic acid (**(±)-2.099**) (1.50 g, 4.82 mmol) and DIPEA (2.52 mL, 14.45 mmol) in CH₂Cl₂ (10 mL) at rt under nitrogen. The resulting solution was stirred at rt for 5 min before (1*R*,3*s*,5*S*,6*r*)-6-aminobicyclo[3.1.0]hexan-3-ol (0.55 g, 4.82 mmol) was added. The resulting solution was stirred at rt for 2 h. The reaction was diluted with sat. aq. NaHCO₃ (20 mL) and extracted with CH₂Cl₂ (2 x 10 mL). The combined organics were passed through a hydrophobic frit and concentrated *in vacuo* to afford the crude product. The crude product was purified by silica chromatography eluting with 0-50% (3:1 EtOH:EtOAc)/EtOAc. The pure fractions were concentrated *in vacuo* to afford (±)-*N*⁵-((1*R*,3*s*,5*S*,6*r*)-3-hydroxybicyclo[3.1.0]hexan-6-yl)-*N*⁷,3-dimethyl-3-phenyl-2,3-dihydrobenzofuran-5,7-dicarboxamide (**(±)-2.103**) (1.69 g, 4.16 mmol, 86% yield) as a white solid (80% pure by NMR). ¹H NMR and LCMS data consistent with single enantiomer.

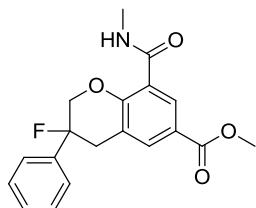
(*S*)-*N*⁵-((1*R*,3*R*,5*S*,6*r*)-3-hydroxybicyclo[3.1.0]hexan-6-yl)-*N*⁷,3-dimethyl-3-phenyl-2,3-dihydrobenzofuran-5,7-dicarboxamide ((*S*)-2.103)



(±)-*N*⁵-((1*R*,3*R*,5*S*,6*r*)-3-hydroxybicyclo[3.1.0]hexan-6-yl)-*N*⁷,3-dimethyl-3-phenyl-2,3-dihydrobenzofuran-5,7-dicarboxamide (**(±)-2.103**) (1.690 g, 4.16 mmol) was dissolved in EtOH (36 mL) and injected onto the column (Column: 250 mm x 30 mm Chiralpak AD-H (5 μm, Batch ADH0CE-PC014), in 2.0 mL aliquots, which was eluted with 50% (EtOH + 0.2% isopropylamine)/heptane, flow rate = 30 mL/min, detection wavelength = 230 nm. Appropriate fractions for isomer 1 were bulked and labelled peak 1. Appropriate fractions for isomer 2 were bulked bulked and labelled peak 2. The bulked pure fractions from peak 2 were concentrated *in vacuo* to afford (*S*)-*N*⁵-((1*R*,3*R*,5*S*,6*r*)-3-hydroxybicyclo[3.1.0]hexan-6-yl)-*N*⁷,3-dimethyl-3-phenyl-2,3-dihydrobenzofuran-5,7-dicarboxamide (**(*S*)-2.103**) (0.645 g, 1.56 mmol) as a white solid. LCMS (formic, ES⁺) t_R = 0.87 min, *m/z* = 407.4; HRMS (C₂₄H₂₆N₂O₄): [M+H]⁺ calculated 407.1971, found 407.1972; ¹H NMR (DMSO-*d*₆, 400 MHz): δ (ppm) 8.29 (d, *J*=3.9 Hz, 1H), 8.21 (d, *J*=2.0 Hz, 1H), 7.86 (q, *J*=4.6 Hz, 1H), 7.71 (d, *J*=2.0 Hz, 1H), 7.22–7.39 (m, 5H), 4.83 (d, *J*=9.0 Hz, 1H), 4.71 (d, *J*=9.0 Hz, 1H),

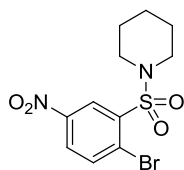
4.56 (d, $J=5.4$ Hz, 1H), 3.78–3.87 (m, 1H), 2.84 (d, $J=4.6$ Hz, 3H), 2.43–2.47 (m, 1H), 2.03 (dd, $J=12.5, 7.1$ Hz, 2H), 1.76 (s, 3H), 1.60 (ddd, $J=12.4, 7.9, 4.4$ Hz, 2H), 1.36–1.46 (m, 2H); ^{13}C NMR (DMSO- d_6 , 101 MHz): δ (ppm) 166.3, 164.1, 159.0, 146.1, 137.5, 129.2, 129.0, 128.1, 127.2, 126.6, 126.3, 116.5, 87.2, 69.9, 49.1, 36.6, 32.8, 26.7, 26.2, 23.4; m.p. 137.9 – 141.3 °C; IR ν_{max} (cm^{-1}) 3300, 1637, 1534, 840, 699; Chiral LC: 4.6 mm x 25 cm Chiralpak AD-H column, 50% (EtOH + 0.2% isopropylamine)/heptane, $t_{\text{R}} = 7.749$ min, *er* 98:2.

(±)-Methyl 3-fluoro-8-(methylcarbamoyl)-3-phenylchromane-6-carboxylate ((±)-2.104)

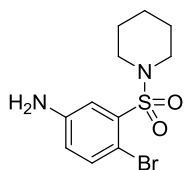


(±)-Methyl 3-(hydroxymethyl)-7-(methylcarbamoyl)-3-phenyl-2,3-dihydrobenzofuran-5-carboxylate **(±)-2.087** (120 mg, 0.352 mmol) was dissolved in dry CH_2Cl_2 (5 mL) at rt under nitrogen. Deoxo-Fluor[®] (50% w/w in THF, 0.259 mL, 0.703 mmol) was added and the resulting solution heated at 40 °C for 1 h. The reaction was allowed to cool before quenching with sat. aq. NaHCO_3 (5 mL) and extracting with CH_2Cl_2 (2 x 5 mL). The combined organics were passed through a hydrophobic frit and concentrated *in vacuo* to afford the crude product. The crude product was purified by formic MDAP. The pure fractions were concentrated *in vacuo* to afford (±)-methyl 3-fluoro-8-(methylcarbamoyl)-3-phenylchromane-6-carboxylate **(±)-2.104** (59 mg, 0.172 mmol, 49% yield) as a white solid. LCMS (formic, ES^+) $t_{\text{R}} = 1.03$ min, $m/z = 344.1$; HRMS ($\text{C}_{19}\text{H}_{18}\text{NO}_4\text{F}$): $[\text{M}+\text{H}]^+$ calculated 344.1298, found 344.1295; ^1H NMR (DMSO- d_6 , 400 MHz): δ (ppm) 8.26 (q, $J=4.5$ Hz, 1H), 8.23 (d, $J=2.0$ Hz, 1H), 7.92 (d, $J=2.0$ Hz, 1H), 7.42–7.60 (m, 5H), 4.47–4.63 (m, 2H), 3.85 (s, 3H), 3.59–3.78 (m, 1H), 3.33–3.43 (m, 1H), 2.83 (d, $J=4.5$ Hz, 3H); ^{19}F NMR (DMSO- d_6 , 376 MHz): δ (ppm) -158.2 (br. s, 1F); ^{13}C NMR (DMSO- d_6 , 151 MHz): δ (ppm) 165.9, 164.9, 154.8, 139.3 (d, $J=19.9$ Hz), 133.7, 130.5, 129.2, 125.1 (d, $J=7.7$ Hz), 123.3, 122.1, 121.7, 91.1 (d, $J=175.8$ Hz), 71.3 (d, $J=22.1$ Hz), 52.6, 40.6, 35.9 (d, $J=23.2$ Hz), 26.9; IR ν_{max} (cm^{-1}) 3431, 2950, 1719, 1648, 1172, 699.

4.4.2. CECR2 Experimental

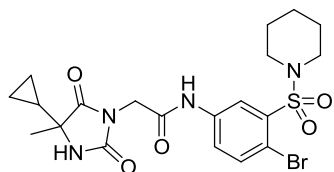
1-((2-Bromo-5-nitrophenyl)sulfonyl)piperidine (3.022)

2-Bromo-5-nitrobenzenesulfonyl chloride **3.021** (1.10 g, 3.66 mmol) was taken up in CH₂Cl₂ (50 mL) under nitrogen and cooled to 0 °C. DIPEA (1.41 mL, 8.05 mmol) was added and the reaction stirred for 5 min before piperidine (0.43 mL, 4.39 mmol) was added. The reaction was stirred at 0 °C for 1 h. The reaction mixture was quenched with sat. aq. NaHCO₃ (50 mL) and extracted with CH₂Cl₂ (2 x 50 mL). The combined organics were filtered through a hydrophobic frit and concentrated *in vacuo* to afford 1-((2-bromo-5-nitrophenyl)sulfonyl)piperidine **3.022** (1.24 g, 3.54 mmol, 97% yield) as an orange gum. LCMS (formic, ES⁺) t_R = 1.24 min, m/z = 349.0, 351.0; HRMS (C₁₁H₁₃BrN₂O₄S): [M+H]⁺ calculated 348.9858, found 348.9844; ¹H NMR (CDCl₃-d, 400 MHz): δ (ppm) 8.91 (d, J=2.7 Hz, 1H), 8.22 (dd, J=8.6, 2.7 Hz, 1H), 7.96 (d, J=8.6 Hz, 1H), 3.32–3.40 (m, 4H), 1.57–1.73 (m, 6H); ¹³C NMR (CDCl₃-d, 101 MHz): δ (ppm) 146.8, 140.8, 137.0, 127.7, 127.2, 126.7, 46.8, 25.6, 23.7.

4-Bromo-3-(piperidin-1-ylsulfonyl)aniline (3.023)

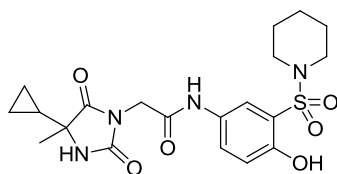
1-((2-Bromo-5-nitrophenyl)sulfonyl)piperidine **3.022** (1.10 g, 3.15 mmol), ammonium chloride (0.25 g, 4.73 mmol) and iron (0.53 g, 9.45 mmol) were dissolved in a 3:1 mixture of EtOH (5.0 mL) and water (1.7 mL). The resulting solution was heated to 70 °C for 2 h. The reaction was allowed to cool then filtered through a plug of Celite, washing with MeOH (20 mL). The resulting solution was concentrated *in vacuo* and then partitioned between sat. aq. NaHCO₃ (20 mL) and CH₂Cl₂ (20 mL). The layers were separated and the aq. phase was extracted with CH₂Cl₂ (2 x 20 mL). The combined organics were passed through a hydrophobic frit and concentrated *in vacuo* to afford the crude product. The crude product was purified by silica chromatography, eluting with 0-50% EtOAc/cyclohexane. The pure fractions were concentrated *in vacuo* to afford 4-bromo-3-(piperidin-1-ylsulfonyl)aniline **3.023** (0.75 g, 2.334 mmol, 74% yield) as an orange gum. LCMS (formic, ES⁺) t_R = 1.02 min, m/z = 319.1, 321.1; HRMS (C₁₁H₁₅BrN₂O₂S): [M+H]⁺ calculated 319.0116, found 319.0112; ¹H NMR (CDCl₃-d, 400 MHz): δ (ppm) 7.39–7.48 (m, 2H), 6.67 (dd, J=8.6, 2.9 Hz, 1H), 3.93 (br. s., 2H), 3.23–3.30 (m, 4H), 1.52–1.69 (m, 6H); ¹³C NMR (CDCl₃-d, 101 MHz): δ (ppm) 145.9, 138.3, 136.2, 119.4, 118.3, 106.9, 46.5, 25.5, 23.8; IR ν_{max} (cm⁻¹) 3374, 2938, 1626, 1590, 1463, 1309, 1140, 719, 578.

(±)-N-(4-Bromo-3-(piperidin-1-ylsulfonyl)phenyl)-2-(4-cyclopropyl-4-methyl-2,5-dioxoimidazolidin-1-yl)acetamide ((±)-3.025)



(±)-2-(4-Cyclopropyl-4-methyl-2,5-dioxoimidazolidin-1-yl)acetic acid (**(±)-3.024**) (319 mg, 1.504 mmol), 4-bromo-3-(piperidin-1-ylsulfonyl)aniline **3.023** (400 mg, 1.253 mmol), and HATU (572 mg, 1.504 mmol) were dissolved in CH₂Cl₂ (10 mL). DIPEA (0.657 mL, 3.76 mmol) was added and the resulting solution was stirred at rt for 2 h. The reaction was quenched with sat. aq. NaHCO₃ (20 mL) and extracted with CH₂Cl₂ (3 x 20 mL). The combined organics were passed through a hydrophobic frit and concentrated *in vacuo* to afford the crude product. The crude product was purified by silica chromatography, eluting with 0-60% EtOAc/cyclohexane. The pure fractions were concentrated *in vacuo* to afford (±)-N-(4-bromo-3-(piperidin-1-ylsulfonyl)phenyl)-2-(4-cyclopropyl-4-methyl-2,5-dioxoimidazolidin-1-yl)acetamide (**(±)-3.025**) (405 mg, 0.789 mmol, 63% yield) as a cream solid. LCMS (formic, ES⁺) t_R = 1.05 min, m/z = 513.2, 515.2; HRMS (C₂₀H₂₅BrN₄O₅S): [M+H]⁺ calculated 513.0807, found 513.0807; ¹H NMR (DMSO-*d*₆, 600 MHz): δ (ppm) 10.71 (s, 1H), 8.98 (s, 1H), 7.91-8.01 (m, 2H), 7.62 (d, *J*=8.6 Hz, 1H), 4.19 (s, 2H), 3.15-3.21 (m, 4H), 1.48-1.56 (m, 6H), 1.40 (s, 3H), 1.12-1.19 (m, 1H), 0.41-0.48 (m, 2H), 0.34-0.39 (m, 1H), 0.26-0.33 (m, 1H); ¹³C NMR (CDCl₃-*d*, 101 MHz): δ (ppm) 176.4, 164.6, 156.5, 138.1, 137.5, 136.3, 124.5, 122.8, 113.9, 62.0, 46.6, 41.5, 25.5, 23.7, 23.0, 17.3, 1.1, 0.3; m.p. 221.5 – 225.0 °C; IR ν_{max} (cm⁻¹) 3308, 1712, 1535, 1454, 1307, 579.

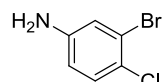
(±)-2-(4-Cyclopropyl-4-methyl-2,5-dioxoimidazolidin-1-yl)-N-(4-hydroxy-3-(piperidin-1-ylsulfonyl)phenyl)acetamide ((±)-3.026)



(±)-N-(4-Bromo-3-(piperidin-1-ylsulfonyl)phenyl)-2-(4-cyclopropyl-4-methyl-2,5-dioxoimidazolidin-1-yl)acetamide (**(±)-3.025**) (50 mg, 0.097 mmol), bis(pinacolato)diboron (50 mg, 0.195 mmol), KOAc (29 mg, 0.292 mmol) and XPhos Pd G2 (8 mg, 9.74 μmol) were dissolved in EtOH (1 mL) at rt under nitrogen. The resulting solution was heated to 100 °C and stirred for 2 h. The reaction was then cooled to 0 °C before aq. 2 M NaOH (0.049 mL, 0.097 mmol) and hydrogen peroxide (35% w/w in water, 0.085 mL, 0.974 mmol) were added sequentially. The resulting solution was stirred at 0 °C for 10 mins. The reaction was quenched by addition of 10% aq. sodium thiosulfate (2 mL) and extracted with CH₂Cl₂ (2 x 5 mL). The combined organics were passed through a hydrophobic frit and

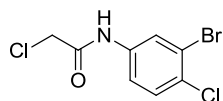
concentrated *in vacuo* to afford the crude product. The crude product was purified by formic MDAP. The pure fractions were concentrated *in vacuo* to afford (\pm)-2-(4-cyclopropyl-4-methyl-2,5-dioximidazolidin-1-yl)-*N*-(4-hydroxy-3-(piperidin-1-ylsulfonyl)phenyl)acetamide (**\pm**)-**3.026** (16 mg, 0.036 mmol, 37% yield) as a white solid. LCMS (formic, ES⁺) t_R = 0.90 min, m/z = 451.3; HRMS (C₂₀H₂₆N₄O₆S): [M+H]⁺ calculated 451.1651, found 451.1648; ¹H NMR (CDCl₃-*d*, 400 MHz): δ (ppm) 8.24 (s, 1H), 7.68 (dd, J =8.8, 2.7 Hz, 1H), 7.63 (d, J =2.7 Hz, 1H), 6.99 (d, J =8.8 Hz, 1H), 5.83 (s, 1H), 4.33 (s, 2H), 3.04–3.14 (m, 4H), 1.64–1.68 (m, 4H), 1.55 (s, 3H), 1.44–1.52 (m, 2H), 1.24–1.31 (m, 1H), 0.57–0.66 (m, 1H), 0.43–0.54 (m, 2H), 0.33–0.42 (m, 1H); *phenol OH not visible*; ¹³C NMR (CDCl₃-*d*, 101MHz): δ (ppm) 176.4, 164.2, 156.4, 152.2, 130.1, 127.8, 119.7, 119.2, 119.1, 61.9, 46.8, 41.6, 25.0, 23.3, 23.0, 17.4, 1.2, 0.3; m.p. 106.7 – 111.7 °C; IR ν_{max} (cm⁻¹) 3309, 2938, 1708, 1452, 579.

3-Bromo-4-chloroaniline (**3.032**)³³⁵



2-Bromo-1-chloro-4-nitrobenzene **3.031** (10.00 g, 42.3 mmol) was suspended in EtOH (30 mL) and water (8.5 mL) Ammonium chloride (3.39 g, 63.4 mmol) and iron (7.09 g, 127 mmol) were added and the reaction heated to 70 °C for 16 h. The reaction mixture was cooled and filtered through a plug of Celite, washing with MeOH (30 mL). The filtrate was concentrated *in vacuo* and the residue partitioned between CH₂Cl₂ and sat. aq. NaHCO₃ (25 mL each). The aq. layer was re-extracted with CH₂Cl₂ (2 x 25 mL). The combined organics were eluted through a hydrophobic frit and concentrated *in vacuo* to give the crude product as an orange solid. The crude product was purified by silica chromatography, eluting with 0-50% EtOAc/cyclohexane. The pure fractions were concentrated *in vacuo* to give 3-bromo-4-chloroaniline **3.032** (7.65 g, 37.1 mmol, 88% yield) as a yellow solid. LCMS (Formic, ES⁺) t_R = 1.01 min; m/z = 206.0; HRMS (C₆H₅BrClN): [M+H]⁺ calculated 205.9367, found 205.9369; ¹H NMR (CDCl₃-*d*, 400 MHz): δ (ppm) 7.19 (d, J =8.6 Hz, 1H), 6.95 (d, J =2.7 Hz, 1H), 6.56 (dd, J =8.6, 2.7 Hz, 1H), 3.70 (br. s., 2H); ¹³C NMR (CDCl₃-*d*, 101 MHz): δ (ppm): 146.0, 130.6, 123.1, 122.6, 119.5, 115.2; m.p. 79.6 – 82.6 °C; IR ν_{max} (cm⁻¹) 3312, 2938, 1708, 1456, 568.

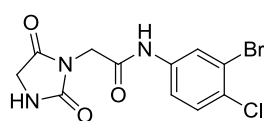
N-(3-Bromo-4-chlorophenyl)-2-chloroacetamide (**3.033**)



DIPEA (3.37 mL, 19.4 mmol) was added to 3-bromo-4-chloroaniline **3.032** (4.00 g, 19.4 mmol) in CH₂Cl₂ (40 mL). 2-Chloroacetyl chloride (1.54 mL, 19.4 mmol) was added and the reaction was stirred at rt for 1 h. The reaction was

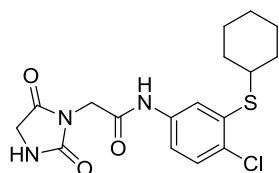
quenched with sat. aq. NaHCO₃ (20 mL) and extracted with CH₂Cl₂ (2 x 20 mL). The organic layers were filtered through a hydrophobic frit and concentrated *in vacuo* to afford the crude product. The crude product was purified by silica chromatography, eluting with 0-50% (3:1 EtOH:EtOAc)/cyclohexane. The pure fractions were concentrated *in vacuo* to afford *N*-(3-bromo-4-chlorophenyl)-2-chloroacetamide **3.033** (4.85 g, 17.1 mmol, 88% yield) as a yellow solid. LCMS (Formic, ES⁺) *t*_R = 1.10 min; *m/z* = 281.9; ¹H NMR (CDCl₃-*d*, 400 MHz): δ (ppm) 8.21 (br. s., 1H), 7.93 (d, *J*=2.4 Hz, 1H), 7.49 (dd, *J*=8.6, 2.4 Hz, 1H), 7.44 (d, *J*=8.6 Hz, 1H), 4.20 (s, 2H).

***N*-(3-Bromo-4-chlorophenyl)-2-(2,5-dioxoimidazolidin-1-yl)acetamide (3.034)**



Imidazolidine-2,4-dione (2.04 g, 20.4 mmol) was added to *N*-(3-bromo-4-chlorophenyl)-2-chloroacetamide **3.033** (4.80 g, 17.0 mmol) and K₂CO₃ (7.03 g, 50.9 mmol) in DMF (15 mL) at rt under nitrogen. The resulting solution was stirred at 70 °C for 1 h before being cooled to rt. The reaction was diluted with CH₂Cl₂ (20 mL) and washed with water (2 x 20 mL). The organic layer was passed through a hydrophobic frit and concentrated *in vacuo* to afford the crude product. The crude product was purified using silica chromatography, eluting with 0-100% (3:1 EtOAc:EtOH)/cyclohexane. The pure fractions were concentrated *in vacuo* to afford *N*-(3-bromo-4-chlorophenyl)-2-(2,5-dioxoimidazolidin-1-yl)acetamide **3.034** (4.62 g, 13.3 mmol, 79% yield) as a white solid. LCMS (Formic, ES⁺) *t*_R = 0.86 min; *m/z* = 348.0; HRMS (C₁₁H₉BrClN₃O₃): [M+H]⁺ calculated 345.9589, found 345.9598; ¹H NMR (DMSO-*d*₆, 400 MHz): δ (ppm) 10.49 (s, 1H), 8.16 (s, 1H), 8.07 (d, *J*=2.4 Hz, 1H), 7.55–7.59 (m, 1H), 7.49–7.50 (m, 1H), 4.18 (s, 2H), 4.01 (s, 2H); ¹³C NMR (DMSO-*d*₆, 101 MHz): δ (ppm) 172.3, 165.9, 157.5, 139.0, 131.1, 127.5, 124.0, 121.8, 120.2, 46.6, 41.3; IR *v*_{max} (cm⁻¹) 3303, 3235, 1700, 1674, 1587, 1523, 1455, 1143, 929, 827, 733, 683.

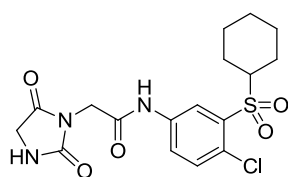
***N*-(4-Chloro-3-(cyclohexylthio)phenyl)-2-(2,5-dioxoimidazolidin-1-yl)acetamide (3.035)**



To a solution of *N*-(3-bromo-4-chlorophenyl)-2-(2,5-dioxoimidazolidin-1-yl)acetamide **3.034** (100 mg, 0.29 mmol) and DIPEA (0.15 mL, 0.87 mmol), in 1,4-dioxane (3 mL) and DMF (2 mL) at 100 °C was added Xantphos (33 mg, 0.06 mmol) and Pd₂dba₃ (26 mg, 0.03 mmol). Cyclohexanethiol (0.04 mL, 0.29 mmol) was added dropwise and the reaction stirred for 1 h. The reaction was allowed to cool before quenching with sat. aq.

Na₂CO₃ (50 mL), and extracting with CH₂Cl₂ (3 x 20 mL). The combined organics were passed through a hydrophobic frit and concentrated *in vacuo* to afford the crude product. The crude product was purified by formic MDAP. The pure fractions were concentrated *in vacuo* to give *N*-(4-chloro-3-(cyclohexylthio)phenyl)-2-(2,5-dioximidazolidin-1-yl)acetamide **3.035** (46 mg, 0.12 mmol, 42% yield) as a white solid. LCMS (Formic, ES⁺) *t*_R = 1.15; *m/z* = 382.1; ¹H NMR (CDCl₃-*d*, 400 MHz): δ (ppm) 8.33 (br. s., 1H), 8.12 (s, 1H), 7.69 (s, 1H), 7.64 (s, 1H), 7.02 (d, *J*=2.0 Hz, 1H), 4.30 (s, 2H), 4.08 (s, 2H), 1.99 (d, *J*=5.1 Hz, 1H), 1.78 (dd, *J*=8.7, 3.8 Hz, 2H), 1.58–1.65 (m, 1H), 1.22–1.50 (m, 7 H).

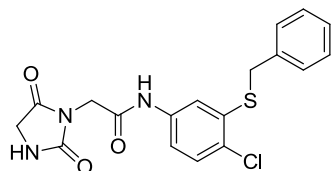
***N*-(4-Chloro-3-(cyclohexylsulfonyl)phenyl)-2-(2,5-dioximidazolidin-1-yl)acetamide (3.036)**



*m*CPBA (46 mg, 0.27 mmol) was added to *N*-(4-chloro-3-(cyclohexylthio)phenyl)-2-(2,5-dioximidazolidin-1-yl)acetamide **3.035** (46 mg, 0.12 mmol) in CH₂Cl₂ (5 mL) at rt under nitrogen. The resulting solution was stirred at rt for 16 h. The reaction was

quenched with sat. aq. Na₂S₂O₃ (10 mL), and extracted with CH₂Cl₂ (10 mL). The organic layer was washed with sat. aq. NaHCO₃, passed through a hydrophobic frit and concentrated *in vacuo* to afford the crude product. The crude product was purified by formic MDAP. The solvent was evaporated *in vacuo* to give *N*-(4-chloro-3-(cyclohexylsulfonyl)phenyl)-2-(2,5-dioximidazolidin-1-yl)acetamide **3.036** (23 mg, 0.06 mmol, 46% yield) as a white solid. LCMS (Formic, ES⁺) *t*_R = 0.92 min; *m/z* = 414.1; HRMS (C₁₇H₂₀ClN₃O₅S): [M+H]⁺ calculated 414.0885, found 414.0880; ¹H NMR (CDCl₃-*d*, 400 MHz): δ (ppm) 9.28 (s, 1H), 7.95–8.08 (m, 2H), 7.42 (d, *J*=8.8 Hz, 1H), 6.63 (s, 1H), 4.35 (s, 2H), 4.06 (s, 2H), 3.43–3.57 (m, 1H), 1.81–1.97 (m, 4 H), 1.69 (d, *J*=9.8 Hz, 1H), 1.41–1.58 (m, 2H), 1.12–1.34 (m, 3H); ¹³C NMR (CDCl₃-*d*, 101 MHz): δ (ppm) 171.6, 165.3, 157.9, 137.3, 135.0, 132.6, 126.9, 125.7, 123.0, 61.5, 46.9, 41.5, 25.1, 25.0, 24.9.

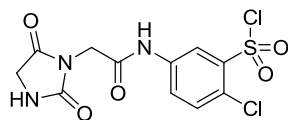
***N*-(3-(Benzylthio)-4-chlorophenyl)-2-(2,5-dioximidazolidin-1-yl)acetamide (3.037)**



To a solution of *N*-(3-bromo-4-chlorophenyl)-2-(2,5-dioximidazolidin-1-yl)acetamide **3.034** (4.60 g, 13.27 mmol) and DIPEA (6.94 mL, 39.8 mmol) in 1,4-dioxane (25 mL) and DMF (17 mL) at 100 °C was added Xantphos (1.54 g, 2.65 mmol) and Pd₂dba₃ (1.22 g, 1.327 mmol). Phenylmethanethiol (1.87 mL, 15.93 mmol) was added dropwise. After 1 h, the reaction was allowed to cool and then partitioned between sat. aq.

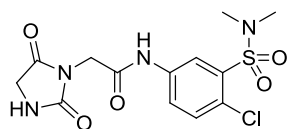
NaHCO₃ (20 mL) and EtOAc (20 mL). A precipitate formed and this was filtered off to give *N*-(3-(benzylthio)-4-chlorophenyl)-2-(2,5-dioxoimidazolidin-1-yl)acetamide **3.037** (4.00 g, 10.26 mmol, 77% yield) as a green solid. LCMS (Formic, ES⁺) t_R = 1.07 min; *m/z* = 390.1; ¹H NMR (DMSO-*d*₆, 400 MHz): δ (ppm) 10.42 (s, 1H), 8.16 (s, 1H), 7.79 (d, *J*=2.2 Hz, 1H), 7.21–7.48 (m, 7 H), 4.22 (s, 2H), 4.19 (s, 2H), 4.02 (s, 2H).

2-Chloro-5-(2-(2,5-dioxoimidazolidin-1-yl)acetamido)benzene-1-sulfonyl chloride (3.039)



To a suspension of *N*-(3-(benzylthio)-4-chlorophenyl)-2-(2,5-dioxoimidazolidin-1-yl)acetamide **3.037** (4.00 g, 10.3 mmol) in MeCN (75 mL), water (3.5 mL) and AcOH (5.0 mL) was added 1,3-dichloro-5,5-dimethylimidazolidine-2,4-dione **3.038** (4.04 g, 20.5 mmol). The resulting solution was stirred at rt for 2 h. The solution was concentrated *in vacuo* and redissolved in CH₂Cl₂ (50 mL), washing with sat. aq. NaHCO₃ (50 mL). The organic layer was passed through a hydrophobic frit and concentrated *in vacuo* to afford the crude product. The crude product was purified by silica chromatography, eluting with 0-100% EtOAc/cyclohexane. The pure fractions were concentrated *in vacuo* to afford 2-chloro-5-(2-(2,5-dioxoimidazolidin-1-yl)acetamido)benzene-1-sulfonyl chloride **3.039** (1.30 g, 3.55 mmol, 35% yield) as a white solid. LCMS (Formic, ES⁺) t_R = 0.50 min; *m/z* = 364.2; ¹H NMR (MeOD-*d*₄, 400 MHz): δ (ppm) 8.54 (d, *J*=2.5 Hz, 1H), 7.97 (dd, *J*=8.8, 2.5 Hz, 1H), 7.73 (d, *J*=8.8 Hz, 1H), 4.36 (s, 2H), 4.09 (s, 2H); *Amide NH and hydantoin NH not visible*; ¹³C NMR (DMSO-*d*₆, 101 MHz): δ (ppm) 172.3, 165.4, 157.5, 145.9, 137.1, 131.1, 125.2, 120.9, 120.4, 46.6, 41.2.

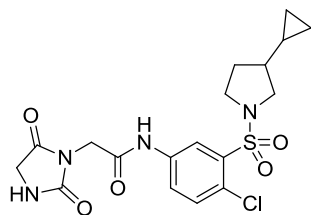
***N*-(4-Chloro-3-(*N,N*-dimethylsulfamoyl)phenyl)-2-(2,5-dioxoimidazolidin-1-yl)acetamide (3.040)**



2-Chloro-5-(2-(2,5-dioxoimidazolidin-1-yl)acetamido)benzene sulfonyl chloride **3.039** (40 mg, 0.109 mmol) was taken up in CH₂Cl₂ (5 mL) under nitrogen and cooled in an ice bath. DIPEA (0.042 mL, 0.240 mmol) was added and the reaction stirred for 5 min before dimethylamine (2M in THF, 0.057 mL, 0.115 mmol) was added and the reaction was stirred for 1 h. The reaction mixture was quenched with sat. aq. NaHCO₃ (10 mL), and washed with 2M HCl aq. (10 mL), then filtered through a hydrophobic frit and concentrated *in vacuo* to give the crude product. The crude product was purified by formic MDAP. The pure fractions were concentrated *in vacuo* to afford *N*-(4-chloro-3-(*N,N*-dimethylsulfamoyl)phenyl)-2-(2,5-dioxoimidazolidin-1-

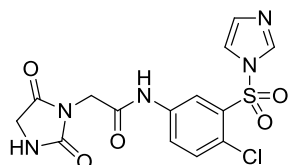
yl)acetamide **3.040** (14 mg, 0.037 mmol, 34% yield) as a white solid. LCMS (Formic ES⁺) t_R = 0.73 min; m/z = 375.2; HRMS (C₁₃H₁₅ClN₄O₅S): [M+H]⁺ calculated 375.0530, found 375.0521; ¹H NMR (DMSO-*d*₆, 400 MHz): δ (ppm) 10.73 (s, 1H), 8.25 (d, J =2.7 Hz, 1H), 8.17 (s, 1H), 7.80 (dd, J =8.8, 2.7 Hz, 1H), 7.64 (d, J =8.8 Hz, 1H), 4.21 (s, 2H), 4.02 (s, 2H), 2.81 (s, 6H).

(±)-*N*-(4-Chloro-3-((3-cyclopropylpyrrolidin-1-yl)sulfonyl)phenyl)-2-(2,5-dioxoimidazolidin-1-yl)acetamide ((±)-3.041)



2-Chloro-5-(2-(2,5-dioxoimidazolidin-1-yl)acetamido)benzene sulfonyl chloride **3.039** (50 mg, 0.137 mmol) was dissolved in CH₂Cl₂ (2 mL) at rt under nitrogen. DIPEA (0.072 mL, 0.410 mmol) was added followed by 3-cyclopropylpyrrolidine (18 mg, 0.164 mmol) and the resulting solution was stirred at rt for 1 h. The reaction was quenched with sat. aq. NaHCO₃ (2 mL) and extracted with CH₂Cl₂ (3 x 2 mL). The combined organics were passed through a hydrophobic frit and concentrated *in vacuo* to afford the crude product. The crude product was purified by formic MDAP. The pure fractions were concentrated *in vacuo* to afford (±)-*N*-(4-chloro-3-((3-cyclopropylpyrrolidin-1-yl)sulfonyl)phenyl)-2-(2,5-dioxoimidazolidin-1-yl)acetamide (**±**)-**3.041** (19 mg, 0.043 mmol, 32% yield) as a white solid. LCMS (formic, ES⁺) t_R = 0.96 min, m/z = 441.1; HRMS (C₁₈H₂₁ClN₄O₅S): [M+H]⁺ calculated 441.0999, found 441.1001; ¹H NMR (MeOD-*d*₄, 400 MHz): δ (ppm) 8.32 (d, J =2.5 Hz, 1H), 7.78 (dd, J =8.6, 2.5 Hz, 1H), 7.56 (d, J =8.6 Hz, 1H), 4.34 (s, 2H), 4.08 (s, 2H), 3.52-3.65 (m, 2H), 3.34-3.42 (m, 1H), 3.12-3.19 (m, 1H), 2.06-2.11 (m, 1H), 1.71-1.86 (m, 1H), 1.57-1.69 (m, 1H), 0.61-0.74 (m, 1H), 0.40-0.51 (m, 2H), 0.11-0.19 (m, 2H); *Amide NH and hydantoin NH not visible*; ¹³C NMR (MeOD-*d*₄, 101 MHz): δ (ppm) 172.4, 165.9, 158.0, 137.4, 136.9, 132.3, 125.9, 124.2, 122.2, 52.4, 46.2, 44.2, 40.5, 30.9, 26.6, 12.6, 2.6, 2.3; m.p. 113.0 – 114.7 °C; IR ν_{max} (cm⁻¹) 3309, 2938, 1708, 1455, 1149, 581.

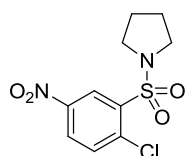
***N*-(3-((1*H*-imidazol-1-yl)sulfonyl)-4-chlorophenyl)-2-(2,5-dioxoimidazolidin-1-yl)acetamide (3.042)**



1*H*-Imidazole (11.15 mg, 0.164 mmol) was added to 2-chloro-5-(2-(2,5-dioxoimidazolidin-1-yl)acetamido)benzene-1-sulfonylchloride **3.039** (60 mg, 0.164 mmol) and DIPEA (0.086 mL, 0.492 mmol) in CH₂Cl₂ (2 mL) at rt under nitrogen. The resulting solution was stirred at rt for 2 h. The reaction was quenched with sat. aq. NaHCO₃ (10 mL) and extracted

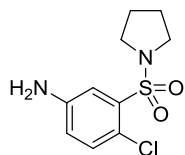
with CH₂Cl₂ (2 x 10 mL). The combined organics were concentrated in *vacuo* to afford the crude product. The crude product was purified by formic MDAP. The pure fractions were concentrated *in vacuo* to afford *N*-(3-((1*H*-imidazol-1-yl)sulfonyl)-4-chlorophenyl)-2-(2,5-dioxoimidazolidin-1-yl)acetamide **3.042** (45 mg, 0.113 mmol, 69% yield) as a white solid. LCMS (formic, ES⁺) t_R = 0.71 min; *m/z* = 398.2; HRMS (C₁₄H₁₂ClN₅O₅S): [M+H]⁺ calculated 398.0326, found 398.0327; ¹H NMR (DMSO-*d*₆, 400 MHz): δ (ppm) 10.85 (s, 1H), 8.58 (d, *J*=2.7 Hz, 1H), 8.36–8.42 (m, 1H), 8.20 (s, 1H), 7.90 (dd, *J*=8.8, 2.7 Hz, 1H), 7.64–7.74 (m, 2H), 7.16 (dd, *J*=1.6, 0.9 Hz, 1H), 4.23 (s, 2H), 4.04 (s, 2H); ¹³C NMR (DMSO-*d*₆, 101 MHz): δ (ppm) 172.3, 166.3, 157.4, 138.9, 138.6, 134.9, 133.7, 131.5, 126.9, 125.2, 121.7, 119.1, 46.6, 41.3; m.p. 149.3 – 152.8 °C; IR ν_{max} (cm⁻¹) 2951, 1715, 1608, 1288, 1251, 773.

1-((2-Chloro-5-nitrophenyl)sulfonyl)pyrrolidine (3.055)



2-Chloro-5-nitrobenzenesulfonyl chloride **3.054** (1.20 g, 4.69 mmol) was taken up in CH₂Cl₂ (50 mL) at 0 °C under nitrogen. DIPEA (1.80 mL, 10.31 mmol) was added and the reaction stirred for 5 min before pyrrolidine (0.39 mL, 4.69 mmol) was added. The reaction was stirred for 2 h at 0 °C after which time the reaction mixture was quenched with sat. aq. NaHCO₃ (50 mL) and extracted with CH₂Cl₂ (2 x 50 mL). The combined organics were filtered through a hydrophobic frit and concentrated *in vacuo* to afford the crude product. The crude product was purified by silica chromatography, eluting with 0-40% EtOAc/cyclohexane. The pure fractions were concentrated in *vacuo* to afford 1-((2-chloro-5-nitrophenyl)sulfonyl)pyrrolidine **3.055** (1.14 g, 3.92 mmol, 84% yield) as a yellow solid. LCMS (Formic, ES⁺) t_R = 1.06, does not ionise; HRMS (C₁₀H₁₁ClN₂O₄S): [M+H]⁺ calculated 291.0206, found 291.0204; ¹H NMR (CDCl₃-*d*, 400 MHz): δ (ppm) 8.91 (d, *J*=2.7 Hz, 1H), 8.33 (dd, *J*=8.8, 2.7 Hz, 1H), 7.74 (d, *J*=8.8 Hz, 1H), 3.41–3.54 (m, 4H), 1.88–2.02 (m, 4H); ¹³C NMR (CDCl₃-*d*, 101 MHz): δ (ppm) 146.2, 139.4, 139.0, 133.2, 127.4, 126.7, 48.1, 25.8; m.p. 95.5 – 101.5 °C; IR ν_{max} (cm⁻¹) 3105, 2970, 1601, 1524, 1337, 603.

4-Chloro-3-(pyrrolidin-1-ylsulfonyl)aniline (3.056)

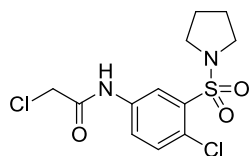


1-((2-Chloro-5-nitrophenyl)sulfonyl)pyrrolidine **3.055** (1.00 g, 3.44 mmol), ammonium chloride (0.28 g, 5.16 mmol) and iron (0.96 g, 17.20 mmol) were dissolved in a 3:1 mixture of EtOH (5.0 mL) and water (1.7 mL). The resulting solution was heated to 70 °C for 2 h. The reaction was allowed to cool then filtered through a plug of Celite, washing with MeOH (20 mL). The resulting solution was concentrated *in*

GSK Confidential – Do not copy

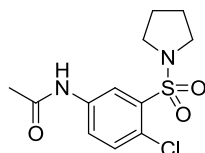
vacuo and then partitioned between sat. aq. NaHCO₃ (10 mL) and CH₂Cl₂ (10 mL). The layers were separated and the aq. layer extracted with CH₂Cl₂ (2 x 10 mL). The combined organics were passed through a hydrophobic frit and concentrated *in vacuo* to afford the crude product. The crude product was purified by silica chromatography, eluting with 0-100% EtOAc/cyclohexane. The pure fractions were concentrated *in vacuo* to afford 4-chloro-3-(pyrrolidin-1-ylsulfonyl)aniline **3.056** (743 mg, 2.85 mmol, 83% yield) as a cream solid. LCMS (Formic, ES⁺) t_R = 0.88 min, *m/z* = 261.2; HRMS (C₁₀H₁₃ClN₂O₂S): [M+H]⁺ calculated 261.0465, found 261.0464; ¹H NMR (CDCl₃-*d*, 400 MHz): δ (ppm) 7.36–7.43 (m, 1H), 7.25 (d, *J*=8.6 Hz, 1H), 6.63–6.79 (m, 1H), 3.94 (br. s., 2H), 3.36–3.46 (m, 4H), 1.82–1.98 (m, 4H); ¹³C NMR (CDCl₃-*d*, 101 MHz): δ (ppm) 145.5, 137.0, 132.6, 119.9, 119.2, 118.0, 47.7, 25.8; m.p. 114.2 – 116.5 °C; IR ν_{max} (cm⁻¹) 3369, 2981, 1616, 1471, 1331, 1158, 586.

2-Chloro-*N*-(4-chloro-3-(pyrrolidin-1-ylsulfonyl)phenyl)acetamide (**3.057**)



DIPEA (0.200 mL, 1.151 mmol) was added to 4-chloro-3-(pyrrolidin-1-ylsulfonyl)aniline **3.056** (100 mg, 0.384 mmol) in CH₂Cl₂ (5 mL) at 0 °C. 2-Chloroacetyl chloride (0.037 mL, 0.460 mmol) was added and the reaction was stirred at rt for 1 h. The reaction was quenched with sat. aq. NaHCO₃ (10 mL) and extracted with CH₂Cl₂ (2 x 10 mL). The organic layers were filtered through a hydrophobic frit and concentrated *in vacuo* to afford 2-chloro-*N*-(4-chloro-3-(pyrrolidin-1-ylsulfonyl)phenyl)acetamide **3.057** (103 mg, 0.305 mmol, 80% yield) as a brown oil. LCMS (Formic, ES⁺) t_R = 0.98 min, *m/z* = 337.1, 339.1; HRMS (C₁₂H₁₄Cl₂N₂O₃S): [M+H]⁺ calculated 337.0180, found 337.0176; ¹H NMR (CDCl₃-*d*, 400 MHz): δ (ppm) 8.66 (br. s., 1H), 8.09 (d, *J*=2.5 Hz, 1H), 8.02 (dd, *J*=8.6, 2.5 Hz, 1H), 7.51 (d, *J*=8.6 Hz, 1H), 4.23 (s, 2H), 3.43–3.48 (m, 4H), 1.92–1.97 (m, 4H); ¹³C NMR (CDCl₃-*d*, 101 MHz): δ (ppm) 164.4, 137.5, 135.9, 132.8, 127.5, 124.6, 122.9, 47.9, 42.8, 25.8; m.p. 113.2 – 119.5 °C; IR ν_{max} (cm⁻¹) 3358, 2978, 1714, 1582, 1465, 1145, 530.

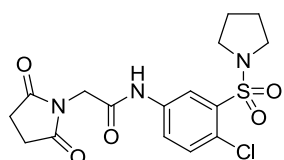
N-(4-Chloro-3-(pyrrolidin-1-ylsulfonyl)phenyl)acetamide (**3.058**)



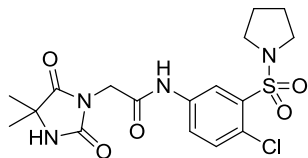
4-Chloro-3-(pyrrolidin-1-ylsulfonyl)aniline **3.056** (50 mg, 0.192 mmol) and DIPEA (0.100 mL, 0.575 mmol) were dissolved in CH₂Cl₂ (1 mL). Acetic anhydride (0.018 mL, 0.192 mmol) was added and the resulting solution was stirred at rt for 1 h. The reaction was quenched with sat. aq. NaHCO₃ (10 mL) and extracted with CH₂Cl₂ (3 x 10 mL). The combined organics were passed through a hydrophobic

frit and concentrated *in vacuo* to afford the crude product. The crude product was purified by formic MDAP. The pure fractions were concentrated *in vacuo* to afford *N*-(4-chloro-3-(pyrrolidin-1-ylsulfonyl)phenyl)acetamide **3.058** (32 mg, 0.106 mmol, 55% yield) as a white solid. LCMS (formic, ES⁺) $t_R = 0.86$ min, $m/z = 303.1$; HRMS (C₁₂H₁₅ClN₂O₃S): [M+H]⁺ calculated 303.0570, found 303.0571; ¹H NMR (CDCl₃-*d*, 400 MHz): δ (ppm) 8.09–8.18 (m, 1H), 7.91–7.99 (m, 2H), 7.48 (d, $J=8.8$ Hz, 1H), 3.40–3.47 (m, 4H), 2.23 (s, 3H), 1.89–1.98 (m, 4H); ¹³C NMR (DMSO-*d*₆, 101 MHz): δ (ppm) 169.4, 139.0, 136.8, 133.0, 124.1, 124.0, 121.2, 48.1, 25.6, 24.5; m.p. 179.5 – 181.3 °C; IR ν_{max} (cm⁻¹) 3336, 2981, 1693, 1593, 1527, 1464, 1326, 1156, 595, 542.

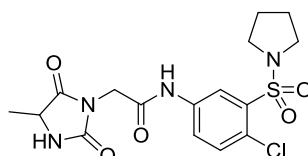
***N*-(4-Chloro-3-(pyrrolidin-1-ylsulfonyl)phenyl)-2-(2,5-dioxopyrrolidin-1-yl)acetamide (3.059)**



4-Chloro-3-(pyrrolidin-1-ylsulfonyl)aniline **3.056** (50 mg, 0.192 mmol), 2-(2,5-dioxopyrrolidin-1-yl)acetic acid (33 mg, 0.211 mmol) and HATU (87 mg, 0.230 mmol) were dissolved in CH₂Cl₂ (2 mL) at rt under air. DIPEA (0.100 mL, 0.575 mmol) was added and the resulting solution was stirred at rt for 1 h. The reaction was quenched with sat. aq. NaHCO₃ (5 mL) and extracted with CH₂Cl₂ (2 x 5 mL). The combined organics were passed through a hydrophobic frit and concentrated *in vacuo* to afford the crude product. The crude product was purified by formic MDAP. The pure fractions were concentrated *in vacuo* to afford *N*-(4-chloro-3-(pyrrolidin-1-ylsulfonyl)phenyl)-2-(2,5-dioxopyrrolidin-1-yl)acetamide **3.059** (40 mg, 0.100 mmol, 52% yield) as a white solid. LCMS (Formic, ES⁺) $t_R = 0.85$ min, $m/z = 400.3$; HRMS (C₁₆H₁₈ClN₃O₅S): [M+H]⁺ calculated 400.0734, found 400.0733; ¹H NMR (CDCl₃-*d*, 400 MHz): δ (ppm) 8.76 (s, 1H), 8.06 (dd, $J=8.8, 2.7$ Hz, 1H), 7.96 (d, $J=2.7$ Hz, 1H), 7.44 (d, $J=8.8$ Hz, 1H), 4.41 (s, 2H), 3.37–3.46 (m, 4H), 2.86 (s, 4H), 1.89–1.95 (m, 4H); ¹³C NMR (CDCl₃-*d*, 101 MHz): δ (ppm) 176.9, 164.3, 136.8, 136.6, 132.7, 126.5, 124.6, 122.6, 47.9, 41.7, 28.3, 25.7; m.p. 195.5 – 198.5 °C; IR ν_{max} (cm⁻¹) 3317, 2972, 1708, 1682, 1529, 1421, 1100, 586, 533.

***N*-(4-Chloro-3-(pyrrolidin-1-ylsulfonyl)phenyl)-2-(4,4-dimethyl-2,5-dioxoimidazolidin-1-yl)acetamide (3.060)**

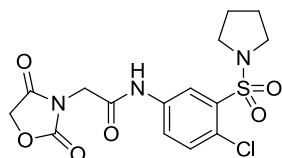
4-Chloro-3-(pyrrolidin-1-ylsulfonyl)aniline **3.056** (50 mg, 0.192 mmol), 2-(4,4-dimethyl-2,5-dioxoimidazolidin-1-yl)acetic acid (39 mg, 0.211 mmol) and HATU (87 mg, 0.230 mmol) were dissolved in CH₂Cl₂ (2 mL) at rt under air. DIPEA (0.10 mL, 0.575 mmol) was added and the resulting solution was stirred at rt for 1 h. The reaction was quenched with sat. aq. NaHCO₃ (5 mL) and extracted with CH₂Cl₂ (2 x 5 mL). The combined organics were passed through a hydrophobic frit and concentrated *in vacuo* to afford the crude product. The crude product was purified by formic MDAP. The pure fractions were concentrated *in vacuo* to afford *N*-(4-chloro-3-(pyrrolidin-1-ylsulfonyl)phenyl)-2-(4,4-dimethyl-2,5-dioxoimidazolidin-1-yl)acetamide **3.060** (57 mg, 0.133 mmol, 69% yield) as a white solid. LCMS (Formic, ES⁺) t_R = 0.87 min, *m/z* = 429.3; HRMS (C₁₇H₂₁ClN₄O₅S): [M+H]⁺ calculated 429.0993, found 429.0995; ¹H NMR (CDCl₃-*d*, 400 MHz): δ (ppm) 8.82 (s, 1H), 8.08 (dd, *J*=8.8, 2.5 Hz, 1H), 7.96 (d, *J*=2.5 Hz, 1H), 7.44 (d, *J*=8.8 Hz, 1H), 6.03 (s, 1H), 4.40 (s, 2H), 3.38–3.46 (m, 4H), 1.90–1.95 (m, 4H), 1.53 (s, 6H); ¹³C NMR (CDCl₃-*d*, 101 MHz): δ (ppm) 177.0, 164.7, 156.0, 136.8, 132.6, 132.7, 126.4, 124.5, 122.6, 59.7, 47.9, 41.6, 25.7, 25.0; m.p. 264.2 – 267.2 °C; IR ν_{max} (cm⁻¹) 3344, 2980, 1714, 1531, 1450, 1304, 595.

(±)-*N*-(4-Chloro-3-(pyrrolidin-1-ylsulfonyl)phenyl)-2-(4-methyl-2,5-dioxoimidazolidin-1-yl)acetamide ((±)-3.061)

2-Chloro-*N*-(4-chloro-3-(pyrrolidin-1-ylsulfonyl)phenyl)acetamide **3.056** (100 mg, 0.297 mmol), (±)-5-methylimidazolidine-2,4-dione (37 mg, 0.326 mmol), and K₂CO₃ (53 mg, 0.386 mmol) were dissolved in acetone (1 mL). The resulting solution was heated to 70 °C and stirred for 1 h. The reaction was allowed to cool before quenching with sat. aq. NaHCO₃ (10 mL) and extracting with CH₂Cl₂ (3 x 10 mL). The combined organics were passed through a hydrophobic frit and concentrated *in vacuo* to afford the crude product. The crude product was purified by formic MDAP. The pure fractions were concentrated *in vacuo* to afford (±)-*N*-(4-chloro-3-(pyrrolidin-1-ylsulfonyl)phenyl)-2-(4-methyl-2,5-dioxoimidazolidin-1-yl)acetamide ((±)-**3.061**) (82 mg, 0.198 mmol, 67% yield). LCMS (Formic, ES⁺) t_R = 0.82 min, *m/z* = 415.3; HRMS (C₁₆H₁₉ClN₄O₅S): [M+H]⁺ calculated 415.0843, found 415.0844; ¹H NMR (DMSO-*d*₆, 400 MHz): δ (ppm) 8.41 (s, 1H), 8.30–8.37 (m, 1H), 8.27 (d, *J*=2.7 Hz, 1H), 7.80 (dd,

$J=8.8, 2.7$ Hz, 1H), 7.63 (d, $J=8.8$ Hz, 1H), 4.14–4.24 (m, 3H), 3.24–3.35 (m, 4H), 1.79–1.88 (m, 4H), 1.30 (d, $J=6.8$ Hz, 3H); ^{13}C NMR (DMSO- d_6 , 101 MHz): δ (ppm) 175.4, 166.0, 156.4, 138.3, 136.8, 133.2, 124.8, 124.3, 121.7, 52.8, 48.1, 41.2, 25.6, 17.8; m.p. 130.9 – 134.9 °C; IR ν_{max} (cm^{-1}) 3321, 2981, 1702, 1454, 1152, 588.

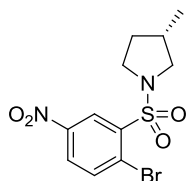
***N*-(4-Chloro-3-(pyrrolidin-1-ylsulfonyl)phenyl)-2-(2,4-dioxooxazolidin-3-yl)acetamide (3.062)**



2-Chloro-*N*-(4-chloro-3-(pyrrolidin-1-ylsulfonyl)phenyl)acetamide

3.056 (50 mg, 0.148 mmol) and potassium 2,4-dioxooxazolidin-3-ide (25 mg, 0.178 mmol) were dissolved in DMF (0.5 mL). The resulting solution was heated to 100 °C and stirred for 2 h. The reaction was allowed to cool, diluted with water (5 mL) and extracted with CH_2Cl_2 (3 x 5 mL). The combined organics were passed through a hydrophobic frit and concentrated *in vacuo* to afford the crude product. The crude product was purified by formic MDAP. The pure fractions were concentrated *in vacuo* to afford *N*-(4-chloro-3-(pyrrolidin-1-ylsulfonyl)phenyl)-2-(2,4-dioxooxazolidin-3-yl)acetamide **3.062** (33 mg, 0.082 mmol, 55% yield) as a white solid. LCMS (formic, ES^+) $t_{\text{R}} = 0.89$ min, $m/z = 402.2$; HRMS ($\text{C}_{15}\text{H}_{16}\text{ClN}_3\text{O}_6\text{S}$): $[\text{M}+\text{H}]^+$ calculated 402.0527, found 402.0523; ^1H NMR (DMSO- d_6 , 400 MHz): δ (ppm) 10.75 (s, 1H), 8.26 (d, $J=2.7$ Hz, 1H), 7.80 (dd, $J=8.8, 2.7$ Hz, 1H), 7.66 (d, $J=8.8$ Hz, 1H), 5.04 (s, 2H), 4.32 (s, 2H), 3.28–3.33 (m, 4H), 1.82–1.87 (m, 4H); ^{13}C NMR (DMSO- d_6 , 101 MHz): δ (ppm) 171.4, 165.0, 156.2, 138.0, 136.9, 133.2, 125.1, 124.5, 121.9, 69.2, 48.1, 42.6, 25.6; m.p. 230.6 – 233.1 °C; IR ν_{max} (cm^{-1}) 3343, 2980, 1745, 1683, 1446, 1157, 534.

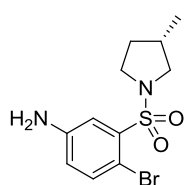
(*S*)-1-((2-Bromo-5-nitrophenyl)sulfonyl)-3-methylpyrrolidine ((*S*)-3.066)



2-Bromo-5-nitrobenzene-1-sulfonyl chloride **3.021** (1.70 g, 5.66 mmol) was taken up in CH_2Cl_2 (5 mL) under nitrogen and cooled in an ice bath. DIPEA (2.17 mL, 12.45 mmol) was added and the reaction stirred for 5 min before (*S*)-3-methylpyrrolidine hydrochloride (0.69 g, 5.66 mmol) was added. The reaction was stirred for 1 h before warming to rt. The reaction mixture was quenched with sat. aq. NaHCO_3 (10 mL) and extracted with CH_2Cl_2 (2 x 20 mL). The combined organics were washed with 2M HCl aq. (10 mL), filtered through a hydrophobic frit and concentrated *in vacuo* to give the crude product. The crude product was purified by silica chromatography, eluting with 0-40% EtOAc/cyclohexane. The pure fractions were

concentrated *in vacuo* to afford (S)-1-((2-bromo-5-nitrophenyl)sulfonyl)-3-methylpyrrolidine (**S**)-**3.066** (1.77 g, 5.08 mmol, 90% yield) as a yellow solid. LCMS (Formic, ES⁺) t_R = 1.17 min, m/z = 349.1, 351.1; ¹H NMR (CDCl₃-*d*, 400 MHz): δ (ppm) 8.89 (d, J =2.7 Hz, 1H), 8.21 (dd, J =8.8, 2.7 Hz, 1H), 7.95 (d, J =8.8 Hz, 1H), 3.56–3.67 (m, 2H), 3.45 (ddd, J =9.5, 8.6, 7.1 Hz, 1H), 2.98 (dd, J =9.4, 7.9 Hz, 1H), 2.28–2.43 (m, 1H), 2.09 (dtd, J =12.7, 6.6, 3.9 Hz, 1H), 1.53–1.67 (m, 1H), 1.07 (d, J =6.6 Hz, 3H); ¹³C NMR (CDCl₃-*d*, 101 MHz): δ (ppm) 146.8, 141.2, 127.7, 127.2, 126.6, 126.1, 59.6, 54.8, 47.9, 33.7, 17.4; IR ν_{max} (cm⁻¹) 3000, 1595, 1528, 1331, 1153, 1125, 1057, 1022, 880, 842, 774, 739, 697, 670.

(S)-4-Bromo-3-((3-methylpyrrolidin-1-yl)sulfonyl)aniline ((S)-3.067)



(S)-1-((2-Bromo-5-nitrophenyl)sulfonyl)-3-methylpyrrolidine (**S**)-**3.066**

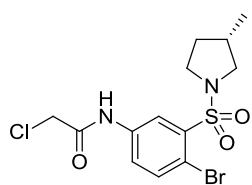
(2.92 g, 8.36 mmol), ammonium chloride (0.67 g, 12.54 mmol) and iron

(2.36 g, 41.8 mmol) were dissolved in a 3:1 mixture of EtOH (20 mL) and

water (7 mL). The resulting solution was heated to 70 °C for 2 h. The

reaction was allowed to cool then filtered through a plug of Celite, washing with MeOH (50 mL). The resulting solution was concentrated *in vacuo* and then partitioned with sat. aq. NaHCO₃ (20 mL) and CH₂Cl₂ (20 mL). The layers were separated and the aq. extracted with CH₂Cl₂ (2 x 20 mL). The combined organics were passed through a hydrophobic frit and concentrated *in vacuo* to afford (S)-4-bromo-3-((3-methylpyrrolidin-1-yl)sulfonyl)aniline (**S**)-**3.067** (2.62 g, 8.21 mmol, 98% yield) as an orange gum. LCMS (formic, ES⁺) t_R = 1.00 min, m/z = 319.1, 321.1; HRMS (C₁₁H₁₅BrN₂O₂S): [M+H]⁺ calculated 319.0116, found 319.0114; ¹H NMR (CDCl₃-*d*, 400 MHz): δ (ppm) 7.41–7.49 (m, 2H), 6.67 (dd, J =8.4, 2.8 Hz, 1H), 3.92 (br. s., 2H), 3.51–3.62 (m, 2H), 3.33–3.44 (m), 2.88–2.96 (m, 1H), 2.26–2.38 (m, 1H), 1.99–2.09 (m, 1H), 1.50–1.57 (m, 1H), 1.05 (d, J =6.6 Hz, 3H); ¹³C NMR (CDCl₃-*d*, 101 MHz): δ (ppm) 146.0, 138.8, 136.0, 119.4, 118.4, 106.8, 54.4, 47.5, 33.8, 33.6, 17.5; IR ν_{max} (cm⁻¹) 3467, 3371, 1591, 1468, 1328, 1142, 584.

(S)-N-(4-Bromo-3-((3-methylpyrrolidin-1-yl)sulfonyl)phenyl)-2-chloroacetamide ((S)-3.068)



DIPEA (0.273 mL, 1.566 mmol) was added to (S)-4-bromo-3-((3-

methylpyrrolidin-1-yl)sulfonyl)aniline (**S**)-**3.067** (500 mg, 1.566 mmol)

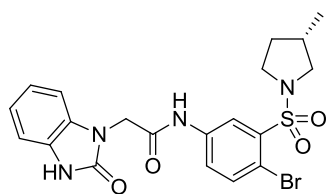
in CH₂Cl₂ (5 mL). 2-Chloroacetyl chloride (0.125 mL, 1.566 mmol) was

added and the reaction was stirred at rt for 1 h. The reaction was

quenched with sat. NaHCO₃ (20 mL) and extracted with CH₂Cl₂ (2 x 20 mL). The organic layers

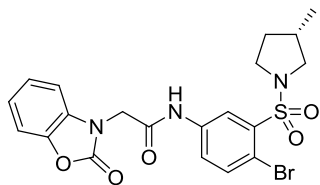
were filtered through a hydrophobic frit and concentrated *in vacuo* to afford the crude product. This was purified by silica chromatography, eluting with 0-50% (3:1 EtOH:EtOAc)/cyclohexane. The pure fractions were concentrated *in vacuo* to afford (*S*)-*N*-(4-bromo-3-((3-methylpyrrolidin-1-yl)sulfonyl)phenyl)-2-chloroacetamide (**S**-3.068 (554 mg, 1.400 mmol, 89% yield) as a yellow oil. LCMS (formic, ES⁺) t_R = 1.08 min, m/z = 395.3, 397.3; HRMS (C₁₃H₁₆BrClN₂O₃S): [M+H]⁺ calculated 394.9832, found 394.9830; ¹H NMR (CDCl₃-*d*, 400 MHz): δ (ppm) 8.49 (br. s., 1H), 8.10 (d, J =2.7 Hz, 1H), 7.93 (dd, J =8.8, 2.7 Hz, 1H), 7.73 (d, J =8.8 Hz, 1H), 4.22 (s, 2H), 3.56–3.64 (m, 2H), 3.43 (td, J =9.0, 7.2 Hz, 1H), 2.96 (dd, J =9.0, 8.1 Hz, 1H), 2.28–2.43 (m, 1H), 2.02–2.12 (m, 1H), 1.53–1.61 (m, 1H), 1.07 (d, J =6.6 Hz, 3H); ¹³C NMR (CDCl₃-*d*, 101 MHz): δ (ppm) 164.3, 139.3, 136.5, 136.3, 124.5, 123.1, 115.1, 54.6, 47.7, 42.8, 33.8, 33.6, 17.4; IR ν_{max} (cm⁻¹) 3301, 2961, 1718, 1532, 1460, 1150, 591.

(*S*)-*N*-(4-Bromo-3-((3-methylpyrrolidin-1-yl)sulfonyl)phenyl)-2-(2-oxo-2,3-dihydro-1*H*-benzo[*d*]imidazol-1-yl)acetamide (S**-3.065)**



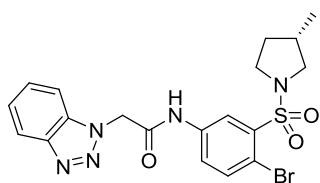
(*S*)-*N*-(4-Bromo-3-((3-methylpyrrolidin-1-yl)sulfonyl)phenyl)-2-chloroacetamide (**S**-3.068 (50 mg, 0.126 mmol), 1,3-dihydro-2*H*-benzo[*d*]imidazol-2-one (19 mg, 0.139 mmol), and K₂CO₃ (23 mg, 0.164 mmol) were dissolved in acetone (1 mL). The resulting solution was heated to 70 °C and stirred for 1 h. The reaction was allowed to cool before quenching with sat. aq. NaHCO₃ (10 mL) and extracting with CH₂Cl₂ (2 x 10 mL). The combined organics were passed through a hydrophobic frit and concentrated *in vacuo* to afford the crude product. The crude product was purified by formic MDAP. The pure fractions were concentrated *in vacuo* to afford (*S*)-*N*-(4-bromo-3-((3-methylpyrrolidin-1-yl)sulfonyl)phenyl)-2-(2-oxo-2,3-dihydro-1*H*-benzo[*d*]imidazol-1-yl)acetamide (**S**-3.065 (7 mg, 0.014 mmol, 11% yield) as an off-white solid. LCMS (formic, ES⁺) t_R = 1.03 min, m/z = 493.2, 495.2; HRMS (C₂₀H₂₁BrN₄O₄S): [M+H]⁺ calculated 493.0545, found 493.0544; ¹H NMR (MeOD-*d*₄, 400 MHz): δ (ppm) 8.33 (d, J =2.4 Hz, 1H), 7.69–7.79 (m, 2H), 7.06–7.15 (m, 4H), 4.76 (s, 2H), 3.49–3.60 (m, 2H), 3.35–3.43 (m, 1H), 2.92 (dd, J =9.4, 7.7 Hz, 1H), 2.25–2.39 (m, 1H), 1.99–2.12 (m, 1H), 1.57 (dd, J =12.3, 8.4 Hz, 1H), 1.03 (d, J =6.8 Hz, 3H); Amide NH and benzoimidazolone NH not visible.

(S)-N-(4-Bromo-3-((3-methylpyrrolidin-1-yl)sulfonyl)phenyl)-2-(2-oxobenzo[d]oxazol-3(2H)-yl)acetamide ((S)-3.069)



(S)-N-(4-Bromo-3-((3-methylpyrrolidin-1-yl)sulfonyl)phenyl)-2-chloroacetamide **(S)-3.068** (50 mg, 0.126 mmol), benzo[d]oxazol-2(3H)-one (20 mg, 0.152 mmol) and K₂CO₃ (23 mg, 0.164 mmol) were dissolved in acetone (1 mL). The resulting solution was heated to 60 °C and stirred for 1 h. The reaction was allowed to cool before quenching with sat. aq. NaHCO₃ (10 mL) and extracting with CH₂Cl₂ (3 x 10 mL). The combined organics were passed through a hydrophobic frit and concentrated *in vacuo* to afford the crude product. The crude product was purified by formic MDAP. The pure fractions were concentrated *in vacuo* to afford (S)-N-(4-bromo-3-((3-methylpyrrolidin-1-yl)sulfonyl)phenyl)-2-(2-oxobenzo[d]oxazol-3(2H)-yl)acetamide **(S)-3.069** (35 mg, 0.071 mmol, 56% yield) as a cream solid. LCMS (formic, ES⁺) t_R = 1.15 min, m/z = 394.0, 396.0; HRMS (C₂₀H₂₀BrN₃O₅S): [M+H]⁺ calculated 494.0385, found 494.0384; ¹H NMR (CDCl₃-d, 400 MHz): δ (ppm) 8.95 (s, 1H), 8.11 (d, J=2.7 Hz, 1H), 7.94 (dd, J=8.8, 2.7 Hz, 1H), 7.64 (d, J=8.8 Hz, 1H), 7.13–7.27 (m, 3H), 7.10 (dd, J=7.5, 1.6 Hz, 1H), 4.73 (s, 2H), 3.52–3.63 (m, 2H), 3.40 (td, J=9.0, 7.1 Hz, 1H), 2.92 (dd, J=9.4, 7.9 Hz, 1H), 2.27–2.38 (m, 1H), 1.98–2.10 (m, 1H), 1.57 (dq, J=12.3, 8.5 Hz, 1H), 1.04 (d, J=6.6 Hz, 3H); ¹³C NMR (CDCl₃-d, 101 MHz): δ (ppm) 164.5, 155.1, 142.7, 138.6, 137.2, 136.3, 130.8, 124.7, 124.4, 123.2, 123.0, 114.3, 110.4, 109.1, 54.6, 47.8, 45.7, 33.8, 33.6, 17.4.

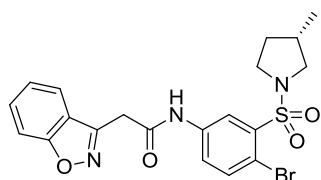
(S)-2-(1H-Benzo[d][1,2,3]triazol-1-yl)-N-(4-bromo-3-((3-methylpyrrolidin-1-yl)sulfonyl)phenyl)acetamide ((S)-3.070)



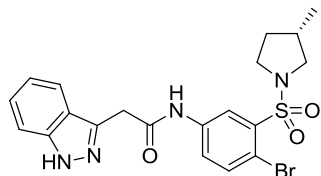
(S)-4-Bromo-3-((3-methylpyrrolidin-1-yl)sulfonyl)aniline **(S)-3.067** (50 mg, 0.157 mmol), 2-(1H-benzo[d][1,2,3]triazol-1-yl)acetic acid (28 mg, 0.157 mmol) and HATU (89 mg, 0.235 mmol) were dissolved in CH₂Cl₂ (2 mL) at rt under air. DIPEA (0.082 mL, 0.470 mmol) was added and the resulting solution was stirred at rt for 1 h. The reaction was quenched with sat. aq. NaHCO₃ (5 mL) and extracted with CH₂Cl₂ (2 x 5 mL). The combined organics were passed through a hydrophobic frit and concentrated *in vacuo* to afford the crude product. The crude product was purified by formic MDAP. The pure fractions were concentrated *in vacuo* to afford (S)-2-(1H-benzo[d][1,2,3]triazol-1-yl)-N-(4-bromo-3-((3-methylpyrrolidin-1-yl)sulfonyl)phenyl)acetamide **(S)-3.070** (59 mg, 0.123 mmol, 79%

yield) as a white solid. LCMS (formic, ES⁺) t_R = 1.13 min, m/z = 478.1, 480.1; HRMS (C₁₉H₂₀BrN₅O₃S): [M+H]⁺ calculated 478.0548, found 478.0551; ¹H NMR (DMSO-*d*₆, 400 MHz): δ (ppm) 11.02 (s, 1H), 8.30 (d, J =2.8 Hz, 1H), 8.07 (d, J =8.3 Hz, 1H), 7.80–7.89 (m, 2H), 7.70–7.77 (m, 1H), 7.57 (ddd, J =8.2, 7.1, 1.0 Hz, 1H), 7.43 (ddd, J =8.2, 7.1, 1.0 Hz, 1H), 5.74 (s, 2H), 3.37–3.50 (m, 2H), 3.23–3.33 (m, 1H), 2.82 (dd, J =9.3, 7.8 Hz, 1H), 2.24 (dq, J =14.7, 7.2 Hz, 1H), 1.90–2.03 (m, 1H), 1.48 (dq, J =12.3, 8.3 Hz, 1H), 0.93 (d, J =6.8 Hz, 3H); ¹³C NMR (DMSO-*d*₆, 101 MHz): δ (ppm) 165.0, 145.0, 138.3, 138.1, 136.2, 133.8, 127.4, 124.0, 123.9, 121.6, 119.0, 112.5, 110.9, 54.2, 50.4, 47.3, 33.0, 32.8, 17.1.

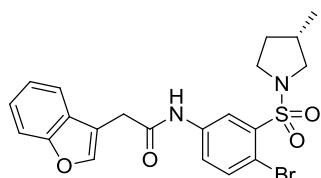
(S)-2-(Benzo[*d*]isoxazol-3-yl)-*N*-(4-bromo-3-((3-methylpyrrolidin-1-yl)sulfonyl)phenyl)acetamide ((S)-3.071)



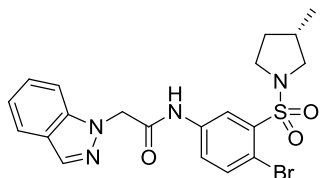
(S)-4-Bromo-3-((3-methylpyrrolidin-1-yl)sulfonyl)aniline **(S)-3.067** (50 mg, 0.157 mmol) was dissolved in CH₂Cl₂ (3 mL). 2-(Benzo[*d*]isoxazol-3-yl)acetic acid (28 mg, 0.157 mmol) and DIPEA (0.082 mL, 0.470 mmol) were added and the solution stirred at rt for 5 min. T3P (50% w/w in EtOAc, 1.438 mL, 0.157 mmol) was added and the reaction was stirred at rt for 1 h. The reaction was concentrated *in vacuo* and the residue was partitioned between CH₂Cl₂ and sat. NaHCO₃ (15 mL each). The aq. layer was re-extracted with CH₂Cl₂ (15 mL). The combined organics were eluted through a hydrophobic frit then concentrated *in vacuo* to give the crude product. The crude product was purified by formic MDAP. The pure fractions were concentrated *in vacuo* to afford (S)-2-(benzo[*d*]isoxazol-3-yl)-*N*-(4-bromo-3-((3-methylpyrrolidin-1-yl)sulfonyl)phenyl)acetamide **(S)-3.071** (41 mg, 0.086 mmol, 55% yield) as a white solid. LCMS (formic, ES⁺) t_R = 1.21 min; m/z = 478.1, 480.1; HRMS (C₂₀H₂₀BrN₃O₄S): [M+H]⁺ calculated 478.0436, found 478.0432; ¹H NMR (DMSO-*d*₆, 400 MHz): δ (ppm) 10.91 (br. s., 1H), 8.33 (d, J =2.4 Hz, 1H), 7.92 (d, J =8.1 Hz, 1H), 7.81 (d, J = 8.6 Hz, 1H), 7.72–7.78 (m, 2H), 7.67 (ddd, J = 7.5, 7.5, 1.2 Hz, 1H), 7.41 (dd, J =7.5, 7.5 Hz, 1H), 4.22 (s, 2H), 3.38–3.51 (m, 2H), 3.25–3.29 (m, 1H), 2.79–2.86 (m, 1H), 2.26 (dq, J =14.5, 7.2 Hz, 1H), 1.94–2.06 (m, 1H), 1.50 (dq, J =12.2, 8.3 Hz, 1H), 0.95 (d, J =6.6 Hz, 3H); ¹³C NMR (DMSO-*d*₆, 101 MHz): δ (ppm) 167.0, 162.9, 154.3, 139.0, 138.8, 136.6, 130.8, 124.4, 124.2, 123.2, 121.9, 121.9, 112.7, 110.1, 54.7, 47.8, 33.7, 33.5, 33.4, 17.6; m.p. 61.3 – 64.9 °C; IR ν_{max} (cm⁻¹) 3326, 2961, 1674, 1583, 1522, 1459, 1380, 1322, 1141, 750.

(S)-N-(4-Bromo-3-((3-methylpyrrolidin-1-yl)sulfonyl)phenyl)-2-(1H-indazol-3-yl)acetamide ((S)-3.072)

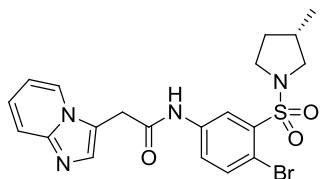
(S)-4-Bromo-3-((3-methylpyrrolidin-1-yl)sulfonyl)aniline **3.067** (32 mg, 0.100 mmol) was reacted with 2-(1H-indazol-3-yl)acetic acid (25 mg, 0.140 mmol) according to general procedure C to afford (S)-N-(4-bromo-3-((3-methylpyrrolidin-1-yl)sulfonyl)phenyl)-2-(1H-indazol-3-yl)acetamide **(S)-3.072** (10 mg, 0.022 mmol, 19%). LCMS (formic, ES⁺) t_R = 1.11 min; m/z = 477.0, 479.0; ¹H NMR (DMSO-*d*₆, 600 MHz): δ (ppm) 8.32–8.40 (m, 1H), 7.80 (d, *J*=8.7 Hz, 3H), 7.45–7.56 (m, 1H), 7.30–7.38 (m, 1H), 7.07–7.13 (m, 1H), 4.05 (s, 2H), 3.44–3.50 (m, 2H), 3.27–3.31 (m, 1H), 2.77–2.88 (m, 1H), 2.20–2.31 (m, 1H), 1.94–2.07 (m, 1H), 1.44–1.55 (m, 1H), 0.97 (d, *J*=6.6 Hz, 3H); Indazole NH and amide NH not visible.

(S)-2-(Benzofuran-3-yl)-N-(4-bromo-3-((3-methylpyrrolidin-1-yl)sulfonyl)phenyl)acetamide ((S)-3.073)

(S)-4-Bromo-3-((3-methylpyrrolidin-1-yl)sulfonyl)aniline **(S)-3.067** (50 mg, 0.157 mmol) and 2-(benzofuran-3-yl)acetic acid (33 mg, 0.188 mmol) were dissolved in CH₂Cl₂ (2 mL) at rt under air. DIPEA (0.082 mL, 0.470 mmol) was added, followed by T3P (50% w/w in EtOAc, 0.131 mL, 0.219 mmol) and the resulting solution was stirred at rt for 1 h. The reaction was quenched with sat. aq. NaHCO₃ (5 mL) and extracted with CH₂Cl₂ (2 x 5 mL). The combined organics were passed through a hydrophobic frit and concentrated *in vacuo* to afford the crude product. The crude product was purified by formic MDAP. The pure fractions were concentrated *in vacuo* to afford (S)-2-(benzofuran-3-yl)-N-(4-bromo-3-((3-methylpyrrolidin-1-yl)sulfonyl)phenyl)acetamide **(S)-3.073** (48 mg, 0.101 mmol, 64% yield) as a cream solid. LCMS (formic, ES⁺) t_R = 1.29 min, m/z = 477.1, 479.1; HRMS (C₂₁H₂₁BrN₂O₄S): [M+H]⁺ calculated 477.0484, found 477.0491; ¹H NMR (CDCl₃-*d*, 400 MHz): δ (ppm) 8.04 (s, 1H), 7.98 (dd, *J*=8.7, 2.5 Hz, 1H), 7.90 (d, *J*=2.5 Hz, 1H), 7.73 (s, 1H), 7.61–7.66 (m, 2H), 7.53 (d, *J*=8.1 Hz, 1H), 7.35 (td, *J*=7.7, 1.3 Hz, 1H), 7.24–7.31 (m, 1H), 3.84 (s, 2H), 3.48–3.58 (m, 2H), 3.36 (td, *J*=9.0, 7.2 Hz, 1H), 2.89 (dd, *J*=9.0, 8.2 Hz, 1H), 2.20–2.35 (m, 1H), 1.97–2.06 (m, 1H), 1.53 (dq, *J*=12.3, 8.6 Hz, 1H), 1.01 (d, *J*=6.5 Hz, 3H); ¹³C NMR (CDCl₃-*d*, 101 MHz): δ (ppm) 168.5, 155.5, 143.4, 138.6, 137.5, 136.2, 127.2, 125.0, 124.7, 123.1, 122.8, 119.6, 113.9, 113.2, 111.8, 54.6, 47.7, 33.8, 33.6, 32.8, 17.4; m.p. 134.0 – 138.5 °C; IR ν_{max} (cm⁻¹) 3338, 2964, 1673, 1583, 1521, 1453, 1143, 746, 587.

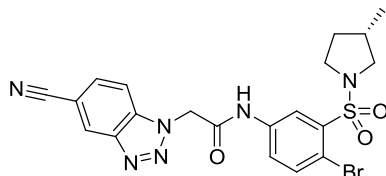
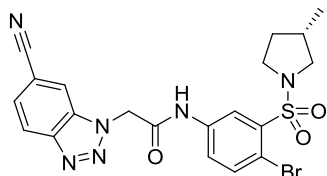
(S)-N-(4-Bromo-3-((3-methylpyrrolidin-1-yl)sulfonyl)phenyl)-2-(1H-indazol-1-yl)acetamide ((S)-3.074)

(S)-4-Bromo-3-((3-methylpyrrolidin-1-yl)sulfonyl)aniline (**(S)-3.067** (32 mg, 0.100 mmol) was reacted with 2-(1H-indazol-1-yl)acetic acid (25 mg, 0.140 mmol) according to general procedure C to afford (S)-N-(4-bromo-3-((3-methylpyrrolidin-1-yl)sulfonyl) phenyl)-2-(1H-indazol-1-yl)acetamide (**(S)-3.074** (7 mg, 0.016 mmol, 14%). LCMS (formic, ES⁺) t_R = 1.17 min; m/z = 477.0, 479.0; ¹H NMR (DMSO-*d*₆, 600 MHz): δ (ppm) 8.32 (d, J=2.6 Hz, 1H), 8.12 (s, 1H), 7.78–7.84 (m, 2H), 7.74 (dd, J=8.7, 2.6 Hz, 1H), 7.67 (d, J=8.7 Hz, 1H), 7.41 (dd, J=7.5, 7.5 Hz, 1H), 7.17 (dd, J=7.5, 7.5 Hz, 1H), 5.36 (s, 2H), 3.46 (dd, J=9.4, 7.2 Hz, 2H), 3.28 (dd, J=7.9, 1.9 Hz, 1H), 2.82 (dd, J=9.4, 7.9 Hz, 1H), 2.20–2.29 (m, 1H), 1.94–2.02 (m, 1H), 1.43–1.53 (m, 1H), 0.93 (d, J=6.6 Hz, 3H); Amide NH not visible.

(S)-N-(4-Bromo-3-((3-methylpyrrolidin-1-yl)sulfonyl)phenyl)-2-(imidazo[1,2-a]pyridin-3-yl)acetamide ((S)-3.075)

(S)-4-Bromo-3-((3-methylpyrrolidin-1-yl)sulfonyl)aniline (**(S)-3.067** (50 mg, 0.157 mmol), 2-(imidazo[1,2-a]pyridin-3-yl)acetic acid (28 mg, 0.157 mmol) and HATU (89 mg, 0.235 mmol) were dissolved in CH₂Cl₂ (2 mL) at rt under air. DIPEA (0.082 mL, 0.470 mmol) was added and the resulting solution was stirred at rt for 1 h. The reaction was quenched with sat. aq. NaHCO₃ (5 mL) and extracted with CH₂Cl₂ (2 x 5 mL). The combined organics were passed through a hydrophobic frit and concentrated *in vacuo* to afford the crude product. The crude product was purified by formic MDAP. The pure fractions were concentrated *in vacuo* to afford (S)-N-(4-bromo-3-((3-methylpyrrolidin-1-yl)sulfonyl)phenyl)-2-(imidazo[1,2-a]pyridin-3-yl)acetamide **3.075** (66 mg, 0.138 mmol, 88% yield) as a white solid. LCMS (formic, ES⁺) t_R = 0.69 min, m/z = 477.2, 479.2; ¹H NMR (DMSO-*d*₆, 400 MHz): δ (ppm) 10.70 (s, 1H), 8.40 (d, J=7.0 Hz, 1H), 8.31 (d, J=2.5 Hz, 1H), 7.81 (d, J=8.5 Hz, 1H), 7.75 (dd, J=8.5, 2.5, 1H), 7.56 (d, J=9.0 Hz, 1H), 7.50 (s, 1H), 7.24 (ddd, J=9.0, 6.8, 1.3 Hz, 1H), 6.93 (td, J=6.8, 1.0 Hz, 1H), 4.14 (s, 2H), 3.38–3.49 (m, 2H), 3.23–3.32 (m, 1H), 2.82 (dd, J=9.3, 7.8 Hz, 1H), 2.24 (dq, J=14.7, 7.2 Hz, 1H), 1.92–2.03 (m, 1H), 1.49 (dq, J=12.3, 8.3 Hz, 1H), 0.94 (d, J=6.8 Hz, 3H); ¹³C NMR (DMSO-*d*₆, 101MHz): d (ppm) 167.7, 162.9, 144.8, 138.7, 138.1, 136.0, 132.6, 125.0, 123.8, 121.4, 118.4, 116.9, 111.9, 111.6, 54.2, 47.3, 33.0, 32.8, 31.7, 17.1;

(S)-N-(4-Bromo-3-((3-methylpyrrolidin-1-yl)sulfonyl)phenyl)-2-(6-cyano-1H-benzo[d][1,2,3]triazol-1-yl)acetamide ((S)-3.076) and **(S)-N-(4-bromo-3-((3-methylpyrrolidin-1-yl)sulfonyl)phenyl)-2-(5-cyano-1H-benzo[d][1,2,3]triazol-1-yl)acetamide ((S)-3.077)**



(S)-N-(4-Bromo-3-((3-methylpyrrolidin-1-yl)sulfonyl)phenyl)-2-chloroacetamide (S)-3.068 (50

mg, 0.126 mmol), 1H-benzo[d][1,2,3]triazole-5-carbonitrile (22 mg, 0.152 mmol), and K₂CO₃ (23 mg, 0.164 mmol) were dissolved in acetone (1 mL). The resulting solution was heated to 60 °C and stirred for 1 h. The reaction was allowed to cool before quenching with sat. aq. NaHCO₃ (10 mL) and extracting with CH₂Cl₂ (3 x 10 mL). The combined organics were passed through a hydrophobic frit and concentrated *in vacuo* to afford the crude product. The crude product was purified by formic MDAP. The fractions containing the desired products were concentrated *in vacuo* to afford a mixture of regioisomers. The regioisomers were dissolved in EtOH (5mL) and injected onto the column (column: 250 mm x 30 mm Chiralpak AD-H, 5 μm), eluting with 50% EtOH/heptane, flow rate = 43 mL min⁻¹, detection wavelength 280 nm. The pure fractions were concentrated *in vacuo* to afford first eluter (S)-N-(4-bromo-3-((3-methylpyrrolidin-1-yl)sulfonyl)phenyl)-2-(6-cyano-1H-benzo[d][1,2,3]triazol-1-yl)acetamide **(S)-3.076** (19 mg, 0.038 mmol, 30% yield) as a white solid and second eluter (S)-N-(4-bromo-3-((3-methylpyrrolidin-1-yl)sulfonyl)phenyl)-2-(5-cyano-1H-benzo[d][1,2,3]triazol-1-yl)acetamide **(S)-3.077** (15 mg, 0.030 mmol, 24% yield) as a white solid.

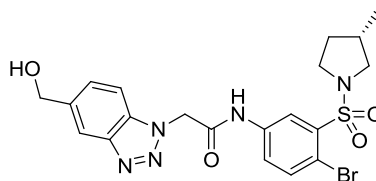
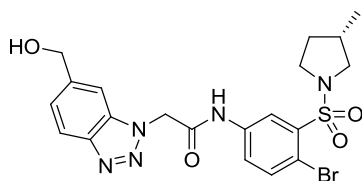
(S)-N-(4-Bromo-3-((3-methylpyrrolidin-1-yl)sulfonyl)phenyl)-2-(6-cyano-1H-benzo[d][1,2,3]triazol-1-yl)acetamide ((S)-3.076):

LCMS (formic, ES⁺) t_R = 1.10 min, m/z = 503.1, 505.1; HRMS (C₂₀H₁₉BrN₆O₃S): [M+H]⁺ calculated 503.0501, found 503.0504; ¹H NMR (DMSO-*d*₆, 600 MHz): δ (ppm) 11.05 (s, 1H), 8.68 (d, J=1.5 Hz, 1H), 8.27–8.34 (m, 2H), 7.77–7.86 (m, 2H), 7.72 (dd, J=8.7, 2.6 Hz, 1H), 5.82 (s, 2H), 3.38–3.51 (m, 2H), 3.25–3.29 (m, 1H), 2.83 (dd, J=9.4, 7.7 Hz, 1H), 2.25 (td, J=7.8, 6.8 Hz, 1H), 1.93–2.04 (m, 1H), 1.49 (dd, J=12.3, 8.4 Hz, 1H), 0.94 (d, J=6.8 Hz, 3H); ¹³C NMR (DMSO-*d*₆, 151 MHz): δ (ppm) 164.6, 146.2, 138.3, 137.8, 136.2, 133.4, 126.2, 124.0, 121.6, 120.8, 118.6, 117.9, 112.5, 109.6, 54.2, 50.8, 47.3, 33.0, 32.8, 17.1.

(S)-*N*-(4-Bromo-3-((3-methylpyrrolidin-1-yl)sulfonyl)phenyl)-2-(5-cyano-1*H*-benzo[*d*][1,2,3]triazol-1-yl)acetamide (**(S)**-3.077):

LCMS (formic, ES⁺) t_R = 1.10 min, m/z = 503.1, 505.1; HRMS (C₂₀H₁₉BrN₆O₃S): [M+H]⁺ calculated 503.0501, found 503.0497; ¹H NMR (DMSO-*d*₆, 400 MHz): δ (ppm) 11.06 (s, 1H), 8.82 (t, *J*=1.1 Hz, 1H), 8.30 (d, *J*=2.7 Hz, 1H), 8.12 (d, *J*=8.6 Hz, 1H), 7.95 (dd, *J*=8.6, 1.5 Hz, 1H), 7.83 (d, *J*=8.6 Hz, 1H), 7.73 (dd, *J*=8.6, 2.7 Hz, 1H), 5.82 (s, 2H), 3.40–3.48 (m, 2H), 3.23–3.29 (m, 1H), 2.82 (dd, *J*=9.3, 7.6 Hz, 1H), 2.19–2.30 (m, 1H), 1.93–2.05 (m, 1H), 1.48 (dd, *J*=12.2, 8.3 Hz, 1H), 0.89–0.99 (m, 3H); ¹³C NMR (DMSO-*d*₆, 151 MHz): δ (ppm) 164.7, 144.1, 138.3, 138.0, 136.2, 135.7, 129.7, 125.8, 124.0, 121.6, 118.7, 113.0, 112.6, 106.6, 54.1, 50.7, 47.3, 33.0, 32.8, 17.1.

(S)-*N*-(4-Bromo-3-((3-methylpyrrolidin-1-yl)sulfonyl)phenyl)-2-(6-(hydroxymethyl)-1*H*-benzo[*d*][1,2,3]triazol-1-yl)acetamide (**(S)**-3.078) and *(S)*-*N*-(4-bromo-3-((3-methylpyrrolidin-1-yl)sulfonyl)phenyl)-2-(5-(hydroxymethyl)-1*H*-benzo[*d*][1,2,3]triazol-1-yl)acetamide (**(S)**-3.079)



(S)-*N*-(4-Bromo-3-((3-methylpyrrolidin-1-yl)sulfonyl)phenyl)-2-chloroacetamide (**(S)**-3.068

(150 mg, 0.379 mmol), (1*H*-benzo[*d*][1,2,3]triazol-5-yl)methanol (68 mg, 0.455 mmol) and K₂CO₃ (68 mg, 0.493 mmol) were dissolved in acetone (5 mL) at rt under air. The resulting solution was heated to 60 °C for 2 h. The reaction was allowed to cool before quenching with sat. aq. NaHCO₃ (10 mL) and extracting with CH₂Cl₂ (2 x 10 mL). The combined organics were passed through a hydrophobic frit and concentrated *in vacuo* to afford the crude product. The crude product was purified by formic MDAP to afford a mixture of regioisomers. The regioisomers were dissolved in EtOH (5mL) and injected onto the column (column: 250 mm x 30 mm Chiralpak AD-H, 5 μm), eluting with 50% EtOH/heptane, flow rate = 43 mL min⁻¹, detection wavelength 280 nm. The pure fractions were concentrated *in vacuo* to afford first eluter *(S)*-*N*-(4-bromo-3-((3-methylpyrrolidin-1-yl)sulfonyl)phenyl)-2-(6-(hydroxymethyl)-1*H*-benzo[*d*][1,2,3]triazol-1-yl)acetamide (**(S)**-3.078 (46 mg, 0.90 mmol, 24% yield) and second eluter *(S)*-*N*-(4-bromo-3-((3-methylpyrrolidin-1-yl)sulfonyl)phenyl)-2-(5-(hydroxymethyl)-1*H*-benzo[*d*][1,2,3]triazol-1-yl)acetamide (**(S)**-3.079 (43 mg, 0.085 mmol, 22% yield).

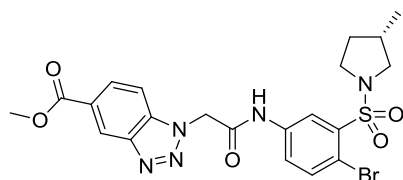
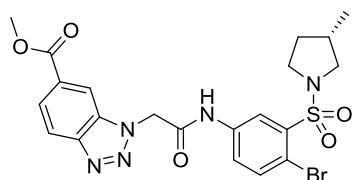
(S)-*N*-(4-Bromo-3-((3-methylpyrrolidin-1-yl)sulfonyl)phenyl)-2-(6-(hydroxymethyl)-1*H*-benzo[d][1,2,3]triazol-1-yl)acetamide ((**S**)-3.078):

LCMS (formic, ES⁺) t_R = 0.96 min, m/z = 508.1, 510.2; HRMS (C₂₀H₂₂BrN₅O₄S): [M+H]⁺ calculated 508.0654, found 508.0653; ¹H NMR (CDCl₃-d, 600 MHz): δ (ppm) 8.12 (d, J=2.0, Hz, 1H), 7.68 (d, J=8.4 Hz, 1H), 7.57 (s, 1H), 7.46–7.51 (m, 1H), 7.41 (d, J=8.8 Hz, 1H), 7.07 (d, J=9.2 Hz, 1H), 5.47 (br. s., 2H), 4.69 (br. s., 2H), 4.30 (br. s., 1H), 3.35–3.46 (m, 2H), 3.20–3.26 (m, 1H), 2.77 (t, J=8.8 Hz, 1H), 2.13–2.23 (m, 1H), 1.87–1.95 (m, 1H), 1.38–1.47 (m, 1H), 0.92 (d, J= 6.6 Hz, 3H); Amide NH not visible; ¹³C NMR (CDCl₃-d, 151 MHz): δ (ppm) 164.9, 144.7, 142.3, 138.3, 137.2, 135.9, 134.0, 124.6, 123.7, 122.9, 119.0, 114.1, 107.1, 64.2, 63.6, 54.5, 47.6, 33.7, 33.5, 17.3.

(S)-*N*-(4-bromo-3-((3-methylpyrrolidin-1-yl)sulfonyl)phenyl)-2-(5-(hydroxymethyl)-1*H*-benzo[d][1,2,3]triazol-1-yl)acetamide ((**S**)-3.079):

LCMS (formic, ES⁺) t_R = 0.97 min, m/z = 508.1, 510.2; HRMS (C₂₀H₂₂BrN₅O₄S): [M+H]⁺ calculated 508.0654, found 508.0655; ¹H NMR (CDCl₃-d, 400 MHz): δ (ppm) 9.42 (br. s., 1H), 8.17 (d, J=2.6 Hz, 1H), 7.79 (s, 1H), 7.72 (dd, J=8.6, 2.6 Hz, 1H), 7.55 (d, J=8.6 Hz, 1H), 7.45–7.52 (m, 1H), 7.37–7.45 (m, 1H), 5.51 (s, 2H), 4.75 (s, 2H), 3.45–3.56 (m, 2H), 3.28–3.37 (m, 1H), 2.86 (dd, J=9.3, 8.1 Hz, 1H), 2.19–2.35 (m, 1H), 1.93–2.08 (m, 1H), 1.43–1.58 (m, 1H), 0.99 (d, J=6.6 Hz, 3H); OH not visible; ¹³C NMR (CDCl₃-d, 151 MHz): δ (ppm) 165.0, 145.3, 138.8, 138.3, 138.1, 136.2, 133.1, 126.9, 124.0, 121.6, 115.7, 112.5, 110.5, 62.7, 54.2, 50.5, 47.3, 33.0, 32.8, 17.1.

Methyl (S)-1-(2-((4-bromo-3-((3-methylpyrrolidin-1-yl)sulfonyl)phenyl)amino)-2-oxoethyl)-1*H*-benzo[d][1,2,3]triazole-5-carboxylate ((S)-3.080) and methyl (S)-1-(2-((4-bromo-3-((3-methylpyrrolidin-1-yl)sulfonyl)phenyl)amino)-2-oxoethyl)-1*H*-benzo[d][1,2,3]triazole-6-carboxylate ((S)-3.081)



(S)-*N*-(4-Bromo-3-((3-methylpyrrolidin-1-yl)sulfonyl)phenyl)-2-chloroacetamide

(S)-3.068 (50 mg, 0.126 mmol), methyl 1*H*-benzo[d][1,2,3]triazole-5-carboxylate (27 mg, 0.152 mmol) and K₂CO₃ (23 mg, 0.164 mmol) were dissolved in acetone (1 mL). The resulting solution was heated to 60 °C and stirred for 1 h. The reaction was allowed to cool before

quenching with sat. aq. NaHCO₃ (10 mL) and extracting with CH₂Cl₂ (3 x 10 mL). The combined organics were passed through a hydrophobic frit and concentrated *in vacuo* to afford the crude product. The crude product was purified by formic MDAP to afford a mixture of regioisomers. The regioisomers were dissolved in EtOH (5mL) and injected onto the column (column: 250 mm x 30 mm Chiralpak IF, 5 μm), eluting with MeOH + 2% isopropylamine, flow rate = 43 mL min⁻¹, detection wavelength 280 nm. The pure fractions were concentrated *in vacuo* to afford first eluter methyl (S)-1-(2-((4-bromo-3-((3-methylpyrrolidin-1-yl)sulfonyl)phenyl)amino)-2-oxoethyl)-1H-benzo[d][1,2,3]triazole-5-carboxylate **3.081** (13 mg, 0.024 mmol, 19% yield) and second eluter methyl (S)-1-(2-((4-bromo-3-((3-methylpyrrolidin-1-yl)sulfonyl)phenyl)amino)-2-oxoethyl)-1H-benzo[d][1,2,3]triazole-6-carboxylate (**S**)-**3.080** (19 mg, 0.035 mmol, 28% yield).

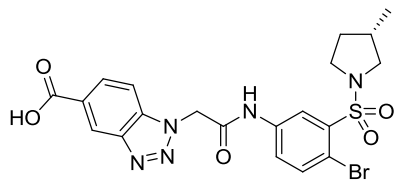
Methyl (S)-1-(2-((4-bromo-3-((3-methylpyrrolidin-1-yl)sulfonyl)phenyl)amino)-2-oxoethyl)-1H-benzo[d][1,2,3]triazole-6-carboxylate ((S)-3.080):

LCMS (formic, ES⁺) t_R = 1.13 min, m/z = 536.1, 538.1; HRMS (C₂₁H₂₂BrN₅O₄S): [M+H]⁺ calculated 536.0603, found 536.0602; ¹H NMR (DMSO-*d*₆, 400 MHz): δ (ppm) 8.64–8.71 (m, 1H), 8.30 (d, J=2.4 Hz, 1H), 8.13 (dd, J=8.8, 1.5 Hz, 1H), 8.00 (d, J=8.8 Hz, 1H), 7.77–7.85 (m, 1H), 7.68–7.76 (m, 1H), 5.79 (s, 2H), 3.93 (s, 3H), 3.37–3.48 (m, 2H), 3.24–3.27 (m, 1H), 2.81 (dd, J=9.4, 7.7 Hz, 1H), 2.24 (td, J=7.8, 6.7 Hz, 1H), 1.92–2.03 (m, 1H), 1.48 (dd, J=12.2, 8.3 Hz, 1H), 0.93 (d, J=6.6 Hz, 3H); *Amide NH not visible*; ¹³C NMR (DMSO-*d*₆, 151 MHz): δ (ppm) 165.9, 164.9, 144.7, 138.2, 136.2, 136.2, 136.2, 127.6, 125.7, 124.1, 121.6, 121.3, 112.4, 111.6, 54.2, 52.4, 50.7, 47.3, 33.0, 32.8, 17.1.

Methyl (S)-1-(2-((4-bromo-3-((3-methylpyrrolidin-1-yl)sulfonyl)phenyl)amino)-2-oxoethyl)-1H-benzo[d][1,2,3] triazole-5-carboxylate ((S)-3.081):

LCMS (formic, ES⁺) t_R = 1.13 min, m/z = 536.1, 538.1; HRMS (C₂₁H₂₂BrN₅O₄S): [M+H]⁺ calculated 536.0603, found 536.0600; ¹H NMR (DMSO-*d*₆, 400 MHz): δ (ppm) 8.82 (t, J=1.1 Hz, 1H), 8.30 (d, J=2.7 Hz, 1H), 8.12 (d, J=8.6 Hz, 1H), 7.95 (dd, J=8.6, 1.5 Hz, 1H), 7.83 (d, J=8.6 Hz, 1H), 7.73 (dd, J=8.6, 2.7 Hz, 1H), 5.82 (s, 2H), 3.92 (s, 3H), 3.40–3.48 (m, 2H), 3.23–3.29 (m, 1H), 2.82 (dd, J=9.3, 7.6 Hz, 1H), 2.19–2.30 (m, 1H), 1.93–2.05 (m, 1H), 1.46–1.50 (m, 1H), 0.95 (d, J= 6.6 Hz, 3H); *Amide NH not visible*; ¹³C NMR (DMSO-*d*₆, 151 MHz): δ (ppm) 165.9, 165.0, 147.0, 138.3, 138.2, 136.2, 133.8, 128.5, 124.1, 124.0, 121.5, 119.4, 113.7, 112.4, 54.2, 52.5, 50.8, 47.3, 33.0, 32.8, 17.1.

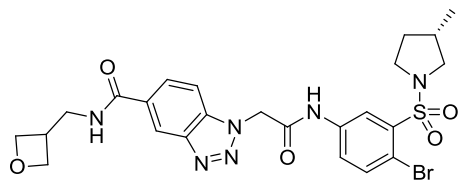
(S)-1-(2-((4-Bromo-3-((3-methylpyrrolidin-1-yl)sulfonyl)phenyl)amino)-2-oxoethyl)-1H-benzo[d][1,2,3]triazole-5-carboxylic acid ((S)-3.080a)



LiOH (31 mg, 1.272 mmol) and ethyl (S)-1-(2-((4-bromo-3-((3-methylpyrrolidin-1-yl)sulfonyl)phenyl)amino)-2-oxoethyl)-1H-benzo[d][1,2,3]triazole-5-carboxylate **(S)-3.080** (350 mg, 0.636 mmol) were dissolved in THF (0.5

mL) and water (0.5 mL). The resulting solution was stirred at 50 °C for 2 h. The reaction was allowed to cool before being acidified with 2 M HCl aq. (20 mL) and extracted with EtOAc (2 x 20 mL). The combined organics were passed through a hydrophobic frit and concentrated *in vacuo* to afford (S)-1-(2-((4-bromo-3-((3-methylpyrrolidin-1-yl)sulfonyl)phenyl)amino)-2-oxoethyl)-1H-benzo[d][1,2,3]triazole-5-carboxylic acid **(S)-3.080a** (284 mg, 0.544 mmol, 86% yield) as a white solid. LCMS (formic, ES⁺) t_R = 1.02 min, m/z = 522.1, 524.1; ¹H NMR (MeOD-*d*₄, 400 MHz): δ (ppm) 8.71–8.75 (m, 1H), 8.35 (d, J =2.4 Hz, 1H), 8.24 (dd, J =8.8, 1.5 Hz, 1H), 7.84 (d, J =8.3 Hz, 1H), 7.71–7.80 (m, 2H), 5.74 (s, 2H), 3.49–3.66 (m, 2H), 3.38 (dt, J =8.5, 1.3 Hz, 1H), 2.92 (dd, J =9.5, 7.8 Hz, 1H), 2.26–2.37 (m, 1H), 2.02–2.08 (m, 1H), 1.57 (dd, J =12.2, 8.5 Hz, 1H), 0.98–1.07 (m, 3H); Acid OH and amide NH not visible.

(S)-1-(2-((4-Bromo-3-((3-methylpyrrolidin-1-yl)sulfonyl)phenyl)amino)-2-oxoethyl)-N-(oxetan-3-ylmethyl)-1H-benzo[d][1,2,3]triazole-5-carboxamide ((S)-3.082)

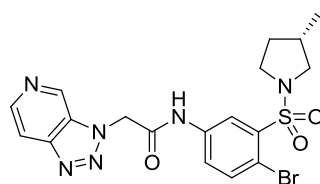
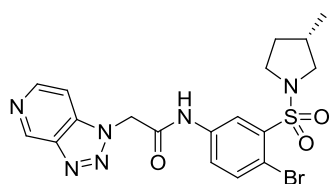


(S)-1-(2-((4-Bromo-3-((3-methylpyrrolidin-1-yl)sulfonyl)phenyl)amino)-2-oxoethyl)-1H-benzo[d][1,2,3]triazole-5-carboxylic acid **(S)-3.080a** (40 mg, 0.077 mmol), oxetan-3-ylmethanamine,

hydrochloride (13 mg, 0.107 mmol) and HATU (35 mg, 0.092 mmol) were dissolved in CH₂Cl₂ (2 mL). DIPEA (0.040 mL, 0.230 mmol) was added and the resulting solution was stirred at rt for 1 h. The reaction was quenched with sat. aq. NaHCO₃ (5 mL) and extracted with CH₂Cl₂ (2 x 5 mL). The combined organics were passed through a hydrophobic frit and concentrated *in vacuo* to afford the crude product. The crude product was purified by HPH MDAP. The pure fractions were concentrated *in vacuo* to afford (S)-1-(2-((4-bromo-3-((3-methylpyrrolidin-1-yl)sulfonyl)phenyl)amino)-2-oxoethyl)-N-(oxetan-3-ylmethyl)-1H-benzo[d][1,2,3]triazole-5-carboxamide **(S)-3.082** (15 mg, 0.026 mmol, 34% yield) as a white solid. LCMS (formic, ES⁺) t_R = 0.95 min, m/z = 591.3, 593.2; HRMS (C₂₄H₂₇BrN₆O₅S): [M+H]⁺ calculated 591.1025, found 591.1026; ¹H NMR (CDCl₃-*d*, 400 MHz): δ (ppm) 9.88 (s, 1H), 8.37 (s, 1H), 8.15 (d, J =2.5 Hz,

1H), 7.91 (dd, $J=8.8, 1.5$ Hz, 1H), 7.84 (dd, $J=8.8, 2.5$ Hz, 1H), 7.47–7.61 (m, 3H), 5.65 (s, 2H), 4.87 (dd, $J=7.8, 6.4$ Hz, 2H), 4.56 (t, $J=6.0$ Hz, 2H), 3.81 (t, $J=6.2$ Hz, 2H), 3.45–3.56 (m, 2H), 3.27–3.42 (m, 2H), 2.86 (t, $J=8.6$ Hz, 1H), 2.28 (dd, $J=15.8, 7.2$ Hz, 1H), 1.95–2.07 (m, 1H), 1.46–1.59 (m, 1H), 1.00 (d, $J=6.6$ Hz, 3H); ^{13}C NMR (CDCl_3 - d , 101MHz): δ (ppm) 167.4, 164.1, 145.0, 138.5, 137.2, 136.2, 135.1, 131.5, 127.7, 124.8, 123.1, 118.4, 114.4, 75.2, 54.6, 47.6, 42.7, 35.0, 33.8, 33.5, 17.4, 0.0; m.p. 131.5 – 137.0 °C; IR ν_{max} (cm^{-1}) 3267, 2970, 1639, 1531, 1300, 1152, 621, 585.

(S)-2-(1H-[1,2,3]triazolo[4,5-c]pyridin-3-yl)-N-(4-bromo-3-((3-methylpyrrolidin-1-yl)sulfonyl)phenyl)acetamide ((S)-3.083) and **(S)-2-(3H-[1,2,3]triazolo[4,5-c]pyridin-3-yl)-N-(4-bromo-3-((3-methylpyrrolidin-1-yl)sulfonyl)phenyl)acetamide ((S)-3.084)**



Method 1: (S)-N-(4-Bromo-3-((3-methylpyrrolidin-1-yl)sulfonyl)phenyl)-2-

chloroacetamide **(S)-3.068** (350 mg, 0.885 mmol), 1H-[1,2,3]triazolo[4,5-c]pyridine (127 mg, 1.061 mmol) and K_2CO_3 (159 mg, 1.150 mmol) were dissolved in acetone (3 mL). The resulting solution was heated to 80 °C and stirred for 12 h. The reaction was allowed to cool before quenching with sat. aq. NaHCO_3 (10 mL) and extracting with CH_2Cl_2 (3 x 10 mL). The combined organics were passed through a hydrophobic frit and concentrated *in vacuo* to afford the crude product. The crude product was purified by TFA MDAP. Fractions containing the desired products were collected separately and concentrated *in vacuo* to afford (S)-2-(3H-[1,2,3]triazolo[4,5-c]pyridin-3-yl)-N-(4-bromo-3-((3-methylpyrrolidin-1-yl)sulfonyl)phenyl)acetamide **(S)-8.084** (59 mg, 0.123 mmol, 14% yield) as a white solid and **(S)-3.083** which required further purification. This was re-purified using formic MDAP. The pure fractions were concentrated *in vacuo* to afford (S)-2-(1H-[1,2,3]triazolo[4,5-c]pyridin-3-yl)-N-(4-bromo-3-((3-methylpyrrolidin-1-yl)sulfonyl)phenyl)acetamide **(S)-8.083** (67 mg, 0.140 mmol, 16% yield) as a white solid.

Method 2: Synthesis of (S)-2-(1H-[1,2,3]Triazolo[4,5-c]pyridin-1-yl)-N-(4-bromo-3-((3-methylpyrrolidin-1-yl)sulfonyl)phenyl)acetamide ((S)-8.083): *tert*-Butyl 2-(1H-[1,2,3]triazolo[4,5-c]pyridin-1-yl)acetate **3.120** (176 mg, 0.752 mmol) was dissolved in HCl (4 M in dioxane, 1.566 mL, 6.27 mmol) and stirred at 40 °C overnight. The reaction was

GSK Confidential – Do not copy

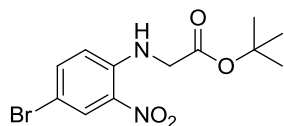
concentrated *in vacuo* to afford the crude acid. (S)-4-Bromo-3-((3-methylpyrrolidin-1-yl)sulfonyl)aniline (**S**-3.067 (200 mg, 0.627 mmol) dissolved in CH₂Cl₂ (10 mL) was added to the crude acid. HATU (286 mg, 0.752 mmol) and DIPEA (0.328 mL, 1.880 mmol) were added, and the resulting solution was stirred at rt for 2 h. The reaction was quenched with sat. aq. NaHCO₃ (10 mL) and extracted with CH₂Cl₂ (3 x 10 mL). The combined organics were passed through a hydrophobic frit and concentrated *in vacuo* to afford the crude product. The crude product was purified by silica chromatography, eluting with 0-50% EtOAc/cyclohexane. The pure fractions were concentrated *in vacuo* to afford (S)-2-(1H-[1,2,3]triazolo[4,5-c]pyridin-1-yl)-N-(4-bromo-3-((3-methylpyrrolidin-1-yl)sulfonyl)phenyl) acetamide (**S**-3.083 (220 mg, 0.459 mmol, 73% yield) as a cream solid.

(S)-2-(1H-[1,2,3]triazolo[4,5-c]pyridin-3-yl)-N-(4-bromo-3-((3-methylpyrrolidin-1-yl)sulfonyl)phenyl)acetamide ((S)-3.083):

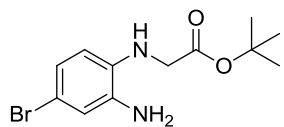
LCMS (formic, ES⁺) t_R = 0.91 min, m/z = 479.2, 481.2; HRMS (C₁₈H₁₉BrN₆O₃S): [M+H]⁺ calculated 479.0501, found 479.0500; ¹H NMR (MeOD-*d*₄, 400 MHz): δ (ppm) 9.89–10.00 (m, 1H), 8.67–8.80 (m, 1H), 8.38 (d, *J*=2.5 Hz, 2H), 7.76 (d, *J*=8.7 Hz, 1H), 7.67 (dd, *J*=8.7, 2.5 Hz, 1H), 5.93 (s, 2H), 3.47–3.57 (m, 2H), 3.34–3.41 (m, 1H), 2.90 (dd, *J*=9.3, 7.8 Hz, 1H), 2.24–2.36 (m, 1H), 2.00–2.04 (m, 1H), 1.47–1.61 (m, 1H), 1.01 (d, *J*=6.6 Hz, 3H); Amide NH not visible; ¹³C NMR (MeOD-*d*₄, 101 MHz): δ (ppm) 164.0, 142.1, 140.9, 140.0, 138.9, 137.7, 136.8, 136.0, 124.2, 122.3, 113.6, 109.5, 54.3, 50.9, 47.4, 33.6, 33.1, 16.2; m.p. 141.5 – 143.0 °C; IR ν_{max} (cm⁻¹) 3572, 2957, 1704, 1586, 1610, 1462, 1316, 1138, 818, 618.

(S)-2-(3H-[1,2,3]triazolo[4,5-c]pyridin-3-yl)-N-(4-bromo-3-((3-methylpyrrolidin-1-yl)sulfonyl)phenyl)acetamide ((S)-3.084):

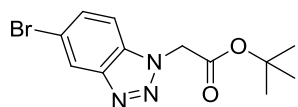
LCMS (formic, ES⁺) t_R = 0.98 min, m/z = 479.2, 481.2; HRMS (C₁₈H₁₉BrN₆O₃S): [M+H]⁺ calculated 479.0501, found 479.0501; ¹H NMR (DMSO-*d*₆, 400 MHz): δ (ppm) 11.09 (s, 1H), 9.47 (d, *J*=1.5 Hz, 1H), 8.55 (d, *J*=5.9 Hz, 1H), 8.31 (d, *J*=2.7 Hz, 1H), 8.16 (dd, *J*=5.9, 1.5 Hz, 1H), 7.84 (d, *J*=8.7 Hz, 1H), 7.73 (dd, *J*=8.7, 2.7 Hz, 1H), 5.91 (s, 2H), 3.38–3.50 (m, 2H), 3.23–3.33 (m, 1H), 2.82 (dd, *J*=9.4, 7.7 Hz, 1H), 2.18–2.31 (m, 1H), 1.93–2.03 (m, 1H), 1.48 (dq, *J*=12.2, 8.3 Hz, 1H), 0.94 (d, *J*=6.6 Hz, 3H); ¹³C NMR (DMSO-*d*₆, 101 MHz): δ (ppm) 164.7, 148.2, 141.2, 138.3, 138.1, 136.7, 136.3, 131.1, 124.0, 121.6, 113.3, 112.6, 54.2, 51.3, 47.3, 33.1, 32.8, 17.1.

***tert*-Butyl (4-bromo-2-nitrophenyl)glycinate (3.086)**³³⁶

4-Bromo-1-fluoro-2-nitrobenzene **3.085** (1.0 g, 4.55 mmol) and *tert*-butyl glycinate, hydrochloride (0.800 g, 4.77 mmol) were dissolved in EtOH (20 mL). TEA (0.634 mL, 4.55 mmol) was added and the reaction refluxed for 6 h. The reaction was allowed to cool, upon which a precipitate formed. The precipitate was filtered off and collected to afford *tert*-butyl (4-bromo-2-nitrophenyl)glycinate **3.086** (0.884 g, 2.67 mmol, 59% yield) as an orange solid. LCMS (formic, ES⁺) $t_R = 1.34$ min, $m/z = 275.1, 277.1$; ¹H NMR (DMSO-*d*₆, 400 MHz): δ (ppm) 8.37 (s, 1H), 8.20 (d, $J=2.4$ Hz, 1H), 7.68 (dd, $J=9.0, 2.4$ Hz, 1H), 6.91 (d, $J=9.0$ Hz, 1H), 4.17 (d, $J=5.6$ Hz, 2H), 1.45 (s, 9H); ¹³C NMR (DMSO-*d*₆, 101 MHz): δ (ppm) 169.1, 144.1, 139.2, 132.3, 128.2, 117.9, 106.3, 82.1, 45.4, 28.2; m.p. 139.6 – 142.1 °C; IR ν_{max} (cm⁻¹) 3339, 2980, 1732, 1563, 1507, 1240, 1147.

***tert*-Butyl (2-amino-4-bromophenyl)glycinate (3.087)**³³⁶

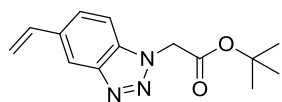
tert-Butyl (4-bromo-2-nitrophenyl)glycinate **3.086** (0.80 g, 2.416 mmol) was suspended in EtOH (30 mL) and water (8 mL). Ammonium chloride (0.194 g, 3.62 mmol) and iron (0.675 g, 12.08 mmol) were added and the reaction heated to 70 °C for 2 h. The reaction mixture was filtered through a 10 g Celite cartridge which was washed with MeOH (30 mL). The filtrate was concentrated *in vacuo* and the residue partitioned between CH₂Cl₂ and water (25 mL each). The aq. layer was re-extracted with CH₂Cl₂ (2 x 25 mL). The combined organics were eluted through a hydrophobic frit and concentrated *in vacuo* to give *tert*-butyl (2-amino-4-bromophenyl)glycinate **3.087** (670 mg, 2.225 mmol, 92% yield) as a cream solid. LCMS (formic, ES⁺) $t_R = 1.13$ min, 301.2, 303.1; HRMS (C₁₂H₁₈BrN₂O₂): [M+H]⁺ calculated 301.0552, found 301.0562; ¹H NMR (DMSO-*d*₆, 400 MHz): δ (ppm) 6.71 (d, $J=2.2$ Hz, 1H), 6.58 (dd, $J=8.5, 2.2$ Hz, 1H), 6.18 (d, $J=8.5$ Hz, 1H), 5.01 (s, 1H), 4.83 (s, 2H), 3.77 (d, $J=6.4$ Hz, 2H), 1.42 (s, 9H); ¹³C NMR (DMSO-*d*₆, 101 MHz): δ (ppm) 170.9, 138.0, 135.0, 119.6, 116.4, 111.7, 109.1, 81.1, 46.3, 28.2; m.p. 100.5 – 105.0 °C; IR ν_{max} (cm⁻¹) 3389, 2982, 1724, 1505, 1362, 1234, 1151.

***tert*-Butyl 2-(5-bromo-1H-benzo[d][1,2,3]triazol-1-yl)acetate (3.088)**

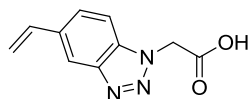
tert-Butyl (2-amino-4-bromophenyl)glycinate **3.087** (500 mg, 1.660 mmol) was suspended in water (2.0 mL) at 0 °C under air. AcOH (0.8 mL) was added followed by sodium nitrite (126 mg, 1.826 mmol) and the resulting

suspension was then placed in a pre-heated stirrer hotplate and stirred at 80 °C for 10 min before allowing to cool to rt. The reaction was diluted with water and extracted with CH₂Cl₂ (3 x 20 mL). The combined organics were passed through a 10 g SCX column, washing with MeOH and concentrated *in vacuo* to afford the crude product. The crude product was purified by silica chromatography, eluting with 0-25% EtOAc/cyclohexane. The pure fractions were concentrated *in vacuo* to afford *tert*-butyl 2-(5-bromo-1*H*-benzo[*d*][1,2,3]triazol-1-yl)acetate **3.088** (284 mg, 0.910 mmol, 55% yield) as a pale pink solid. LCMS (formic, ES⁺) *t*_R = 1.13 min, *m/z* = 312.1, 314.1; HRMS (C₁₂H₁₄BrN₃O₂): [M+H]⁺ calculated 312.0348, found 312.0342; ¹H NMR (DMSO-*d*₆, 400 MHz): δ (ppm) 8.37 (d, *J*=2.0 Hz, 1H), 7.85 (d, *J*=8.8 Hz, 1H), 7.74 (dd, *J*=8.8, 2.0 Hz, 1H), 5.68 (s, 2H), 1.40 (s, 9H); ¹³C NMR (DMSO-*d*₆, 101 MHz): δ (ppm) 166.5, 146.7, 133.1, 131.0, 122.0, 117.0, 113.3, 83.1, 50.0, 28.1; m.p. 148.4 – 152.4 °C; IR *v*_{max} (cm⁻¹) 2982, 1739, 1153, 806.

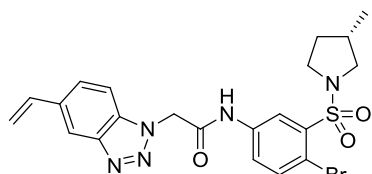
***tert*-Butyl 2-(5-vinyl-1*H*-benzo[*d*][1,2,3]triazol-1-yl)acetate (3.089)**



tert-Butyl 2-(5-bromo-1*H*-benzo[*d*][1,2,3]triazol-1-yl)acetate **3.088** (350 mg, 1.121 mmol), trifluoro(vinyl)borate, potassium salt (300 mg, 2.242 mmol), and XPhos Pd G2 (88 mg, 0.112 mmol) were dissolved in THF (5 mL) at rt under nitrogen. TEA (0.469 mL, 3.36 mmol) was added and the reaction heated at 100 °C under mw irradiation for 2 h. The reaction was diluted with water (10 mL) and extracted with EtOAc (3 x 10 mL). The combined organics were passed through a hydrophobic frit and concentrated *in vacuo* to afford the crude product. The crude product was purified by silica chromatography, eluting with 0-40% EtOAc/cyclohexane. The pure fractions were concentrated *in vacuo* to afford *tert*-butyl 2-(5-vinyl-1*H*-benzo[*d*][1,2,3]triazol-1-yl)acetate **3.089** (181 mg, 0.698 mmol, 62% yield) as a cream solid. LCMS (formic, ES⁺) *t*_R = 1.10 min, *m/z* = 260.2; ; HRMS (C₁₄H₁₇N₃O₂): [M+H]⁺ calculated 260.1399, found 260.1392; ¹H NMR (CDCl₃-*d*, 400 MHz): δ (ppm) 8.04 (d, *J*=1.0 Hz, 1H), 7.68 (dd, *J*=8.6, 1.0 Hz, 1H), 7.44 (d, *J*=8.6 Hz, 1H), 6.89 (dd, *J*=17.6, 11.0 Hz, 1H), 5.84 (d, *J*=17.6 Hz, 1H), 5.36 (d, *J*=11.0 Hz, 1H), 5.33 (s, 2H), 1.45–1.50 (m, 9H); ¹³C NMR (CDCl₃-*d*, 101 MHz): δ (ppm) 165.2, 146.7, 136.2, 134.3, 133.2, 126.1, 117.7, 114.5, 109.3, 83.7, 50.0, 27.9.

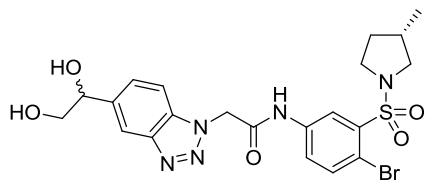
2-(5-Vinyl-1H-benzo[d][1,2,3]triazol-1-yl)acetic acid (3.089a)

HCl (4 M in dioxane, 1.7 mL, 6.94 mmol) was added to *tert*-butyl 2-(5-vinyl-1H-benzo[d][1,2,3]triazol-1-yl)acetate **3.089** (180 mg, 0.694 mmol) at rt under air. The reaction was stirred at 40 °C overnight. The reaction was allowed to cool and then concentrated *in vacuo* to afford 2-(5-vinyl-1H-benzo[d][1,2,3]triazol-1-yl)acetic acid **3.089a** (136 mg, 0.669 mmol, 96 % yield) as a yellow solid. LCMS (formic, ES⁺) $t_R = 0.77$ min, $m/z = 204.3$; ¹H NMR (DMSO-*d*₆, 400 MHz): δ (ppm) 8.08 (s, 1H), 7.73–7.85 (m, 2H), 6.92 (dd, $J=17.6, 11.0$ Hz, 1H), 5.96 (d, $J=17.6$ Hz, 1H), 5.64 (s, 2H), 5.34 (d, $J=11.0$ Hz, 1H); *Acid OH not visible*; ¹³C NMR (DMSO-*d*₆, 101 MHz): δ (ppm) 169.0, 146.1, 136.7, 134.1, 133.8, 126.1, 117.1, 115.2, 111.5, 49.3.

***N*-(4-Bromo-3-((3-methylpyrrolidin-1-yl)sulfonyl)phenyl)-2-(5-vinyl-1H-benzo[d][1,2,3]triazol-1-yl)acetamide ((S)-3.090)**

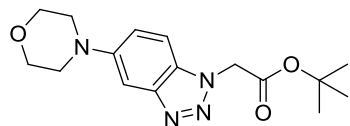
2-(5-Vinyl-1H-benzo[d][1,2,3]triazol-1-yl)acetic acid **3.089a** (122 mg, 0.601 mmol), (*S*)-4-bromo-3-((3-methylpyrrolidin-1-yl)sulfonyl)aniline (**S**)-**3.067** (160 mg, 0.501 mmol), and HATU (229 mg, 0.601 mmol) were dissolved in CH₂Cl₂ (10 mL). DIPEA (0.263 mL, 1.504 mmol) was added and the resulting solution was stirred at rt for 2 h. The reaction was quenched with sat. aq. NaHCO₃ (10 mL) and extracted with CH₂Cl₂ (3 x 10 mL). The combined organics were passed through a hydrophobic frit and concentrated *in vacuo* to afford the crude product. The crude product was purified by silica chromatography, eluting with 0-50% EtOAc/cyclohexane. The pure fractions were concentrated *in vacuo* to afford (*S*)-*N*-(4-bromo-3-((3-methylpyrrolidin-1-yl)sulfonyl)phenyl)-2-(5-vinyl-1H-benzo[d][1,2,3]triazol-1-yl)acetamide (**S**)-**3.090** (153 mg, 0.303 mmol, 61% yield) as a cream solid. LCMS (formic, ES⁺) $t_R = 1.18$ min, $m/z = 504.2, 506.2$; HRMS (C₂₁H₂₂BrN₅O₃S): [M+H]⁺ calculated 504.0705, found 504.0706; ¹H NMR (DMSO-*d*₆, 400 MHz): δ (ppm) 8.31 (d, $J=2.7$ Hz, 1H), 8.10 (s, 1H), 7.68–7.90 (m, 4H), 6.93 (dd, $J=17.5, 11.0$ Hz, 1H), 5.97 (d, $J=17.5$ Hz, 1H), 5.71 (s, 2H), 5.34 (d, $J=11.0$ Hz, 1H), 3.38–3.52 (m, 2H), 3.15–3.28 (m, 1H), 2.80–2.84 (m, 1H), 2.22–2.27 (m, 1H), 1.92–2.05 (m, 1H), 1.47–1.51 (m, 1H), 0.94 (d, $J=6.8$ Hz, 3H); *Amide NH not visible*; ¹³C NMR (DMSO-*d*₆, 101 MHz): δ (ppm) 165.5, 146.1, 138.8, 138.6, 136.7, 134.2, 134.1, 126.1, 124.5, 122.1, 117.2, 115.2, 113.0, 113.1, 111.6, 54.7, 51.0, 47.8, 33.5, 33.4, 17.6; m.p. 140.9 – 146.9 °C; IR ν_{max} (cm⁻¹) 3275, 2971, 1697, 1586, 1459, 1151, 586.

***N*-(4-Bromo-3-(((*S*)-3-methylpyrrolidin-1-yl)sulfonyl)phenyl)-2-(5-((*R*)-1,2-dihydroxyethyl)-1*H*-benzo[*d*][1,2,3]triazol-1-yl)acetamide (3.091)**, mixture of diastereomers



AD-mix- β (0.140 g, 0.099 mmol) was added to a stirred solution of (*S*)-*N*-(4-bromo-3-((3-methylpyrrolidin-1-yl)sulfonyl)phenyl)-2-(5-vinyl-1*H*-benzo[*d*][1,2,3]triazol-1-yl)acetamide (**S**)-**3.090** (50 mg, 0.099 mmol) in *i*PrOH (1 mL) and water (1 mL). The reaction mixture was stirred at rt for 4 h. A further 2 eq. of AD-mix- β were added and the reaction stirred at rt for 16 h. The reaction was quenched by the addition of 10% aq. sodium sulfite solution (10 mL) and the mixture stirred for 5 min. The mixture was extracted with EtOAc (3 x 10 mL). The combined organics were passed through a hydrophobic frit and concentrated *in vacuo* to afford the crude product. The crude product was purified by formic MDAP. The pure fractions were concentrated *in vacuo* to afford *N*-(4-bromo-3-(((*S*)-3-methylpyrrolidin-1-yl)sulfonyl)phenyl)-2-(5-((*R*)-1,2-dihydroxyethyl)-1*H*-benzo[*d*][1,2,3]triazol-1-yl)acetamide **3.091** (8 mg, 0.014 mmol, 14% yield) as a white solid and a mixture of diastereomers. LCMS (formic, ES⁺) t_R = 0.89 min, m/z = 538.2, 540.1; HRMS (C₂₁H₂₄BrN₅O₅S): [M+H]⁺ calculated 538.0760, found 538.0765; ¹H NMR (MeOD-*d*₄, 400 MHz): δ (ppm) 8.35 (d, J =2.0 Hz, 1H), 8.06 (d, J =1.0 Hz, 1H), 7.70–7.79 (m, 3H), 7.65 (dd, J =8.7, 2.0 Hz, 1H), 5.67 (s, 2H), 4.86–4.94 (m, 1H), 3.72 (dd, J =6.0, 2.6 Hz, 2H), 3.47–3.60 (m, 2H), 3.35–3.42 (m, 1H), 2.91 (dd, J =9.4, 7.7 Hz, 1H), 2.24–2.38 (m, 1H), 2.06–2.10 (m, 1H), 1.51–1.62 (m, 1H), 1.02 (d, J =6.6 Hz, 3H); Amide NH and alcohol OHs not visible; Diastereotopic protons not visible; ¹³C NMR (MeOD-*d*₄, 101 MHz): δ (ppm) 164.9, 145.3, 139.5, 139.0, 137.9, 136.0, 133.6, 126.8, 124.1, 122.1, 116.0, 113.4, 109.9, 74.1, 67.2, 54.3, 33.6, 33.0, 16.9, 16.2, -0.6.

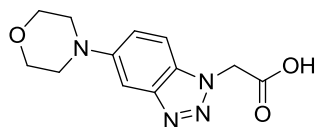
***tert*-Butyl 2-(5-morpholino-1*H*-benzo[*d*][1,2,3]triazol-1-yl)acetate (3.092)**



tert-Butyl 2-(5-bromo-1*H*-benzo[*d*][1,2,3]triazol-1-yl)acetate **3.088** (200 mg, 0.641 mmol), Cs₂CO₃ (626 mg, 1.922 mmol), Pd₂(dba)₃ (29 mg, 0.032 mmol), and RuPhos (30 mg, 0.064 mmol) were dissolved in toluene (1 mL) at rt under nitrogen. Morpholine (0.084 mL, 0.961 mmol) was added and the resulting solution was stirred at 80 °C under mw irradiation for 1 h. The reaction was diluted with water (5 mL) and extracted with CH₂Cl₂ (3 x 10 mL). The combined organics were passed through a hydrophobic frit and concentrated *in vacuo* to afford the crude product. The crude product was purified by silica chromatography eluting

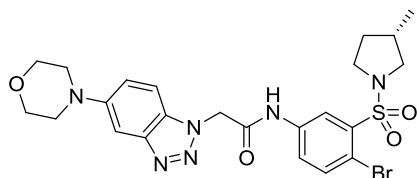
with 0-50% EtOAc/cyclohexane. The pure fractions were concentrated *in vacuo* to afford *tert*-butyl 2-(5-morpholino-1*H*-benzo[*d*][1,2,3]triazol-1-yl)acetate **3.092** (70 mg, 0.220 mmol, 34% yield) as a cream solid. LCMS (formic, ES⁺) $t_R = 0.93$ min, $m/z = 319.3$; ¹H NMR (CDCl₃-*d*, 400 MHz): δ (ppm) 7.43 (d, $J=2.2$ Hz, 1H), 7.38 (d, $J=9.0$ Hz, 1H), 7.31 (dd, $J=9.0, 2.2$ Hz, 1H), 5.29 (s, 2H), 3.85–4.02 (m, 4H), 3.16–3.27 (m, 4H), 1.47 (s, 9H).

2-(5-Morpholino-1*H*-benzo[*d*][1,2,3]triazol-1-yl)acetic acid (**3.092a**)



HCl (4 M in dioxane, 393 μ L, 1.570 mmol) was added to *tert*-butyl 2-(5-morpholino-1*H*-benzo[*d*][1,2,3]triazol-1-yl)acetate **3.092** (50 mg, 0.157 mmol) at rt under air. The reaction was stirred at 40 °C for 4 h. A further 4 eq. of HCl (4 M in dioxane, 157 μ L, 0.628 mmol) was added and the reaction left stirring at 40 °C overnight. The reaction was allowed to cool and then concentrated *in vacuo* to afford 2-(5-morpholino-1*H*-benzo[*d*][1,2,3]triazol-1-yl)acetic acid **3.092a** (40 mg, 0.153 mmol, 97% yield) as a yellow solid. LCMS (formic, ES⁺) $t_R = 0.58$ min, $m/z = 263.2$; ¹H NMR (MeOD-*d*₄, 400 MHz): δ (ppm) 8.27 (d, $J=2.4$ Hz, 1H), 7.99 (d, $J=9.0$ Hz, 1H), 7.88 (dd, $J=9.0, 2.4$ Hz, 1H), 5.70 (s, 2H), 4.09–4.16 (m, 4H), 3.74–3.78 (m, 4H); Acid OH not visible.

(*S*)-*N*-(4-Bromo-3-((3-methylpyrrolidin-1-yl)sulfonyl)phenyl)-2-(5-morpholino-1*H*-benzo[*d*][1,2,3]triazol-1-yl)acetamide ((*S*)-**3.093**)

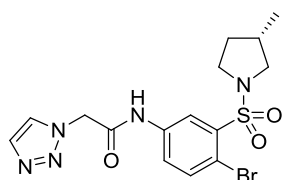


2-(5-Morpholino-1*H*-benzo[*d*][1,2,3]triazol-1-yl)acetic acid **3.092a** (41 mg, 0.157 mmol), (*S*)-4-bromo-3-((3-methylpyrrolidin-1-yl)sulfonyl)aniline (**S**)-**3.067** (50 mg, 0.157 mmol), and HATU (72 mg, 0.188 mmol) were dissolved in CH₂Cl₂ (10 mL). DIPEA (0.082 mL, 0.470 mmol) was added and the resulting solution was stirred at rt for 2 h. The reaction was quenched with sat. aq. NaHCO₃ (10 mL) and extracted with CH₂Cl₂ (3 x 10 mL). The combined organics were passed through a hydrophobic frit and concentrated *in vacuo* to afford the crude product. The crude product was purified by formic MDAP. The fractions which contained the desired product were concentrated *in vacuo* and purified by silica chromatography, eluting with 0-100% EtOAc/cyclohexane. The pure fractions were concentrated *in vacuo* to afford (*S*)-*N*-(4-bromo-3-((3-methylpyrrolidin-1-yl)sulfonyl)phenyl)-2-(5-morpholino-1*H*-benzo[*d*][1,2,3]triazol-1-yl)acetamide (**S**)-**3.093** (15 mg, 0.027 mmol, 17% yield) as a white solid. LCMS (formic, ES⁺) $t_R =$

GSK Confidential – Do not copy

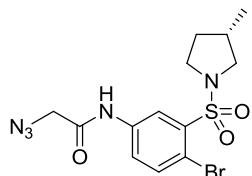
1.05 min, m/z = 563.1, 565.1; HRMS ($C_{23}H_{27}BrN_6O_4S$): $[M+H]^+$ calculated 563.1076, found 563.1080; 1H NMR (MeOD- d_4 , 400 MHz): δ (ppm) 8.34 (d, $J=2.4$ Hz, 1H), 7.68–7.78 (m, 2H), 7.65 (d, $J=9.0$ Hz, 1H), 7.38–7.44 (m, 1H), 7.29–7.35 (m, 1H), 5.61 (s, 2H), 3.84–3.92 (m, 4H), 3.47–3.58 (m, 2H), 3.35–3.39 (m, 1H), 3.14–3.25 (m, 4H), 2.86–2.94 (m, 1H), 2.24–2.36 (m, 1H), 2.03–2.08 (m, 1H), 1.51–1.65 (m, 1H), 1.01 (d, $J=6.7$ Hz, 3H); Amide NH not visible; ^{13}C NMR (MeOD- d_4 , 101 MHz): δ (ppm) 164.9, 149.8, 146.6, 138.9, 137.9, 136.0, 129.5, 124.0, 122.3, 121.6, 113.5, 110.5, 101.7, 66.6, 60.2, 54.3, 50.4, 33.6, 33.1, 16.2, 12.9; m.p. 122.3 – 125.9 °C; IR ν_{max} (cm^{-1}) 2964, 1698, 1586, 1459, 1114, 619, 586.

(S)-N-(4-Bromo-3-((3-methylpyrrolidin-1-yl)sulfonyl)phenyl)-2-(1H-1,2,3-triazol-1-yl)acetamide ((S)-3.095)



(S)-4-Bromo-3-((3-methylpyrrolidin-1-yl)sulfonyl)aniline **(S)-3.067** (40 mg, 0.125 mmol), 2-(1H-1,2,3-triazol-1-yl)acetic acid **3.094**, hydrochloride (25 mg, 0.150 mmol) and HATU (72 mg, 0.188 mmol) were dissolved in CH_2Cl_2 (2 mL) at rt under air. DIPEA (0.066 mL,

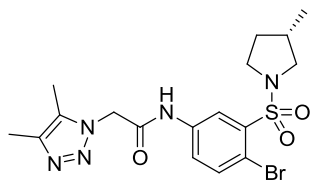
0.376 mmol) was added and the resulting solution was stirred at rt for 2 h. The reaction was quenched by the addition of sat. aq. $NaHCO_3$ (10 mL) and extracted with CH_2Cl_2 (2 x 10 mL). The combined organics were passed through a hydrophobic frit and concentrated *in vacuo* to afford the crude product. The crude product was purified by formic MDAP. The pure fractions were concentrated *in vacuo* to afford (S)-N-(4-bromo-3-((3-methylpyrrolidin-1-yl)sulfonyl)phenyl)-2-(1H-1,2,3-triazol-1-yl)acetamide **(S)-3.095** (36 mg, 0.084 mmol, 67% yield) as a white solid. LCMS (formic, ES^+) t_R = 0.83 min, m/z = 428.2, 430.2; HRMS ($C_{15}H_{18}BrN_5O_3S$): $[M+H]^+$ calculated 428.0397, found 428.0394; 1H NMR ($CDCl_3-d$, 400 MHz): δ (ppm) 9.33 (s, 1H), 8.23 (d, $J=2.5$ Hz, 1H), 7.92 (s, 1H), 7.86 (s, 1H), 7.81 (dd, $J=8.6, 2.5$ Hz, 1H), 7.65 (d, $J=8.6$ Hz, 1H), 5.40 (s, 2H), 3.52–3.61 (m, 2H), 3.33–3.44 (m, 1H), 2.91 (dd, $J=9.4, 7.9$ Hz, 1H), 2.24–2.35 (m, 1H), 1.98–2.09 (m, 1H), 1.55 (dq, $J=12.4, 8.5$ Hz, 1H), 1.03 (d, $J=6.6$ Hz, 3H); ^{13}C NMR ($CDCl_3-d$, 101 MHz): δ (ppm) 163.8, 138.7, 137.0, 136.2, 134.0, 126.1, 124.8, 123.3, 114.6, 54.6, 53.2, 47.7, 33.8, 33.6, 17.4; m.p. 65.8 – 71.1 °C; IR ν_{max} (cm^{-1}) 2970, 1704, 1585, 1531, 1459, 1142, 840, 557.

(S)-2-Azido-N-(4-bromo-3-((3-methylpyrrolidin-1-yl)sulfonyl)phenyl)acetamide ((S)-3.096)

(S)-4-Bromo-3-((3-methylpyrrolidin-1-yl)sulfonyl)aniline **(S)-3.067**

(500 mg, 1.566 mmol), 2-azidoacetic acid (158 mg, 1.566 mmol), and HATU (715 mg, 1.880 mmol) were dissolved in CH₂Cl₂ (5 mL) at rt under air. DIPEA (0.819 mL, 4.70 mmol) was added and the resulting

solution was stirred at rt for 2 h. The reaction was quenched with sat. aq. NaHCO₃ (20 mL) and extracted with CH₂Cl₂ (2 x 20 mL). The combined organics were passed through a hydrophobic frit and concentrated *in vacuo* to afford the crude product. The crude product was purified by silica chromatography eluting with 0-100% EtOAc/cyclohexane. The pure fractions were concentrated *in vacuo* to afford (S)-2-azido-N-(4-bromo-3-((3-methylpyrrolidin-1-yl)sulfonyl)phenyl)acetamide **(S)-3.096** (590 mg, 1.467 mmol, 94% yield) as a yellow oil. LCMS (formic, ES⁺) t_R = 1.08 min, m/z = 400.1, 402.1; ; HRMS (C₁₃H₁₆BrN₅O₃S): [M+H]⁺ calculated 402.0232, found 402.0231; ¹H NMR (CDCl₃-d, 400 MHz): δ (ppm) 8.39 (br. s., 1H), 8.09 (d, J=2.7 Hz, 1H), 7.94 (dd, J=8.8, 2.7 Hz, 1H), 7.71 (d, J=8.8 Hz, 1H), 4.17 (s, 2H), 3.54–3.64 (m, 2H), 3.36–3.47 (m, 1H), 2.95 (dd, J=9.4, 7.9 Hz, 1H), 2.35 (ddd, J=14.9, 6.6, 2.2 Hz, 1H), 2.03–2.12 (m, 1H), 1.59 (dq, J=12.3, 8.5 Hz, 1H), 1.06 (d, J=6.6 Hz, 3H); ¹³C NMR (CDCl₃-d, 101 MHz): δ (ppm) 165.1, 139.2, 136.6, 136.3, 124.5, 123.0, 114.7, 54.6, 52.9, 47.7, 33.8, 33.6, 17.4; m.p. 80.5 – 83.2 °C; IR ν_{max} (cm⁻¹) 3339, 2960, 2097, 1715, 1598, 1530, 1146, 618, 586, 538.

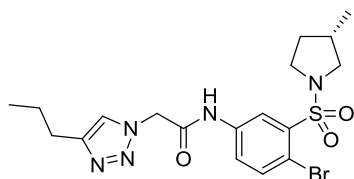
((S)-N-(4-Bromo-3-((3-methylpyrrolidin-1-yl)sulfonyl)phenyl)-2-(4,5-dimethyl-1H-1,2,3-triazol-1-yl)acetamide ((S)-3.097)

(S)-2-Azido-N-(4-bromo-3-((3-methylpyrrolidin-1-yl)sulfonyl)phenyl)acetamide **(S)-3.096** (50 mg, 0.124 mmol), but-2-yne (10 mg, 0.186 mmol), and Cp^{*}RuCl(PPh₃)₂ (3 mg, 3.73 μmol) were dissolved in THF (1 mL) at rt under nitrogen. The resulting

solution was stirred at 65 °C for 2 h. The reaction was quenched with water (2 mL) and extracted with CH₂Cl₂ (2 x 2 mL). The combined organics were passed through a hydrophobic frit and concentrated *in vacuo* to afford the crude product. The crude product was purified by formic MDAP. The pure fractions were concentrated *in vacuo* to afford ((S)-N-(4-bromo-3-((3-methylpyrrolidin-1-yl)sulfonyl)phenyl)-2-(4,5-dimethyl-1H-1,2,3-triazol-1-yl)acetamide **(S)-3.097** (35 mg, 0.077 mmol, 62% yield) as a cream solid. LCMS (Formic, ES⁺) t_R = 0.99 min, m/z = 456.2, 458.2; HRMS (C₁₇H₂₂BrN₅O₃S): [M+H]⁺ calculated 456.0705, found 456.0705; ¹H

NMR (CDCl₃-d, 400 MHz): δ (ppm) 9.44 (s, 1H), 8.20 (d, $J=2.7$ Hz, 1H), 7.84 (dd, $J=8.8, 2.7$ Hz, 1H), 7.65 (d, $J=8.8$ Hz, 1H), 5.22 (s, 2H), 3.52–3.61 (m, 2H), 3.35–3.44 (m, 1H), 2.92 (dd, $J=9.4, 7.9$ Hz, 1H), 2.26–2.37 (m, 7H), 1.99–2.09 (m, 1H), 1.49–1.62 (m, 1H), 1.04 (d, $J=6.6$ Hz, 3H); ¹³C NMR (CDCl₃-d, 101 MHz): δ (ppm) 164.1, 141.2, 138.9, 137.2, 136.1, 131.3, 124.7, 123.3, 114.5, 54.6, 51.4, 47.7, 33.8, 33.6, 17.4, 10.3, 7.9.

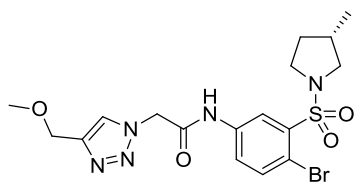
(S)-N-(4-Bromo-3-((3-methylpyrrolidin-1-yl)sulfonyl)phenyl)-2-(4-propyl-1H-1,2,3-triazol-1-yl)acetamide ((S)-3.098)



(S)-2-Azido-N-(4-bromo-3-((3-methylpyrrolidin-1-yl)sulfonyl)phenyl)acetamide **(S)-3.096** (50 mg, 0.124 mmol), pent-1-yne (0.03 mL, 0.249 mmol), sodium ascorbate (4 mg, 0.019 mmol) and Cu(OAc)₂·H₂O (3 mg, 0.012 mmol) were

dissolved in degassed MeOH (1 mL). The resulting solution was stirred at 100 °C under mw irradiation for 30 min. The reaction was diluted with water (10 mL) and extracted with CH₂Cl₂ (3 x 10 mL). The combined organics were passed through a hydrophobic frit and concentrated *in vacuo* to afford the crude product. The crude product was purified by formic MDAP. The pure fractions were concentrated *in vacuo* to afford (S)-N-(4-bromo-3-((3-methylpyrrolidin-1-yl)sulfonyl)phenyl)-2-(4-propyl-1H-1,2,3-triazol-1-yl)acetamide **(S)-3.098** (26 mg, 0.055 mmol, 45% yield) as a white solid. LCMS (Formic, ES⁺) $t_R = 1.09$ min, $m/z = 470.2, 472.2$; HRMS (C₁₈H₂₄BrN₅O₃S): [M+H]⁺ calculated 470.0861, found 470.0863; ¹H NMR (CDCl₃-d, 400 MHz): δ (ppm) 8.87 (s, 1H), 8.14 (d, $J=2.7$ Hz, 1H), 7.82 (dd, $J=8.6, 2.7$ Hz, 1H), 7.67 (d, $J=8.6$ Hz, 1H), 7.54 (s, 1H), 5.24 (s, 2H), 3.50–3.63 (m, 2H), 3.40 (td, $J=9.0, 7.1$ Hz, 1H), 2.93 (dd, $J=9.4, 7.9$ Hz, 1H), 2.75 (t, $J=7.6$ Hz, 2H), 2.26–2.39 (m, 1H), 2.01–2.11 (m, 1H), 1.71–1.78 (m, 3H), 1.50–1.61 (m, 1H), 0.97–1.07 (m, 5H); ¹³C NMR (CDCl₃-d, 101 MHz): δ (ppm) 163.3, 149.0, 139.0, 136.7, 136.2, 124.7, 123.3, 122.7, 114.9, 54.6, 53.4, 47.7, 33.8, 33.6, 27.6, 22.5, 17.4, 13.8; IR ν_{max} (cm⁻¹) 3276, 2961, 1705, 1586, 1531, 1459, 1143, 650, 536.

(S)-N-(4-Bromo-3-((3-methylpyrrolidin-1-yl)sulfonyl)phenyl)-2-(4-(methoxymethyl)-1H-1,2,3-triazol-1-yl)acetamide ((S)-3.099)

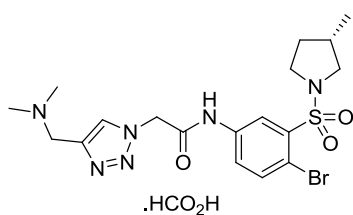


(S)-2-Azido-N-(4-bromo-3-((3-methylpyrrolidin-1-yl)sulfonyl)phenyl)acetamide **(S)-3.096** (50 mg, 0.124 mmol), 3-methoxyprop-1-yne (10 mg, 0.137 mmol), CuSO₄·5H₂O (2 mg, 6.21 μ mol) and sodium ascorbate (4 mg, 0.019 mmol)

GSK Confidential – Do not copy

were dissolved in a mixture of CH₂Cl₂ (1.0 mL) and water (1.0 mL). The resulting solution was stirred at rt for 16 h. The reaction was diluted with water (10 mL) and extracted with CH₂Cl₂ (3 x 10 mL). The combined organics were passed through a hydrophobic frit and concentrated *in vacuo* to afford the crude product. The crude product was purified by formic MDAP. The pure fractions were concentrated *in vacuo* to afford (*S*)-*N*-(4-bromo-3-((3-methylpyrrolidin-1-yl)sulfonyl)phenyl)-2-(4-(methoxymethyl)-1*H*-1,2,3-triazol-1-yl)acetamide (**S**)-**3.099** (29 mg, 0.061 mmol, 49% yield) as a white solid. LCMS (Formic, ES⁺) *t*_R = 0.96 min, *m/z* = 472.2, 474.2; HRMS (C₁₇H₂₂BrN₅O₄S): [M+H]⁺ calculated 472.0654, found 472.0658; ¹H NMR (CDCl₃-*d*, 400 MHz): δ (ppm) 9.17 (s, 1H), 8.19 (d, *J*=2.7 Hz, 1H), 7.81–7.92 (m, 2H), 7.67 (d, *J*=8.6 Hz, 1H), 5.33 (s, 2H), 4.64 (s, 2H), 3.53–3.62 (m, 2H), 3.44 (s, 3H), 3.36–3.43 (m, 1H), 2.93 (dd, *J*=9.4, 7.9 Hz, 1H), 2.28–2.39 (m, 1H), 2.00–2.10 (m, 1H), 1.51–1.64 (m, 1H), 1.04 (d, *J*=6.8 Hz, 3H); ¹³C NMR (CDCl₃-*d*, 101 MHz): δ (ppm) 163.7, 145.6, 138.8, 137.0, 136.2, 124.8, 124.5, 123.3, 114.6, 65.8, 58.5, 54.6, 53.3, 47.8, 33.8, 33.6, 17.4; IR *v*_{max} (cm⁻¹) 2964, 1706, 1586, 1532, 1459, 1139, 620, 536.

(*S*)-*N*-(4-Bromo-3-((3-methylpyrrolidin-1-yl)sulfonyl)phenyl)-2-(4-((dimethylamino)methyl)-1*H*-1,2,3-triazol-1-yl)acetamide, formic acid salt (**S**)-**3.100**

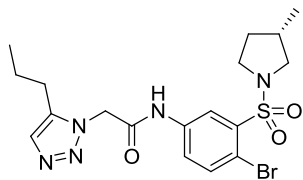


(*S*)-2-Azido-*N*-(4-bromo-3-((3-methylpyrrolidin-1-yl)sulfonyl)phenyl)acetamide (**S**)-**3.096** (50 mg, 0.124 mmol), *N,N*-dimethylprop-2-yn-1-amine (0.02 mL, 0.137 mmol), CuSO₄·5H₂O (2 mg, 6.21 μmol) and sodium ascorbate (4 mg, 0.019 mmol) were dissolved in a mixture of CH₂Cl₂ (1.0 mL)

and water (1.0 mL). The resulting solution was stirred at rt for 16 h. The reaction was diluted with water (10 mL) and extracted with CH₂Cl₂ (3 x 10 mL). The combined organics were passed through a hydrophobic frit and concentrated *in vacuo* to afford the crude product. The crude product was purified by formic MDAP. The pure fractions were concentrated *in vacuo* to afford (*S*)-*N*-(4-bromo-3-((3-methylpyrrolidin-1-yl)sulfonyl)phenyl)-2-(4-((dimethylamino)methyl)-1*H*-1,2,3-triazol-1-yl)acetamide, formic acid salt (**S**)-**3.100** (39 mg, 0.073 mmol, 59% yield) as a white solid. LCMS (Formic, ES⁺) *t*_R = 0.60 min, *m/z* = 485.2, 487.2; HRMS (C₁₈H₂₅BrN₆O₃S): [M+H]⁺ calculated 485.0970, found 485.0975; ¹H NMR (DMSO-*d*₆, 600 MHz): δ (ppm) 10.91 (s, 1H), 8.31 (d, *J*=2.8 Hz, 1H), 8.00 (s, 1H), 7.82 (d, *J*=8.8 Hz, 1H), 7.72 (dd, *J*=8.8, 2.8 Hz, 1H), 5.34 (s, 2H), 3.55 (s, 2H), 3.47 (dd, *J*=9.5, 7.0 Hz, 1H), 3.42 (td, *J*=8.8, 4.0 Hz, 1H), 3.29 (dt, *J*=9.5, 7.7 Hz, 1H), 2.80–2.85 (m, 1H), 2.22–2.29 (m, 1H), 2.18 (s, 6H), 1.96–2.03

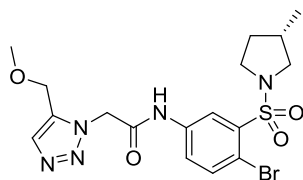
(m, 1H), 1.46-1.53 (m, 1H), 0.95 (d, $J=7.0$ Hz, 3H); NOE was observed upon irradiation of 8.00 to 5.34, 3.55, and 2.18; ^{13}C NMR (CDCl_3 - d , 101 MHz): δ (ppm) 163.6, 139.0, 137.4, 136.3, 134.7, 133.9, 124.5, 122.7, 114.3, 54.5, 52.6, 51.3, 47.6, 45.0, 33.8, 33.6, 17.4.

(S)-N-(4-Bromo-3-((3-methylpyrrolidin-1-yl)sulfonyl)phenyl)-2-(5-propyl-1H-1,2,3-triazol-1-yl)acetamide ((S)-3.101)



(S)-2-Azido-*N*-(4-bromo-3-((3-methylpyrrolidin-1-yl)sulfonyl)phenyl)acetamide **(S)-3.096** (40 mg, 0.099 mmol), pent-1-yne (0.02 mL, 0.149 mmol), and $\text{Cp}^*\text{RuCl}(\text{PPh}_3)_2$ (2 mg, 2.98 μmol) were dissolved in THF (1 mL) at rt under nitrogen. The resulting solution was stirred at 65 °C for 2 h. The reaction was quenched with water (2 mL) and extracted with CH_2Cl_2 (2 x 2 mL). The combined organics were passed through a hydrophobic frit and concentrated *in vacuo* to afford the crude product. The crude product was purified by formic MDAP. The pure fractions were concentrated *in vacuo* to afford (S)-*N*-(4-bromo-3-((3-methylpyrrolidin-1-yl)sulfonyl)phenyl)-2-(5-propyl-1H-1,2,3-triazol-1-yl)acetamide **(S)-3.101** (24 mg, 0.051 mmol, 51% yield) as a cream solid. LCMS (Formic, ES^+) $t_{\text{R}} = 1.08$ min, $m/z = 470.3, 472.3$; HRMS ($\text{C}_{18}\text{H}_{24}\text{BrN}_5\text{O}_3\text{S}$): $[\text{M}+\text{H}]^+$ calculated 470.0861, found 470.0865; ^1H NMR ($\text{DMSO}-d_6$, 400 MHz): δ (ppm) 10.94 (s, 1H), 8.30 (d, $J=2.6$ Hz, 1H), 7.83 (d, $J=8.6$ Hz, 1H), 7.73 (dd, $J=8.6, 2.6$ Hz, 1H), 7.57 (s, 1H), 5.29 (s, 2H), 3.39–3.52 (m, 2H), 3.30–3.34 (m, 1H), 2.84 (dd, $J=9.4, 7.5$ Hz, 1H), 2.63 (t, $J=7.5$ Hz, 2H), 2.18–2.34 (m, 1H), 1.93–2.07 (m, 1H), 1.63–1.64 (m, 2H), 1.51 (dq, $J=12.3, 8.3$ Hz, 1H), 0.89–1.03 (m, 6H); ^{13}C NMR ($\text{DMSO}-d_6$, 101 MHz): δ (ppm) 165.4, 139.1, 138.9, 138.6, 136.7, 131.9, 124.4, 121.9, 113.0, 54.7, 50.6, 47.8, 33.6, 33.4, 24.7, 21.3, 17.6, 14.0; m.p. 145.0 – 150.0 °C; IR ν_{max} (cm^{-1}) 2970, 1693, 1531, 1461, 584.

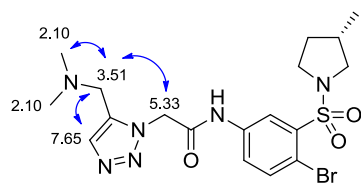
(S)-N-(4-Bromo-3-((3-methylpyrrolidin-1-yl)sulfonyl)phenyl)-2-(5-(methoxymethyl)-1H-1,2,3-triazol-1-yl)acetamide ((S)-3.102)



(S)-2-Azido-*N*-(4-bromo-3-((3-methylpyrrolidin-1-yl)sulfonyl)phenyl)acetamide (50 mg, 0.124 mmol), 3-methoxyprop-1-yne **(S)-3.096** (13 mg, 0.186 mmol), and $\text{Cp}^*\text{RuCl}(\text{PPh}_3)_2$ (3 mg, 3.73 μmol) were dissolved in THF (1 mL) at rt under nitrogen. The resulting solution was stirred at 65 °C for 18 h. The reaction was quenched with water (2 mL) and extracted with CH_2Cl_2 (2 x 2 mL). The combined organics were passed through a hydrophobic frit and concentrated *in vacuo* to afford the crude product. The crude product

was purified by formic MDAP. The pure fractions were concentrated *in vacuo* to afford (*S*)-*N*-(4-bromo-3-((3-methylpyrrolidin-1-yl)sulfonyl)phenyl)-2-(5-(methoxymethyl)-1*H*-1,2,3-triazol-1-yl)acetamide (**S**)-**3.102** (13 mg, 0.028 mmol, 22% yield) as a cream solid. LCMS (Formic, ES⁺) t_R = 0.97 min, m/z = 472.2, 474.2; HRMS (C₁₇H₂₂BrN₅O₄S): [M+H]⁺ calculated 472.0654, found 472.0651; ¹H NMR (CDCl₃-*d*, 400 MHz): δ (ppm) 8.78 (s, 1H), 8.10 (d, J =2.7 Hz, 1H), 7.87 (dd, J =8.6, 2.7 Hz, 1H), 7.75 (s, 1H), 7.68 (d, J =8.6 Hz, 1H), 5.34 (s, 2H), 4.65 (s, 2H), 3.53–3.63 (m, 2H), 3.37–3.46 (m, 4H), 2.94 (dd, J =9.4, 7.9 Hz, 1H), 2.27–2.40 (m, 1H), 2.01–2.11 (m, 1H), 1.52–1.64 (m, 1H), 1.05 (d, J =6.6 Hz, 3H); ¹³C NMR (CDCl₃-*d*, 101 MHz): δ (ppm) 163.8, 139.0, 136.9, 136.2, 134.6, 134.1, 124.7, 123.1, 114.7, 62.6, 58.7, 54.6, 52.0, 47.7, 33.8, 33.6, 17.4; m.p. 63.1 – 69.9 °C; IR ν_{max} (cm⁻¹) 2970, 1699, 1585, 1532, 1460, 1153, 585.

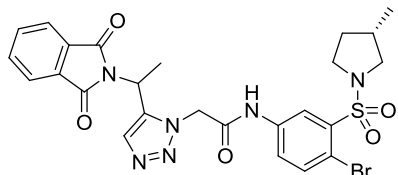
(S)-N-(4-Bromo-3-((3-methylpyrrolidin-1-yl)sulfonyl)phenyl)-2-(5-((dimethylamino)methyl)-1*H*-1,2,3-triazol-1-yl)acetamide, formic acid salt ((S)-3.103)



(*S*)-2-azido-*N*-(4-bromo-3-((3-methylpyrrolidin-1-yl)sulfonyl)phenyl)acetamide (**S**)-**3.096** (150 mg, 0.373 mmol), *N,N*-dimethylprop-2-yn-1-amine (47 mg, 0.559 mmol), and Cp**Ru*Cl(PPh₃)₂ (9 mg, 0.011 mmol) were

dissolved in THF (3 mL) at rt under nitrogen. The resulting solution was stirred at 65 °C for 2 h. The reaction was quenched with water (2 mL) and extracted with CH₂Cl₂ (2 x 2 mL). The combined organics were passed through a hydrophobic frit and concentrated *in vacuo* to afford the crude product. The crude product was purified by silica chromatography, eluting with 0-25% EtOH/EtOAc. The pure fractions were concentrated *in vacuo* to afford the second crude product. The second crude was purified by HPH MDAP. The pure fractions were concentrated *in vacuo* to afford (*S*)-*N*-(4-bromo-3-((3-methylpyrrolidin-1-yl)sulfonyl)phenyl)-2-(5-((dimethylamino)methyl)-1*H*-1,2,3-triazol-1-yl)acetamide (**S**)-**3.103** (82 mg, 0.169 mmol, 45% yield) as a cream solid. LCMS (Formic, ES⁺) t_R = 0.63 min, m/z = 485.3, 487.2; HRMS (C₁₈H₂₅BrN₆O₃S): [M+H]⁺ calculated 485.0970, found 485.0969; ¹H NMR (DMSO-*d*₆, 600 MHz): δ (ppm) 8.27 (d, J =2.6 Hz, 1H), 7.81 (d, J =8.5 Hz, 1H), 7.71 (dd, J =8.5, 2.6 Hz, 1H), 7.65 (s, 1H), 5.33 (s, 2H), 3.51 (s, 2H), 3.47 (dd, J =9.5, 7.0 Hz, 1H), 3.40-3.45 (m, 1H), 3.29 (dt, J =9.6, 7.7 Hz, 1H), 2.83 (dd, J =9.2, 7.7 Hz, 1H), 2.20-2.30 (m, 1H), 2.10 (s, 6H), 1.95-2.02 (m, 1H), 1.45-1.54 (m, 1H), 0.95 (d, J =7.0 Hz, 3H); NOE was observed upon irradiation of 3.51 to 5.33, 7.65 and 2.10; ¹³C NMR (DMSO-*d*₆, 101 MHz): δ (ppm) 164.9, 138.3, 138.2, 136.2, 135.2, 133.1, 123.9, 121.4, 112.2, 54.2, 50.9, 50.8, 47.3, 44.7, 33.0, 32.8, 17.1.

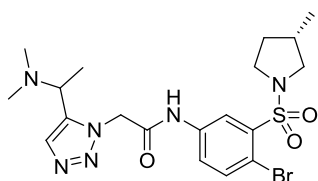
***N*-(4-Bromo-3-(((*S*)-3-methylpyrrolidin-1-yl)sulfonyl)phenyl)-2-(5-(1-(1,3-dioxisoindol-2-yl)ethyl)-1*H*-1,2,3-triazol-1-yl)acetamide (3.104)**, mixture of diastereomers



(*S*)-2-Azido-*N*-(4-bromo-3-((3-methylpyrrolidin-1-yl)sulfonyl)phenyl)acetamide (**S**)-3.096 (60 mg, 0.149 mmol), (\pm)-2-(but-3-yn-2-yl)isoindoline-1,3-dione (**\pm**)-3.109 (45 mg, 0.224 mmol), and Cp**RuCl*(PPh₃)₂ (4 mg, 4.47 μ mol) were

dissolved in THF (3 mL) at rt under nitrogen. The resulting solution was stirred at 65 °C for 2 h. The reaction was allowed to cool before quenching with water (5 mL) and extracting with CH₂Cl₂ (2 x 5 mL). The combined organics were passed through a hydrophobic frit and concentrated *in vacuo* to afford the crude product. The crude product was purified using HPH MDAP. The pure fractions were concentrated *in vacuo* to afford *N*-(4-bromo-3-(((*S*)-3-methylpyrrolidin-1-yl)sulfonyl)phenyl)-2-(5-(1-(1,3-dioxisoindolin-2-yl)ethyl)-1*H*-1,2,3-triazol-1-yl)acetamide **3.104** (38 mg, 0.063 mmol, 42% yield) as a colourless gum and a mixture of diastereomers. LCMS (formic, ES⁺) t_R = 1.08 min, m/z = 601.3, 603.3; ¹H NMR (CDCl₃-*d*, 400 MHz): δ (ppm) 8.04 (s, 1H), 7.86 (t, J =2.4 Hz, 1H), 7.69–7.73 (m, 1H), 7.62–7.70 (m, 4H), 7.53 (d, J =8.6 Hz, 1H), 7.33–7.38 (m, 1H), 5.66 (q, J =7.1 Hz, 1H), 5.37 (d, J =16.9 Hz, 1H), 5.10 (d, J =16.9 Hz, 1H), 3.49–3.59 (m, 2H), 3.32–3.43 (m, 1H), 2.87–2.96 (m, 1H), 2.27–2.39 (m, 1H), 2.02–2.10 (m, 1H), 1.99 (d, J =7.1 Hz, 3H), 1.59–1.61 (m, 1H), 1.06 (d, J =6.6 Hz, 3H); *Diastereotopic protons not visible.*

***N*-(4-Bromo-3-(((*S*)-3-methylpyrrolidin-1-yl)sulfonyl)phenyl)-2-(5-(1-(dimethylamino)ethyl)-1*H*-1,2,3-triazol-1-yl)acetamide (3.105)**, mixture of diastereomers

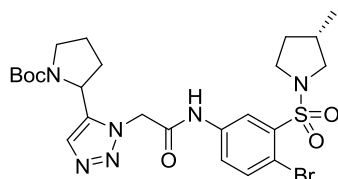


To a solution of *N*-(4-bromo-3-(((*S*)-3-methylpyrrolidin-1-yl)sulfonyl)phenyl)-2-(5-(1-(1,3-dioxisoindolin-2-yl)ethyl)-1*H*-1,2,3-triazol-1-yl)acetamide, mixture of diastereomers **3.104** (28 mg, 0.047 mmol) in EtOH (2 mL) was added hydrazine hydrate (7 μ L, 0.070 mmol). The mixture was stirred at rt for 10 min then at reflux for a further 30 min. The mixture was allowed to cool to rt before the addition of a 2 M solution of NaOH (10 mL). The EtOH was evaporated and the residual aq. suspension was then extracted with EtOAc (3 x 10 mL). The combined organics were passed through a hydrophobic frit and concentrated *in vacuo* to give the *free primary amine* which was used without further purification. The *free primary amine* was dissolved in MeOH (2 mL). Formaldehyde (37% w/w

GSK Confidential – Do not copy

in water, 9 μ L, 0.116 mmol) and STAB (25 mg, 0.116 mmol) were added and the resulting solution stirred at rt for 2 h. The reaction was quenched with water (2 mL) and extracted with CH_2Cl_2 (2 x 5 mL). The combined organics were passed through a hydrophobic frit and concentrated *in vacuo* to afford the crude product. The crude product was purified by HPH MDAP. The pure fractions were concentrated *in vacuo* to afford *N*-(4-bromo-3-(((*S*)-3-methylpyrrolidin-1-yl)sulfonyl)phenyl)-2-(5-(1-(dimethylamino)ethyl)-1*H*-1,2,3-triazol-1-yl)acetamide **3.105** (9 mg, 0.019 mmol, 40% yield) as a white solid and a mixture of diastereomers. LCMS (formic, ES^+), $t_{\text{R}} = 0.65$ min, $m/z = 499.3, 501.4$; ^1H NMR (MeOD- d_4 , 400 MHz): δ (ppm) 8.35 (d, $J=2.4$ Hz, 1H), 7.79 (d, $J=8.6$ Hz, 1H), 7.73 (dd, $J=8.6, 2.4$ Hz, 1H), 7.69 (s, 1H), 5.42 (ABq, $J=16.9$ Hz, 2H), 4.04 (q, $J=6.6$ Hz, 1H), 3.52–3.62 (m, 2H), 3.38–3.44 (m, 1H), 2.90–2.96 (m, 1H), 2.28–2.39 (m, 1H), 2.19 (s, 6H), 2.07–2.13 (m, 1H), 1.55–1.64 (m, 1H), 1.41 (d, $J=6.6$ Hz, 3H), 1.04 (d, $J=6.8$ Hz, 3H); *Amide NH not visible; Diastereotopic protons not visible.*

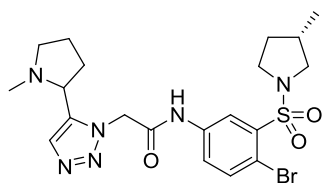
tert-Butyl 2-(1-(2-((4-bromo-3-(((*S*)-3-methylpyrrolidin-1-yl)sulfonyl)phenyl)amino)-2-oxoethyl)-1*H*-1,2,3-triazol-5-yl)pyrrolidine-1-carboxylate (3.106), mixture of diastereomers



(*S*)-2-Azido-*N*-(4-bromo-3-((3-methylpyrrolidin-1-yl)sulfonyl)phenyl)acetamide (**S**)-**3.096** (60 mg, 0.149 mmol), *tert*-butyl 2-ethynylpyrrolidine-1-carboxylate (44 mg, 0.224 mmol), and $\text{Cp}^*\text{RuCl}(\text{PPh}_3)_2$ (4 mg, 4.47 μ mol) were dissolved in THF (1 mL)

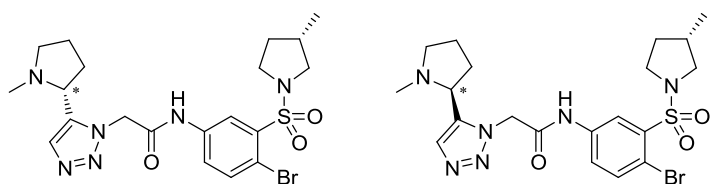
at rt under nitrogen. The resulting solution was stirred at 65 $^\circ\text{C}$ for 2 h. The reaction was quenched with water (2 mL) and extracted with CH_2Cl_2 (2 x 2 mL). The combined organics were passed through a hydrophobic frit and concentrated *in vacuo* to afford the crude product. The crude product was purified by HPH MDAP. The pure fractions were concentrated *in vacuo* to afford *tert*-butyl 2-(1-(2-((4-bromo-3-(((*S*)-3-methylpyrrolidin-1-yl)sulfonyl)phenyl)amino)-2-oxoethyl)-1*H*-1,2,3-triazol-5-yl)pyrrolidine-1-carboxylate **3.106** (73 mg, 0.122 mmol, 82% yield) as a white solid and a mixture of diastereomers. LCMS (Formic, ES^+) $t_{\text{R}} = 1.20$ min, $m/z = 597.2, 599.2$; ^1H NMR (CDCl_3 - d , 400 MHz): δ (ppm) 8.85 (s, 1H), 8.19 (br. s., 1H), 7.80 (d, $J=6.1$ Hz, 1H), 7.66 (d, $J=8.8$ Hz, 1H), 7.60 (s, 1H), 5.36–5.45 (m, 1H), 5.19 (br. s., 1H), 4.91–4.96 (m, 1H), 3.55–3.65 (m, 4H), 3.37–3.46 (m, 1H), 2.88–2.99 (m, 1H), 2.32–2.45 (m, 2H), 2.03–2.10 (m, 2H), 1.92–2.00 (m, 1H), 1.58–1.64 (m, 2H), 1.44 (br. s., 9H), 1.06 (d, $J=6.6$, 3H); *Diastereotopic protons not visible.*

***N*-(4-Bromo-3-(((*S*)-3-methylpyrrolidin-1-yl)sulfonyl)phenyl)-2-(5-(1-methylpyrrolidin-2-yl)-1*H*-1,2,3-triazol-1-yl)acetamide (3.107)**, mixture of diastereomers



HCl (4 M in dioxane, 2 mL, 8.00 mmol) was added to *tert*-butyl 2-(1-(2-((4-bromo-3-(((*S*)-3-methylpyrrolidin-1-yl)sulfonyl)phenyl)amino)-2-oxoethyl)-1*H*-1,2,3-triazol-5-yl)pyrrolidine-1-carboxylate, mixture of diastereomers **3.106** (70 mg, 0.117 mmol) at rt under air. The resulting solution was stirred at rt for 4 h. The reaction was concentrated *in vacuo* to afford the *free secondary amine*. The *free secondary amine* was dissolved in MeOH (1 mL) and formaldehyde (37% w/w in water, 0.012 mL, 0.151 mmol) was added, followed by STAB (32 mg, 0.151 mmol) and the resulting solution stirred at rt for 2 h. The reaction was quenched with water (2 mL) and extracted with CH₂Cl₂ (2 x 5 mL). The combined organics were passed through a hydrophobic frit and concentrated *in vacuo* to afford the crude product. The crude product was purified by HPH MDAP. The pure fractions were concentrated *in vacuo* to afford *N*-(4-bromo-3-(((*S*)-3-methylpyrrolidin-1-yl)sulfonyl)phenyl)-2-(5-(1-methylpyrrolidin-2-yl)-1*H*-1,2,3-triazol-1-yl) acetamide **3.107** (45 mg, 0.087 mmol, 87% yield) as a white solid and a mixture of diastereomers. LCMS (formic, ES⁺), *t*_R = 0.67 min, *m/z* = 511.2, 513.2; HRMS (C₂₀H₂₇BrN₆O₃S): [M+H]⁺ calculated 511.1127, found 511.1127; ¹H NMR (CDCl₃-*d*, 400 MHz): δ (ppm) 9.54 (s, 1H), 8.11 (d, *J*=2.7 Hz, 1H), 7.85 (dd, *J*=8.6, 2.7 Hz, 1H), 7.66 (s, 1H), 7.64 (d, *J*=8.6 Hz, 1H), 5.52 (d, *J*=16.0 Hz, 1H), 5.35 (d, *J*=16.0 Hz, 1H), 3.51–3.62 (m, 3H), 3.34–3.42 (m, 1H), 3.16–3.25 (m, 1H), 2.91 (dd, *J*=9.4, 7.9 Hz, 1H), 2.28–2.41 (m, 3H), 2.24 (s, 3H), 2.03–2.08 (m, 1H), 1.96–2.01 (m, 1H), 1.85–1.94 (m, 2H), 1.50–1.61 (m, 1H), 1.03 (d, *J*=6.6 Hz, 3H); ¹³C NMR (CDCl₃-*d*, 101 MHz): δ (ppm) 164.3, 139.3, 138.9, 137.3, 136.2, 133.4, 124.7, 123.0, 114.3, 60.4, 56.4, 54.6, 52.1, 47.7, 40.8, 33.8, 33.6, 31.9, 23.0, 17.4.

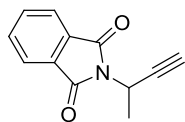
***(S,R*)*-N-(4-Bromo-3-(((*S*)-3-methylpyrrolidin-1-yl)sulfonyl)phenyl)-2-(5-(1-methylpyrrolidin-2-yl)-1*H*-1,2,3-triazol-1-yl)acetamide ((*S,R**)-3.107)** and ***(S,S*)*-N-(4-bromo-3-(((*S*)-3-methylpyrrolidin-1-yl)sulfonyl)phenyl)-2-(5-(1-methylpyrrolidin-2-yl)-1*H*-1,2,3-triazol-1-yl)acetamide ((*S,S**)-3.107)**



N-(4-bromo-3-(((*S*)-3-methylpyrrolidin-1-yl)sulfonyl)phenyl)-2-(5-(1-(dimethylamino)ethyl)-1*H*-1,2,3-triazol-1-yl)

acetamide **3.107** was dissolved in EtOH (1 mL) and injected onto the column (column: 250 mm x 30 mm Chiralpak AD-H, 5 μ m), eluting with 40% (EtOH + 2% isopropylamine)/(heptane + 2% isopropylamine), flow rate = 30 mL min⁻¹, detection wavelength 215 nm. The pure fractions from peak 1 were concentrated *in vacuo* to afford (*S,R**)-*N*-(4-Bromo-3-(((*S*)-3-methylpyrrolidin-1-yl)sulfonyl)phenyl)-2-(5-(1-methylpyrrolidin-2-yl)-1*H*-1,2,3-triazol-1-yl) acetamide (**(*S,R**)-3.107**) (10 mg, 0.020 mmol) as a white solid and the pure fractions from peak 2 were concentrated *in vacuo* to afford (*S,S**)-*N*-(4-bromo-3-(((*S*)-3-methylpyrrolidin-1-yl)sulfonyl)phenyl)-2-(5-(1-methylpyrrolidin-2-yl)-1*H*-1,2,3-triazol-1-yl)acetamide (**(*S,S**)-3.107**) (11 mg, 0.022 mmol) as a white solid. *Data consistent with distereomeric mixture (3.107)*; Chiral LC: 4.6 mm x 250 mm Chiralpak AD-H column, 40% (EtOH + 2% isopropylamine)/heptane, (**(*S,R**)-3.107**): t_R = 10.292 min; *dr* 98:2; (**(*S,S**)-3.107**): t_R = 13.782 min; *dr* 98:1.

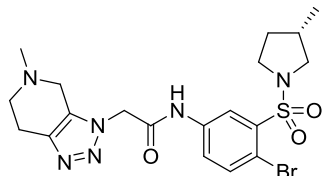
(\pm)-2-(But-3-yn-2-yl)isoindoline-1,3-dione (3.109**)**³³⁷



TEA (1.193 mL, 8.56 mmol) and methanesulfonic anhydride (746 mg, 4.28 mmol) were added to but-3-yn-2-ol (**(\pm)-3.108**) (0.224 mL, 2.85 mmol) in CH₂Cl₂ (2 mL) at rt under air. The resulting solution was stirred at rt for 1 h. The reaction was diluted with water (5 mL) and extracted with CH₂Cl₂ (3 x 5 mL). The combined organics were passed through a hydrophobic frit and concentrated *in vacuo* to afford the crude *mesylate* intermediate. The crude *mesylate* intermediate was dissolved in DMF (3 mL). Potassium 1,3-dioxoisoindolin-2-ide (793 mg, 4.28 mmol) was added and the reaction stirred at 80 °C for 1 h. The reaction was quenched with ice water (10 mL) and extracted with CH₂Cl₂ (3 x 10 mL). The combined organics were pass through a hydrophobic frit and concentrated *in vacuo* to afford the crude product. The crude product was purified by silica chromatography, eluting with 0-80% EtOAc/cyclohexane. The pure fractions were concentrated *in vacuo* to afford (\pm)-2-(but-3-yn-2-yl)isoindoline-1,3-dione (**(\pm)-3.109**) (220 mg, 1.104 mmol, 39% yield) as a white solid. LCMS (formic, ES⁺) t_R = 0.94 min, *no m/z*; HRMS (C₁₂H₉NO₂): [M+H]⁺ calculated 200.0712, found 200.0704; ¹H NMR (CDCl₃-*d*, 400 MHz): δ (ppm) 7.85–7.92 (m, 2H), 7.72–7.78 (m, 2H), 5.24 (qd, *J*=7.3, 2.5 Hz, 1H), 2.36 (d, *J*=2.5 Hz,

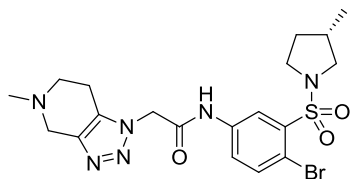
1H), 1.74 (d, $J=7.3$ Hz, 3H); ^{13}C NMR (CDCl_3 - d , 101 MHz): δ (ppm) 166.9, 134.1, 131.9, 123.4, 81.1, 71.2, 36.9, 20.0; IR ν_{max} (cm^{-1}) 3266, 2980, 1712, 1386, 719.

(S)-N-(4-Bromo-3-((3-methylpyrrolidin-1-yl)sulfonyl)phenyl)-2-(5-methyl-4,5,6,7-tetrahydro-3H-[1,2,3]triazolo[4,5-c]pyridin-3-yl)acetamide ((S)-3.110)



Iodomethane (6.23 μl , 0.100 mmol) was added to (S)-2-(3H-[1,2,3]triazolo[4,5-c]pyridin-3-yl)-N-(4-bromo-3-((3-methylpyrrolidin-1-yl)sulfonyl)phenyl)acetamide **(S)-3.084** (40 mg, 0.083 mmol) in MeCN (2 mL) at rt under air. The resulting solution was refluxed at 80 $^{\circ}\text{C}$ for 8 h. The reaction mixture was allowed to cool and concentrated *in vacuo* to afford the *methyl pyridinium intermediate*. The residue was dissolved in a 1:1 mixture of MeOH (1 mL) and water (1 mL) before NaBH_4 (7 mg, 0.184 mmol) was added and the resulting solution was stirred at rt for 30 min. The reaction was quenched with water (5 mL) and extracted with EtOAc (3 x 5 mL). The combined organics were passed through a hydrophobic frit and concentrated *in vacuo* to afford the crude product. The crude product was purified by HPH MDAP. The pure fractions were concentrated *in vacuo* to afford (S)-N-(4-bromo-3-((3-methylpyrrolidin-1-yl)sulfonyl)phenyl)-2-(5-methyl-4,5,6,7-tetrahydro-3H-[1,2,3]triazolo[4,5-c]pyridin-3-yl) acetamide **(S)-3.110** (12 mg, 0.025 mmol, 29% yield) as a white solid. LCMS (formic, ES^+) t_{R} = 0.66 min, m/z = 497.2, 499.2; HRMS ($\text{C}_{19}\text{H}_{25}\text{BrN}_6\text{O}_3\text{S}$): $[\text{M}+\text{H}]^+$ calculated 497.0969, found 497.0970; ^1H NMR (CDCl_3 - d , 400 MHz): δ (ppm) 9.27 (br. s., 1H), 8.20 (d, $J=2.7$ Hz, 1H), 7.86 (dd, $J=8.8, 2.7$ Hz, 1H), 7.67 (d, $J=8.8$ Hz, 1H), 5.18 (s, 2H), 3.66 (s, 2H), 3.52–3.63 (m, 2H), 3.35–3.46 (m, 1H), 2.89–2.99 (m, 3H), 2.76–2.86 (m, 2H), 2.54 (s, 3H), 2.26–2.39 (m, 1H), 1.99–2.11 (m, 1H), 1.58 (dq, $J=12.3, 8.5$ Hz, 1H), 1.05 (d, $J=6.8$ Hz, 3H); ^{13}C NMR (CDCl_3 - d , 101 MHz): δ (ppm) 163.6, 142.2, 139.0, 137.0, 136.2, 132.6, 124.7, 123.3, 114.7, 54.6, 52.1, 51.6, 49.5, 47.7, 45.1, 33.8, 33.6, 22.2, 17.4; m.p. 106.5 – 109.5 $^{\circ}\text{C}$; IR ν_{max} (cm^{-1}) 2970, 1705, 1585, 1534, 1460, 1148, 621, 589.

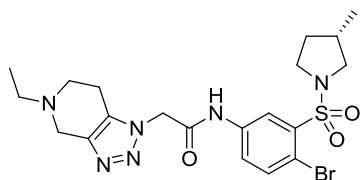
(S)-N-(4-Bromo-3-((3-methylpyrrolidin-1-yl)sulfonyl)phenyl)-2-(5-methyl-4,5,6,7-tetrahydro-1H-[1,2,3]triazolo[4,5-c]pyridin-1-yl)acetamide ((S)-3.111)



Iodomethane (8 μL , 0.125 mmol) was added to (S)-2-(1H-[1,2,3]triazolo[4,5-c]pyridin-1-yl)-N-(4-bromo-3-((3-methylpyrrolidin-1-yl)sulfonyl)phenyl)acetamide **(S)-3.083** (50 mg, 0.104 mmol) in MeCN (2 mL) at rt under air. The resulting

solution was refluxed at 80 °C for 4 h. The reaction was allowed to cool and concentrated *in vacuo* to afford the *methyl pyridinium intermediate*. The residue was dissolved in a 1:1 mixture of MeOH (1 mL) and water (1 mL) before NaBH₄ (9 mg, 0.184 mmol) was added and the resulting solution was stirred at rt for 30 min. The reaction was quenched with water (5 mL) and extracted with EtOAc (3 x 5 mL). The combined organics were passed through a hydrophobic frit and concentrated *in vacuo* to afford the crude product. The crude product was purified by HPH MDAP. The pure fractions were concentrated *in vacuo* to afford (*S*)-*N*-(4-bromo-3-((3-methylpyrrolidin-1-yl)sulfonyl)phenyl)-2-(5-methyl-4,5,6,7-tetrahydro-1*H*-[1,2,3]triazolo [4,5-*c*]pyridin-1-yl)acetamide (**S**)-**3.111** (20 mg, 0.039 mmol, 38% yield) as a white solid. LCMS (formic, ES⁺) t_R = 0.62 min, *m/z* = 497.2, 499.2; HRMS (C₁₉H₂₄BrN₅O₃S): [M+H]⁺ calculated 497.0967, found 497.0964; ¹H NMR (MeOD-*d*₄, 400 MHz): δ (ppm) 8.36 (d, *J*=2.7 Hz, 1H), 7.65–7.80 (m, 2H), 5.29 (s, 2H), 3.66 (s, 2H), 3.49–3.62 (m, 2H), 3.39 (ddd, *J*=9.6, 8.4, 7.2 Hz, 1H), 2.82–2.96 (m, 5H), 2.51–2.57 (m, 3H), 2.27–2.40 (m, 1H), 1.99–2.12 (m, 3H), 1.51–1.65 (m, 1H), 1.04 (d, *J*=6.6 Hz, 3H); *Amide NH not visible*; ¹³C NMR (MeOD-*d*₄, 101 MHz): δ (ppm) 164.5, 141.2, 139.0, 137.8, 136.0, 132.4, 124.0, 122.1, 113.5, 54.3, 51.1, 50.6, 50.2, 47.4, 43.6, 33.6, 33.1, 19.7, 16.3; m.p. 71.2 – 75.2 °C; IR ν_{max} (cm⁻¹) 2970, 1704, 1586, 1532, 1459, 1304, 1143, 620, 587.

(S)-N-(4-Bromo-3-((3-methylpyrrolidin-1-yl)sulfonyl)phenyl)-2-(5-ethyl-4,5,6,7-tetrahydro-1*H*-[1,2,3]triazolo[4,5-*c*]pyridin-1-yl)acetamide ((S)-3.112)

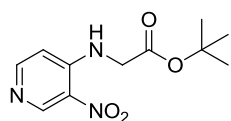


Iodoethane (33 mg, 0.209 mmol) was added to (*S*)-2-(1*H*-[1,2,3]triazolo[4,5-*c*]pyridin-1-yl)-*N*-(4-bromo-3-((3-methylpyrrolidin-1-yl)sulfonyl)phenyl)acetamide (**S**)-**3.083** (100 mg, 0.209 mmol) in MeCN (2 mL) at rt under air. The

resulting solution was refluxed for 18 h. The reaction was allowed to cool and concentrated *in vacuo* to afford the *ethyl pyridinium intermediate*. The intermediate was dissolved in a 1:1 mixture of MeOH (1 mL) and water (1 mL), NaBH₄ (17 mg, 0.459 mmol) was added and the resulting solution was stirred at rt for 30 min. The reaction was quenched with sat. aq. NaHCO₃ (5 mL) and extracted with CH₂Cl₂ (3 x 5 mL). The combined organics were passed through a hydrophobic frit and concentrated *in vacuo* to afford the crude product. The crude product was purified by HPH MDAP. The pure fractions were concentrated *in vacuo* to afford (*S*)-*N*-(4-bromo-3-((3-methylpyrrolidin-1-yl)sulfonyl)phenyl)-2-(5-ethyl-4,5,6,7-tetrahydro-1*H*-[1,2,3]triazolo [4,5-*c*]pyridin-1-yl)acetamide (**S**)-**3.112** (21 mg, 0.041 mmol, 20% yield) as

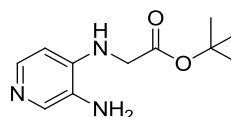
a white solid. LCMS (formic, ES⁺) t_R = 0.63 min, m/z = 511.3, 513.3; HRMS (C₂₀H₂₇BrN₆O₃S): [M+H]⁺ calculated 511.1114, found 511.1125; ¹H NMR (CDCl₃-*d*, 400 MHz): δ (ppm) 9.75 (br. s., 1H), 8.22 (d, J =2.7 Hz, 1H), 7.78 (dd, J =8.8, 2.7 Hz, 1H), 7.62 (d, J =8.8 Hz, 1H), 5.20 (s, 2H), 3.78 (s, 2H), 3.48–3.58 (m, 2H), 3.34–3.41 (m, 1H), 2.82–2.96 (m, 5H), 2.76 (q, J =7.3 Hz, 2H), 2.23–2.36 (m, 1H), 1.96–2.07 (m, 1H), 1.54 (dd, J =12.5, 8.6 Hz, 1H), 1.18–1.25 (m, 3H), 1.02 (d, J =6.6 Hz, 3H); ¹³C NMR (CDCl₃-*d*, 101 MHz): δ (ppm) 164.0, 142.0, 138.8, 137.3, 136.1, 132.6, 124.7, 123.1, 114.3, 54.6, 51.2, 49.3, 48.7, 47.7, 33.7, 33.6, 20.3, 17.4, 12.2, 1.9; m.p. 88.0 – 90.4 °C; IR ν_{\max} (cm⁻¹) 3262, 2965, 1704, 1586, 1533, 1459.

***tert*-Butyl (3-nitropyridin-4-yl)glycinate (3.117)**



4-Chloro-3-nitropyridine **3.116** (3.00 g, 18.92 mmol) and *tert*-butyl glycinate, hydrochloride (3.33 g, 19.87 mmol) were dissolved in EtOH (20 mL). TEA (2.64 mL, 18.92 mmol) was added and the reaction refluxed for 6 h. The reaction was allowed to cool before concentrating *in vacuo*. The residue was partitioned between sat. aq. NaHCO₃ (20 mL) and CH₂Cl₂ (20 mL). The layers were separated and the aq. layer was extracted with CH₂Cl₂ (2 x 20 mL). The combined organics were passed through a hydrophobic frit and concentrated *in vacuo* to afford the crude product. The crude was purified by silica chromatography, eluting with 0-80% EtOAc/cyclohexane. The pure fractions were concentrated *in vacuo* to afford *tert*-butyl (3-nitropyridin-4-yl)glycinate **3.117** (1.58 g, 6.24 mmol, 33% yield) as a yellow solid. LCMS (Formic, ES⁺) t_R = 0.61 min, m/z = 254.2; HRMS (C₁₁H₁₅N₃O₄): [M+H]⁺ calculated 254.1141, found 254.1136; ¹H NMR (CDCl₃-*d*, 400 MHz): δ (ppm) 9.27 (s, 1H), 8.59 (s, 1H), 8.36 (d, J =6.1 Hz, 1H), 6.58 (d, J =6.1 Hz, 1H), 4.02 (d, J =5.1 Hz, 2H), 1.55 (s, 9H); ¹³C NMR (DMSO-*d*₆, 101 MHz): δ (ppm) 168.6, 153.3, 149.0, 148.5, 130.0, 109.6, 82.3, 44.9, 28.2; m.p. 91.2 – 93.3 °C; IR ν_{\max} (cm⁻¹) 3346, 1727, 1623, 1355, 1164, 826, 550.

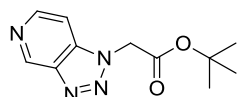
***tert*-Butyl (3-aminopyridin-4-yl)glycinate (3.118)**



tert-Butyl (3-nitropyridin-4-yl)glycinate **3.117** (1.50 g, 5.92 mmol) was suspended in EtOH (30 mL) and water (8 mL). Ammonium chloride (0.48 g, 8.88 mmol) and iron (1.65 g, 29.6 mmol) were added and the reaction heated to 70 °C for 2 h. The reaction mixture was filtered through a 10 g Celite cartridge washing with MeOH (30mL). The filtrate was concentrated *in vacuo* and the residue partitioned between CH₂Cl₂ and water (25 mL each). The aq. layer was re-extracted with

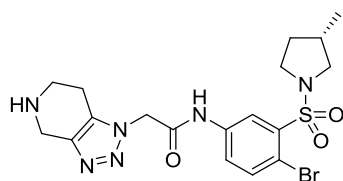
CH₂Cl₂ (2 x 25 mL). The combined organics were eluted through a hydrophobic frit and concentrated *in vacuo* to give *tert*-butyl (3-aminopyridin-4-yl)glycinate **3.118** (1.21 g, 5.42 mmol, 91% yield) as an orange gum. LCMS (formic, ES⁺) *t*_R = 0.39 min, *m/z* = 224.3; ¹H NMR (CDCl₃-*d*, 400 MHz): δ (ppm) 8.00 (d, *J*=5.4 Hz, 1H), 7.95 (s, 1H), 6.37 (d, *J*=5.4 Hz, 1H), 4.67–4.76 (m, 1H), 3.86 (d, *J*=5.1 Hz, 2H), 3.18 (s, 2H), 1.53 (s, 9H).

***tert*-Butyl 2-(1*H*-[1,2,3]triazolo[4,5-*c*]pyridin-1-yl)acetate (3.119)**



tert-Butyl (3-aminopyridin-4-yl)glycinate **3.118** (1.00 g, 4.48 mmol) was suspended in water (10 mL) at 0 °C under air. AcOH (10 mL) was added, followed by sodium nitrite (0.371 g, 5.37 mmol) and the resulting suspension was then placed in a pre-heated stirrer hotplate and stirred at 80 °C for 10 min before it was allowed to cool to rt. The reaction was diluted with water (5 mL) and extracted with CH₂Cl₂ (3 x 20 mL). The combined organics were passed through a hydrophobic frit and concentrated *in vacuo* to afford the crude product. The crude product was purified by silica chromatography, eluting with 0-100% EtOAc/cyclohexane. The pure fractions were concentrated *in vacuo* to afford *tert*-butyl 2-(1*H*-[1,2,3]triazolo[4,5-*c*]pyridin-1-yl)acetate **3.119** (0.39 mg, 1.665 mmol, 37% yield) as a white solid. LCMS (formic, ES⁺) *t*_R = 0.68 min, *m/z* = 235.2; HRMS (C₁₁H₁₄N₄O₂): [M+H]⁺ calculated 235.1195, found 235.1192; ¹H NMR (CDCl₃-*d*, 400 MHz): δ (ppm) 9.51 (d, *J*=1.5 Hz, 1H), 8.62 (d, *J*=5.9 Hz, 1H), 7.44 (dd, *J*=5.9, 1.5 Hz, 1H), 5.36 (s, 2H), 1.48 (s, 9H); ¹³C NMR (DMSO-*d*₆, 101 MHz): δ (ppm) 166.4, 145.2, 144.3, 142.9, 137.5, 106.1, 83.2, 49.8, 28.0; m.p. 96.7 – 98.2 °C; IR *v*_{max} (cm⁻¹) 2978, 1745, 1607, 1369, 1234, 1154, 1081.

(*S*)-*N*-(4-Bromo-3-((3-methylpyrrolidin-1-yl)sulfonyl)phenyl)-2-(4,5,6,7-tetrahydro-1*H*-[1,2,3]triazolo[4,5-*c*]pyridin-1-yl)acetamide ((*S*)-3.120)

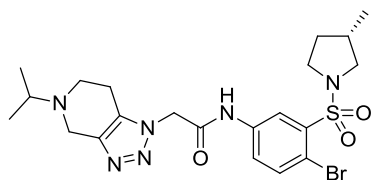


Method 1: (*S*)-2-(1*H*-[1,2,3]triazolo[4,5-*c*]pyridin-1-yl)-*N*-(4-bromo-3-((3-methylpyrrolidin-1-yl) sulfonyl) phenyl) acetamide (**(*S*)-3.083**) (30 mg, 0.063 mmol) was dissolved in a 1:1:1 mixture of MeOH, EtOH and AcOH (12 mL). The resulting solution was hydrogenated over Rh/C on the H-cube apparatus with a flow rate of 1 mL min⁻¹. The apparatus was set up to allow the reaction mixture to cycle through the H-cube for 24 h. The reaction mixture was then concentrated *in vacuo* to afford the crude product. The crude product was purified by HPH MDAP. The pure fractions were concentrated *in vacuo* to afford (*S*)-*N*-(4-bromo-3-((3-methylpyrrolidin-1-yl)sulfonyl)phenyl)-2-(4,5,6,7-tetrahydro-

1*H*-[1,2,3]triazolo[4,5-*c*]pyridin-1-yl)acetamide (**S**)-**3.120** (9 mg, 0.018 mmol, 29% yield) as a cream solid.

Method 2: (*S*)-2-(1*H*-[1,2,3]triazolo[4,5-*c*]pyridin-1-yl)-*N*-(4-bromo-3-((3-methylpyrrolidin-1-yl)sulfonyl)phenyl) acetamide (**S**)-**3.083** (750 mg, 1.565 mmol) and 5% Pt/C B103032-5 JM26 (75 mg, 1.565 mmol) were dissolved in MeOH (3.6 mL) and AcOH (0.1 mL). The resulting solution was placed in a HP ChemSCAN reactor and stirred at 50 °C under 240 psi of hydrogen for 48 h. The reaction was filtered through Celite, washing with MeOH and concentrated *in vacuo* to afford (*S*)-*N*-(4-bromo-3-((3-methylpyrrolidin-1-yl)sulfonyl)phenyl)-2-(4,5,6,7-tetrahydro-1*H*-[1,2,3]triazolo[4,5-*c*]pyridin-1-yl)acetamide (**S**)-**3.120** (500 mg, 1.034 mmol, 66% yield) as a cream solid. LCMS (formic, ES⁺) *t*_R = 0.61 min, *m/z* = 483.2, 485.2; HRMS (C₁₈H₂₃BrN₆O₃S): [M+H]⁺ calculated 483.0814, found 483.0814; ¹H NMR (MeOD-*d*₄, 400 MHz): δ (ppm) 8.31 (d, *J*=2.5 Hz, 1H), 7.82 (d, *J*=8.7 Hz, 1H), 7.73 (dd, *J*=8.7, 2.5 Hz, 1H), 5.28 (s, 2H), 3.95–4.00 (m, 2H), 3.50–3.60 (m, 2H), 3.37 (s, 2H), 3.12 (s, 2H), 2.88–2.97 (m, 1H), 2.76–2.82 (m, 2H), 2.28–2.40 (m, 1H), 2.02–2.13 (m, 1H), 1.52–1.65 (m, 1H), 1.04 (d, *J*=6.6 Hz, 3H); Amide NH not visible; ¹³C NMR (CDCl₃-*d*, 101 MHz): δ (ppm) 163.9, 142.7, 138.9, 137.1, 136.2, 132.9, 124.7, 123.2, 114.5, 54.6, 51.1, 47.7, 42.4, 42.3, 33.8, 33.6, 21.6, 17.4; m.p. 140.0 – 144.8 °C; IR ν_{max} (cm⁻¹) 2959, 1701, 1586, 1533, 1459, 1301, 1149, 621.

(S)-N-(4-Bromo-3-((3-methylpyrrolidin-1-yl)sulfonyl)phenyl)-2-(5-isopropyl-4,5,6,7-tetrahydro-1*H*-[1,2,3]triazolo[4,5-*c*]pyridin-1-yl)acetamide ((S)-3.113)

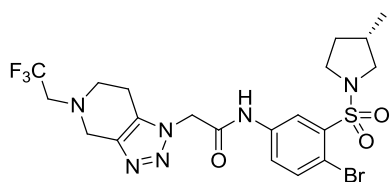


(*S*)-*N*-(4-Bromo-3-((3-methylpyrrolidin-1-yl)sulfonyl)phenyl)-2-(4,5,6,7-tetrahydro-1*H*-[1,2,3]triazolo[4,5-*c*]pyridin-1-yl)acetamide (**S**)-**3.120** (35 mg, 0.072 mmol) and K₂CO₃ (30 mg, 0.217 mmol) were dissolved in acetone

(1 mL). 2-Iodopropane (18 mg, 0.109 mmol) was added and the resulting solution stirred at 80 °C for 4 h. A further 1 eq. of 2-iodopropane was added and the resulting solution stirred at 80 °C for a further 4 h. The reaction was allowed to cool, diluted with water (2 mL) and extracted with CH₂Cl₂ (2 x 2 mL). The combined organics were passed through a hydrophobic frit and concentrated *in vacuo* to afford the crude product. The crude product was purified by HPH MDAP. The pure fractions were concentrated *in vacuo* to afford (*S*)-*N*-(4-bromo-3-((3-methylpyrrolidin-1-yl)sulfonyl)phenyl)-2-(5-isopropyl-4,5,6,7-tetrahydro-1*H*-[1,2,3]triazolo[4,5-*c*]pyridin-1-yl)acetamide (**S**)-**3.113** (22 mg, 0.042 mmol, 58% yield) as a white solid. LCMS (formic, ES⁺) *t*_R = 0.64 min, *m/z* = 525.3, 527.3; HRMS (C₂₁H₂₉BrN₆O₃S): [M+H]⁺

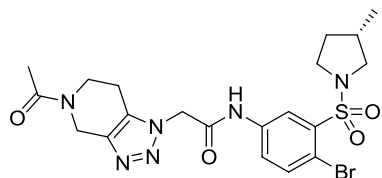
calculated 525.1283, found 525.1280; ^1H NMR (MeOD- d_4 , 400 MHz): δ (ppm) 8.36 (d, $J=2.7$ Hz, 1H), 7.77 (s, 1H), 7.70–7.75 (m, 1H), 3.78 (s, 2H), 3.50–3.59 (m, 2H), 3.36–3.44 (m, 1H), 3.01–3.10 (m, 1H), 2.93 (d, $J=5.1$ Hz, 3H), 2.81–2.87 (m, 2H), 2.29–2.40 (m, 1H), 2.08–2.12 (m, 1H), 2.02–2.04 (m, 1H), 1.52–1.64 (m, 1H), 1.17–1.22 (m, 7H), 1.05 (d, $J=6.6$ Hz, 3H); *Amide NH not visible*; ^{13}C NMR (MeOD- d_4 , 101 MHz): δ (ppm) 164.6, 142.0, 139.0, 137.8, 136.0, 133.1, 124.1, 122.3, 116.7, 56.9, 54.3, 53.8, 50.2, 45.4, 44.1, 33.7, 33.0, 20.4, 17.2, 16.2.

(S)-N-(4-Bromo-3-((3-methylpyrrolidin-1-yl)sulfonyl)phenyl)-2-(5-(2,2,2-trifluoroethyl)-4,5,6,7-tetrahydro-1H-[1,2,3]triazolo[4,5-c]pyridin-1-yl)acetamide ((S)-3.114)



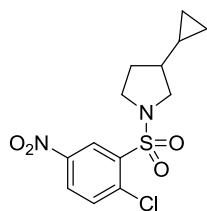
(S)-N-(4-Bromo-3-((3-methylpyrrolidin-1-yl)sulfonyl)phenyl)-2-(4,5,6,7-tetrahydro-1H-[1,2,3]triazolo[4,5-c]pyridin-1-yl)acetamide **(S)-3.120** (40 mg, 0.083 mmol) was dissolved in THF (1 mL) at rt under nitrogen. The resulting

solution was heating to 70 °C, followed by sequential addition of phenylsilane (0.02 mL, 0.165 mmol) and TFA (0.01 mL, 0.145 mmol). The resulting solution was stirred at 70 °C for 1 h. The reaction was allowed to cool, quenched with sat. aq. NaHCO_3 (2 mL) and extracted with CH_2Cl_2 (3 x 2 mL). The combined organics were passed through a hydrophobic frit and concentrated *in vacuo* to afford the crude product. The crude product was purified by formic MDAP. The pure fractions were concentrated *in vacuo* to afford (S)-N-(4-bromo-3-((3-methylpyrrolidin-1-yl)sulfonyl)phenyl)-2-(5-(2,2,2-trifluoroethyl)-4,5,6,7-tetrahydro-1H-[1,2,3]triazolo[4,5-c]pyridin-1-yl)acetamide **(S)-3.114** (20 mg, 0.035 mmol, 43% yield) as a white solid. LCMS (formic, ES^+) $t_{\text{R}} = 1.10$ min, $m/z = 565.0$, 567.0; HRMS ($\text{C}_{20}\text{H}_{24}\text{BrF}_3\text{N}_6\text{O}_3\text{S}$): $[\text{M}+\text{H}]^+$ calculated 565.0844, found 565.0842; ^1H NMR (MeOD- d_4 , 400 MHz): δ (ppm) 8.36 (d, $J=2.5$ Hz, 1H), 7.78 (d, $J=8.6$ Hz, 1H), 7.72 (dd, $J=8.6$, 2.4 Hz, 1H), 5.29 (s, 2H), 3.94 (s, 2H), 3.51–3.61 (m, 2H), 3.34–3.43 (m, $J=9.8$ Hz, 3H), 3.11 (t, $J=5.9$ Hz, 2H), 2.93 (dd, $J=9.5$, 7.8 Hz, 1H), 2.85 (t, $J=5.7$ Hz, 2H), 2.29–2.39 (m, 1H), 2.06–2.11 (m, 1H), 1.53–1.64 (m, 1H), 1.05 (d, $J=6.6$ Hz, 3H); *Amide NH not visible*; ^{13}C NMR (MeOD- d_4 , 101 MHz): δ (ppm) 165.0, 141.0, 138.9, 137.7, 135.9, 135.0, 132.7, 127.2, 123.0 (q, $J=193.2$ Hz), 113.7, 55.9, 54.4, 50.2, 49.7, 49.1, 47.7 (q, $J=21.3$ Hz), 33.6, 33.2, 26.6, 19.8, 16.3; ^{19}F NMR (MeOD- d_4 , 376 MHz): δ (ppm) -71.50.

(S)-2-(5-Acetyl-4,5,6,7-tetrahydro-1H-[1,2,3]triazolo[4,5-c]pyridin-1-yl)-N-(4-bromo-3-((3-methylpyrrolidin-1-yl)sulfonyl)phenyl)acetamide ((S)-3.115)

(S)-N-(4-Bromo-3-((3-methylpyrrolidin-1-yl)sulfonyl)phenyl)-2-(4,5,6,7-tetrahydro-1H-[1,2,3]triazolo[4,5-c]pyridin-1-yl)acetamide **(S)-3.120** (35 mg, 0.072 mmol) was dissolved in CH₂Cl₂ (1 mL) at rt under nitrogen. DIPEA

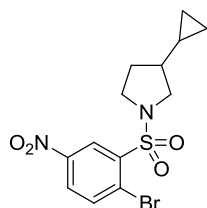
(0.038 mL, 0.217 mmol) was added followed by Ac₂O (10 μL, 0.109 mmol). The resulting solution was stirred at rt for 1 h. The reaction was quenched with sat. aq. NaHCO₃ (2 mL) and extracted with CH₂Cl₂ (3 x 2 mL). The combined organics were passed through a hydrophobic frit and concentrated *in vacuo* to afford the crude product. The crude product was purified by formic MDAP. The pure fractions were concentrated *in vacuo* to afford (S)-2-(5-acetyl-4,5,6,7-tetrahydro-1H-[1,2,3]triazolo[4,5-c]pyridin-1-yl)-N-(4-bromo-3-((3-methylpyrrolidin-1-yl)sulfonyl)phenyl)acetamide **(S)-3.115** (20 mg, 0.039 mmol, 53% yield) as a white solid. LCMS (formic, ES⁺) t_R = 0.89 min. m/z = 525.2, 527.2; HRMS (C₂₀H₂₅BrN₆O₄S): [M+H]⁺ calculated 525.0920, found 525.0920; ¹H NMR (DMSO-*d*₆, 400 MHz, 373 K): δ (ppm) ¹H NMR (DMSO-*d*₆, 400 MHz): d (ppm) 8.36 (d, J=2.7 Hz, 1H), 7.78 (d, J=8.6 Hz, 1H), 7.71 (dd, J=8.6, 2.7 Hz, 1H), 4.64 (s, 2H), 3.79 (t, J=5.7 Hz, 2H), 3.42–3.55 (m, 2H), 3.29–3.39 (m, 1H), 2.89 (dd, J=9.7, 7.2 Hz, 1H), 2.81 (t, J=5.7 Hz, 4H), 2.31 (dd, J=14.3, 7.2 Hz, 1H), 2.12 (s, 3H), 1.99–2.09 (m, 1H), 1.52 (dd, J=12.2, 7.8 Hz, 1H), 1.01 (d, J=6.8 Hz, 3H); Amide NH not visible.

(±)-1-((2-Chloro-5-nitrophenyl)sulfonyl)-3-cyclopropylpyrrolidine ((±)-3.121)

2-Chloro-5-nitrobenzenesulfonyl chloride **3.054** (1.10 g, 4.30 mmol) was taken up in CH₂Cl₂ (50 mL) under nitrogen and cooled to 0 °C. DIPEA (1.65 mL, 9.45 mmol) was added and the reaction stirred for 5 min before (±)-3-cyclopropylpyrrolidine (0.48 g, 4.30 mmol) was added. The reaction was stirred at 0 °C for 2 h. The reaction mixture was quenched with sat. NaHCO₃ (50 mL) and extracted with CH₂Cl₂ (2 x 50 mL). The combined organics were filtered through a hydrophobic frit and concentrated *in vacuo* to give the crude product. The crude product was purified by silica chromatography, eluting with 0-40% cyclohexane/EtOAc. The pure fractions were concentrated *in vacuo* to afford (±)-1-((2-chloro-5-nitrophenyl)sulfonyl)-3-cyclopropylpyrrolidine **(±)-3.121** (1.28 g, 3.87 mmol, 90% yield) as a yellow gum. LCMS (formic, ES⁺) t_R = 1.23 min, m/z = 331.2; HRMS (C₁₃H₁₅ClN₂O₄S): [M+H]⁺ calculated 331.0519, found 331.0510; ¹H NMR (CDCl₃-*d*, 400 MHz): δ (ppm) 8.92 (d, J=2.7 Hz, 1H), 8.33 (dd, J=8.8,

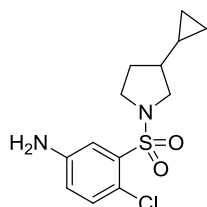
2.7 Hz, 1H), 7.71 (d, $J=8.8$ Hz, 1H), 3.58–3.69 (m, 2H), 3.45 (ddd, $J=9.7, 8.3, 7.2$ Hz, 1H), 3.21 (dd, $J=9.5, 7.8$ Hz, 1H), 2.03–2.15 (m, 1H), 1.80 (dq, $J=12.5, 8.3$ Hz, 1H), 1.60–1.69 (m, 1H), 0.63–0.76 (m, 1H), 0.43–0.55 (m, 2H), 0.08–0.22 (m, 2H); ^{13}C NMR (CDCl_3 - d , 101 MHz): δ (ppm) 146.2, 139.4, 139.0, 133.2, 127.4, 126.7, 52.9, 47.8, 44.4, 31.5, 13.0, 3.7, 3.4; IR ν_{max} (cm^{-1}) 3098, 1601, 1524, 1344, 1162, 884.

(±)-1-((2-Bromo-5-nitrophenyl)sulfonyl)-3-cyclopropylpyrrolidine ((±)-3.122)



2-Bromo-5-nitrobenzenesulfonyl chloride **3.021** (1.30 g, 4.33 mmol) was taken up in CH_2Cl_2 (50 mL) under nitrogen and cooled in an ice bath. DIPEA (1.66 mL, 9.52 mmol) was added and the reaction stirred for 5 min before (±)-3-cyclopropylpyrrolidine (0.48 g, 4.33 mmol) was added. The reaction was stirred for 2 h at 0 °C. The reaction mixture was quenched with sat. NaHCO_3 (50 mL) and extracted with CH_2Cl_2 (2 x 50 mL). The combined organics were filtered through a hydrophobic frit and concentrated *in vacuo* to give the crude product. This was purified by silica chromatography, eluting with 0-30% cyclohexane/EtOAc. The pure fractions were concentrated *in vacuo* to afford (±)-1-((2-bromo-5-nitrophenyl)sulfonyl)-3-cyclopropylpyrrolidine ((±)-**3.122**) (1.38 g, 3.68 mmol, 85% yield) as a yellow gum. LCMS (formic, ES^+) $t_{\text{R}} = 1.24$ min, $m/z = 375.2, 377.2$; HRMS ($\text{C}_{13}\text{H}_{15}\text{BrN}_2\text{O}_4\text{S}$): $[\text{M}+\text{H}]^+$ calculated 375.0014, found 375.0013; ^1H NMR (CDCl_3 - d , 400 MHz): δ (ppm) 8.91 (d, $J=2.8$ Hz, 1H), 8.22 (dd, $J=8.7, 2.8$ Hz, 1H), 7.96 (d, $J=8.6$ Hz, 1H), 3.58–3.68 (m, 2H), 3.41–3.52 (m, 1H), 3.21 (dd, $J=9.5, 7.6$ Hz, 1H), 2.04–2.16 (m, 1H), 1.81 (dq, $J=12.3, 8.4$ Hz, 1H), 1.55–1.71 (m, 1H), 0.62–0.77 (m, 1H), 0.43–0.55 (m, 2H), 0.08–0.23 (m, 2H); ^{13}C NMR (CDCl_3 - d , 101 MHz): δ (ppm) 146.8, 141.2, 136.9, 127.7, 127.2, 126.6, 53.0, 47.9, 44.4, 31.5, 13.0, 3.7, 3.4; IR ν_{max} (cm^{-1}) 3103, 1597, 1526, 1341, 1161, 880, 606.

(±)-4-Chloro-3-((3-cyclopropylpyrrolidin-1-yl)sulfonyl)aniline ((±)-3.123)

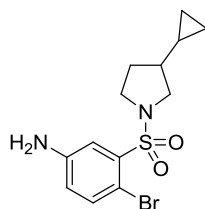


(±)-1-((2-Chloro-5-nitrophenyl)sulfonyl)-3-cyclopropylpyrrolidine ((±)-**3.121**) (1.25 g, 3.78 mmol), ammonium chloride (0.30 g, 5.67 mmol) and iron (0.63 g, 11.34 mmol) were dissolved in EtOH (5.0 mL) and water (1.7 mL). The resulting solution was heated to 70 °C for 2 h. The reaction was allowed to cool then filtered through a plug of Celite, washing with MeOH (20 mL). The resulting solution was concentrated *in vacuo* and then partitioned between sat. aq. NaHCO_3 (20 mL) and CH_2Cl_2 (20 mL). The layers were separated and the aq. layer extracted with CH_2Cl_2

GSK Confidential – Do not copy

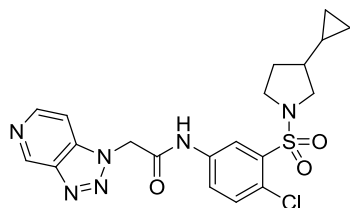
(2 x 20 mL). The combined organics were passed through a hydrophobic frit and concentrated *in vacuo* to afford (±)-4-chloro-3-((3-cyclopropylpyrrolidin-1-yl)sulfonyl)aniline (±)-**3.123** (1.11 g, 3.69 mmol, 98% yield) as a yellow gum. LCMS (formic, ES⁺) $t_R = 1.07$ min, $m/z = 301.1$; HRMS (C₁₃H₁₇ClN₂O₂S): [M+H]⁺ calculated 301.0778, found 301.0771; ¹H NMR (CDCl₃-*d*, 400 MHz): δ (ppm) 7.41 (d, *J*=2.7 Hz, 1H), 7.26 (d, *J*=8.5 Hz, 1H), 6.75 (dd, *J*=8.5, 2.7 Hz, 1H), 3.91 (br. s., 2H), 3.53–3.63 (m, 2H), 3.39 (ddd, *J*=9.5, 8.3, 7.1 Hz, 1H), 3.15 (dd, *J*=9.5, 7.7 Hz, 1H), 1.98–2.09 (m, 1H), 1.74 (dq, *J*=12.3, 8.4 Hz, 1H), 1.56–1.61 (m, 1H), 0.60–0.74 (m, 1H), 0.41–0.52 (m, 2H), 0.08–0.18 (m, 2H); ¹³C NMR (CDCl₃-*d*, 101 MHz): δ (ppm) 145.4, 137.1, 132.5, 120.1, 119.2, 118.0, 52.5, 47.4, 44.3, 31.5, 13.1, 3.6, 3.3; IR ν_{max} (cm⁻¹) 3375, 1596, 1468, 1323, 1159, 590.

(±)-4-Bromo-3-((3-cyclopropylpyrrolidin-1-yl)sulfonyl)aniline ((±)-**3.124**)



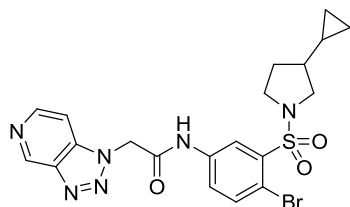
(±)-1-((2-Bromo-5-nitrophenyl)sulfonyl)-3-cyclopropylpyrrolidine (±)-**3.122** (1.30 g, 3.46 mmol), ammonium chloride (0.28 g, 5.20 mmol) and iron (0.58 g, 10.39 mmol) were dissolved in EtOH (5.0 mL) and water (1.7 mL). The resulting solution was heated to 70 °C for 2 h. The reaction was allowed to cool then filtered through a plug of Celite, washing with MeOH (20 mL). The resulting solution was concentrated *in vacuo* and then partitioned between sat. aq. NaHCO₃ (20 mL) and CH₂Cl₂ (20 mL). The layers were separated and the aq. layer extracted with CH₂Cl₂ (2 x 20 mL). The combined organics were passed through a hydrophobic frit and concentrated *in vacuo* to afford the crude product. The crude product was purified by silica chromatography, eluting with 0-100% EtOAc/cyclohexane. The pure fractions were concentrated *in vacuo* to afford (±)-4-bromo-3-((3-cyclopropylpyrrolidin-1-yl)sulfonyl)aniline (±)-**3.124** (1.19 g, 3.45 mmol, 99% yield) as an orange gum. LCMS (formic, ES⁺) $t_R = 1.10$ min, $m/z = 345.2$, 347.2; HRMS (C₁₃H₁₇BrN₂O₂S): [M+H]⁺ calculated 345.0272, found 345.0270; ¹H NMR (CDCl₃-*d*, 400 MHz): δ (ppm) 7.40–7.48 (m, 2H), 6.67 (dd, *J*=8.4, 2.8 Hz, 1H), 3.94 (br. s., 2H), 3.51–3.63 (m, 2H), 3.39 (ddd, *J*=9.5, 8.2, 7.2 Hz, 1H), 3.15 (dd, *J*=9.4, 7.7 Hz, 1H), 1.97–2.11 (m, 1H), 1.69–1.82 (m, 1H), 1.54–1.66 (m, 1H), 0.62–0.75 (m, 1H), 0.39–0.54 (m, 2H), 0.07–0.20 (m, 2H); ¹³C NMR (CDCl₃-*d*, 101 MHz): δ (ppm) 146.0, 138.8, 136.0, 119.4, 118.4, 106.9, 52.5, 47.4, 44.3, 31.5, 13.2, 3.6, 3.3; IR ν_{max} (cm⁻¹) 3374, 1591, 1462, 1312, 1156, 544.

(±)-2-(1*H*-[1,2,3]Triazolo[4,5-*c*]pyridin-1-yl)-*N*-(4-chloro-3-((3-cyclopropylpyrrolidin-1-yl)sulfonyl)phenyl)acetamide ((±)-3.125)



tert-Butyl 2-(1*H*-[1,2,3]triazolo[4,5-*c*]pyridin-1-yl)acetate **3.119** (187 mg, 0.798 mmol) was dissolved in HCl (4 M in dioxane, 1.66 mL, 6.65 mmol) and stirred at rt for 16 h. The reaction mixture was concentrated *in vacuo* to afford the crude acid. (±)-4-Chloro-3-((3-cyclopropylpyrrolidin-1-yl)sulfonyl)aniline (**±**)-**3.123** (200 mg, 0.665 mmol), and HATU (303 mg, 0.798 mmol) were added and the mixture dissolved in CH₂Cl₂ (10 mL). DIPEA (0.348 mL, 1.995 mmol) was added and the resulting solution was stirred at rt for 2 h. The reaction was quenched with sat. aq. NaHCO₃ (10 mL) and extracted with CH₂Cl₂ (3 x 10 mL). The combined organics were passed through a hydrophobic frit and concentrated *in vacuo* to afford the crude product. The crude product was purified by silica chromatography, eluting with 0-100% EtOAc/cyclohexane. The pure fractions were concentrated *in vacuo* to afford (±)-2-(1*H*-[1,2,3]triazolo[4,5-*c*]pyridin-1-yl)-*N*-(4-chloro-3-((3-cyclopropylpyrrolidin-1-yl)sulfonyl)phenyl)acetamide (**±**)-**3.125** (241 mg, 0.523 mmol, 79% yield) as a cream solid. LCMS (formic, ES⁺) *t*_R = 0.98 min, *m/z* = 461.3; HRMS (C₂₀H₂₁ClN₆O₃S): [M+H]⁺ calculated 461.1163, found 461.1161; ¹H NMR (CDCl₃-*d*, 400 MHz): δ (ppm) 9.45 (d, *J*=1.1 Hz, 1H), 9.16 (s, 1H), 8.58 (d, *J*=6.0 Hz, 1H), 8.25 (d, *J*=2.7 Hz, 1H), 7.82 (dd, *J*=8.8, 2.7 Hz, 1H), 7.65 (dd, *J*=6.0, 1.1 Hz, 1H), 7.43 (d, *J*=8.8 Hz, 1H), 5.67 (s, 2H), 3.51–3.58 (m, 2H), 3.30–3.39 (m, 1H), 3.12 (dd, *J*=9.7, 7.7 Hz, 1H), 1.97–2.06 (m, 1H), 1.73 (dd, *J*=12.5, 8.6 Hz, 1H), 1.51–1.63 (m, 1H), 0.55–0.67 (m, 1H), 0.37–0.48 (m, 2H), 0.05–0.12 (m, 2H); m.p. 63.7 – 68.8 °C; IR *v*_{max} (cm⁻¹) 3008, 1590, 1465, 1156, 839, 556.

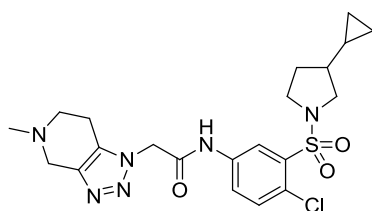
(±)-2-(1*H*-[1,2,3]Triazolo[4,5-*c*]pyridin-1-yl)-*N*-(4-bromo-3-((3-cyclopropylpyrrolidin-1-yl)sulfonyl)phenyl)acetamide ((±)-3.126)



tert-Butyl 2-(1*H*-[1,2,3]triazolo[4,5-*c*]pyridin-1-yl)acetate **3.119** (163 mg, 0.695 mmol) was dissolved in HCl (4 M in dioxane, 1.45 mL, 5.79 mmol) and stirred at 40 °C for 16 h. The reaction mixture was concentrated *in vacuo* to afford the crude acid. (±)-4-Bromo-3-((3-cyclopropylpyrrolidin-1-yl)sulfonyl)aniline (**±**)-**3.124** (200 mg, 0.579 mmol), and HATU (264 mg, 0.695 mmol) were added and the mixture dissolved in CH₂Cl₂ (10 mL). DIPEA (0.304 mL, 1.738 mmol) was added and the resulting solution was stirred at rt for 2 h. The reaction was quenched with sat. aq. NaHCO₃ (10 mL) and extracted

with CH₂Cl₂ (3 x 10 mL). The combined organics were passed through a hydrophobic frit and concentrated *in vacuo* to afford the crude product. The crude product was purified by silica chromatography, eluting with 0-50% EtOAc/cyclohexane. The pure fractions were concentrated *in vacuo* to afford (±)-2-(1*H*-[1,2,3]triazolo[4,5-*c*]pyridin-1-yl)-*N*-(4-bromo-3-((3-cyclopropylpyrrolidin-1-yl)sulfonyl)phenyl)acetamide (±)-**3.126** (222 mg, 0.439 mmol, 76% yield) as a cream solid. LCMS (formic, ES⁺) t_R = 0.97 min, *m/z* = 505.2, 507.2; HRMS (C₂₀H₂₁BrN₆O₃S): [M+H]⁺ calculated 505.0657, found 505.0658; ¹H NMR (CDCl₃-*d*, 400 MHz): δ (ppm) 9.54 (d, *J*=0.7 Hz, 1H), 9.06 (s, 1H), 8.67 (d, *J*=4.5 Hz, 1H), 8.12 (d, *J*=2.7 Hz, 1H), 7.99 (dd, *J*=8.6, 2.7 Hz, 1H), 7.59–7.71 (m, 2H), 5.64 (s, 2H), 3.55–3.65 (m, 2H), 3.38–3.47 (m, 1H), 3.17 (dd, *J*=9.4, 7.7 Hz, 1H), 2.04–2.13 (m, 1H), 1.80 (dq, *J*=12.3, 8.4 Hz, 1H), 1.57–1.69 (m, 1H), 0.61–0.73 (m, 1H), 0.40–0.53 (m, 2H), 0.07–0.19 (m, 2H); ¹³C NMR (CDCl₃-*d*, 101 MHz): δ (ppm) 163.5, 145.3, 144.7, 138.5, 137.4, 137.0, 136.5, 125.1, 125.0, 123.2, 114.7, 104.9, 52.9, 51.4, 47.9, 44.4, 31.4, 13.0, 3.7, 3.4; m.p. 74.3 – 77.8 °C; IR ν_{max} (cm⁻¹) 3207, 1701, 1587, 1387, 1158, 833, 556.

(±)-*N*-(4-Chloro-3-((3-cyclopropylpyrrolidin-1-yl)sulfonyl)phenyl)-2-(5-methyl-4,5,6,7-tetrahydro-1*H*-[1,2,3]triazolo[4,5-*c*]pyridin-1-yl)acetamide (±)-3.127****

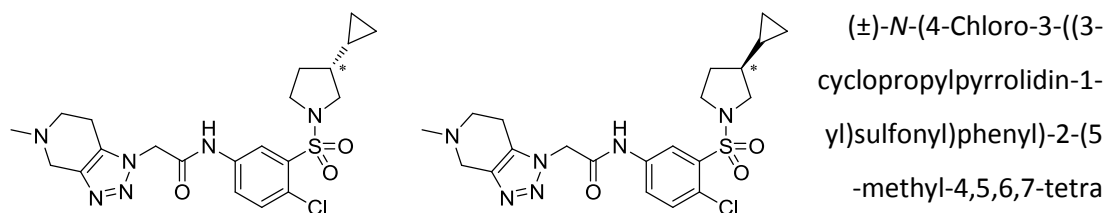


Iodomethane (0.16 mL, 2.169 mmol) was added to (±)-2-(1*H*-[1,2,3]triazolo[4,5-*c*]pyridin-1-yl)-*N*-(4-chloro-3-((3-cyclopropylpyrrolidin-1-yl)sulfonyl)phenyl)acetamide (±)-**3.125** (1.00 g, 2.169 mmol) in MeCN (20 mL) at rt under air.

The resulting solution was refluxed at 80 °C for 2 h. The reaction was allowed to cool and concentrated *in vacuo* to afford the *methyl pyridinium intermediate*. The residue was dissolved in MeOH (10 mL) and water (10 mL), before NaBH₄ (0.18 g, 4.77 mmol) was added and the resulting solution stirred at rt for 30 min. The reaction was quenched with water (20 mL) and extracted with CH₂Cl₂ (3 x 20 mL). The combined organics were passed through a hydrophobic frit and concentrated *in vacuo* to afford (±)-*N*-(4-chloro-3-((3-cyclopropylpyrrolidin-1-yl)sulfonyl)phenyl)-2-(5-methyl-4,5,6,7-tetrahydro-1*H*-[1,2,3]triazolo[4,5-*c*]pyridin-1-yl)acetamide (±)-**3.127** (762 mg, 1.591 mmol, 73% yield) as a white solid. LCMS (formic, ES⁺) t_R = 0.68 min, *m/z* = 479.3; HRMS (C₂₁H₂₇ClN₆O₃S): [M+H]⁺ calculated 479.1632, found 479.1629; ¹H NMR (CDCl₃-*d*, 400 MHz): δ (ppm) 8.98 (s, 1H), 8.13 (d, *J*=2.7 Hz, 1H), 7.91 (dd, *J*=8.8, 2.7 Hz, 1H), 7.46 (d, *J*=8.8 Hz, 1H), 5.16 (s, 2H), 3.70 (s, 2H), 3.53–3.62 (m, 2H), 3.39 (ddd, *J*=9.5, 8.3, 7.2 Hz, 1H), 3.15 (dd, *J*=9.5, 7.8 Hz, 1H), 2.80–2.89 (m, 4H), 2.56

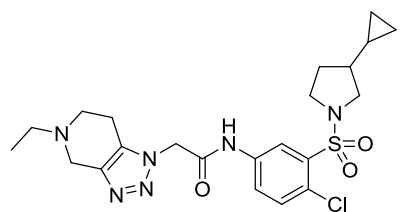
(s, 3H), 1.99–2.10 (m, 1H), 1.76 (dq, $J=12.2, 8.4$ Hz, 1H), 1.56–1.66 (m, 1H), 0.60–0.71 (m, 1H), 0.41–0.52 (m, 2H), 0.09–0.18 (m, 2H); ^{13}C NMR (CDCl_3 -*d*, 101 MHz): δ (ppm) 163.6, 143.0, 137.3, 136.1, 132.6, 132.2, 127.3, 124.7, 123.1, 77.2, 52.7, 51.4, 51.4, 47.6, 45.1, 44.3, 31.4, 20.6, 13.0, 3.7, 3.3; m.p. 91.8 – 97.8 °C; IR ν_{max} (cm^{-1}) 2950, 1705, 1535, 1464, 1157, 591.

(*S)-*N*-(4-Chloro-3-((3-cyclopropylpyrrolidin-1-yl)sulfonyl)phenyl)-2-(5-methyl-4,5,6,7-tetrahydro-1*H*-[1,2,3]triazolo[4,5-*c*]pyridin-1-yl)acetamide ((*S**)-3.127)** and **(*R**)-*N*-(4-chloro-3-((3-cyclopropylpyrrolidin-1-yl)sulfonyl)phenyl)-2-(5-methyl-4,5,6,7-tetrahydro-1*H*-[1,2,3]triazolo[4,5-*c*]pyridin-1-yl)acetamide ((*R**)-3.127)**



(\pm)-*N*-(4-Chloro-3-((3-cyclopropylpyrrolidin-1-yl)sulfonyl)phenyl)-2-(5-methyl-4,5,6,7-tetrahydro-1*H*-[1,2,3]triazolo[4,5-*c*]pyridin-1-yl)acetamide (\pm)-3.127 was dissolved in EtOH (1 mL) and injected onto the column (column: 250 mm x 20 mm Chiralpak IG, 5 μm), eluting with 50% (EtOH + 0.2% isopropylamine)/(heptane + 0.2% isopropylamine), flow rate = 15 mL min^{-1} , detection wavelength 215 nm. The pure fractions from peak 1 were concentrated *in vacuo* to afford (*S**)-*N*-(4-chloro-3-((3-cyclopropylpyrrolidin-1-yl)sulfonyl)phenyl)-2-(5-methyl-4,5,6,7-tetrahydro-1*H*-[1,2,3]triazolo[4,5-*c*]pyridin-1-yl)acetamide (*S**)-3.127 (16 mg, 0.033 mmol) as a white solid and the pure fractions from peak 2 were concentrated *in vacuo* to afford (*R**)-*N*-(4-chloro-3-((3-cyclopropylpyrrolidin-1-yl)sulfonyl)phenyl)-2-(5-methyl-4,5,6,7-tetrahydro-1*H*-[1,2,3]triazolo[4,5-*c*]pyridin-1-yl)acetamide (*R**)-3.127 (15 mg, 0.031 mmol) as a white solid. *Data consistent with racemate* (\pm)-3.127; Chiral LC: 4.6 mm x 250 mm Chiralpak IG column, 80% (EtOH + 2% isopropylamine)/heptane, (*S**)-3.127: t_{R} = 17.354 min; *er* >99:1; (*R**)-3.127: t_{R} = 23.739 min; *er* >99:1.

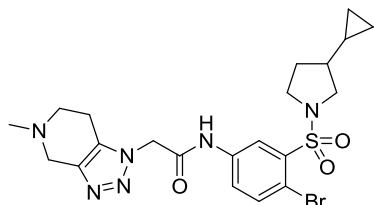
(\pm)-*N*-(4-Chloro-3-((3-cyclopropylpyrrolidin-1-yl)sulfonyl)phenyl)-2-(5-ethyl-4,5,6,7-tetrahydro-1*H*-[1,2,3]triazolo[4,5-*c*]pyridin-1-yl)acetamide ((\pm)-3.128)



Iodoethane (27 mg, 0.174 mmol) was added to (\pm)-2-(1*H*-[1,2,3]triazolo[4,5-*c*]pyridin-1-yl)-*N*-(4-chloro-3-((3-cyclopropylpyrrolidin-1-yl)sulfonyl)phenyl)acetamide (\pm)-3.125 (80 mg, 0.174 mmol) in MeCN (2 mL) at rt under air. The resulting solution was refluxed at 80 °C for 2 h. The reaction was allowed to cool and

concentrated *in vacuo* to afford the *ethyl pyridinium intermediate*. The residue was dissolved in MeOH (1 mL) and water (1 mL), before NaBH₄ (14 mg, 0.382 mmol) was added and the resulting solution stirred at rt for 30 min. The reaction was quenched with water (5 mL) and extracted with EtOAc (3 x 5 mL). The combined organics were passed through a hydrophobic frit and concentrated *in vacuo* to afford the crude product. The crude product was purified by HPH MDAP. The pure fractions were concentrated *in vacuo* to afford (±)-*N*-(4-chloro-3-((3-cyclopropylpyrrolidin-1-yl)sulfonyl)phenyl)-2-(5-ethyl-4,5,6,7-tetrahydro-1*H*-[1,2,3]triazolo[4,5-*c*]pyridin-1-yl)acetamide (±)-**3.128** (33 mg, 0.066 mmol, 38% yield) as a white solid. LCMS (formic, ES⁺) t_R = 0.70 min, *m/z* = 493.3; HRMS (C₂₂H₂₉ClN₆O₃S): [M+H]⁺ calculated 493.1789, found 493.1790; ¹H NMR (CDCl₃-*d*, 400 MHz): δ (ppm) 9.16 (s, 1H), 8.13 (d, *J*=2.7 Hz, 1H), 7.90 (dd, *J*=8.8, 2.7 Hz, 1H), 7.46 (d, *J*=8.8 Hz, 1H), 5.15 (s, 2H), 3.81 (s, 2H), 3.53–3.63 (m, 2H), 3.34–3.44 (m, 1H), 3.15 (dd, *J*=9.5, 7.6 Hz, 1H), 2.92–2.99 (m, 2H), 2.85–2.92 (m, 2H), 2.78 (q, *J*=7.1 Hz, 2H), 1.99–2.10 (m, 1H), 1.76 (dq, *J*=12.3, 8.5 Hz, 1H), 1.53–1.66 (m, 1H), 1.19–1.27 (m, 3H), 0.59–0.73 (m, 1H), 0.40–0.53 (m, 2H), 0.08–0.17 (m, 2H); ¹³C NMR (CDCl₃-*d*, 101 MHz): δ (ppm) 163.7, 142.4, 137.3, 136.2, 132.6, 132.4, 127.2, 124.7, 123.1, 52.7, 51.3, 51.2, 49.2, 48.7, 47.6, 44.3, 31.4, 20.3, 13.0, 12.1, 3.7, 3.3; m.p. 84.6 – 88.2 °C; IR ν_{max} (cm⁻¹) 2970, 1704, 1537, 1465, 1157, 591.

(±)-*N*-(4-Bromo-3-((3-cyclopropylpyrrolidin-1-yl)sulfonyl)phenyl)-2-(5-methyl-4,5,6,7-tetrahydro-1*H*-[1,2,3]triazolo[4,5-*c*]pyridin-1-yl)acetamide (±)-**3.129**

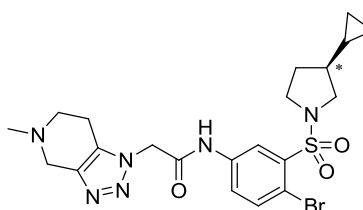
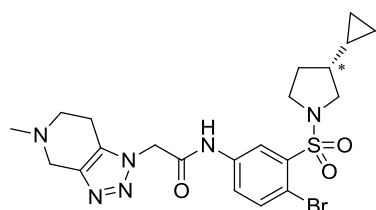


Iodomethane (42 mg, 0.297 mmol) was added to (±)-2-(1*H*-[1,2,3]triazolo[4,5-*c*]pyridin-1-yl)-*N*-(4-bromo-3-((3-cyclopropylpyrrolidin-1-yl)sulfonyl)phenyl)acetamide (±)-**3.126** (150 mg, 0.297 mmol) in MeCN (2 mL) at rt under air.

The resulting solution was refluxed at 80 °C for 2 h. The reaction was allowed to cool and concentrated *in vacuo* to afford the *methyl pyridinium intermediate*. The residue was dissolved in MeOH (1 mL) and water (1 mL), before NaBH₄ (25 mg, 0.653 mmol) was added and the resulting solution was stirred at rt for 30 min. The reaction was quenched with water (5 mL) and extracted with EtOAc (3 x 5 mL). The combined organics were passed through a hydrophobic frit and concentrated *in vacuo* to afford the crude product. The crude product was purified by HPH MDAP. The pure fractions were concentrated *in vacuo* to afford (±)-*N*-(4-bromo-3-((3-cyclopropylpyrrolidin-1-yl)sulfonyl)phenyl)-2-(5-methyl-4,5,6,7-tetrahydro-1*H*-[1,2,3]triazolo[4,5-*c*]pyridin-1-yl)acetamide (±)-**3.129** (67 mg, 0.128 mmol, 43% yield) as

a white solid. LCMS (formic, ES⁺) t_R = 0.69 min, m/z = 523.2, 525.2; HRMS (C₂₁H₂₇BrN₆O₃S): [M+H]⁺ calculated 523.1127, found 523.1124; ¹H NMR (CDCl₃-d, 400 MHz): δ (ppm) 9.23 (s, 1H), 8.18 (d, J =2.7 Hz, 1H), 7.83 (dd, J =8.8, 2.7 Hz, 1H), 7.66 (d, J =8.8 Hz, 1H), 5.18 (s, 2H), 3.68 (s, 2H), 3.53–3.62 (m, 2H), 3.35–3.43 (m, 1H), 3.15 (dd, J =9.5, 7.6 Hz, 1H), 2.78–2.87 (m, 4H), 2.54 (s, 3H), 2.03–2.09 (m, 1H), 1.76 (dq, J =12.3, 8.4 Hz, 1H), 1.54–1.66 (m, 1H), 0.61–0.72 (m, 1H), 0.40–0.52 (m, 2H), 0.08–0.17 (m, 2H); ¹³C NMR (CDCl₃-d, 101 MHz): δ (ppm) 163.7, 143.0, 138.9, 137.0, 136.2, 132.4, 124.7, 123.3, 114.7, 52.8, 51.4, 51.4, 51.4, 47.7, 45.2, 44.3, 31.4, 20.6, 13.1, 3.7, 3.4.

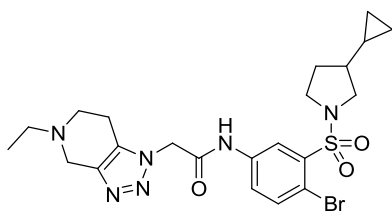
(S*)-N-(4-Bromo-3-((3-cyclopropylpyrrolidin-1-yl)sulfonyl)phenyl)-2-(5-methyl-4,5,6,7-tetrahydro-1H-[1,2,3]triazolo[4,5-c]pyridin-1-yl)acetamide ((S*)-3.129) and **(R*)-N-(4-bromo-3-((3-cyclopropylpyrrolidin-1-yl)sulfonyl)phenyl)-2-(5-methyl-4,5,6,7-tetrahydro-1H-[1,2,3]triazolo[4,5-c]pyridin-1-yl)acetamide ((R*)-3.129)**



(±)-N-(4-bromo-3-((3-cyclopropylpyrrolidin-1-yl)sulfonyl)phenyl)-2-(5-methyl-4,5,6,7-tetrahydro-1H-[1,2,3]triazolo[4,5-c]pyridin-1-yl)acetamide (±)-3.129

(±)-N-(4-bromo-3-((3-cyclopropylpyrrolidin-1-yl)sulfonyl)phenyl)-2-(5-methyl-4,5,6,7-tetrahydro-1H-[1,2,3]triazolo[4,5-c]pyridin-1-yl)acetamide (±)-3.129 was dissolved in EtOH (5 mL) and injected onto the column (column: 250 mm x 20 mm Chiralpak IG, 5 μ m), eluting with 95% (EtOH + 0.2% isopropylamine)/CH₂Cl₂, flow rate = 15 mL min⁻¹, detection wavelength 215 nm. The pure fractions from peak 1 were concentrated *in vacuo* to afford (S*)-N-(4-bromo-3-((3-cyclopropylpyrrolidin-1-yl)sulfonyl)phenyl)-2-(5-methyl-4,5,6,7-tetrahydro-1H-[1,2,3]triazolo[4,5-c]pyridin-1-yl)acetamide (S*)-3.129 (20 mg, 0.038 mmol) as a white solid and the pure fractions from peak 1 were concentrated *in vacuo* to afford (R*)-N-(4-bromo-3-((3-cyclopropylpyrrolidin-1-yl)sulfonyl)phenyl)-2-(5-methyl-4,5,6,7-tetrahydro-1H-[1,2,3]triazolo[4,5-c]pyridin-1-yl)acetamide (R*)-3.129 (24 mg, 0.046 mmol) as white solids. Data consistent with racemate (±)-3.129; Chiral LC: 4.6 mm x 250 mm Chiralpak IG column, 80% (EtOH + 2% isopropylamine)/heptane, (S*)-3.129: t_R = 9.785 min; *er* >99:1; (R*)-3.129: t_R = 12.045 min; *er* >99:1.

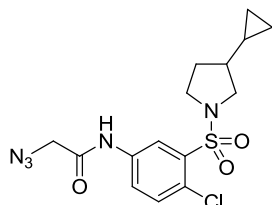
(±)-N-(4-Bromo-3-((3-cyclopropylpyrrolidin-1-yl)sulfonyl)phenyl)-2-(5-ethyl-4,5,6,7-tetrahydro-1H-[1,2,3]triazolo[4,5-c]pyridin-1-yl)acetamide ((±)-3.130)



Iodoethane (70 mg, 0.495 mmol) was added to (±)-2-(1H-[1,2,3]triazolo[4,5-c]pyridin-1-yl)-N-(4-bromo-3-((3-cyclopropylpyrrolidin-1-yl)sulfonyl)phenyl)acetamide **(±)-3.126** (50 mg, 0.099 mmol) in MeCN (2 mL) at rt under air. The resulting solution was refluxed at 80 °C for 2 h.

The reaction was allowed to cool and concentrated *in vacuo* to afford the *ethyl pyridinium intermediate*. The residue was dissolved in MeOH (1 mL) and water (1 mL), before NaBH₄ (8 mg, 0.218 mmol) was added and the resulting solution stirred at rt for 30 min. The reaction was quenched with water (5 mL) and extracted with EtOAc (3 x 5 mL). The combined organics were passed through a hydrophobic frit and concentrated *in vacuo* to afford the crude product. The crude product was purified by HPH MDAP. The pure fractions were concentrated *in vacuo* to afford (±)-N-(4-bromo-3-((3-cyclopropylpyrrolidin-1-yl)sulfonyl)phenyl)-2-(5-ethyl-4,5,6,7-tetrahydro-1H-[1,2,3]triazolo[4,5-c]pyridin-1-yl)acetamide **(±)-3.130** (16 mg, 0.030 mmol, 30% yield) as a white solid. LCMS (formic, ES⁺) t_R = 0.71 min, m/z = 537.2, 539.2; HRMS (C₂₂H₂₉BrN₆O₃S): [M+H]⁺ calculated 537.1283, found 537.1281; ¹H NMR (CDCl₃-d, 400 MHz): δ (ppm) 9.46 (s, 1H), 8.19 (d, J=2.7 Hz, 1H), 7.82 (dd, J=8.7, 2.7 Hz, 1H), 7.65 (d, J=8.7 Hz, 1H), 5.17 (s, 2H), 3.83 (s, 2H), 3.52–3.61 (m, 2H), 3.33–3.44 (m, 1H), 3.15 (dd, J=9.5, 7.6 Hz, 1H), 2.87–3.02 (m, 4H), 2.80 (q, J=7.6 Hz, 2H), 1.98–2.10 (m, 1H), 1.76 (dq, J=12.4, 8.3 Hz, 1H), 1.54–1.67 (m, 1H), 1.24 (t, J=7.1 Hz, 3H), 0.61–0.73 (m, 1H), 0.40–0.51 (m, 2H), 0.07–0.18 (m, 2H); ¹³C NMR (CDCl₃-d, 101 MHz): δ (ppm) 163.8, 141.9, 138.9, 137.1, 136.1, 132.4, 124.7, 123.2, 114.6, 52.7, 51.3, 51.1, 49.2, 48.6, 47.7, 44.3, 31.4, 20.2, 13.1, 12.0, 3.7, 3.3.

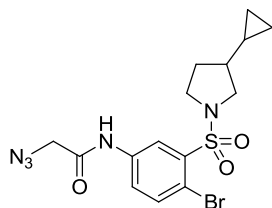
(±)-2-Azido-N-(4-chloro-3-((3-cyclopropylpyrrolidin-1-yl)sulfonyl)phenyl)acetamide ((±)-3.131)



(±)-4-Chloro-3-((3-cyclopropylpyrrolidin-1-yl)sulfonyl)aniline **(±)-3.123** (400 mg, 1.330 mmol), 2-azidoacetic acid (148 mg, 1.463 mmol), and HATU (607 mg, 1.596 mmol) were dissolved in CH₂Cl₂ (5 mL) at rt under air. DIPEA (0.695 mL, 3.99 mmol) was added and the resulting solution was stirred at rt for 1 h. The reaction was quenched with sat. aq. NaHCO₃ (20 mL) and extracted with CH₂Cl₂ (2 x 20 mL). The combined organics were passed through

a hydrophobic frit and concentrated *in vacuo* to afford the crude product. The crude product was purified by silica chromatography eluting with 0-50% EtOAc/cyclohexane. The pure fractions were concentrated *in vacuo* to afford (\pm)-2-azido-*N*-(4-chloro-3-((3-cyclopropylpyrrolidin-1-yl)sulfonyl)phenyl)acetamide (**(\pm)-3.131**) (455 mg, 1.185 mmol, 89% yield) as a pale yellow gum. LCMS (formic, ES⁺) t_R = 1.17 min, m/z = 428.2, 430.2; HRMS (C₁₅H₁₈ClN₅O₃S): [M+H]⁺ calculated 384.0897, found 384.0894; ¹H NMR (CDCl₃-*d*, 400 MHz): δ (ppm) 8.49 (s, 1H), 8.09 (d, J =2.7 Hz, 1H), 7.94 (dd, J =8.8, 2.7 Hz, 1H), 7.69 (d, J =8.8 Hz, 1H), 4.16 (s, 2H), 3.52–3.65 (m, 2H), 3.40 (ddd, J =9.5, 8.4, 7.1 Hz, 1H), 3.16 (dd, J =9.5, 7.7 Hz, 1H), 2.03–2.07 (m, 1H), 1.78 (dq, J =12.3, 8.4 Hz, 1H), 1.55–1.69 (m, 1H), 0.62–0.73 (m, 1H), 0.38–0.53 (m, 2H), 0.06–0.21 (m, 2H); ¹³C NMR (CDCl₃-*d*, 101 MHz): δ (ppm) 165.2, 137.3, 136.0, 132.6, 127.2, 124.6, 122.8, 52.9, 52.7, 47.6, 44.3, 31.5, 13.1, 3.6, 3.3; IR ν_{max} (cm⁻¹) 3325, 2104, 1589, 1524, 1465, 1155, 588.

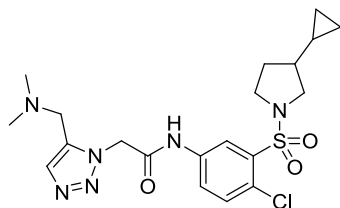
(\pm)-2-Azido-*N*-(4-bromo-3-((3-cyclopropylpyrrolidin-1-yl)sulfonyl)phenyl)acetamide
(\pm)-3.132



(\pm)-4-Bromo-3-((3-cyclopropylpyrrolidin-1-yl)sulfonyl)aniline (**(\pm)-3.124**) (500 mg, 1.448 mmol), 2-azidoacetic acid (161 mg, 1.593 mmol), and HATU (661 mg, 1.738 mmol) were dissolved in CH₂Cl₂ (5 mL) at rt under air. DIPEA (0.757 mL, 4.34 mmol) was added and the

resulting solution was stirred at rt for 1 h. The reaction was quenched with sat. aq. NaHCO₃ (20 mL) and extracted with CH₂Cl₂ (2 x 20 mL). The combined organics were passed through a hydrophobic frit and concentrated *in vacuo* to afford the crude product. The crude product was purified by silica chromatography eluting with 0-50% EtOAc/cyclohexane. The pure fractions were concentrated *in vacuo* to afford (\pm)-2-azido-*N*-(4-bromo-3-((3-cyclopropylpyrrolidin-1-yl)sulfonyl)phenyl)acetamide (**(\pm)-3.132**) (552 mg, 1.289 mmol, 89% yield) as a pale yellow gum. LCMS (formic, ES⁺) t_R = 1.17 min, m/z = 428.2, 430.2; HRMS (C₁₅H₁₈BrN₅O₃S): [M+H]⁺ calculated 428.0392, found 428.0392; ¹H NMR (CDCl₃-*d*, 400 MHz): δ (ppm) 8.49 (s, 1H), 8.09 (d, J =2.7 Hz, 1H), 7.94 (dd, J =8.8, 2.7 Hz, 1H), 7.69 (d, J =8.8 Hz, 1H), 4.16 (s, 2H), 3.52–3.65 (m, 2H), 3.40 (ddd, J =9.5, 8.4, 7.1 Hz, 1H), 3.16 (dd, J =9.5, 7.7 Hz, 1H), 2.03–2.07 (m, 1H), 1.78 (dq, J =12.3, 8.4 Hz, 1H), 1.55–1.69 (m, 1H), 0.62–0.73 (m, 1H), 0.38–0.53 (m, 2H), 0.06–0.21 (m, 2H); ¹³C NMR (CDCl₃-*d*, 101 MHz): δ (ppm) 165.4, 138.9, 136.7, 136.3, 124.6, 123.0, 114.6, 52.9, 52.8, 47.7, 44.3, 31.4, 13.1, 3.7, 3.4; IR ν_{max} (cm⁻¹) 3347, 2102, 1588, 1525, 1322, 1152, 585.

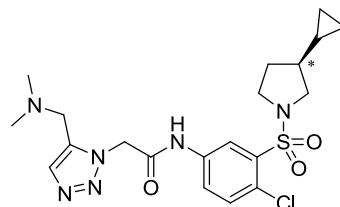
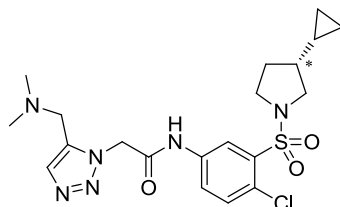
(±)-N-(4-Chloro-3-((3-cyclopropylpyrrolidin-1-yl)sulfonyl)phenyl)-2-(5-((dimethylamino)methyl)-1H-1,2,3-triazol-1-yl)acetamide ((±)-3.133)



(±)-2-Azido-N-(4-chloro-3-((3-cyclopropylpyrrolidin-1-yl)sulfonyl)phenyl)acetamide (**±**)-**3.131** (80 mg, 0.208 mmol), *N,N*-dimethylprop-2-yn-1-amine (17 mg, 0.208 mmol), and Cp**RuCl*(PPh₃)₂ (5 mg, 6.25 μmol) were dissolved in THF (3 mL)

at rt under nitrogen. The resulting solution was stirred at 65 °C for 1 h. The reaction was diluted with water (2 mL) and extracted with CH₂Cl₂ (3 x 2 mL). The combined organics were passed through a hydrophobic frit and concentrated *in vacuo* to afford the crude product. The crude product was purified HPH MDAP. The pure fractions were concentrated *in vacuo* to afford (±)-*N*-(4-chloro-3-((3-cyclopropylpyrrolidin-1-yl)sulfonyl)phenyl)-2-(5-((dimethylamino)methyl)-1H-1,2,3-triazol-1-yl)acetamide (**±**)-**3.133** (48 mg, 0.103 mmol, 50% yield) as a cream solid. LCMS (Formic, ES⁺) *t_R* = 0.70 min, *m/z* = 467.3; HRMS (C₂₀H₂₇ClN₆O₃S): [M+H]⁺ calculated 467.1632, found 467.1633; ¹H NMR (CDCl₃-*d*, 400 MHz): δ (ppm) 10.25 (s, 1H), 8.04 (dd, *J*=8.8, 2.5 Hz, 1H), 7.79 (d, *J*=2.5 Hz, 1H), 7.70 (s, 1H), 7.46 (d, *J*=8.8 Hz, 1H), 5.25 (s, 2H), 3.66 (s, 2H), 3.51–3.61 (m, 2H), 3.38 (ddd, *J*=9.5, 8.3, 7.1 Hz, 1H), 3.14 (dd, *J*=9.5, 7.6 Hz, 1H), 2.40 (s, 6H), 2.03–2.07 (m, 1H), 1.75 (dq, *J*=12.3, 8.4 Hz, 1H), 1.53–1.64 (m, 1H), 0.61–0.71 (m, 1H), 0.41–0.51 (m, 2H), 0.10–0.15 (m, 2H); ¹³C NMR (CDCl₃-*d*, 101 MHz): δ (ppm) 163.6, 137.3, 136.7, 134.8, 133.9, 132.7, 126.8, 124.6, 122.5, 52.6, 52.5, 51.2, 47.5, 44.9, 44.3, 31.4, 13.1, 3.7, 3.3.

(*S)-N-(4-Chloro-3-((3-cyclopropylpyrrolidin-1-yl)sulfonyl)phenyl)-2-(5-((dimethylamino)methyl)-1H-1,2,3-triazol-1-yl)acetamide ((*S**)-3.133) and (*R**)-N-(4-chloro-3-((3-cyclopropylpyrrolidin-1-yl)sulfonyl)phenyl)-2-(5-((dimethylamino)methyl)-1H-1,2,3-triazol-1-yl)acetamide ((*R**)-3.133)**



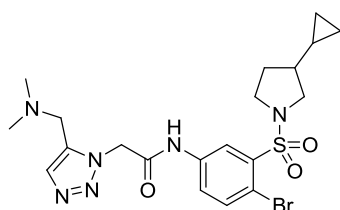
(±)-*N*-(4-Chloro-3-((3-cyclopropylpyrrolidin-1-yl)sulfonyl)phenyl)-2-(5-((dimethylamino)methyl)-1H-1,2,3-triazol-1-yl)acetamide (**±**)-**3.133** was dissolved in MeCN (2 mL) and injected onto the column

(column: 250 mm x 30 mm Chiralpak AS-H, 5 μm), eluting with 15% (MeCN + 0.2% isopropylamine)/MTBE, flow rate = 30 mL min⁻¹, detection wavelength 215 nm. The pure fractions from peak 1 were concentrated *in vacuo* to afford (*S**)-*N*-(4-chloro-3-((3-

GSK Confidential – Do not copy

cyclopropylpyrrolidin-1-yl)sulfonyl)phenyl)-2-(5-((dimethylamino)methyl)-1*H*-1,2,3-triazol-1-yl)acetamide (**S***)-**3.133** (11 mg, 0.024 mmol) as a white solid and the pure fractions from peak 2 were concentrated *in vacuo* to afford (*S**)-*N*-(4-chloro-3-((3-cyclopropylpyrrolidin-1-yl)sulfonyl)phenyl)-2-(5-((dimethylamino)methyl)-1*H*-1,2,3-triazol-1-yl)acetamide (**R***)-**3.133** (10 mg, 0.021 mmol) as a white solid. *Data consistent with racemate ((±)-3.133)*; Chiral LC: 4.6 mm x 250 mm Chiralpak AS-H column, 10% (MeCN + 0.2% isopropylamine)/MTBE, (**S***)-**3.133**: $t_R = 27.003$ min; *er* >99:1; (**R***)-**3.133**: $t_R = 31.278$ min; *er* 98:2.

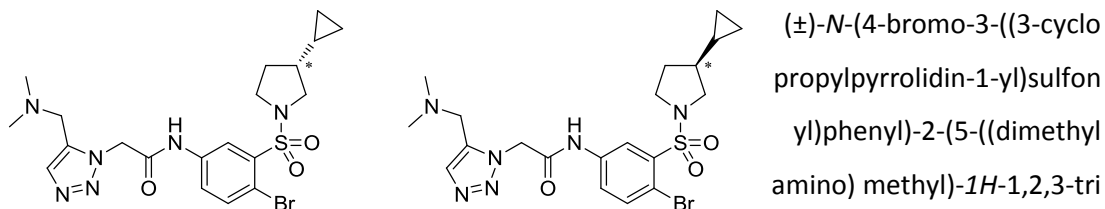
(±)-*N*-(4-Bromo-3-((3-cyclopropylpyrrolidin-1-yl)sulfonyl)phenyl)-2-(5-((dimethylamino)methyl)-1*H*-1,2,3-triazol-1-yl)acetamide ((±)-3.134)



(±)-2-Azido-*N*-(4-bromo-3-((3-cyclopropylpyrrolidin-1-yl)sulfonyl)phenyl)acetamide (**±**)-**3.132** (40 mg, 0.093 mmol), *N,N*-dimethylprop-2-yn-1-amine (8 mg, 0.093 mmol), and Cp**RuCl*(PPh₃)₂ (2 mg, 2.80 μmol) were dissolved in THF (3 mL)

at rt under nitrogen. The resulting solution was stirred at 65 °C for 1 h. The reaction mixture was diluted with water (2 mL) and extracted with CH₂Cl₂ (3 x 2 mL). The combined organics were passed through a hydrophobic frit and concentrated *in vacuo* to afford the crude product. The crude product was purified by HPH MDAP. The pure fractions were concentrated *in vacuo* to afford (±)-*N*-(4-bromo-3-((3-cyclopropylpyrrolidin-1-yl)sulfonyl)phenyl)-2-(5-((dimethylamino)methyl)-1*H*-1,2,3-triazol-1-yl)acetamide (**±**)-**3.134** (36 mg, 0.070 mmol, 75% yield) as a cream solid. LCMS (Formic, ES⁺) $t_R = 0.71$ min, $m/z = 511.2, 513.2$; HRMS (C₂₀H₂₇BrN₆O₃S): [M+H]⁺ calculated 511.1127, found 511.1127; ¹H NMR (CDCl₃-*d*, 400 MHz): δ (ppm) 10.27 (s, 1H), 7.95 (dd, *J*=8.8, 2.7 Hz, 1H), 7.81 (d, *J*=2.7 Hz, 1H), 7.63–7.72 (m, 2H), 5.24 (s, 2H), 3.65 (s, 2H), 3.51–3.60 (m, 2H), 3.38 (ddd, *J*=9.5, 8.5, 7.1 Hz, 1H), 3.14 (dd, *J*=9.5, 7.5 Hz, 1H), 2.40 (s, 6H), 2.05 (dd, *J*=7.5, 0.9 Hz, 1H), 1.77 (dd, *J*=12.5, 8.5 Hz, 1H), 1.53–1.68 (m, 1H), 0.60–0.73 (m, 1H), 0.40–0.52 (m, 2H), 0.10–0.15 (m, 2H); ¹³C NMR (CDCl₃-*d*, 101 MHz): δ (ppm) 163.6, 139.0, 137.4, 136.3, 134.8, 133.9, 124.5, 122.7, 114.3, 52.7, 52.6, 51.3, 47.6, 45.0, 44.4, 31.4, 13.1, 3.7, 3.4.

(S*)-N-(4-Bromo-3-((3-cyclopropylpyrrolidin-1-yl)sulfonyl)phenyl)-2-(5-((dimethylamino) methyl)-1H-1,2,3-triazol-1-yl)acetamide ((S*)-3.134) and **(R*)-N-(4-bromo-3-((3-cyclopropylpyrrolidin-1-yl)sulfonyl)phenyl)-2-(5-((dimethylamino) methyl)-1H-1,2,3-triazol-1-yl)acetamide ((R*)-3.134)**



(±)-N-(4-bromo-3-((3-cyclopropylpyrrolidin-1-yl)sulfonyl)phenyl)-2-(5-((dimethylamino) methyl)-1H-1,2,3-triazol-1-yl)acetamide (±)-3.134 was dissolved in MeCN (2 mL) and injected onto the column (column: 250 mm x 30 mm Chiralpak AS-H, 5 μm), eluting with 15% (MeCN + 0.2% isopropylamine)/MTBE, flow rate = 30 mL min⁻¹, detection wavelength 215 nm. The pure fractions from peak 1 were concentrated *in vacuo* to afford (S*)-N-(4-bromo-3-((3-cyclopropylpyrrolidin-1-yl)sulfonyl)phenyl)-2-(5-((dimethylamino) methyl)-1H-1,2,3-triazol-1-yl)acetamide (S*)-3.134 (14 mg, 0.027 mmol) as a white solid and the pure fractions from peak 2 were concentrated *in vacuo* to afford (R*)-N-(4-Bromo-3-((3-cyclopropylpyrrolidin-1-yl)sulfonyl)phenyl)-2-(5-((dimethylamino) methyl)-1H-1,2,3-triazol-1-yl)acetamide (R*)-3.134 (14 mg, 0.027 mmol) as a white solid. *Data consistent with racemate ((±)-3.134)*; Chiral LC: 4.6 mm x 250 mm Chiralpak AS-H column, 10% (MeCN + 0.2% isopropylamine)/MTBE, (S*)-3.134: $t_R = 33.336$ min; *er* >99:1; (R*)-3.134 : $t_R = 37.937$ min; *er* 98:2.

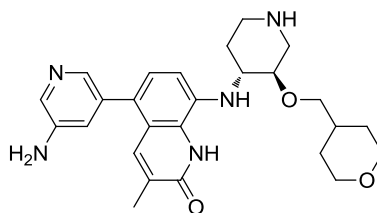
4.5. Biological Data Experimental

ATAD2 TR-FRET Binding Assay

Compounds were titrated from 10 mM in 100% DMSO, and 100 nL was transferred to a low-volume black 384-well microtiter plate using a Labcyte Echo 555. A Thermo Scientific Multidrop Micro was used to dispense 5 μL of 5 nM FLAG-6His-Tev-ATAD2(981–1121) in 50 mM Hepes, 150 mM NaCl, 5% Glycerol, 1 mM CHAPS, and 1 mM DTT at pH 7.4, in the presence of 100 nM Alexa Fluor 488-labeled ligand. After equilibrating for 30 min in the dark at rt, the ATAD2 protein–fluorescent ligand interaction was detected using TR-FRET following a 5 μL addition of 1.5 nM Lanthascreen Elite Tb-anti His antibody (Invitrogen, PV5863) in assay buffer. Time-resolved fluorescence (TRF) was then detected on a TRF laser equipped PerkinElmer Envision multimode plate reader (excitation = 337 nm; emission 1 = 520 nm; emission 2 = 495 nm; dual wavelength bias dichroic = 400, 505 nm). TR-FRET ratio was

GSK Confidential – Do not copy

calculated using the following equation: ratio = ((acceptor fluorescence at 520 nm)/(donor fluorescence at 495 nm)) × 1000. TR FRET ratio data was normalized to a mean of 16 replicates per microtiter plate of both 10 μM **4.01** and 100% DMSO controls.



4.01

IC₅₀ values were determined for each of the compounds tested by fitting the fluorescence ratio data to a four parameter curve fit of the following form was then applied.

$$y = \frac{a - d}{1 + (x/c)^b} + d$$

Where 'a' is the minimum, 'b' is the Hill slope, 'c' is the pIC₅₀ and 'd' is the maximum.

CECR2 TR-FRET Binding Assay

Compounds were titrated from 10 mM in 100% DMSO, and 100 nL was transferred to a low-volume black 384-well microtiter plate using a Labcyte Echo 555. A Thermo Scientific Multidrop Micro was used to dispense 5 μL of 6H-FLAG-tev-CECR2 (424-543) in 50 mM Hepes, 150 mM NaCl, 5% Glycerol, 1 mM CHAPS, and 1 mM DTT at pH 7.4, in the presence of 200 nM Alexa Fluor 647-labeled ligand. After equilibrating for 15 min at rt, the CECR2 protein–fluorescent ligand interaction was detected using TR-FRET following a 5 μL addition of 3 nM Eu-W1024-labeled Anti-6xHis antibody in assay buffer. Time-resolved fluorescence (TRF) was then detected on a TRF laser equipped PerkinElmer Envision multimode plate reader (excitation = 315 nm; emission 1 = 665 nm; emission 2 = 615 nm). TR-FRET ratio was calculated using the following equation: ratio = ((acceptor fluorescence at 665 nm)/(donor fluorescence at 615 nm)) × 1000. TR FRET ratio data was normalized to a mean of 16 replicates per microtiter plate of both no protein and 100% DMSO controls. IC₅₀ values were determined for each of the compounds tested by fitting the fluorescence ratio data to a four parameter curve fit of the following form was then applied.

$$y = \frac{a - d}{1 + (x/c)^b} + d$$

5. Appendix

Table 5.01a. Single Shot BROMOscan data from DiscoverX

BRD	3.112	3.103	3.111	3.130	3.128	3.113
ATAD2A	100	100	100	100	100	99
ATAD2B	0	36	83	100	100	100
BAZ2A	56	3	73	7	8	30
BAZ2B	21	20	62	29	41	47
BRD1	97	94	93	95	73	97
BRD2(1)	90	75	43	48	37	54
BRD2(2)	96	95	66	89	10	1
BRD3(1)	97	84	36	50	39	57
BRD3(2)	97	96	68	96	56	77
BRD4(1)	88	80	67	31	26	92
BRD4(2)	100	97	97	99	66	34
BRD7	48	69	70	72	60	66
BRD9	95	91	98	93	84	92
BRDT(1)	96	66	76	84	63	70
BRDT(2)	97	96	94	100	95	78
BRPF1	93	88	98	100	90	99
BRPF3	98	91	100	95	95	50
CECR2	100	100	100	99	100	100
CREBBP	0	75	0	1	1	2
EP300	2	0	25	8	0	1
FALZ	92	94	99	99	89	93
GCN5L2	99	100	100	100	100	100
PBRM1(2)	58	13	88	100	82	64
PBRM1(5)	11	11	93	18	23	31
PCAF	73	99	93	99	89	83
SMARCA2	0	0	58	0	0	9
SMARCA4	0	0	48	0	5	3
TAF1(2)	99	98	100	100	100	100
TAF1L(2)	76	96	100	100	100	100
TRIM24	19	30	48	46	46	45
TRIM33	25	14	38	30	48	38
WDR9(2)	97	85	100	89	44	100

Continued overleaf...

GSK Confidential – Do not copy

Table 5.01b. Single Shot BROMOscan data from DiscoverX

BRD	(S,S*)- 3.107	(S,R*)- 3.107	(S*)- 3.134	(S*)- 3.133	(S*)- 3.127	(S*)- 3.129
ATAD2A	99	100	99	99	100	98
ATAD2B	100	100	100	100	100	100
BAZ2A	59	74	91	65	54	57
BAZ2B	51	62	38	0	58	52
BRD1	99	99	94	67	89	96
BRD2(1)	94	89	51	23	96	94
BRD2(2)	87	1	35	28	97	99
BRD3(1)	95	92	41	38	97	96
BRD3(2)	97	63	81	67	100	100
BRD4(1)	100	99	90	84	100	89
BRD4(2)	85	0	57	8	100	100
BRD7	93	82	73	45	75	66
BRD9	100	98	90	71	97	99
BRDT(1)	92	84	83	63	100	99
BRDT(2)	89	57	87	70	100	100
BRPF1	100	100	98	72	96	87
BRPF3	85	100	92	55	92	96
CECR2	100	100	100	100	99	100
CREBBP	15	3	0	4	1	0
EP300	1	0	0	0	0	0
FALZ	99	96	98	93	95	95
GCN5L2	100	100	100	100	100	100
PBRM1(2)	60	49	98	75	97	99
PBRM1(5)	19	13	31	6	0	11
PCAF	100	100	100	100	100	100
SMARCA2	4	0	0	0	0	3
SMARCA4	0	1	8	6	0	0
TAF1(2)	100	100	100	100	100	100
TAF1L(2)	99	98	95	87	81	82
TRIM24	47	48	57	39	11	8
TRIM33	20	20	32	10	54	51
WDR9(2)	100	100	98	81	95	98

Figure 5.01. Graph to show correlation between CLND solubility and CAD solubility.

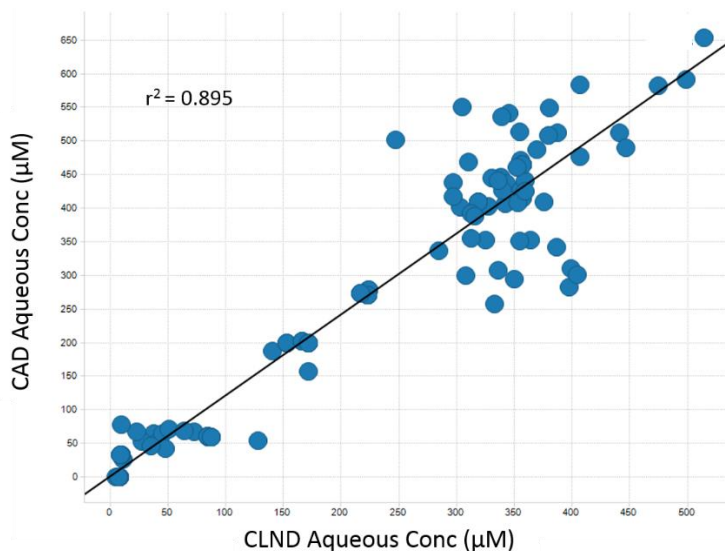
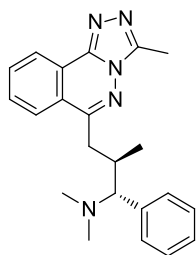
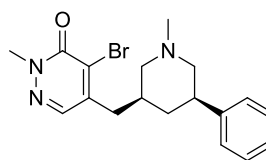


Figure 5.02. PCAF Chemical probes L-Moses (5.01) and GSK4028 (5.02).^{266, 267}

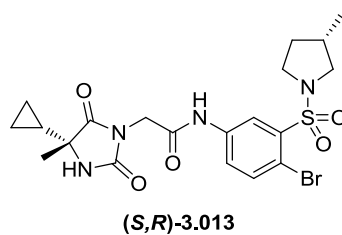


L-Moses, **5.01**
PCAF $pK_d = 6.9$
GCN5 $pK_d = 6.3$



GSK4027, **5.02**
PCAF $pK_d = 8.9$
GCN5 $pK_d = 8.9$

Table 5.02. Data on (S,R)-3.013.



	(S,R)-3.013
CECR2 pIC_{50} (n) / ATAD2 pIC_{50} (n)	6.9(4) / 7.0(8)
Selectivity ^a	1x(A)
BRD4 BD1 pIC_{50} (n)	<4.3(4)
ChromLogD _{7.4}	4.8
CLND Solubility ($\mu\text{g mL}^{-1}$)	146
AMP	147

^a(A) denotes selectivity for ATAD2 over CECR2

Figure 5.03. NOESY spectrum for 3.100.

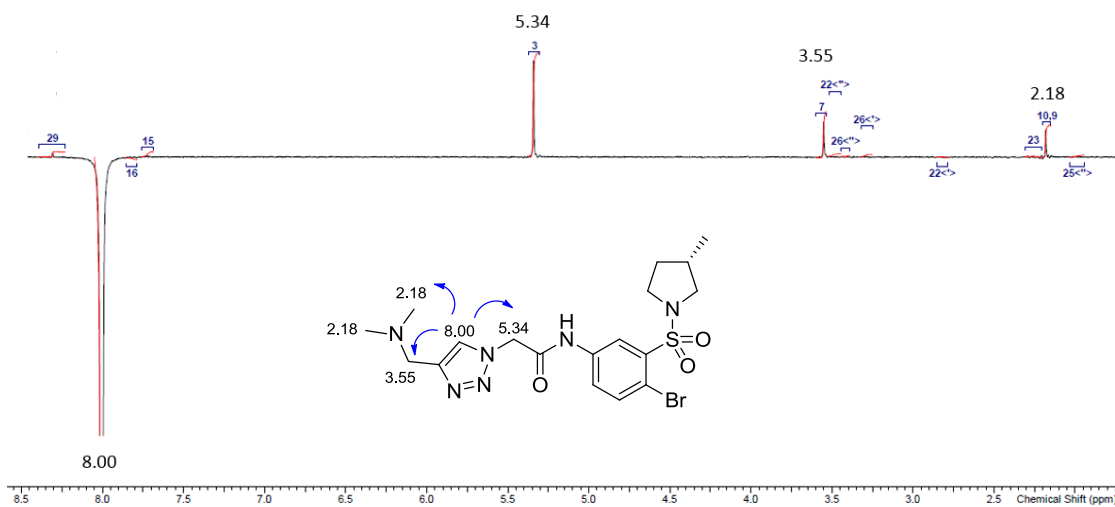
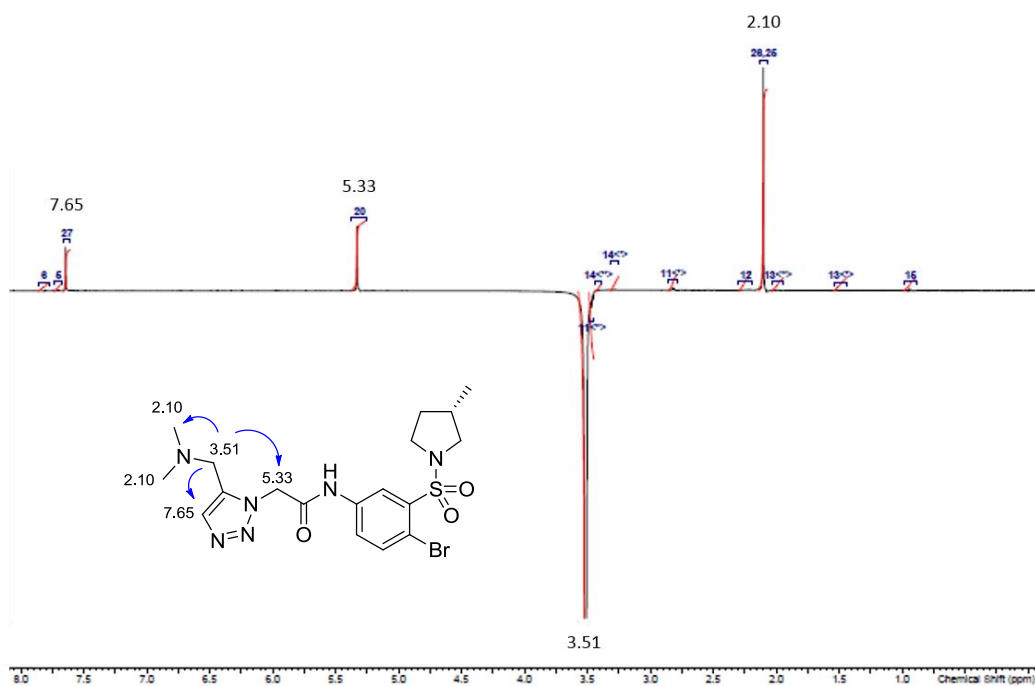


Figure 5.04. NOESY spectrum for 3.103.



6. References

1. Hughes, J.; Rees, S.; Kalindjian, S.; Philpott, K. Principles of early drug discovery. *Br. J. Pharmacol.* **2011**, *162*, 1239-1249.
2. Scannell, J. W.; Bosley, J. When Quality Beats Quantity: Decision Theory, Drug Discovery, and the Reproducibility Crisis. *PLoS One* **2016**, *11*, e0147215.
3. Dolgos, H.; Trusheim, M.; Gross, D.; Halle, J.-P.; Ogden, J.; Osterwalder, B.; Sedman, E.; Rossetti, L. Translational Medicine Guide transforms drug development processes: the recent Merck experience. *Drug Discov. Today* **2016**, *21*, 517-526.
4. Waring, M. J.; Arrowsmith, J.; Leach, A. R.; Leeson, P. D.; Mandrell, S.; Owen, R. M.; Pairaudeau, G.; Pennie, W. D.; Pickett, S. D.; Wang, J.; Wallace, O.; Weir, A. An analysis of the attrition of drug candidates from four major pharmaceutical companies. *Nat. Rev. Drug Discov.* **2015**, *14*, 475.
5. Cook, D.; Brown, D.; Alexander, R.; March, R.; Morgan, P.; Satterthwaite, G.; Pangalos, M. N. Lessons learned from the fate of AstraZeneca's drug pipeline: a five-dimensional framework. *Nat. Rev. Drug Discov.* **2014**, *13*, 419.
6. Morgan, P.; Brown, D. G.; Lennard, S.; Anderton, M. J.; Barrett, J. C.; Eriksson, U.; Fidock, M.; Hamrén, B.; Johnson, A.; March, R. E.; Matcham, J.; Mettetal, J.; Nicholls, D. J.; Platz, S.; Rees, S.; Snowden, M. A.; Pangalos, M. N. Impact of a five-dimensional framework on R&D productivity at AstraZeneca. *Nat. Rev. Drug Discov.* **2018**, *17*, 167.
7. Morgan, P.; Van Der Graaf, P. H.; Arrowsmith, J.; Feltner, D. E.; Drummond, K. S.; Wegner, C. D.; Street, S. D. A. Can the flow of medicines be improved? Fundamental pharmacokinetic and pharmacological principles toward improving Phase II survival. *Drug Discov. Today* **2012**, *17*, 419-424.
8. McGinnity, D. F.; Soars, M. G.; Urbanowicz, R. A.; Riley, R. J. Evaluation of fresh and cryopreserved hepatocytes as in vitro drug metabolism tools for the prediction of metabolic clearance. *Drug Metab. Dispos.* **2004**, *32*, 1247-1253.
9. Waring, M. J. Defining optimum lipophilicity and molecular weight ranges for drug candidates-Molecular weight dependent lower log D limits based on permeability. *Bioorg. Med. Chem. Lett.* **2009**, *19*, 2844-2851.
10. Waring, M. J.; Johnstone, C. A quantitative assessment of hERG liability as a function of lipophilicity. *Bioorg. Med. Chem. Lett.* **2007**, *17*, 1759-1764.
11. Arnott, J. A.; Planey, S. L. The influence of lipophilicity in drug discovery and design. *Expert Opin. Drug Discov.* **2012**, *7*, 863-875.
12. A. P. Hill; Young, R. J. Getting physical in drug discovery: a contemporary perspective on solubility and hydrophobicity. *Drug Discov. Today* **2011**, *15*, 648-655.
13. Waring, M. J. Lipophilicity in drug discovery. *Expert Opin. Drug Discov.* **2010**, *5*, 235-248.
14. Bayliss, M. K.; Butler, J.; Feldman, P. L.; Green, D. V. S.; Leeson, P. D.; Palovich, M. R.; Taylor, A. J. Quality guidelines for oral drug candidates: dose, solubility and lipophilicity. *Drug Discov. Today* **2016**, *21*, 1719-1727.
15. Young, R. J.; Green, D. V. S.; Luscombe, C. N.; Hill, A. P. Getting physical in drug discovery II: the impact of chromatographic hydrophobicity measurements and aromaticity. *Drug Discov. Today* **2011**, *16*, 822-830.
16. Di, L.; Fish, P. V.; Mano, T. Bridging solubility between drug discovery and development. *Drug Discov. Today* **2012**, *17*, 486-495.
17. Alsenz, J.; Kansy, M. High throughput solubility measurement in drug discovery and development. *Adv. Drug Deliv. Rev.* **2007**, *59*, 546-567.

18. Williams, H. D.; Trevaskis, N. L.; Charman, S. A.; Shanker, R. M.; Charman, W. N.; Pouton, C. W.; Porter, C. J. H. Strategies to Address Low Drug Solubility in Discovery and Development. *Pharmacol. Rev.* **2013**, *65*, 315-499.
19. Baiwei, L.; Pease, J. H. A high throughput solubility assay for drug discovery using microscale shake-flask and rapid UHPLC-UV-CLND quantification. *J. Pharm. Biomed. Anal.* **2016**, *122*, 126-140.
20. Kestranek, A.; Chervenak, A.; Longenberger, J.; Placko, S. Chemiluminescent nitrogen detection (CLND) to measure kinetic aqueous solubility. *Curr. Protoc. Chem. Biol.* **2013**, *5*, 269-280.
21. Di, L.; Kerns, E. H. Profiling drug-like properties in discovery research. *Curr. Opin. Chem. Biol.* **2003**, *7*, 402-408.
22. Kansy, M.; Senner, F.; Gubernator, K. Physicochemical high throughput screening: parallel artificial membrane permeation assay in the description of passive absorption processes. *J. Med. Chem.* **1998**, *41*, 1007-1010.
23. Schürmann, M.; Janning, P.; Ziegler, S.; Waldmann, H. Small-Molecule Target Engagement in Cells. *Cell Chem. Bio.* **2016**, *23*, 435-441.
24. Durham, T. B.; Blanco, M.-J. Target Engagement in Lead Generation. *Bioorg. Med. Chem. Lett.* **2015**, *25*, 998-1008.
25. Yan, Y.; Marriott, G. Analysis of protein interactions using fluorescence technologies. *Curr. Opin. Chem. Biol.* **2003**, *7*, 635-640.
26. Jacqmin, P.; McFadyen, L.; Wade, J. R. A receptor theory-based semimechanistic PD model for the CCR5 noncompetitive antagonist maraviroc. *Br. J. Clin. Pharmacol.* **2008**, *65*, 95-106.
27. Rosario, M. C.; Jacqmin, P.; Dorr, P.; James, I.; Jenkins, T. M.; Abel, S.; Van Der Ryst, E. Population pharmacokinetic/ pharmacodynamic analysis of CCR5 receptor occupancy by maraviroc in healthy subjects and HIV-positive patients. *Br. J. Clin. Pharmacol.* **2008**, *65*, 86-94.
28. Hopkins, A. L.; Keserü, G. M.; Leeson, P. D.; Rees, D. C.; Reynolds, C. H. The role of ligand efficiency metrics in drug discovery. *Nat. Rev. Drug Discov.* **2014**, *13*, 105.
29. Hopkins, A. L.; Groom, C. R.; Alex, A. Ligand efficiency: a useful metric for lead selection. *Drug Discov. Today* **2004**, *9*, 430-431.
30. Mortenson, P. N.; Murray, C. W. Assessing the lipophilicity of fragments and early hits. *J. Comput. Aided Mol. Des.* **2011**, *25*, 663-667.
31. Xie, Q.; Soutto, M.; Xu, X.; Zhang, Y.; Johnson, C. H. Bioluminescence Resonance Energy Transfer (BRET) Imaging in Plant Seedlings and Mammalian Cells. In *Molecular Imaging: Methods and Protocols*, Shah, K., Ed. Humana Press: Totowa, NJ, 2011; pp 3-28.
32. Machleidt, T.; Woodroffe, C. C.; Schwinn, M. K.; Méndez, J.; Robers, M. B.; Zimmerman, K.; Otto, P.; Daniels, D. L.; Kirkland, T. A.; Wood, K. V. NanoBRET—A Novel BRET Platform for the Analysis of Protein–Protein Interactions. *ACS Chem. Biol.* **2015**, *10*, 1797-1804.
33. Philpott, M.; Rogers, C. M.; Yapp, C.; Wells, C.; Lambert, J.-P.; Strain-Damerell, C.; Burgess-Brown, N. A.; Gingras, A.-C.; Knapp, S.; Müller, S. Assessing cellular efficacy of bromodomain inhibitors using fluorescence recovery after photobleaching. *Epigenetics & Chromatin* **2014**, *7*, 14.
34. Sweet, M. J.; Hume, D. A. Endotoxin signal transduction in macrophages. *J. Leukoc. Biol.* **1996**, *60*, 8-26.
35. Lloyd, C. M.; Minto, A. W.; Dorf, M. E.; Proudfoot, A.; Wells, T. N. C.; Salant, D. J.; Gutierrez-Ramos, J.-C. RANTES and Monocyte Chemoattractant Protein–1 (MCP-1) Play an

- Important Role in the Inflammatory Phase of Crescentic Nephritis, but Only MCP-1 Is Involved in Crescent Formation and Interstitial Fibrosis. *J. Exp. Med.* **1997**, 185, 1371-1380.
36. Baeck, C.; Wehr, A.; Karlmark, K. R.; Heymann, F.; Vucur, M.; Gassler, N.; Huss, S.; Klussmann, S.; Eulberg, D.; Luedde, T.; Trautwein, C.; Tacke, F. Pharmacological inhibition of the chemokine CCL2 (MCP-1) diminishes liver macrophage infiltration and steatohepatitis in chronic hepatic injury. *Gut* **2012**, 61, 416-426.
37. Mukherjee, S. *The Gene An Intimate History*. **2016**, Penguin Random House: UK, p392-393.
38. Carey, N. The Epigenetics Revolution. In *The Epigenetics Revolution*, Icon Book Ltd: UK: 2011.
39. Carey, N. *Junk DNA*. Icon Books Ltd: UK: 2015.
40. Franklin, R. E.; Gosling, R. G. Molecular Configuration in Sodium Thymonucleate. *Nature* **1953**, 171, 740.
41. Watson, J. D.; Crick, F. H. C. Molecular Structure of Nucleic Acids: A Structure for Deoxyribose Nucleic Acid. *Nature* **1953**, 171, 737.
42. Wilkins, M. H. F.; Stokes, A. R.; Wilson, H. R. Molecular Structure of Nucleic Acids: Molecular Structure of Deoxypentose Nucleic Acids. *Nature* **1953**, 171, 738.
43. Watson, J. D.; Crick, F. H. C. Genetical Implications of the Structure of Deoxyribonucleic Acid. *Nature* **1953**, 171, 964.
44. Crick, F. Central Dogma of Molecular Biology. *Nature* **1970**, 227, 561.
45. Consortium, I. H. G. S. Finishing the euchromatic sequence of the human genome. *Nature* **2004**, 431, 931-945.
46. C. H. Arrowsmith; C. Bountra; P. V. Fish; K. Lee; Schapira, M. Epigenetic protein families: a new frontier for drug discovery. *Nat. Rev. Drug Discov.* **2012**, 11, 384-400.
47. Teif, V. B.; Rippe, K. Predicting nucleosome positions on the DNA: combining intrinsic sequence preferences and remodeler activities. *Nucleic Acids Res.* **2009**, 37, 5641-5655.
48. Mehler, M. F. Epigenetic principles and mechanisms underlying nervous system functions in health and disease. *Prog. Neurobiol.* **2008**, 86, 305-341.
49. G. Zhang; S. G. Smith; Zhou, M. Discovery of Chemical Inhibitors of Human Bromodomains. *Chem. Rev.* **2015**, 115, 11625-11668.
50. A. Csordas. On the biological role of histone acetylation. *Biochem. J* **1990**, 265, 23-38.
51. P. A. Marks; V. M. Richon; R. Breslow; Rifkind, R. A. Histone deacetylase inhibitors as new cancer drugs. *Curr. Opin. Oncol.* **2001**, 13, 477-483.
52. Brand, M.; Measures, A. M.; B. G. Wilson; Cortopassi, W. A.; Alexander, R.; Hoss, M.; Hewings, D. S.; Rooney, T. P. C.; Paton, R. S.; Conway, S. J. Small Molecule Inhibitors of Bromodomain-Acetyl-lysine Interactions. *ACS Chem. Biol.* **2015**, 10, 22-39.
53. S. Ropero; Esteller, M. The role of histone deacetylases (HDACs) in human cancer. *Mol. Oncol.* **2007**, 1, 19-25.
54. T. Jenuwein; Allis, C. D. Translating the histone code. *Science* **2001**, 293, 1074-1080.
55. Lee, K. K.; Workman, J. L. Histone acetyltransferase complexes: one size doesn't fit all. *Nat. Rev. Mol. Cell Bio.* **2007**, 8, 284-295.
56. D. Bandyopadhyay; N. A. Okan; E. Bales; L. Nascimento; P. A. Cole; Medrano, E. E. Down-regulation of p300/CBP histone acetyltransferase activates a senescence checkpoint in human melanocytes. *Cancer Res.* **2002**, 62, 6231-6239.
57. Ito, K.; Caramori, G.; Lim, S.; Oates, T.; Chung, K. F.; Barnes, P. J.; Adcock, I. M. Expression and activity of histone deacetylases in human asthmatic airways. *Am. J. Respir. Crit. Care Med.* **2002**, 166, 392-396.

58. P. Barnes; Adcock, I. M.; Ito, K. Histone acetylation and deacetylation: Importance in inflammatory lung diseases. *Eur. Respir. J.* **2005**, *25*, 552-563.
59. K. Mantelingu; Reddy, B. A. A.; Swaminathan, V.; Kishore, A. H.; Siddappa, N. B.; Kumar, G. V. P.; Nagashankar, G.; Natesh, N.; Roy, S.; Sadhale, P. P.; Ranga, U.; Narayana, C.; Kundu, T. K. Specific Inhibition of p300-HAT Alters Global Gene Expression and Represses HIV Replication. *Chem. Biol.* **2007**, *14*, 645-657.
60. Ryu, Y.-K.; Park, H.-Y.; Go, J.; Kim, Y.-H.; Hwang, J. H.; Choi, D.-H.; Noh, J.-R.; Rhee, M.; Han, P.-L.; Lee, C.-H.; Kim, K.-S. Effects of histone acetyltransferase inhibitors on L-DOPA-induced dyskinesia in a murine model of Parkinson's disease. *J. Neural Transm.* **2018**, *125*, 1319-1331.
61. F. J. Dekker; Haisma, H. J. Histone acetyl transferases as emerging drug targets. *Drug Discov. Today* **2009**, *14*, 942-948.
62. S. A. Gayther; S. J. Batley; L. Linger; A. Bannister; K. Thorpe; S. Chin; Y. Daigo; P. Russell; A. Wilson; Sowter, H. M.; Delhanty, J. D. A.; B. A. J. Ponder; T. Kouzarides; Caldas, C. Mutations truncating the EP300 acetylase in human cancers. *Nat. Genet.* **2000**, *24*, 300-303.
63. Eliseeva, E. D.; Valkov, V.; Jung, M.; Jung, M. O. Characterization of novel inhibitors of histone acetyltransferases. *Mol. Cancer Ther.* **2007**, *6*, 2391-2398.
64. Dahlin, J. L.; Nelson, K. M.; Strasser, J. M.; Barsyte-Lovejoy, D.; Szewczyk, M. M.; Organ, S.; Cuellar, M.; Singh, G.; Shrimp, J. H.; Nguyen, N.; Meier, J. L.; Arrowsmith, C. H.; Brown, P. J.; Baell, J. B.; Walters, M. A. Assay interference and off-target liabilities of reported histone acetyltransferase inhibitors. *Nat. Commun.* **2017**, *8*, 1527.
65. Costi, R.; Di Santo, R.; Artico, M.; Miele, G.; Valentini, P.; Novellino, E.; Cereseto, A. Cinnamoyl Compounds as Simple Molecules that Inhibit p300 Histone Acetyltransferase. *J. Med. Chem.* **2007**, *50*, 1973-1977.
66. Chimenti, F.; Bizzarri, B.; Maccioni, E.; Secci, D.; Bolasco, A.; Chimenti, P.; Fioravanti, R.; Granese, A.; Carradori, S.; Tosi, F.; Ballario, P.; Vernarecci, S.; Filetici, P. A Novel Histone Acetyltransferase Inhibitor Modulating Gcn5 Network: Cyclopentylidene-[4-(4'-chlorophenyl)thiazol-2-yl]hydrazone. *J. Med. Chem.* **2009**, *52*, 530-536.
67. Bowers, E. M.; Yan, G.; Mukherjee, C.; Orry, A.; Wang, L.; Holbert, M. A.; Crump, N. T.; Hazzalin, C. A.; Liszczak, G.; Yuan, H.; Larocca, C.; Saldanha, S. A.; Abagyan, R.; Sun, Y.; Meyers, D. J.; Marmorstein, R.; Mahadevan, L. C.; Alani, R. M.; Cole, P. A. Virtual Ligand Screening of the p300/CBP Histone Acetyltransferase: Identification of a Selective Small Molecule Inhibitor. *Chem. Biol.* **2010**, *17*, 471-482.
68. Mai, A.; Rotili, D.; Tarantino, D.; Nebbioso, A.; Castellano, S.; Sbardella, G.; Tini, M.; Altucci, L. Identification of 4-hydroxyquinolines inhibitors of p300/CBP histone acetyltransferases. *Bioorg. Med. Chem. Lett.* **2009**, *19*, 1132-1135.
69. Haberland, M.; Montgomery, R. L.; Olson, E. N. The many roles of histone deacetylases in development and physiology: implications for disease and therapy. *Nat. Rev. Genet.* **2009**, *10*, 32.
70. Bradner, J. E.; West, N.; Grachan, M. L.; Greenberg, E. F.; Haggarty, S. J.; Warnow, T.; Mazitschek, R. Chemical phylogenetics of histone deacetylases. *Nat. Chem. Biol.* **2010**, *6*, 238.
71. McClure, J. J.; Li, X.; Chou, C. J. Advances and Challenges of HDAC Inhibitors in Cancer Therapeutics. In *Adv. Cancer Res.*, Tew, K. D.; Fisher, P. B., Eds. Academic Press: 2018; Vol. 138, pp 183-211.
72. Marks, A. P.; Breslow, R. Dimethyl sulfoxide to vorinostat: development of this histone deacetylase inhibitor as an anticancer drug. *Nat. Biotechnol.* **2007**, *25*, 84-90.
73. S. G. Mack. To selectivity and beyond. *Nat. Biotechnol.* **2010**, *28*, 1259-1266.

74. X. Qian; G. Ara; E. Mills; Rochelle, W. J. L.; Lichenstein, H. S.; Jeffers, M. Activity of the histone deacetylase inhibitor belinostat (PXD101) in preclinical models of prostate cancer. *Int. J. Cancer* **2008**, *122*, 1400-1410.
75. Z. Qiao; Ren, S.; Li, W.; Wang, X.; He, M.; Guo, Y.; Sun, L.; He, Y.; Ge, Y.; Yu, Q. Chidamide, a novel histone deacetylase inhibitor, synergistically enhances gemcitabine cytotoxicity in pancreatic cancer cells. *Biochem. Biophys. Res. Commun.* **2013**, *434*, 95-101.
76. Suzuki, T.; Ando, T.; Tsuchiya, K.; Fukazawa, N.; Saito, A.; Mariko, Y.; Yamashita, T.; Nakanishi, O. Synthesis and Histone Deacetylase Inhibitory Activity of New Benzamide Derivatives. *J. Med. Chem.* **1999**, *42*, 3001-3003.
77. Hu, E.; Dul, E.; Sung, C.-M.; Chen, Z.; Kirkpatrick, R.; Zhang, G.-F.; Johanson, K.; Liu, R.; Lago, A.; Hofmann, G.; Macarron, R.; De Los Frailes, M.; Perez, P.; Krawiec, J.; Winkler, J.; Jaye, M. Identification of Novel Isoform-Selective Inhibitors within Class I Histone Deacetylases. *J. Pharmacol. Exp. Ther.* **2003**, *307*, 720-728.
78. Iyer, S. P.; Foss, F. F. Romidepsin for the treatment of peripheral T-cell lymphoma. *Oncologist* **2015**, *20*, 1084-1091.
79. Falkenberg, K. J.; Johnstone, R. W. Histone deacetylases and their inhibitors in cancer, neurological diseases and immune disorders. *Nat. Rev. Drug Discov.* **2014**, *13*, 673.
80. Rubin, E. H.; Agrawal, N. G. B.; Friedman, E. J.; Scott, P.; Mazina, K. E.; Sun, L.; Du, L.; Ricker, J. L.; Frankel, S. R.; Gottesdiener, K. M.; Wagner, J. A.; Iwamoto, M. A Study to Determine the Effects of Food and Multiple Dosing on the Pharmacokinetics of Vorinostat Given Orally to Patients with Advanced Cancer. *Clin. Cancer Res.* **2006**, *12*, 7039-7045.
81. S. R. Haynes; C. Dollard; F. Winston; S. Beck; J. Trowsdale; Dawid, I. B. The bromodomain: a conserved sequence found in human, Drosophila and yeast proteins. *Nucleic Acids Res.* **1992**, *20*, 2603-0.
82. G. Zhang; R. Sanchez; Zhou, M. Scaling the Druggability Landscape of Human Bromodomains, a New Class of Drug Targets. *J. Med. Chem.* **2012**, *55*, 7342-7345.
83. N. H. Theodoulou; N. C. O. Tomkinson; R. K. Prinjha; Humphreys, P. G. Progress in the Development of non-BET Bromodomain Chemical Probes. *ChemMedChem* **2016**, *11*, 477-487.
84. Perry, M. M.; Durham, A. L.; Austin, P. J.; Adcock, I. M.; Chung, K. F. BET Bromodomains Regulate Transforming Growth Factor- β -induced Proliferation and Cytokine Release in Asthmatic Airway Smooth Muscle. *J. Biol. Chem.* **2015**, *290*, 9111-9121.
85. Zhang, G.; Liu, R.; Zhong, Y.; Plotnikov, A. N.; Zhang, W.; Zeng, L.; Rusinova, E.; Gerona-Nevarro, G.; Moshkina, N.; Joshua, J.; Chuang, P. Y.; Ohlmeyer, M.; He, J. C.; Zhou, M.-M. Down-regulation of NF- κ B Transcriptional Activity in HIV-associated Kidney Disease by BRD4 Inhibition. *J. Biol. Chem.* **2012**, *287*, 28840-28851.
86. Bisgrove, D. A.; Mahmoudi, T.; Henklein, P.; Verdin, E. Conserved P-TEFb-interacting domain of BRD4 inhibits HIV transcription. *Proc. Natl. Acad. Sci.* **2007**, *104*, 13690-13695.
87. Schulz, D.; Mugnier, M. R.; Paulsen, E.-M.; Kim, H.-S.; Chung, C.-w. W.; Tough, D. F.; Rioja, I.; Prinjha, R. K.; Papavasiliou, F. N.; Debler, E. W. Bromodomain Proteins Contribute to Maintenance of Bloodstream Form Stage Identity in the African Trypanosome. *PLoS Biol.* **2015**, *13*, e1002316.
88. Fu, W.; Farache, J.; Clardy, S. M.; Hattori, K.; Mander, P.; Lee, K.; Rioja, I.; Weissleder, R.; Prinjha, R. K.; Benoist, C.; Mathis, D. Epigenetic modulation of type-1 diabetes via a dual effect on pancreatic macrophages and β cells. In *eLife*, 2014; Vol. 3, p e04631.
89. Khan, Y. M.; Kirkham, P.; Barnes, P. J.; Adcock, I. M. Brd4 Is Essential for IL-1 β -Induced Inflammation in Human Airway Epithelial Cells. *PLoS One* **2014**, *9*, e95051.

90. French, C. A.; Ramirez, C. L.; Kolmakova, J.; Hickman, T. T.; Cameron, M. J.; Thyne, M. E.; Kutok, J. L.; Toretsky, J. A.; Tadavarthy, A. K.; Kees, U. R.; Fletcher, J. A.; Aster, J. C. BRD–NUT oncoproteins: a family of closely related nuclear proteins that block epithelial differentiation and maintain the growth of carcinoma cells. *Oncogene* **2007**, *27*, 2237.
91. French, C. A. NUT midline carcinoma. *Cancer Genet. Cytogenet.* **2010**, *203*, 16-20.
92. Doroshow, D. B.; Eder, J. P.; LoRusso, P. M. BET inhibitors: a novel epigenetic approach. *Ann. Oncol.* **2017**, *28*, 1776-1787.
93. Braun, T.; Gardin, C. Investigational BET bromodomain protein inhibitors in early stage clinical trials for acute myelogenous leukemia (AML). *Expert Opin. Investig. Drugs* **2017**, *26*, 803-811.
94. Zuber, J.; Shi, J.; Wang, E.; Rappaport, A. R.; Herrmann, H.; Sison, E. A.; Magoon, D.; Qi, J.; Blatt, K.; Wunderlich, M.; Taylor, M. J.; Johns, C.; Chicas, A.; Mulloy, J. C.; Kogan, S. C.; Brown, P.; Valent, P.; Bradner, J. E.; Lowe, S. W.; Vakoc, C. R. RNAi screen identifies Brd4 as a therapeutic target in acute myeloid leukaemia. *Nature* **2011**, *478*, 524.
95. Basheer, F.; Huntly, B. J. P. BET bromodomain inhibitors in leukemia. *Exp. Hematol.* **2015**, *43*, 718-731.
96. Chen, C.; Liu, Y.; Lu, C.; Cross, J. R.; Morris, J. P.; Shroff, A. S.; Ward, P. S.; Bradner, J. E.; Thompson, C.; Lowe, S. W. Cancer-associated IDH2 mutants drive an acute myeloid leukemia that is susceptible to Brd4 inhibition. *Genes Dev.* **2013**, *27*, 1974-1985.
97. Mertz, J. A.; Conery, A. R.; Bryant, B. M.; Sandy, P.; Balasubramanian, S.; Mele, D. A.; Bergeron, L.; Sims, R. J. Targeting MYC dependence in cancer by inhibiting BET bromodomains. *Proc. Natl. Acad. Sci.* **2011**, *108*, 16669-16674.
98. Baratta, M. G.; Schinzel, A. C.; Zwang, Y.; Bandopadhyay, P.; Bowman-Colin, C.; Kutt, J.; Curtis, J.; Piao, H.; Wong, L. C.; Kung, A. L.; Beroukhim, R.; Bradner, J. E.; Drapkin, R.; Hahn, W. C.; Liu, J. F.; Livingston, D. M. An in-tumor genetic screen reveals that the BET bromodomain protein, BRD4, is a potential therapeutic target in ovarian carcinoma. *Proc. Natl. Acad. Sci.* **2015**, *112*, 232-237.
99. Wyce, A.; Degenhardt, Y.; Bai, Y.; Le, B.; Korenchuk, S.; Crouthamel, M.-C.; McHugh, C. F.; Vessella, R.; Creasy, C. L.; Tummino, P. J.; Barbash, O. Inhibition of BET bromodomain proteins as a therapeutic approach in prostate cancer. *Oncotarget* **2013**, *4*, 2419-2429.
100. Henssen, A.; Thor, T.; Odersky, A.; Heukamp, L.; El-Hindy, N.; Beckers, A.; Speleman, F.; Althoff, K.; Schäfers, S.; Schramm, A.; Sure, U.; Fleischhack, G.; Eggert, A.; Schulte, J. H. BET bromodomain protein inhibition is a therapeutic option for medulloblastoma. *Oncotarget* **2013**, *4*, 2080-2095.
101. Cheng, Z.; Gong, Y.; Ma, Y.; Lu, K.; Lu, X.; Pierce, L. A.; Thompson, R. C.; Muller, S.; Knapp, S.; Wang, J. Inhibition of BET Bromodomain Targets Genetically Diverse Glioblastoma. *Clin. Cancer Res.* **2013**, *19*, 1748-1759.
102. Tolani, B.; Gopalakrishnan, R.; Punj, V.; Matta, H.; Chaudhary, P. M. Targeting Myc in KSHV-associated primary effusion lymphoma with BET bromodomain inhibitors. *Oncogene* **2013**, *33*, 2928.
103. Bernasconi, E.; Gaudio, E.; Kwee, I.; Bertoni, F. Assessment of the Antiproliferative Activity of a BET Bromodomain Inhibitor as Single Agent and in Combination in Non-Hodgkin Lymphoma Cell Lines. In *Histone Deacetylases: Methods and Protocols*, Sarkar, S., Ed. Springer New York: New York, NY, 2016; pp 305-312.
104. Wu, Z.; Hu, Z.; Han, X.; Li, Z.; Zhu, Q.; Wang, Y.; Zheng, Q.; Yan, J. The BET-Bromodomain Inhibitor JQ1 synergized ABT-263 against colorectal cancer cells through suppressing c-Myc-induced miR-1271-5p expression. *Biomed. Pharmacother.* **2017**, *95*, 1574-1579.

105. Shao, Q.; Kannan, A.; Lin, Z.; Stack, B. C.; Suen, J. Y.; Gao, L. BET Protein Inhibitor JQ1 Attenuates Myc-Amplified MCC Tumor Growth *In Vivo*. *Cancer Res.* **2014**, *74*, 7090-7102.
106. Ozer, H. G.; El-Gamal, D.; Powell, B.; Hing, Z. A.; Blachly, J. S.; Harrington, B.; Mitchell, S.; Grieselhuber, N. R.; Williams, K.; Lai, T.-H.; Alinari, L.; Baiocchi, R. A.; Brinton, L.; Baskin, E.; Cannon, M.; Beaver, L.; Goettl, V. M.; Lucas, D. M.; Woyach, J. A.; Sampath, D.; Lehman, A. M.; Yu, L.; Zhang, J.; Ma, Y.; Zhang, Y.; Spevak, W.; Shi, S.; Severson, P.; Shellooe, R.; Carias, H.; Tsang, G.; Dong, K.; Ewing, T.; Marimuthu, A.; Tantoy, C.; Walters, J.; Sanftner, L.; Rezaei, H.; Nespi, M.; Matusow, B.; Habets, G.; Ibrahim, P.; Zhang, C.; Mathé, E. A.; Bollag, G.; Byrd, J. C.; Lapalombella, R. BRD4 Profiling Identifies Critical Chronic Lymphocytic Leukemia Oncogenic Circuits and Reveals Sensitivity to PLX51107, a Novel Structurally Distinct BET Inhibitor. *Cancer Discov.* **2018**, *8*, 458-477.
107. Puissant, A.; Frumm, S. M.; Alexe, G.; Bassil, C. F.; Qi, J.; Chanthery, Y. H.; Nekritz, E. A.; Zeid, R.; Gustafson, W. C.; Greninger, P.; Garnett, M. J.; McDermott, U.; Benes, C. H.; Kung, A. L.; Weiss, W. A.; Bradner, J. E.; Stegmaier, K. Targeting MYCN in Neuroblastoma by BET Bromodomain Inhibition. *Cancer Discov.* **2013**, *3*, 308-323.
108. Segura, M. F.; Fontanals-Cirera, B.; Gaziel-Sovran, A.; Guijarro, M. V.; Hanniford, D.; Zhang, G.; González-Gomez, P.; Morante, M.; Jubierre, L.; Zhang, W.; Darvishian, F.; Ohlmeyer, M.; Osman, I.; Zhou, M.-M.; Hernando, E. BRD4 Sustains Melanoma Proliferation and Represents a New Target for Epigenetic Therapy. *Cancer Res.* **2013**, *73*, 6264.
109. Chaidos, A.; Caputo, V.; Gouvedenou, K.; Liu, B.; Marigo, I.; Chaudhry, M. S.; Rotolo, A.; Tough, D. F.; Smithers, N. N.; Bassil, A. K.; Chapman, T. D.; Harker, N. R.; Barbash, O.; Tummino, P.; Al-Mahdi, N.; Haynes, A. C.; Cutler, L.; Le, B.; Rahemtulla, A.; Roberts, I.; Kleijnen, M.; Witherington, J. J.; Parr, N. J.; Prinjha, R. K.; Karadimitris, A. Potent antimyeloma activity of the novel bromodomain inhibitors I-BET151 and I-BET762. *Blood* **2014**, *123*, 697.
110. da Motta, L. L.; Ledaki, I.; Purshouse, K.; Haider, S.; De Bastiani, M. A.; Baban, D.; Morotti, M.; Steers, G.; Wigfield, S.; Bridges, E.; Li, J. L.; Knapp, S.; Ebner, D.; Klamt, F.; Harris, A. L.; McIntyre, A. The BET inhibitor JQ1 selectively impairs tumour response to hypoxia and downregulates CA9 and angiogenesis in triple negative breast cancer. *Oncogene* **2016**, *36*, 122.
111. Rhyasen, G. W.; Hattersley, M. M.; Yao, Y.; Dulak, A.; Wang, W.; Petteruti, P.; Dale, I. L.; Boiko, S.; Cheung, T.; Zhang, J.; Wen, S.; Castriotta, L.; Lawson, D.; Collins, M.; Bao, L.; Ahdesmaki, M. J.; Walker, G.; O'Connor, G.; Yeh, T. C.; Rabow, A. A.; Dry, J. R.; Reimer, C.; Lyne, P.; Mills, G. B.; Fawell, S. E.; Waring, M. J.; Zinda, M.; Clark, E.; Chen, H. AZD5153: A Novel Bivalent BET Bromodomain Inhibitor Highly Active against Hematologic Malignancies. *Mol. Cancer Ther.* **2016**, *15*, 2563-2574.
112. Boi, M.; Gaudio, E.; Bonetti, P.; Kwee, I.; Bernasconi, E.; Tarantelli, C.; Rinaldi, A.; Testoni, M.; Cascione, L.; Ponzoni, M.; Mensah, A. A.; Stathis, A.; Stussi, G.; Riveiro, M. E.; Herait, P.; Inghirami, G.; Cvitkovic, E.; Zucca, E.; Bertoni, F. The BET Bromodomain Inhibitor OTX015 Affects Pathogenetic Pathways in Preclinical B-cell Tumor Models and Synergizes with Targeted Drugs. *Clin. Cancer Res.* **2015**, *21*, 1628.
113. Ba, M.; Long, H.; Yan, Z.; Wang, S.; Wu, Y.; Tu, Y.; Gong, Y.; Cui, S. BRD4 promotes gastric cancer progression through the transcriptional and epigenetic regulation of c-MYC. *J. Cell. Biochem.* **2018**, *119*, 973-982.
114. Delmore, Jake E.; Issa, Ghayas C.; Lemieux, Madeleine E.; Rahl, Peter B.; Shi, J.; Jacobs, Hannah M.; Kastiris, E.; Gilpatrick, T.; Paranal, Ronald M.; Qi, J.; Chesi, M.; Schinzel, Anna C.; McKeown, Michael R.; Heffernan, Timothy P.; Vakoc, Christopher R.; Bergsagel, P. L.; Ghobrial, Irene M.; Richardson, Paul G.; Young, Richard A.; Hahn, William C.; Anderson,

- Kenneth C.; Kung, Andrew L.; Bradner, James E.; Mitsiades, Constantine S. BET Bromodomain Inhibition as a Therapeutic Strategy to Target c-Myc. *Cell* **2011**, 146, 904-917.
115. Jang, M. K.; Mochizuki, K.; Zhou, M.; Jeong, H.-S.; Brady, J. N.; Ozato, K. The Bromodomain Protein Brd4 Is a Positive Regulatory Component of P-TEFb and Stimulates RNA Polymerase II-Dependent Transcription. *Mol. Cell* **2005**, 19, 523-534.
116. Whyte, Warren A.; Orlando, David A.; Hnisz, D.; Abraham, Brian J.; Lin, Charles Y.; Kagey, Michael H.; Rahl, Peter B.; Lee, Tong I.; Young, Richard A. Master Transcription Factors and Mediator Establish Super-Enhancers at Key Cell Identity Genes. *Cell* **2013**, 153, 307-319.
117. Lovén, J.; Hoke, Heather A.; Lin, Charles Y.; Lau, A.; Orlando, David A.; Vakoc, Christopher R.; Bradner, James E.; Lee, Tong I.; Young, Richard A. Selective Inhibition of Tumor Oncogenes by Disruption of Super-Enhancers. *Cell* **2013**, 153, 320-334.
118. Coude, M.; Braun, T.; Berrou, J.; Dupont, M.; Bertrand, S.; Masse, A.; Raffloux, E.; Itzykson, R.; Delord, M.; Riveiro, M. E.; Herait, P.; Baruchel, A.; Dombret, H.; Gardin, C. BET inhibitor OTX015 targets BRD2 and BRD4 and decreases c-MYC in acute leukemia cells. *Oncotarget* **2015**, 6, 17698.
119. <https://clinicaltrials.gov/ct2/home>. (24/10/2018).
120. Zhang, Q.-g.; Qian, J.; Zhu, Y.-c. Targeting bromodomain-containing protein 4 (BRD4) benefits rheumatoid arthritis. *Immunol. Lett.* **2015**, 166, 103-108.
121. Liu, Z.; Wang, P.; Chen, H.; Wold, E. A.; Tian, B.; Brasier, A. R.; Zhou, J. Drug Discovery Targeting Bromodomain-Containing Protein 4. *J. Med. Chem.* **2017**, 60, 4533-4558.
122. Tough, D. F.; Tak, P. P.; Tarakhovskiy, A.; Prinjha, R. K. Epigenetic drug discovery: breaking through the immune barrier. *Nat. Rev. Drug Discov.* **2016**, 15, 835.
123. Klein, K.; Kabala, P. A.; Grabiec, A. M.; Gay, R. E.; Kolling, C.; Lin, L.-L.; Gay, S.; Tak, P. P.; Prinjha, R. K.; Ospelt, C.; Reedquist, K. A. The bromodomain protein inhibitor I-BET151 suppresses expression of inflammatory genes and matrix degrading enzymes in rheumatoid arthritis synovial fibroblasts. *Ann. Rheum. Dis.* **2016**, 75, 422.
124. Meng, S.; Zhang, L.; Tang, Y.; Tu, Q.; Zheng, L.; Yu, L.; Murray, D.; Cheng, J.; Kim, S. H.; Zhou, X.; Chen, J. BET Inhibitor JQ1 Blocks Inflammation and Bone Destruction. *J. Dent. Res.* **2014**, 93, 657-662.
125. Park-Min, K.-H.; Lim, E.; Lee, M. J.; Park, S. H.; Giannopoulou, E.; Yarilina, A.; van der Meulen, M.; Zhao, B.; Smithers, N.; Witherington, J.; Lee, K.; Tak, P. P.; Prinjha, R. K.; Ivashkiv, L. B. Inhibition of osteoclastogenesis and inflammatory bone resorption by targeting BET proteins and epigenetic regulation. *Nat. Commun.* **2014**, 5, 5418.
126. Nicodeme, E.; Jeffrey, K. L.; Schaefer, U.; Beinke, S.; Dewell, S.; Chung, C.-w.; Chandwani, R.; Marazzi, I.; Wilson, P.; Coste, H.; White, J.; Kirilovsky, J.; Rice, C. M.; Lora, J. M.; Prinjha, R. K.; Lee, K.; Tarakhovskiy, A. Suppression of inflammation by a synthetic histone mimic. *Nature* **2010**, 468, 1119.
127. Schilderink, R.; Bell, M.; Reginato, E.; Patten, C.; Rioja, I.; Hilbers, F. W.; Kabala, P. A.; Reedquist, K. A.; Tough, D. F.; Tak, P. P.; Prinjha, R. K.; de Jonge, W. J. BET bromodomain inhibition reduces maturation and enhances tolerogenic properties of human and mouse dendritic cells. *Mol. Immunol.* **2016**, 79, 66-76.
128. Bandukwala, H. S.; Gagnon, J.; Togher, S.; Greenbaum, J. A.; Lamperti, E. D.; Parr, N. J.; Molesworth, A. M. H.; Smithers, N.; Lee, K.; Witherington, J.; Tough, D. F.; Prinjha, R. K.; Peters, B.; Rao, A. Selective inhibition of CD4+ T-cell cytokine production and autoimmunity by BET protein and c-Myc inhibitors. *Proc. Natl. Acad. Sci.* **2012**, 109, 14532.

129. Mele, D. A.; Salmeron, A.; Ghosh, S.; Huang, H.-R.; Bryant, B. M.; Lora, J. M. BET bromodomain inhibition suppresses T(H)17-mediated pathology. *J. Exp. Med.* **2013**, *210*, 2181-2190.
130. McLure, K. G.; Gesner, E. M.; Tsujikawa, L.; Kharenko, O. A.; Attwell, S.; Campeau, E.; Wasiaik, S.; Stein, A.; White, A.; Fontano, E.; Suto, R. K.; Wong, N. C. W.; Wagner, G. S.; Hansen, H. C.; Young, P. R. RVX-208, an Inducer of ApoA-I in Humans, Is a BET Bromodomain Antagonist. *PLoS One* **2014**, *8*, e83190.
131. Nadeem, A.; Al-Harbi, N. O.; Al-Harbi, M. M.; El-Sherbeeney, A. M.; Ahmad, S. F.; Siddiqui, N.; Ansari, M. A.; Zoheir, K. M. A.; Attia, S. M.; Al-Hosaini, K. A.; Al-Sharary, S. D. Imiquimod-induced psoriasis-like skin inflammation is suppressed by BET bromodomain inhibitor in mice through RORC/IL-17A pathway modulation. *Pharmacol. Res.* **2015**, *99*, 248-257.
132. Prinjha, R. K.; Witherington, J.; Lee, K. Place your BETs: the therapeutic potential of bromodomains. *Trends Pharmacol. Sci.* **2012**, *33*, 146-153.
133. Huang, B.; Yang, X.-D.; Zhou, M.-M.; Ozato, K.; Chen, L.-F. Brd4 Coactivates Transcriptional Activation of NF- κ B via Specific Binding to Acetylated RelA. *Mol. Cell. Biol.* **2009**, *29*, 1375-1387.
134. A. C. Belkina; Denis, G. V. BET domain co-regulators in obesity, inflammation and cancer. *Nat. Rev. Cancer* **2012**, *12*, 465-477.
135. Arkin, Michelle R.; Tang, Y.; Wells, James A. Small-Molecule Inhibitors of Protein-Protein Interactions: Progressing toward the Reality. *Chem. Biol.* **2014**, *21*, 1102-1114.
136. P. Filippakopoulos; S. Picaud; M. Mangos; T. Keates; J. Lambert; D. Barsyte-Lovejoy; I. Felletar; R. Volkmer; S. M.; T. Pawson; A. Gringras; C. Arrowsmith; Knapp, S. Histone Recognition and Large-Scale Structural Analysis of the Human Bromodomain Family. *Cell* **2012**, *149*, 214-231.
137. S. G. Smith; Zhou, M. The Bromodomain: A New Target in Emerging Epigenetic Medicine. *ACS Chem. Biol.* **2016**, *11*, 598-608.
138. Cox, O. B.; Krojer, T.; Collins, P.; Monteiro, O.; Talon, R.; Bradley, A.; Fedorov, O.; Amin, J.; Marsden, B. D.; Spencer, J.; von Delft, F.; Brennan, P. E. A poised fragment library enables rapid synthetic expansion yielding the first reported inhibitors of PHIP(2), an atypical bromodomain. *Chem. Sci.* **2016**, *7*, 2322-2330.
139. F. A. Romero; A. M. Taylor; T. D. Crawford; V. Tsui; A. Côté; Magnuson, S. Disrupting Acetyl-Lysine Recognition: Progress in the Development of Bromodomain Inhibitors. *J. Med. Chem.* **2016**, *59*, 1271-1298.
140. Filippakopoulos, P.; Qi, J.; Picaud, S.; Shen, Y.; Smith, W. B.; Fedorov, O.; Morse, E. M.; Keates, T.; Hickman, T. T.; Felletar, I.; Philpott, M.; Munro, S.; McKeown, M. R.; Wang, Y.; Christie, A. L.; West, N.; Cameron, M. J.; Schwartz, B.; Heightman, T. D.; La Thangue, N.; French, C. A.; Wiest, O.; Kung, A. L.; Knapp, S.; Bradner, J. E. Selective inhibition of BET bromodomains. *Nature* **2010**, *468*, 1067.
141. O. Mirguet; R. Gosmini; J. Toum; C. A. Clément; M. Barnathan; J. Brusq; J. E. Mardaunt; R. M. Grimes; M. Crowe; O. Pinaeu; M. Ajakane; A. Daugan; P. Jeffrey; L. Cutler; A. C. Haynes; N. N. Smithers; C. Chung; P. Bamborough; I. J. Uings; A. Lewis; J. Witherington; N. Parr; R. K. Prinjha; Nicodeme, E. Discovery of Epigenetic Regulator I-BET762: Lead Optimization to Afford a Clinical Candidate Inhibitor of the BET Bromodomains. *J. Med. Chem.* **2013**, *56*, 7501-7515.
142. Berthon, C.; Raffoux, E.; Thomas, X.; Vey, N.; Gomez-Roca, C.; Yee, K.; Taussig, D. C.; Rezai, K.; Roumier, C.; Herait, P.; Kahatt, C.; Quesnel, B.; Michallet, M.; Recher, C.; Lokiec, F.; Preudhomme, C.; Dombret, H. Bromodomain inhibitor OTX015 in patients with acute leukaemia: a dose-escalation, phase 1 study. *The Lancet Haematology* **2016**, *3*, e186-e195.

143. Stathis, A.; Zucca, E.; Bekradda, M.; Gomez-Roca, C.; Delord, J.-P.; de La Motte Rouge, T.; Uro-Coste, E.; de Braud, F.; Pelosi, G.; French, C. A. Clinical Response of Carcinomas Harboring the BRD4–NUT Oncoprotein to the Targeted Bromodomain Inhibitor OTX015/MK-8628. *Cancer Discov.* **2016**, *6*, 492-500.
144. Shapiro, G. I.; Dowlati, A.; LoRusso, P. M.; Eder, J. P.; Anderson, A.; Do, K. T.; Kagey, M. H.; Sirard, C.; Bradner, J. E.; Landau, S. B. Abstract A49: Clinically efficacy of the BET bromodomain inhibitor TEN-010 in an open-label substudy with patients with documented NUT-midline carcinoma (NMC). *Mol. Cancer Ther.* **2015**, *14*, A49-A49.
145. Mirguet, O.; Lamotte, Y.; Donche, F.; Toum, J.; Gellibert, F.; Bouillot, A.; Gosmini, R.; Nguyen, V.-L.; Delannée, D.; Seal, J.; Blandel, F.; Boullay, A.-B.; Boursier, E.; Martin, S.; Brusq, J.-M.; Krysa, G.; Riou, A.; Tellier, R.; Costaz, A.; Huet, P.; Dudit, Y.; Trottet, L.; Kirilovsky, J.; Nicodeme, E. From ApoA1 upregulation to BET family bromodomain inhibition: Discovery of I-BET151. *Bioorg. Med. Chem. Lett.* **2012**, *22*, 2963-2967.
146. Seal, J.; Lamotte, Y.; Donche, F.; Bouillot, A.; Mirguet, O.; Gellibert, F.; Nicodeme, E.; Krysa, G.; Kirilovsky, J.; Beinke, S.; McCleary, S.; Rioja, I.; Bamborough, P.; Chung, C.-W.; Gordon, L.; Lewis, T.; Walker, A. L.; Cutler, L.; Lugo, D.; Wilson, D. M.; Witherington, J.; Lee, K.; Prinjha, R. K. Identification of a novel series of BET family bromodomain inhibitors: Binding mode and profile of I-BET151 (GSK1210151A). *Bioorg. Med. Chem. Lett.* **2012**, *22*, 2968-2972.
147. Wilson, A. J.; Stubbs, M.; Liu, P.; Ruggeri, B.; Khabele, D. The BET inhibitor INCB054329 reduces homologous recombination efficiency and augments PARP inhibitor activity in ovarian cancer. *Gynecol. Oncol.* **2018**, *149*, 575-584.
148. Duan, Y.-C.; Guan, Y.; Qin, W.; Zhai, X.; Yu, B.; Liu, H.-M. Targeting Brd4 for Cancer therapy: Inhibitors and Degraders. *MedChemComm* **2018**.
149. Gehling, V. S.; Hewitt, M. C.; Vaswani, R. G.; Leblanc, Y.; Côté, A.; Nasveschuk, C. G.; Taylor, A. M.; Harmange, J.-C.; Audia, J. E.; Pardo, E.; Joshi, S.; Sandy, P.; Mertz, J. A.; Sims, R. J.; Bergeron, L.; Bryant, B. M.; Bellon, S.; Poy, F.; Jayaram, H.; Sankaranarayanan, R.; Yellapantula, S.; Bangalore Srinivasamurthy, N.; Birudukota, S.; Albrecht, B. K. Discovery, Design, and Optimization of Isoxazole Azepine BET Inhibitors. *ACS Med. Chem. Lett.* **2013**, *4*, 835-840.
150. Theodoulou, N. H.; Tomkinson, N. C. O.; Prinjha, R. K.; Humphreys, P. G. Clinical progress and pharmacology of small molecule bromodomain inhibitors. *Curr. Opin. Chem. Biol.* **2016**, *33*, 58-66.
151. McDaniel, K. F.; Wang, L.; Soltwedel, T.; Fidanze, S. D.; Hasvold, L. A.; Liu, D.; Mantei, R. A.; Pratt, J. K.; Sheppard, G. S.; Bui, M. H.; Faivre, E. J.; Huang, X.; Li, L.; Lin, X.; Wang, R.; Warder, S. E.; Wilcox, D.; Albert, D. H.; Magoc, T. J.; Rajaraman, G.; Park, C. H.; Hutchins, C. W.; Shen, J. J.; Edalji, R. P.; Sun, C. C.; Martin, R.; Gao, W.; Wong, S.; Fang, G.; Elmore, S. W.; Shen, Y.; Kati, W. M. Discovery of N-(4-(2,4-Difluorophenoxy)-3-(6-methyl-7-oxo-6,7-dihydro-1H-pyrrolo[2,3-c]pyridin-4-yl)phenyl)ethanesulfonamide (ABBV-075/Mivebresib), a Potent and Orally Available Bromodomain and Extraterminal Domain (BET) Family Bromodomain Inhibitor. *J. Med. Chem.* **2017**, *60*, 8369-8384.
152. Wang, L.; Pratt, J. K.; Soltwedel, T.; Sheppard, G. S.; Fidanze, S. D.; Liu, D.; Hasvold, L. A.; Mantei, R. A.; Holms, J. H.; McClellan, W. J.; Wendt, M. D.; Wada, C.; Frey, R.; Hansen, T. M.; Hubbard, R.; Park, C. H.; Li, L.; Magoc, T. J.; Albert, D. H.; Lin, X.; Warder, S. E.; Kovar, P.; Huang, X.; Wilcox, D.; Wang, R.; Rajaraman, G.; Petros, A. M.; Hutchins, C. W.; Panchal, S. C.; Sun, C.; Elmore, S. W.; Shen, Y.; Kati, W. M.; McDaniel, K. F. Fragment-Based, Structure-Enabled Discovery of Novel Pyridones and Pyridone Macrocycles as Potent Bromodomain and Extra-Terminal Domain (BET) Family Bromodomain Inhibitors. *J. Med. Chem.* **2017**, *60*, 3828-3850.

153. Chung, C.-w.; Dean, A. W.; Woolven, J. M.; Bamborough, P. Fragment-Based Discovery of Bromodomain Inhibitors Part 1: Inhibitor Binding Modes and Implications for Lead Discovery. *J. Med. Chem.* **2012**, *55*, 576-586.
154. Gosmini, R.; Nguyen, V. L.; Toum, J.; Simon, C.; Brusq, J.-M. G.; Krysa, G.; Mirguet, O.; Riou-Eymard, A. M.; Boursier, E. V.; Trottet, L.; Bamborough, P.; Clark, H.; Chung, C.-w.; Cutler, L.; Demont, E. H.; Kaur, R.; Lewis, A. J.; Schilling, M. B.; Soden, P. E.; Taylor, S.; Walker, A. L.; Walker, M. D.; Prinjha, R. K.; Nicodème, E. The Discovery of I-BET726 (GSK1324726A), a Potent Tetrahydroquinoline ApoA1 Up-Regulator and Selective BET Bromodomain Inhibitor. *J. Med. Chem.* **2014**, *57*, 8111-8131.
155. Ruthenburg, A. J.; Li, H.; Patel, D. J.; David Allis, C. Multivalent engagement of chromatin modifications by linked binding modules. *Nat. Rev. Mol. Cell Bio.* **2007**, *8*, 983.
156. McGinty, R. K.; Tan, S. Recognition of the nucleosome by chromatin factors and enzymes. *Curr. Opin. Struct. Biol.* **2016**, *37*, 54-61.
157. Speranzini, V.; Pilotto, S.; Sixma, T. K.; Mattevi, A. Touch, act and go: landing and operating on nucleosomes. *The EMBO Journal* **2016**.
158. Miller, T. C. R.; Simon, B.; Rybin, V.; Grötsch, H.; Curtet, S.; Khochbin, S.; Carlomagno, T.; Müller, C. W. A bromodomain–DNA interaction facilitates acetylation-dependent bivalent nucleosome recognition by the BET protein BRDT. *Nat. Commun.* **2016**, *7*, 13855.
159. Waring, M. J.; Chen, H.; Rabow, A. A.; Walker, G.; Bobby, R.; Boiko, S.; Bradbury, R. H.; Callis, R.; Clark, E.; Dale, I.; Daniels, D. L.; Dulak, A.; Flavell, L.; Holdgate, G.; Jowitt, T. A.; Kikhney, A.; McAlister, M.; Méndez, J.; Ogg, D.; Patel, J.; Petteruti, P.; Robb, G. R.; Robers, M. B.; Saif, S.; Stratton, N.; Svergun, D. I.; Wang, W.; Whittaker, D.; Wilson, D. M.; Yao, Y. Potent and selective bivalent inhibitors of BET bromodomains. *Nat. Chem. Biol.* **2016**, *12*, 1097.
160. Bradbury, R. H.; Callis, R.; Carr, G. R.; Chen, H.; Clark, E.; Feron, L.; Glossop, S.; Graham, M. A.; Hattersley, M.; Jones, C.; Lamont, S. G.; Ouvry, G.; Patel, A.; Patel, J.; Rabow, A. A.; Roberts, C. A.; Stokes, S.; Stratton, N.; Walker, G. E.; Ward, L.; Whalley, D.; Whittaker, D.; Wrigley, G.; Waring, M. J. Optimization of a Series of Bivalent Triazolopyridazine Based Bromodomain and Extraterminal Inhibitors: The Discovery of (3R)-4-[2-[4-[1-(3-Methoxy-[1,2,4]triazolo[4,3-b]pyridazin-6-yl)-4-piperidyl]phenoxy]ethyl]-1,3-dimethyl-piperazin-2-one (AZD5153). *J. Med. Chem.* **2016**, *59*, 7801-7817.
161. Tanaka, M.; Roberts, J. M.; Seo, H.-S.; Souza, A.; Paulk, J.; Scott, T. G.; DeAngelo, S. L.; Dhe-Paganon, S.; Bradner, J. E. Design and characterization of bivalent BET inhibitors. *Nat. Chem. Biol.* **2016**, *12*, 1089.
162. Suh, J. L.; Watts, B.; Stuckey, J. I.; Norris-Drouin, J. L.; Cholensky, S. H.; Dickson, B. M.; An, Y.; Mathea, S.; Salah, E.; Knapp, S.; Khan, A.; Adams, A. T.; Strahl, B. D.; Sagum, C. A.; Bedford, M. T.; James, L. I.; Kireev, D. B.; Frye, S. V. Quantitative Characterization of Bivalent Probes for a Dual Bromodomain Protein, Transcription Initiation Factor TFIID Subunit 1. *Biochemistry* **2018**, *57*, 2140-2149.
163. Picaud, S.; Leonards, K.; Lambert, J.-P.; Dovey, O.; Wells, C.; Fedorov, O.; Monteiro, O.; Fujisawa, T.; Wang, C.-Y.; Lingard, H.; Tallant, C.; Nikbin, N.; Guetzoyan, L.; Ingham, R.; Ley, S. V.; Brennan, P.; Muller, S.; Samsonova, A.; Gingras, A.-C.; Schwaller, J.; Vassiliou, G.; Knapp, S.; Filippakopoulos, P. Promiscuous targeting of bromodomains by bromosporine identifies BET proteins as master regulators of primary transcription response in leukemia. *Sci. Adv.* **2016**, *2*.
164. Proschak, E.; Stark, H.; Merk, D. Polypharmacology by Design: A Medicinal Chemist's Perspective on Multitargeting Compounds. *J. Med. Chem.* **2018**.

165. Bhadury, J.; Nilsson, L. M.; Veppil Muralidharan, S.; Green, L. C.; Li, Z.; Gesner, E. M.; Hansen, H. C.; Keller, U. B.; McLure, K. G.; Nilsson, J. A. BET and HDAC inhibitors induce similar genes and biological effects and synergize to kill in Myc-induced murine lymphoma. *Proc. Natl. Acad. Sci.* **2014**, *111*, E2721-E2730.
166. Atkinson, S. J.; Soden, P. E.; Angell, D. C.; Bantscheff, M.; Chung, C.-w.; Giblin, K. A.; Smithers, N.; Furze, R. C.; Gordon, L.; Drewes, G.; Rioja, I.; Witherington, J.; Parr, N. J.; Prinjha, R. K. The structure based design of dual HDAC/BET inhibitors as novel epigenetic probes. *MedChemComm* **2014**, *5*, 342-351.
167. Amemiya, S.; Yamaguchi, T.; Hashimoto, Y.; Noguchi-Yachide, T. Synthesis and evaluation of novel dual BRD4/HDAC inhibitors. *Biorg. Med. Chem.* **2017**, *25*, 3677-3684.
168. Shao, M.; He, L.; Zheng, L.; Huang, L.; Zhou, Y.; Wang, T.; Chen, Y.; Shen, M.; Wang, F.; Yang, Z.; Chen, L. Structure-based design, synthesis and in vitro antiproliferative effects studies of novel dual BRD4/HDAC inhibitors. *Bioorg. Med. Chem. Lett.* **2017**, *27*, 4051-4055.
169. Zhang, Z.; Hou, S.; Chen, H.; Ran, T.; Jiang, F.; Bian, Y.; Zhang, D.; Zhi, Y.; Wang, L.; Zhang, L.; Li, H.; Zhang, Y.; Tang, W.; Lu, T.; Chen, Y. Targeting epigenetic reader and eraser: Rational design, synthesis and in vitro evaluation of dimethylisoxazoles derivatives as BRD4/HDAC dual inhibitors. *Bioorg. Med. Chem. Lett.* **2016**, *26*, 2931-2935.
170. Carlino, L.; Rastelli, G. Dual Kinase-Bromodomain Inhibitors in Anticancer Drug Discovery: A Structural and Pharmacological Perspective. *J. Med. Chem.* **2016**, *59*, 9305-9320.
171. Ciceri, P.; Müller, S.; O'Mahony, A.; Fedorov, O.; Filippakopoulos, P.; Hunt, J. P.; Lasater, E. A.; Pallares, G.; Picaud, S.; Wells, C.; Martin, S.; Wodicka, L. M.; Shah, N. P.; Treiber, D. K.; Knapp, S. Dual kinase-bromodomain inhibitors for rationally designed polypharmacology. *Nat. Chem. Biol.* **2014**, *10*, 305.
172. Wernig, G.; Kharas, M. G.; Okabe, R.; Moore, S. A.; Leeman, D. S.; Cullen, D. E.; Gozo, M.; McDowell, E. P.; Levine, R. L.; Doukas, J.; Mak, C. C.; Noronha, G.; Martin, M.; Ko, Y. D.; Lee, B. H.; Soll, R. M.; Tefferi, A.; Hood, J. D.; Gilliland, D. G. Efficacy of TG101348, a Selective JAK2 Inhibitor, in Treatment of a Murine Model of JAK2V617F-Induced Polycythemia Vera. *Cancer Cell* **2008**, *13*, 311-320.
173. Chen, L.; Yap, J. L.; Yoshioka, M.; Lanning, M. E.; Fountain, R. N.; Raje, M.; Scheenstra, J. A.; Strovel, J. W.; Fletcher, S. BRD4 Structure–Activity Relationships of Dual PLK1 Kinase/BRD4 Bromodomain Inhibitor BI-2536. *ACS Med. Chem. Lett.* **2015**, *6*, 764-769.
174. Liu, S.; Yosief, H. O.; Dai, L.; Huang, H.; Dhawan, G.; Zhang, X.; Muthengi, A. M.; Roberts, J.; Buckley, D. L.; Perry, J. A.; Wu, L.; Bradner, J. E.; Qi, J.; Zhang, W. Structure-guided Design and Development of Potent and Selective Dual Bromodomain 4 (BRD4)/Polo-like Kinase 1 (PLK1) Inhibitors. *J. Med. Chem.* **2018**.
175. Andrews, F. H.; Singh, A. R.; Joshi, S.; Smith, C. A.; Morales, G. A.; Garlich, J. R.; Durden, D. L.; Kutateladze, T. G. Dual-activity PI3K–BRD4 inhibitor for the orthogonal inhibition of MYC to block tumor growth and metastasis. *Proc. Natl. Acad. Sci.* **2017**, *114*, E1072-E1080.
176. Wang, J.; Erazo, T.; Ferguson, F. M.; Buckley, D. L.; Gomez, N.; Muñoz-Guardiola, P.; Diéguez-Martínez, N.; Deng, X.; Hao, M.; Masefski, W.; Fedorov, O.; Offei-Addo, N. K.; Park, P. M.-C.; Dai, L.; DiBona, A.; Becht, K.; Kim, N. D.; McKeown, M. R.; Roberts, J. M.; Zhang, J.; Sim, T.; Alessi, D. R.; Bradner, J. E.; Lizcano, J. M.; Blacklow, S. C.; Qi, J.; Xu, X.; Gray, N. S. Structural and atropisomeric factors governing the selectivity of pyrimido-benzodiazepinones as inhibitors of kinases and bromodomains. *ACS Chem. Biol.* **2018**.
177. Singh, A. R.; Joshi, S.; Burgoyne, A. M.; Sicklick, J. K.; Ikeda, S.; Kono, Y.; Garlich, J. R.; Morales, G. A.; Durden, D. L. Single Agent and Synergistic Activity of the “First-in-Class” Dual

- PI3K/BRD4 Inhibitor SF1126 with Sorafenib in Hepatocellular Carcinoma. *Mol. Cancer Ther.* **2016**, 15, 2553-2562.
178. Valeur, E.; Guéret, S. M.; Adihou, H.; Gopalakrishnan, R.; Lemurell, M.; Waldmann, H.; Grossmann, T. N.; Plowright, A. T. New Modalities for Challenging Targets in Drug Discovery. *Angew. Chem. Int. Ed.* **2017**, 56, 10294-10323.
179. Raina, K.; Crews, C. M. Targeted protein knockdown using small molecule degraders. *Curr. Opin. Chem. Biol.* **2017**, 39, 46-53.
180. Ottis, P.; Crews, C. M. Proteolysis-Targeting Chimeras: Induced Protein Degradation as a Therapeutic Strategy. *ACS Chem. Biol.* **2017**, 12, 892-898.
181. Qin, C.; Hu, Y.; Zhou, B.; Fernandez-Salas, E.; Yang, C.-Y.; Liu, L.; McEachern, D.; Przybranowski, S.; Wang, M.; Stuckey, J.; Meagher, J.; Bai, L.; Chen, Z.; Lin, M.; Yang, J.; Ziazadeh, D. N.; Xu, F.; Hu, J.; Xiang, W.; Huang, L.; Li, S.; Wen, B.; Sun, D.; Wang, S. Discovery of QCA570 as an Exceptionally Potent and Efficacious Proteolysis Targeting Chimera (PROTAC) Degradator of the Bromodomain and Extra-Terminal (BET) Proteins Capable of Inducing Complete and Durable Tumor Regression. *J. Med. Chem.* **2018**, 61, 6685-6704.
182. Lu, J.; Qian, Y.; Altieri, M.; Dong, H.; Wang, J.; Raina, K.; Hines, J.; Winkler, James D.; Crew, Andrew P.; Coleman, K.; Crews, Craig M. Hijacking the E3 Ubiquitin Ligase Cereblon to Efficiently Target BRD4. *Chem. Biol.* **2015**, 22, 755-763.
183. Bondeson, D. P.; Mares, A.; Smith, I. E. D.; Ko, E.; Campos, S.; Miah, A. H.; Mulholland, K. E.; Routly, N.; Buckley, D. L.; Gustafson, J. L.; Zinn, N.; Grandi, P.; Shimamura, S.; Bergamini, G.; Faelh-Savitski, M.; Bantscheff, M.; Cox, C.; Gordon, D. A.; Willard, R. R.; Flanagan, J. J.; Casillas, L. N.; Votta, B. J.; den Besten, W.; Famm, K.; Kruidenier, L.; Carter, P. S.; Harling, J. D.; Churcher, I.; Crews, C. M. Catalytic in vivo protein knockdown by small-molecule PROTACs. *Nat. Chem. Biol.* **2015**, 11, 611.
184. Zhou, B.; Hu, J.; Xu, F.; Chen, Z.; Bai, L.; Fernandez-Salas, E.; Lin, M.; Liu, L.; Yang, C.-Y.; Zhao, Y.; McEachern, D.; Przybranowski, S.; Wen, B.; Sun, D.; Wang, S. Discovery of a Small-Molecule Degradator of Bromodomain and Extra-Terminal (BET) Proteins with Picomolar Cellular Potencies and Capable of Achieving Tumor Regression. *J. Med. Chem.* **2018**, 61, 462-481.
185. Bai, L.; Zhou, B.; Yang, C.-Y.; Ji, J.; McEachern, D.; Przybranowski, S.; Jiang, H.; Hu, J.; Xu, F.; Zhao, Y.; Liu, L.; Fernandez-Salas, E.; Xu, J.; Dou, Y.; Wen, B.; Sun, D.; Meagher, J.; Stuckey, J.; Hayes, D. F.; Li, S.; Ellis, M. J.; Wang, S. Targeted Degradation of BET Proteins in Triple-Negative Breast Cancer. *Cancer Res.* **2017**, 77, 2476-2487.
186. Zengerle, M.; Chan, K.-H.; Ciulli, A. Selective Small Molecule Induced Degradation of the BET Bromodomain Protein BRD4. *ACS Chem. Biol.* **2015**, 10, 1770-1777.
187. Gadd, M. S.; Testa, A.; Lucas, X.; Chan, K.-H.; Chen, W.; Lamont, D. J.; Zengerle, M.; Ciulli, A. Structural basis of PROTAC cooperative recognition for selective protein degradation. *Nat. Chem. Biol.* **2017**, 13, 514.
188. Riching, K. M.; Mahan, S.; Corona, C. R.; McDougall, M.; Vasta, J. D.; Robers, M. B.; Urh, M.; Daniels, D. L. Quantitative Live-Cell Kinetic Degradation and Mechanistic Profiling of PROTAC Mode of Action. *ACS Chem. Biol.* **2018**.
189. Chan, K.-H.; Zengerle, M.; Testa, A.; Ciulli, A. Impact of Target Warhead and Linkage Vector on Inducing Protein Degradation: Comparison of Bromodomain and Extra-Terminal (BET) Degradators Derived from Triazolodiazepine (JQ1) and Tetrahydroquinoline (I-BET726) BET Inhibitor Scaffolds. *J. Med. Chem.* **2018**, 61, 504-513.
190. Raina, K.; Lu, J.; Qian, Y.; Altieri, M.; Gordon, D.; Rossi, A. M. K.; Wang, J.; Chen, X.; Dong, H.; Siu, K.; Winkler, J. D.; Crew, A. P.; Crews, C. M.; Coleman, K. G. PROTAC-induced

- BET protein degradation as a therapy for castration-resistant prostate cancer. *Proc. Natl. Acad. Sci.* **2016**, 113, 7124-7129.
191. Bolden, Jessica E.; Tasdemir, N.; Dow, Lukas E.; van Es, Johan H.; Wilkinson, John E.; Zhao, Z.; Clevers, H.; Lowe, Scott W. Inducible In Vivo Silencing of Brd4 Identifies Potential Toxicities of Sustained BET Protein Inhibition. *Cell Rep.* **2014**, 8, 1919-1929.
192. Sudhir, S. S.; Vivek, R. Thrombocytopenia in Adults: A Practical Approach to Evaluation and Management. *South. Med. J.* **2006**, 99, 491-498.
193. Baud, M. G. J.; Lin-Shiao, E.; Cardote, T.; Tallant, C.; Pschibul, A.; Chan, K.-H.; Zengerle, M.; Garcia, J. R.; Kwan, T. T. L.; Ferguson, F. M.; Ciulli, A. A bump-and-hole approach to engineer controlled selectivity of BET bromodomain chemical probes. *Science* **2014**, 346, 638.
194. Baud, M. G. J.; Lin-Shiao, E.; Zengerle, M.; Tallant, C.; Ciulli, A. New Synthetic Routes to Triazolo-benzodiazepine Analogues: Expanding the Scope of the Bump-and-Hole Approach for Selective Bromo and Extra-Terminal (BET) Bromodomain Inhibition. *J. Med. Chem.* **2016**, 59, 1492-1500.
195. Runcie, A. C.; Zengerle, M.; Chan, K. H.; Testa, A.; van Beurden, L.; Baud, M. G. J.; Epemolu, O.; Ellis, L. C. J.; Read, K. D.; Coulthard, V.; Brien, A.; Ciulli, A. Optimization of a "bump-and-hole" approach to allele-selective BET bromodomain inhibition. *Chem. Sci.* **2018**.
196. Zhang, G.; Plotnikov, A. N.; Rusinova, E.; Shen, T.; Morohashi, K.; Joshua, J.; Zeng, L.; Mujtaba, S.; Ohlmeyer, M.; Zhou, M.-M. Structure-Guided Design of Potent Diazobenzene Inhibitors for the BET Bromodomains. *J. Med. Chem.* **2013**, 56, 9251-9264.
197. Gacias, M.; Gerona-Navarro, G.; Plotnikov, Alexander N.; Zhang, G.; Zeng, L.; Kaur, J.; Moy, G.; Rusinova, E.; Rodriguez, Y.; Matikainen, B.; Vincek, A.; Joshua, J.; Casaccia, P.; Zhou, M.-M. Selective Chemical Modulation of Gene Transcription Favors Oligodendrocyte Lineage Progression. *Chem. Biol.* **2014**, 21, 841-854.
198. Raux, B.; Voitovich, Y.; Derviaux, C.; Lugari, A.; Rebuffet, E.; Milhas, S.; Priet, S.; Roux, T.; Trinquet, E.; Guillemot, J.-C.; Knapp, S.; Brunel, J.-M.; Fedorov, A. Y.; Collette, Y.; Roche, P.; Betzi, S.; Combes, S.; Morelli, X. Exploring Selective Inhibition of the First Bromodomain of the Human Bromodomain and Extra-terminal Domain (BET) Proteins. *J. Med. Chem.* **2016**, 59, 1634-1641.
199. Hügler, M.; Lucas, X.; Weitzel, G.; Ostrovskiy, D.; Breit, B.; Gerhardt, S.; Einsle, O.; Günther, S.; Wohlwend, D. 4-Acyl Pyrrole Derivatives Yield Novel Vectors for Designing Inhibitors of the Acetyl-Lysine Recognition Site of BRD4(1). *J. Med. Chem.* **2016**, 59, 1518-1530.
200. Cheung, K.; Lu, G.; Sharma, R.; Vincek, A.; Zhang, R.; Plotnikov, A. N.; Zhang, F.; Zhang, Q.; Ju, Y.; Hu, Y.; Zhao, L.; Han, X.; Meslamani, J.; Xu, F.; Jaganathan, A.; Shen, T.; Zhu, H.; Rusinova, E.; Zeng, L.; Zhou, J.; Yang, J.; Peng, L.; Ohlmeyer, M.; Walsh, M. J.; Zhang, D. Y.; Xiong, H.; Zhou, M.-M. BET N-terminal bromodomain inhibition selectively blocks Th17 cell differentiation and ameliorates colitis in mice. *Proc. Natl. Acad. Sci.* **2017**, 114, 2952.
201. Picaud, S.; Wells, C.; Felletar, I.; Brotherton, D.; Martin, S.; Savitsky, P.; Diez-Dacal, B.; Philpott, M.; Bountra, C.; Lingard, H.; Fedorov, O.; Müller, S.; Brennan, P. E.; Knapp, S.; Filippakopoulos, P. RVX-208, an inhibitor of BET transcriptional regulators with selectivity for the second bromodomain. *Proc. Natl. Acad. Sci.* **2013**, 110, 19754.
202. Kharenko, O. A.; Gesner, E. M.; Patel, R. G.; Norek, K.; White, A.; Fontano, E.; Suto, R. K.; Young, P. R.; McLure, K. G.; Hansen, H. C. RVX-297- a novel BD2 selective inhibitor of BET bromodomains. *Biochem. Biophys. Res. Commun.* **2016**, 477, 62-67.

203. Jahagirdar, R.; Attwell, S.; Marusic, S.; Bendele, A.; Shenoy, N.; McLure, K. G.; Gilham, D.; Norek, K.; Hansen, H. C.; Yu, R.; Tobin, J.; Wagner, G. S.; Young, P. R.; Wong, N. C. W.; Kulikowski, E. RVX-297, a BET Bromodomain Inhibitor, Has Therapeutic Effects in Preclinical Models of Acute Inflammation and Autoimmune Disease. *Mol. Pharmacol.* **2017**, *92*, 694.
204. Wang, Q.; Li, Y.; Xu, J.; Wang, Y.; Leung, E. L.-H.; Liu, L.; Yao, X. Selective inhibition mechanism of RVX-208 to the second bromodomain of bromo and extraterminal proteins: insight from microsecond molecular dynamics simulations. *Sci. Rep.* **2017**, *7*, 8857.
205. Su, J.; Liu, X.; Zhang, S.; Yan, F.; Zhang, Q.; Chen, J. A theoretical insight into selectivity of inhibitors toward two domains of bromodomain-containing protein 4 using molecular dynamics simulations. *Chem. Biol. Drug Des.* **2018**, *91*, 828-840.
206. Law, R. P.; Atkinson, S. J.; Bamborough, P.; Chung, C.-w.; Demont, E. H.; Gordon, L. J.; Lindon, M.; Prinjha, R. K.; Watson, A. J. B.; Hirst, D. J. Discovery of Tetrahydroquinoxalines as Bromodomain and Extra-Terminal Domain (BET) Inhibitors with Selectivity for the Second Bromodomain. *J. Med. Chem.* **2018**, *61*, 4317-4334.
207. Preston, A.; Atkinson, S. J.; Seal, J.; Mitchell, D. J.; Watson, R. J.; Gray, J.; Woolven, J. M.; Chung, C.; Rianjongdee, F.; Prinjha, R. K.; Lindon, M.; Demont, E. H. The Design and Synthesis of a Highly Selective and in vivo capable Inhibitor of the Second Bromodomain (BD2) of the Bromodomain and Extra Terminal Domain (BET) Family of Proteins. *Manuscript in preparation* **2018**.
208. Seal, J.; Atkinson, S. J.; Aylott, H. E.; Harrison, L.; Hayhow, T.; Mitchell, D. J.; Preston, A.; Watson, R. J.; Woolven, J. M.; Wall, I. D.; Chung, C.; Gray, J.; Michon, A.; Grandi, P.; Taylor, S.; Prinjha, R. K.; Rioja, I.; Demont, E. H. The Optimisation of a Novel, Weak Bromo and Extra Terminal Domain (BET) Bromodomain Fragment Ligand to a Potent and Selective Second Bromodomain (BD2) Inhibitor. *Manuscript in preparation* **2018**.
209. Freire, E. Do enthalpy and entropy distinguish first in class from best in class? *Drug Discov. Today* **2008**, *13*, 869-874.
210. Demont, E. H.; Watson, R. J. *Unpublished GSK work*.
211. Z. Li; J. Zhang; C. Brouwer; C. Yang; N. W. Reich; He, C. Bronsted Acid Catalyzed Addition of Phenols, Carboxylic Acids, and Tosylamides to Simple Olefins. *Org. Lett.* **2006**, *8*, 4175-4178.
212. Baldwin, J. E. Rules for ring closure. *J. Chem. Soc., Chem. Commun.* **1976**, 734-736.
213. Baldwin, J. E.; Thomas, R. C.; Kruse, L. I.; Silberman, L. Rules for ring closure: ring formation by conjugate addition of oxygen nucleophiles. *J. Org. Chem.* **1977**, *42*, 3846-3852.
214. S. K. Chittimalla; T. Chang; Liu, T.; Hsieh, H.; Liao, C. Reactions of 2-hydroxybenzophenones with Corey-Chaykovsky reagent. *Tetrahedron* **2008**, *64*, 2586-2595.
215. Duan, X.; Zeng, J.; Zhang, Z.; Zi, G. A Facile Two-Step Synthesis of 2-Arylbenzofurans Based on the Selective Cross McMurry Couplings. *J. Org. Chem.* **2007**, *72*, 10283-10286.
216. Aslam, S. N.; Stevenson, P. C.; Phythian, S. J.; Veitch, N. C.; Hall, D. R. Synthesis of cicerfuran, an antifungal benzofuran, and some related analogs. *Tetrahedron* **2006**, *62*, 4214-4226.
217. J. Mangas-Sanchez; Busto, E.; Gotor-Fernandez, V.; Gotor, V. Straightforward Synthesis of Enantiopure 2,3-Dihydrobenzofurans by a Sequential Stereoselective Biotransformation and Chemical Intramolecular Cyclization. *Org. Lett.* **2010**, *12*, 3498-3501.
218. Zweifel, G.; Ayyangar, N. R.; Brown, H. C. Hydroboration. XVII. An examination of several representative dialkylboranes as selective hydroborating agents. *J. Am. Chem. Soc.* **1963**, *85*, 2072-2076.

219. Kabalka, G. W.; Shoup, T. M.; Goudgoan, M. N. Sodium perborate: a mild and convenient reagent for efficiently oxidizing organoboranes. *J. Org. Chem.* **1989**, *54*, 5930-5933.
220. Brown, H. C.; Knight, E. F.; Scouten, C. G. Hydroboration. XXXVI. Direct route to 9-borabicyclo[3.3.1]nonane via the cyclic hydroboration of 1,5-cyclooctadiene. 9-Borabicyclo[3.3.1]nonane as a uniquely selective reagent for the hydroboration of olefins. *J. Am. Chem. Soc.* **1974**, *96*, 7765-7770.
221. Brown, H. C.; Zweifel, G. Hydroboration. VIII. Bis(3-methyl-2-butylborane) as a selective reagent for the hydroboration of alkenes and dienes. *J. Am. Chem. Soc.* **1961**, *83*, 1241-1246.
222. Brown, H. C.; Pfaffenberger, C. D. Thexylborane as a convenient reagent for the cyclic hydroboration of dienes. Stereospecific syntheses via cyclic hydroboration. *J. Am. Chem. Soc.* **1967**, *89*, 5475-5477.
223. Brown, H. C.; Weissman, S. A.; Perumal, P. T.; Dhokte, U. P. Hydroboration. 85. Synthesis and hydroboration of (-)-2-phenylapopinene. Comparison of mono(2-phenylapoisopinocampheyl)borane with its 2-methyl and 2-ethyl analogs for the chiral hydroboration of representative alkenes. *J. Org. Chem.* **1990**, *55*, 1217-1223.
224. Eissenstat, M.; Delahanty, G.; Topin, A.; Rajendran, G. R. Resistance-repellent retroviral protease inhibitors. WO 2005110428, 2005.
225. Hossain, N. Preparation of coumaranspiro[2,1]cyclohexanes as modulators of chemokine receptor activity. WO 2005037814, 2005.
226. Hossain, N.; Ivanova, S.; Mensonides-Harsema, M. Preparation of tricyclic spiropiperidines or spiropyrrolidines useful against disorders affected by modulation of chemokine receptors. WO 2004005295, 2004.
227. Lim, J.; Jeon, I.; Lyons, C. B.; Laufersweiler, M. C.; Tan, L.; Baek, J. B. Carboxylic Acid-Terminated Hyperbranched Polybenzoxazole and Its Polyarm-Star Block Copolymers. *Macromolecules* **2009**, *42*, 1541-1553.
228. X. Wang; Anil, G.; Caille, S.; Hu, J.; Preston, J. P.; Ronk, M.; Walker, S. Highly Enantioselective Hydrogenation of Styrenes Directed by 2'-Hydroxyl Groups. *Org. Lett.* **2011**, *13*, 1881-1883.
229. Guram, A. S.; King, A. O.; Allen, J. G.; Wang, X.; Schenkel, L. B.; Chan, J.; Bunel, E. E.; Faul, M. M.; Larsen, R. D.; Martinelli, M. J.; Reider, P. J. New Air-Stable Catalysts for General and Efficient Suzuki-Miyaura Cross-Coupling Reactions of Heteroaryl Chlorides. *Org. Lett.* **2006**, *8*, 1787-1789.
230. Guram, A. S.; Wang, X.; Bunel, E. E.; Faul, M. M.; Larsen, R. D.; Martinelli, M. J. New Catalysts for Suzuki-Miyaura Coupling Reactions of Heteroatom-Substituted Heteroaryl Chlorides. *J. Org. Chem.* **2007**, *72*, 5104-5112.
231. Kinzel, T.; Zhang, Y.; Buchwald, S. L. A New Palladium Precatalyst Allows for the Fast Suzuki-Miyaura Coupling Reactions of Unstable Polyfluorophenyl and 2-Heteroaryl Boronic Acids. *J. Am. Chem. Soc.* **2010**, *132*, 14073-14075.
232. Altman, R. A.; Fors, B. P.; Buchwald, S. L. Pd-catalyzed amination reactions of aryl halides using bulky biarylmonophosphine ligands. *Nat. Protoc.* **2007**, *2*, 2881.
233. T. Kinzel; Zhang, Y.; Buchwald, S. L. A New Palladium Precatalyst Allows for the Fast Suzuki-Miyaura Coupling Reactions of Unstable Polyfluorophenyl and 2-Heteroaryl Boronic Acids. *J. Am. Chem. Soc.* **2010**, *132*, 14073-14075.
234. Organ, M. G.; Avola, S.; Dubovyk, I.; Hadei, N.; Kantchev, E. A. B.; O'Brien, C. J.; Valente, C. A user-friendly, all-purpose Pd-NHC (NHC = N-heterocyclic carbene) precatalyst for the Negishi reaction: a step towards a universal cross-coupling catalyst. *Chem. Eur. J.* **2006**, *12*, 4749-4755.

235. M. W. Khan; Alam, M. J.; Rashid, M. A.; Chowdhury, R. A new structural alternative in benzo[b]furans for antimicrobial activity. *Bioorg. Med. Chem.* **2005**, *13*, 4796-4805.
236. M. Saitoh; Kunitomo, J.; Kimura, E.; Iwashita, H.; Uno, Y.; Onishi, T.; Uchiyama, N.; Kawamoto, T.; Tanaka, T.; Mol, C. D.; Dougan, D. R.; Textor, G. P.; Snell, G. P.; Takizawa, M.; Itoh, F.; Kori, M. 2-{3-[4-(Alkylsulfinyl)phenyl]-1-benzofuran-5-yl}-5-methyl-1,3,4-oxadiazole Derivatives as Novel Inhibitors of Glycogen Synthase Kinase-3 β with Good Brain Permeability. *J. Med. Chem.* **2009**, *52*, 6270-6286.
237. http://jmcct.com/products-services/product_p502.html.
238. Preston, A.; Wheelhouse, K. *Unpublished GSK work*.
239. Ndubaku, C. O.; Crawford, J. J.; Drobnick, J.; Aliagas, I.; Campbell, D.; Dong, P.; Dornan, L. M.; Duron, S.; Epler, J.; Gazzard, L.; Heise, C. E.; Hoeflich, K. P.; Jakubiak, D.; La, H.; Lee, W.; Lin, B.; Lyssikatos, J. P.; Maksimoska, J.; Marmorstein, R.; Murray, L. J.; O'Brien, T.; Oh, A.; Ramaswamy, S.; Wang, W.; Zhao, X.; Zhong, Y.; Blackwood, E.; Rudolph, J. Design of Selective PAK1 Inhibitor G-5555: Improving Properties by Employing an Unorthodox Low-pKa Polar Moiety. *ACS Med. Chem. Lett.* **2015**, *6*, 1241-1246.
240. Cruciani, G.; Carosati, E.; De Boeck, B.; Ethirajulu, K.; Mackie, C.; Howe, T.; Vianello, R. MetaSite: Understanding Metabolism in Human Cytochromes from the Perspective of the Chemist. *J. Med. Chem.* **2005**, *48*, 6970-6979.
241. Diaz, P.; Gendre, F.; Stella, L.; Charpentier, B. New synthetic retinoids obtained by palladium-catalyzed tandem cyclisation-hydride capture process. *Tetrahedron* **1998**, *54*, 4579-4590.
242. Trost, B. M.; Thiel, O. R.; Tsui, H.-C. Total Syntheses of Furaquinocin A, B, and E. *J. Am. Chem. Soc.* **2003**, *125*, 13155-13164.
243. Li, X.-T.; Gu, Q.-S.; Dong, X.-Y.; Meng, X.; Liu, X.-Y. A Copper Catalyst with a Cinchona-Alkaloid-Based Sulfonamide Ligand for Asymmetric Radical Oxytrifluoromethylation of Alkenyl Oximes. *Angew. Chem. Int. Ed.* **2018**, *57*, 7668-7672.
244. Trost, B. M.; Fullerton, T. J. New synthetic reactions. Allylic alkylation. *J. Am. Chem. Soc.* **1973**, *95*, 292-294.
245. Vachhani, D. D.; Butani, H. H.; Sharma, N.; Bhoya, U. C.; Shah, A. K.; Van der Eycken, E. V. Domino Heck/borylation sequence towards indolinone-3-methyl boronic esters: trapping of the σ -alkylpalladium intermediate with boron. *Chem. Commun.* **2015**, *51*, 14862-14865.
246. Yoon, H.; Jang, Y. J.; Lautens, M. Diastereoselective Pd-Catalyzed Domino Heck/Arylborylation Sequence Forming Borylated Chromans. *Synthesis* **2016**, *48*, 1483-1490.
247. Ishiyama, T.; Murata, M.; Miyaura, N. Palladium(0)-Catalyzed Cross-Coupling Reaction of Alkoxydiboron with Haloarenes: A Direct Procedure for Arylborylation Esters. *J. Org. Chem.* **1995**, *60*, 7508-7510.
248. Thompson, A. L. S.; Kabalka, G. W.; Akula, M. R.; Huffman, J. W. The Conversion of Phenols to the Corresponding Aryl Halides Under Mild Conditions. *Synthesis* **2005**, *2005*, 547-550.
249. Molander, G. A.; Trice, S. L. J.; Dreher, S. D. Palladium-Catalyzed, Direct Boronic Acid Synthesis from Aryl Chlorides: A Simplified Route to Diverse Boronate Ester Derivatives. *J. Am. Chem. Soc.* **2010**, *132*, 17701-17703.
250. Webb, K. S.; Levy, D. A facile oxidation of boronic acids and boronic esters. *Tetrahedron Lett.* **1995**, *36*, 5117-5118.
251. Gadge, S. T.; Bhanage, B. M. Recent developments in palladium catalysed carbonylation reactions. *RSC Advances* **2014**, *4*, 10367-10389.

252. Brennführer, A.; Neumann, H.; Beller, M. Palladium-Catalyzed Carbonylation Reactions of Aryl Halides and Related Compounds. *Angew. Chem. Int. Ed.* **2009**, *48*, 4114-4133.
253. Baburajan, P.; Elango, K. P. Co₂(CO)₈ as a convenient in situ CO source for the direct synthesis of benzamides from aryl halides (Br/I) via aminocarbonylation. *Tetrahedron Lett.* **2014**, *55*, 1006-1010.
254. Huchet, Q. A.; Kuhn, B.; Wagner, B.; Fischer, H.; Kansy, M.; Zimmerli, D.; Carreira, E. M.; Müller, K. On the polarity of partially fluorinated methyl groups. *J. Fluorine Chem.* **2013**, *152*, 119-128.
255. Gillis, E. P.; Eastman, K. J.; Hill, M. D.; Donnelly, D. J.; Meanwell, N. A. Applications of Fluorine in Medicinal Chemistry. *J. Med. Chem.* **2015**, *58*, 8315-8359.
256. Singh, R. P.; Shreeve, J. n. M. Recent Advances in Nucleophilic Fluorination Reactions of Organic Compounds- Using Deoxofluor and DAST. *Synthesis* **2002**, 2002, 2561-2578.
257. Dax, K.; Albert, M.; Hammond, D.; Illaszewicz, C.; Purkarthofer, T.; Tscherner, M.; Weber, H. Rearrangements in the Course of Fluorination by Diethylaminosulfur Trifluoride at C-2 of Glycopyranosides: Some New Parameters. *Monatsh. Chem.* **2002**, *133*, 427-448.
258. Mossine, A. V.; Brooks, A. F.; Makaravage, K. J.; Miller, J. M.; Ichiishi, N.; Sanford, M. S.; Scott, P. J. H. Synthesis of [18F]Arenes via the Copper-Mediated [18F]Fluorination of Boronic Acids. *Org. Lett.* **2015**, *17*, 5780-5783.
259. Kati, W. Abstract DDT01-05: ABBV-744: A first-in-class highly BDII-selective BET bromodomain inhibitor. *Cancer Res.* **2018**, *78*, DDT01-05-DDT01-05.
260. Moustakim, M.; Clark, P. G. K.; Hay, D. A.; Dixon, D. J.; Brennan, P. E. Chemical probes and inhibitors of bromodomains outside the BET family. *MedChemComm* **2016**, *7*, 2246-2264.
261. Sweis, R. F. Target (In)Validation: A Critical, Sometimes Unheralded, Role of Modern Medicinal Chemistry. *ACS Med. Chem. Lett.* **2015**, *6*, 618-621.
262. Weiss, W. A.; Taylor, S. S.; Shokat, K. M. Recognizing and exploiting differences between RNAi and small-molecule inhibitors. *Nat. Chem. Biol.* **2007**, *3*, 739.
263. Frye, S. V. The art of the chemical probe. *Nat. Chem. Biol.* **2010**, *6*, 159.
264. M. E. Bunnage; E. L. P. Chekler; Jones, L. H. Target validation using chemical probes. *Nat. Chem. Biol.* **2013**, *9*, 195-199.
265. P. Filippakopoulos; J. Qi; S. Picaud; Y. Shen; W. B. Smith; O. Fedorov; E. M. Morse; T. Keates; T. T. Hickman; I. Felletar; M. Philpott; S. Munro; M. R. McKeown; Y. Wang; A. L. Christie; N. West; M. J. Cameron; B. Schwartz; T. D. Heightman; N. La Thangue; C. A. French; O. Weist; A. L. Kung; S. Knapp; Bradner, J. E. Selective inhibition of BET bromodomains. *Nature* **2010**, *468*, 1067-1073.
266. Humphreys, P. G.; Bamborough, P.; Chung, C.-w.; Craggs, P. D.; Gordon, L.; Grandi, P.; Hayhow, T. G.; Hussain, J.; Jones, K. L.; Lindon, M.; Michon, A.-M.; Renaux, J. F.; Suckling, C. J.; Tough, D. F.; Prinjha, R. K. Discovery of a Potent, Cell Penetrant, and Selective p300/CBP-Associated Factor (PCAF)/General Control Nonderepressible 5 (GCN5) Bromodomain Chemical Probe. *J. Med. Chem.* **2017**, *60*, 695-709.
267. Moustakim, M.; Clark, P. G. K.; Trulli, L.; Fuentes de Arriba, A. L.; Ehebauer, M. T.; Chaikuad, A.; Murphy, E. J.; Mendez-Johnson, J.; Daniels, D.; Hou, C.-F. D.; Lin, Y.-H.; Walker, J. R.; Hui, R.; Yang, H.; Dorrell, L.; Rogers, C. M.; Monteiro, O. P.; Fedorov, O.; Huber, K. V. M.; Knapp, S.; Heer, J.; Dixon, D. J.; Brennan, P. E. Discovery of a PCAF Bromodomain Chemical Probe. *Angew. Chem. Int. Ed.* **2017**, *56*, 827-831.
268. Fedorov, O.; Lingard, H.; Wells, C.; Monteiro, O. P.; Picaud, S.; Keates, T.; Yapp, C.; Philpott, M.; Martin, S. J.; Felletar, I.; Marsden, B. D.; Filippakopoulos, P.; Müller, S.; Knapp,

- S.; Brennan, P. E. [1,2,4]Triazolo[4,3-a]phthalazines: Inhibitors of Diverse Bromodomains. *J. Med. Chem.* **2014**, *57*, 462-476.
269. Rooney, T. P. C.; Filippakopoulos, P.; Fedorov, O.; Picaud, S.; Cortopassi, W. A.; Hay, D. A.; Martin, S.; Tumber, A.; Rogers, C. M.; Philpott, M.; Wang, M.; Thompson, A. L.; Heightman, T. D.; Pryde, D. C.; Cook, A.; Paton, R. S.; Müller, S.; Knapp, S.; Brennan, P. E.; Conway, S. J. A Series of Potent CREBBP Bromodomain Ligands Reveals an Induced-Fit Pocket Stabilized by a Cation- π Interaction. *Angew. Chem. Int. Ed.* **2014**, *53*, 6126-6130.
270. Picaud, S.; Fedorov, O.; Thanasopoulou, A.; Leonards, K.; Jones, K.; Meier, J.; Olzscha, H.; Monteiro, O.; Martin, S.; Philpott, M.; Tumber, A.; Filippakopoulos, P.; Yapp, C.; Wells, C.; Che, K. H.; Bannister, A.; Robson, S.; Kumar, U.; Parr, N.; Lee, K.; Lugo, D.; Jeffrey, P.; Taylor, S.; Vecellio, M. L.; Bountra, C.; Brennan, P. E.; O'Mahony, A.; Velichko, S.; Müller, S.; Hay, D.; Daniels, D. L.; Urh, M.; La Thangue, N. B.; Kouzarides, T.; Prinjha, R.; Schwaller, J.; Knapp, S. Generation of a Selective Small Molecule Inhibitor of the CBP/p300 Bromodomain for Leukemia Therapy. *Cancer Res.* **2015**, *75*, 5106-5119.
271. Unzue, A.; Xu, M.; Dong, J.; Wiedmer, L.; Spiliotopoulos, D.; Cafilisch, A.; Nevado, C. Fragment-Based Design of Selective Nanomolar Ligands of the CREBBP Bromodomain. *J. Med. Chem.* **2016**, *59*, 1350-1356.
272. Xu, M.; Unzue, A.; Dong, J.; Spiliotopoulos, D.; Nevado, C.; Cafilisch, A. Discovery of CREBBP Bromodomain Inhibitors by High-Throughput Docking and Hit Optimization Guided by Molecular Dynamics. *J. Med. Chem.* **2016**, *59*, 1340-1349.
273. Bronner, S. M.; Murray, J.; Romero, F. A.; Lai, K. W.; Tsui, V.; Cyr, P.; Beresini, M. H.; de Leon Boenig, G.; Chen, Z.; Choo, E. F.; Clark, K. R.; Crawford, T. D.; Jayaram, H.; Kaufman, S.; Li, R.; Li, Y.; Liao, J.; Liang, X.; Liu, W.; Ly, J.; Maher, J.; Wai, J.; Wang, F.; Zheng, A.; Zhu, X.; Magnuson, S. A Unique Approach to Design Potent and Selective Cyclic Adenosine Monophosphate Response Element Binding Protein, Binding Protein (CBP) Inhibitors. *J. Med. Chem.* **2017**, *60*, 10151-10171.
274. Denny, R. A.; Flick, A. C.; Coe, J.; Langille, J.; Basak, A.; Liu, S.; Stock, I.; Sahasrabudhe, P.; Bonin, P.; Hay, D. A.; Brennan, P. E.; Pletcher, M.; Jones, L. H.; Chekler, E. L. P. Structure-Based Design of Highly Selective Inhibitors of the CREB Binding Protein Bromodomain. *J. Med. Chem.* **2017**, *60*, 5349-5363.
275. Romero, F. A.; Murray, J.; Lai, K. W.; Tsui, V.; Albrecht, B. K.; An, L.; Beresini, M. H.; de Leon Boenig, G.; Bronner, S. M.; Chan, E. W.; Chen, K. X.; Chen, Z.; Choo, E. F.; Clagg, K.; Clark, K.; Crawford, T. D.; Cyr, P.; de Almeida Nagata, D.; Gascoigne, K. E.; Grogan, J. L.; Hatzivassiliou, G.; Huang, W.; Hunsaker, T. L.; Kaufman, S.; Koenig, S. G.; Li, R.; Li, Y.; Liang, X.; Liao, J.; Liu, W.; Ly, J.; Maher, J.; Masui, C.; Merchant, M.; Ran, Y.; Taylor, A. M.; Wai, J.; Wang, F.; Wei, X.; Yu, D.; Zhu, B.-Y.; Zhu, X.; Magnuson, S. GNE-781, A Highly Advanced Potent and Selective Bromodomain Inhibitor of Cyclic Adenosine Monophosphate Response Element Binding Protein, Binding Protein (CBP). *J. Med. Chem.* **2017**, *60*, 9162-9183.
276. Lai, K. W.; Romero, F. A.; Tsui, V.; Beresini, M. H.; de Leon Boenig, G.; Bronner, S. M.; Chen, K.; Chen, Z.; Choo, E. F.; Crawford, T. D.; Cyr, P.; Kaufman, S.; Li, Y.; Liao, J.; Liu, W.; Ly, J.; Murray, J.; Shen, W.; Wai, J.; Wang, F.; Zhu, C.; Zhu, X.; Magnuson, S. Design and synthesis of a biaryl series as inhibitors for the bromodomains of CBP/P300. *Bioorg. Med. Chem. Lett.* **2018**, *28*, 15-23.
277. Clark, P. G. K.; Vieira, L. C. C.; Tallant, C.; Fedorov, O.; Singleton, D. C.; Rogers, C. M.; Monteiro, O. P.; Bennett, J. M.; Baronio, R.; Müller, S.; Daniels, D. L.; Méndez, J.; Knapp, S.; Brennan, P. E.; Dixon, D. J. LP99: Discovery and Synthesis of the First Selective BRD7/9 Bromodomain Inhibitor. *Angew. Chem. Int. Ed.* **2015**, *54*, 6217-6221.

278. Hay, D. A.; Rogers, C. M.; Fedorov, O.; Tallant, C.; Martin, S.; Monteiro, O. P.; Müller, S.; Knapp, S.; Schofield, C. J.; Brennan, P. E. Design and synthesis of potent and selective inhibitors of BRD7 and BRD9 bromodomains. *MedChemComm* **2015**, *6*, 1381-1386.
279. Karim, R. M.; Schönbrunn, E. An Advanced Tool To Interrogate BRD9. *J. Med. Chem.* **2016**, *59*, 4459-4461.
280. Martin, L. J.; Koegl, M.; Bader, G.; Cockcroft, X.-L.; Fedorov, O.; Fiegen, D.; Gerstberger, T.; Hofmann, M. H.; Hohmann, A. F.; Kessler, D.; Knapp, S.; Knesl, P.; Kornigg, S.; Müller, S.; Nar, H.; Rogers, C.; Rumpel, K.; Schaaf, O.; Steurer, S.; Tallant, C.; Vakoc, C. R.; Zeeb, M.; Zoephel, A.; Pearson, M.; Boehmelt, G.; McConnell, D. Structure-Based Design of an in Vivo Active Selective BRD9 Inhibitor. *J. Med. Chem.* **2016**, *59*, 4462-4475.
281. Theodoulou, N. H.; Bamborough, P.; Bannister, A. J.; Becher, I.; Bit, R. A.; Che, K. H.; Chung, C.-w.; Dittmann, A.; Drewes, G.; Drewry, D. H.; Gordon, L.; Grandi, P.; Leveridge, M.; Lindon, M.; Michon, A.-M.; Molnar, J.; Robson, S. C.; Tomkinson, N. C. O.; Kouzarides, T.; Prinjha, R. K.; Humphreys, P. G. Discovery of I-BRD9, a Selective Cell Active Chemical Probe for Bromodomain Containing Protein 9 Inhibition. *J. Med. Chem.* **2016**, *59*, 1425-1439.
282. Clegg, M.; Tomkinson, N. C. O.; Prinjha, R. K.; Humphreys, P. G. Advancements in the Development of non-BET Bromodomain Chemical Probes. *Manuscript in preparation* **2018**.
283. Caron, C.; Lestrat, C.; Marsal, S.; Escoffier, E.; Curtet, S.; Virolle, V.; Barbry, P.; Debernardi, A.; Brambilla, C.; Brambilla, E.; Rousseaux, S.; Khochbin, S. Functional characterization of ATAD2 as a new cancer/testis factor and a predictor of poor prognosis in breast and lung cancers. *Oncogene* **2010**, *29*, 5171-5181.
284. Zou June, X.; Revenko Alexey, S.; Li Li, B.; Gemo Abigael, T.; Hong-Wu, C. ANCCA, an estrogen-regulated AAA+ ATPase coactivator for ERα, is required for coregulator occupancy and chromatin modification. *Proc. Natl. Acad. Sci.* **2007**, *104*, 18067-18072.
285. Boussouar, F.; Jamshidikia, M.; Morozumi, Y.; Rousseaux, S.; Khochbin, S. Malignant genome reprogramming by ATAD2. *Biochimica et Biophysica Acta (BBA) - Gene Regulatory Mechanisms* **2013**, *1829*, 1010-1014.
286. Vidler, L. R.; Brown, N.; Knapp, S.; Hoelder, S. Druggability Analysis and Structural Classification of Bromodomain Acetyl-lysine Binding Sites. *J. Med. Chem.* **2012**, *55*, 7346-7359.
287. Hussain, M.; Zhou, Y.; Song, Y.; Hameed, H. M. A.; Jiang, H.; Tu, Y.; Zhang, J. ATAD2 in cancer: a pharmacologically challenging but tractable target. *Expert Opin. Ther. Targets* **2018**, *22*, 85-96.
288. Chaikuad, A.; Petros, A. M.; Fedorov, O.; Xu, J.; Knapp, S. Structure-based approaches towards identification of fragments for the low-druggability ATAD2 bromodomain. *MedChemComm* **2014**, *5*, 1843-1848.
289. Harner, M. J.; Chauder, B. A.; Phan, J.; Fesik, S. W. Fragment-Based Screening of the Bromodomain of ATAD2. *J. Med. Chem.* **2014**, *57*, 9687-9692.
290. Demont, E. H.; Chung, C.-w.; Furze, R. C.; Grandi, P.; Michon, A.-M.; Wellaway, C.; Barrett, N.; Bridges, A. M.; Craggs, P. D.; Diallo, H.; Dixon, D. P.; Douault, C.; Emmons, A. J.; Jones, E. J.; Karamshi, B. V.; Locke, K.; Mitchell, D. J.; Mouzon, B. H.; Prinjha, R. K.; Roberts, A. D.; Sheppard, R. J.; Watson, R. J.; Bamborough, P. Fragment-Based Discovery of Low-Micromolar ATAD2 Bromodomain Inhibitors. *J. Med. Chem.* **2015**, *58*, 5649-5673.
291. Bamborough, P.; Chung, C.-w.; Furze, R. C.; Grandi, P.; Michon, A.-M.; Sheppard, R. J.; Barnett, H.; Diallo, H.; Dixon, D. P.; Douault, C.; Jones, E. J.; Karamshi, B.; Mitchell, D. J.; Prinjha, R. K.; Rau, C.; Watson, R. J.; Werner, T.; Demont, E. H. Structure-Based Optimization of Naphthyridones into Potent ATAD2 Bromodomain Inhibitors. *J. Med. Chem.* **2015**, *58*, 6151-6178.

292. Bamborough, P.; Chung, C.-w.; Demont, E. H.; Furze, R. C.; Bannister, A. J.; Che, K. H.; Diallo, H.; Douault, C.; Grandi, P.; Kouzarides, T.; Michon, A.-M.; Mitchell, D. J.; Prinjha, R. K.; Rau, C.; Robson, S.; Sheppard, R. J.; Upton, R.; Watson, R. J. A Chemical Probe for the ATAD2 Bromodomain. *Angew. Chem. Int. Ed.* **2016**, *55*, 11382-11386.
293. Bamborough, P.; Chung, C.-w.; Furze, R. C.; Grandi, P.; Michon, A.-M.; Watson, R. J.; Mitchell, D. J.; Barnett, H.; Prinjha, R. K.; Rau, C.; Sheppard, R. J.; Werner, T.; Demont, E. H. Aiming to Miss a Moving Target: Bromo and Extra Terminal Domain (BET) Selectivity in Constrained ATAD2 Inhibitors. *J. Med. Chem.* **2018**.
294. Fernández-Montalván, A. E.; Berger, M.; Kuroopka, B.; Koo, S. J.; Badock, V.; Weiske, J.; Puetter, V.; Holton, S. J.; Stöckigt, D.; ter Laak, A.; Centrella, P. A.; Clark, M. A.; Dumelin, C. E.; Sigel, E. A.; Soutter, H. H.; Troast, D. M.; Zhang, Y.; Cuzzo, J. W.; Keefe, A. D.; Roche, D.; Rodeschini, V.; Chaikuad, A.; Díaz-Sáez, L.; Bennett, J. M.; Fedorov, O.; Huber, K. V. M.; Hübner, J.; Weinmann, H.; Hartung, I. V.; Gorjánácz, M. Isoform-Selective ATAD2 Chemical Probe with Novel Chemical Structure and Unusual Mode of Action. *ACS Chem. Biol.* **2017**, *12*, 2730-2736.
295. Zhang, Q.; Bai, B.; Mei, X.; Wan, C.; Cao, H.; Dan, L.; Wang, S.; Zhang, M.; Wang, Z.; Wu, J.; Wang, H.; Huo, J.; Ding, G.; Zhao, J.; Xie, Q.; Wang, L.; Qiu, Z.; Zhao, S.; Zhang, T. Elevated H3K79 homocysteinylation causes abnormal gene expression during neural development and subsequent neural tube defects. *Nat. Commun.* **2018**, *9*, 3436.
296. Footz, T. K.; Brinkman-Mills, P.; Banting, G. S.; Maier, S. A.; Riazzi, M. A.; Bridgland, L.; Hu, S.; Birren, B.; Minoshima, S.; Shimizu, N.; Pan, H.; Nguyen, T.; Fang, F.; Fu, Y.; Ray, L.; Wu, H.; Shaull, S.; Phan, S.; Yao, Z.; Chen, F.; Huan, A.; Hu, P.; Wang, Q.; Loh, P.; Qi, S.; Roe, B. A.; McDermid, H. E. Analysis of the Cat Eye Syndrome Critical Region in Humans and the Region of Conserved Synteny in Mice: A Search for Candidate Genes at or near the Human Chromosome 22 Pericentromere. *Genome Res.* **2001**, *11*, 1053-1070.
297. C. E. Dawe; M. K. Kooistra; N. A. Fairbridge; A. C. Pizio; McDermid, H. E. Role of chromatin remodeling gene *Cecr2* in neurulation and inner ear development. *Dev. Dyn.* **2011**, *240*, 372-383.
298. Thompson, P. J.; Norton, K. A.; Niri, F. H.; Dawe, C. E.; McDermid, H. E. CECR2 Is Involved in Spermatogenesis and Forms a Complex with SNF2H in the Testis. *J. Mol. Biol.* **2012**, *415*, 793-806.
299. G. S. Banting; O. Barak; T. M. Ames; A. C. Burnham; M. D. Kardel; N. S. Cooch; C. E. Davidson; R. Godbout; H. E. Mcdermid; Shiekhattar, R. CECR2, a protein involved in neurulation, forms a novel chromatin remodeling complex with SNF2L. *Hum. Mol. Genet.* **2004**, *14*, 513-524.
300. Lee, S.-K.; Park, E.-J.; Lee, H.-S.; Lee, Y. S.; Kwon, J. Genome-wide screen of human bromodomain-containing proteins identifies *Cecr2* as a novel DNA damage response protein. *Mol. Cells* **2012**, *34*, 85-91.
301. M. Toyoshima; H. L. Howie; M. Imakura; R. M. Walsh; J. E. Annis; A. N. Chang; J. Frazier; B. N. Chau; A. Loboda; P. S. Linsley; M. A. Cleary; Park, J. R.; Grandori, C. Functional genomics identifies therapeutic targets for MYC-driven cancer. *Proc. Natl. Acad. Sci. U. S. A.* **2012**, *109*, 9545-50.
302. Crawford, T. D.; Audia, J. E.; Bellon, S.; Burdick, D. J.; Bommi-Reddy, A.; Côté, A.; Cummings, R. T.; Duplessis, M.; Flynn, E. M.; Hewitt, M.; Huang, H.-R.; Jayaram, H.; Jiang, Y.; Joshi, S.; Kiefer, J. R.; Murray, J.; Nasveschuk, C. G.; Neiss, A.; Pardo, E.; Romero, F. A.; Sandy, P.; Sims, R. J.; Tang, Y.; Taylor, A. M.; Tsui, V.; Wang, J.; Wang, S.; Wang, Y.; Xu, Z.; Zawadzke, L.; Zhu, X.; Albrecht, B. K.; Magnuson, S. R.; Cochran, A. G. GNE-886: A Potent and Selective Inhibitor of the Cat Eye Syndrome Chromosome Region Candidate 2 Bromodomain (CECR2). *ACS Med. Chem. Lett.* **2017**, *8*, 737-741.

303. Fedorov, O.; Castex, J.; Tallant, C.; Owen, D. R.; Martin, S.; Aldeghi, M.; Monteiro, O.; Filippakopoulos, P.; Picaud, S.; Trzupek, J. D.; Gerstenberger, B. S.; Bountra, C.; Willmann, D.; Wells, C.; Philpott, M.; Rogers, C.; Biggin, P. C.; Brennan, P. E.; Bunnage, M. E.; Schüle, R.; Günther, T.; Knapp, S.; Müller, S. Selective targeting of the BRG/PB1 bromodomains impairs embryonic and trophoblast stem cell maintenance. *Sci. Adv.* **2015**, 1.
304. Gerstenberger, B. S.; Trzupek, J. D.; Tallant, C.; Fedorov, O.; Filippakopoulos, P.; Brennan, P. E.; Fedele, V.; Martin, S.; Picaud, S.; Rogers, C.; Parikh, M.; Taylor, A.; Samas, B.; O'Mahony, A.; Berg, E.; Pallares, G.; Torrey, A. D.; Treiber, D. K.; Samardjiev, I. J.; Nasipak, B. T.; Padilla-Benavides, T.; Wu, Q.; Imbalzano, A. N.; Nickerson, J. A.; Bunnage, M. E.; Muller, S.; Knapp, S.; Owen, D. R. Identification of a Chemical Probe for Family VIII Bromodomains through Optimization of a Fragment Hit. *J. Med. Chem.* **2016**, 59, 4800-4811.
305. Sutherell, C. L.; Tallant, C.; Monteiro, O. P.; Yapp, C.; Fuchs, J. E.; Fedorov, O.; Siejka, P.; Müller, S.; Knapp, S.; Brenton, J. D.; Brennan, P. E.; Ley, S. V. Identification and Development of 2,3-Dihydropyrrolo[1,2-a]quinazolin-5(1H)-one Inhibitors Targeting Bromodomains within the Switch/Sucrose Nonfermenting Complex. *J. Med. Chem.* **2016**, 59, 5095-5101.
306. Myriantopoulos, V.; Gaboriaud-Kolar, N.; Tallant, C.; Hall, M.-L.; Grigoriou, S.; Brownlee, P. M.; Fedorov, O.; Rogers, C.; Heidenreich, D.; Wanior, M.; Drosos, N.; Mexia, N.; Savitsky, P.; Bagratuni, T.; Kastritis, E.; Terpos, E.; Filippakopoulos, P.; Müller, S.; Skaltsounis, A.-L.; Downs, J. A.; Knapp, S.; Mikros, E. Discovery and Optimization of a Selective Ligand for the Switch/Sucrose Nonfermenting-Related Bromodomains of Polybromo Protein-1 by the Use of Virtual Screening and Hydration Analysis. *J. Med. Chem.* **2016**, 59, 8787-8803.
307. Crawford, T. D.; Tsui, V.; Flynn, E. M.; Wang, S.; Taylor, A. M.; Côté, A.; Audia, J. E.; Beresini, M. H.; Burdick, D. J.; Cummings, R.; Dakin, L. A.; Duplessis, M.; Good, A. C.; Hewitt, M. C.; Huang, H.-R.; Jayaram, H.; Kiefer, J. R.; Jiang, Y.; Murray, J.; Nasveschuk, C. G.; Pardo, E.; Poy, F.; Romero, F. A.; Tang, Y.; Wang, J.; Xu, Z.; Zawadzke, L. E.; Zhu, X.; Albrecht, B. K.; Magnuson, S. R.; Bellon, S.; Cochran, A. G. Diving into the Water: Inducible Binding Conformations for BRD4, TAF1(2), BRD9, and CECR2 Bromodomains. *J. Med. Chem.* **2016**, 59, 5391-5402.
308. E. M. Flynn; O. W. Huang; F. Poy; S. F. Bellon; Y. Tang; Cochran, A. G. A Subset of Human Bromodomains Recognizes Butyryllysine and Crotonyllysine Histone Peptide Modifications. *Structure* **2015**, 23, 1801-1814.
309. Zhang, X.; Chen, K.; Wu, Y.-D.; Wiest, O. Protein dynamics and structural waters in bromodomains. *PLoS One* **2017**, 12, e0186570.
310. Aldeghi, M.; Ross, G. A.; Bodkin, M. J.; Essex, J. W.; Knapp, S.; Biggin, P. C. Large-scale analysis of water stability in bromodomain binding pockets with grand canonical Monte Carlo. *Comms. Chem.* **2018**, 1, 19.
311. Bent, H. A. Structural chemistry of donor-acceptor interactions. *Chem. Rev.* **1968**, 68, 587-648.
312. Thirman, J.; Engelage, E.; Huber, S. M.; Head-Gordon, M. Characterizing the interplay of Pauli repulsion, electrostatics, dispersion and charge transfer in halogen bonding with energy decomposition analysis. *PCCP* **2018**, 20, 905-915.
313. Clark, T. sigma-Holes. *WIREs Comput. Mol. Sci* **2013**, 3, 13-20.
314. Hardegger, L. A.; Kuhn, B.; Spinnler, B.; Anselm, L.; Ecabert, R.; Stihle, M.; Gsell, B.; Thoma, R.; Diez, J.; Benz, J.; Plancher, J.-M.; Hartmann, G.; Banner, D. W.; Haap, W.; Diederich, F. Systematic Investigation of Halogen Bonding in Protein-Ligand Interactions. *Angew. Chem. Int. Ed.* **2011**, 50, 314-318.

315. Auffinger, P.; Hays, F. A.; Westhof, E.; Ho, P. S. Halogen bonds in biological molecules. *Proc. Natl. Acad. Sci. U. S. A.* **2004**, 101, 16789-16794.
316. C. Mispelaere-Canivet; Spindler, F.; Perrio, S.; Beslin, P. Pd₂(dba)₃/Xantphos-catalyzed cross-coupling of thiols and aryl bromides/triflates. *Tetrahedron* **2005**, 61, 5253-5259.
317. Demont, E. H.; Bamborough, P.; Chung, C.; Craggs, P. D.; Fallon, D.; Gordon, L. J.; Grandi, P.; Hobbs, C. I.; Hussain, J.; Jones, E. J.; Gall, A. L.; Michon, A.; Mitchell, D. J.; Prinjha, R. K.; Roberts, A. D.; Sheppard, R. J.; Watson, R. J. 1,3-Dimethyl Benzimidazolones Are Potent, Selective Inhibitors of the BRPF1 Bromodomain. *ACS Med. Chem. Lett.* **2014**, 5, 1190-1195.
318. Pu, Y.; Christesen, A.; Ku, Y. A simple and highly effective oxidative chlorination protocol for the preparation of arenesulfonyl chlorides. *Tetrahedron Lett.* **2010**, 51, 418-421.
319. Bamborough, P. Unpublished work.
320. Hao, M.-H. Theoretical Calculation of Hydrogen-Bonding Strength for Drug Molecules. *J. Chem. Theory Comput.* **2006**, 2, 863-872.
321. Young, R. J.; Green, D. V. S.; Luscombe, C. N.; Hill, A. P. Getting physical in drug discovery II: the impact of chromatographic hydrophobicity measurements and aromaticity. *Drug Discovery Today* **2011**, 16, 822-830.
322. Hill, A. P.; Young, R. J. Getting physical in drug discovery: a contemporary perspective on solubility and hydrophobicity. *Drug Discov. Today* **2010**, 15, 648-655.
323. Luo, R. Z.; Zablocki, M.-M. Azabenzimidazolones as prostaglandin D2 receptor binding inhibitors and their preparation, pharmaceutical compositions and use in the treatment of diseases. WO 2010045276, 2009.
324. Molander, G. A.; Brown, A. R. Suzuki-Miyaura Cross-Coupling Reactions of Potassium Vinyltrifluoroborate with Aryl and Heteroaryl Electrophiles. *J. Org. Chem.* **2006**, 71, 9681-9686.
325. Hentges, S. G.; Sharpless, K. B. Asymmetric induction in the reaction of osmium tetroxide with olefins. *J. Am. Chem. Soc.* **1980**, 102, 4263-4265.
326. Sharpless, K. B.; Amberg, W.; Bennani, Y. L.; Crispino, G. A.; Hartung, J.; Jeong, K. S.; Kwong, H. L.; Morikawa, K.; Wang, Z. M. The osmium-catalyzed asymmetric dihydroxylation: a new ligand class and a process improvement. *J. Org. Chem.* **1992**, 57, 2768-2771.
327. Surry, D. S.; Buchwald, S. L. Dialkylbiaryl phosphines in Pd-catalyzed amination: a user's guide. *Chem. Sci.* **2011**, 2, 27-50.
328. Wuitschik, G.; Carreira, E. M.; Wagner, B.; Fischer, H.; Parrilla, I.; Schuler, F.; Rogers-Evans, M.; Müller, K. Oxetanes in Drug Discovery: Structural and Synthetic Insights. *J. Med. Chem.* **2010**, 53, 3227-3246.
329. Lee, B.-Y.; Park, S. R.; Jeon, H. B.; Kim, K. S. A new solvent system for efficient synthesis of 1,2,3-triazoles. *Tetrahedron Lett.* **2006**, 47, 5105-5109.
330. Boren, B. C.; Narayan, S.; Rasmussen, L. K.; Zhang, L.; Zhao, H.; Lin, Z.; Jia, G.; Fokin, V. V. Ruthenium-Catalyzed Azide-Alkyne Cycloaddition: Scope and Mechanism. *J. Am. Chem. Soc.* **2008**, 130, 8923-8930.
331. Caferro, T., R.; Chamberlain, S. D.; Donaldson, K. H.; Harris, P. A.; Gaul, M. D.; Uehling, D. E.; Vanderwall, D. E. Preparation of alkynyl thienopyrimidines as protein tyrosine kinase inhibitors useful against cancer and other disorders WO2003053446, 2002.
332. Savall, B. M.; Wu, D.; De Angelis, M.; Carruthers, N. I.; Ao, H.; Wang, Q.; Lord, B.; Bhattacharya, A.; Letavic, M. A. Synthesis, SAR, and Pharmacological Characterization of Brain Penetrant P2X7 Receptor Antagonists. *ACS Med. Chem. Lett.* **2015**, 6, 671-676.

333. <https://www.helgroup.com//reactor-systems/hydrogenation-catalysis/catalyst-screening/cat96/>. (19/10/2013).
334. Andrews, K. G.; Faizova, R.; Denton, R. M. A practical and catalyst-free trifluoroethylation reaction of amines using trifluoroacetic acid. *Nat. Commun.* **2017**, *8*, 15913.
335. Andresen, B. M. A., Neville J.; Miller, Thomas A. Preparation of aminopyridine derivatives for use as spleen tyrosine kinase (Syk) inhibitors. WO2013US68190, 2013.
336. Sawayama, Y. A., Keiji; Yamai, Yusuke; Iwamoto, Kohei; Kiyoshige, Saori Preparation of benzimidazole derivatives for inhibiting voltage-gated sodium channel Nav1.7. CAN165:236079, 2016.
337. Gu, Y. G.; Weitzberg, M.; Clark, R. F.; Xu, X.; Li, Q.; Zhang, T.; Hansen, T. M.; Liu, G.; Xin, Z.; Wang, X.; Wang, R.; McNally, T.; Camp, H.; Beutel, B. A.; Sham, H. L. Synthesis and Structure–Activity Relationships of N-{3-[2-(4-Alkoxyphenoxy)thiazol-5-yl]-1-methylprop-2-ynyl}carboxy Derivatives as Selective Acetyl-CoA Carboxylase 2 Inhibitors. *J. Med. Chem.* **2006**, *49*, 3770-3773.